REDUCTION ROASTING
OF NICKELIFERROUS ORE
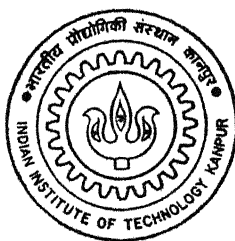# IN MULTIPLE HEARTH FURNACE

by

NILOY KUMAR NATH

DEPARTMENT OF MATERIALS AND METALLURGICAL ENGINEERING

INDIAN INSTITUTE OF TECHNOLOGY KANPUR

MARCH, 1995

REDUCTION ROASTING
OF NICKELIFERROUS ORE
IN MULTIPLE HEARTH FURNACE

A Thesis Submitted
in Partial Fulfilment of the Requirements
for the Degree of
DOCTOR OF PHILOSOPHY

By
NILOY KUMAR NATH

to the
DEPARTMENT OF MATERIALS AND METALLURGICAL ENGINEERING
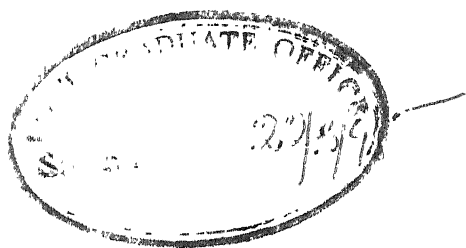## INDIAN INSTITUTE OF TECHNOLOGY KANPUR
MARCH, 1995

MME - 1995 - D - NAT - RED -

Certificate

Certified that the work contained in this thesis entitled "**Reduction Roasting of Nickelifer-rous Ore in Multiple Hearth Furnace**", by *Niloy Kumar Nath,* has been carried out under our supervision and that this work has not been submitted elsewhere for a degree or diploma.

(DR. NIRUPAM CHAKRABORTI)
Associate Professor,
Department of Materials and Metallurgical Engineering,
Indian Institute of Technology,
Kanpur-208016, INDIA

(DR. RAJIV SHEKHAR)
Assistant Professor,
Department of Materials and Metallurgical Engineering,
Indian Institute of Technology,
Kanpur-208016, INDIA

March, 1995

To

My   Parents :

my source of inspiration.

SYNOPSIS

Economic extraction of nickel from the lateritic nickeliferrous ore found in India, and many other parts of the tropical regions of the world is gaining wide spread interest, since there is a limited resource of sulfide based nickel ore deposits, and the demand for this economically and strategically important metal is ever increasing.

The extraction process of nickel from lateritic ore involves energy intensive reduction process of the ore followed by leaching and electrowinning techniques to extract nickel. The overall economy of the process depends on the efficiency of the reduction process due to high cost of fuels like oil, coal or natural gas.

In this thesis a comprehensive study of the reduction process is undertaken, starting from the single pellet reduction kinetics study, to the final modeling of an industrial reduction roasting furnace like Multiple Hearth Furnace. The work can be subdivided into three parts:

- Ore characterization and single pellet reduction kinetics study.

- Computer simulation and experimental study of reduction in fixed bed reactors.

- Computer simulation of the reduction process in Multiple Hearth Furnace.

Ore Characterization and Single Pellet Reduction Kinetics study

The run of mines ore is characterized by using various technique like SEM, EDAX, DTA, X-ray diffraction, chemical analysis and BET surface area measurements. The ore contains a very high amount of iron oxide (54 wt %) and small amount of nickel oxide (1.22 wt %) and has a very high moisture content and complex mineralogy.

Single pellet reduction study is conducted in a thermogravimetric setup to experimentally determine the kinetic parameters for both iron oxide and nickel oxide. Iron oxide reduction rate is

directly calculated from the thermogravimetric readings while reduction rate of nickel is estimated by leaching and chemical analysis. The experimental data is analyzed by using the established gas solid reaction kinetic models, with necessary modifications for non-isothermal reduction and effect of product gas formation. Furthermore a complex oxide reduction mechanism for nickel is also proposed considering the formation of $(Fe_{1-x}Ni_x)_2O_3$ complex oxide, from the minerals like goethite present in the ore. According to this mechanism unlocked NiO formation takes place only after the partial reduction of this complex oxide to form wüstite (Fe_xO) and nickel oxide (NiO).

Macrostructure of the reduced pellet is then computationally simulated to get a better insight of the reaction mechanism and visualization of the process.

Experimental and Modeling study of Reduction in Fixed Bed Reactors

Under industrial conditions, packed bed of ore pellets are reduced by reducing gases, where gas flow or gas solid contact can take place in either of the two typical modes : (i) Gas flowing vertically through the bed, as in Shaft furnace; or (ii) Gas flowing horizontally over the bed, as in Multiple Hearth Furnace and Rotary kiln. Both the situations were considered in the present work.

Reduction in a Fixed Bed Reactor with Gas Flowing through the Bed

Reduction under vertical gas flow condition is experimentally studied in a cylindrical setup. A mathematical model is then developed to simulate the process. Here, the heat and mass transfer in the bed is dominated by forced convection. In this study the fluid flow field through the packed bed of pellets is calculated from a differential form of Ergun's equation, and the void fraction variation in a packed bed of spheres is taken from literature. The computation involves steady state solution of the fluid flow in the packed bed by Ergun's equation, and simultaneous transient state solution of : (i) Solid phase thermal energy balance, (ii) Gas phase thermal energy balance, (iii) Gas phase mass or species balance, and (iv) Solid phase mass or species balance equations. The experimental and simulated results showed reasonably good matching. The effect of parameters like gas composition, pellet size etc. are also studied computationally.

Reduction in a Fixed Bed Reactor with Gas Flowing over the Bed

Reduction under horizontal gas flow condition is experimentally studied in a rectangular reactor, and a model is also developed to simulate the process. The heat and mass transfer in the gaseous phase over the bed is dominated by convection; and inside the bed it is governed by diffusion. The computation involves steady state solution of the fluid flow field over the bed by using a stream function and vorticity formulation, and simultaneous transient state solution of gas-solid heat and mass transfer, and reaction kinetics, as mentioned earlier. The experimental and simulated results showed reasonably good matching. The effect of parameters like gas velocity, gas composition, pellet size etc. are also studied computationally.

Modeling of the Reduction Process in Multiple Hearth Furnace

Industrially reduction of this type of ore can be done in a rotary kiln, shaft furnace or multiple hearth furnace (MHF). Since the reduction process is very slow and good control of gas composition is necessary for efficient reduction; MHF is considered to be the most promising for this purpose. Already a pilot plant study of the reduction process in MHF is undertaken by Regional Research Laboratory (RRL), Bhubaneswar. A model for the reduction process in MHF is therefore done based on the specifications of the MHF used in RRL Bhubaneswar.

Finite difference method is used for the solution of cylindrical axi-symmetric (r-z) equations. The solution technique involves Crank-Nicholson scheme and first order upwinding for the convective terms. This model will help in optimizing the process parameters, scaleup of the furnace and finally for the process control of the furnace under operating conditions.

Concluding Remarks

Different aspects of the reduction process of nickeliferrous ore is studied in this investigation, keeping in mind the prevailing process of reduction under industrial conditions. The single pellet reduction kinetics study showed considerable decrease in rate constant value with time due to the effect of product gas formation and non-isothermal reduction. Appreciably high reducibility of nickel is observed at 900 K and 1000 K, and selective reducibility is found to be better at 900 K for single pellet reduction.

The experimental and simulated results of nickel reduction under packed bed conditions are found to be in reasonably good agreement; considering the difficulties and limitations of the

experimental techniques. In general reduction kinetics is found to be considerably faster at 1000 K than at 900 K under packed bed conditions. The experimental and simulated results gave better match for complex oxide reduction mechanism of nickel, particularly in the regions where iron reduction is below 33 %, i.e. in the wüstite formation range. This indicates that the complex oxide reduction mechanism is more appropriate for defining the reduction kinetics of nickel in this type of lateritic nickeliferrous ore. The parametric study on input gas composition showed strong effect of water vapor on reduction kinetics, and the effect is more severe at 900 K than at 1000 K. The effect of pellet size is not very significant in the range of 2 to 8 mm pellet diameter, for reduction in packed bed conditions. The packed bed model is then extended to simulate the reduction process in a multiple hearth furnace. The results of three intermediate hearths are computed where most of the reduction takes place.

ACKNOWLEDGEMENT

Contents

List of Figures

xvii

List of Tables

List of symbols

B_{Vol}	Bed volume of a MHF hearth
C	Concentration
C_A	Reactant gas concentration
C_B	Solid concentration
D_e	Effective diffusivity in the core region, defined by eqn (3 1)
D'_e	Effective diffusivity in the product layer
D_M	Molecular diffusivity
D_K	Knudsen diffusivity
d_p	Particle or pellet diameter defined by eqn.(4 2)
f_1	Laminar resistance term defined by eqn.(4 5)
f_2	Turbulent resistance term defined by eqn.(4 6)
F	Flow rate
$g_{Fg(X)}$	Non-dimensional time for chemical control kinetics, defined by eqn (3.15)
G_H	Non-dimensional gas concentration.
k	Rate constant
k_A	Rate constant for two-layer model
$k_{/rg}$	Rate constant for grain model
k_f	Film mass transfer coefficient
K_{eq}	Equilibrium ratio of product gas and reactant gas
K_T	Thermal conductivity of pellet
l_w	Wall thickness
M_x	Solid mixing parameter
$n_1,\ n_2$	Mole fraction of iron oxide and nickel oxide $(n_1 + n_2 = 1)$
N_{sh}	Nusselt's number in the core region
N'_{sh}	Nusselt's number in the product layer
N_u	Nusselt's number
p	Porosity
P	Pressure
P_e	Peclet number
$P_{H_2},\ P_{H_2O}$	Partial pressure of hydrogen and water vapor
$P_{Fp(X)}$	Non-dimensional time for diffusion control kinetics, defined by eqn (3.17)
q	Heat of reaction
Q	Activation Energy
r	Radial position in the pellet
R	Universal gas constant
R_e	Reynold's number
R_G	Reaction term for mass or species balance

R_h	Ratio of partial pressure of water vapor and hydrogen, defined by eqn.(3 37)
R_{kg}	Rate of Solid input
R_{obs}	Observed reduction rate, defined by eqns (3 26) and (3.29)
R_p	Pellet radius
R_{st}	Residence time of solid in a hearth
R_T	Reaction term for non-isothermal reaction
S_c	Schmidt number
t	Time
t_c	Critical time for product layer formation, defined by eqn.(3 23)
t^*	Non-dimensional time, defined by eqn.(3 8)
T	Temperature
u	Superficial gas velocity
V	Velocity
V_{ol}	Volume flow rate of gas in the MHF hearths
Z	Non-dimensional temperature, defined in eqn (3.32)

Greek symbols:

$\triangle$	Finite Difference
∇	'Del' differential operator
$\triangle G$	Free Energy change due to reaction
$\triangle H$	Enthalpy change due to reaction
$\triangle S$	Entropy change due to reaction
α	Thermal or mass diffusivity
μ	Gas viscosity
ϕ	Non-dimensional parameter for two-layer model, defined in eqn.(3.24)
ϕ_s	Particle shape factor for packed bed
ρ	Density
σ	Non-dimensional parameter for grain model, defined in eqn.(3 12)
τ	Tortuosity factor
ε	Non-dimensional radial position
φ	Represents ant property which can be transported and diffused
ψ	Stream Function
ξ	Amplification factor defined by eqn.(4.33)
ϵ	Bed porosity or void fraction
ω	Vorticity

Subscripts and superscripts:

av	Average value
b	Bulk concentration
b	Packed Bed
eq	Equilibrium condition
g	Grain
g	Gaseous Phase
G	Gas concentration
H	Hydrogen
i	As super script to denote imaginary number ($\sqrt{-1}$) in eqn (4 33)
i	Used as a counter to denote grid number
i	Variable Oxide (1 Nickel,2 Iron)
int	Initial condition
m	Interfacial position between the product layer and the core region
o	Initial Concentration
o	Standard state
p	Pellet or particle
s	Pellet surface
s	Solid Phase
sc	Shrinking core
w	Solid Wall
*	Dimensionless quantity
'	Product layer

Chapter 1

INTRODUCTION

The present study deals with the economic extraction of nickel from lateritic nickeliferrous ore The laterite ores are oxides of complex mineralogy, and nickel is present in it as lattice substitute for iron or magnesium in minerals like goethite and serpentine respectively. Since the Indian ore predominantly consists of the iron bearing goethite phase it is known as nickeliferrous ore, and this type of ores are also known as limonitic ores Nickeliferrous laterite ores are located in the Sukinda region of Orissa in India, as an overburden of the chromite ore The nickeliferrous overburden generated from the chromite mines is in the order of 9 million tones per annum averaging about 0.7 % Nickel, which is dumped as waste. The total reserve of this overburden ore is estimated to be about 154 million tones [1]. At present almost the total nickel requirement of India is met by imports, and so the department of mines has shown interest in exploring the possibility of extracting nickel and cobalt from this ore for the future needs in the country. At present various research organizations in India, like National Metallurgical Laboratory, Jamshedpur; Regional Research Laboratory, Bhubaneswar etc., are involved in the recovery of nickel and cobalt by reduction-roast-ammoniacal leach, and electrowinning process [1, 2, 3, 4]. In this process different types of reductants, such as fuel oil, natural gas, coal, could be used for metallization of nickel and cobalt.

Nickel ores occur in both sulfide and oxide forms. The production from sulfide ores have predominated over the oxide ores, since it is much simpler and more economical to extract nickel from sulfide ores. However there is a limited resource of sulfide ores and about 80 % of the nickel ore deposits are present in its oxide form. Due to these reasons, as the demand for nickel increased steadily, production from oxide ores gradually increased. Figure 1.1 [5] demonstrates the shift in emphasis from sulfide to laterite over the last 35 year period as more and more laterite

deposits were developed to the commercial stage World nickel from laterite sources increased steadily from less than 5 % to about 25 % in 1960, 35 % in 1970 and 44 % in 1980 During the 1960's several factors contributed to the renewed interest and massive investment in laterites. These included steady increase in nickel demand and the prospect of continuing low energy costs (hence, low production cost for the energy-intensive extraction from laterites). Currently, nickel production from laterites as a percentage of overall production appears to have stabilized at about 45 % level. This plateau has been caused by the increase in energy costs and shutdown of uneconomic establishments during the early 1980's due to this reason

Nickel is an economically and strategically important alloying element that is increasingly being used for making stainless steel, super alloys, maraging steel and consumed in the field of chemical processing, space research, nuclear reactor engineering The present world production of nickel has exceeded 0 5 million tons per annum. Nickel is a valuable alloying constituent in a wide range of alloys mainly for improving the mechanical properties, heat and corrosion resistance of the alloy. Due to the high cost of nickel some of the nickel products have been substituted by other materials like, titanium, aluminium, plastics etc. Figure 1.2 [5] compares the growth in consumption of a number of such materials. It can be concluded that due to high cost of metals like nickel and copper, their consumption have maintained a lower growth rate, and are used specifically for those purposes where it cannot be substituted.

1.1 Nickel Ores

India has no known reserves of sulfide ores In the lateritic ores nickel is present in the form of solid solutions with iron or magnesium bearing minerals, and so physical upgrading methods are not applicable. The only method which has been employed is tumbling followed by screening. This method separates or eliminates part of the silica based gangue minerals. Therefore, in laterite ore processing, the feed to the extraction plant is low grade with 1 % to 3 % Nickel compared to 8 % to 15 % Nickel in the flotation concentrates fed to the sulfide ore processing plants In addition, when processing sulfide concentrates, the heat generated by sulfide oxidation can be used advantageously, whereas no such internal fuel is available in the case of laterite ores. Furthermore the laterites contain a large amount of free and combined water, and the removal of this water requires a lot of energy Therefore, the recovery of nickel from oxide ores requires two to six times the energy needed for the recovery of nickel from sulfide concentrates

LATERITE   PRODUCTION   (%)

1950	1960	1970	1980	1985 - 87
4	25	34	44	45 (est)
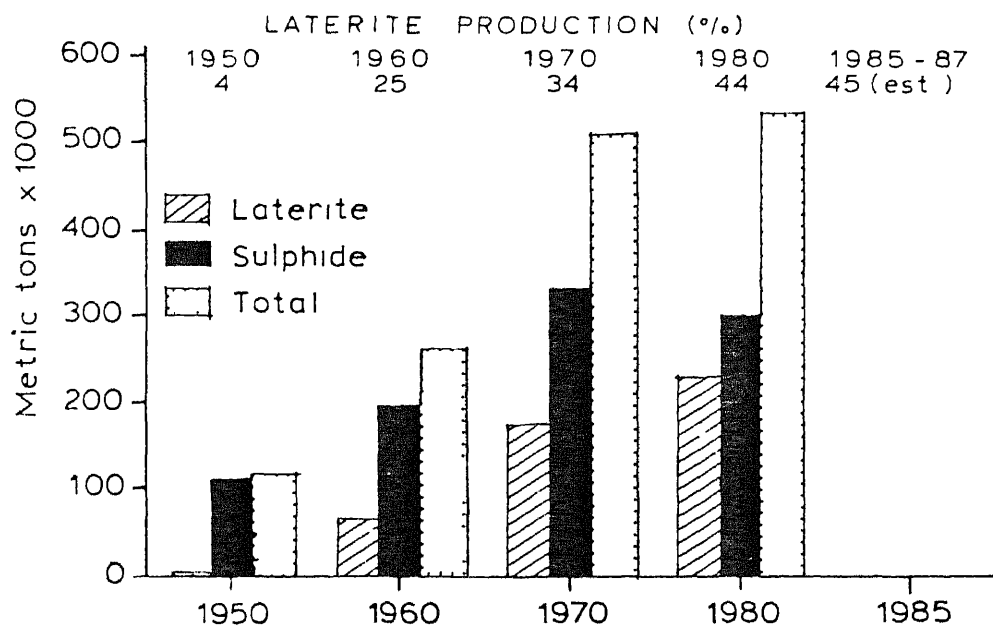
Figure 1.1: Non-socialist world nickel mine production [5].
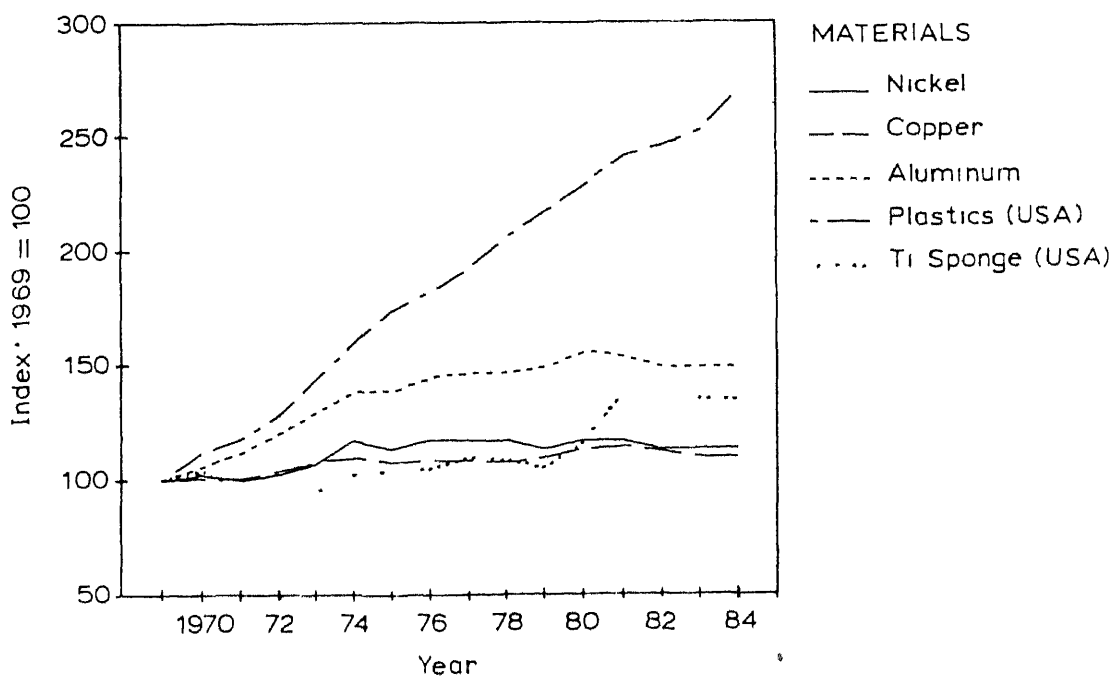
Figure 1.2: Growth rate of selected materials [5].

The lateiite ores can be processed by the following methods to recover the nickel values :

1. Pyrometallurgical Processing

2 Pyrometallurgical Processing followed by Hydrometallurgical Processing

3. Hydrometallurgical Processing

1.1.1 Pyrometallurgical Processing

Pyrometallurgical processing consists of drying the ore to eliminate free moisture, heating the ore to a temperature of about 800 K to 1000 K to drive off combined water of crystallization (which is released above 800 K), and to selectively reduce the ore under a reducing atmosphere, and smelting the ore to recover a metal/matte phase containing over 90 % of the nickel and a slag containing the unwanted oxides

The reduced ore is smelted in the normal procedure in an electric furnace at 1800 to 1900 K During smelting, the reduced nickel and iron melt to form a ferronickel bath with 25-40 % nickel, and the gangue silicates form a molten slag. The ferronickel is tapped from the furnace and is sent for further refining in order to oxidize phosphorus and remove sulfur, to produce ferronickel or stainless steel.

In matte smelting operation, sulfur is incorporated in the feed to the electric furnace. This operation produces a matte instead of ferronickel in the electric furnace. This matte is latter converted to eliminate iron to produce high concentration of nickel sulfide. This nickel sulfide can be roasted and reduced to produce metallic nickel. Pyrometallurgical processing is applicable in the case of ores with less than 25 % iron.

Over 75 % of the nickel produced from the oxide ores of nickel is currently being extracted by total pyrometallurgical processing [6, 7] which is ideal because the more economical high-grade ore bodies have a low iron content. However, in the future, the lower-grade high iron ore bodies are likely to be important sources of nickel and the methods described in the next two sections are likely to attract more attention.

1.1.2 Pyrometallurgical Processing followed by Hydrometallurgy

An ore with a high iron content cannot be readily treated by total pyrometallurgical route because in the smelting stage the grade of ferronickel/matte produced will be low, and the high iron content of the slag makes it highly corrosive towards the refractories at the smelting temperatures of 1750 K and above. For such an ore, an attractive methods involves, the pyrometallurgical reduction process followed by the leaching of the metallic nickel with ammoniacal ammonium-carbonate solution under oxygen atmosphere to obtain a leached solution containing nickel The nickel present in the solution can be precipitated in the form of a basic carbonate [$3Ni(OH)_2 2NiCO_3$] On calcination at 1000 to 1100 K, the carbonate decomposes to nickel oxide which can be reduced to yield metallic nickel When the leach solution contains other metals like cobalt, nickel can be recovered by solvent extraction methods or by electro deposition techniques This route is followed by the Greenvale plant in Australia [8], and in the pilot plant studies in Regional Research Laboratory, Bhubaneswar, India [1, 2]

1.1.3 Hydrometallurgical Processing

Although a number of hydrometallurgical processes have been studied, the process that is used in commercial practice and is receiving attention is the high pressure acid leaching process. This process is suited for high-iron (> 40 %) ores with a low serpentine or magnesium containing minerals. Serpentines consume a large amount of acid, therefore, for high-serpentine ores, this process is not attractive.

The foregoing process is in commercial use at a plant in Moa Bay (Cuba) [9]. In this plant, the limonitic ore is first screened to remove rock and serpentine and then subjected to sulfuric acid leaching at 525 K. In order to maintain water in liquid state, a pressure of about 40 atm is applied. The metals in the leach solution are precipitated in the form of sulfides by precipitation with H_2S at 400 K temperature and 10 atm pressure. This produces a sulfide precipitate of about 55 % Ni, 0.3 % Fe and rest sulfur. This precipitate has to be dissolved and the solution refined to produce refined nickel. This procedure is not widely used due to pollution problems caused by the chemicals, and highly corrosive condition of the leaching process

1.2 Scope of the Present Work

In the present investigation we have systematically studied the reduction process of nickeliferrous ore under various conditions The Indian nickeliferrous ore contains high amount of iron and small amount of nickel, for which the pyrometallurgical route followed by leaching is considered to be the most suitable Since the overall efficiency of the extraction process will mainly depend on the energy intensive reduction process, it is studied thoroughly starting from the single pellet reduction kinetics to modeling of an industrial furnace namely Multiple hearth roaster. There are various reduction roasting furnaces in operation for reducing this type of ores like Shaft furnace [10], Rotary kiln [6] and Multihearth furnace [2]. The performance criteria of the roasters are not known quantitatively, and good mathematical models for studying the performance of the furnaces are not available, resulting in inefficiency and arbitrary choice of furnaces for the roasting operations Simulation of the process, and modeling of the roasting furnaces are complicated due to the simultaneous occurrence of various phenomena like gas flow, gas solid heat & mass transfer, and reaction kinetics of the ore under varying conditions inside the furnace. Therefore this type of modeling study can quantitatively study the efficiency and advantages of each furnaces under any specific condition. The effect of various operating parameters can also be studied and adjusted for achieving better efficiency, if a model incorporating all the important parameters are available. Keeping in view all these goals we have studied the performance of fixed bed reactors for gas flow over the bed and gas flow through the bed conditions which are the basic two modes of gas solid contact in the industrial reactors. Based on the flow over the bed condition a model for Multihearth furnace is developed Similar models can also be made for Shaft furnaces based on the flow through the bed study.

1.3 Layout of the Thesis

In the next Chapter literature review of the previous work in the related areas are briefly discussed.

In the third Chapter characterization of the Indian nickeliferrous ore is described and its reduction kinetics with hydrogen is presented and analyzed. The effect of non-isothermal reduction and effect of product gas formation were incorporated in the gas solid reaction kinetic models to make them more general and widely applicable under different conditions.

The fourth Chapter briefly outlines the necessity for mathematical modeling in extractive metallurgy, and the numerical methods used in the present investigation.

The performance of fixed bed reactors are presented in the fourth and fifth Chapters Theoretical models were developed and matched with experimental data to validate the models

In the seventh Chapter development of the mathematical model for multiple hearth furnace is described and the effect of some of the important parameters are discussed.

Concluding remarks and suggestions for future work are given in the next two Chapters; Appendix and references are given subsequently.

Chapter 2

LITERATURE REVIEW

A brief review of the current state of research on the extraction process of nickel from lateritic ore is presented in this Chapter. Industrial processes like reduction roasting of nickeliferrous ore involves various subjects or related topics like ore characterization, reaction kinetics, heat and mass transfer, mathematical modeling etc., which has to be studied and integrated to get an overall understanding of the process. The important aspects of the process are discussed in the following sections :

2.1 Nickeliferrous Ore and its Characteristics

The oxide ores of nickel are referred to as laterites. The laterite ores are formed by a process of weathering, and occurs mainly in the tropical regions and are generally classified as follows [11] :

1. A redish brown laterite overburden, to a depth of several meters from the surface, containing about 1 to 1 5 % Nickel with 40 to 50 % iron. This is also known as limonitic ores. The limonites mainly contains goethite [$(FeNi)O(OH).nH_2O$] which has nickel in solid solution with iron oxide.

2. The layer below the limonitic zone is the serpentinic [$Mg_6Si_4O_{16}(OH)_8$] zone, in which Mg has been substituted in varying degrees by nickel, iron and cobalt. It contains about 1.5 to 4 % nickel with 10 to 15 % iron.

3. Below these layers is a rocky zone containing less than 1 % nickel and 10 % iron.

Table 2 1: Composition of the Indian lateritic nickeliferrous ore reported in literature

Components	Nayak [1]	Bodas [3]	Singh et al [4]	Present Work
Ni	1 06	0 82	1 12	1 22
Co	0.04	0 057	0 064	-
Fe	54.71	24 35	49.3	54 65
Cr_2O_3	1.65	1 35	3 46	2.54
MgO	1.25	0 23	1.08	0.33
Al_2O_3	1 42	3 37	5 36	4 90
SiO_2	9.72	52 31	5.05	36 36
L O.I[†]	13 70	0 90	15 02	-

[†] Loss On Ignition

It may be noted here that the Indian nickel ore found in the sukinda region of Orissa is limonitic in nature and the serpentine ore zone is absent in this ore body [9] The composition of the ore reported by various investigators are given in table 2.1

Electron Probe Micro-Analysis (EPMA) study of NiO concentration in different mineral species of laterite ore is reported by Onodera et al., [11]; and is given below :

1 Serpentine : NiO 2-5 %, rarely more than 15 %. The greater the density, higher the content of NiO, particularly in the 2.65-2 96 T/m^3 density region where it came to 5-15 %

2 Limonite · NiO assay about 3-8 %. It can be spotted by its reddish color.

3. Unaltered quartz : An insignificant amount of nickel was determined in it.

4. Magnetite and Chromite · No NiO could be determined in these minerals.

5 Talc and kaolinite : an insignificant amount of NiO was observed

6 Enstate and forsterite : NiO assay shows a wide range of distribution up to 10 %.

In limonitic and serpentinic ore, nickel is present in the form of a solid solution. Here physical beneficiation methods are not very successful. Magnetic separation method for separating iron, nickel and chromium containing goethite phase from non-magnetic Al-Si-O phase have been tried and it is found that the method is more successful for larger size fractions [11]. Since the Indian lateritic ore has very fine clay like structure, the magnetic separation method is not very

effective. It is found that the finer ore fractions contains higher percentage of Ni, Fe, Co etc, and so differential settling time is used to remove larger particle fractions [11]. This method is generally used to partially upgrade the ore

2.2 Differential Thermal Analysis (DTA) and Thermo-Gravimetry (TG)

The DTA and TG curves for the two major nickel bearing minerals namely goethite and serpentine is shown in figure 2.1, as reported by Onodera et al [11]. We can approximately estimate the relative concentration of goethite and serpentine in the ore by comparing their characteristic DTA peaks.

Figure 2 2 shows the DTA peaks of a typical lateritic ore [9]. The first endothermic peak (W) at around 400 K is due to the removal of free moisture in the ore. The second endothermic peak (G) at around 573 K is due to the dehydration of goethite to hematite. Nickel is present as a lattice substitute for iron in the goethite phase, therefore the dehydration of goethite can be represented as :

$$2(Fe_{1-x}Ni_x)OOH \rightarrow (Fe_{1-x}Ni_x)_2O_3 + H_2O \qquad (2 1)$$

The presence of nickel in goethite is very difficult to identify, since it has very small amount of nickel and the change in lattice parameter due to nickel will be very small since their atomic radii are very similar. It has been reported by Cores et al. [12] that mixture of $NiO\text{-}Fe_3O_4$ when heated above 730 K produce complex oxides like nickel ferrites :

$$NiO + Fe_3O_4 \rightarrow NiFe_2O_4 + FeO \qquad (2.2)$$

It is also reported that the reduction of mixture of oxides of nickel and iron results in the formation of a series of solid solutions Ni_xFe_{1-x} which is confirmed by X-ray analysis [12].

Loss of constitutional water from magnesium complex mineral at 820 K gives rise to a medium size endothermic peak(S), which is associated with the phase transformations shown below [11].

$$(Mg_{1-x}Ni_x)_3Si_2O_5(OH) = 2(Mg_{1-x}Ni_x)O + (Mg_{1-x}Ni_x)Si_2O_5 + 2H_2O \qquad (2.3)$$
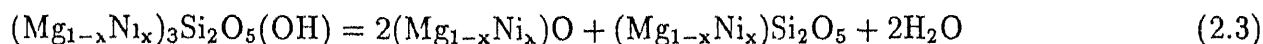
Crystallographic transformations of serpentine to olivine (or forsterite), which is indicated by a strong exothermic peak at 1073 K

$$4(Mg_{1-x}Ni_x)O + 2(Mg_{1-x}Ni_x)Si_2O_5 = 3(Mg_{1-x}Ni_x)_2Si_2O_4 + SiO_2 \tag{2.4}$$
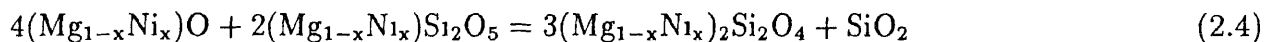
2.3   Pyrometallurgical Processing followed by Hydrometallurgy

Pyrometallurgical processing consists of drying the ore to eliminate free moisture, heating the ore to a temperature of 650 - 950 K to drive off the free and combined water of crystallization. If the iron content of the ore is less than 25 %, it can be directly smelted to recover the metal or ferronickel in the matte phase containing over 90 % Ni But this cannot be achieved with high percentage of iron in the ore

When making a comparison between the hydrometallurgical processing of laterite and sulfide ores, it is the energy required to roast the laterite ore, along with its inability to be concentrated, that makes it more costly to treat than the sulfides.

Notwithstanding this necessity for a high temperature reduction roast step, the ammonia ammonium-carbonate leach system does have the following advantages over an acid digestion of laterite ores, a process which does not require a roasting step.

1. The leach medium (NH_3 and CO_2)can be recovered for reuse.

2. Only the nickel and cobalt are kept in solution and the problems of removing undesirable contaminants (e.g. Fe, Al, and Mg) are not experienced.

3 Corrosion problems are less severe.

A simplified flow sheet of the pyrometallurgical processing for nickel extraction is shown in figure 2.3. The unit operation steps involved can now be discussed in little more details, and the Australian plant practice for nickel extraction reported by Reid [8] can be referred for this. The ore is initially stockpiled to partially dry it in atmosphere to about 25 % moisture which is reduced to 2-3 % in rotary kiln dryers. Both oil and coal can be used for this, although coal is preferred due to economic reasons. For coal firing spreader grate stoker air heaters with gas
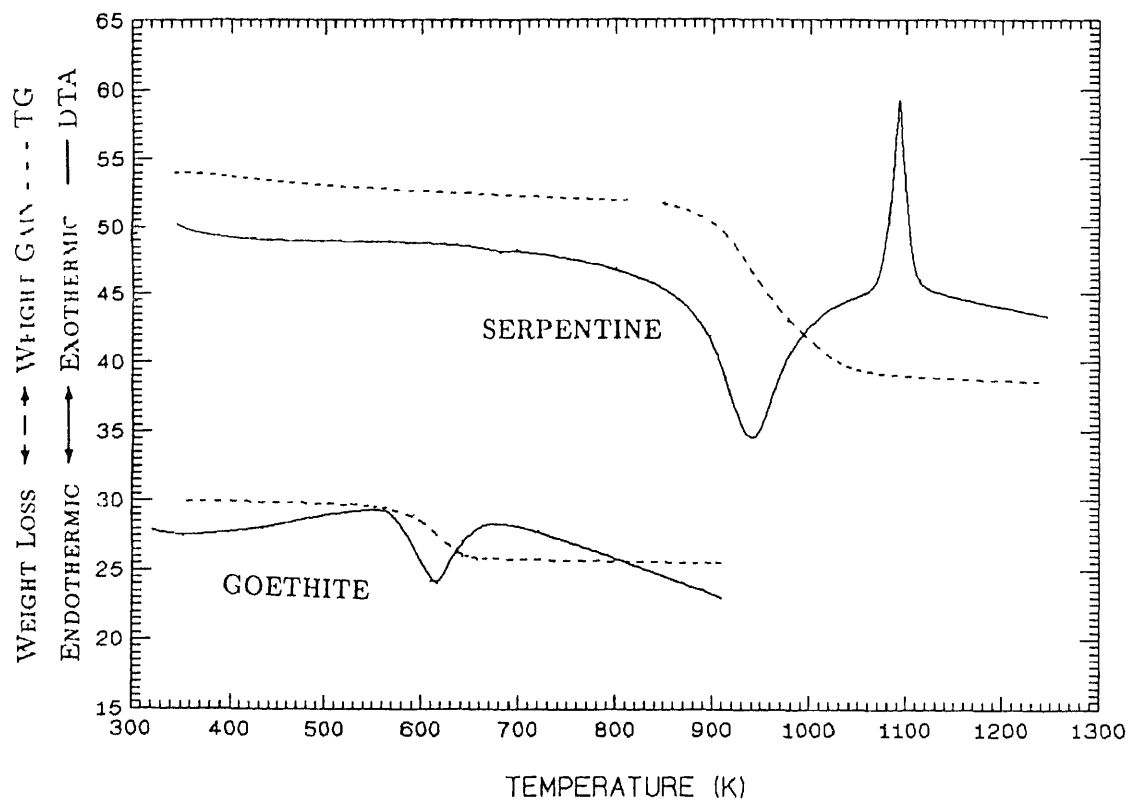
Figure 2 1· Thermal gravity - differential thermal analysis for serpentine and goethite [11].
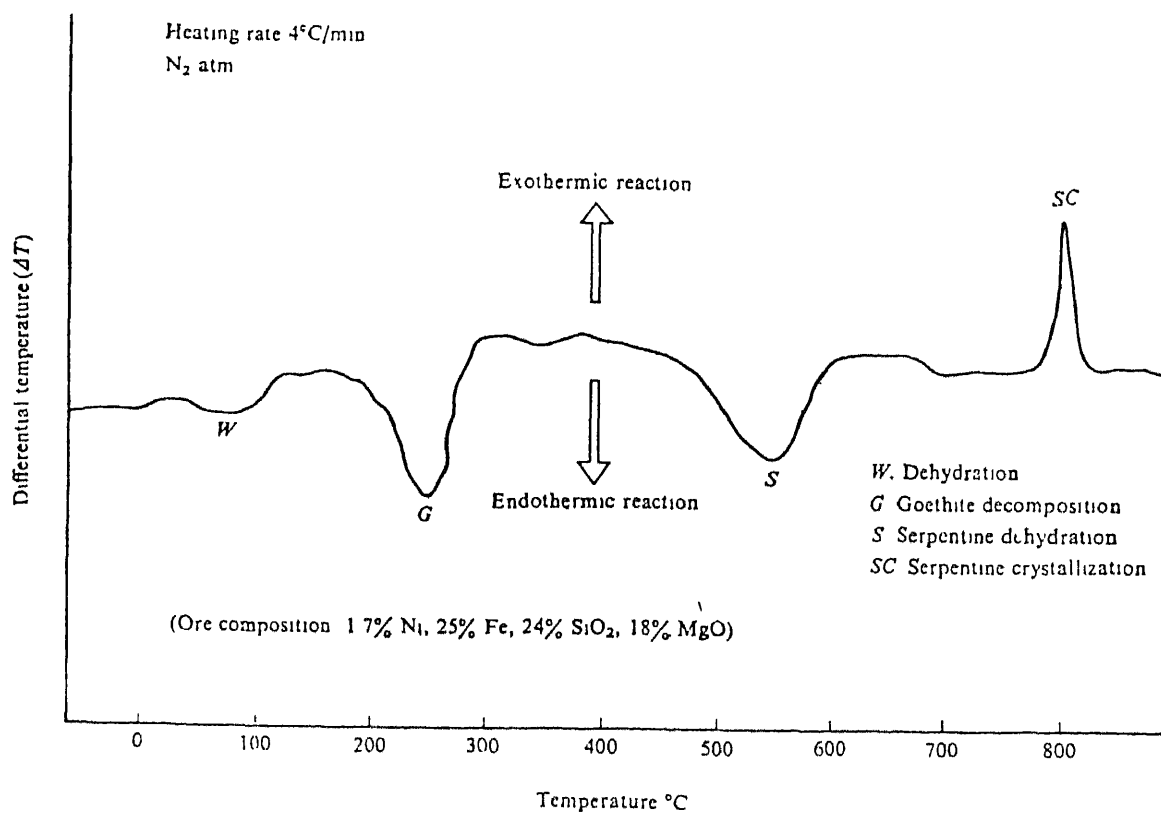
Figure 2.2: Differential thermal analysis of a typical laterite ore [9].

ducting to the dryers are needed The coal consumption is about 0 035 t/t of ore dried. The dried ore is hammer milled and then dry ground to a size of about 60 % minus 45 micron in ball mills in case of lumpy ores

The dried ore is then fed into a reduction roasting furnace, and Reid [8] has reported that mixing the ore with 2 5 % fuel oil enhances the efficiency of nickel and cobalt reduction The reduction of the nickel and cobalt in the ore (along with the unavoidable production of 5 to 7 % metallic iron) is obtained by operating the oil fired combustion chambers with sub-stoichiometric air to generate hydrogen and carbon monoxide gases in the roasters.

The optimum temperature of reduction is reported to be in the range of 1000 - 1100 K [1, 4, 8], and the reduction efficiency drops rapidly both above and below this range At lower temperatures incomplete reduction occurs and at higher temperatures phase transformations occurs with the formation of forsterites (or olivine) and ferrites which irreversively captures some of the nickel and cobalt from serpentine and limonite fractions of the ore respectively.

The effect of particle size on nickel extraction shows that all size fractions coarser than 45 μm showed significant improvement in nickel extraction efficiency on further grinding. However sizes below 45 μm showed no such significant improvement, thereby indicating that significant surface area already had been exposed so that the micropore penetration limitation to nickel extraction was no longer important [8].

When operating under the reducing conditions, which maximize the reduction of nickel and cobalt, near about 20 % of the iron content of the ore is also reduced to the metallic state. This unfortunately adversely affects the leaching step, because most of the reduced nickel and cobalt form alloys with this metallic iron.

2.4 Thermodynamics and Kinetics of Selective Reduction

According to Ellingham diagram shown in figure 2.4 [13] the descending order of free energy of formation (or tendency to get reduced) for Nickel and iron oxides are as follows :

$$Fe_2O_3 < NiO < Fe_3O_4 < FeO$$
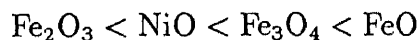
Iron oxide reduction takes place in step wise manner :

$$Fe_2O_3 \rightarrow Fe_3O_4 \rightarrow FeO \rightarrow Fe$$
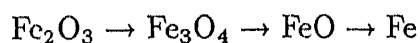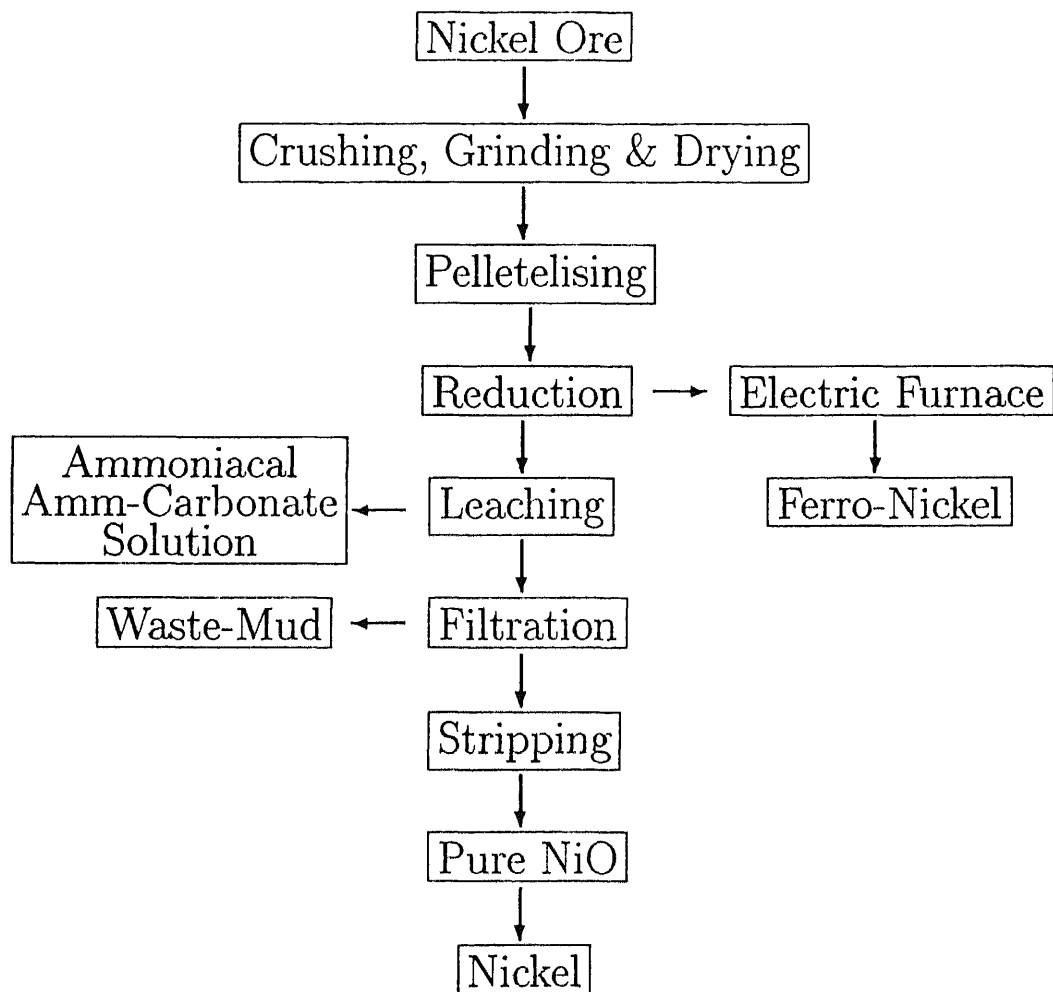
Figure 2 3: Flowsheet for nickel extraction by Pyrometallurgical process [9].

Table 2.2· Product gas composition by substoichiometric combustion of non-coking coal.

Gas	Bodas et al [3]	Singh et al. [4]
CO	20 3	29.2
CO_2	31.6	24.6
H_2	35.5	30.1
CH_4	4 15	1 2
O_2	1.6	2 8
N_2	6 9	12.1

Therefore according to the Ellingham diagram Fe_2O_3 will first get reduced to Fe_3O_4; then NiO will be reduced and after that reduction of Fe_3O_4 and FeO will take place. Therefore preferential reduction of NiO before the reduction of Fe_3O_4 and FeO to metallic iron is possible in principle

Industrially hydrocarbon fuels like natural gas, pulverized coal, fuel oil etc are used to provide both the energy and reducing gas required for the process. The composition of the gas produced by oxygen deficient combustion of such fuels reported in literature [3, 4] is shown in table 2 2.

Samanta et al. [14] have studied the reducibility of various reducing gases, and their findings are shown in figure 2 5. The figure shows that the reducibility of H_2 increases very rapidly with temperature making it a stronger reducing agent than CO above 1150 K. Below this temperature CO is a stronger reducing agent. So at around 1073 K, the optimum temperature for Ni-ore reduction, both CO and H_2 will have comparable reducibility.

The reduction of iron and nickel oxides with CO and H_2 either together or individually can be studied by the Fe-Ni-O-C system and Fe-Ni-O-H systems shown in figure 2 6, which indicates the composition and temperature limits of reactions encountered during the reduction of various oxides. A diagram in this form was first used by Edstrom [15, 16] for iron oxide reduction. The stability region of the Ni-O phases were taken from the similar diagrams reported by Samanta et al , and Ray et al. [14, 9]. Industrially reducing condition can be produced by partial combustion of hydrocarbon fuel or coal under oxygen deficient condition to produce a mixture of CO/CO_2 and H_2/H_2O, and the typical ratio of CO/CO_2 (or H_2/H_2O) achieved is in the range of 0.5 to 0 7 before reduction and finally becomes 0.1 to 0.2 after the completion of reduction. From figure 2.6 it can be predicted that metallic nickel and magnetite would be the predominant phases, but in reality the metallic phase contains 30-50 % Fe and the oxide phase always contains wüstite
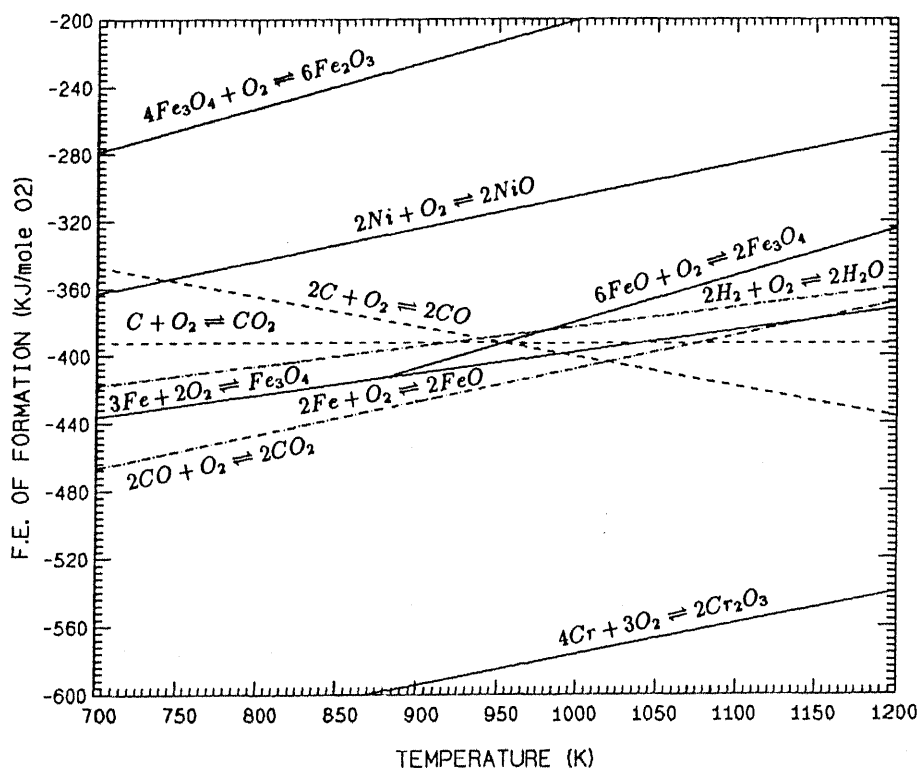
Figure 2.4: The standard free energy of formation of oxides; the standard states being the pure condensed phases and gases at 1 atm pressure [13].
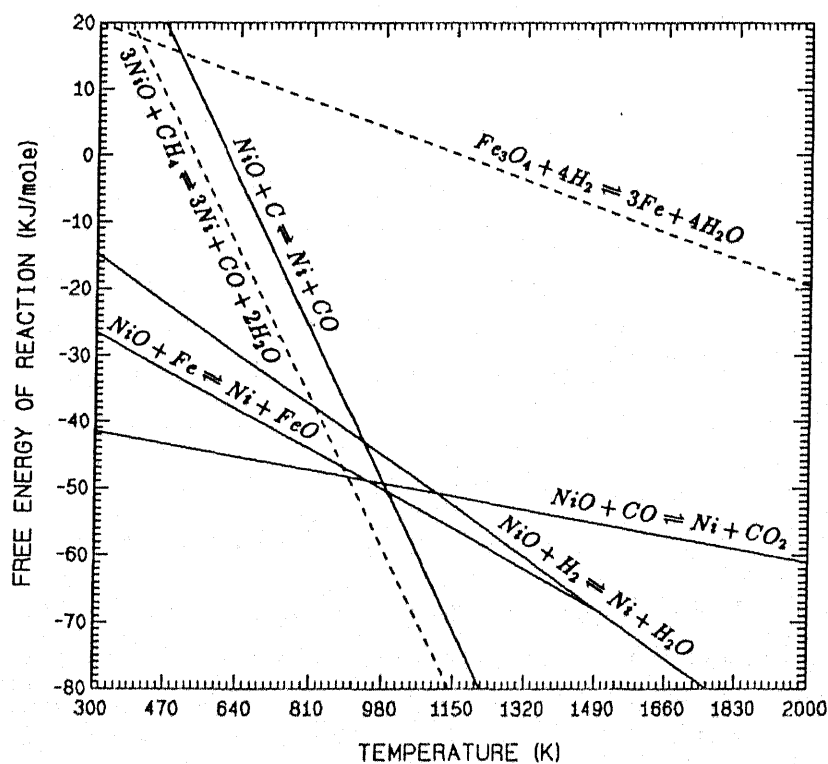
Figure 2.5: Free energy change for nickel oxide reduction as a function of temperature [14].

and magnetite The amount of reduction varies between 80 % and 95 % of Ni depending on reduction time and conditions.

Any gas solid reduction process is limited by the temperature at which it can operate If the temperature is too high the solid reactants will agglomerate and for nickel ore the formation of olivine further restricts it to a range below 1100 K; if the temperature is too low the reaction rate will not allow an acceptable rate of reduction.

Cores et al. [12] have studied the joint reduction under non-isothermal conditions of an iron concentrate and nickel oxide, with the use of coal and hydrogen as reducing agents The results of 25 % NiO and 75 % Fe_3O_4 are shown in figure 2 7(a) and (b) for reduction with coal and hydrogen respectively. The figures show distinct peaks for nickel and iron oxide reduction. For hydrogen the peaks for NiO and Fe_2O_3 reduction are at around 623 K and 723 K respectively For reduction with coal peaks for maximum reduction of NiO is at around 1013 K and for Fe_3O_4 it is at about 1183 K These results however are not directly applicable for nickel ore reduction since it contains various phases and its reduction kinetics varies considerably from the pure oxides of iron and nickel.

2.5   Reduction of Pure Oxides and Ores of Nickel and Iron

Reduction kinetics of pure nickel oxide (NiO) were studied extensively by various investigators [17, 18, 19, 20, 21, 22] to study the gas solid reaction mechanism, since it is a simple oxide and directly reduces to metallic nickel without forming any intermediate oxides. The activation energy of NiO reduction with hydrogen and carbon monoxide, reported in literature is given in table A.18 and A.20 in Appendix A. The effect of water vapor formed during hydrogen reduction of nickel oxide were studied by Bandrowski et al. and Pluschkell et al. [20, 21], and its effect on rate constant is given below.

Bandrowski et al. [20] $k = k^\circ \left[1 + 3.37 P_{H_2O}\right]^{-1}$

Pluschkell et al. [21] $k = k^\circ \left[\sqrt{P_{H_2}} \left(1 + 2.71 \times 10^{-2} \exp(5838/T) \frac{P_{H_2O}}{P_{H_2}}^2\right)\right]^{-1}$

Reduction of iron oxide with hydrogen and carbon monoxide were also studied extensively due to its importance in iron making through blast furnace and sponge iron route Iron oxide reduction is complicated by the presence of three oxide phases namely hematite (Fe_2O_3), mag-
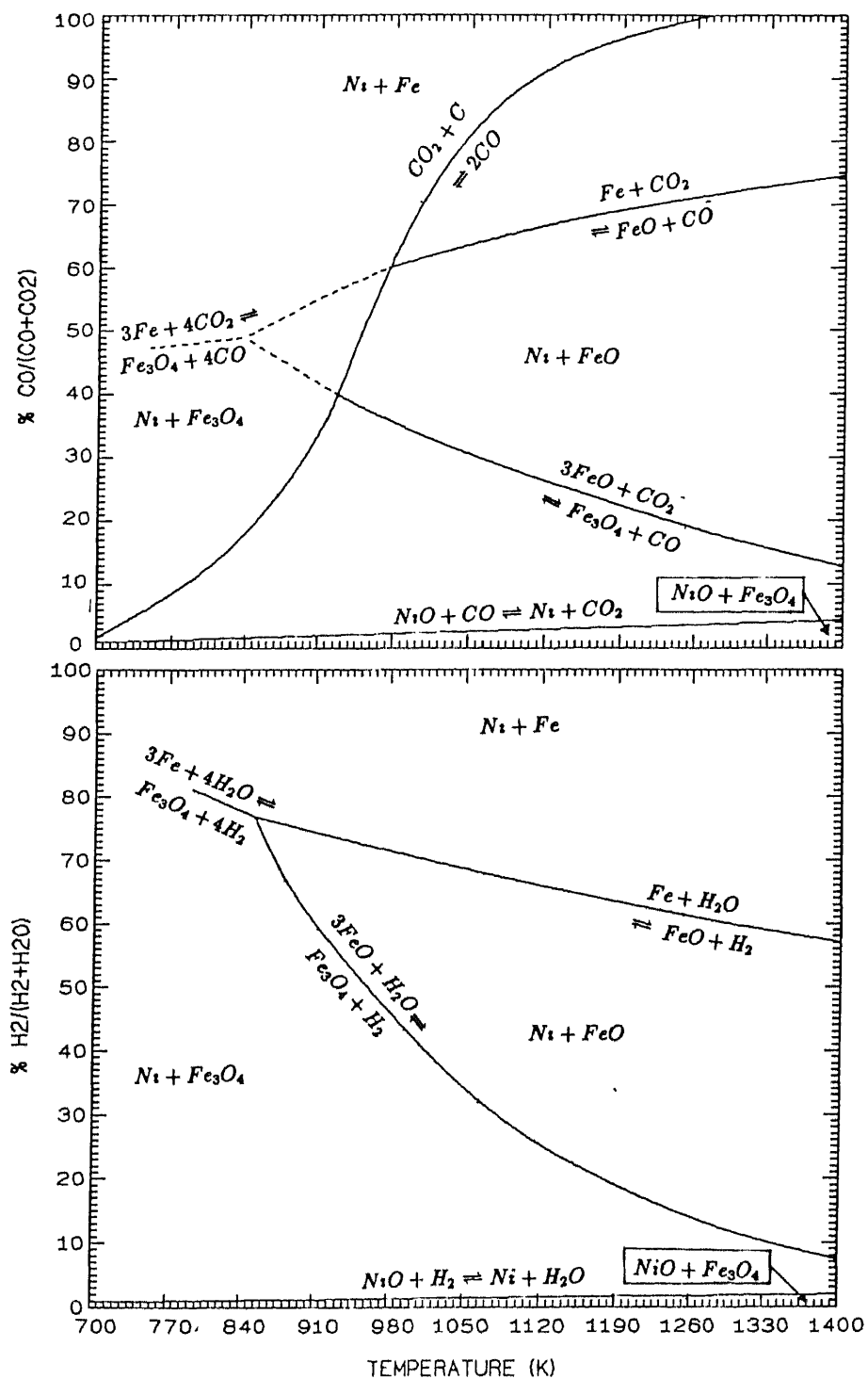
Figure 2 6: Fe-Ni-O-H and Fe-Ni-O-C system at 1 atm pressure [9, 14, 16].
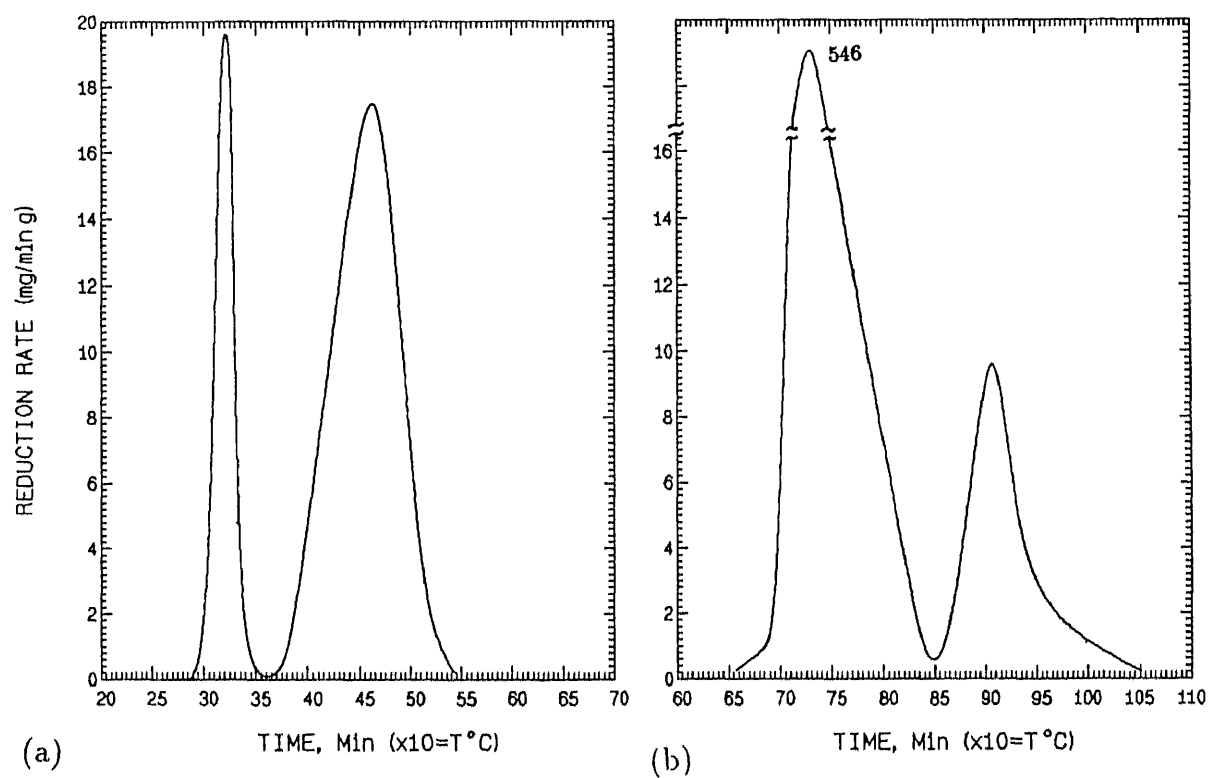
Figure 2 7: Specific reduction rate vs. temperature (and time) for reduction with : (a) Hydrogen and (b) Coal [12].

nctite (Fe_3O_4) and wüstite (Fe_xO); and the reduction of iron ore which is generally in the form of hematite takes place in step wise manner citedancy,bits,benesch. The activation energy of iron oxide reduction reported in literature is given in table A.19 and A 21 of Appendix A. Presence of water vapor sharply diminishes the reducibility of iron oxides by hydrogen. Apart from the thermodynamic effect of the product phase gas, it has other effects like poisoning effect whereby it gets attached in the oxide surface and makes the reduction process slow.

Apart from these there are other specific and abrupt changes in reducibility of iron oxides with hydrogen and carbon monoxide which are listed below :

1 The wüstite (Fe_xO) phase is unstable below 833 K and so there is change in reaction mechanism above this temperature

2 There is an anomalous decrease in reducibility of hematite or magnetite with hydrogen in the range of 850 - 950 K, as reported by various investigators studying the reducibility of iron in that range [23, 24, 25].

3 There is a similar anomalous decrease in reducibility of iron oxide with carbon monoxide in the range of 950 - 1250 K [26]

4 During reduction at high temperature ranges (1000 - 1500 K) grain coarsening and change in pore structure takes place which may abruptly changes the mechanism of reaction.

The anomalous behavior of reduction kinetics of iron oxide by H_2 as reported by McKewan [24] is shown in figure 2.8, and similar behavior for CO as reported by Themelis and Gauvin [26] is shown in figure 2.9.

Reduction kinetics of mixture of iron and nickel oxides were also studied by Szekely and Hostaoglu, and Cores et al. [12, 27] They have taken pure oxides of iron and nickel and physically mixed them so that the individual grains are still either pure iron or nickel oxide particles. Chemical control condition where selective reduction occurs, and diffusion control condition where selective reduction does not occur, were studied and the typical curves for chemical control and diffusion control conditions are shown in figure 2.10 and figure 2.11 respectively Cores et al. [12] have studied the combined effect of time and temperature for reduction with hydrogen and coal, shown in in figure 2.7.

However in actual lateritic ores, nickel and iron are mixed in the molecular level such that nickel occupies some of the iron lattice sites in the goethite phase; and magnesium lattice sites in
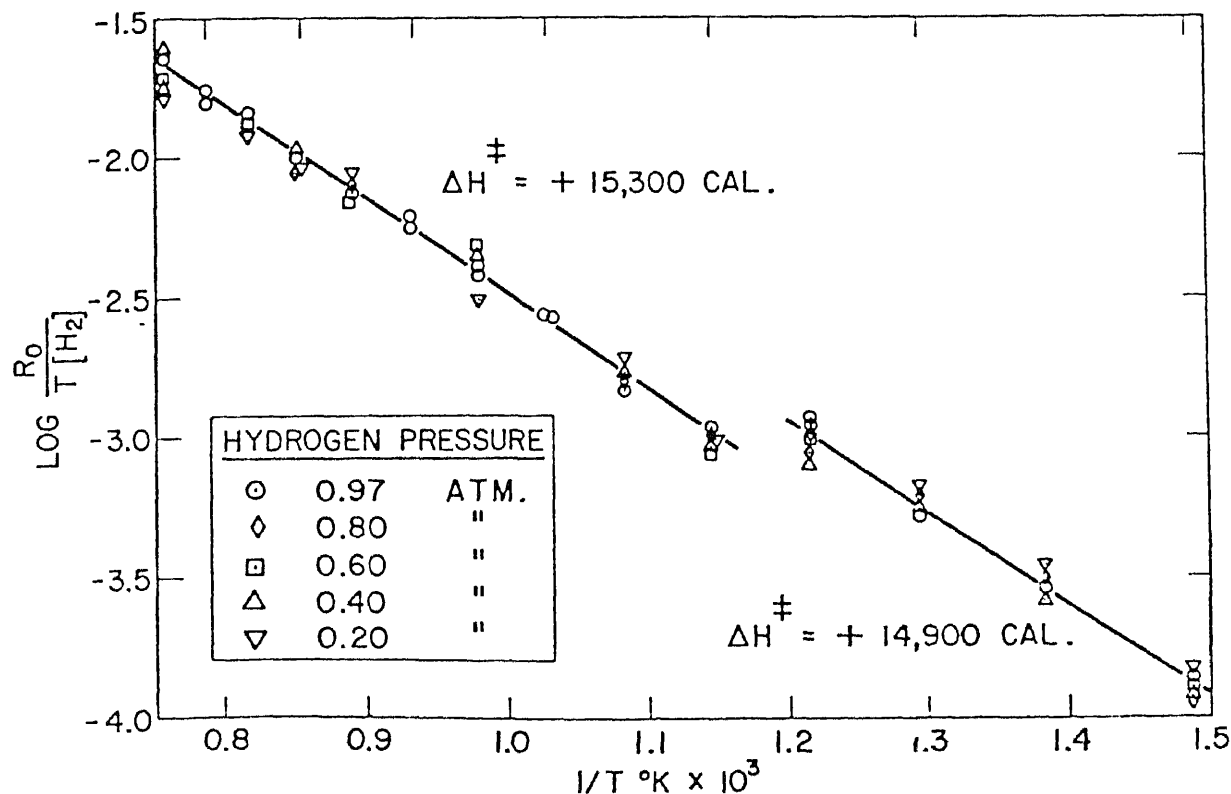
Figure 2 8: Rate constant data for reduction of iron oxide spheres with hydrogen [24].
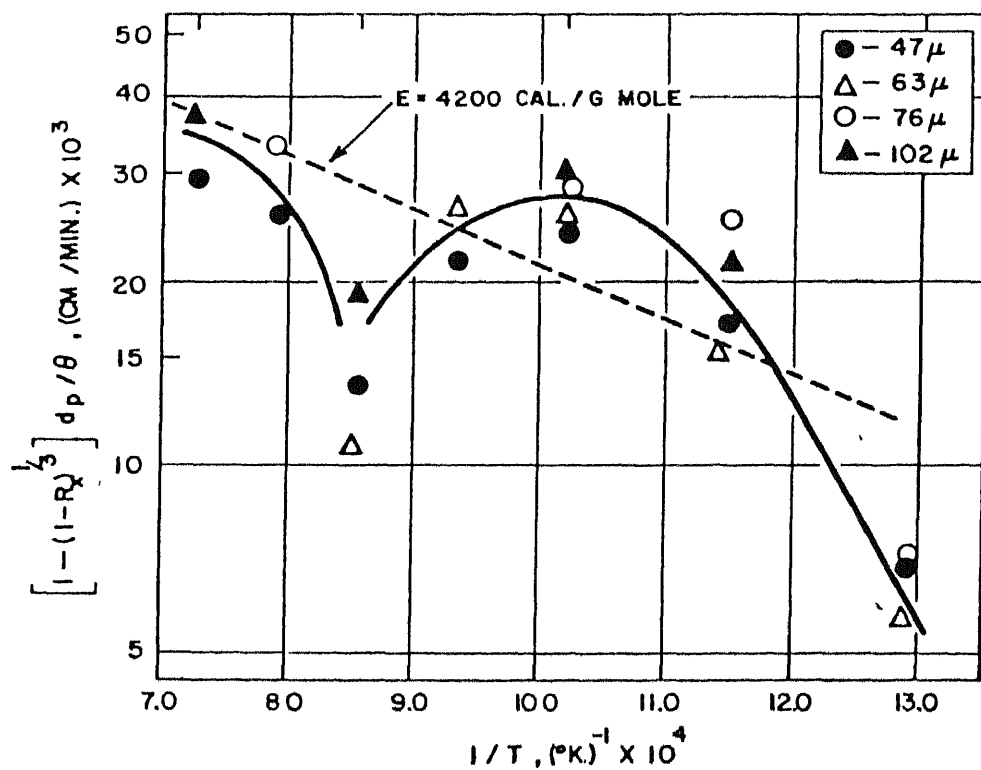
Figure 2.9: Effect of temperature on the rate constant of iron oxide reduction with CO [26].
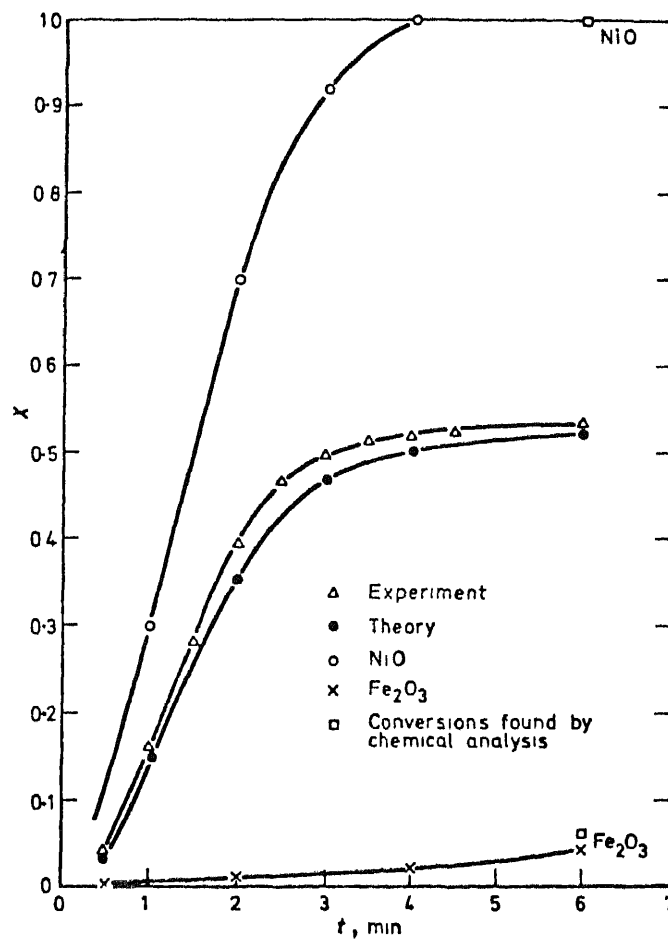
Figure 2 10· Conversion with time for reaction of disk 0.0635 cm thick, 50 % hematite and 50 % nickel oxide, with hydrogen at 608 K, in the region of chemical control kinetics [27]
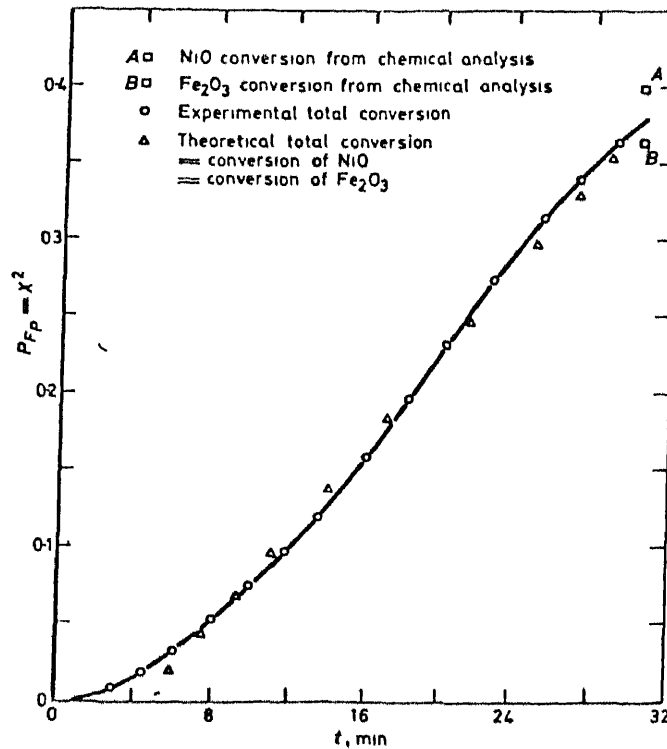
Figure 2.11: Conversion with time for reaction of disk 1.96 cm thick, 50 % hematite and 50 %

Table 2 3 Chemical Compositions of the Ore Samples (in Wt %), studied by Kawahara et al [30].

Ore Sample	Ni	Co	Fe	Al_2O_3	MgO	SiO_2	L.O.I.[†]	MgO/SiO_2
A	1 71	0.069	6 52	1.13	24 9	33 1	22.6	0.75
B	1.69	0 129	43.86	11 10	1.3	5.4	15.3	0 24
C	1 88	0.092	15 56	2 33	21 8	36 7	14 7	0 59
D	2 13	0 102	19 46	3.81	18.0	29.6	13 9	0 61
E	1.22	0.136	48.26	6 69	1 5	6 9	11.5	0 22

[†] Loss On Ignition

the serpentine phase, since iron and nickel have very close atomic radii (Fe=1 2412 A°; Ni=1.2458 A°) [28], while nickel and magnesium have very close ionic radii (Ni^{2+}=0 78, Mg^{2+}=0.78) [29]. The molecular level mixing of nickel or nickel oxide with other phases has a very significant effect on its reducibility. The reducibility of nickel present in the lateritic ores is considerably different from the reducibility of pure nickel oxides as revealed by the study on reducibility of lateritic ores by Kawahara et al. [30]. They have chosen five ore sample ABCDE and their composition is shown in table 2.3 The phase relationship of the samples are given below.

1. Sample A consists of serpentine and free silica.

2 Sample C and D consists of serpentine and hematite.

3. Sample B and E consists of hematite and goethite

4. The reduced ore consists of olivine and metallic iron or iro nickel alloy.

5. The peak intensity of the metallic iron (or Fe-Ni) in the reduced ores varies with the type of ore. Sample A shows strong Olivine peaks and weak metallic peaks, where as sample E shows strong peaks for Fe-Ni and weak peaks for olivine.

The relationship between the percent nickel reduction after 40 minutes of reduction with hydrogen, and the iron content of the ore is shown in figure 2 12 The figure clearly indicates that the reducibility of nickel increases with increasing iron content in the ore. This effect of iron can be related to the MgO/SiO_2 ratio. The reducibility of nickel decreases with increase in magnesium-silicate content or MgO/SiO_2 ratio of the ore.

It is well known that nickel oxide ores containing high magnesia contents, exhibit poor reducibility at high reduction temperatures This phenomenon has been attributed to the formation of olivine, a Ni-Fe-Mg-ortosilicate [8, 31]. Since the ionic radius Ni^{2+} is close to that of Mg^{2+} (0 068 and 0 065 nm, respectively), nickel can readily exchange places with magnesium silicates. Once nickel is tied up in this form, it cannot be reduced by gaseous reduction even by pure hydrogen at 1223 K The nickel activity in a solid solution of Mg_2SiO_4 and Ni_2SiO_4 is very low at nickel concentrations below 5 mass % [31], which explains the poor reducibility. The poor nickel reduction obtained for sample A can be accounted for by the formation of olivine phase. On the other hand Mg-silicate content of sample E is too low to incorporate a significant formation of the nickel in the olivine phase at high temperatures

To have a better understanding of the increase in reducibility of nickel with increasing iron content of the ore, consider the phase relationship shown in figure 2.13 [30]. This phase diagram represents the $SiO_2(+Al_2O_3) - MgO - FeO$ system. In this phase diagram, region I consists of pyroxine + SiO_2, region II of olivine + pyroxine + SiO_2, region III of olivine + SiO_2, region IV of olivine + pyroxene and region V of magnesio-wüstite + olivine.

As samples A, C and D lies in region IV consisting of olivine they are difficult to reduce Samples B and E are located in region V and are thus more easily reduced. The order A $\rightarrow$ C $\rightarrow$ D $\rightarrow$ B $\rightarrow$ E as indicated in figure 2.13 agrees well with the order of nickel reducibility Therefore this phase diagram of $SiO_2(+Al_2O_3) - MgO - FeO$ is an excellent first order method for predicting the reducibility of nickel ores.

The Sukinda ore, which is limonitic in nature with high iron content and negligible amount of magnesium has very good reducibility. Figure 2.14 shows the effect of temperature on reducibility of the ore with high volatile, non-coking coal, whose combustion product gas composition is given in table 2 2.

Comparing the reducibility of pure nickel oxide mixed with iron oxide (figure 2.7), with reducibility of lateritic ores (figure 2.12 and 2.14) it can be seen that the reducibility of lateritic ores are considerably slower and occurs at much higher temperatures. This is due to the formation of complex oxide phases with other oxides or minerals.
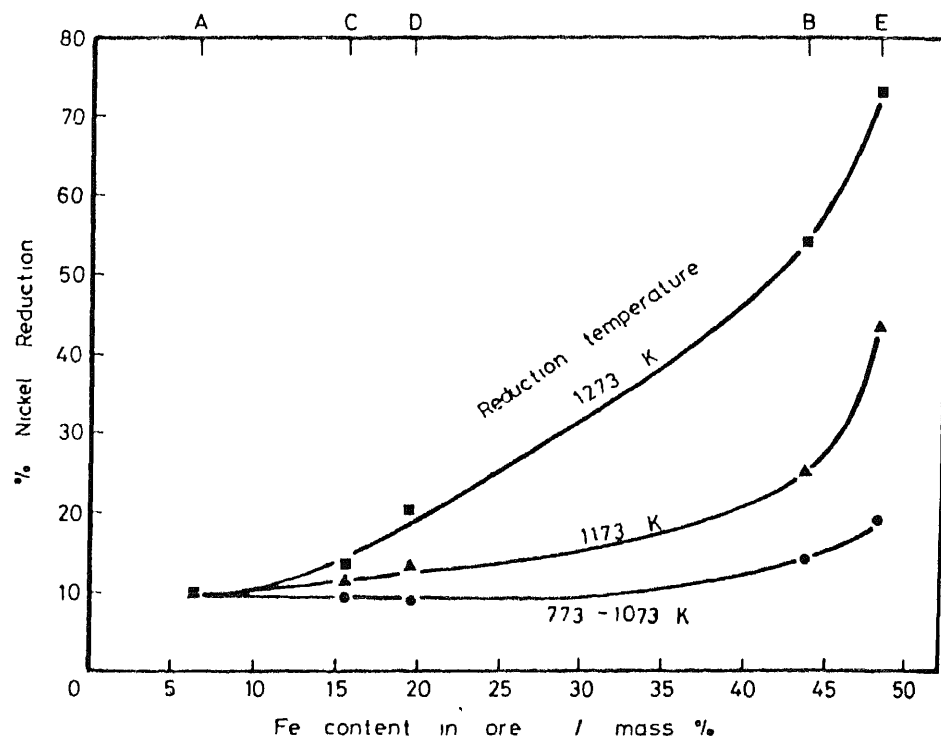
Figure 2.12. Relation between percent reduction of nickel and iron content in ore when reduction was carried out for 40 minutes [30].
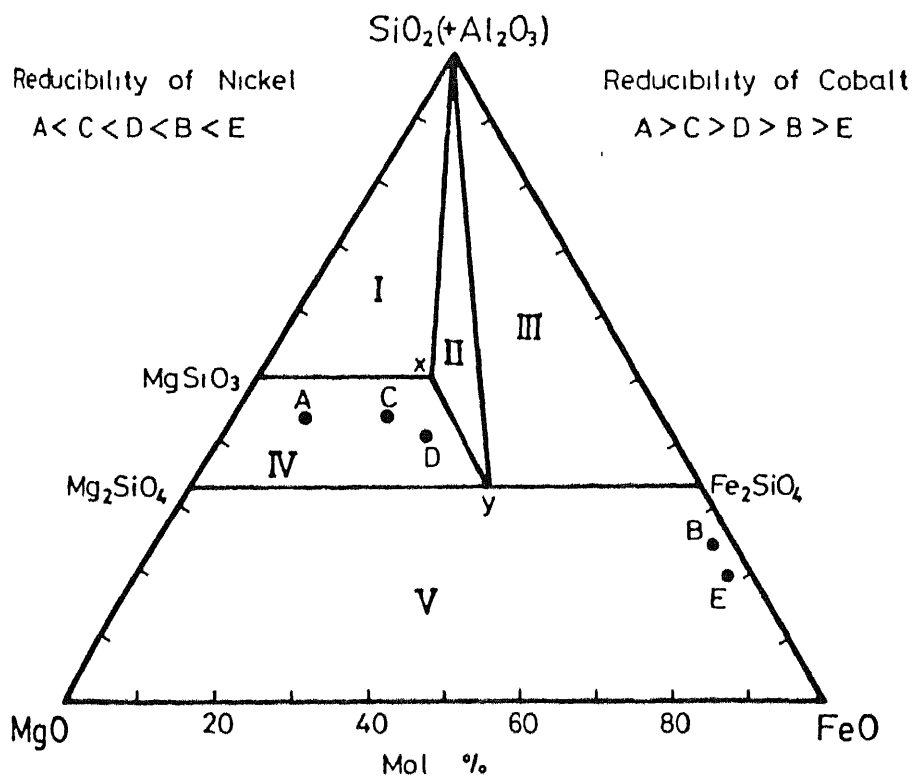
Figure 2.13: Phase diagram of $SiO_2(+Al_2O_3)$ -- MgO — FeO system showing the position of the
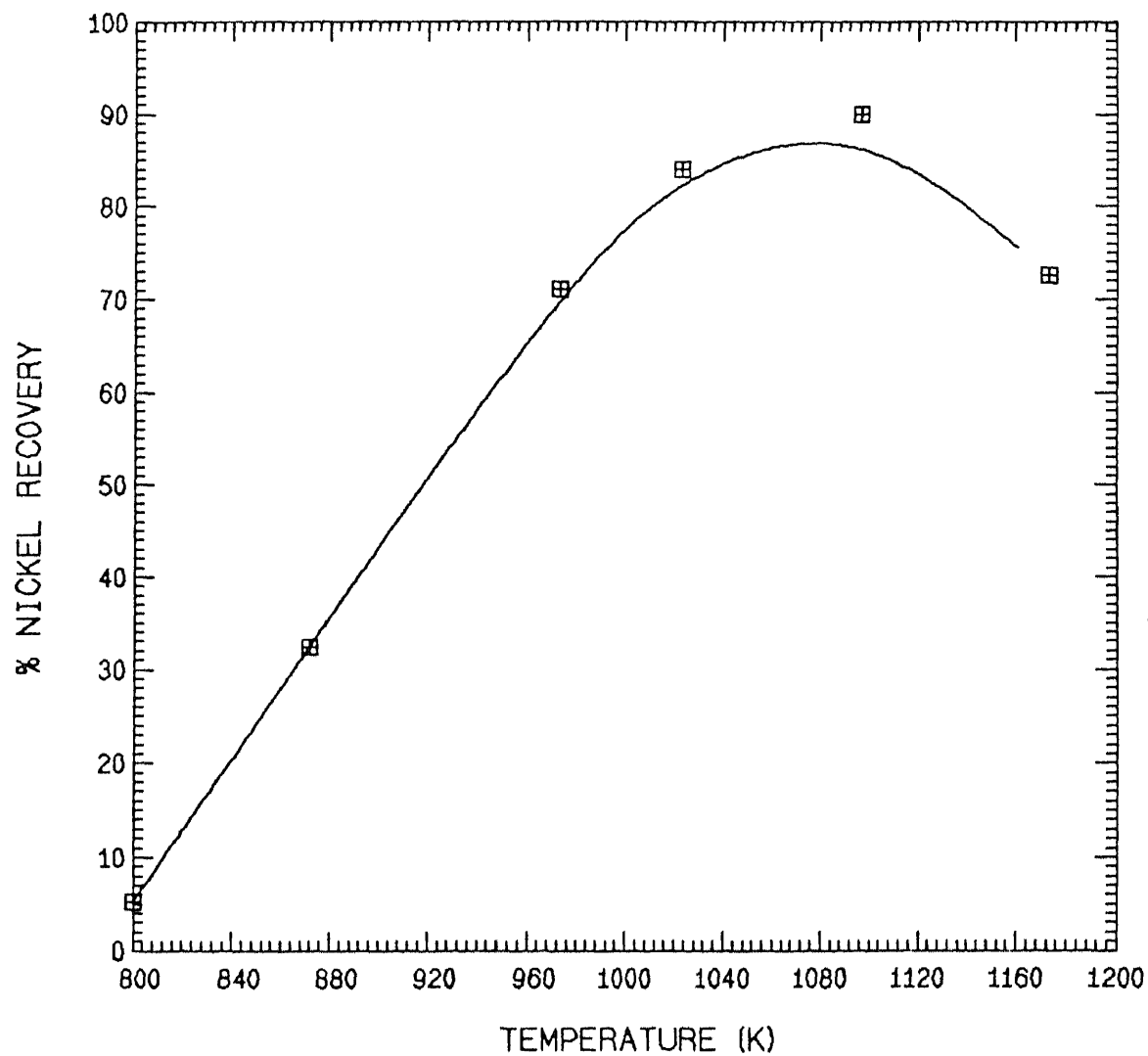
Figure 2.14: Effect of temperature on nickel reduction [4]

2.6 Gas-Solid Reaction Kinetic Models

The rate of gas-solid reaction forming a product gas and a solid product depends on the kinetics of steps like

1. Diffusion of the gas from the bulk phase to the pellet surface.

2. Diffusion of the gaseous reactant from the pellet surface to the reaction interface

3. Chemical reaction kinetics at the gas solid reaction interface.

The slowest kinetic step determines the overall kinetics of the reaction. Step(1) is kept relatively fast under experimental conditions of single pellet reduction so that other two kinetic steps depending on the inter-pellet diffusivity and chemical reaction rate can be studied more systematically.

If the diffusion rate is much faster than the chemical reaction rate, the overall reaction rate becomes chemical controlled. This condition is more prevalent at lower temperatures when chemical kinetics is slower. Under this condition the reaction occurs homogeneously throughout the pellet and the relation between non-dimensional time t^* and fraction reacted X is given by :

$$t^* = 1 - (1 - X)^{1/3} \tag{2.5}$$

$$\text{Where, } t^* = k/r_g \frac{C_{Ao}^n}{\rho_m} t \tag{2.6}$$

This is latter modified by Szekely et al.,and Sohn and Szekely [18, 32], and according to them under this condition the shape of the grains constituting the pellet will determine the reaction rate such that :

$$t^* = 1 - (1 - X)^{1/F_g} \tag{2.7}$$

Where, Grain shape factor $F_g=3$ for spherical; 2 for cylindrical; 1 for plate shaped grains.

At lower temperatures reaction of many finely shaped particles follow nucleation and growth kinetics characterized by an S - shaped conversion-vs-time relationship [19] given by :

$$t^* = [-ln(1 - X)]^{1/n} \tag{2 8}$$

The value of n is reported to be 2 804 to 2.856 for H_2 reduction of nickel oxide [19].

At the initial stages all the reactions are chemically controlled, but as the reaction proceeds formation of product layer takes place and the reaction becomes diffusion controlled when the chemical kinetics is much faster than the diffusion through the product layer. Under this condition the reaction rate is given by [18, 33]

$$\left.\begin{aligned}
t^* &= \tfrac{R_p^2 K/r_g}{2F_p D_e} \{X^2\}, & F_p = 1 \ (Plate) \\
&= \tfrac{R_p^2 K/r_g}{2F_p D_e} \{X + (1 - X)\ln(1 - X)\}, & F_p = 2 \ (Cylinder) \\
&= \tfrac{R_p^2 K/r_g}{2F_p D_e} \{1 - 3(1 - X)^{2/3} + 2(1 - X)\}, & F_p = 3 \ (Sphere)
\end{aligned}\right\} \tag{2 9}$$

In the intermediate regime where both chemical kinetics and diffusion kinetics rates are comparable we can addup the time required for the reaction due to chemical kinetics and diffusion kinetics, which is based on the law of additive reaction time [19, 34] · Therefore this gives rise to the generalized rate of chemical kinetics since it contains both the chemical kinetics and diffusion kinetics terms.

This model is generally referred to as Grain Model [35] since it takes into consideration the size and shape of both the pellet and the grains constituting the pellet. Where as previous models were based on pellet shapes only.

It can be noted here that the grain model is based on the approximate theory of additive reaction time and so correction factors can be added for the intermediate regimes by conducting experiments in that range as reported by Evans and Ranade [35, 36]. A more rigorously derived model of gas solid reaction kinetics is also developed for spherical pellets as reported by Isida and Wen, Aushman and Watson, and Rao [37, 38, 39]. In this model, completely reacted product phase formation is considered only after a critical time t_c The critical time for complete conversion at the surface can be quite high for chemical control kinetics, while it is much lower for diffusion control kinetics. Before the product layer formation reaction takes place throughout the pellet following a set of equations. After the product layer formation reaction occurs only in the partially reacted core, and the reaction kinetics is defined by a different set of equations considering different physical properties like pore diffusivity for the product layer. Since two set of equations are employed to define the reaction kinetics before and after the product layer formation or critical time t_c, this model is referred to here as 'Two Layer Model'. The application

of this model for analyzing gas solid reaction is described in Chapter 3 and the derivation of the model equations are discussed in Appendix B

Gas solid reaction kinetics model are developed on the basis of isothermal condition. But during reaction temperature may increase or decrease depending on the exothermic or endothermic nature of the reaction respectively The change in temperature will change the reaction rate constant value which follow exponential relationship with temperature according to Arrhenius equation.

$$k = k^o \exp(-Q/RT) \tag{2.10}$$

Temperature correction have been incorporated in reaction kinetic model by Bandyopadhyay et al [40] assuming a homogeneous reaction mechanism, and their methodology was successfully applied for the carbon gassification reaction [41]. The carbon gasification reaction however follows a Langmuir-Hinselwood type of kinetics and therefore, the expressions provided by these authors are not directly applicable in the present situation. During this study we have appropriately modified the formulation of Bandyopadhyay et al [40, 41], and is given in Chapter 3.

The product gas formed during reaction often plays an important role of slowing down the reaction kinetics due to various reasons like the free energy of the product phase becomes less negative due to the presence of product gas phase and also other specific effects like poisoning of the gas solid reaction interface etc

2.7 Leaching

Industrial leaching tanks [8] are agitated mechanically by turbines. In order to minimize problems with high density material settling to the bottom of the vessel, each discharge is by means of a dip pipe from the bottom of the tank, rather than conventional overflow. The air injection is through the center of the agitator shaft, utilizing a slip seal. The air bubles are dispersed as they rise through the turbine blades.

Contrary to most metallurgical leaching processes, the kinetics of extraction of nickel and cobalt from lateritic ores are not enhanced by elevated slurry temperatures This is particularly unfortunate in view of the available sensible heat content of the hot calcine discharge from the roasters One reason for this is that, progressively more cobalt, and to a lasser extent nickel, is co-precipitated with iron as the temperature rises.

The ammonia ammonium-carbonate electrolyte is unusual in that the reagents are not irreversively consumed in the leaching process and are recovered from the pregnant liquor and tailing streams for reuse. The recovery process (steam distillation) generates a leach liquor of approximately 130 g/l NH_3 and 100 g/l CO_2, which is reintroduced in the leaching circuit.

In laboratory scale, leaching is done in an autoclave shown in figure 2.17. Mechanical stirrers were used to agitate the liquor. For heating the solution steam or electric heating coils can be used

2.7.1   Leaching Mechanism

During leaching the reduced iron first goes in the solution, when nickel and cobalt remains undissolved. To eliminate the iron in the solution, preconditioning of the reduced sample was done in high concentration of ammonia and carbon-dioxide. Air is purged during preconditioning to oxidize ferrous iron to ferric iron. The chemical reactions taking place during preconditioning [3] are as follows :

$$2Fe + O_2 + 2H_2O + 4(NH_4)CO_3 \rightarrow 2FeCO_3(NH_4)_2CO_3 + 4NH_4OH$$

$$FeCO_3(NH_4)_2CO_3 + 2H2O + O_2 \rightarrow 2Fe_2(CO_3)_3(NH_4)_2CO_3 + 4NH_4OH$$

$$Fe(CO_3)_3(NH_4)_2CO_3 + 6NH_4OH \rightarrow 2Fe(OH)_3 + 4(NH_4)_2CO_3$$
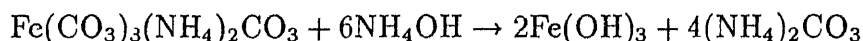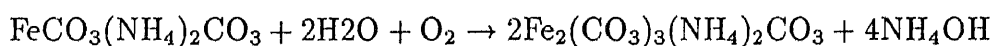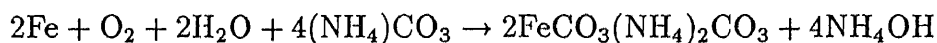
The preconditioning is done in 1:1 solid:liquid ratio. It is found that preconditioning time of 30 minutes is sufficient to precipitate iron completely.

The preconditioned slurry is then leached in an autoclave under oxygen atmosphere at around 70 C. The reactions involved in the dissolution of freshly reduced nickel (and Cobalt), in presence of oxygen, in ammoniacal solution are :

$$Ni = Ni^{+2} + 2e^-$$

$$Ni^{+2} + nNH_4CO_3 = (Ni(NH_3)_n)(CO_3)_2 + (n-2)HCO_3 + 2H^+$$

$$2H^+ + \frac{1}{2}O_2 + 2e^- = H_2O$$

$$Ni + nNH_4CO_3 + 2O_2 = (Ni(NH_3)_n)(CO_3)_2 + (n-2)HCO_3 + H_2O$$
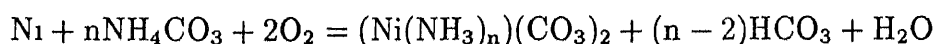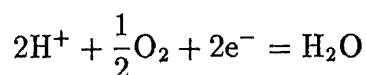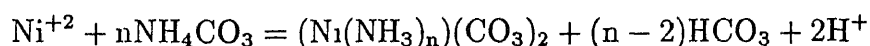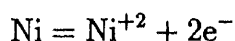
Where n is the co-ordination number of nickel in the complex formed and is usually 4 to 6. The use of NH_3 and CO_2 solutions to leach nickel from ores containing both nickel and cobalt was

originally developed by Caron [42]. Schrader et al. [43] in their studies on Ni-NH$_3$-H$_2$O system have found that nickel hydroxide precipitates at pH$\approx$ 6 in the absence of NH$_3$ and NH$_4^+$. When these are present the formation of nickel hydroxide starts at pH 10. A solution of 10M NH$_3$ shows a pH value of $\approx$ 12 They have further elaborated that to keep Ni in solution the pH must be below 10 and the solution should be stable. To this end, a buffer must be used to keep the pH in the range of 8 to 9 Ammonium carbonate fulfills this role upto 10 mole concentration The simplest amine complexes are formed as soon as the pH is above 2.5. At pH$\approx$ 6, all nickel in the solution is present as nickel diamine Ni(NH$_3$)$_2^{+2}$ complex, changing to tetramine Ni(NH$_3$)$_4^{+2}$ complex above pH 6, and to hexamine complex Ni(NH$_3$)$_6^{+2}$ at pH 8, and is converted to insoluble Ni(OH)$_2$ at pH 10 In the concentration range of 70 g/l of NH$_3$ and 35 g/l of CO$_2$ the solution pH remains stable at 9.5.

For efficient utilization of leaching solution the solid liquid ratio is kept as high as possible, without affecting the recovery of nickel to a large extent The effect of solid liquid ratio on nickel recovery and leaching kinetics is shown in figure 2.15 [4], and the change in concentration of leaching reagents with time is shown in figure 2.16. Industrially solid liquid ratio of 1:3 is reported by Caron [42], and there are in general several tanks or thickeners in series under counter current flow of solid and liquid for leaching and washing to fully recover the reduced nickel content in the slurry. The final nickel concentration in the pregnant solution is in the range of 8 to 12 g/l

The reduced metallic phase of nickel ore forms Fe-Ni alloy and the leaching kinetics of this system have been studied by Jandova and Pedlik [44]. Their findings for this alloy system is shown in figure 2.18. The leaching behavior of the various Fe-Ni alloy under the same conditions of leaching varies depending on their composition and structure. Nickel from all the Fe-Ni alloys starts to dissolve immediately and its major portion passes into the solution within the first 60 min of the leaching process The rate of nickel dissolution increases with increasing content of the γ-Fe-Ni alloy and decreases with increasing content of α-Fe-Ni alloy The leaching behavior of the Fe-Ni35 alloy, containing both α-ferro-nickel and γ-ferro-nickel alloys, represents a transition step between pure α-Fe-Ni and γ-Fe-Ni alloys.

The results confirm the necessity of controlling the reductive roasting of laterite ores in order to minimize the amount of α-Fe-Ni alloy in the reduced laterites. Metallic phases with a higher γ-Fe-Ni alloy content show, in addition to a faster rate of nickel dissolution, a higher resistance against potential passivation.
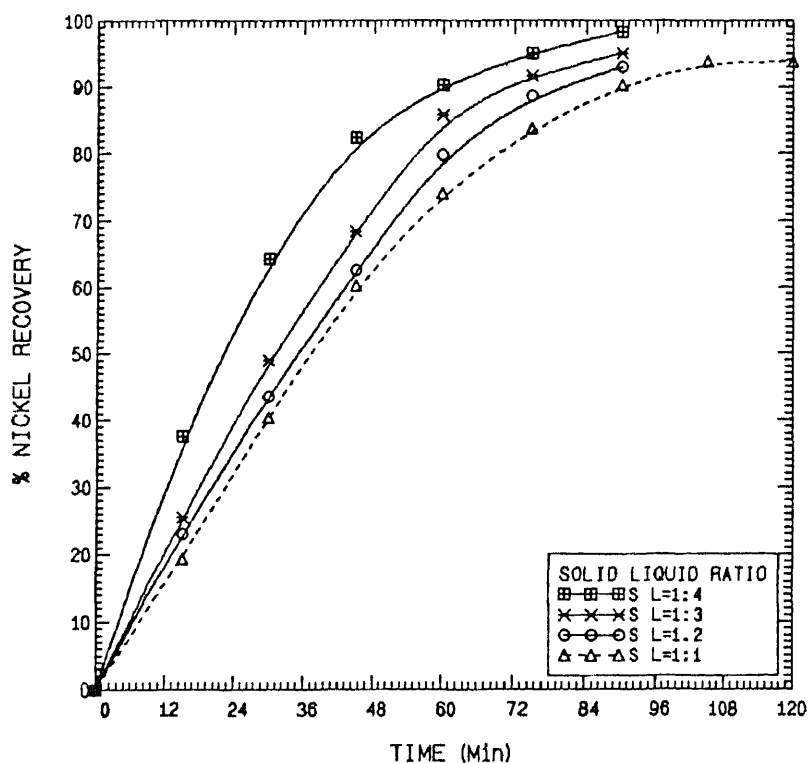
Figure 2 15: Effect of solid liquid ratio on leaching kinetics [4].
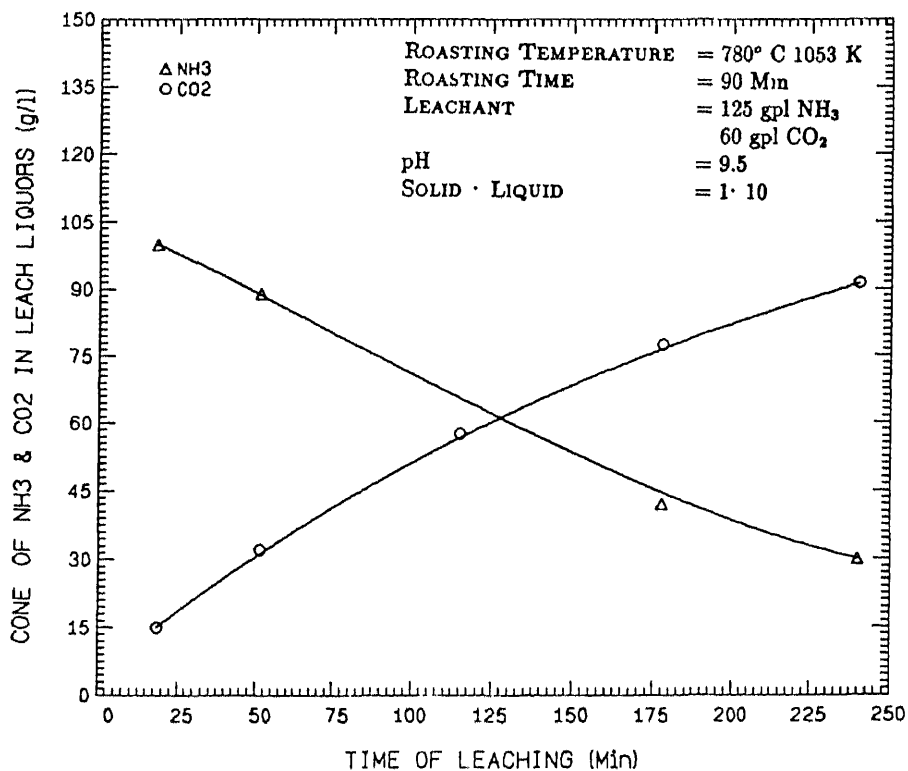
Figure 2 16: Variation of ammonia and carbon dioxide in the leaching solution with time [3].
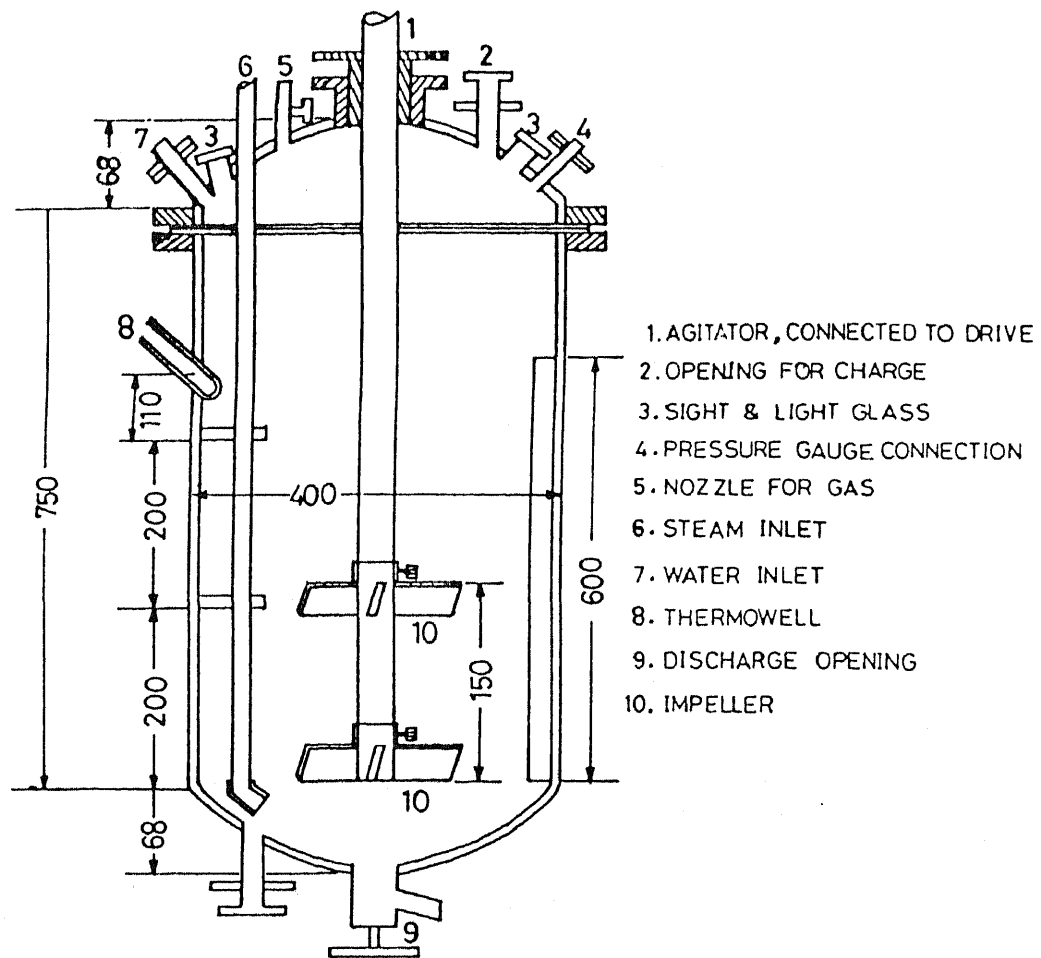
Figure 2.17: Diagram of an Autoclave used for leaching purpose [45].
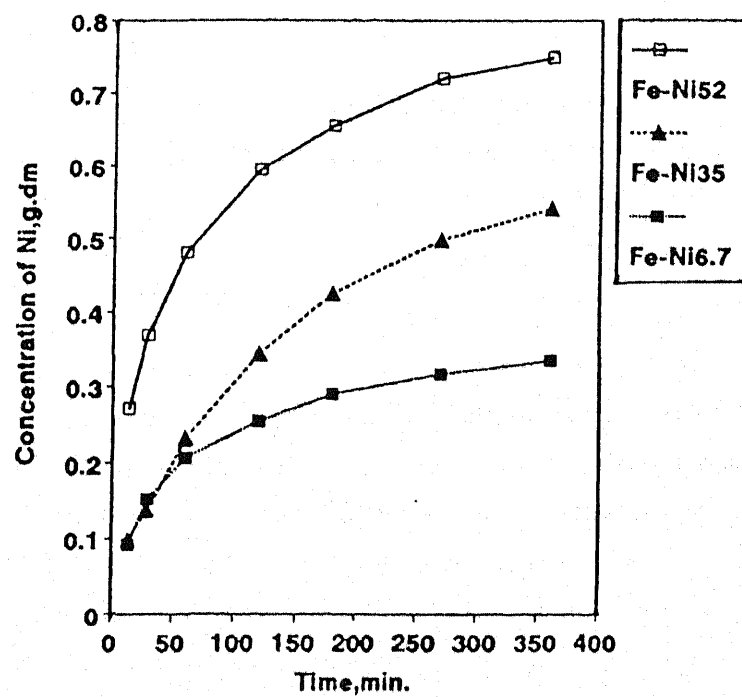
Figure 2.18: Dissolution of nickel from various Fe-Ni alloy samples as a function of time in 400 ml of oxygenated solution of 1.9 $Kmol.m^{-3}$ NH_3, 1.4 $Kmol.m^{-3}$ $(NH_4)_2CO_3$ at 313 K. Initial weight of alloy particles were : Fe-Ni52 0.77 g, Fe-Ni35 1.15 g, Fe-Ni6.7 6.0 g [44].

Although ammonium-carbonate is the most common buffer reagent used in nickel leaching, other salts can also be used for this purpose. Room temperature leaching using ammonium salts of carbonate and sulfite under simultaneous grinding and leaching conditions have been reported by Im and Johnston [46] The leaching kinetics is very similar in both the cases although the final recovery is marginally better for the carbonate containing solution.

Leaching under high temperature is studied by Dubeck and Im [47]. High temperature leaching showed very fast rate of leaching initially and thereafter decreased dramatically with time. This is in sharp contrast to the room temperature leaching experience and common leaching trends The results also showed a better leaching capability of sulfites than carbonates under high temperature conditions. From the study they have concluded that for better leaching kinetics high temperature leaching can be employed with rapid quenching facility by circulating water to cool the solution below 350 K once the desired nickel concentration is reached

2.8 Modeling of Fixed Bed Reactors

For industrial reactors the concentration of the fluid reactant is usually a function of time and position in the reactor The models for the reaction of individual entities of solid cannot therefore be applied directly, since they are developed for a constant environment surrounding the solid. An additional complication arises if the temperature of the solid varies with position or time.

For reactors therefore it is necessary to employ additional equations describing the variation of fluid reactant concentration and temperature within the reactor Such equations will contain convective and diffusive terms arising from the transport of mass, momentum or heat during the bulk motion of the fluid A preliminary step is therefore to arrive at some quantitative description of the flow of the fluid within the reactor.

Evans and Sohn [48] have studied reaction in a packed bed reactor with gas moving through the bed in plug flow condition. Reaction kinetics of the pellets were defined by grain model considering uniform size and isothermal condition. A typical computational result obtained by them is shown in figure 2.19. Ranade and Evans [36] have studied the reduction of packed bed of iron ore, and verified the computed results by comparing with the experimentally obtained overall extent of reduction with the simulated behavior. The results showed good agreement between the experimental and computed data as shown in figure 2.20.

For a more detailed study flow distribution in a packed bed has to be evaluated. Fluid
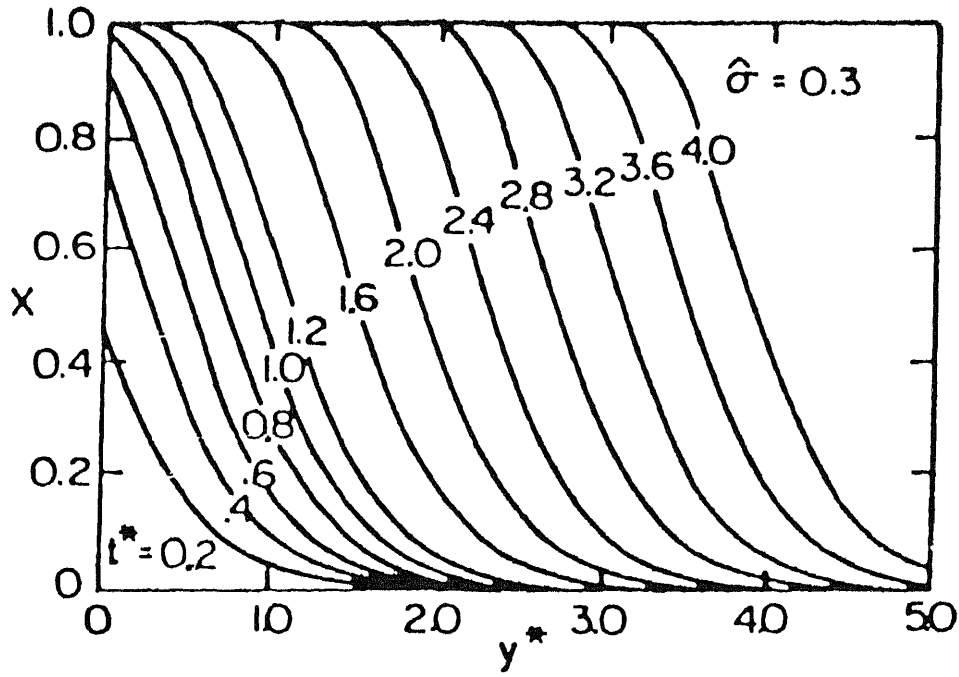
Figure 2 19: Extent of reaction *vs.* position in bed for reaction modulus $\sigma = 0\ 3$ in a fixed bed reactor [48].
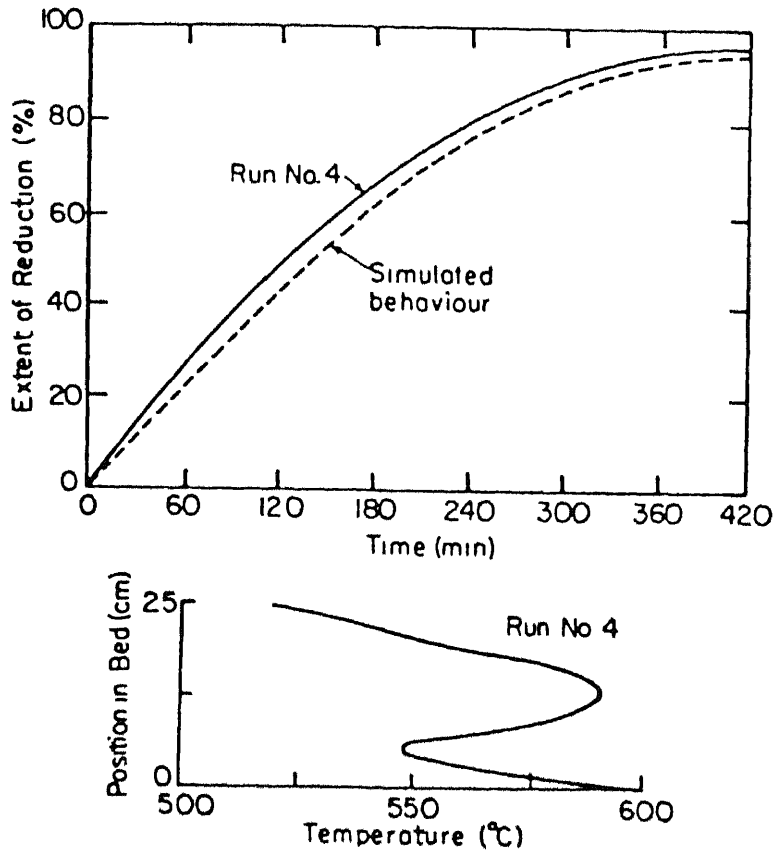
Figure 2 20

flow through a packed solid bed is defined by Ergun's equation which, depends on the void fraction variation and pellet size distribution in the bed Void fraction variation in a packed bed of identical spheres in a cylindrical tube and other configurations have been studied by Benenati and Brosilow [49] Szekely and Poveromo [50] have used the Benenati and Brosilow's data by fitting a second order curve through them to compute the flow distribution under various configurations which is then experimentally verified. A similar approach has been taken in the present study for computing the flow distribution in the intermediate Reynold's number region, which will be discussed in more details in Chapter 5.

For fixed bed reactors with gas flowing over the bed, there will be no gas velocity inside the bed and gas phase mass transfer will be governed by the diffusivity of the reactant gas. Under this condition only the gas velocity profile over the bed needs to be computed. Once the gas velocity profile is known and the reaction kinetics defined by grain model; the other parameters like temperature and gas composition profile in the bed is computed by using the energy and mass balance equations.

The strategy followed for modeling fixed bed reactors can also be extended for modeling industrial furnaces with moving bed conditions. The only difference arise due to the solid motion In most of the industrial furnaces used for roasting operations, gas and solid moves counter current to each other, and so after starting from a initial condition it will reach a steady state after some time. If the attainment of steady state is slow for the process the time of computation from the initial conditions may be quite large.

2.9 Different Types of Roasters

Various kinds of roasting like, oxidation of sulfides, chlorination, reduction roasting etc are done to facilitate subsequent extraction processes like leaching, smelting etc. Reduction roasting of lateritic ore to crude metallic state is done to make the product porous and readily soluble in the leach solution.

Different kinds of furnaces can be used for the roasting operation according to the properties of the ore like reaction kinetics thermal characteristics etc. Therefore, in sulfide oxidation roasting; where the reaction is highly exothermic and kinetics is fast, fluidized bed roasting with air is the most economic and efficient process. However for the reduction roasting of lateritic ores, fluidized bed roasting is not very efficient since the process is not autogenous and the kinetics is

slow. For the reduction roasting of lateritic ores three different types of roasters are mainly used, namely : Shaft Furnace, Rotary Kiln and Multiple Hearth Furnace (MHF). All the three types of roasters are used industrially for the reduction roasting of laterite ores. All the roasters have some advantages and disadvantages which make one of them more suitable than the other under some specific conditions. Therefore a brief description and a comparative study of the roasters should be helpful for identifying the most suitable roaster under some given constraint.

2.9.1 Shaft Furnace

Vertical shaft furnaces are generally used for producing ferro-nickel by selective reduction of briquetes or pellets formed from laterite ores. A cross sectional view of the shaft furnace used at Falconbridge in Dominicana is shown in figure 2 21 [10]. Reducing gas is produced by sub-stoichiometric combustion of naptha with air in a Shell gassifier. The reduced ore is melted in an electric furnace to yield a large amount of discard slag and ferro-nickel with a grade of approximately 36 % nickel. Because of the segregated gas flow, the briquetes move through a wide range of gas composition and temperature. Ores in fine powder form cannot be used in a shaft furnace since it will choke the gas flow through the furnace. The temperature control within the furnace is also not very accurate so that there may be partial sintering of the ore feed. This method is more suitable for the ores containing less amount of iron oxide. For ores containing high percentage of iron oxide, it will produce excess of reduced iron which will be difficult to leach, or else it will produce low grade ferro-nickel on direct smelting.

2.9.2 Rotary Kiln

Rotary kilns are used extensively for drying operations for their simplicity of operation and high productivity. For reduction roasting of laterites also it is used in various plants mainly for producing ferronickel. Rotary kiln is made of steel shell and is lined with fire clay brick of about 100 mm thick and generally has a small inclination of about 2.5 %. Plant practice for laterite reduction in a rotary kiln is described by Watanabe et al. [6]. Pilot plant study of rotary kiln operation with the lateritic ore found in India is reported by Nayak [1]. A schematic diagram of a rotary kiln and its operation is shown in figure 2 22 [6]. As shown in the figure, briquetes were fed continuously into the grate, then supplied to the kiln after a counter current heat exchange with hot gas. Within the kiln, the briquetes travel at an average speed of 6 m/h. During traveling countercurrent to the flow of hot gas produced by the combustion of fuel coal, all the smelting
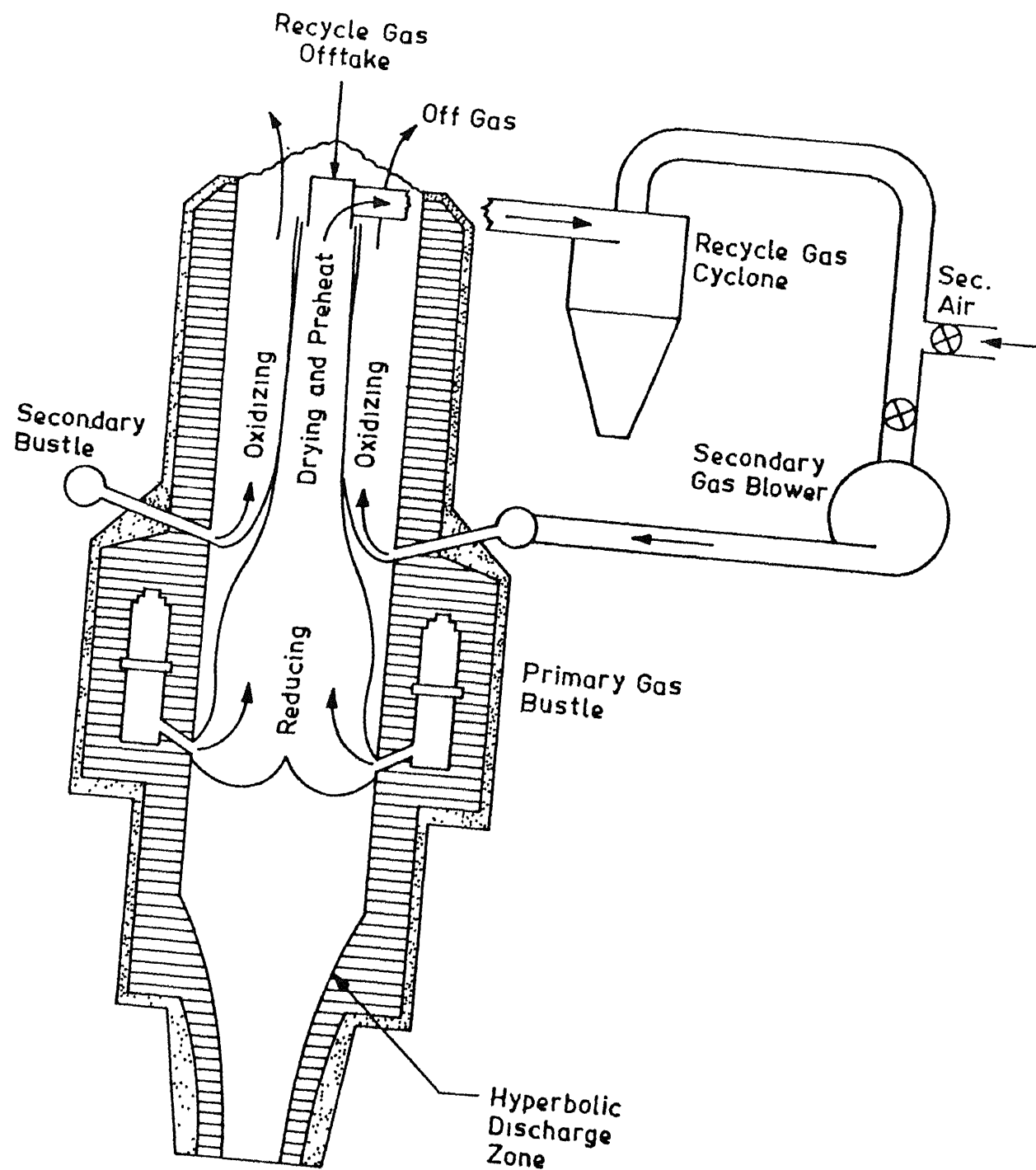
Figure 2.21: Cross section of the shaft furnace used at Falconbridge Dominicana [10].

steps, dehydration, reduction, collapse of briquetes, slag formation, agglomeration of reduced metal particles etc. take place. The carbonaceous materials inserted into the briquetes act as a fuel and reductant. The most important technical factors for carrying out a stable operation are the constant feeding rate of briquetes and the attainment of a stable temperature profile. Inferior quality of briquetes, varying feeding rate or scattering of carbonaceous fuel can cause local overheating or overcooling and increase in fine dust formation. Temperature profile and reaction kinetics behavior within the kiln is shown in figure 2 23. The temperature of the wet gas after passing through the grate is around 360 K.

During the movement half way through the kiln, dehydration, vaporization of crystallized water in the ore and dissociation of limestone can be completed. When the reduction of iron and nickel oxides by reducing gas and carbonaceous materials begins, the briquetes perseumably collapse due to the volume expansion and gradually becomes softened. When materials move upto about 30 m from the exit of the kiln, the temperature of the materials rises to about 1100 C. At this stage the slag forming reaction begins to occur parallel to the reduction. Reduction of iron and nickel oxides to metals occur almost simultaneously regardless of the great difference in free energy of formation between those oxides.

The rotary kiln operation is more suitable for ferro nickel production from low iron containing ores of both limonitic and serpentinic nature. Control of gas composition and temperature profile is not very accurate and local overheating and sintering is always a problem. Due to its lower residence time the temperature of operation is much higher to attain faster reduction kinetics. Control of gas composition and temperature profile is not very accurate and so there is considerable reduction of iron to its metallic state accompanied by local overheating and sintering. This will cause considerable difficulty for the subsequent extraction of nickel through leaching technique. However sintering and excess of metallic iron will cause no problem for direct smelting of the roasted ore to produce ferro-nickel.

2.9.3 Multiple Hearth Furnace

Multiple Hearth Furnace is a refractory lined cylindrical vessel made of plate steel, fitted with seven to twelve refractory hearths. Figure 2.24 shows a typical MHF used for roasting operations in Regional Research Laboratory, Bhubaneswar as reported by Banerjee et al. [2]. It consists of a steel vertical shaft attached with cast iron arms with oblique paddle like rabbles. the solid ore enters the roaster from the top and moves down due to the rotation of the rabble arms along the
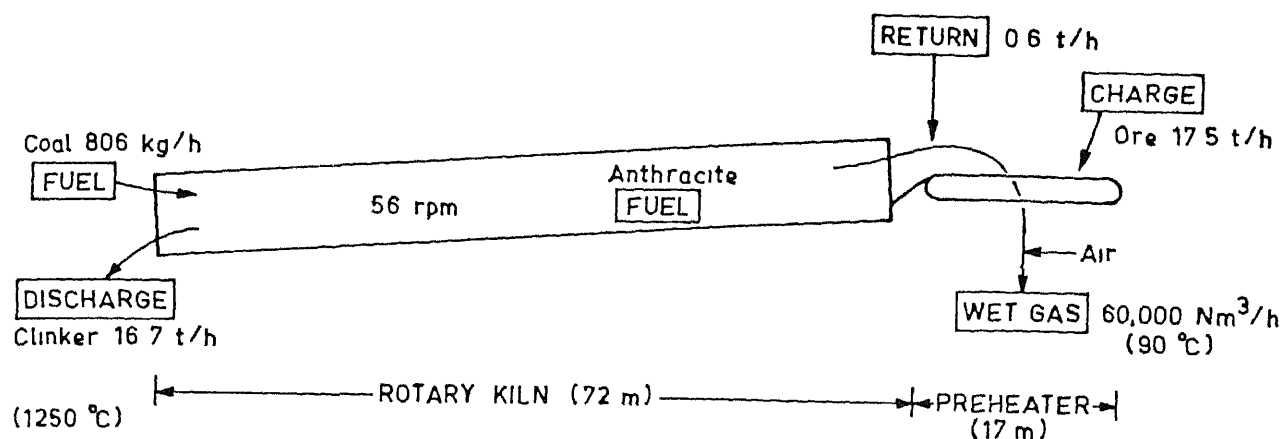
Figure 2 22: Rotary kiln operation at Nippon Yakin Kagyo Co. Ltd [6].
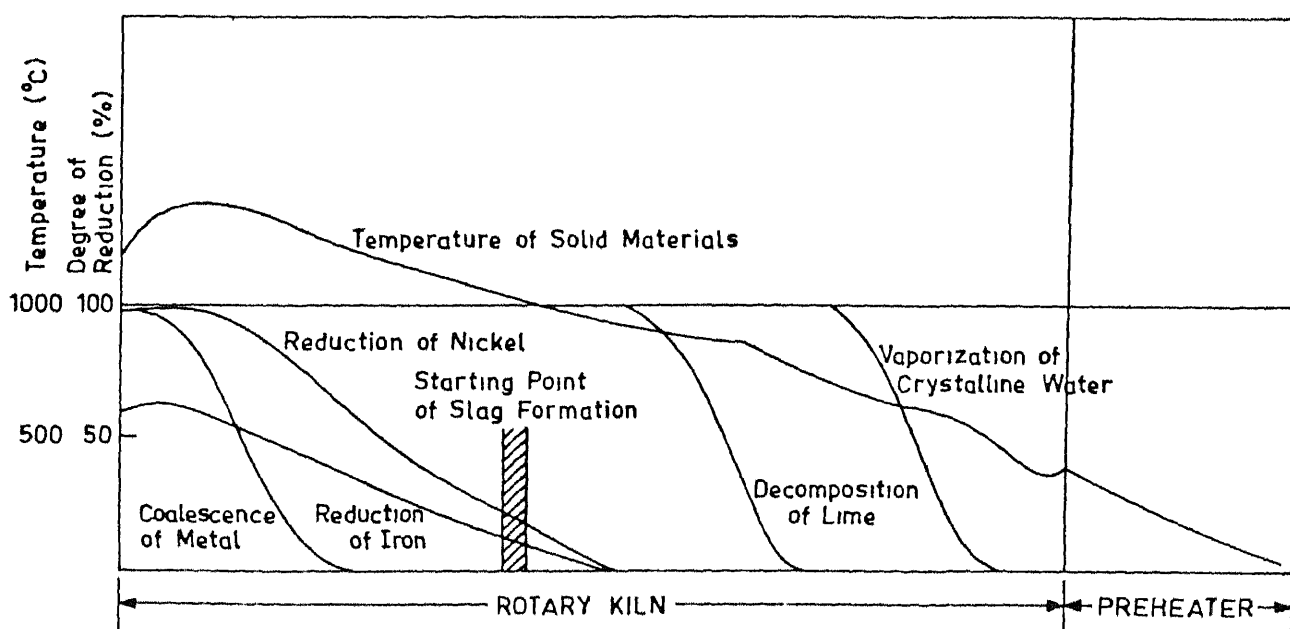
Figure 2.23: Reduction procedure inside the firring kiln [6]

hearth plane at about 0 5 - 3 rpm. Usually the hearths are built with a small slope, and the rabble blades are kept slightly inclined so that the ore can drift slowly in a radial direction and drop to the next hearth on completion of its residence time in the previous one. The ore finally exits from the bottom of the roaster. The total residence time of the ore in MHF is about 1 5 hours. Oil fired combustion chambers, usually placed in the lower hearth regions are operated under sub-stoichiometric condition of about 50 % of the theoretical combustion air required to ensure a strong reducing atmosphere in the roaster. Heating rate is kept low to have practically all the nickel reduced to the metallic phase before it reaches 1030 K. Above this temperature there is a phase change during which any unreduced NiO combines with iron silicate, and then it becomes much more difficult to reduce. Time required for heating the furnace and average temperature in the hearths during the reduction process is shown in figure 2 25 [2] It is seen from the figure that the furnace is heated slowly to the operating temperature, and the temperature is maintained within a narrow range in the hearths Residence time in the roaster is about 1.5 hours, during which period most of the nickel present in the limonitic phase is reduced to metallic nickel, and most of the iron oxide present is also reduced to FeO state and a small fraction to metallic iron. The iron and nickel content of the serpentinic fraction $(Mg, Fe, Ni)_6 Si_4 O_{10}(OH)_8$ is essentially not reduced The hot reduced ore leaving the roaster will quickly reoxidize and become insoluble to the ammonia leach solution if exposed to air. This necessitates cooling the ore down to about 400 K under non-oxidizing atmosphere in rotary coolers or screw feeders, cooled by circulating water. Flue dust passing out in the roaster gas is removed in the dust collectors and returned to the roaster.

The attractive features of the MHF roaster [51], is that it can treat an unlimited variety of ores without elaborate material preparation, operating control parameters are few and easily adjustable, operation lost time is very little, and above all, it produces calcines of very consistent quality. Accurate control of gas composition and temperature profile is possible at different hearth positions. The process is also best suited for slow reaction kinetic systems requiring good temperature and gas concentration control and efficiency under slow reaction kinetics.

Since the reduction of laterite ores have to maintain some ideal condition to maximize the nickel reduction with minimum iron reduction, and a reasonably high reaction kinetics; a sound mathematical modeling of the process is essential for overall efficiency of the process. Modeling of MHF were previously done by Gupta et al. [51] and Saharoy et al. [52] for sulfide ore roasting Gupta et al have developed a two-dimensional steady state model in (x,z) coordinate system for computing simultaneous heat and mass transfer in MHF to estimate the temperature and

composition of the solid and gaseous phase within the furnace. The average distance traveled by the ore particles in θ-direction was denoted by 'x' and the average distance traveled by the gas phase was denoted by 'z' In a further development, Saharoy et al. developed a three-dimensional model for MHF in cylindrical coordinate system Their results on the effect of preheating temperature were mutually consistent, but the gas composition and temperature profile obtained by the three dimensional model were more realistic in nature.

However these models have considered uniform gas velocity or plug flow condition and have not computed the gas velocity profile over the solid bed of ores The gas velocity profile over the bed will primarily determine the mass transfer of the reactant gas to the reacting solid surface which may be the rate controlling step for the overall reaction kinetics in the MHF. Therefore a more rigorous model of MHF, incorporating the gas velocity profile over the solid bed is envisaged, and is described in more details in Chapter 7.
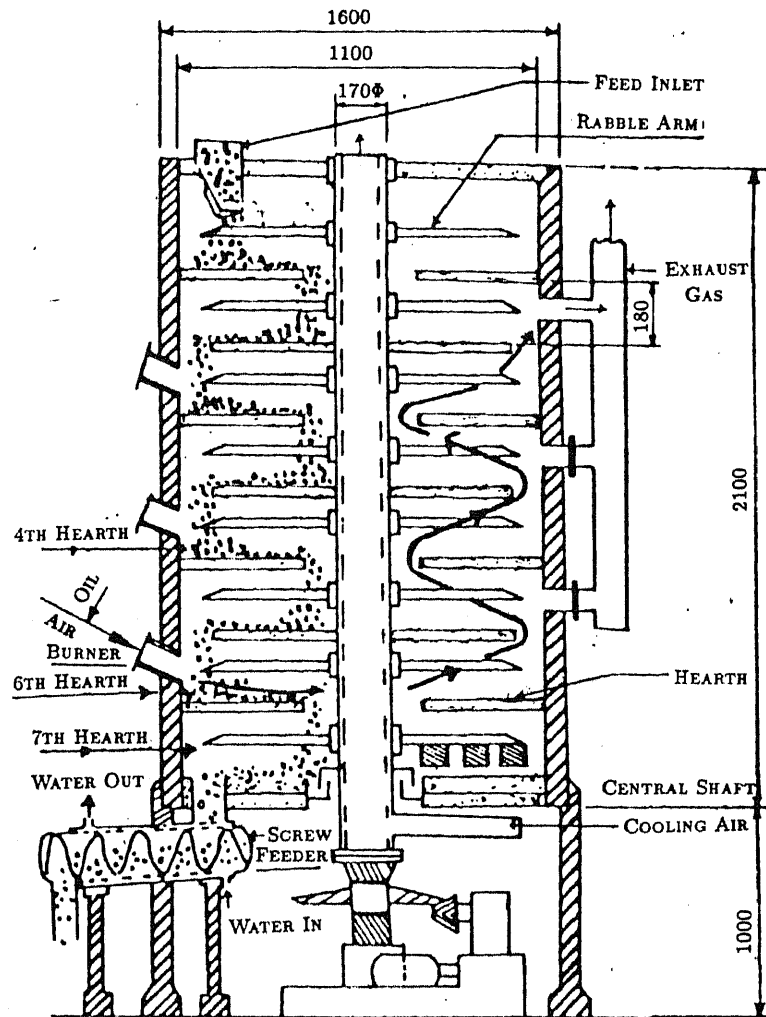
All dimensions are in mm :

Figure 2.24: Cross sectional view of the Multiple Hearth Furnace used in RRL, Bhubaneswar [2].
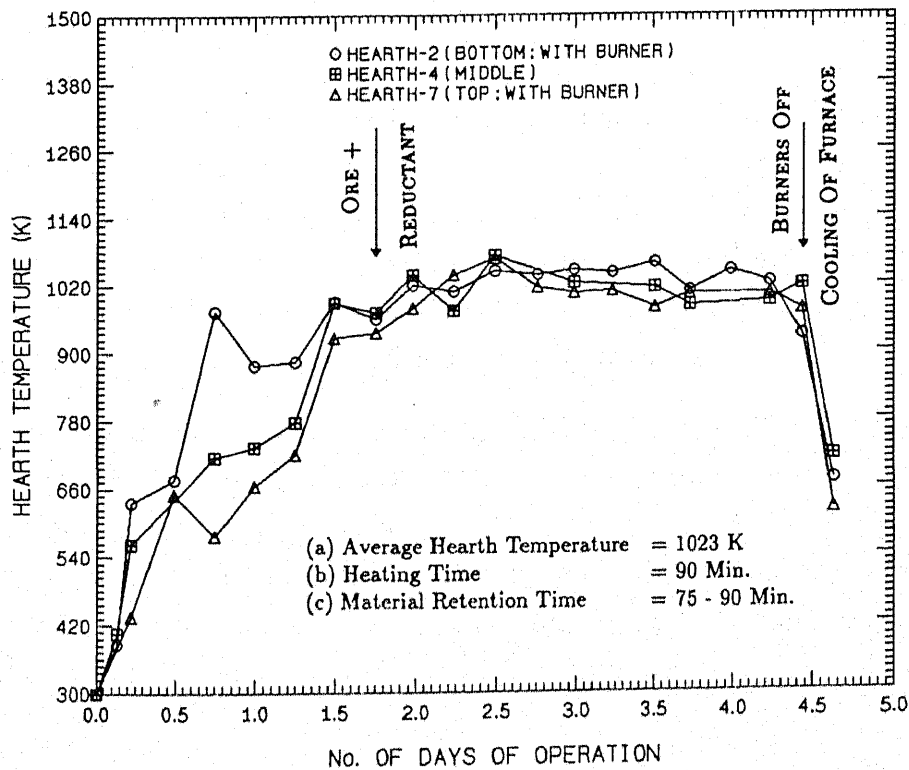
Figure 2.25: Temperature profile in the MHF hearths [2].

Chapter 3

CHARACTERIZATION AND REDUCTION KINETICS STUDY OF NICKELIFERROUS ORE

3.1 Introduction

The lateritic nickeliferrous ore found in India, contains very high percentage of iron and small amount of nickel. For this type of ore, as discussed in the previous Chapters, reduction roasting followed by leaching is the most suitable route for extraction of nickel. The ore has a complex mineralogy and the reduction mechanism of this type of ores are not very well defined. Therefore the ore obtained from RRL Bhubaneswar [53], was first characterized and then its reduction kinetics with hydrogen was studied to evaluate the mechanism of reduction and estimate the kinetic parameters. Industrially reduction roasting operation of this type of ores can be accomplished in furnaces where the solid bed of ore pellets or briquetes are in moving condition. For studying the reduction process under fixed and moving bed condition; study of the reduction process of the individual pellets under known conditions are essential and will be the basis for further study of the process under fixed and moving bed conditions.

Pellet reduction experiments are conducted at 800 K, 900 K and 1000 K, within which range this type of ores are generally reduced [4, 14, 31]. The experimental results are then analyzed by the established gas solid reaction models to estimate the various reaction kinetic parameters. The effect of non-isothermal reduction and product gas formation are incorporated in the model, to formulate a more generalized model, which can predict the reduction rate under industrial

conditions where pellet size, temperature of reduction and gas concentration (H_2/H_2O ratio) can vary by a large extent.

In view of the above mentioned observations, the following studies were conducted during the present investigation :

- Ore characterization using Chemical Analysis, DTA, SEM, EDAX, BET and X-ray Powder Diffraction techniques.

- Single pellet reduction using hydrogen in a thermogravimetric setup.

- Characterization of the reduced material using Chemical analysis, X-ray Powder Diffraction, SEM and EDAX.

- Evaluation of precise reaction rate constants and other kinetic parameters using existing gas-solid reaction models.

- Prediction of reduced pellet structure.

3.2   Characterization of the Ore

Chemical analysis of the ore is done to determine the amount of iron, nickel, chromium and residual gangue by standard quantitative analysis method. A known weight of the ore is heated in a mixture of concentrated hydrochloric and nitric acid to dissolve the amount of iron, nickel and chromium present in the ore. The filtered solution is then used to determine the amount of iron, nickel and chromium, and the residue is weighed to estimate the amount of gangue present in the ore. Chemical analysis has shown that Sukinda laterite contains a very high percentage of iron oxide (about 54.65 Wt %). In comparison, the amount of nickel oxide is significantly small (about 1.22 Wt %). The detailed composition of the ore is given in table 3.1.

The nickeliferrous ore predominantly consists of goethite [(FeNi)O(OH).nH_2O] which has nickel in solid solution with iron oxide and a small amount of complex magnesium silicate in the form of serpentine [$Mg_6Si_4O_{16}(OH)_8$], in which magnesium is usually substituted by varying degrees of nickel, iron and cobalt. This ore was subjected to a thorough characterization using a number of techniques as described below.

3.2.1 Differential Thermal Analysis (DTA) and Thermo-Gravimetry (TG)

Differential thermal analysis, when carried out on lateritic ore, gives a good indication of the expected behavior of the ore during pyrometallurgical processing. The endothermic and exothermic peaks obtained by this method indicates the energy requirements at those specific temperatures. Any loss or gain in weight during heating is shown by the thermogravimetry curve.

It is also known that the DTA studies of limonitic ore with high iron content (50-60 % Fe_2O_3) usually do not show any serpentine peaks where Mg-silicate may exist in the form of talc. Such ores are easier to reduce because of olivine recrystallization and the consequent locking up of NiO does not occur in this case.

Results of the DTA-TG analysis of Sukinda nickel ore, conducted in a Linseis thermobalance (model No. L81/042) is shown in figure 3 1 It shows very prominent W and G peaks and sharp weightloss curve at those regions, indicating high content of free moisture and combined water of crystallization associated with goethite. The serpentine peaks (S and SC) are very small here, which indicates negligible amount of magnesium based complex mineral is present in this ore. Low content of magnesium is also evident from the EDAX analysis of the ore given in table 3.1.

Table 3 1· Ore composition by chemical analysis and EDAX analysis, given in weight percentage.

Components	As Received Ore	Preheated Ore		Reduced and Leached Ore	
		Chemical Analysis	EDAX Analysis	Chemical Analysis	EDAX Analysis
NiO	0.76	1.22	1.75	0.05	0.55
Fe_2O_3	33.83	54.65	53 56	55.34	53 55
Cr_2O_3	1.57	2.54	3.15	2.65	2.34
GANGUE	25.74	41.59	41.59	41.96	42.56
SiO_2	-	-	36.36	-	36.92
Al_2O_3	-	-	4.90	-	5.70
MgO	-	-	0.33	-	0.94
$Free\ Moisture$	28.60	-	-	-	-
$Water\ of\ Crystl.$	9.50	-	-	-	-

ORE COMPOSITION

1 % Ni, 38 % Fe, 31 % SiO$_2$, 2 % MgO

ENDOTHERMIC REACTION

⇑

EXOTHERMIC REACTION

⇓
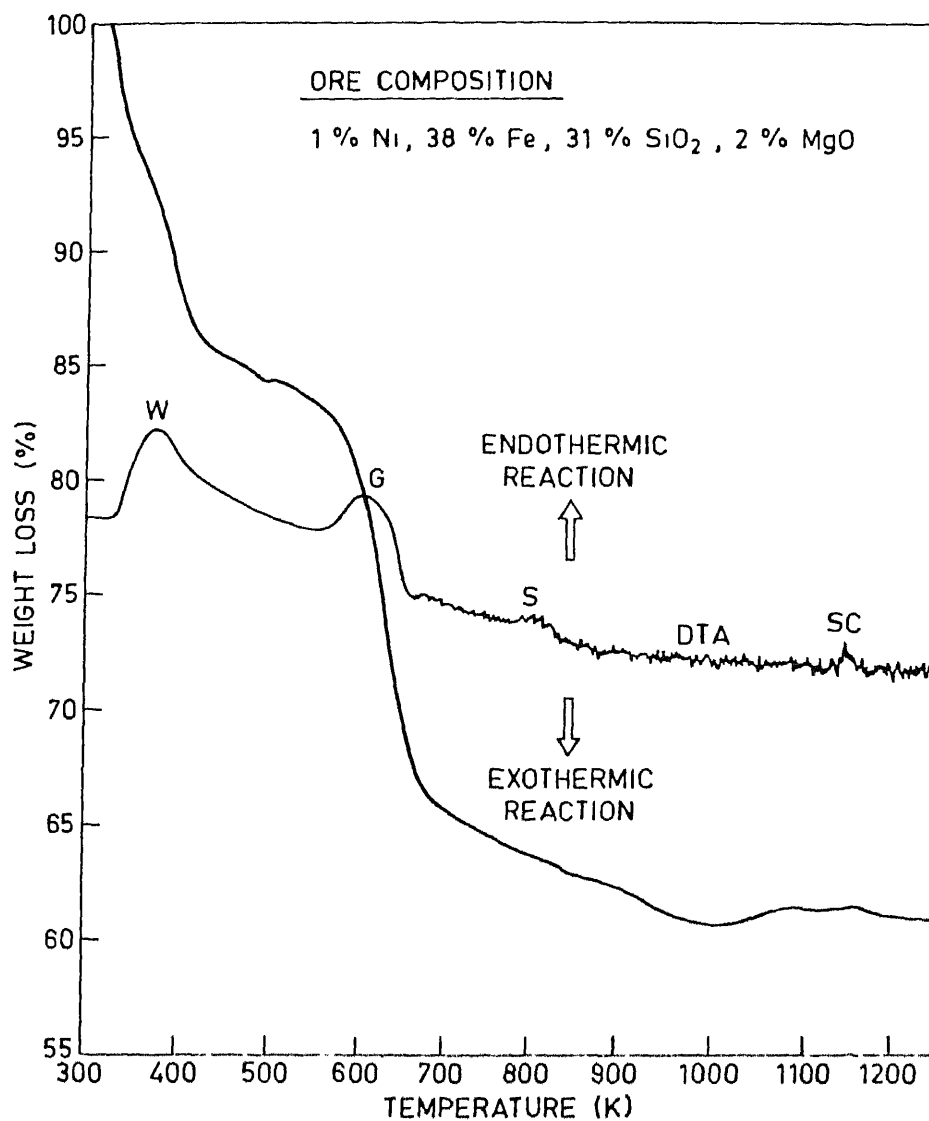
DTA OF SUKHINDA NICKELIFERROUS (LETERITIC) ORE

W : Dehydration (350 K)

G : Goethite decomposition (600 K)
$$2\,FeOOH \rightarrow Fe_2O_3 + H_2O$$

S : Dehydration of serpentine (800 K)
$$Mg_6Si_4O_{10}(OH)_8 \rightarrow 3Mg_2SiO_4 + 4H_2O + SiO_2$$

SC : Serpentine recrystallization (1100 K)
$$Serpentine \rightarrow Olivine$$

Figure 3 1. Differential thermal analysis of the Sukinda lateritic nickeliferrous ore.

3.2.2 Powder Diffraction studies

The results of the chemical analysis were further supported by a direct identification of phases through powder diffraction studies in a Seifert ISO-Debyflex1001 X-ray machine using Cr-Kα radiation. Powder diffraction charts for the gangue, the ore at room temperature and the ore heated at 850 K are shown in figure 3.2 and the peaks identified for various phases from X-ray powder diffraction file [54] are indicated by numbers shown below the charts in the figure. The peak angles and the corresponding intensities are given in table A.1, and the standard peaks for the reducible phases and the gangue minerals are given in table A.4 and A.3 respectively of Appendix A.

The gangue mineral contains mainly silica and other minerals like Al_2SiO_5 and Mg-Al-Si-O complex minerals. The peaks for gangue minerals will be present in all the powder diffraction charts as a constant factor in a reduced intensity corresponding to its approximate concentration of 42 %.

A preheating temperature of 850 K is chosen to completely dehydrate the ore above the serpentine dehydration peak 'S' at around 800 K as shown in figure 3.1. The change in peak intensity between ore at room temperature and preheated at 850 K will indicate the phase transformations in the ore due to preheating. The peaks for goethite ($FeOOH$) shows a considerable decrease in intensity in the 850 K heated sample compared to the corresponding room temperature peaks, indicating almost complete break down of goethite structure. The peak around 40° is coincident with peaks of gangue minerals and so may not indicate any considerable presence of goethite at 850 K. The peaks of $\gamma - Fe_2O_3$ showed considerable increase in intensity in the 850 K heated sample, which is formed due to the decomposition of goethite. Some of the peaks of $\gamma - Fe_2O_3$ are coincident with $FeOOH$ and their increase in intensity indicates formation of Fe_2O_3 rather than the formation of $FeOOH$. The peaks of $(Fe_{2/3}Ni_{1/3})OOH$ are very similar to $FeOOH$ and could not be studied separately. The presence of chromium in the ore as a mixed oxide with iron is confirmed by the presence $FeCr_2O_4$ peaks and its increase in intensity in the 850 K heated sample indicates goethite like hydrated structure at room temperature

3.2.3 SEM, EDAX and BET characterization of the Ore

Scanning electron microscope studies are done in a JEOL JSM-840A unit. The SEM micrographs shown in figure 3.3 indicates that there are in general two types of grains in the ore. The more
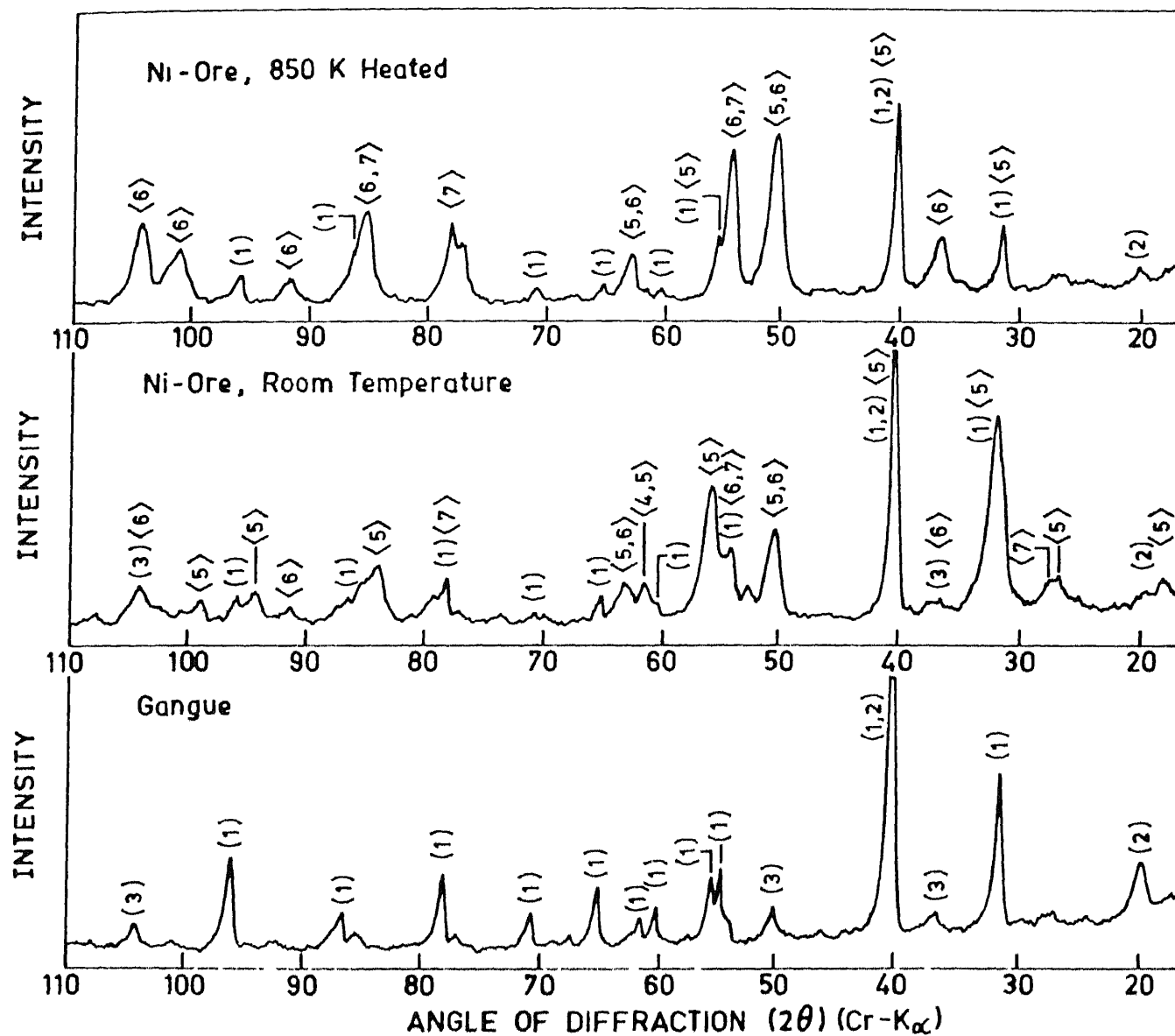
Figure 3.2. X-ray powder diffraction analysis of gangue, and nickel ore at room temperature and 850 K preheated sample.

abundant matrix phase has no definite grain size or shape and contains relatively higher concentration of all the reducible and economically important metals like iron, nickel and chromium. The other type of grains embedded in the matrix phase has more or less distinct shape and sharp corners and have higher concentration of silicon and aluminium and are essentially particles of alumino-silicate complex gangue minerals The EDAX measurements showed slightly higher percentage of nickel than chemical analysis, since the the peaks are too small and so the effect of background may be there.

The grain size and shape of this type of clay mineral is enigmatic and can vary widely according to the techniques used for its measurements The weighted average grain size obtained by coulter counter method is about 5 μm. However a much smaller grain size of about 0.2 μm (considering spherical grain) was obtained by BET surface area measurements. The BET measurements have given higher specific surface area may be due to the presence of internal pore structure within the grains measured by coulter counter method. The grain size measured by BET technique is considered to be more appropriate for determining kinetic parameters like intrapellet knudsen diffusivity and rate constant values [17, 18]

3.3   Experimental Technique

As discussed in the previous Chapter, reduction of nickel oxide by CO or H_2 is thermodynamically more favorable than the reduction of iron oxides, as the corresponding free energy values are more negative [14, 31] Selective reduction of nickel oxide in the laterite ore is therefore possible in principle.

During this study 'Large', 'Medium' and 'Small' sized spherical pellets of the ore with approximate radii of 0 35, 0.45 and 0.62 cm respectively were made using 0.2 % polyvinyle alcohol solution as binder and preheated to 850 K for two hours to remove the free and combined water of crystallization, and also to break the complex mineral structure as far as possible. The pellets are then reduced by hydrogen at 800 K, 900 K and 1000 K Further details of the experiments are provided below.

LINE PROFILE

AREA SCAN
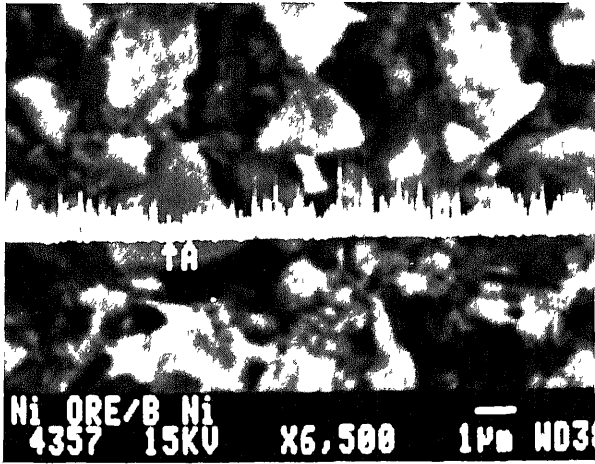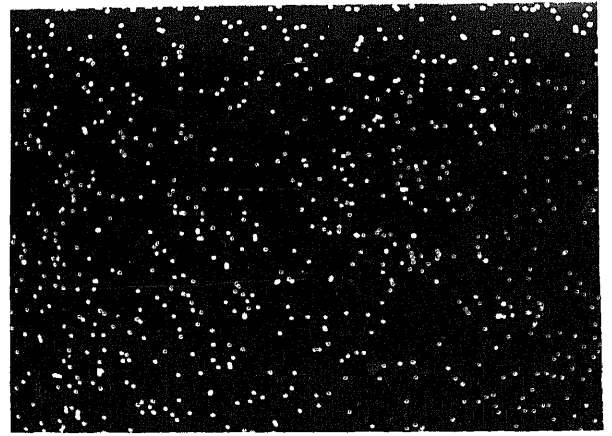
(a) NICKEL — $1\mu m$ NICKEL — $1\mu m$
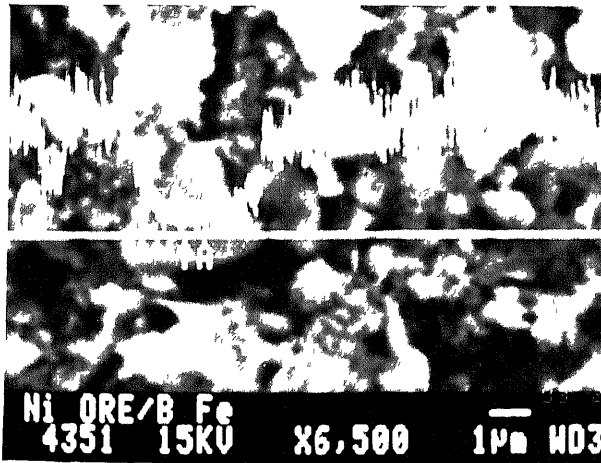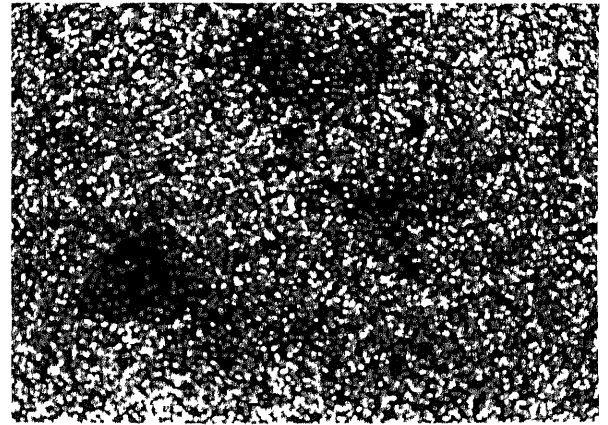
(b) IRON — $1\mu m$ IRON — $1\mu m$
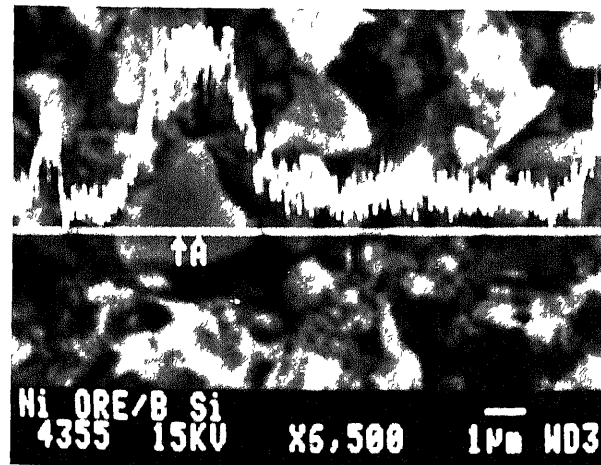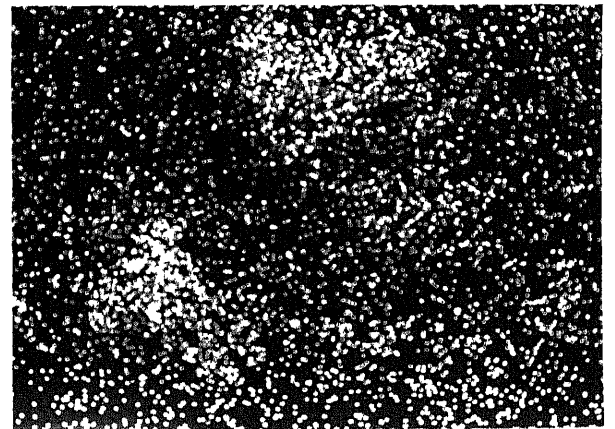
(c) SILICON — $1\mu m$ SILICON — $1\mu m$

Figure 3 3. EDAX analysis of nickel ore

3.3.1   Thermogravimetric Setup

All the gas-solid reaction experiments reported here were conducted in a thermogravimetric (TG) apparatus shown in figure 3.4. Similar experimental setup was earlier used by Bandyopadhyay et al [40, 55] for studying the kinetics of carbon gasification reaction. It consisted of a vertical furnace, a mulite tube as reaction chamber, gas inlet and outlet pipes, a thermocouple for the control and measurement of temperature, sample hanging assembly and a single pan semi-micro balance (Sartorius make) with readability of 10^{-4} gm for continuous recording of instantaneous weight

A kanthal wound vertical furnace of 53 cm length was used in the study. A mulite tube of 62 cm length and 5 cm internal diameter was employed as the reaction chamber, which was fitted with two brass flanges (one at the top and the other at the bottom) to provide air tight covers. Both the flanges were fitted with copper tubes brazed on them for water cooling. Silicon rubber gaskets and high temperature sealants were used to make the set-up air tight.

The description and the precautions taken for the thermogravimetric study are as follows :

1. The single pan balance was placed on a wooden platform with a central hole, and an inconel rod was connected to the balance. The sample bucket holder was suspended to the constant temperature zone of the reactor tube with the help of flexible nichrome wires through a hook in the inconel rod. The cylindrical sample holder was made of stainless steel wire mesh for easy passage of gas through it.

2. The furnace had about 6 cm long uniform temperature zone, where the sample could be conveniently placed. The thermocouple was used for both control and measurement of temperature at the reaction zone.

3 The furnace was controlled by Leeds and Northrup model 6260 Electromax temperature controller actuated by chromel - alumel thermocouple. The power supply circuit consisted of a temperature controller and a variable autotransformer for accurate control of temperature. The thermocouple was also connected to a digital millivoltmeter to measure the temperature in the reaction zone.

4 The length of the mulite tube reaction chamber was taken sufficiently large to preheat the gas upto the sample temperature in the reaction zone
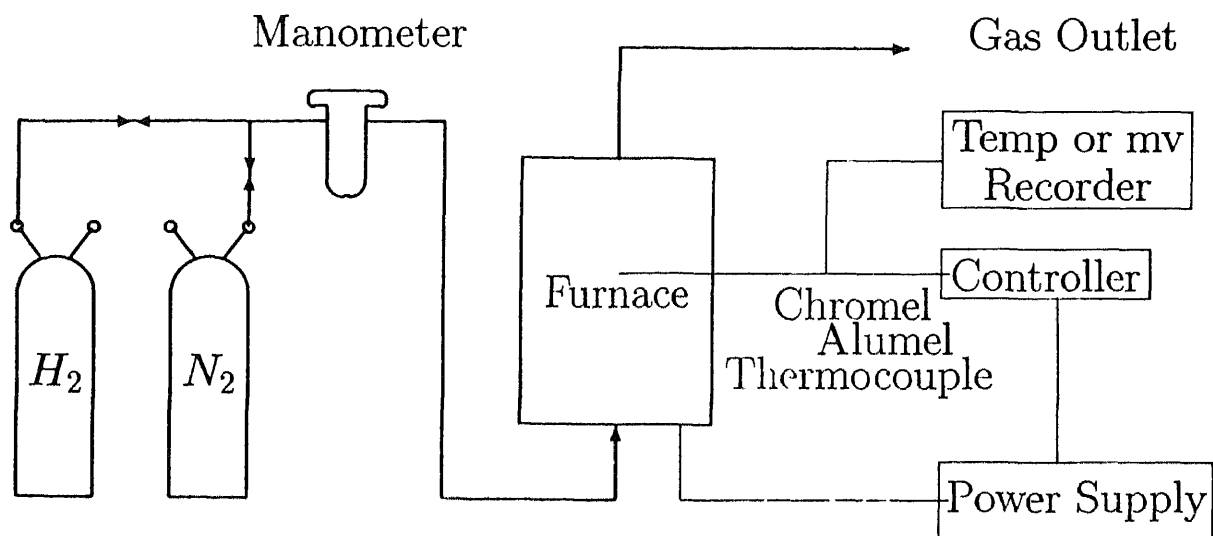
Figure 3.4: Schematic diagram of the experimental setup.

5. The pellet samples were first placed in the reaction zone and held for 1 hour to attain the furnace temperature. From calculations based on heating kinetics at the center of a sphere, the time of homogenization is found to be sufficient to attain the furnace temperature through out the pellet [56]

6 The tube-furnace was then flushed with nitrogen to form an inert atmosphere before hydrogen was passed at a superficial velocity of 4 cm/sec.

The setup for passing the gases for conducting the experiments is shown in figure 3 5. The arrangements for temperature control and measurement in the reaction zone is also shown in the figure. The manometer was first calibrated for hydrogen flow rate by measuring the height difference for different flow rates of hydrogen. The height difference and flow rates were then plotted and fitted with a third order polynomial as shown in figure A.1 given in the Appendix A From the fitted curve we can get the manometer height difference for any selected flow rate within the range of calibration.

3.3.2 Technique of Reduced Nickel and Iron Analysis

The nickel content of the pellets reduced for different time periods were analyzed by leaching representative samples in ammoniacal ammonium-carbonate solution in an autoclave for 2.5 hours at around 340K, using pure oxygen at 1 atmosphere pressure. A liter of leaching solution contained 300 cc of 0.81 gm/cc ammonia solution, and 100 gms of ammonium-carbonate The leached solution containing nickel was then filtered and precipitated by dimethyl glyoxime (DMG) and weighed to estimate the amount of nickel reduced. Weight of nickel is about 20.32 % of the total weight of the Ni-DMG complex precipitate.

In our laboratory this method worked quite satisfactorily, producing reproducible result. Similar techniques were used by other research groups and the results are already documented in the literature [8, 14, 31].

The nickel analysis technique and the pertinent chemical reactions [4, 9, 57] are summarized in figure 3 6

After obtaining the nickel fraction reduced at various times, a fourth order polynomial was fitted through the experimental points to get the overall time versus nickel fraction reduced curve. The weight loss due to nickel oxide reduction was calculated from the fitted curve and subtracted
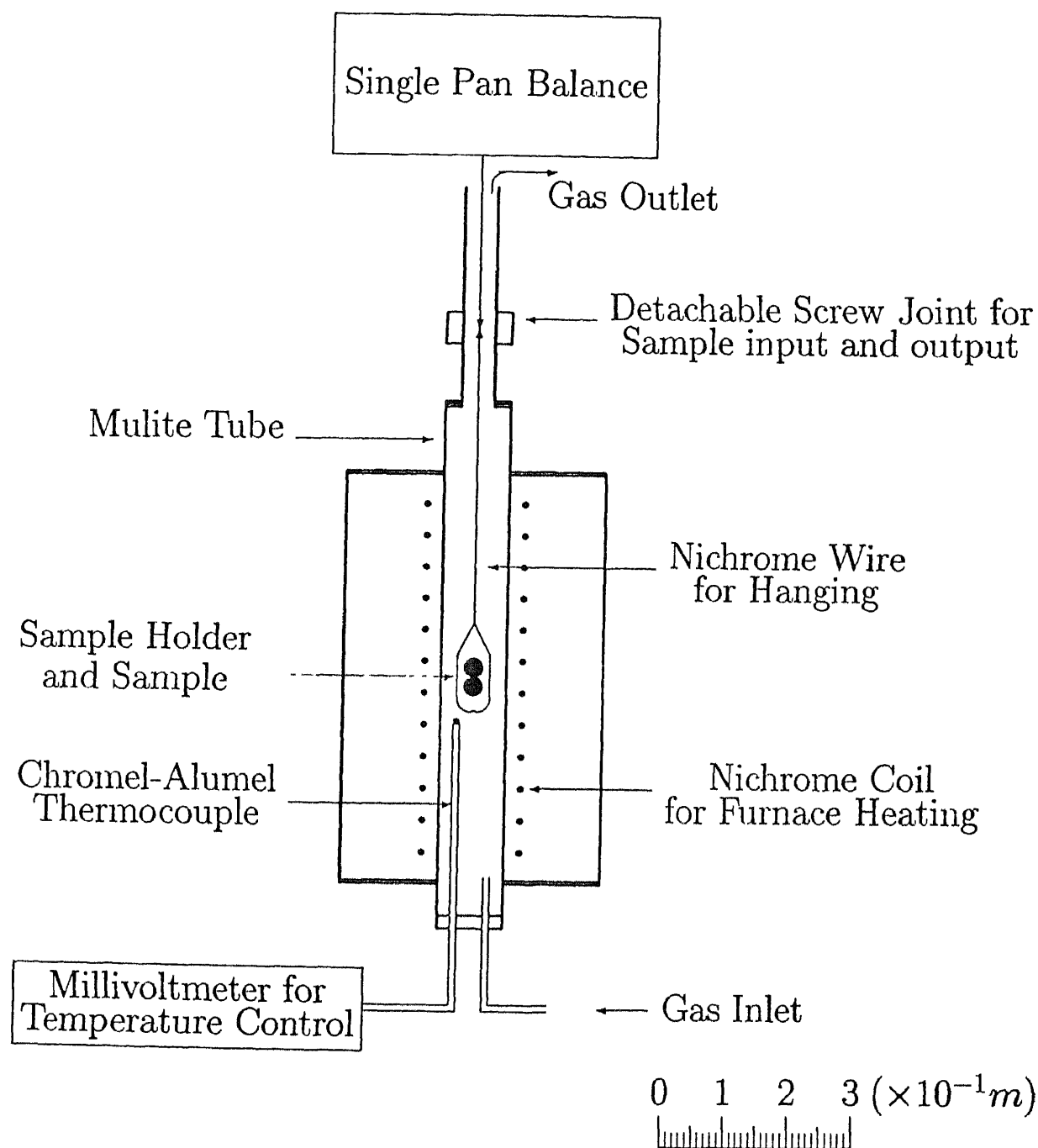
Figure 3.5: Thermogravimetric set up for single pellet reduction experiments.

NICKEL ANALYSIS

The reduced Nickel ore pellets are dissolved in Ammonical Ammonium-Carbonate solution, and leached at $65^{\circ}C$ for 3 hours under Oxygen atmosphere

$$FeNi + O_2 + 8NH_3 + 3CO_2 + H_2O = Ni(NH_3)_6^{+2} + Fe^{+2} + 2NH_4^+ + 3CO_3^{-2}$$

$\downarrow$
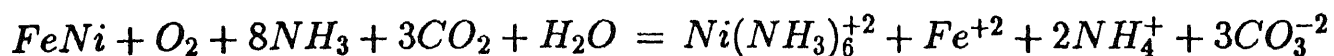
The Iron first goes into solution as Fe^{+2} and then precipitates over the ore particles under oxidizing condition.

$$4Fe^{+2} + O_2 + 2H_2O + 8OH^- = 4Fe(OH)_3$$

$\downarrow$
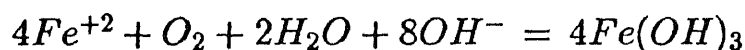
The filtered solution containing Nickel-Ammonium complex is then precipitated by Dimethyl-glyoxime and, measured by gravimetric method
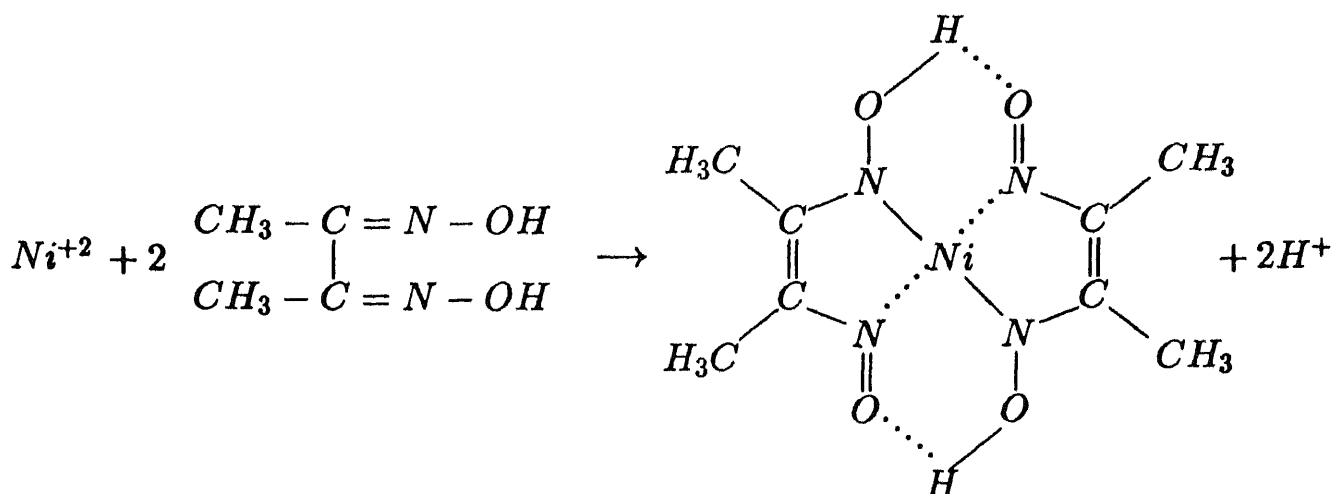
Figure 3.6: Flow chart for reduced nickel analysis.

from the time versus weight loss results obtained from the experiment to get the weight loss for iron oxide reduction, from which fraction of iron oxide reduced can be calculated directly.

Since one data point for nickel reduction is obtained from one experiment, five or more experiments had to be conducted at a particular condition for different time periods to get the curve for nickel reduction However iron reduction curve or data points are obtained in a continuous fashion for all the experiments Three such points for nickel reduction and the corresponding iron reduction curves are shown in figure 3.7. The iron reduction curves showed good matching among them, indicating good reproducibility of the experimental results.

3.4   Experimental Results and Discussion

Single pellet reduction data obtained during this investigation are plotted in figure 3 8(a), (b) and (c), and the experimental data for nickel and iron are given in tables A 8 to A 13 in Appendix A

The reduction rate of iron oxide and nickel oxide at 800 K are very similar, and showed negligible selective reducibility as shown in figure 3 8(a). Although pure nickel oxide can be completely reduced by hydrogen at around 800 K [18, 19], but due to the complex mineral structure of the ore, its reduction rate is considerably slower. In the present study maximum reduction of nickel oxide is less than 50 % after 40 minutes of reduction.

The reduction rate of nickel oxide is much higher than the iron oxide at 900 K as shown in figure 3 8(b) The effect of pellet size is also prominent at this temperature. Investigators [23, 58] have reported an anomalous decrease in reduction rate of iron oxide around this temperature, which may be the cause for good selective reducibility of nickel oxide at this temperature.

Reduction rate of both nickel oxide and iron oxide is much faster at 1000 K as shown in figure 3.8(c). Since reduction rate of iron oxide is also considerably fast at this temperature, good selective reducibility is not observed.

Comparing the reduction kinetic results it can be concluded that best selective reducibility and most prominent effect of pellet size is observed at 900 K. The reduction rate of nickel oxide and iron oxide is considerably faster at 1000 K, so for faster reduction and good selective reducibility, some temperature between 900 K and 1000 K will be suitable.

Phase transformations taking place during the reduction process at 800 K, 900 K and 1000 K
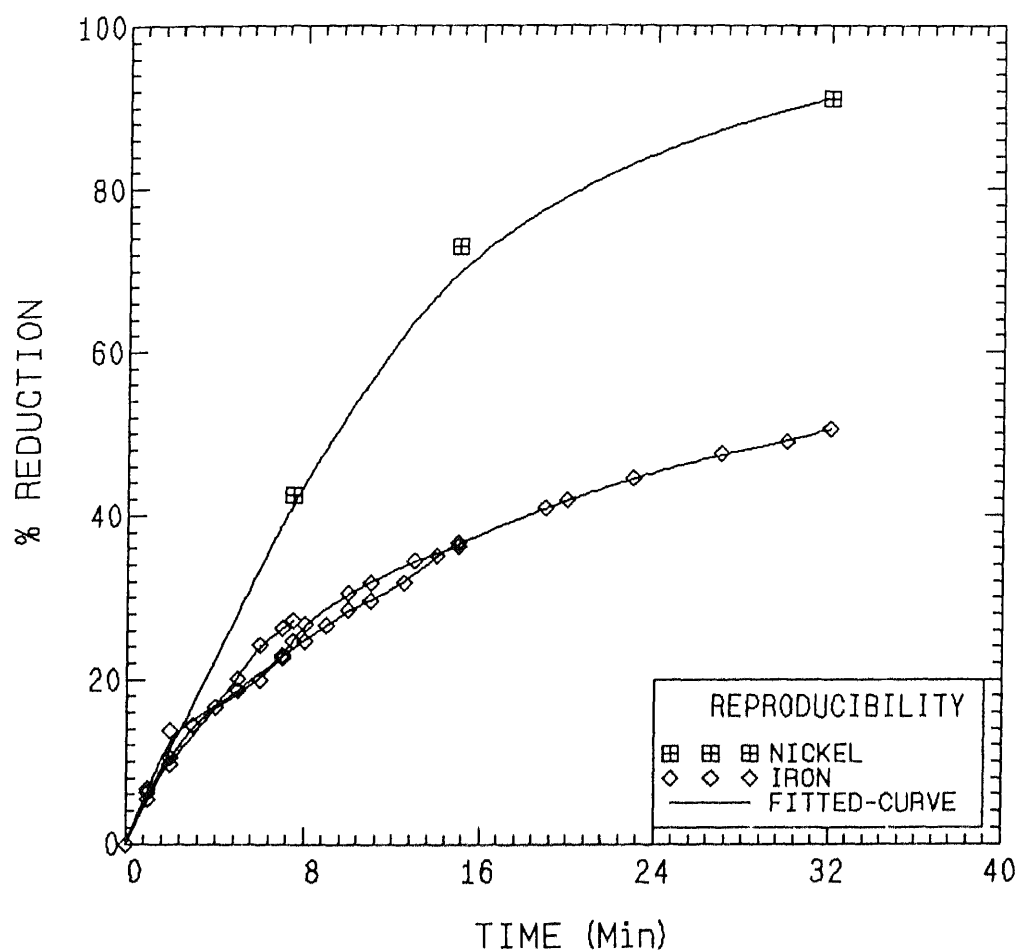
Figure 3 7: Nickel data points and the corresponding reduction rates for iron, for the medium size pellets reduced at 900 K, showing the reproducibility for iron reduction.
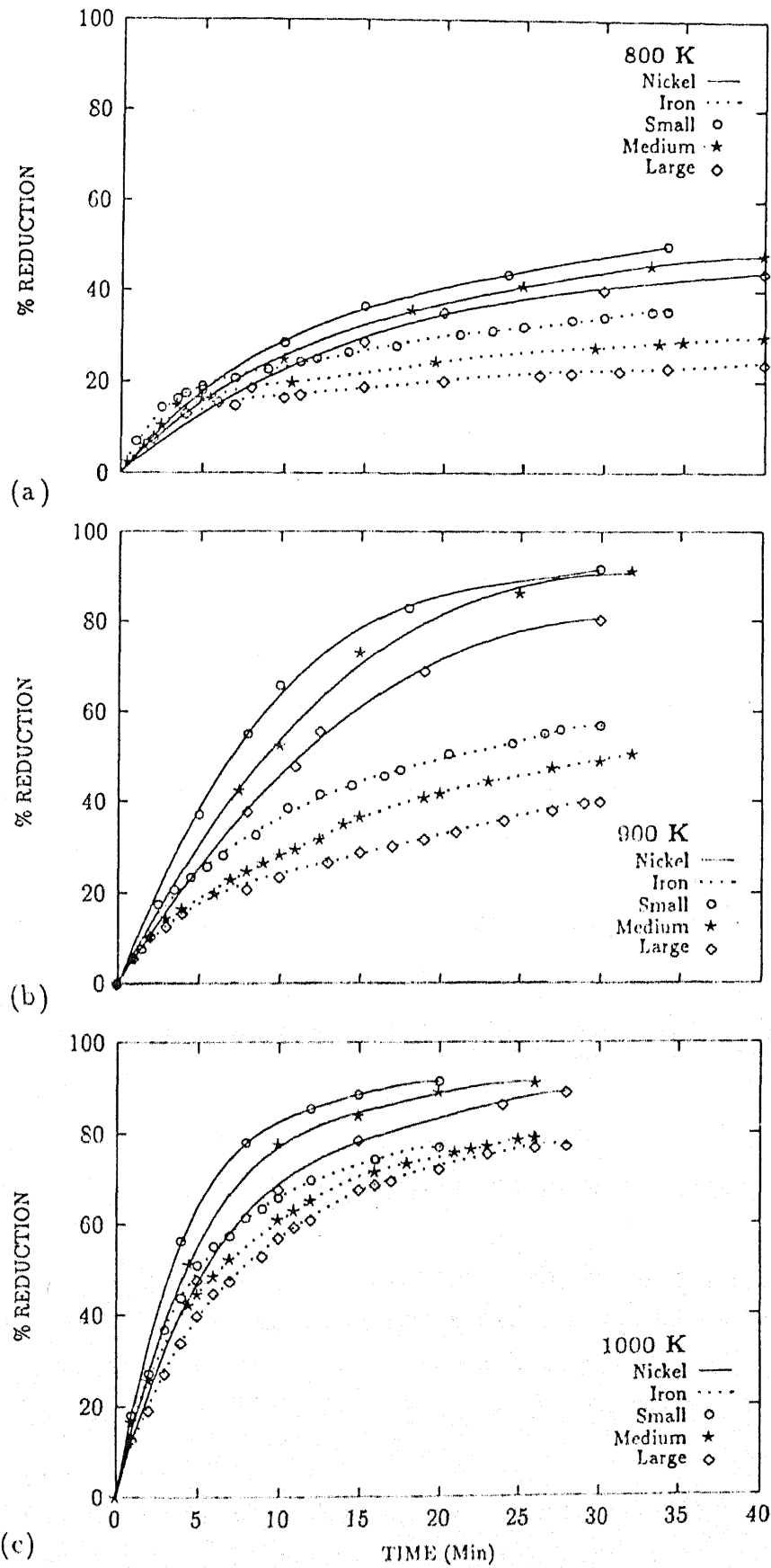
Figure 3.8: Experimental data points and the fitted curves for nickel ore pellet reduced at : (a) 800 K (b) 900 K (c) 1000 K

are analyzed by comparing the X-ray powder diffraction of 'Small' pellets reduced for 30 minutes at these temperatures. Diffraction charts for reduced pellets in figure 3 9 shows increasing peak intensity for metallic iron and nickel and corresponding decrease in peak intensity for iron oxides. The maximum intensity peak for reduced iron and nickel at an angle of 68 8°, has an intensity ratio of about 1:3·6 for corresponding reduction at 800 K, 900 K and 1000 K, from which we can roughly estimate that 10 %, 30 % and 60 % metallization has taken place under the given conditions. Since concentration of nickel is very low and its peaks coincided with metallic iron peaks it could not be studied separately. The peaks identified and the corresponding intensities for the X-ray study of the reduced ore is given in table A.2, and the standard peaks for the reducible phase, partially reduced phase and the reduced metallic phase are given in table A.4, A 5 and A 6 of Appendix A.

The change in iron and nickel distribution after leaching can be observed by comparing the SEM/EDAX photographs shown in figure 3.3 and figure 3.10 for the unreduced ore, and the reduced and leached ore respectively The comparative decrease in nickel concentration in the matrix in figure 3.10 indicates the extraction of reduced nickel by leaching operation. The line scan of the leached ore showed almost constant iron concentration throughout the ore matrix This may be due to the reason that the reduced iron is oxidized and reprecipitated in the ore during leaching operation, and while doing so it precipitated homogeneously. The decrease in nickel concentration in the leached ore can also be observed by comparing the X-ray peak intensity for nickel obtained by EPMA analysis of the unreduced, and the reduced and leached ore as shown in figure 3.11.

We have subjected the experimental data for pellet reduction to a rigorous analysis, as outlined in the following sections.

3.5   Estimation of various Parameters

In the present case of gas solid reduction, the situation is complicated by the presence of two reducible metallic oxides namely nickel oxide and iron oxides. Although we are mainly interested in the reduction of nickel oxide; but iron oxide is the major constituent of the ore, and so it will predominantly effect the thermal characteristics and gas concentration in the pellet during reduction

Previously Szekely and Hastaoglu [27] have utilized the grain model for reducing pellets

Figure 3 9 X-ray powder diffraction analysis of nickel ore reduced at 800 K, 900 K and 1000 K.

62

LINE PROFILE AREA SCAN
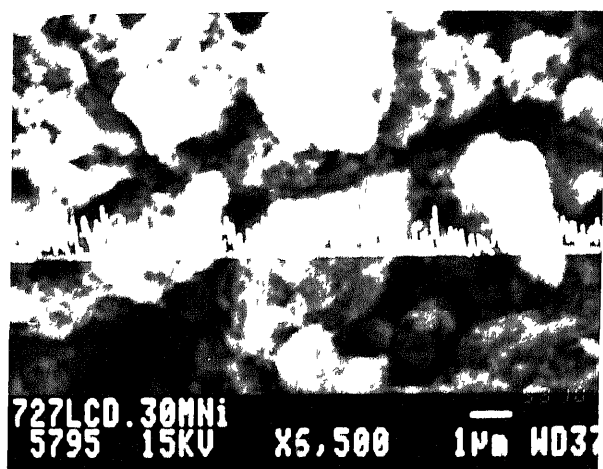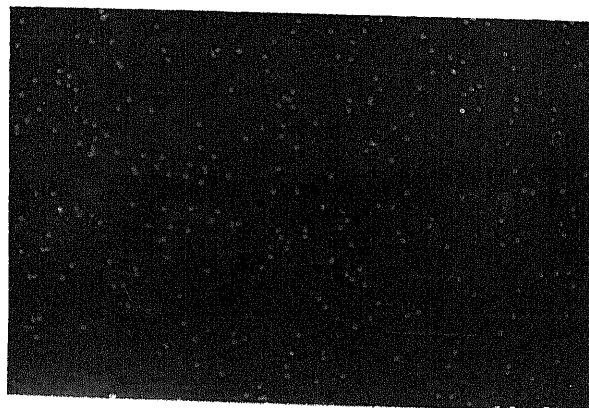
(a) NICKEL $\overline{1\mu m}$ NICKEL $\overline{1\mu m}$
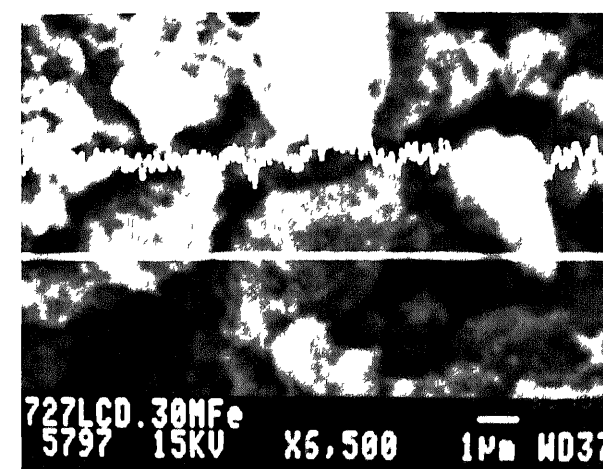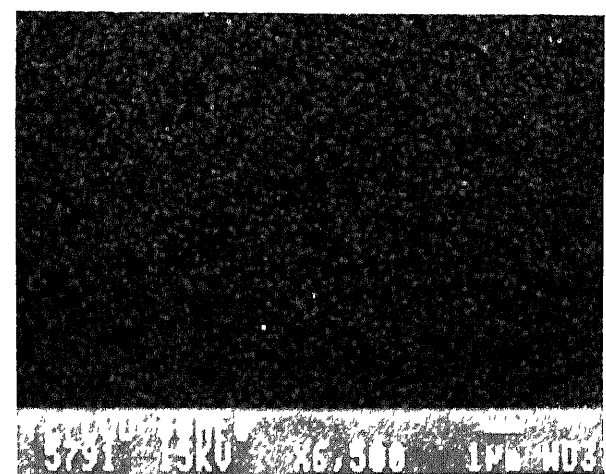
(b) IRON $\overline{1\mu m}$ IRON $\overline{1\mu m}$
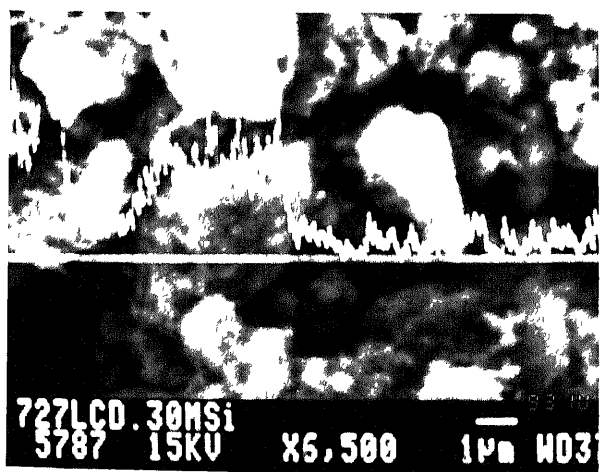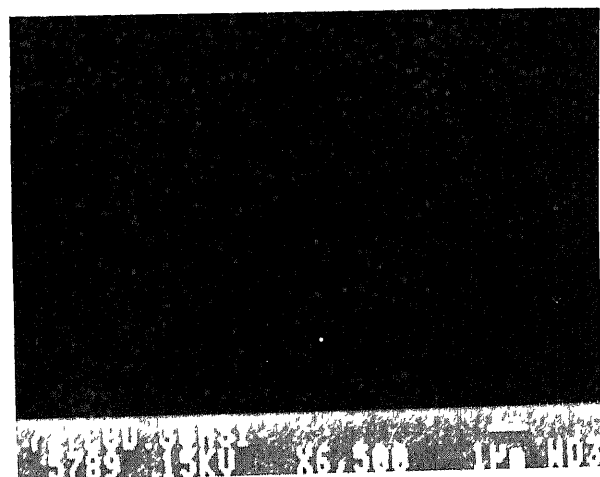
(c) SILICON $\overline{1\mu m}$ SILICON $\overline{1\mu m}$

Figure 3.10: EDAX analysis of reduced and leached ore.
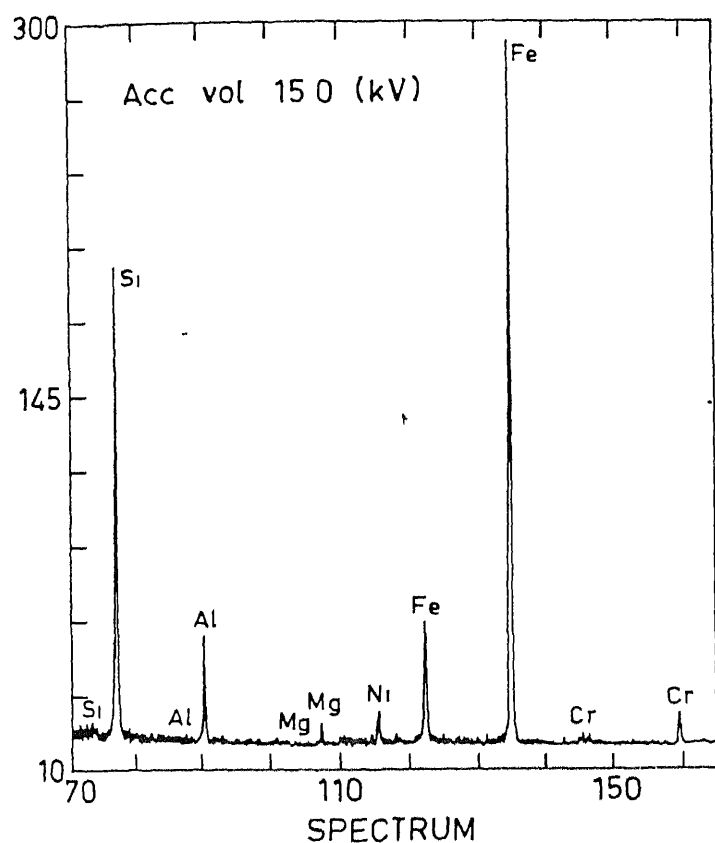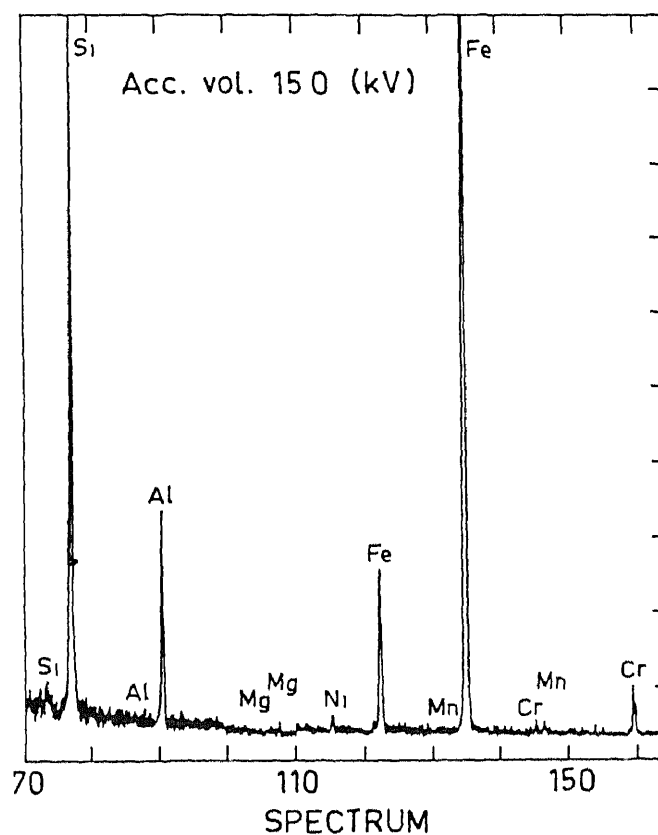
Figure 3.11: X-ray peaks obtained by EPMA analysis of : (a) The unreduced ore (b) The reduced and leached ore.

containing mixture of nickel oxide and hematite, a similar approach is taken in the present study. In general same equations are used for the two oxides The parameters like diffusivity (D_e, D'_e), pellet radius (R_p), grain radius (r_g), pellet and grain shape factor $(F_p$ and $F_g)$ are same for both the cases; but the rate constant value (k denoted by $k_{/rg}$ and k_A in the two models discussed later), fraction reduced or solid concentration (X or C_B), shrinking core radius and core radius (ε_{sc} and ε_m), heat of reaction ($\triangle H$), equilibrium constant (K_{eq}) are different for the two metallic oxides A subscript 'ı' is used to denote variable quantity in the section for effect of non-ısothermal reaction and product gas formation; where $ı = 1$ denotes nickel oxide and $ı = 2$ denotes iron oxide. In the general discussion for the models the subscript 'i' is not used for simplification. The same equations are used first for iron oxide reduction and then for nickel oxide reduction.

The parameter values and the equations to estimate them are given in table (3.2). The diffusion coefficient, physical properties of solid, gas and the thermal properties are given in table A 24, A 25, A 26, and A.27 in Appendix A. To simplify the model equations solid density is considered to be the gram equivalent density of the pellets with respect to removable oxygen concentration ([O]) or reactant gas ([H_2]) Therefore the density of solid becomes $C_{Bo} = 3[Fe_2O_3] + [NiO]$ per unit volume of the pellet, such that the parameters like porosity, stoichiometric factor are incorporated in the solid density and doesn't appear in the model equations. In a similar approach effective diffusivity is defined as .

$$D_e = \frac{p}{\tau}\left(\frac{1}{\frac{1}{D_M} + \frac{1}{D_K}}\right)$$

(3.1)

to incorporate the parameters like porosity and tortuosity factor.

Due to higher rate of reduction, and accompanying change in porosity and internal pore structure at higher temperatures; an enhanced effect of temperature is considered for knudsen diffusivity compared to theoretical value where the porosity and pore structure is constant. Enhanced effect of temperature on diffusivity is also reported in literature for pellet reduction [36]

Porosity of the preheated pellets are measured by water displacement method. A pellet of known weight and volume is dipped in a measuring cylinder containing water. The increase in water level gives the intrinsic volume of the pellet from which porosity can be easily calculated. Tortuosity factor is taken to be the inverse of pellet porosity and knudsen diffusivity is calculated from the standard relations [18].

Table 3.2: Parameter values for single pellet reduction.

PARAMETERS	VALUES	IN SI UNITS	REF.
Gas Density	$C_{Ab} = 12187.5/T$	$(mole/m^3)$	
Intrinsic Solid Density	3714	(kg/m^3)	
Pellet Porosity	$p = 0.5645$		
Apparent density of pellet	1617.4	(kg/m^3)	
Mole fraction NiO	$n1 = 0.016$		
Mole fraction Fe_2O_3	$n2 = 0.984$		
Equivalent solid density	$C_{Bo} = 16871$	$(mole/m^3)$	
Thermal Conductivity of solid	$K_s = 0.63$	$(W/m.K)$	[59]
Pellet radius : Small/Medium/Large	$R_p = 3.5/4.5/6.2$	$(\times 10^{-3}\ m)$	
BET area of preheated Pellet	44.7	(m^2/gm)	
Grain Radius (Fg=1)	$r_g = 6.024 \times 10^{-3}$	(μm)	
Superficial gas velocity	$u = 0.04$	(m/s)	
Gas viscosity	$\mu = 3.633 \times 10^{-6} \exp(-598/T)$	$(Pa\ s)$	[60]
Schmidt number	$S_c = \dfrac{\mu}{\rho_{H_2} D_{AB}}$		
Particle Reynold's number	$R_{e,p} = \dfrac{2R_p u \rho_{H_2}}{\mu}$		
Film mass transfer coefficient	$k_f = \frac{D_{AB}}{R_p}(1 + 0.3 R_{e,p}^{1/2} S_c^{1/3})$	(m/s)	[39]
REACTION PARAMETERS :			
Effective Pellet Diffusivity	$\dfrac{1}{D_e} = \dfrac{\tau}{p\left(\frac{1}{D_K} + \frac{1}{D_{AB}}\right)}$	(m^2/s)	
Product layer diffusivity	$D'_e = D_e \times 994 \exp(-5197/T)$		

The parameters like equilibrium constant, rate constant, heat of reaction which are different for different iron oxides are estimated on the basis of Lever rule. The equilibrium constant value for iron oxides estimated by Lever rule is shown in figure 3.12.

3.6 Structural Model for Gas-Solid reaction : Grain Model

Extensive theoretical and experimental research on the reduction of high quality nickel oxide was carried out by Szekely et al., and Sohn et al., [18, 19, 32]. The mathematical model developed by these researchers can be considered to be a significant improvement over the conventional shrinking core model [33], as the shape and size of both the pellet as well as the particles constituting the pellets were taken into consideration. A schematic diagram of a pellet showing the reduction in the individual grains, as assumed in grain model is shown in figure 3.13 [61]. Due to this modification it is generally referred to as grain model [35, 62]. The gas-solid reaction kinetics was assumed to be controlled either by the the rate of chemical reaction or by the rate of diffusion of the reacting gas through the product layer. The slower of these two was assumed to determine the rate.

The basic assumptions for the reaction kinetic models are given below :

- Irreversible reaction.

- Diffusion within the pellet is by equimolar counter diffusion.

- The reaction is first order with respect to the gaseous phase.

- Gas concentration within the pellet is described by pseudo-steady state approximation.

- Diffusion of reactant gases through the product layer of individual grains is not rate limiting.

- The solid structure is macroscopically uniform and is unaffected by the reaction.

- The system is isothermal. (Correction factors are incorporated later to consider its effect)

$$
\left.
\begin{array}{lll}
Pellet\ Volume & : & V_p \\
Pellet\ area & : & A_p \\
Grain\ Volume & : & V_g \\
Grain\ Area & : & A_g
\end{array}
\right\}
\tag{3.2}
$$
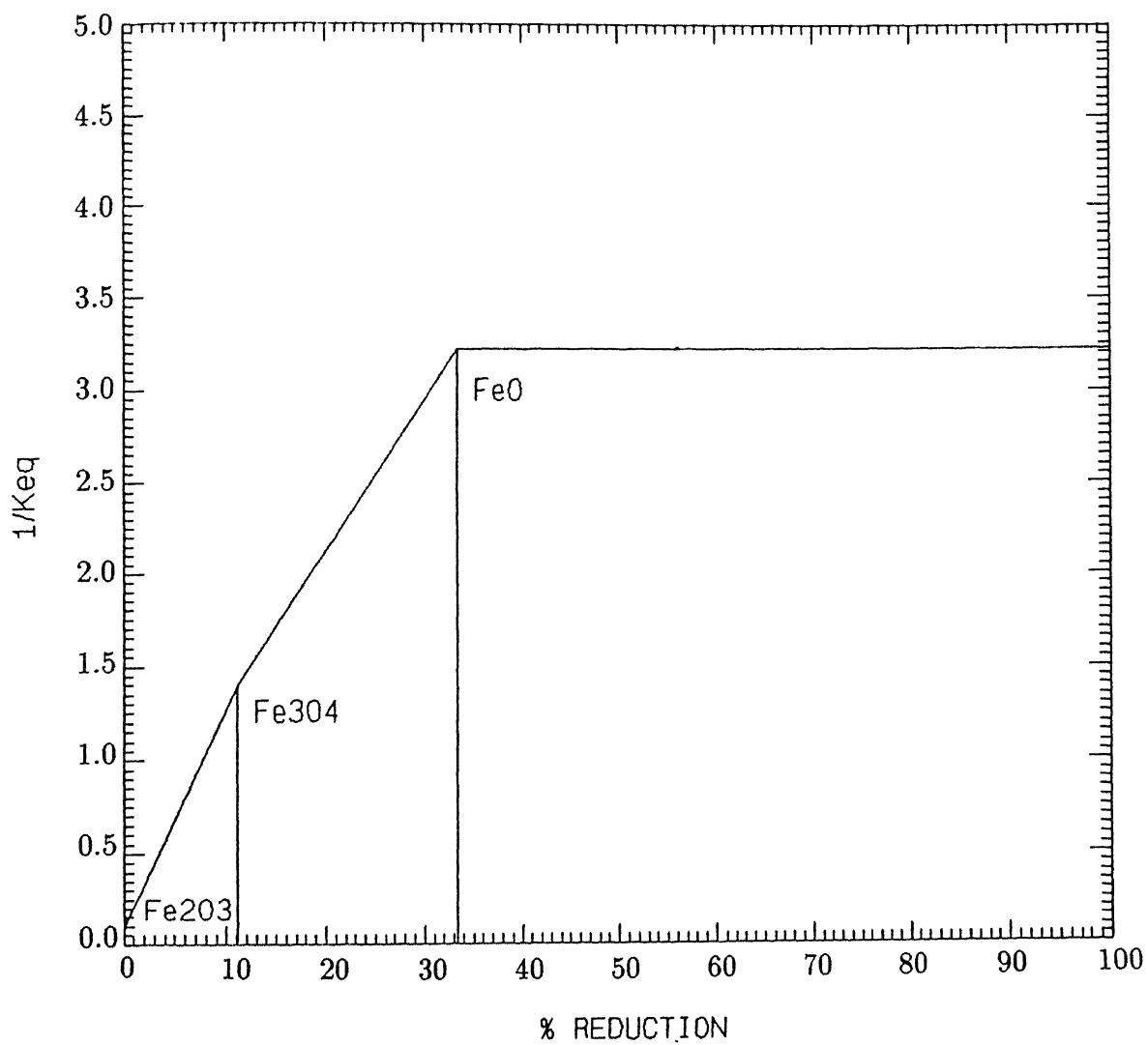
Figure 3.12: Estimation of equilibrium constant of iron oxides by Lever rule.
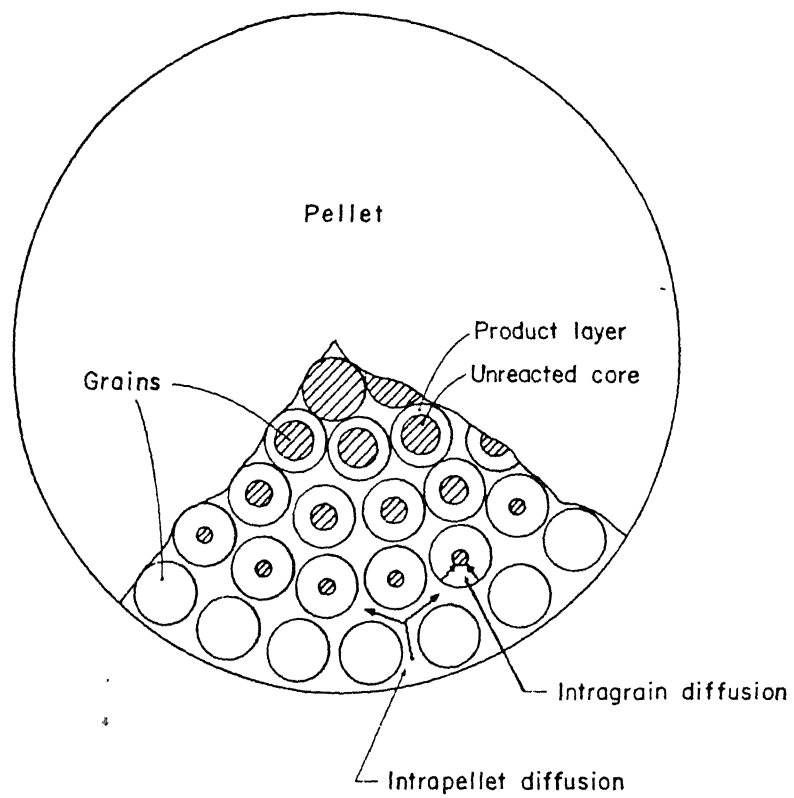
Figure 3.13: Schematic representation of the grain model [61].

$$Structure\ Factor\ :\ Fg,\ Fp\quad = 3\ for\ sphere \atop \left. = 2\ for\ cylinder \atop = 1\ for\ plate \right\} \tag{3.3}$$

$$\left. \begin{array}{rcl} (H_2) + [NiO] &=& (H_2O) + [Ni] \\ (A) + [B] &=& (C) + [D] \end{array} \right\} \tag{3.4}$$
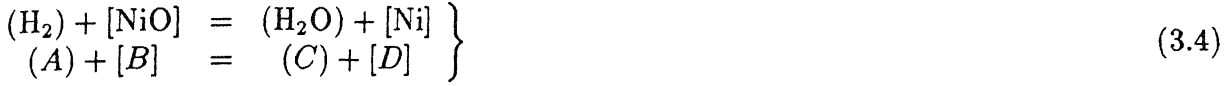
For conservation of gaseous reactant :

$$De\ \nabla^2 C_A - V_A = 0 \tag{3.5}$$

For conservation of solid reactant :

$$C_{Bo}\frac{dr_g}{dt} = kC_A \tag{3.6}$$

The reaction term V_A is written as :

$$V_A = kC_A\frac{A_g}{V_g}\left(\frac{A_g r_g}{V_g F_g}\right)^{Fg-1} \tag{3.7}$$

Non-dimensionalizing the equations :

$$\left. \begin{array}{lll} \text{Dimensionless concentration} &:& \psi = \frac{C_A}{C_{Ab}} \\[4pt] \text{Dimensionless pellet radius} &:& \eta = \frac{A_p R_p}{F_p V_p} \\[4pt] \text{Dimensionless grain radius} &:& \varepsilon = \frac{A_g r_g}{F_g V_g} \\[4pt] \text{Dimensionless time} &:& t^* = \left(\frac{kC_{Ab}}{C_{Bo}}\frac{A_g}{F_g V_g}\right)t = \left(\frac{k/r_g C_{Ab}}{C_{Bo}}\right)t \end{array} \right\} \tag{3.8}$$

So eqn.(3.5) and (3.6) becomes :

$$\nabla^2\psi - 2F_g F_p \sigma^2 \psi^n \varepsilon^{Fg-1} = 0 \tag{3.9}$$

$$\frac{\partial\varepsilon}{\partial t^*} = -\psi^n \tag{3.10}$$

Boundary conditions for eqn.(3.9) and (3.10) :

$$\left. \begin{array}{ll} \varepsilon = 1, & at\ t^* = 0 \\ \psi = 1, & at\ \eta = 1 \\ \dfrac{\partial \psi}{\partial \eta} = 0, & at\ \eta = 0 \end{array} \right\} \tag{3.11}$$

Here in eqn.(3.9) σ is a dimensionless parameter and physically signifies the ratio of, the ability to react chemically, and the ability to transport the gaseous reactant through the product phase. The magnitude of σ determines the exact control mechanism.

$$\sigma = \frac{V_p}{A_p} \sqrt{\frac{kF_p}{2D_e}\left(\frac{A_g}{F_g V_g}\right)} = R_p \sqrt{\frac{k_{/rg}}{6D_e}} \tag{3.12}$$

And the overall extent of reaction 'X' is given by :

$$X = \frac{\displaystyle\int_0^1 \eta^{F_p-1}(1-\varepsilon)^{F_g} d\eta}{\displaystyle\int_0^1 \eta^{F_p-1} d\eta} \tag{3.13}$$

3.6.1 For Asymptotic behavior of σ :

when $\sigma \to 0$, Chemical control Kinetics ($\sigma < 0.3$)

Uniform Reduction.

$\psi = 1$, for all t

$\varepsilon = 1 - t$, for $0 \le t \le 1$

$\varepsilon = 0$, for $t \ge 1$

ε is not a function of η

From the above conditions applied to eqn.(3.13), we get the relation given by eqn.(2.7) discussed in Chapter 2 :

$$t^*_{\sigma \to 0} = 1 - (1-x)^{1/F_g} \tag{3.14}$$

By conducting experiments in this condition the grain shape factor F_g can be estimated. Again by putting the value of t we get :

$$1 - (1-x)^{1/F_g} = g_{F_g}(x) = \frac{C_{Ab}}{C_{Bo}} k_{/rg} t \tag{3.15}$$

From the slope of the $g_{Fg}(x)$ *vs.* t curve or at least from the linear part we can get the value of K, the intrinsic rate parameter. And by conducting the experiments at different temperatures we can get the Activation energy.

When $\sigma \to \infty$: Diffusion Control Kinetics($\sigma > 3.0$)

This is represented by shrinking core model :

$$P_{Fp}(x) = \frac{t^*}{\sigma^2} \tag{3.16}$$

Where, $P_{F_p}(x)$ is given by the eqn.(2.9) given in Chapter 2 :

$$
\begin{aligned}
P_{Fp}(x) \quad &= X^2, & For\ Fp &= 1\ (Plate) \\
&= X + (1 - X)\ln(1 - X), & For\ Fp &= 2\ (Cylinder) \\
&= 1 - 3(1 - X)^{2/3} + 2(1 - X), & For\ Fp &= 3\ (Sphere)
\end{aligned}
\tag{3.17}
$$

The derivation of the equation for spherical pellets ($F_p = 3$) is given in the Appendix B. The eqn.(3.16) in dimensional form becomes :

$$P_{Fp}(X) = \frac{2FpD_eC_{AO}t}{R_p^2(1 - \varepsilon)C_{Bo}} \tag{3.18}$$

Thus plotting $P_{Fp}(x)$ against t, the value of D_e (effective diffusivity in pellet) can be estimated from the slope.

Intermediate region $(0.3 < \sigma < 3.0)$

Szekely et al., and Sohn et al. [18, 19, 32, 34] had also considered an intermediate regime where the intrinsic rate of chemical reaction is comparable with that of the diffusion process. Under this condition both chemical kinetics and product layer diffusion is significant. In such a case one can add up the time required for these two processes on the basis of 'The Law of Additive Reaction Time', giving rise to a generalized rate expression which takes into account both diffusion and the chemical control processes. It should be pointed out that this expression for the reduction rate at the intermediate region is not exact as it is based upon the approximate law of additive reaction times which takes the time required to attain a certain fraction of conversion as the sum

total of times required for attaining the same conversion under chemical control kinetics when diffusion is infinitely fast, and diffusion controlled kinetics when chemical reaction is infinitely fast.

$$
\begin{pmatrix}
\text{Time required} \\
\text{to attain} \\
\text{a certain} \\
\text{conversion}
\end{pmatrix}
=
\begin{pmatrix}
\text{Time required to attain} \\
\text{the same conversion} \\
\text{if the interpellet diffusion} \\
\text{is infinitely fast}
\end{pmatrix}
+
\begin{pmatrix}
\text{Time required to attain} \\
\text{the same conversion} \\
\text{if the reaction of grains} \\
\text{are infinitely fast}
\end{pmatrix}
$$

$$
t^* = t^*_{\sigma \to 0} + t^*_{\sigma \to \infty}
\tag{3.19}
$$

The effect of external mass transfer can also be incorporated by adding an extra term for it to get :

$$
t^* = g_{Fg}(X) + \sigma^2 \left\{ P_{Fp}(X) + \frac{2X}{N_{Sh}} \right\}
\tag{3.20}
$$

Where N_{sh} is the modified Sherwood number given by :

$$
N_{sh} = \frac{R_p k_f}{D_e}
\tag{3.21}
$$

N_{sh} may play an important role in determining the overall rate for larger values of σ (for smaller value of mass transfer is very fast and the reaction is chemically controlled). The effect of external mass transfer becomes unimportant when $N'_{sh} > 30$

The weight loss data from the thermogravimetric setup can be readily converted into fraction reacted as a function of time. Utilizing the grain model of Szekely et al., Sohn and Szekely [18, 32], one can utilize the following relationship for the calculation of the rate constant :

$$
k_{/rg} = \frac{g_{Fg}(X)}{\frac{C_{Ab} \cdot t}{C_{Bo}} - \frac{R_p^2}{6D_e} \left(P_{Fp}(X) + \frac{2X}{N_{Sh}} \right)}
\tag{3.22}
$$

3.7 Two Layer Model

In an analogous approach, primarily used by various researchers in the field of iron oxide reduction [37, 38, 39], completely reduced product layer formation is considered after a critical time t_c, given

by :

$$t_c = \frac{C_{Bo}\left[1 + \frac{1}{N_{Sh}}(\phi \coth \phi - 1)\right]}{k_A C_{Ab}} \tag{3.23}$$

Where, $\quad \phi = R_p\sqrt{\frac{k_A}{D_e}} \tag{3.24}$

This scheme of reaction, could be more appropriately termed as the two layer model, since different set of rate expressions are used for the two time periods, before the product layer formation $(t < t_c)$ and after the product layer formation $(t > t_c)$. The derivation of the two layer model equations used in this study are given in Appendix B. Figure 3.14 shows the different zones during reduction and the typical concentration profiles for reduced nickel, iron and water vapor formed after 15 minutes of reduction at 900 K. The figure shows that completely reduced layer has been formed for nickel denoted by $\varepsilon_{m,1}$, while it is still not complete for iron $(\varepsilon_{m,2})$.

Before the product layer formation $(t < t_c)$, the fraction reacted and the observed reaction rate are obtained as :

$$X = \frac{3k_A C_{Ab} t(\phi \coth \phi - 1)}{C_{Bo} \phi^2 \left\{1 + \frac{1}{N_{Sh}}(\phi \coth \phi - 1)\right\}} \tag{3.25}$$

$$R_{obs} = \frac{4\pi R_p D_e C_{Ab}(\phi \coth \phi - 1)}{1 + \frac{1}{N_{Sh}}(\phi \coth \phi - 1)} \tag{3.26}$$

while after the product layer formation $(t > t_c)$

$$\frac{k_A C_{Ab} t}{C_{Bo}} = 1 + \left(1 - \frac{D_e}{D'_e}\right)\ln\left(\frac{\varepsilon_m \sinh \phi}{\sinh \phi_m}\right) + \frac{D_e}{D'_e}(\phi_m \coth \phi_m - 1) \times$$
$$\left(1 - \varepsilon_m + \frac{\varepsilon_m}{N'_{Sh}}\right) + \frac{D_e \phi^2}{6 D'_e}\left\{(1 - \varepsilon_m)^2(1 + 2\varepsilon_m) + \frac{2}{N'_{Sh}}(1 - \varepsilon_m{}^3)\right\} \tag{3.27}$$

$$X = 1 - \varepsilon^3 + \frac{3\varepsilon_m}{\phi^2}(\phi_m \coth \phi_m - 1) \tag{3.28}$$

$$R_{obs} = \frac{4\pi D_e R_m C_{Ab}(\phi_m \coth \phi_m - 1)}{1 + \frac{D_e}{D'_e}\left(1 - \varepsilon_m + \frac{\varepsilon_m}{N'_{Sh}}\right)(\phi_m \coth \phi_m - 1)} \tag{3.29}$$

H2:H2O

PRODUCT PHASE CONE. --->

NiO:Ni

Fe2O3:Fe

$\varepsilon_{(m)1} = 0.937$

$\varepsilon_{(sc)1} = 0.707$

$C_{A(sc)1} = 0.794$

$C_{A(sc)2} = 0.901$

$\varepsilon_{(sc)2} = 0.879$

$\varepsilon_{(m)2} = 1.000$

H2:H2O

NiO:Ni

Fe2O3:Fe

PRODUCT PHASE CONCENTRATION

NON DIMENSIONAL RADIUS
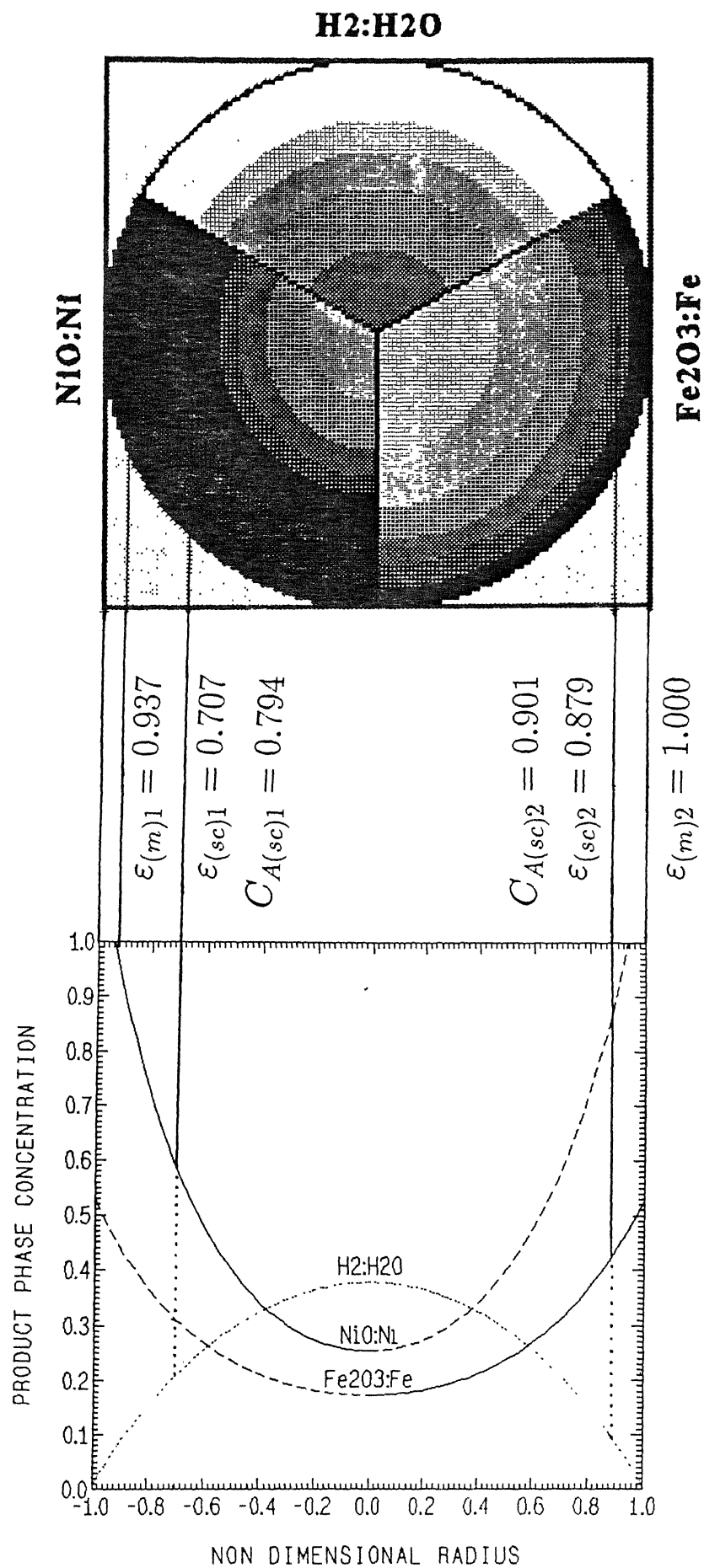
Figure 3.14: Two layer model predictions for Large pellet, reduced at 900 K for 15 minutes.

Where, $\quad \phi_m = \varepsilon_m \phi$ $\hfill$ (3.30)

Calculation of the rate constant requires an interactive solution of eqn.(3.25) before and eqn.(3.27) and (3.28) after the product layer formation time t_c. During this study a Newton-Raphson solver was used to accomplish this.

3.8 . Comparison of results obtained from Grain Model and Two-layer Model

The values of the reaction rate constants calculated from the above mentioned models are shown in figure 3.15-3.16. It is important to point out that the trends predicted by both the models are rather well in accord, and use of either of them is justified under the present situation. Some of the sharp kinks which are observed in the two-layer model predictions (figure 3.15-3.16) are perhaps arising out of the approximate numerical solution of the model equations at the transition time $(t = t_c)$, rather than some actual physical phenomena.

For both the models same rate constant value k, denoted by $k_{/rg}$ for grain model and k_A for two-layer model is used. The intrinsic rate constant at a particular temperature is evaluated by zero radii extrapolation of the rate constant data from the two models for the three different pellet sizes. Zero radii extrapolation is done to eliminate the effect of diffusivity and non-isothermal effect on the rate constant, and this method was successfully utilized in a previous work [41].

The activation energy for nickel oxide reduction is then evaluated by fitting an exponential Arrhenius type equation through the intrinsic rate constant data for the three temperatures as shown in figure 3.17. The activation energy for iron oxide could not be obtained by fitting the three rate constant values for the three temperatures since there was very little increase in its value from temperature 800 K to 900 K, and so the activation energy was assumed to be a step function of temperaturer, one in the range of 800 K to 900 K and another for 900 K to 1000 K as shown in figure 3.17. This anomalous behavior of iron oxide reduction is also reported by various investigators studying its reduction kinetics in this temperature range [23, 24, 25, 58] as shown in figure (2.8) for H_2 and figure (2.9) for CO. The Arrhenius equations for the rate constants evaluated from the experimental study is given in table A.22 in Appendix A. The activation energy of reduction obtained in the present study is well in accordance with similar studies reported in literature, as shown in table (A.18) and (A.19) in Appendix A.
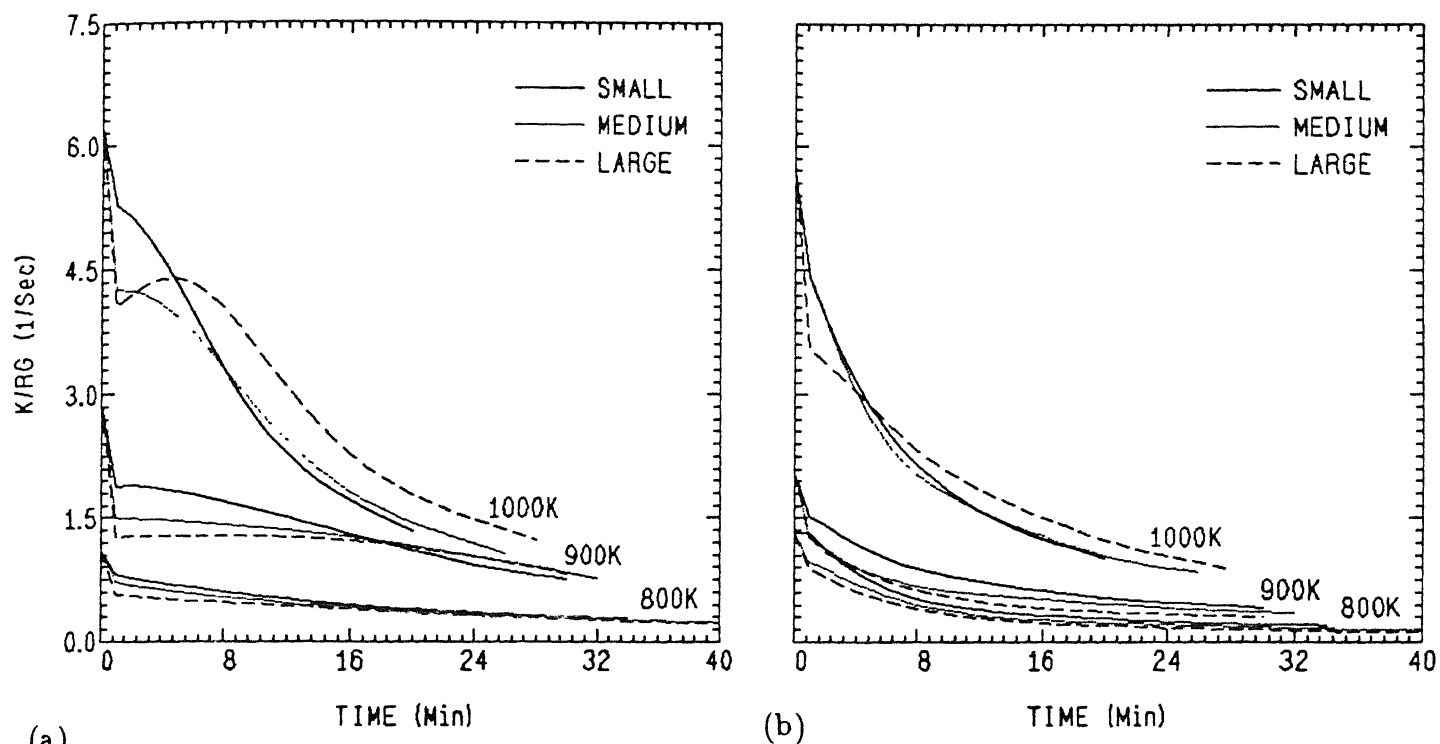
Figure 3.15: Rate constant variation with time for grain model, for the reduction of : (a) Nickel and (b) Iron
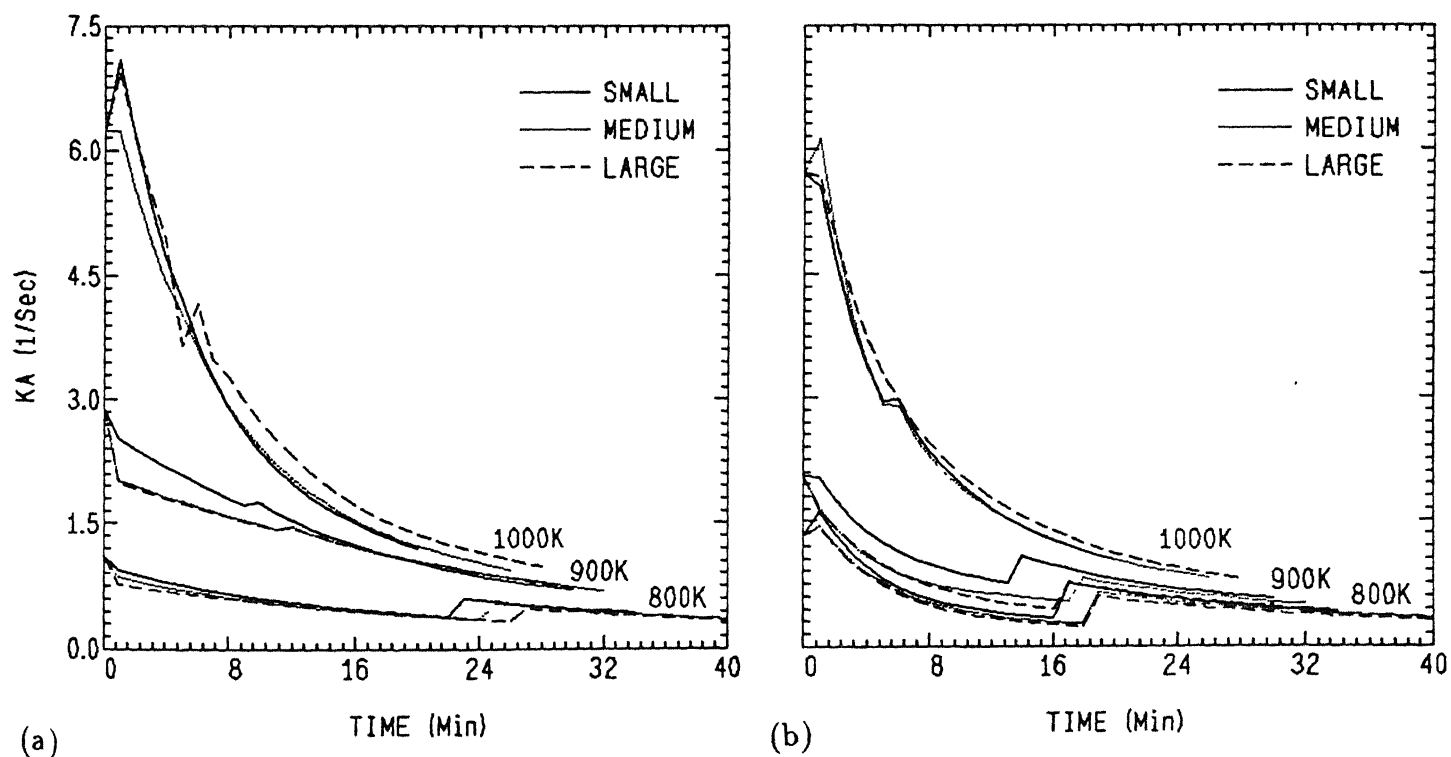
Figure 3.16: Rate constant variation with time for two layer model, for the reduction of : (a) Nickel and (b) Iron

The activation energy of reduction of nickel and iron with carbon monoxide is shown in table A.20 and A.21, and the rate constant equations estimated from the literature data is given in table A.23 of Appendix A. The rate constant value can not be used directly from literature since the grain size and shape of the ore or oxide used may not be same as used here. Therefore the the reported values for reduction with hydrogen is compared with the present experimental results and that ratio is used as the basis for estimating the rate constant for reduction with CO. The reported studies where rate constant values for both CO and H_2 are given is used for this purpose. The Arrhenius plot for the rate constant variation with temperature for reduction with CO thus obtained is shown in figure 3.18.

3.9 Modification of Rate Constant due to Non-isothermal effect and Product Gas formation

As evident from figure 3.15-3.16, both the kinetic models considered here predict progressive lowering of reaction rate constant as a function of time. This trend however, requires some more explanation.

The pellets of finite size are likely to offer a considerable thermal resistance, due to which a temperature gradient may exist between the surface and center of the pellet, and reaction actually may proceed non-isothermally. In order to have an accurate prediction of the reaction rate constant, the corrections due to this non-isothermal behavior need to be accounted for, along with the pertinent corrections due to the formation of water vapor which is also known to affect the reaction rate. Similar temperature corrections were attempted earlier by Bandyopadhyay et al. [41]. During this study we have appropriately modified the formulation of Bandyopadhyay et al. [40, 41], so that the appropriate differential equation becomes :

$$\sum_{i=1}^{i=2} R_i \Delta H_i = \frac{K_T T_s}{R_p^2 \varepsilon^2} \frac{\partial}{\partial \varepsilon} \left(\varepsilon^2 \frac{\partial Z}{\partial \varepsilon} \right) \tag{3.31}$$

$$Where : \left. \begin{array}{rl} \sum_{i=1}^{i=2} R_i \Delta H_i & = C_{Bo} \left\{ n_1 \Delta H_1 \frac{dX_1}{dt} + n_2 \Delta H_2 \frac{dX_2}{dt} \right\} \\ Z & = \frac{T}{T_s} \end{array} \right\} \tag{3.32}$$

the required boundary conditions are :
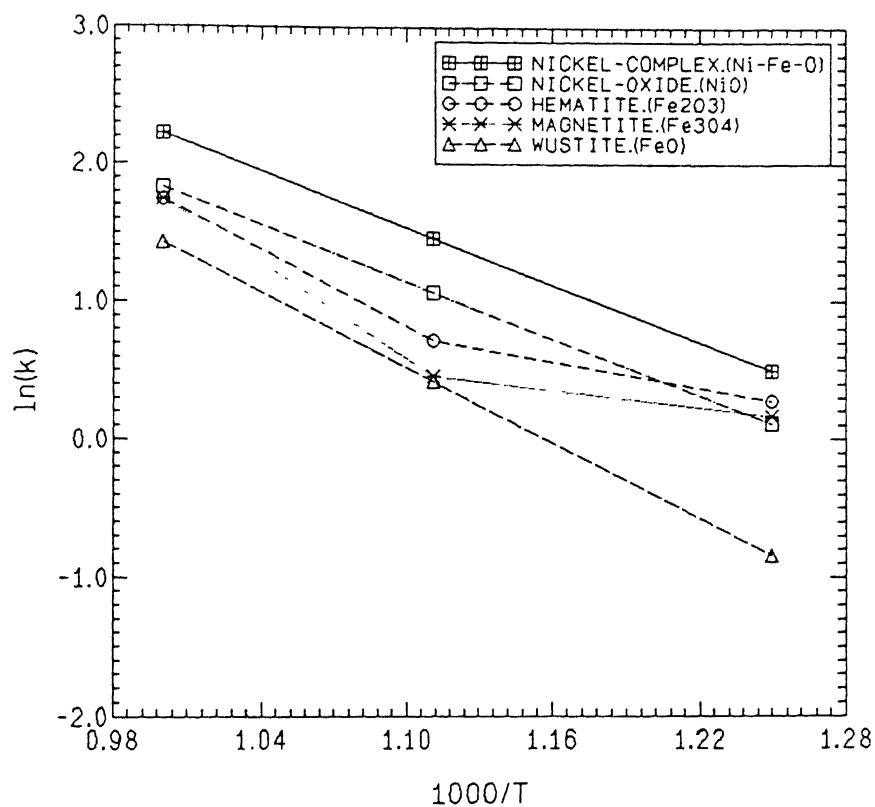
Figure 3.17: Experimentally obtained rate constant variation with temperature for the reduction of nickel and iron with Hydrogen.
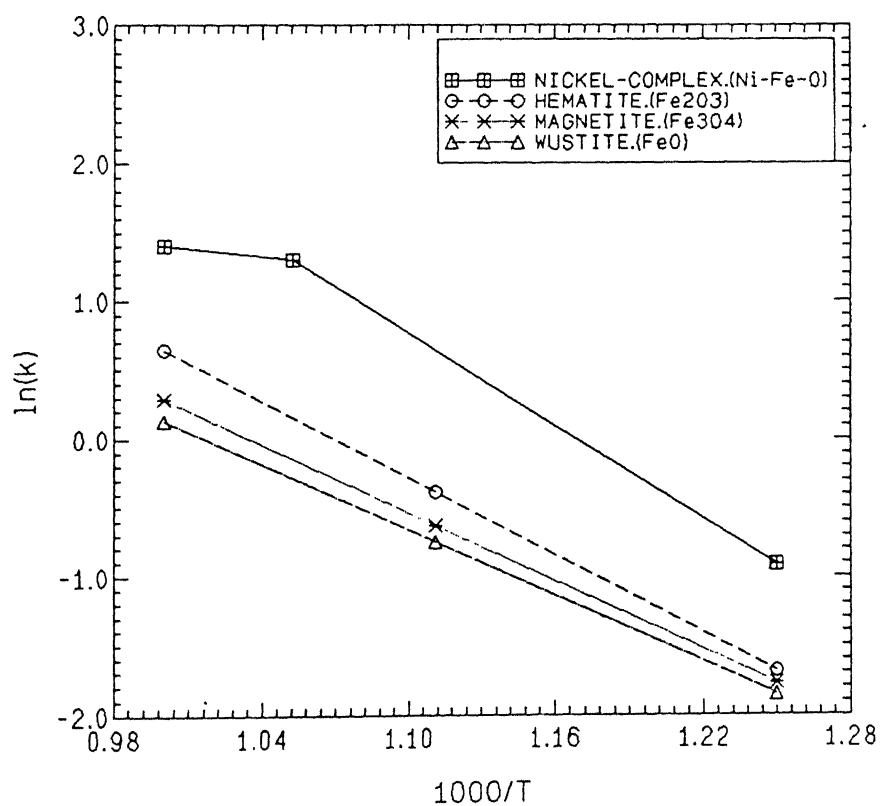
Figure 3.18: Temperature dependence of rate constant for nickel and iron reduction with Carbon monoxide, taken from literature.

$$\left.\begin{array}{lll} At\ the\ center\ \cdot & \varepsilon = 0, \dfrac{\partial Z}{\partial \varepsilon} = 0 \\ At\ the\ outer\ surface. & \varepsilon = 1, Z = 1 \end{array}\right\}$$

and the solution obtained is :

$$Z = 1 - \frac{R \Delta H R_p{}^2}{6 K_T T_s}(1 - \varepsilon^2) \tag{3 33}$$

The reaction interface is assumed to be the shrinking core radius given by :

$$\varepsilon_{sc} = r_{sc}/R_p = (1 - X)^{1/3} \tag{3.34}$$

and the temperature at the reaction interface is obtained by putting $\varepsilon = \varepsilon_{sc}$ in eqn.(3.33). The temperature variation at the reaction interface with time for different conditions are shown in figure 3 19. We can calculate the temperature corrected rate constant value by using the reaction interface temperature in the Arrhenius equation for rate constant as shown below

$$k^o = k^o_{T_s} exp\left(-\frac{Q}{RT_m}\right) \tag{3.35}$$

Furthermore, it is a well documented fact [20, 21, 25, 63, 64] that the rate of reaction slows down due to water vapor formation, and the actual measurements of the rate constant k become progressively lower with time, showing a large deviation from its initial values. Proceeding analogous to some previous studies, [63, 64] this retardation effect of water vapor is incorporated in the following form of rate equation :

$$-\frac{\partial X}{\partial t} = k^o P_{H_2}\left(1 - \frac{\frac{P_{H_2O}}{P_{H_2}}}{K_{eq}}\right) = k^o P_{H_2}\left(1 - \frac{R_h}{K_{eq}}\right) \tag{3.36}$$

where,

$$R_h = \frac{P_{H_2O}}{P_{H_2}} \tag{3 37}$$

From the above eqn.(3.36) we get :
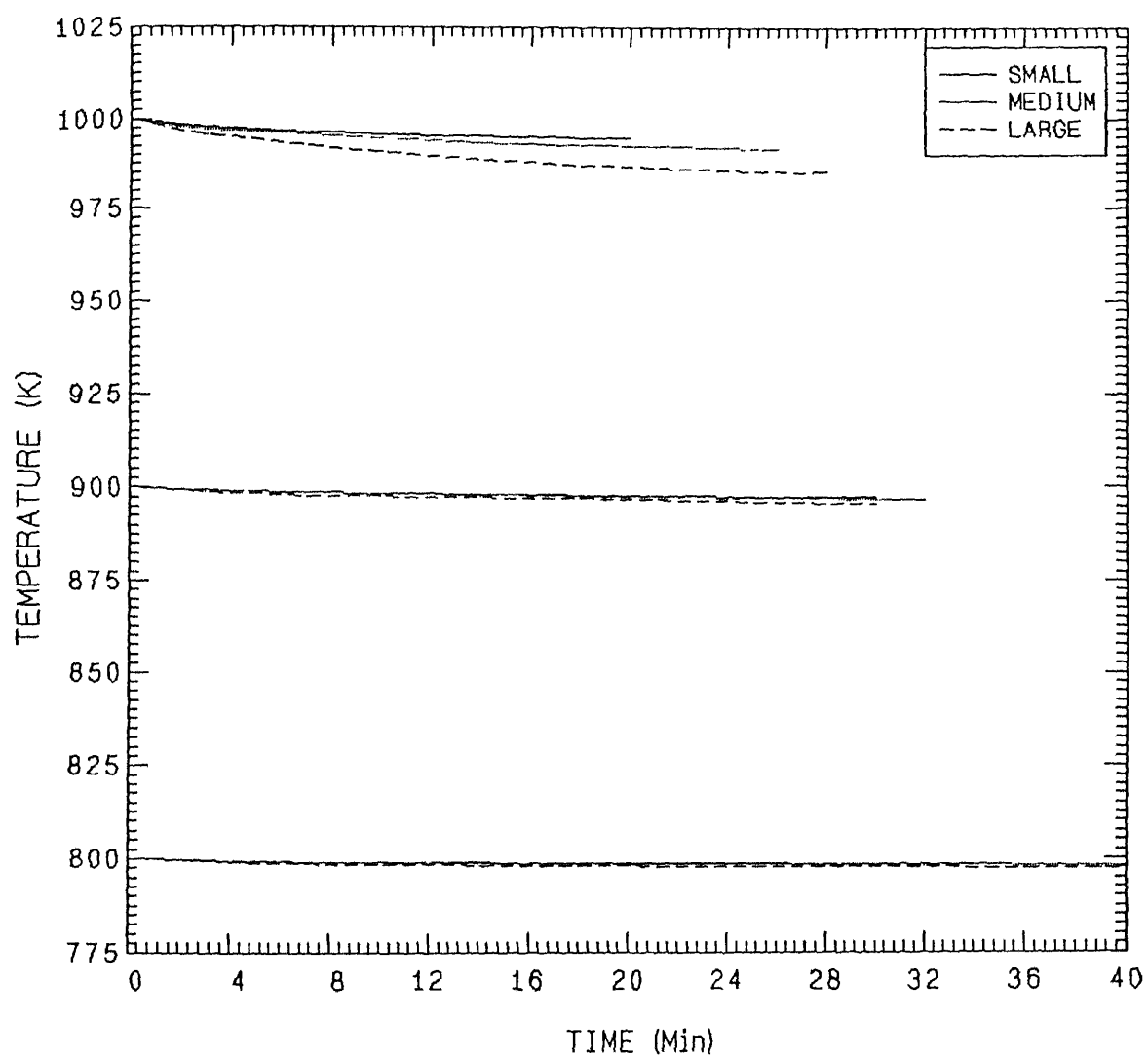
Figure 3.19: Temperature variation with time at the reaction interface.

$$k = k^o \left(1 - \frac{R_h}{K_{eq}}\right) \tag{3.38}$$

Where, Water Vapor Correction Factor for rate constant is $\left(1 - \frac{R_h}{K_{eq}}\right)$

Gas concentration at the reaction interface can be obtained by two-layer model eqn.(3 39) and (3 40), before and after the product layer formation respectively. The above mentioned equations can be obtained by putting $\varepsilon = \varepsilon_{sc,t}$) in eqn (3.47) and (3 51), discussed later in the section for pellet structure prediction

Gas concentration at the reaction interface before the product layer formation $(t \leq t_c)$:

$$(C_A)_{sc,t} = \frac{C_{Ab} \sinh(\phi \varepsilon_{sc,t})}{\varepsilon_{sc,t} \sinh \phi \left\{1 + \frac{1}{N_{sh}}(\phi \coth \phi - 1)\right\}} \tag{3 39}$$

Gas concentration at the reaction interface after the product layer formation $(t \geq t_c)$:

$$(C_A)_{sc,t} = \frac{C_{Am} \varepsilon_m \sinh(\phi \varepsilon_{sc,t})}{\varepsilon_{sc,t} \sinh \phi_m} \tag{3.40}$$

Where C_{Am} is given by eqn (3 49).

The gas concentration inside the pellet is determined on basis of overall reaction rate; which can be approximated by the reaction rate constant of iron, since it is the major constituent of the reactive solid phase. However the reaction interface $(\varepsilon = \varepsilon_{sc,t})$ is taken separately for iron and nickel oxides, i.e. all parameters in eqn.(3.39) and (3.40) are for iron oxide except ε_{sc} In general higher water vapor concentration is predicted for nickel; since it has higher reduction rate and correspondingly lower radii value of reaction interface, which gave higher water vapor concentration at the reaction interface. The assumed reaction interface position and the corresponding gas composition is schematically shown in figure 3.14.

Using two equations on the basis of t_c often becomes inconvenient, under such conditions the gas concentration at the reaction interface can be approximated by substituting ε_m by ε_{sc} in eqn (3 49) for the gas concentration at the interface between product layer and partially reduced core; which gives :

$$C_{sc} = \frac{C_{Ab}}{1 + \frac{D_e}{D_e'}(\phi_{sc} \coth \phi_{sc} - 1)\left(1 - \varepsilon_{sc} + \frac{\varepsilon_{sc}}{N_{sh}}\right)} \tag{3.41}$$

This equation is used to predict the gas concentration at the reaction interface (by taking $\frac{D_e}{D_e^l} = 1$), for calculating the rate constant value $(k_{/rg})$ in the fixed bed and moving bed reactor models. Although eqn (3 41) is obtained from two layer model eqn (3 49) it can be easily used with grain model equations since the rate constant value and its variation is very similar in both the cases (as shown by figure 3 15 and 3 16).

Alternatively water vapor concentration at the reaction interface can also be predicted from grain model equations. Substituting k (equivalent to $k_{/rg}$) from eqn.(3 38) to eqn (3 22) we get :

$$(k_{/rg})_\imath = (k_{/rg}^{\,o})_\imath \left(1 - \frac{(R_h)_\imath}{(K_{eq})_\imath}\right) = \frac{g_{Fg}(X)_\imath}{\frac{C_{Ab}t}{C_{Bo}} - \frac{R_p^2}{6D_e}\left(P_{Fp}(X)_\imath + \frac{2X_\imath}{N_{Sh}}\right)} \qquad (3.42)$$

$$(R_h)_\imath = (K_{eq})_\imath \left[1 - \frac{g_{Fg}(X)_\imath}{(k_{/rg}^{\,o})_\imath \left\{\frac{C_{Ab}t}{C_{Bo}} - \frac{R_p^2}{6D_e}\left(P_{Fp}(X)_\imath + 2\frac{X_\imath}{N_{Sh}}\right)\right\}}\right] \qquad (3.43)$$

It should be clarified here that the water vapor concentration obtained from eqn.(3 43) is dependent on the accuracy of the K_{eq} value used. Equation (3.43) is used separately for iron oxide and nickel oxide reduction, and they should give comparable results although they may not give exactly same value since the reaction interface for the two oxides are not same. In the present study, nickel oxide reduction data predicted higher H_2O concentration as expected; since it has higher reduction rate and correspondingly lower radii value for the reaction interface.

The effect of water vapor on iron oxide reduction is taken directly from the thermodynamic equilibrium constants for iron oxide reduction. The variation of equilibrium constant value with iron oxide reduction is shown in figure 3.12. For hematite reduction the thermodynamic equilibrium constant value is too high and so a reasonably high value of '10' is taken for numerical stability.

The thermodynamic equilibrium constant (K_{eq}) for nickel oxide reduction is very high for any significant effect of water vapor on its reduction rate, but in actual situation it is found to effect its reduction rate significantly as reported in literature [20, 21] In the present investigation the effect of water vapor on nickel oxide reduction reported by Pluschkell et al. [21] is used. The parameters used for predicting the water vapor concentration are given in table atpg in Appendix A, and the predicted concentration at the reaction interface is shown in figure 3 20. In general eqn.(3 43) and eqn.(3 39 & 3.40) gave reasonably good match as shown in figure 3 20(b).
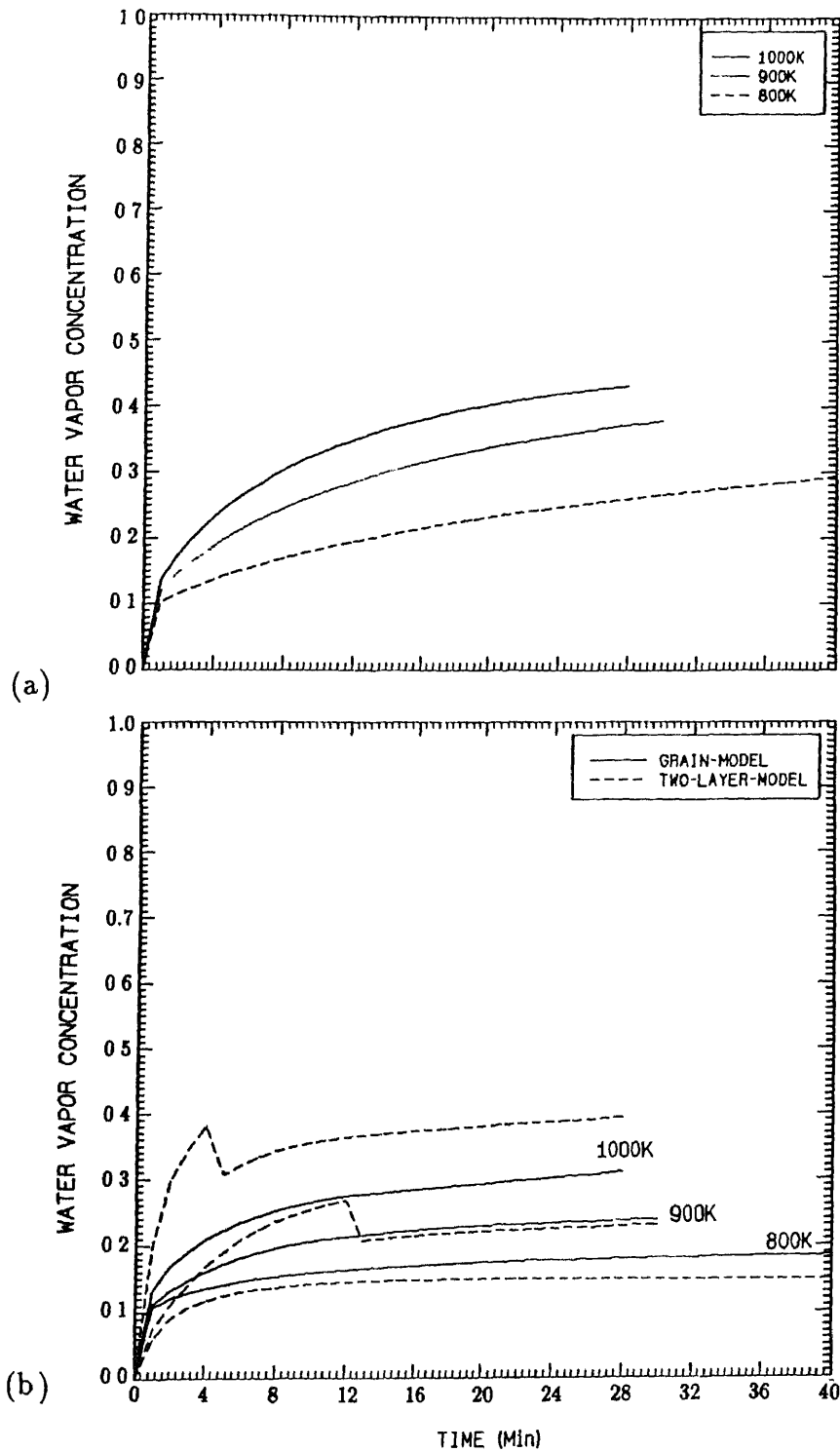
Figure 3.20: Water vapor concentration variation with time at the reaction interface.
(a) For nickel reduction in large pellets at 800 K, 900 K and 1000 K by grain model.
(b) For iron reduction in large pellets at 800 K, 900 K, and 1000 K by grain model and two-layer model.

The temperature and water vapor corrections were added to the initial k value, and the results are shown in figure 3.21. The curve now closely resembles the ones shown in figure 3.15-3.16, giving a strong indication that the reaction slows down with time, predominantly because of these two factors.

3.10 Complex Oxide Mechanism for Nickel Reduction in Nickeliferrous Ore

The property of a complex mineral like nickeliferrous ore can vary significantly from physical mixtures of pure oxides of nickel and iron It is known that nickel and iron is present as solid solution, forming complex oxides or minerals like goethite and serpentine Since the Indian nickel ore contains negligible amount of serpentine, we can concentrate on the possible mechanism of reduction of goethite Nickel is present as a lattice substitute for iron in the goethite phase, and the steps for the formation of metallic iron or nickel from goethite can be summarized below

$$(Fe_{1-x}Ni_x)OOH \xrightarrow{\Delta} (Fe_{1-x}Ni_x)_2O_3 \xrightarrow{[H]} (Fe_{1-x}Ni_x)_3O_4 \xrightarrow{[H]} \begin{matrix} FeO \\ NiO \end{matrix} \xrightarrow{[H]} \begin{matrix} Fe \\ Ni \end{matrix} \qquad (3.44)$$
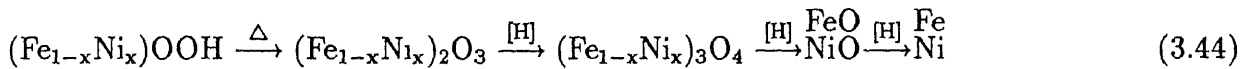
From the above eqn.(3.44) we can infer that the ore becomes reducible after the first step, but selective reduction of nickel is not possible in the second and third steps, since it is locked in the predominantly iron containing complex oxides which reduces in a similar fashion as hematite (Fe_2O_3) and magnetite (Fe_3O_4). Only after the third step i.e. after the formation of wüstite (Fe_xO) and NiO, they can get reduced separately giving rise to selective reduction.

Initially we have considered nickel and iron oxides as separate entity without any interaction or condition imposed due to this locked structure. But the packed bed experimental results showed considerable deviation from the predicted values, which can be explained by this complex oxide reduction mechanism. Therefore modification for this complex oxide mechanism is incorporated in the grain model. It is considered that the amount of NiO free to get reduced increases linearly from 0 to 100 % as the reduction of iron proceeds from 0 to 33 % i.e. when wüstite formation is complete. This can be implemented as follows · If X_{Fe} is below 33 % then

$$\left(\frac{dX_{Ni}}{dt}\right)_A = \left(\frac{dX_{Ni}}{dt}\right)_C \times \frac{X_{Fe}}{0.33} \qquad (3.45)$$

else
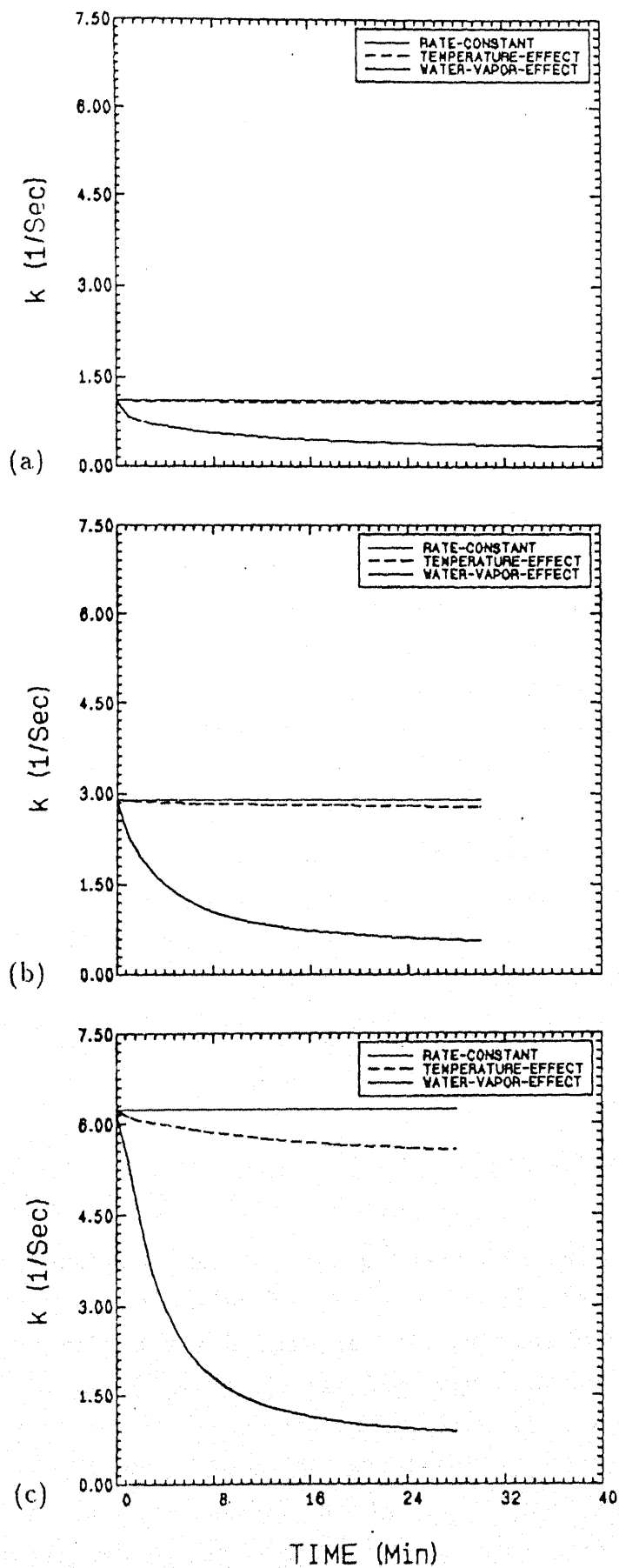
Figure 3.21: Predicted rate constant variation due to non-isothermal effect and, water vapor effect on nickel reduction in large pellets at : (a) 800 K (b) 900 K (c) 1000 K.

$$\left(\frac{dX_{Ni}}{dt}\right)_A = \left(\frac{dX_{Ni}}{dt}\right)_C \times 1\ 0 \tag{3.46}$$

(Where, the subscripts stands for . A - Actual reduction rate ; C - Calculated reduction rate considering free NiO)

This essentially means that the reduction rate of nickel is initially slower due to the locked condition and afterwards getting freed from the locked structure, its reduction rate increases rapidly to reach the experimental points as shown schematically in figure 3.22. By using a fitted curve through the experimental points we got the reaction rate constant A, but if we consider the complex oxide mechanism, it will have slower rate B1 initially and faster rate B2 afterwards, before and after the complete formation of free NiO Therefore the effective rate constant of nickel can be both higher and lower than the experimentally obtained rate constant A according to the presence of NiO in partially locked or free condition as shown by the range t1 and t2 in the figure 3.22 This implies that the actual reduction rate constant of free NiO shown by B2, is higher than the experimentally obtained rate constant A. For getting the exact value of B2 some guess values have to be taken initially and computed to match the single pellet experimental results. If the guess value gives good matching with all the experimental results we can consider it to be the actual rate constant B2 for the free NiO In the present case the rate constant value B2 for free NiO is found to be 1 5 times the experimentally obtained rate constant value A The initial rate of reduction shown by B1 is taken care of by the eqn (3.45). The iron oxide reduction rate is unaffected by this complex oxide mechanism since the complex oxide behaves like iron reduction, and also due to the fact that very small amount of nickel is present in the complex oxide

3.11 Estimation of Pellet Reduction Rate

The procedure for estimating the reduction rate considering the effects of non-isothermal reduction and product gas formation can be discussed now. Initially the fraction reduced 'X' at any temperature can be predicted by calculating the rate constants from Arrhenius equation and then directly using the model equations : eqn.(3 20) for grain model or eqn.(3 29) for two-layer model, since initially there is no effect of non-isothermal reaction or product gas formation. The value of 'X' thus obtained can then be used to compute the temperature by using eqn.(3 33), and product gas concentration at the reaction interface by using eqn.(3.43) or eqn.(3.39 and 3.40). Similarly correction factors for all the subsequent steps can be computed from the 'X' values
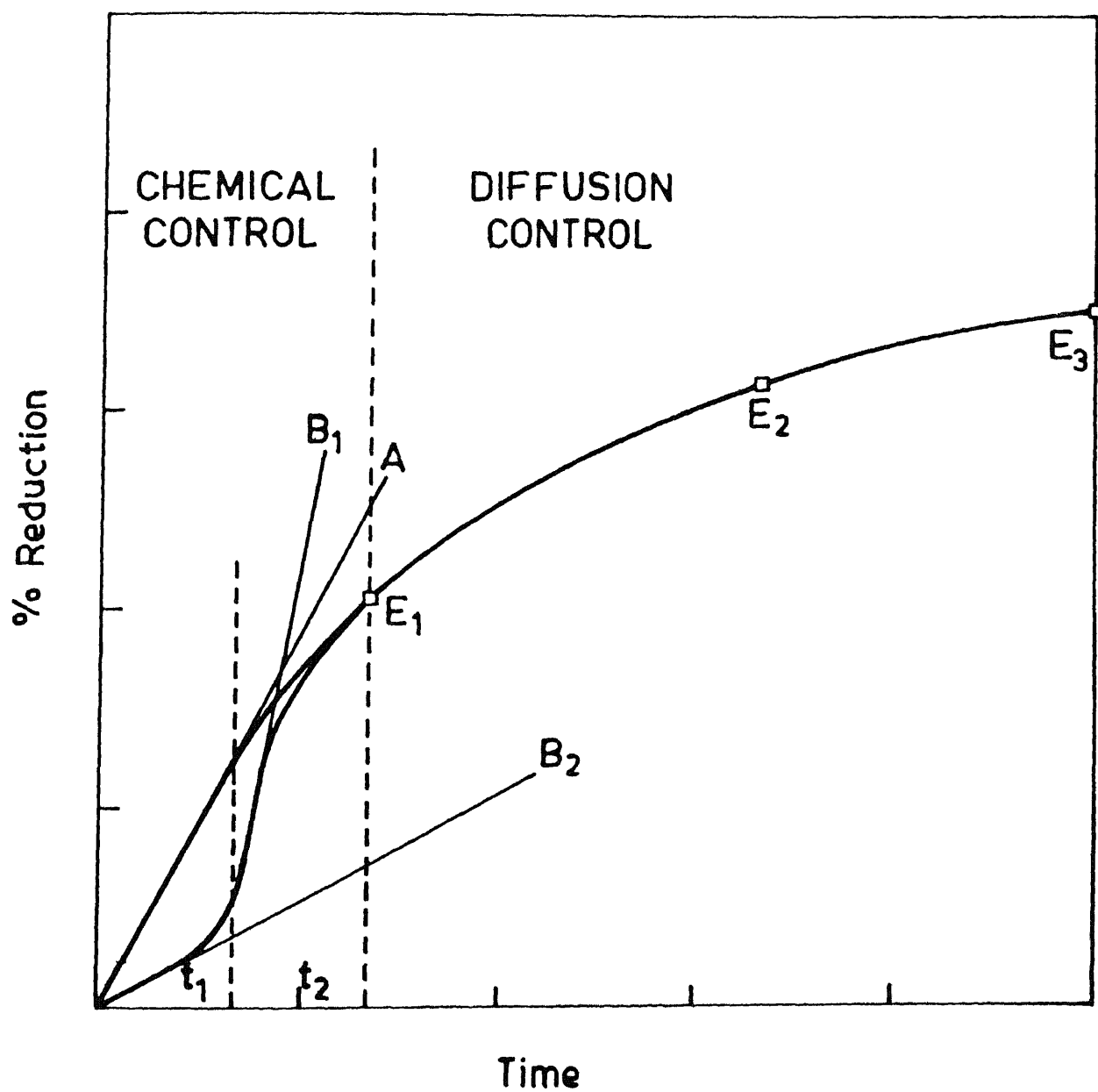
Figure 3.22: Schematic diagram for nickel reduction by complex oxide mechanism.

of the previous time step. The flow chart for the computer code used for the estimating the reduction rate of the pellets is shown in figure C.1 in Appendix C. The matching between the experimental pellet reduction data and the predictions done by the grain model, modified grain model for complex oxide mechanism of nickel reduction, and two-layer model are shown in figure 3 23, 3 24 and 3 25

Finally it should be mentioned that both the models used here have some positive features and limitations, and so an effort is made here to compare the two. The grain model is more often employed as it is relatively simpler and easy to use. It is also more versatile and can be used for all the three general pellet shapes and grain shapes. The two-layer model is on the other hand very rigorously solved using very few simplifying assumptions, trying to follow the exact phenomena of pellet reduction By doing so it became specific and applicable only for spherical pellets with constant area of gas solid reaction which implies $F_g = 1$ for grain model, which is the value used in the present calculations However apart from these limitations it has some unique features, like it can predict the concentration profile of both the solid and the gaseous phases inside the pellet and thereby predict the reduced pellet structure as described in the next section.

3.12   Prediction of Reduced Pellet Structure

As mentioned before the reduction of pellets can proceed by two competing kinetics; either by chemical control kinetics when the diffusion is much faster than chemical reaction rate or by diffusion control kinetics when chemical reaction rate is much faster than the diffusion rate. Chemical control kinetics mostly occurs at lower temperatures, and under this condition the gas can easily diffuse inside the pellet, and reduction proceeds homogeneously throughout the pellet. At relatively higher temperatures chemical reaction rate increases exponentially with temperature following Arrhenius rate equation, where as diffusion increases at much lower rate and thus becomes relatively slower, and so the overall reaction becomes diffusion controlled. Under this condition the reaction proceeds topochemically producing shrinking core type of structure

Since the two types of competing reaction kinetics produce completely different kinds of structures, it may be interesting to know what happens under real conditions when both the kinetic rates are comparable. This will also be helpful for optimizing temperature for selective reduction,
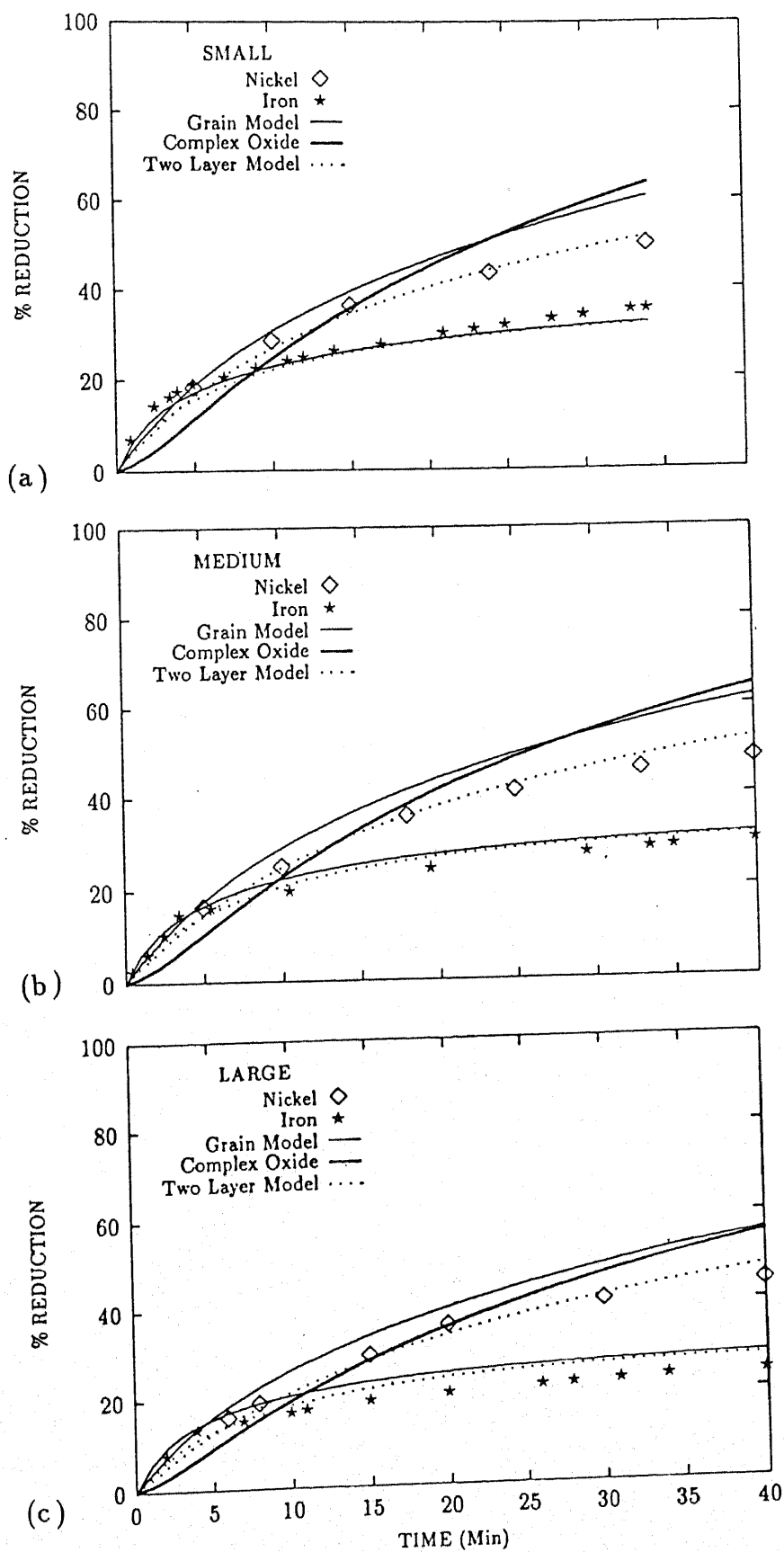
Figure 3.23: Comparison between the experimental data and the predicted results by grain model, two-layer model and complex oxide model at 800 K for : (a) Small (b) Medium and (c) Large pellets.
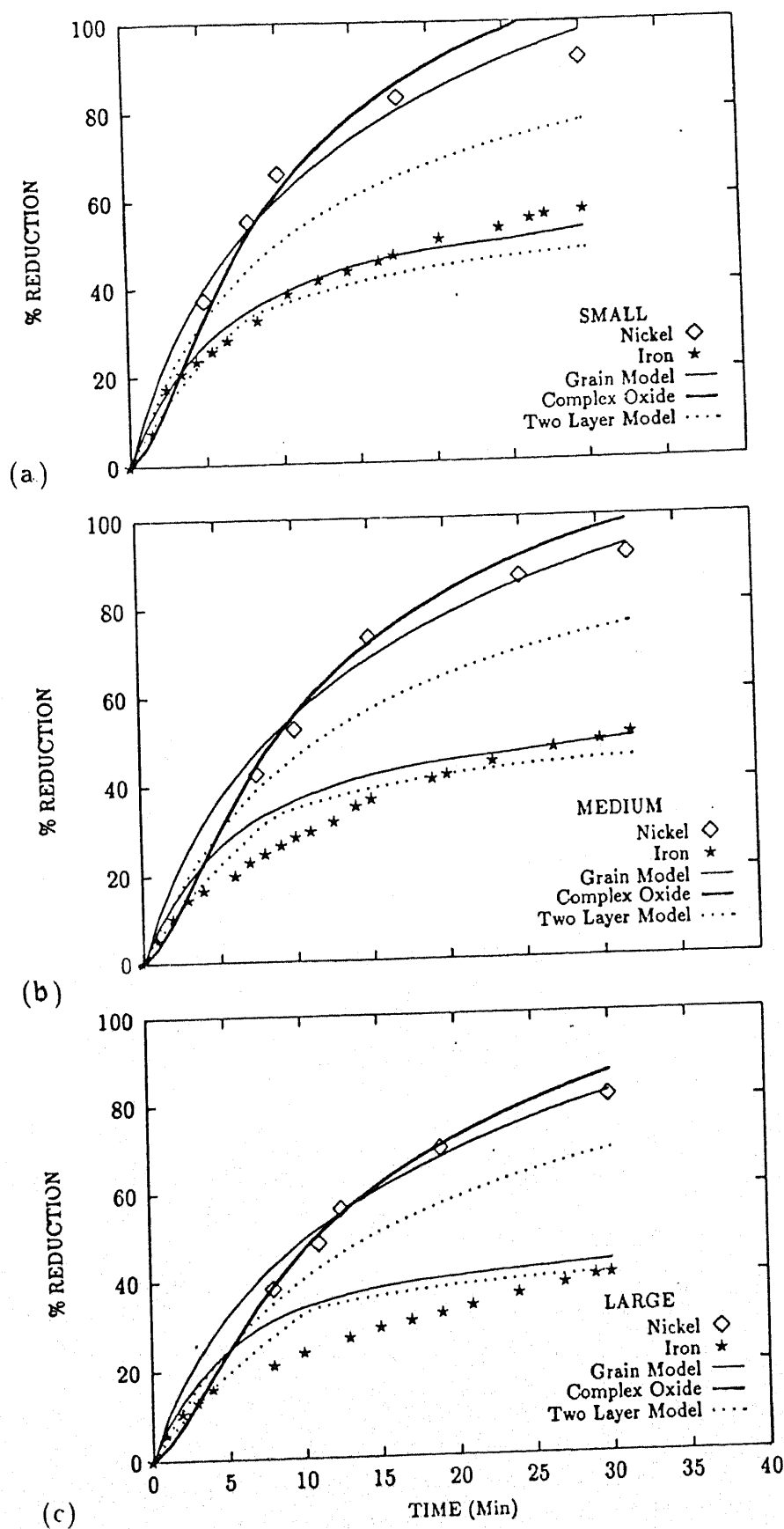
Figure 3.24: Comparison between the experimental data and the predicted results by grain model, two-layer model and complex oxide model at 900 K for : (a) Small (b) Medium and (c) Large pellets.
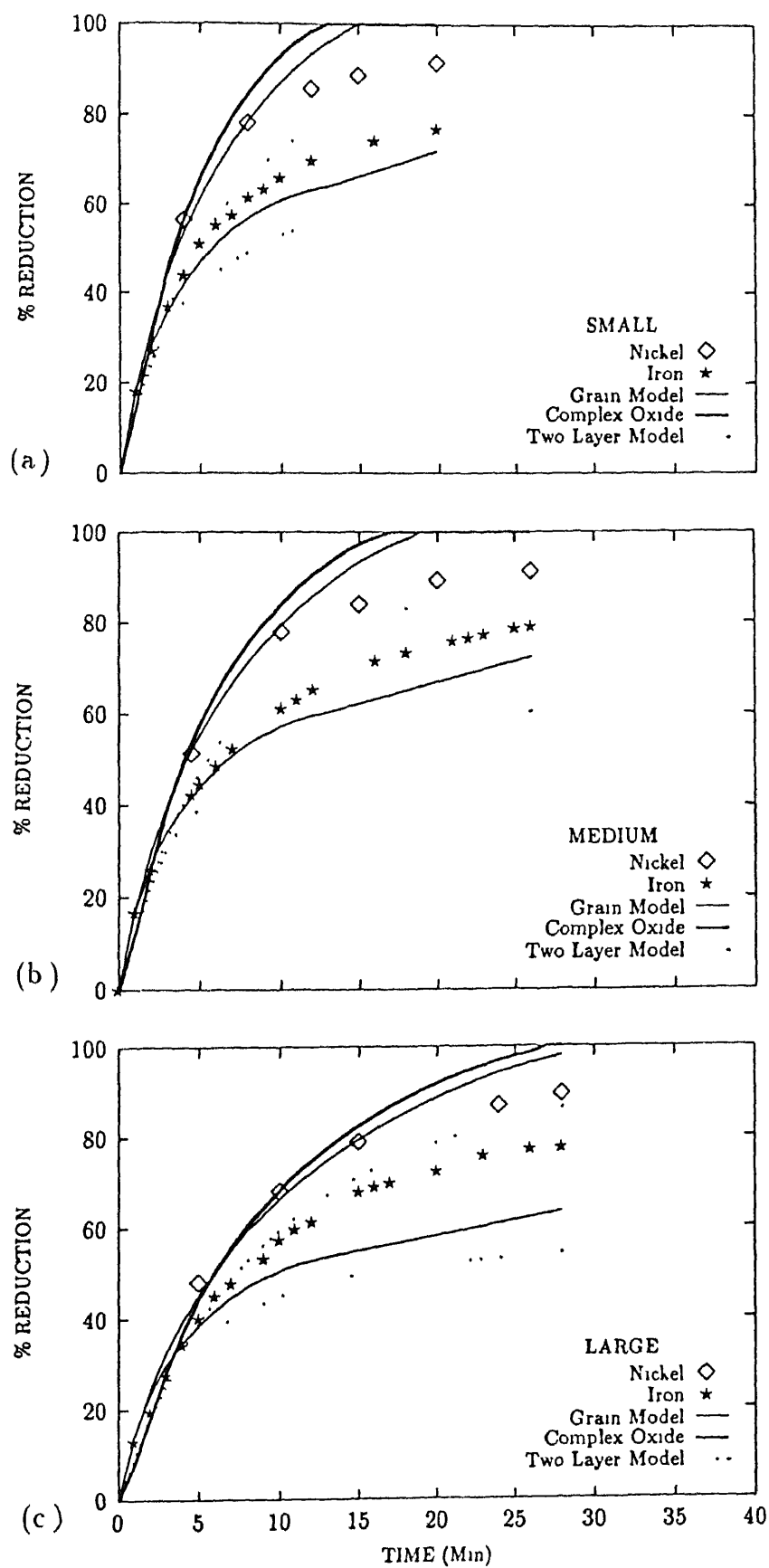
Figure 3.25: Comparison between the experimental data and the predicted results by grain model, two-layer model and complex oxide model at 1000 K for · (a) Small (b) Medium and (c) Laige pellets

since chemical control kinetics at lower temperature should give better selective reduction, but for faster reduction higher temperature is needed Also the effect of pellet size can be visualized, although qualitatively it is known that larger pellet size leads to diffusion control kinetics but too small pellet size can lead to fluidization and permeability problems under industrial conditions Previously reduced pellet structure were studied experimentally for iron oxides [65, 23, 64] and also for pure nickel oxide [17, 58]; but for the present case since the main interest lies in the nickel oxide reduction which constitutes only 1.22 % of the ore, an experimental study of the pellet structure could not be undertaken

For predicting the concentration profile of the two reducible oxides and the gaseous phase we have used the intermediate equations needed for deriving the two-layer model [37, 38, 39]

For $t \leq t_c$:

Gas concentration profile inside a pellet is given by :

$$C_A = \frac{C_{Ab} \sinh(\phi \varepsilon)}{\varepsilon \sinh \phi \left\{ 1 + \frac{1}{N_{sh}} (\phi \coth \phi - 1) \right\}}$$

(3 47)

Solid concentration profile :

$$C_B = C_{Bo} - \int_0^t \frac{k_A C_{Ab} \sinh(\phi \varepsilon) dt}{\varepsilon \sinh \phi \left\{ 1 + \frac{1}{N_{sh}} (\phi \coth \phi - 1) \right\}}$$

(3.48)

For $t \geq t_c$:

Gas concentration at the interface between product layer and partially reduced core $(\varepsilon = \varepsilon_m)$:

$$C_{Am} = \frac{C_{Ab}}{1 + \frac{D_e}{D'_e} (\phi_m \coth \phi_m - 1) \left(1 - \varepsilon_m + \frac{\varepsilon_m}{N_{sh}} \right)}$$

(3.49)

Gas concentration profile in the product layer $(\varepsilon_m \leq \varepsilon \leq 1)$:

$$C_A = \frac{C_{Am} \varepsilon_m \left(1 - \varepsilon + \frac{\varepsilon}{N'_{sh}} \right) + C_{Ab} (\varepsilon - \varepsilon_m)}{\varepsilon \left(1 - \varepsilon_m + \frac{\varepsilon_m}{N'_{sh}} \right)}$$

(3 50)

Gas concentration profile in the partially reduced core ($\varepsilon_m \geq \varepsilon \geq 0$) :

$$C_A = \frac{C_{Am}\varepsilon_m \sinh(\phi\varepsilon)}{\varepsilon \sinh \phi_m} \qquad (3.51)$$

Solid concentration profile in the partially reduced core ($\varepsilon_m \geq \varepsilon \geq 0$) :

$$C_B = C_{Bo}\left[1 - \frac{\sinh(\phi\varepsilon)}{\varepsilon \sinh \phi}\right] + \int_{t_c}^{t} \frac{k_A C_{Ab}\varepsilon_m \sinh(\phi\varepsilon)dt}{\sinh \phi_m \left[1 + \frac{D_e}{D_e'}(\phi_m \coth \phi_m - 1)\left(1 - \varepsilon_m + \frac{\varepsilon_m}{N_{sh}'}\right)\right]} \qquad (3.52)$$

The predicted concentration profile is then integrated over the whole pellet volume to get the average concentration of solid and gas phases :

$$X = \frac{3\int_0^{R_p} r^2(C_B/C_{Bo})dr}{R_p^3} \qquad (3.53)$$

The concentration profiles of the product phase produced during reduction, like water vapor, nickel and iron fraction reduced, are then plotted by using mono-dithering in Star-base graphics The effect of time, temperature and pellet size on the reduced pellet structure is studied here as shown in figure 3.26, 3 27 and 3.28 respectively, the details of which are given below.

figure 3 26 shows the effect of time on pellet reduction Initially the reduction rate is very similar for both the oxides but with progress in time much higher amount of nickel oxide reduction is observed compared to iron oxide. Water vapor concentration is quite high at the initial stage since the reduction rate is much faster initially stages, it is lower at the 15 minute stage and slightly higher at 25 minute stage since the reaction has progressed deeper inside the pellet at the later stage making diffusing out of water vapor more difficult

The effect of temperature on reduction is shown in figure 3.27. The figure shows the reduction is nearly homogeneous at 800 K but close to shrinking core structure at 1000 K. The reduction rate of iron oxide and nickel oxide are comparable at 800 K and it is marginally higher for nickel oxide at 1000 K but at 900 K the reduction rate of nickel oxide is significantly higher than that of iron oxide, giving rise to good selective reduction characteristics According to theory chemical control kinetics at lower temperature should give better selective reduction but in the present study intermediate temperature of 900 K produced best selective reduction This may be due to the complex oxide structure of the ore, and for the anomalous behavior of iron oxide reduction

around this temperature range The water vapor concentration inside the pellet increases with increase in temperature of reduction

The effect of pellet size variation is shown in figure 3 28. Reduction rate of nickel oxide is much faster for smaller pellets and it also showed better selective reducibility. The water vapor concentration inside the pellet is higher for larger pellets since it has to diffuse through a larger distance.

The predicted concentration profile is then integrated over the pellet volume according to eqn (3 53) to obtain the overall fraction reduced 'X' and it is then compared with the experimental results and the computed results from grain model and two-layer model as shown in table 3.3.

Table 3 3 Matching of Integrated data over the pellet volume with the experimental data and computed data by grain model and two-layer model.

Condition	Integrated Value (%)	Experimental Value (%)	Grain Model prediction (%)	Two-layer Model Prediction (%)
Large,15min,800 K				
Nickel	28.17	29 81	33 52	28.17
Iron	17 01	18.66	23 32	21.78
Large,15min,900 K				
Nickel	64.70	60.95	60.23	56 71
Iron	32.09	28.52	38.16	36 26
Large,15min,1000 K				
Nickel	72.19	78.12	79.36	71 15
Iron	61.67	67.25	54.89	49.58
Large,5min,900 K				
Nickel	28.44	25.73	32.40	25 10
Iron	16.79	17 74	24.61	19.53
Large,25min,900 K				
Nickel	76.79	77.80	75.73	63.86
Iron	45.73	37.12	41 86	39.57
Small,15min,900 K				
Nickel	72 23	78.38	73 65	60.72
Iron	33 29	44.43	44 74	40.89
Medium,15min,900 K				
Nickel	71.01	70.36	68 17	56.92
Iron	31.90	36.24	42 04	38.97

The matching of the results are reasonably close and the predicted structures are well in accordance with the expected structures from theoretical considerations and experimental study [17, 23]

3.13 Concluding Remarks

The present study establishes that methodology adopted earlier for analyzing the pure nickel oxide and iron ore reduction can be easily extended for the low grade laterite ores, like the one that is discovered in Sukinda, India. Formation of water vapor as a reaction product, in addition to the non-isothermal nature of the reaction needs to be considered for an accurate description of the reaction mechanism The results of this study will serve as the necessary background for the subsequent study of reduction in packed bed reactors and Multiple hearth furnace
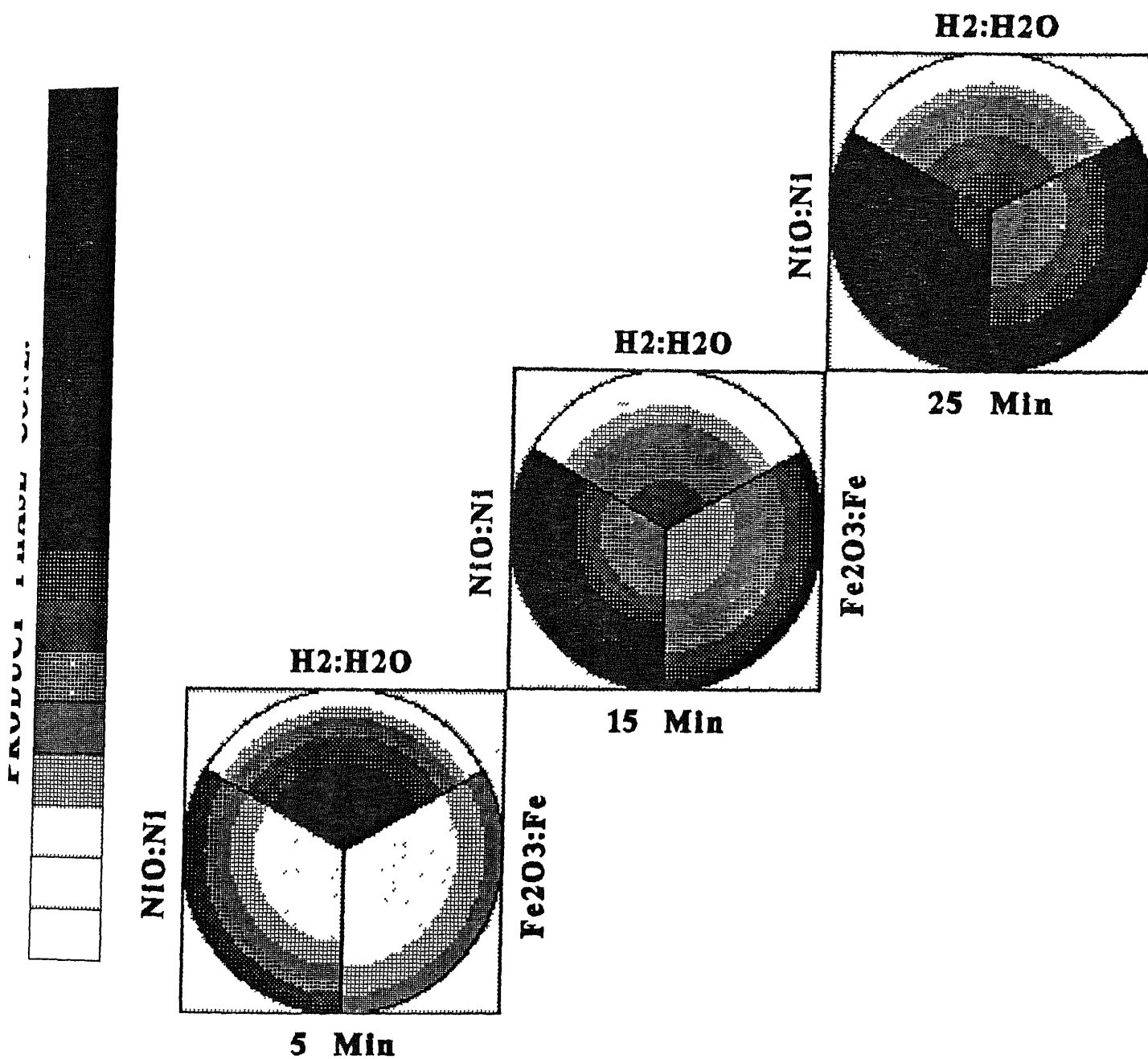
Figure 3.26: Reduced pellet structure of large pellets after 5, 15 and 25 minutes of reduction at 900 K.
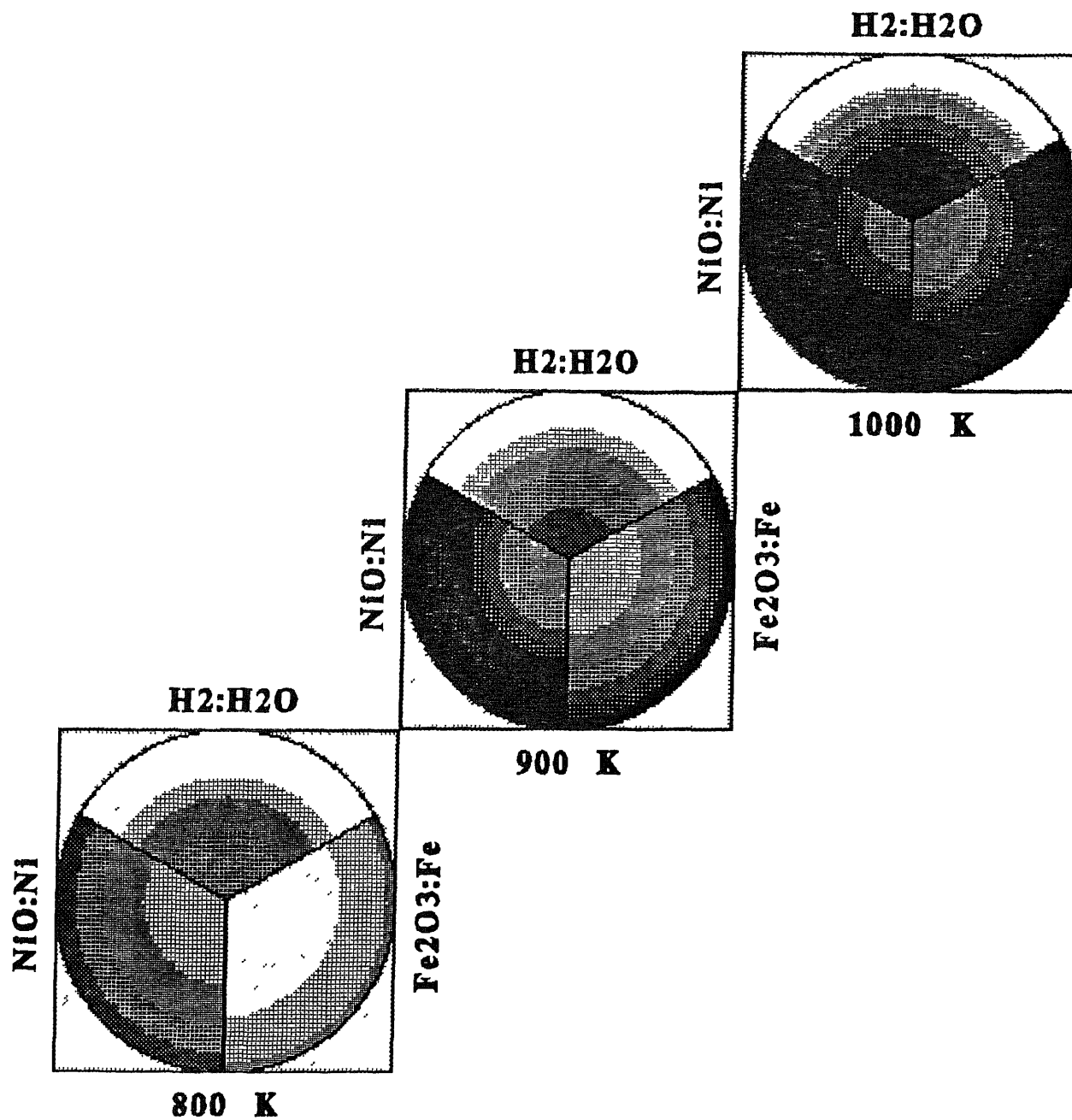
Figure 3 27. Reduced pellet structure of large pellets after 15 minutes of reduction at 800 K, 900 K and 1000 K
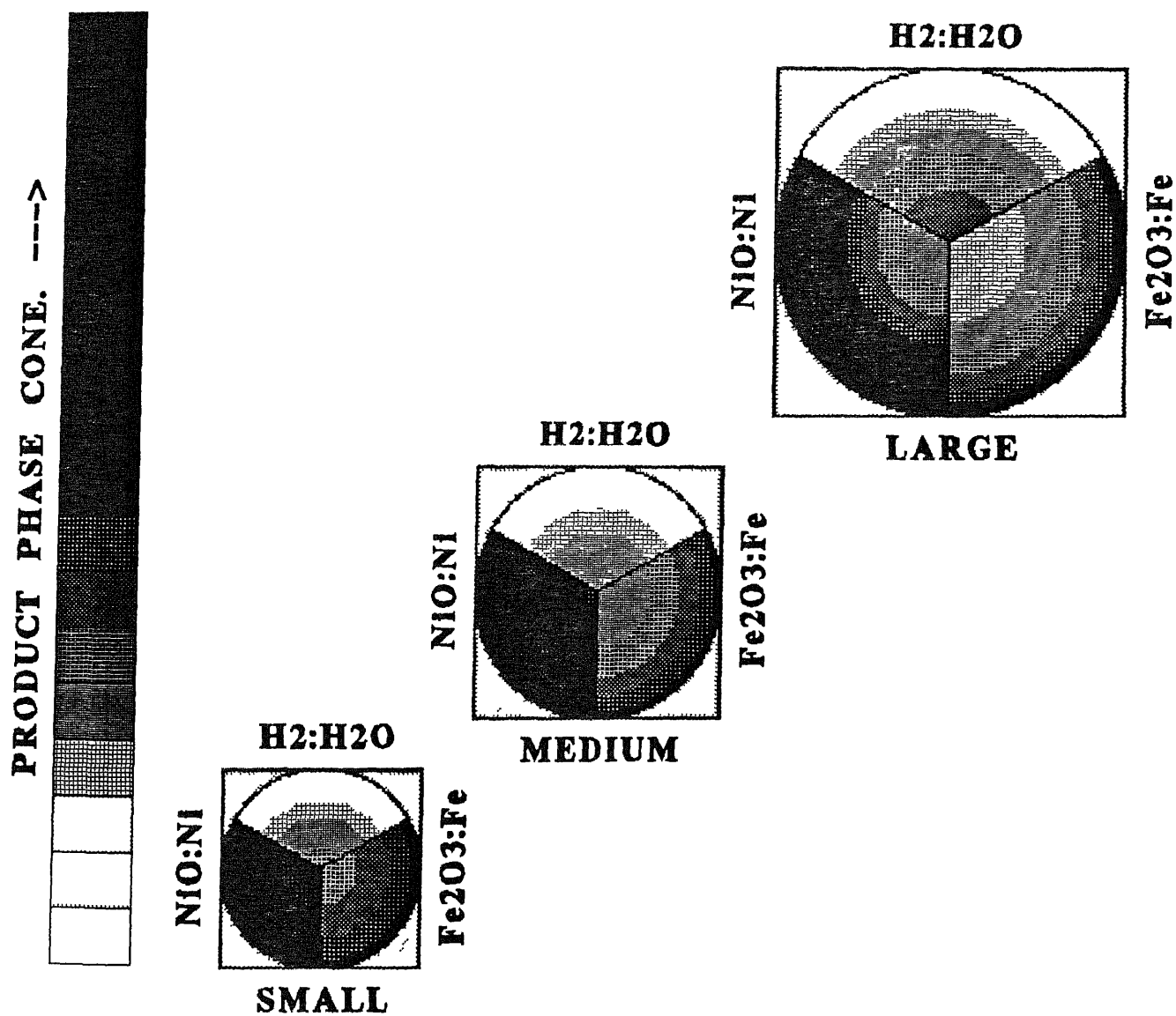
Figure 3.28· Reduced pellet structure of small, medium and large pellets after 15 minutes of reduction at 900 K

Chapter 4

MATHEMATICAL MODELING AND FORMULATION

Pyrometallurgical process operations are carried out industrially in large scale furnaces where various phenomena like gas flow, heat and mass transfer, and gas solid reactions take place simultaneously which are interdependent on each other. For economic operation, optimization of the process parameters are essential. Experimental evaluation of these process parameters for large scale furnaces often becomes too expensive and time consuming. Therefore the effect of various parameters are studied in small scale experimental setups, which are then matched with numerically simulated results. The model thus developed can be easily scaled up to predict the performance of large scale industrial furnaces

The development of mathematical model involves, describing the various phenomena occurring in the process by mathematical equations. The equations involved may be algebraic or differential equations. The type of equations involved and their solution procedure followed in this study is briefly discussed in this Chapter.

4.1   The Role of Mathematical Models

Mathematical models are representation of the process in the form of mathematical equations, which can provide quantitative results for any given condition. This will help in proper designing and optimization of the process parameters, and also for process control during its operation.

Developing a mathematical model needs proper understanding of all the phenomena involved

in the process Therefore, if all the phenomena are not properly described or taken into account, the simulated results may vary widely from the experimental results under certain conditions This indicates that the understanding of the process is not proper or complete for that particular situation and it needs to be investigated more rigorously. Simultaneous experimental and mathematical simulation thus help in proper understanding and evaluation of the various phenomena and mechanisms involved in the process It is important to stress that calculations and measurements are not alternatives, but most often pursued in a complementary fashion. As Szekely [66] pointed out,' mathematical modeling, experimental results, and actual plant scale measurements may all be ingredients of a successful program. Indeed, in many instances several iterations may be required between mathematical modeling and physical measurements before the desired level of understanding finally emerges'.

4.1.1   Development of Mathematical Models

The important steps for the development of mathematical models are schematically shown in figure 4 1 [66]. The first and the most important step is to form a mental picture of the process and identify the key parameters affecting the system. The process phenomena are then expressed in a mathematical form

As shown in the figure 4 1, the next two parallel steps are numerical solution and experimental work Numerical solution is often necessary because purely analytical results will not provide adequate detail, or may not be possible for complicated systems Experimental work will be needed, both for testing the theoretical predictions and also for estimating parameter values like reaction rate constant, thermal conductivity, diffusivity etc., if they are not available in literature.

It can be concluded here that once the problem has been identified, investigation should start with simplified conditions, and then use this as a framework for planning more complicated experimental and computational programs to be pursued in an interactive manner.

4.1.2   The Building Blocks of Mathematical Models

In an industrial process operation various phenomena like fluid flow, reaction between various phases, heat and mass transfer etc goes on simultaneously. To model them, generally a main program is written which initializes the conditions and calls various subroutines written specifically for a particular phenomenon. For example, the reaction kinetics at a particular point of the
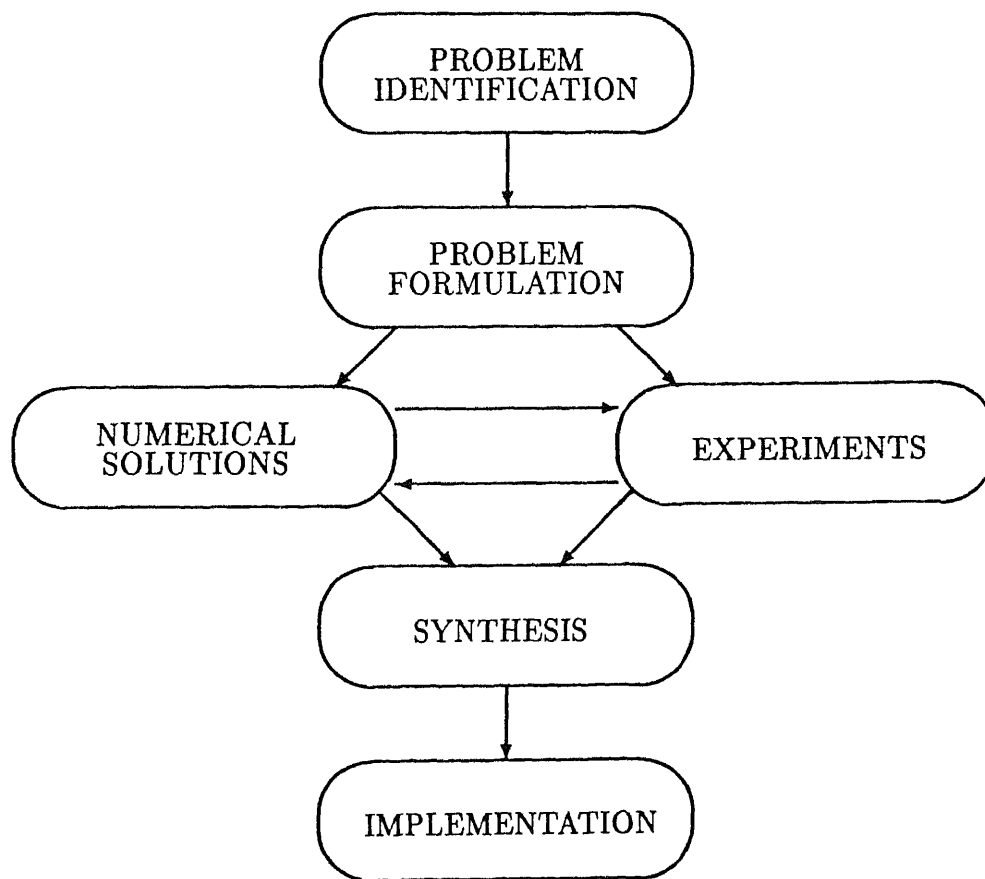
Figure 4.1· The general methodology of mathematical model development [66].

computational domain is calculated on the basis of informations obtained from other subroutines like composition of gas, temperature of gas and solid etc from other subroutines. The other subroutines then takes this information about the reaction rate to recalculate the gas composition, temperature etc in the next time step and this cycle goes on to compute the process dynamics forward in time.

4.2 Modeling Equations

The equations used for modeling the different process phenomena are taken mostly in their differential form The equations for gas velocity profile involves higher order nonlinear equations, which have to be solved iteratively. A number of such equations occur in the heat and mass transfer studies of gas-solid reaction The transport equations for gas and solid thermal energy balance, and gas phase mass balance are second order partial differential equations The solid phase mass balance is usually coupled with the reaction kinetics.

Partial differential equations in Cartesian and cylindrical axi-symmetric coordinate system were considered in the present study. In order to simplify the differential equations and boundary conditions, we made several assumptions as indicated below :

1. The viscous dissipation terms are neglected for computing the gas phase thermal energy balance since it is significant only under very high velocity gradients or turbulent conditions.

2. No radiation effects within the gas phase The effect of radiation is incorporated by considering the gas-solid heat transfer coefficient as a function of temperature.

3. Thermal gradients within the individual particles are neglected This amounts to Newtonian heating or cooling conditions This assumption is valid for all practical purpose for packed bed conditions when the particle Biot number is less than 0 25 [56], for the present systems its value ranged from 0 11 to 0.36 for the fixed bed reactor studies and from 0.16 to 0.30 for the moving bed reactor study. For most of the cases, the Biot number is within the limit of 0 25, and only for the conditions of high temperature and gas velocity it has exceeded the limit; which is neglected for simplifying the calculations

4. The conductivity of both solid and gaseous phase in the packed bed region is taken equal to the overall conductivity of the bed, since the solid phase is not continuous in the packed bed

region and thermal conduction will be partially through the solid particles and partially through the intermediate gaseous phase

5 Diffusivity of the gaseous phase is taken proportional to the void fraction in the packed bed region ($D_b = (1 - \epsilon)D_M$)

4.2.1   Vectorial Ergun's Equation

Pyrometallurgical processing of solid natural resources is frequently performed in the packed beds through which a gas is flown to promote the convective heat and mass transfer, and also to enhance the rate of chemical processes involved   Therefore, flow structures in the packed bed strongly affect the performance of the processes

Extensive investigations have been conducted to obtain the momentum transfer equations characterizing the flow dynamics in packed bed medium. Nevertheless, it is virtually intractable to solve the Navier-Stokes equation for the fluid flow in interparticle regions   A preliminary, yet alternative approach to this problem was devoted to developing the *hydraulic* or *pipe-flow* equations for the one-dimensional flow of fluids through granular beds   Employing this type of approach, Kozeny-Carman equation for laminar flow and Bruke- Plummer equation for turbulent flow were successfully derived making allowance for the mean hydraulic radius of the flow capillaries and for the effect of voidage [59]   Ergun [67] comprehensively correlated these two equations by simply adding the turbulent and the laminar resistance terms to yield an expression of the form ·

$$\frac{\triangle P}{L} = \frac{150\mu V(1 - \epsilon)^2}{d_p\epsilon^3} + \frac{1.75\rho_g V^2(1 - \epsilon)}{d_p\epsilon^3} \tag{4.1}$$

Where v is the superficial velocity and ρ_g is the density of the gas or fluid at the arithmetic average of the end pressures. This additive characteristic of the viscous and kinetic pressure loss terms has been confirmed theoretically from Navier-Stokes equation by Irmay [68]

The particle size d_p in the Ergun's equation is defined in terms of the specific surface area of a unit volume of solid particles S_v as :
$$d_p = \frac{6}{S_v}$$
That is to say, d_p denotes the diameter of equivalent spheres having the same specific surface area as the non-spherical packing employed. For dispersed beds with a wide range of particle

size, it is necessary to calculate a representative mean diameter From the specific surface area we can thus calculate the average or mean diameter :

$$d_p = \frac{1}{\sum_{i=1}^{k} \frac{n_i}{d_{pi}}} \qquad (4.2)$$

where n_i stands for the fractional volume of the i-th classified size segment.

Yoon and Kim have confirmed that the Ergun equation for the fixed bed system is also well applicable to the moving bed system, provided a slip velocity of the fluid relative to the descending solid particles is used instead of the superficial fluid velocity The variation of voidage with gas velocity, or with the descending velocity of the solid particles also have to be taken into consideration [69]

The non-uniform flows associated with the voidage and particle size variations in beds can be accomplished by using the equations of continuity as well as the Ergun equation in their vectorial forms. When gas evolution is relatively negligible, the set of governing equations are as follows :

$$\nabla.V = 0 \qquad (4.3)$$

$$-\nabla P = (f_1 + f_2 \mid \overline{V} \mid)V \qquad (4.4)$$

$$f_1 = \frac{150\mu(1-\epsilon)^2}{(\phi_s d_p)^2 \epsilon^3} \qquad (4.5)$$

$$f_2 = \frac{1.75\rho_g(1-\epsilon)}{(\phi_s d_p)\epsilon^3} \qquad (4.6)$$

Where $\mid \overline{V} \mid = \sqrt{V_r^2 + V_z^2}$ is the gas velocity and f_1 and f_2 stand for the Ergun's coefficient of viscous resistance and turbulent resistance respectively.

This set of equations have been applied in packed bed systems by, Radestock and Jeschar [70], Staneck and Szekely [71], and Szekely and Poveromo [50], resulting in a great amount of information on the behavior of non-uniform flows through layered and other configurations

We now proceed to describe the solution procedure of eqns (4.3) and 4.4 for the fluid flow through two-dimensional or axi-symmetrical beds having spatially variable resistances. The equation of continuity given by eqn.(4.3) can be satisfied by working in terms of the stream function ψ which is defined as .

$$V_r = \frac{1}{r^m}\left(\frac{\partial \psi}{\partial z}\right) \tag{4.7}$$

$$V_z = -\frac{1}{r^m}\left(\frac{\partial \psi}{\partial r}\right) \tag{4 8}$$

Where $m = 0$ for two-dimensional flow and $m = 1$ for axi-symmetrical flow Thus if the terms involving velocity are replaced by the stream function, and the pressure gets eliminated, there will be no need to solve any explicit expression for the continuity condition

The directional components of the Ergun eqn (4 4), can be written as :

$$-\frac{\partial P}{\partial r} = (f_1 + f_2 \mid \overline{V} \mid)V_r \tag{4.9}$$

$$-\frac{\partial P}{\partial z} = (f_1 + f_2 \mid \overline{V} \mid)V_z \tag{4 10}$$

Gas pressure P can be entirely removed from eqns (4.9) and (4.10) by using .

$$\frac{\partial^2 P}{\partial r \partial z} = \frac{\partial^2 P}{\partial z \partial r} \tag{4.11}$$

The resultant equation in terms of stream function is as follows :

$$\left\{\frac{\partial f_1}{\partial r}\frac{\partial \psi}{\partial r} + \frac{\partial f_1}{\partial z}\frac{\partial \psi}{\partial z} + f_1\left(\frac{\partial^2 \psi}{\partial r^2} + \frac{\partial^2 \psi}{\partial z^2} - \frac{m}{r}\frac{\partial \psi}{\partial r}\right)\right\}\sqrt{\left(\frac{\partial \psi}{\partial r}\right)^2 + \left(\frac{\partial \psi}{\partial z}\right)^2}$$
$$+\frac{1}{r^m}\left\{\frac{\partial f_2}{\partial r}\frac{\partial \psi}{\partial r} + \frac{\partial f_2}{\partial z}\frac{\partial \psi}{\partial z} + f_2\left(\frac{\partial^2 \psi}{\partial r^2} + \frac{\partial^2 \psi}{\partial z^2} - \frac{m}{r}\frac{\partial \psi}{\partial r}\right)\right\}\left\{\left(\frac{\partial \psi}{\partial r}\right)^2 + \left(\frac{\partial \psi}{\partial z}\right)^2\right\} +$$
$$+\frac{f_2}{r^m}\left\{\left(\frac{\partial \psi}{\partial r}\right)^2\left(\frac{\partial^2 \psi}{\partial r^2} - \frac{m}{r}\frac{\partial \psi}{\partial r}\right) + \left(\frac{\partial \psi}{\partial z}\right)^2\left(\frac{\partial^2 \psi}{\partial z^2} - \frac{m}{r}\frac{\partial \psi}{\partial r}\right) + 2\left(\frac{\partial \psi}{\partial r}\frac{\partial \psi}{\partial z}\right)\frac{\partial^2 \psi}{\partial r \partial z}\right\} = 0 \tag{4.12}$$

Equation 4.12 in a finite difference form, together with the appropriate boundary conditions, gives the value of ψ at any point in the field, provided that the spatially distributed flow resistance is known Once the solution for ψ has been obtained, velocity can be evaluated by eqns (4 7) and (4 8) Muchi et al. [69] have defined all the terms with respect to molar velocity of gas $(G = \rho_g V)$ instead of gas velocity V, to take into account the incompressible nature of the flow such that the resistance terms f_1 and f_2 becomes :

$$f_1 = \frac{150\mu(1-\epsilon)^2}{\rho_g(\phi_s d_p)^2 \epsilon^3} \tag{4.13}$$

$$f_2 = \frac{1\ 75(1-\epsilon)}{\rho_g(\phi_s d_p)\epsilon^3} \tag{4.14}$$

In all other equations V being replaced by G. They have also mentioned a simpler method for computing the pressure variation inside the bed by combining the divergence of eqn.(4.4) with eqn (4 3), to get :

$$\triangle P = \frac{\partial^2 P}{\partial z^2} + \frac{1}{r^m}\frac{\partial}{\partial r}\left(r^m\frac{\partial P}{\partial r}\right) = -G_r\frac{\partial W}{\partial r} - G_z\frac{\partial W}{\partial z} \tag{4 15}$$

Where, $W = f_1 + f_2 \mid \overline{G} \mid$

This formulation was however not used in the present analysis

The resistance terms f_1 *and* f_2 depend on the pellet or particle size and void fraction ϵ variation in the bed. Void fraction variation in cylindrical packed bed of spheres have been studied by Benenati and Brosilow [49]. The solution technique for Ergun's equation under simplified condition of turbulent flow region is described by Szekely and Poveromo [50] The application and solution techniques for Ergun equation will be discussed in more details in Chapter 3.

4.2.2   Gas Flow Field by Stream Function and Vorticity method

Stream function - vorticity method is one of the most popular methods for solving two-dimensional or axi-symmetric incompressible Navier Stokes equations. The governing equation of motion for two-dimensional Cartesian coordinate system for Newtonian fluids are as follows :

$$\text{x} - \text{Momentum equation :}\quad V_x\frac{\partial V_x}{\partial x} + V_y\frac{\partial V_x}{\partial y} = -\frac{P^o}{\rho_g V^o}\frac{\partial P}{\partial x} + \frac{1}{R_e}\nabla^2 V_x \tag{4.16}$$

$$\text{y} - \text{Momentum equation .}\quad V_x\frac{\partial V_y}{\partial x} + V_y\frac{\partial V_y}{\partial y} = -\frac{P^o}{\rho_g V^o}\frac{\partial P}{\partial y} + \frac{1}{R_e}\nabla^2 V_y \tag{4 17}$$

$$\text{Continuity equation}\quad \frac{\partial V_x}{\partial x} + \frac{\partial V_y}{\partial y} = 0 \tag{4.18}$$

The eqns (4.16 and 4 17) are difficult to deal with due to the lack of separate equation for pressure P To overcome this difficulty stream function (ψ) and vorticity (ω) is introduced as follows

$$\left.\begin{array}{l} V_x = \dfrac{\partial \psi}{\partial y} \\[2mm] V_y = -\dfrac{\partial \psi}{\partial x} \end{array}\right\} \tag{4 19}$$

$$\omega = \frac{\partial V_x}{\partial y} - \frac{\partial V_y}{\partial x} \tag{4.20}$$

It may be mentioned here that vorticity is a vector quantity having three components and is defined as [72, 73] :

$$\omega = \nabla \times \vec{V}$$

For the present situation, since the variation of velocity is neglected along the z-direction for Cartesian and θ-direction for the axisymmetric case; only one component of vorticity becomes significant, and consequently, vorticity can be solved like a pseudo scalar.

We can readily see that existence of eqn (4 19) automatically satisfy continuity equation (4 18) If we substitute the dependent variable with stream function, we shall not be concerned with eqn (4 18) any more. Invoking eqn.(4 19) into (4.20) we obtain the equation for coupling between stream function and vorticity.

$$\omega = \frac{\partial^2 \psi}{\partial x^2} + \frac{\partial^2 \psi}{\partial y^2} \tag{4.21}$$

Now if we differentiate eqn.(4.16) with respect to y and eqn.(4.17) with respect to x and subtract the differentiated eqn (4.17) from the differentiated eqn.(4 16) and rearrange the resulting equation, we shall obtain.

$$\frac{\partial \psi}{\partial y}\frac{\partial \omega}{\partial x} - \frac{\partial \psi}{\partial x}\frac{\partial \omega}{\partial y} = \frac{1}{R_e}\left(\frac{\partial^2 \omega}{\partial x^2} + \frac{\partial^2 \omega}{\partial y^2}\right) \tag{4 22}$$

This is referred to as vorticity transport equation.

Thus we have now a system of simultaneous equations (4.21, 4 22 and 4 19) to be solved for ψ, ω, V_x and V_y. Application of this method and its solution procedure will be discussed in more details in the relevant Chapters

4.3 Numerical Methods

The numerical techniques followed here for solving the partial differential equations describing the process phenomena are discussed in this section. The important aspects which must be taken into account are as follows :

1. Efficient and less time consuming computational technique

2. Accuracy of the computed results

3. Stability criteria of the solution procedure adopted

These aspects are briefly discussed in the following sections.

4.3.1 Finite Difference Method

The two-dimensional differential equations considered here for the process modeling are solved by finite difference technique. The governing equations and the boundary conditions are converted into algebraic form by discretizing them using a Taylor series expansion As per standard procedure, a three point central differencing strategy is used for the second order diffusive terms in the governing differential equations and a two point forward or backward differencing method (depending upon the direction of velocity) is adopted for the convective terms Further details of such discretization procedure is provided by Gupta [51] The system of simultaneous algebraic equations thus obtained were solved by using the line-by-line method, similar procedure was followed earlier and described by Gupta et al [51]. In this method the properties in the nodal points are solved along a particular line, keeping the other unknowns unchanged from the previous iteration values. This results in a pseudo-one-dimensional formulation along the grid line under consideration, which can be solved efficiently by a tridiagonal matrix algorithm [74]. By this method sweeping is done sequentially in a particular direction first from one end of the computational domain to the other; then the sweeping is done in the alternate direction. This method is used because the convergence criteria and the speed of computation is much superior than the pentadiagonal matrix solvers, which is needed when nodal points of both the directions are considered as unknowns.

The solution procedure can be described by considering a two-dimensional transport equation,

having a time dependent term, and convective and diffusive terms in the space directions, and a source term .

$$\frac{\partial \varphi}{\partial t} + V_x \frac{\partial \varphi}{\partial x} + V_y \frac{\partial \varphi}{\partial y} = \alpha \left(\frac{\partial^2 \varphi}{\partial x^2} + \frac{\partial^2 \varphi}{\partial y^2} \right) + R \tag{4 23}$$

Where, V_x and V_y is the x and y direction velocity, α is the coefficient of diffusivity and φ is any property which can be transported and diffused like gas velocity, gas composition and temperature. The second order diffusion terms are discretized by using three point central differencing method The convective terms are discretized by first order upwinding method and for time dimension Crank Nicholson method scheme is employed; which is discussed later in more details

By discretizing the eqn (4 23) and rearranging the terms for i-direction (or x-direction) sweep we will get three unknown terms for the nodal points $i - 1$, i and $i + 1$, which can be written in the form of a tridiagonal matrix as shown below

$$\begin{bmatrix} b(1,j) & c(i,j) & \cdot\cdot & & \cdot & \cdot \\ a(2,j) & b(2,j) & c(2,j) & \cdot\cdot & & \cdot \\ \cdot\cdot & \cdot\cdot & \cdot\cdot & \cdot\cdot\cdot & & \cdot \\ \cdot & a(i,j) & b(i,j) & c(i,j) & & \vdots \\ \vdots & \cdot\cdot & \cdot & \cdot\cdot & & \vdots \\ \vdots & & \cdot\cdot\cdot & \cdot\cdot\cdot & a(n,j) & b(n,j) \end{bmatrix} \begin{bmatrix} \varphi(1,j) \\ \varphi(2,j) \\ \\ \varphi(i,j) \\ \vdots \\ \varphi(n,j) \end{bmatrix}^{k+1} = \begin{bmatrix} d(1,j) \\ d(2,j) \\ \vdots \\ d(i,j) \\ \\ d(n,j) \end{bmatrix}^k \tag{4.24}$$

Where n denotes the total number of nodal points in i–direction. For the first and last nodal points there is no i-1 and i+1 points as they are outside the computational domain, and so appropriate boundary conditions have to be selected which will define those points in terms known values or in terms of nodal points inside the computational domain The system of equations having three unknown terms forming the subdiagonal, diagonal and superdiagonal terms of the matrix is known as tridiagonal matrix, which can be solved very efficiently by using standard tridiagonal matrix solvers [74].

4.3.2 Crank Nicholson Technique

Initial value problem or transient partial differential equations can be discretized with respect to time by explicit method or by implicit method Considering only the viscous term we get the parabolic diffusion equation :

$$\frac{\partial \varphi}{\partial t} = \alpha \frac{\partial^2 \varphi}{\partial x^2} \tag{4.25}$$

For which the explicit is stable only when :

$$0 < \lambda \le \frac{1}{2}; \text{ where, } \lambda = \frac{\Delta t}{(\Delta x)^2} \tag{4 26}$$

Although the explicit scheme is second order accurate in time it is not extensively used for this very restrictive condition in time step. The implicit scheme is unconditionally stable for eqn (4 25), but it is only first order accurate in time. Therefore combining the stability of an implicit method with the accuracy of explicit method, Crank Nicholson method is developed by taking the average of the explicit and implicit schemes [74] ·

$$\frac{\varphi_j^{n+1} - \varphi_j^n}{\Delta t} = \alpha \left[\frac{(\varphi_{j-1} - 2\varphi_j + \varphi_{j+1})^{n+1} + (\varphi_{j-1} - 2\varphi_j + \varphi_{j+1})^n}{(\Delta x)^2} \right] \cdots + 0[(\Delta t)^2 + (\Delta x)^2]$$

Crank Nicholson method is also unconditionally stable and second order accurate in time for eqn.(4.25), and this method is employed for solving the transient PDEs in the present study. Stability analysis of Cranck Nicholson technique with diffusion and convective terms by Von Neuman method is discussed later.

4.3.3 First Order Upwinding

The salient points of transport equations can be discussed with the help of a model equation. having a convective term, a diffusive term and a time dependent term

$$\frac{\partial \varphi}{\partial t} + V_x \frac{\partial \varphi}{\partial x} = \alpha \frac{\partial^2 \varphi}{\partial x^2} \tag{4.27}$$

Focusing on the inertial term or the first order differential term in space :

Central Differencing : $\dfrac{\partial \varphi}{\partial x} = \dfrac{\varphi_{j+1} - \varphi_{j-1}}{2 \triangle x} \quad \cdots + 0[(\triangle x)^2]$ $\qquad\qquad$ (4.28)

First order upwinding gives .

$$\dfrac{\partial \varphi}{\partial x} \;=\; \dfrac{\varphi_j - \varphi_{j-1}}{\triangle x} \;\cdots\; + 0[(\triangle x)] \qquad For \; V_x > 0 \;\Big\}$$
$$\qquad\;=\; \dfrac{\varphi_{j+1} - \varphi_j}{\triangle x} \;\cdots\; + 0[(\triangle x)] \qquad For \; V_x < 0 \;\Big\}$$
$$\qquad\qquad\qquad\qquad\qquad\qquad\qquad\qquad\qquad\qquad (4.29)$$

$$\Rightarrow \quad \dfrac{\partial \varphi}{\partial x} = \dfrac{(nx-1)\varphi_{j-1} + (-1)^{nx}\varphi_j + nx\,\varphi_{j+1}}{\triangle x} \qquad Where, \quad \begin{array}{l} nx = 0 \; for \; V_x > 0 \\ nx = 1 \; for \; V_x < 0 \end{array} \Big\} \;\; (4.30)$$

Therefore we can develop a first order hybrid scheme by combining eqn (4.28) and (4 30) ·

$$\dfrac{\partial \varphi}{\partial x} \;=\; (1-\beta)\left\{ \dfrac{\varphi_{j+1} - \varphi_{j-1}}{2 \triangle x} \right\} + \beta \left\{ \dfrac{(nx-1)\varphi_{j-1} + (-1)^{nx}\varphi_j + nx\varphi_{j+1}}{\triangle x} \right\}$$
$$\qquad\;=\; \dfrac{(2\beta nx - \beta - 1)\varphi_{j-1} + 2\beta(-1)^{nx}\varphi_j + (2\beta nx - \beta + 1)\varphi_{j+1}}{2 \triangle x} \qquad (4.31)$$

4.3.4 Virtual Point Method

The solution for the grid points in the boundary often involves a fictitious grid point at one mesh length $\triangle x$ outside the computational domain. For example temperature gradient in the boundary at $j = J_{Min}$ can be defined in finite difference form as :

$$\dfrac{dT}{dx} \;=\; \dfrac{T_{j+1} - T_{j-1}}{2 \triangle x} \;+\; 0[(\triangle x)^2] \;\Big\}$$
$$or, \qquad\;=\; \dfrac{T_j - T_{j+1}}{\triangle x} \;+\; 0[(\triangle x)] \;\Big\} \qquad\qquad (4\ 32)$$

Where, T_{j-1} is outside the computational domain

The conduction region is assumed to extend to this fictitious point, and the governing conduction equation is then written in finite difference form for the surface point The unknown fictitious temperature is eliminated between these two equations to give the desired equation for the surface grid point. For the Cartesian system, this treatment yields the same result as that obtained from an energy balance for the region represented by the surface grid point. For other coordinate systems, the two are very close. This treatment is simpler than the one involving an energy balance of the control volume and is very useful, particularly for complicated geometries and for flow problems [75] This method of implementation of boundary condition is known as virtual point method and used for the solution of equations in the boundary regions

4.3.5 Von Neuman Stability Analysis

During discretization of the governing equations, stability of the numerical scheme followed were analyzed by Von Neuman method The Von Neuman analysis is local, for a particular grid point
We imagine that the coefficients of the difference equations are so slowly varying as to be considered constant in space and time. In that case, the independent solution, or eigenmodes, of the difference equation are all of the form :

$$\varphi_j^n = \xi^n \exp^{\imath k_j \Delta x} \tag{4.33}$$

Where k is a real spatial wave number (which can have any value) and $\xi = \xi(k)$ is a complex number that depends on k. The key fact is that the time dependence of a single eigen mode is nothing more than successive integer powers of the complex number ξ. Therefore, the difference equations are unstable (have exponentially growing modes) if $\mid \xi(k) \mid > 1$ for some k. The number ξ is called the *amplification factor* at a given wave number k. Analyzing the standard one dimensional transport eqn.(4.27), discretized by Crank Nicholson scheme in time and central in space dimension we get ·

$$\frac{\varphi_j^{n+1} - \varphi_j^n}{\Delta t} + V_x \left\{ \frac{(\varphi_{j+1}^{n+1} - \varphi_{j-1}^{n+1}) + (\varphi_{j+1}^n - \varphi_{j-1}^n)}{4 \, \Delta x} \right\} =$$
$$\alpha \left\{ \frac{(\varphi_{j+1}^{n+1} - 2\varphi_j^{n+1} + \varphi_{j-1}^{n+1}) + (\varphi_{j+1}^n - s\varphi_j^n + \varphi_{j-1}^n)}{2(\Delta x)^2} \right\} \tag{4.34}$$

By using eqn.(4.33) in the above equation and dividing by $\varphi^n \exp^{\imath k_j \Delta x}$ we get :

$$(\xi - 1) + (\xi + 1) \frac{V_x \, \Delta t}{4 \, \Delta x} (\exp^{\imath k \Delta x} - \exp^{-\imath k \Delta x}) = (\xi + 1) \frac{\alpha}{2(\Delta x)^2} (\exp^{\imath k \Delta x} + \exp^{-\imath k \Delta x} - 2) \tag{4.35}$$

Where, $\quad \sin x = \dfrac{\exp^{\imath x} - \exp^{-\imath x}}{2\imath}, \quad \cos x = \dfrac{\exp^{\imath x} + \exp^{-\imath x}}{2}$ \hfill (4.36)

$$\frac{\xi - 1}{\xi + 1} = - \left\{ \frac{V_x \, \Delta t}{2 \, \Delta x} \sin(k \, \Delta x) + \frac{2D \, \Delta t}{\Delta x^2} \sin^2(\frac{k \, \Delta x}{2}) \right\} \tag{4.37}$$

$$\Rightarrow \quad \xi = \frac{1 - \frac{V_x \Delta t}{2\Delta x} \sin(k \, \Delta x) - \frac{2D\Delta t}{\Delta x^2} \sin^2(\frac{k\Delta x}{2})}{1 + \frac{V_x \Delta t}{2\Delta x} \sin(k \, \Delta x) + \frac{2D\Delta t}{\Delta x^2} \sin^2(\frac{k\Delta x}{2})} \tag{4.38}$$

Where, $\xi \leq 1$ for stability The above eqn.(4.38) can be greater than unity only when the term $\frac{V_x \Delta t}{2\Delta x} \sin(k \Delta x)$ is negative. The maximum negative value of $\sin(k \Delta x)$ is '-1' which gives :

$$1 - \frac{D \Delta t}{\Delta x^2} + \frac{v \Delta t}{2 \Delta x} \leq 1 + \frac{D \Delta t}{\Delta x^2} - \frac{V_x \Delta t}{2 \Delta x} \tag{4.39}$$

$$\Rightarrow \quad \Delta x \leq \left| \frac{2D}{V_x} \right| \tag{4 40}$$

The Δx value defined by the above equation limits the step size in $x-$direction This is also known as 'Heuristic Stability Limit' [76].

Now, let the value of the second term $\frac{2D\Delta t}{\Delta x^2} \sin^2(\frac{k\Delta x}{2})$ be denoted by 'f'

$$\text{For Stability} \quad \frac{V_x \Delta t}{2 \Delta x} \leq f \tag{4.41}$$

$$\Delta t \leq \left| \frac{2f \Delta x}{V_x} \right| \tag{4.42}$$

Where $\Delta t \leq \left| \frac{\Delta x}{V_x} \right|$ is the well known Courant-Freidrich-Lewy (CFL) stability condition. So for the present case the stability depends on some factor 2f times the CFL condition. Therefore after choosing 'Δx' according to limit set by eqn.(4.40) we can take the time step 'Δt' according to eqn (4 42) and the value of f can be taken as one.

4.3.6 Non-dimensionalizing the Equations

The equations were non-dimensionalized for simplification and easy scaleup of the models developed. The value of the non-dimensional terms also gives a first hand idea of the relative importance of the different terms present in the equation The standard values used for non-dimensionalizing the terms are given in table 4 1. The standard time used for non-dimensionalizing the equations are local *i.e.* valid only for that particular equation depending on the thermal or the mass diffusion coefficient. The non-dimensional terms obtained for the governing equations are given in table 4.2.

Table 4.1: Standard Values used for non-dimensionalizing the equations.

T_o	$= 1000$ K	Standard Temperature
L_o	$= 0.1$ m	Standard Length
V_o	$= 0.1$ m/s	Standard Velocity

Standard time for Solid Phase Thermal Energy Balance

$$t_s = \frac{L_o^2 \rho_s C_{p,s}}{K_b} \quad \text{Standard Time}$$

Standard time for Gaseous Phase Thermal Energy Balance

$$t_s = \frac{L_o^2 \rho_g C_{p,g}}{K} \quad \text{Standard time (Where } K \Rightarrow K_b \text{ or } K_g)$$

Standard time for Gaseous Phase Mass or Species Balance

$$t_s = \frac{L_o^2}{D_e} \quad \text{Standard time}$$

4.4 Concluding Remarks

The equations and the technique discussed in this Chapter were employed for the process simulation discussed in the subsequent chapters All the computations for the process simulation were done in a local area network (LAN) of HP 9000 Series mini frame systems and workstations.

Table 4.2. List of Non-Dimensional terms

x	$= \dfrac{x'}{L_o}$	Distance along the x-axis
y	$= \dfrac{y'}{L_o}$	Distance along the y-axis
r	$= \dfrac{r'}{L_o}$	Radial distance
z	$= \dfrac{z'}{L_o}$	Distance along the axis
t	$= \dfrac{t'}{t_s}$	Non-dimensional time
T_s	$= \dfrac{T_s'}{T_o}$	Solid Temperature
T_g	$= \dfrac{T_g'}{T_o}$	Gas Temperature
G_H	$= \dfrac{C_A}{C_{Ab}}$	Gas Composition (For hydrogen)
X	$= \dfrac{C_{Bo} - C_B}{C_{Bo}}$	Fraction Reduced
Nu	$= \dfrac{h_v L_o^2}{K_b}$	Nusselt's number for gas to solid heat transfer

Equation of Motion

R_e	$= \dfrac{L_o V_o}{\nu}$	Reynold's number

Solid Phase Thermal Energy Balance

Pe_{Ts}	$= \dfrac{V_o L_o \rho_s C_{p,s}}{K_b}$	Peclet number for thermal convection
$R_{T,i}$	$= \dfrac{q_i C_{Bo,i}}{C_{p,s} T_o}$	Reaction term for heat of reaction

Gaseous Phase Thermal Energy Balance

Pe_{Tg}	$= \dfrac{V_o L_o \rho_g C_{p,g}}{K_g}$	Peclet number for thermal convection

Gaseous Phase Mass or Species Balance

Pe_G	$= \dfrac{V_o L_o}{D_e}$	Peclet number for gas phase mass convection
$R_{G,i}$	$= \dfrac{C_{Bo,i}}{C_{Ao}}$	Reaction term for mass balance

$'$ Dimensional parameter

Chapter 5

REDUCTION IN A FIXED BED REACTOR WITH GAS FLOWING VERTICALLY THROUGH THE BED

This Chapter deals with the experimental and numerical modeling study of gas solid reactions when the reacting gas flows vertically through the packed bed of ore pellets. In industrial furnaces like shaft furnace shown in figure 2.21, the basic mode of gas solid contact is similar to the present situation, but the only difference is that the bed is not static but moving. For studying the process experimentally and to match it with simulated results, static bed reactor was chosen for its simplicity and accuracy of experimental measurements. The extent of nickel reduction at different depths were experimentally determined and compared with numerically simulated results to verify the mathematical model and understand the basic mechanism of reaction. The model thus developed can be used to study the effect of various parameters which will be very difficult and time consuming to study experimentally. The objective of this type of modeling is to study the performance of a reactor, and to predict the overall rate of conversion of the solid contained in the reactor. The first task for this purpose is to arrive at a quantitative description of the rate of reaction of the pellets in the reactor for the specified surroundings. In the present case the grain model described in Chapter 3 is used for this purpose. However, this is only the first task, since in a packed bed the environment surrounding the pellet is affected by the presence of other pellets, most notably by the reaction of the other pellets. A second task is therefore to apply the transport and conservation equations to describe the environment in the reactor, which is a function of time and position.

5.1 Experimental Setup and Procedure

A stainless steel tube of internal diameter 4 cm and length 16 cm which can be enclosed from both sides was used for conducting the experiments, as shown in figure 5 1. Stainless steel tubes were attached to the bottom and top positions for gas inlet and outlet respectively The cylindrical reactor was filled with refractory beads upto about 5 cm height for preheating the reactant gas to furnace temperature. Five layers of pellets separated by wire meshes, having a total height of 9 cm were then placed over the preheating zone of refractory beads The tube was then closed from both sides and made air tight by using a mixture of white cement, asbestos wool and water The entire chamber was inserted in the tubular furnace for conducting the experiments The furnace has a 30 cm long uniform temperature zone in the central region where the tubular reactor can be conveniently placed. The gas flow and other associated arrangements were similar to the setup shown in figure 3.5. The reactor in the furnace was then heated to the reaction temperature and flushed with nitrogen before passing hydrogen at a specified flow rate for conducting the experiments. After the experiment the reactor was taken out and cooled to room temperature under stagnant H_2-H_2O atmosphere to avoid any reoxidation from atmospheric oxygen. After cooling the reactor to room temperature, 3 5 grams of representative pellet samples were collected from each layer and analyzed by the standard chemical analysis method described in figure 3.6 for determining the amount of nickel reduced.

5.2 Mathematical Model for the Process Simulation

For fully describing the reduction process in a fixed bed reactor under vertical gas flow condition, all the process phenomena like gas flow though the bed, gas-solid heat and mass transfer, reaction kinetics of the ore pellets have to be taken into account For this purpose following conservation equations need to be solved in a coupled fashion.

1 Fluid flow through the packed bed of spherical pellets

2. Gaseous phase thermal energy balance.

3 Solid phase thermal energy balance.

4. Gaseous phase mass or species balance.

5. Solid phase mass or species balance.
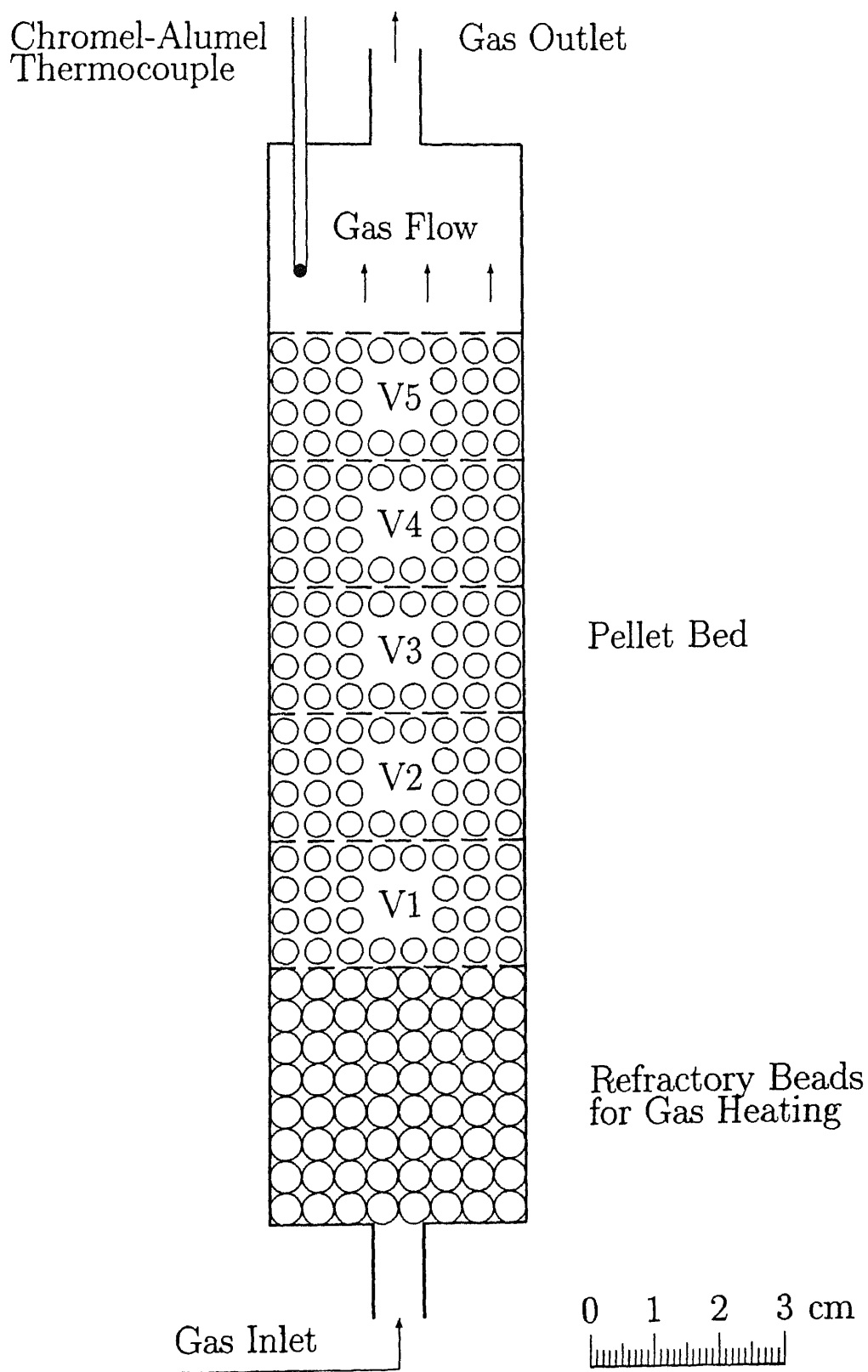
Figure 5 1: Setup for the Vertical gas flow experiments

5.3 Parameter Values for the Process

The parameters used for the process and the dimensions of the cylindrical reactor packed with spherical pellets are given in table 5 1. Gas velocity through packed bed is considered to be in the laminar zone for particle Reynolds number below 5 and turbulent above 150, as shown in figure 5 2 [59] Therefore in the present situation the Reynolds numbers are mostly in the intermediate region (as shown in table 5.1), and so the effect of both the laminar resistance term (f_1) and the turbulent resistance term (f_2) has to be taken under consideration

Void fraction in packed beds are higher near the cylinder wall and varies sinusoidally with decreasing amplitude towards the center In the present study a cylindrical reactor of 4 cm diameter is used, packed with pellets of 0 5 cm diameter. Therefore the ratio of the cylinder diameter and pellet diameter is eight in this case. In the present study the void fraction variation in a cylindrical packed bed of spheres is taken from the experimental results of Benenati and Brosilow [49], and a third order curve is fitted for the data as shown in figure 5.4. The void fraction variation represented by the fitted curve is used for predicting the gas velocity profile inside the packed bed by using Ergun's equation

The manometer calibration for the selected gas velocities is shown in figure A.1 and table A.7 The reaction kinetic parameters like rate constant values are given in table A.22; and the values for diffusivity, heat of reaction, gas-solid heat transfer coefficient etc., are taken from table A 24, A.17 and A.27 in Appendix A.

5.4 Computational Domain

Since there is no angular or theta direction variation of properties, cylindrical axisymmetric equations are used for modeling the process. The computational domain used for this purpose is shown in figure 5 3 Gas inlet boundary is shown by EN, and gas exit is shown by EX. The central line or the axis of symmetry is denoted by C and the cylinder wall is denoted by W The grid points where the equations are solved were shown by circles or dots. The boundary zones in the computational domain with respect to the grid points can be summarized as given below :

C · Center line : $i = 1$; $1 \leq j \leq J_{Max}$

W Wall surface $i = I_{Max}$; $1 \leq j \leq J_{Max}$
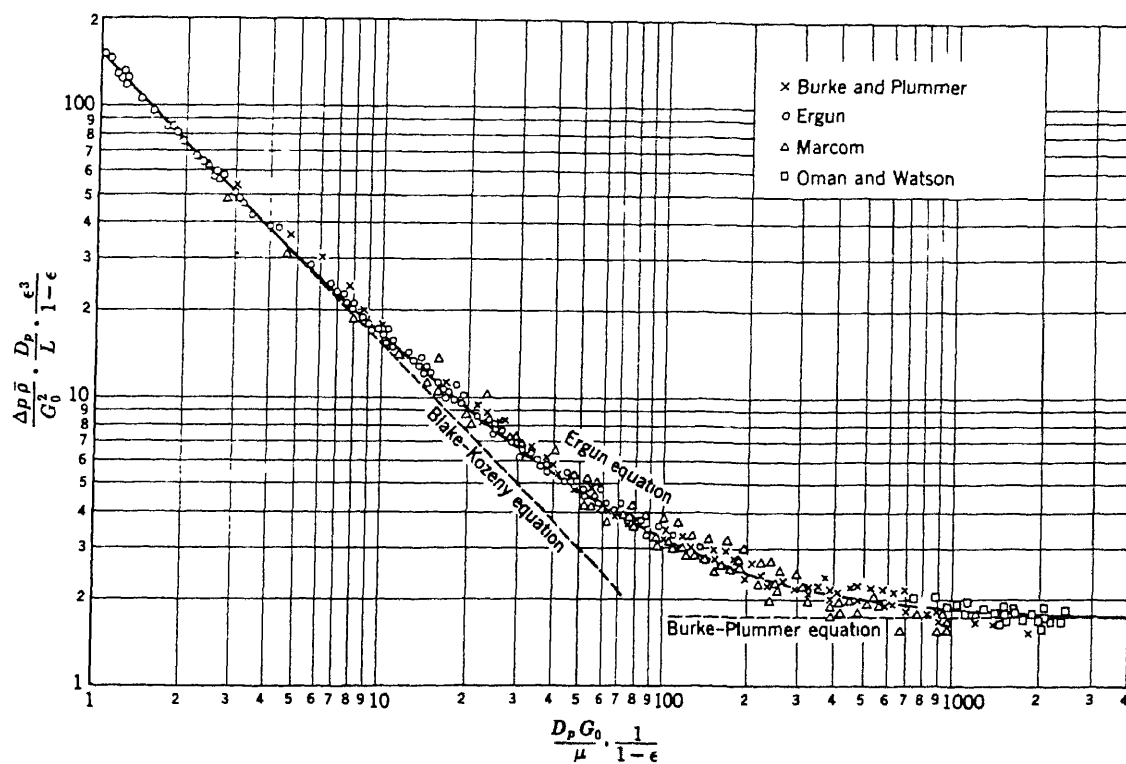
Figure 5.2: Pressure - drop correlation for flow through packed beds [59].

Table 5.1: Reactor dimensions and parameter values for vertical gas flow condition.

PARAMETER	VALUE	UNIT
Reactor Dimensions		(in mm)
Diameter	40	
Heating Zone height	50	
Packed Bed Height	90	
Bed Porosity		(%)
Wall surface	48	
Center	36	
Average bed porosity	40	
Pellet diameter	5	mm
No. of Layers	5	
Gas Velocity	2F, 5F and 8F	
Where F (Volumetric Flow rate)	8 65	cc/sec at 1000 K
or F (Superficial velocity)	0.69	cm/sec at 1000 K
Particle Reynolds number (R_e)		
For 2F, 5F and 8F	3 45, 8.08 and 12 70	
Biot Number for		
2F, 5F and 8F at 900 K	0.33, 0.22, 0 10	
2F, 5F and 8F at 1000 K	0 36, 0.24, 0.11	
Grid Size		
$\triangle r$	0 2	cm
$\triangle z$	0 15	cm
No of Grid Points I_{Max}; J_{Max}	10, 60	
$\triangle t$ (for 900 K)	0 50	sec
$\triangle t$ (for 1000 K)	0 25	sec

EN . Lower boundary or gas Entry $\quad 1 \leq i \leq I_{Max}, j = 1$

EX Upper boundary or gas Exit $\cdot$ $1 \leq i \leq I_{Max}, j = J_{Max}$

5.5   Governing Equations

A quasi-steady state model was used in the present study where the fluid flow equations were solved for steady state condition, since the total number of gas moles or gas volume remained constant during the reduction process, and the equations for all the other parameters like gas-solid temperature, and composition were solved in a transient fashion. Virtual point method is used to implement the boundary conditions The conductivity of both gas and solid was taken equal to the conductivity of the packed bed, and the gas diffusivity was taken proportional to the void fraction of the bed The equations were taken in their non-dimensional form and the non-dimensional terms are explained in the list of non-dimensional terms given in table 4.2 of Chapter 4 The parameters were first initialized, and the inlet gas temperature and composition were taken equal to the initial conditions for gas The wall temperature was taken equal to the initial solid temperature. The initial conditions can be summarized as given below $\cdot$ For $t = 0,$ $(1 \leq i \leq I_{Max}; 1 \leq j \leq J_{Max})$

1 $T_{s(i,j)} = T_{s,int} = T_{s,w}$

2 $T_{g(i,j)} = T_{g,int}$

3 $G_{H(i,j)} = G_{H,int}$

4. $X_{i(i,j)} = 0$

5.5.1   Gas Flow Through Packed Bed : Ergun's Equation

The vectorial form of Ergun's equation was solved for predicting the gas velocity profile in the packed bed The Ergun's equations for cylindrical axisymmetric condition $(m = 1)$, as given by eqn (4 3) to eqn (4.12) in Chapter 4 was used for this purpose
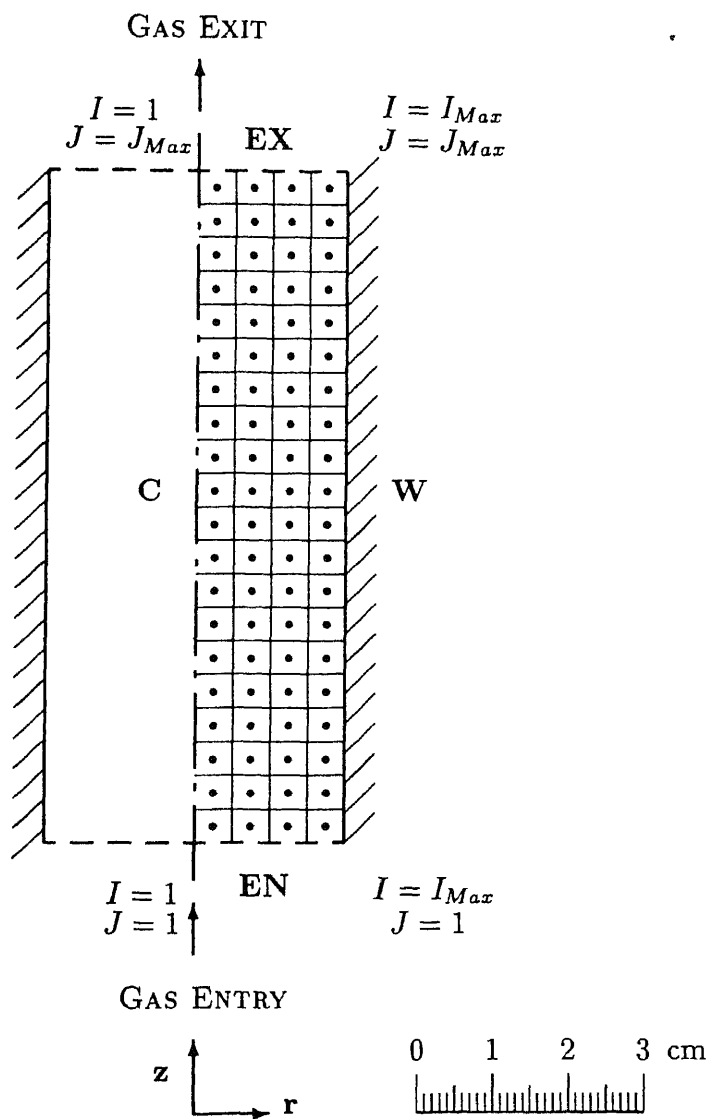
Figure 5.3: Computational domain for the Vertical gas flow condition.

Since the Ergun's equation has higher order and nonlinear terms, it cannot be discretized directly Therefore it has to be simplified and broken down into smaller equations of first and second order, and has to be solved iteratively.

Discretization of the terms were done by central differencing in r-direction and backward differencing in z-direction Central differencing in r-direction is done since the velocity in the lateral or r-direction is not known, and central differencing has second order accuracy compared to first order accuracy for the forward and backward differencing. The gas flow in the z-direction is from the bottom upwards and so backward differencing scheme is adopted according to first order upwinding.

The following terms are defined and discretized separately

$$\psi_{r2} = \left(\frac{\partial \psi}{\partial r}\right)^2; \qquad \psi_{z2} = \left(\frac{\partial \psi}{\partial z}\right)^2$$

$$f_{1r} = \frac{\partial f_1}{\partial r}; \qquad f_{1z} = \frac{\partial f_1}{\partial z}$$

$$f_{2r} = \frac{\partial f_2}{\partial r}; \qquad f_{2z} = \frac{\partial f_2}{\partial z}$$

$$\psi_{rz} = \frac{\partial^2 \psi}{\partial r \partial z} = \frac{\psi_{(i+1,j)} - \psi_{(i+1,j-1)} - \psi_{(i-1,j)} + \psi_{(i-1,j-1)}}{2 \triangle r \triangle z}$$

The equation now simplifies to become ·

$$\left\{ f_{1r}\frac{\partial \psi}{\partial r} + f_{1z}\frac{\partial \psi}{\partial z} + f_1 \left(\frac{\partial^2 \psi}{\partial r^2} + \frac{\partial^2 \psi}{\partial z^2} - \frac{1}{r}\frac{\partial \psi}{\partial r} \right) \right\} \sqrt{\psi_{s2} + \psi_{z2}}$$

$$+ \frac{1}{r}\left\{ f_{2r}\frac{\partial \psi}{\partial r} + f_{2z}\frac{\partial \psi}{\partial z} + f_2 \left(\frac{\partial^2 \psi}{\partial r^2} + \frac{\partial^2 \psi}{\partial z^2} - \frac{1}{r}\frac{\partial \psi}{\partial r} \right) \right\} (\psi_{r2} + \psi_{z2})^2$$

$$+ \frac{f_2}{r}\left\{ \psi_{r2} \left(\frac{\partial^2 \psi}{\partial r^2} - \frac{1}{r}\frac{\partial \psi}{\partial r} \right) + \psi_{z2} \left(\frac{\partial^2 \psi}{\partial z^2} - \frac{1}{r}\frac{\partial \psi}{\partial r} \right) + 2\psi_{rz}\frac{\partial \psi}{\partial r}\frac{\partial \psi}{\partial z} \right\} = 0 \qquad (5.1)$$

The equation now becomes a second order equation which can be solved by the standard tridiagonal matrix method The terms ψ_{r2}, ψ_{z2}, f_{1r}, f_{1z}, f_{2r}, f_{2z} and ψ_{rz} are taken as pseudo-constants, whose values are taken from the previous iteration, and the set of equations are solved in a iterative manner.

Initial Condition : The initial stream function value in the domain is evaluated by :

$$\int_1^1 \partial \psi = -\int_{r=dr}^{r=i\,dr} r V_{z,av} dr \qquad (5.2)$$

$$\Rightarrow \quad \psi = -\frac{r^2}{2}V_{z,av} \tag{5.3}$$

Boundary Conditions

C and W : Constant stream function values at the center and wall surface ·

$$\psi = -\frac{(\imath\ dr)^2}{2}V_{z,av} \tag{5.4}$$

Where, $\imath = 1$ at the center, and $\imath = I_{Max}$ at the wall surface

EN : Zero flux for stream function, by virtual point method :

$$\frac{\partial \psi}{\partial z} = 0 \tag{5 5}$$

EX . Zero gradient for stream function, for smooth transition of flow .

$$\frac{\partial \psi}{\partial z} = 0 \tag{5 6}$$

5.5.2   Solid Phase Thermal Energy Balance

Solid phase thermal energy balance was solved to consider the non-isothermal nature of the reduction process. It will also provide us the information about the gas-solid heat exchange. Both the terms will act as source terms. The equation in its non-dimensional form is given by :

$$\frac{\partial T_s}{\partial t} = \left[\frac{1}{r}\frac{\partial}{\partial r}\left(r\frac{\partial T_s}{\partial r}\right) + \frac{\partial^2 T_s}{\partial z^2}\right] + Nu(T_g - T_s) + \sum_{\imath=1}^{n}R_{T,\imath}\frac{\partial X_\imath}{\partial t} \tag{5.7}$$

Boundary Conditions

The boundary conditions are implemented by virtual point method coupled with eqn (5.7).

C and W : Zero temperature gradient :

$$\frac{\partial T_s}{\partial r} = 0 \tag{5.8}$$

EN . Known gas temperature, and zero solid temperature gradient :

$$T_{g(i,j)} = T_{g,int} \qquad (5\ 9)$$

$$\frac{\partial T_s}{\partial z} = 0 \qquad (5\ 10)$$

EX . Zero temperature gradient .

$$\frac{\partial T_s}{\partial z} = 0 \qquad (5.11)$$

5.5.3 Gaseous Phase Thermal Energy Balance

For considering the effect of non-isothermal reduction and gas-solid heat exchange both the solid phase and gaseous phase thermal energy balance have to be solved simultaneously. The amount of heat lost by the gaseous phase will be equal to the heat gained by the solid phase, and vice-versa The equation in its non-dimensional form is given by :

$$\frac{\partial T_g}{\partial t} + Pe_{T_g}\left(V_r\frac{\partial T_g}{\partial r} + V_z\frac{\partial T_g}{\partial z}\right) = \left[\frac{1}{r}\frac{\partial}{\partial r}\left(r\frac{\partial T_g}{\partial r}\right) + \frac{\partial^2 T_g}{\partial z^2}\right] + Nu(T_s - T_g) \qquad (5\ 12)$$

Boundary Conditions

The boundary conditions are implemented by virtual point method coupled with eqn (5.12).

C   Zero flux condition :

$$\frac{\partial T_g}{\partial r} = 0 \qquad (5.13)$$

W . Known wall or solid temperature :

$$T_{s(i,j)} = T_{s,int} \qquad (5.14)$$

EN · Temperature is defined ·

$$T_{g(i,1)} = T_{g,int} \qquad (5.15)$$

EX . Continuity of gas temperature ·

$$\frac{\partial T_g}{\partial z} = 0 \qquad (5\ 16)$$

5.5.4 Gaseous Phase Mass or Species Balance

The gas phase mass or species balance will determine the reactant gas concentration at different positions of the reactor which will then determine the gas-solid reaction rate. Therefore it will play a vital role in determining the reduction profile in the reactor. The reaction rate will act as a source term for the equation The equation in its non-dimensional form is given by ·

$$\frac{\partial G_H}{\partial t} + Pe_G \left(V_r \frac{\partial G_H}{\partial r} + V_z \frac{\partial G_H}{\partial z} \right) = \left[\frac{1}{r} \frac{\partial}{\partial r} \left(r \frac{\partial G_H}{\partial r} \right) + \frac{\partial^2 G_H}{\partial z^2} \right] + \sum_{i=1}^{n} R_{G,i} \frac{\partial X_i}{\partial t} \tag{5.17}$$

Boundary Conditions

C and W Zero flux condition :

$$\frac{\partial G_H}{\partial r} = 0 \tag{5 18}$$

EN · Gas convection from bulk phase to the packed bed surface :
By neglecting the diffusive terms and the r-direction velocity, and by putting

$$\frac{\partial G_H}{\partial z} = \frac{1}{\Delta z}(G_{H(i,j)} - G_{H,int})R \tag{5.19}$$

in eqn (5.17) we get the inlet boundary condition as ·

$$\frac{\partial G_H}{\partial t} + Pe_G \frac{\partial V_z}{\Delta z}(G_H - G_{H,int}) = \sum_{i=1}^{n} R_{G,i} \frac{\partial X_i}{\partial t} \tag{5.20}$$

EX Continuity of gas composition :

$$\frac{\partial G_H}{\partial z} = 0 \tag{5.21}$$

5.5.5 Solid Phase Mass or Species Balance by Grain Model

The grain model is used for predicting the reduction rate of solid due to its simplicity and accuracy of prediction as described in Chapter 3 The gas concentration at the reaction interface for calculating the reaction rate constant is however calculated from the two layer model eqn.(3.41). This is possible under the present situation for the grain shape factor $F_g = 1$. We have checked

the results without using eqn.(3 41), i.e. by neglecting the gas concentration profile in the pellets, and the the difference in the predicted results were found to be negligible. The reduction rate of solid ore pellets according to grain model is given by :

$$\frac{dX}{dt} = \frac{k_{/rg}C_A}{C_{Bo}\left[1 + 2\sigma^2\left\{\frac{1}{(1-X)^{1/3}} - 1\right\}\right]} \tag{5.22}$$

5.6 Computational Procedure

The computations were done in a local area network of HP 9000 Series miniframe systems and workstations. The grid size and the time steps were determined by using the Von Neuman stability analysis for the Crank Nicholson discretization scheme used, as described in Chapter 4 The solution procedure involves a main program to initialize the conditions, and to call the subroutines for the solution of the different phenomena involved in the process. The time step between the two set of solutions are in the range of 0.25 to 0.5 sec , which can be considered as reasonably small to assume the solution of the equations as simultaneous. The time of computation (real time) is in the range of 5 minutes for 1000 time steps. The solution procedure, description of the main program and its subroutines, and the computer code developed are given in Appendix C.

5.7 Results and Discussion

The results of the experimental and computational study of the reduction process under vertical gas flow condition are discussed in this section. The gas velocity profile in the packed bed is first solved for steady state condition, and then the other parameters were evaluated for transient conditions.

5.7.1 Gas Velocity Profile

The gas velocity profile inside the packed bed was predicted by considering a fitted average void fraction as shown in figure 5 4 Similar procedure was followed earlier by Szekely and Poveromo [50], for their experimental and computational study of fluid flow through packed beds under turbulent conditions. We have replotted their results and compared with the predictions made

by the present code developed, to validate our results as shown in figure 5 5 The matching is found to be quite satisfactory with their results

The gas velocity profile inside the packed bed for the present configuration is shown in figure 5 6, and it is found to be more uniform near the gas entrance and exit positions.

5.7.2 Matching between Experimental and Simulated results

The effect of time and gas velocity on nickel reduction were studied experimentally at 900 K and 1000 K The experimental results were estimated by analyzing representative samples from each layer of the packed bed, and the experimental results for nickel reduction are given in table A.14 and A.15 of Appendix A. For matching with the experimental results, volume averaged values of the computed results in each layer were taken for the parameters studied. The experimental results were then matched with the computationally predicted results at 900 K and 1000 K as shown in figure 5.7 and 5.8 respectively. The percentage reduction of nickel is predicted by both the grain model, shown by small dotted lines, and the complex oxide mechanism shown by thick lines The percentage iron reduction predicted computationally is also plotted and shown by large dots. In the lower most layer, where the gas first enters the packed bed has the highest percentage reduction since hydrogen concentration is maximum at that region. As the gas moves up from the lower layers to the upper layers, hydrogen gas concentration decreases and the concentration of the product gas i.e. water vapor increases, and so the reduction rate falls sharply. In the bottom layer, some of the experimental points were much below the predicted results. This may be due to due to some reoxidation from atmospheric oxygen which may diffuse in during the removal of the reaction chamber from the furnace, or due to some flow maldistribution in the lower region. The intermediate layers showed reasonably good match between the experimental and predicted results. Both the mixed oxide and the complex oxide mechanism used here for predicting nickel reduction showed similar trends However at the topmost layer, where reduction is minimum the matchings are apparently better for complex oxide mechanism.

Therefore, for the subsequent computational study of the process, complex oxide mechanism for nickel reduction is used. Comparing the predicted result for iron and nickel reduction in figure 5.7 and 5.8, it is seen that iron reduction is faster in the upper layers and in the initial period when conversion to wüstite is not complete and so the total NiO is not free to get reduced. Initial iion reduction rate is also faster due to the fact that the reduction of hematite and magnetite is much faster than the wüstite reduction. Some of the experimental data points showed some
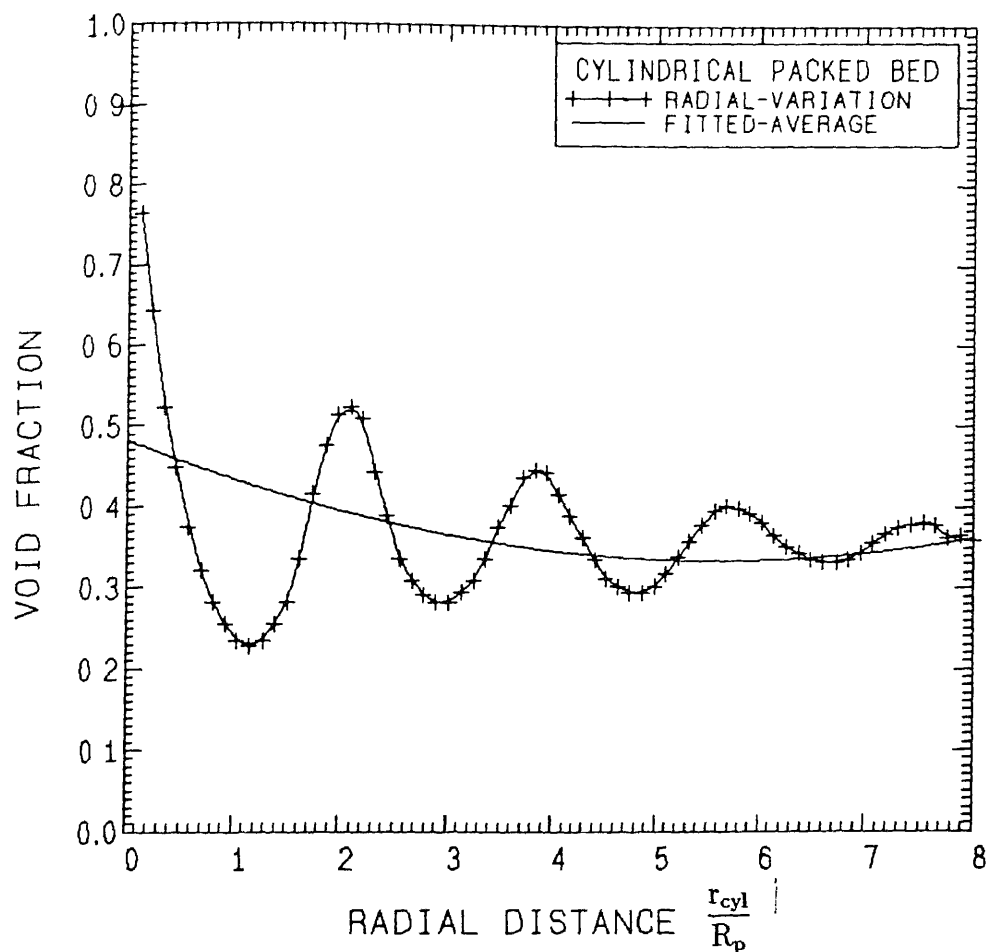
Figure 5 4· Radial variation of void fraction for packed bed of spheres in a cylindrical tube, and the fitted curve showing the average void fraction variation [49].
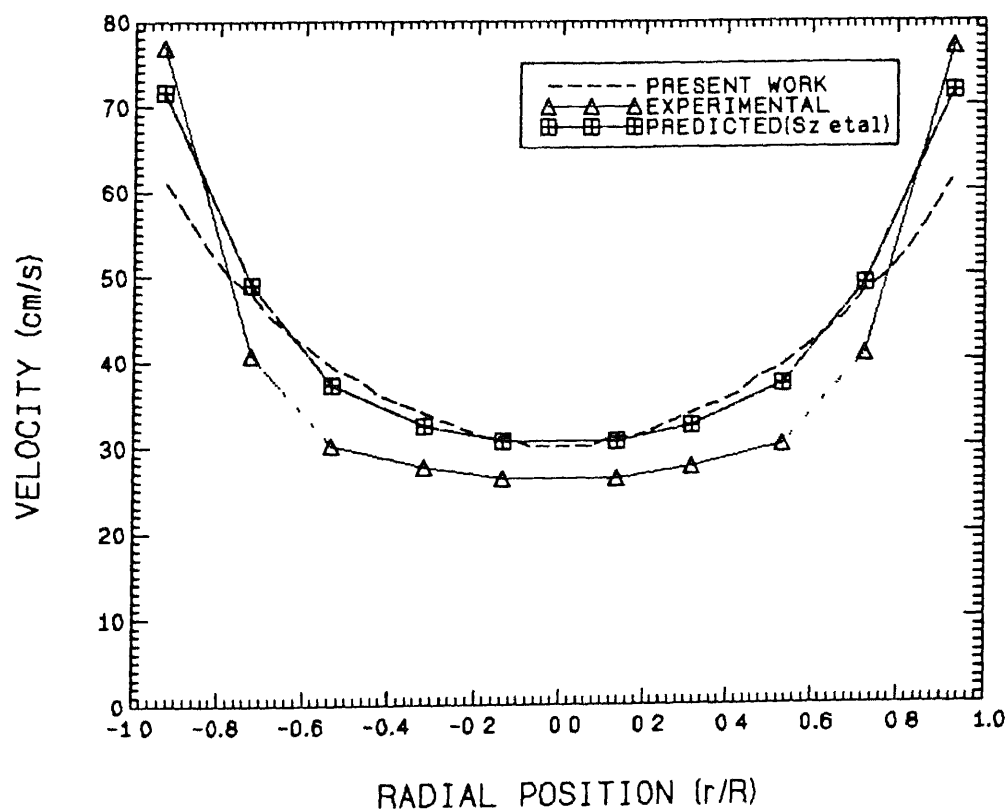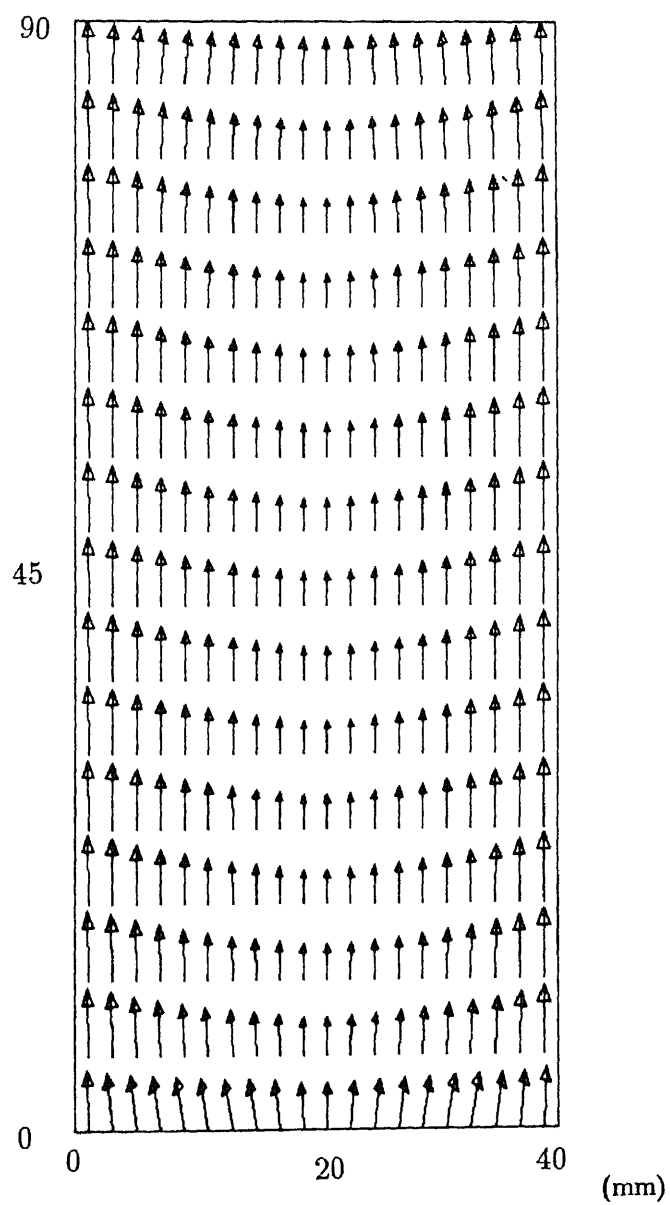
Figure 5.6: Vector plot for the gas velocity profile inside the packed bed.

(a)

(b)
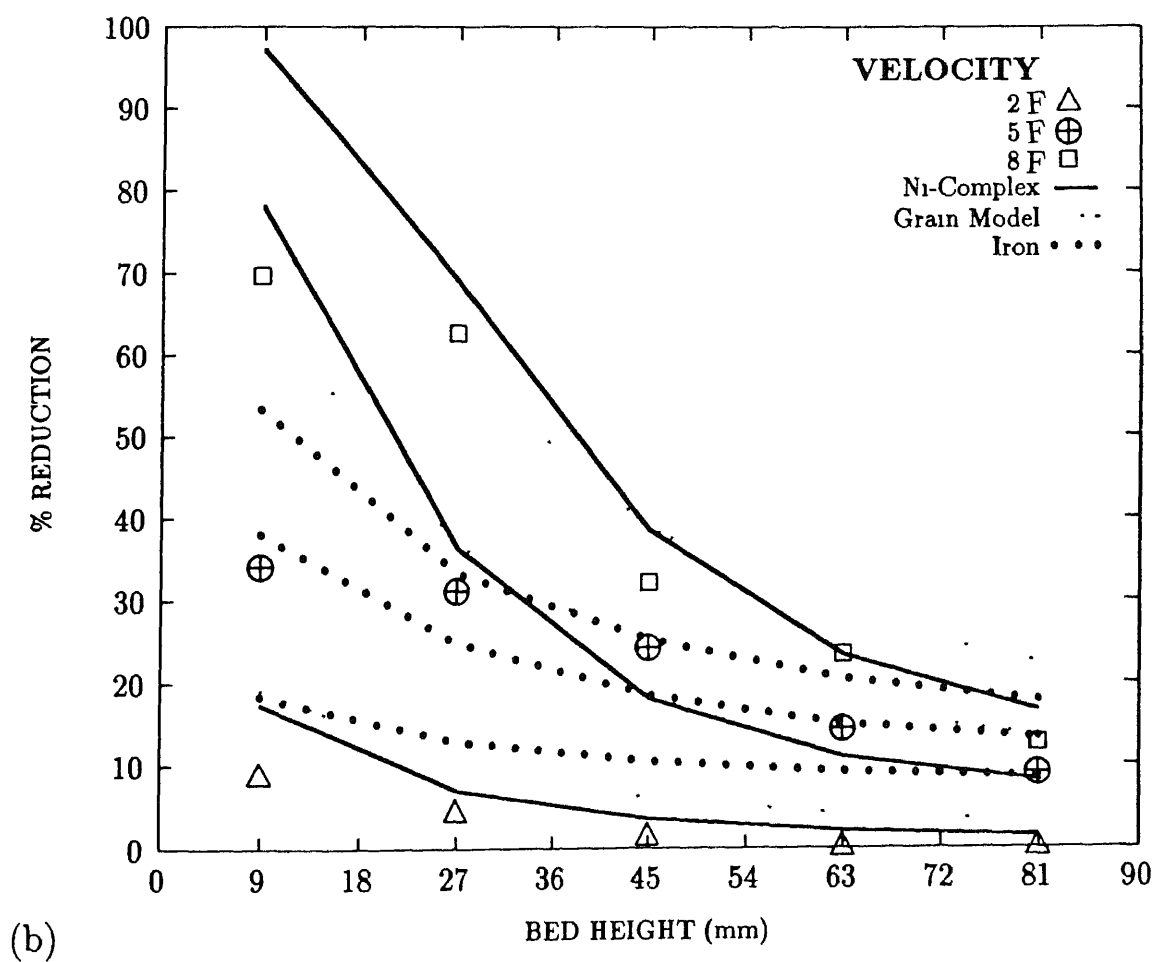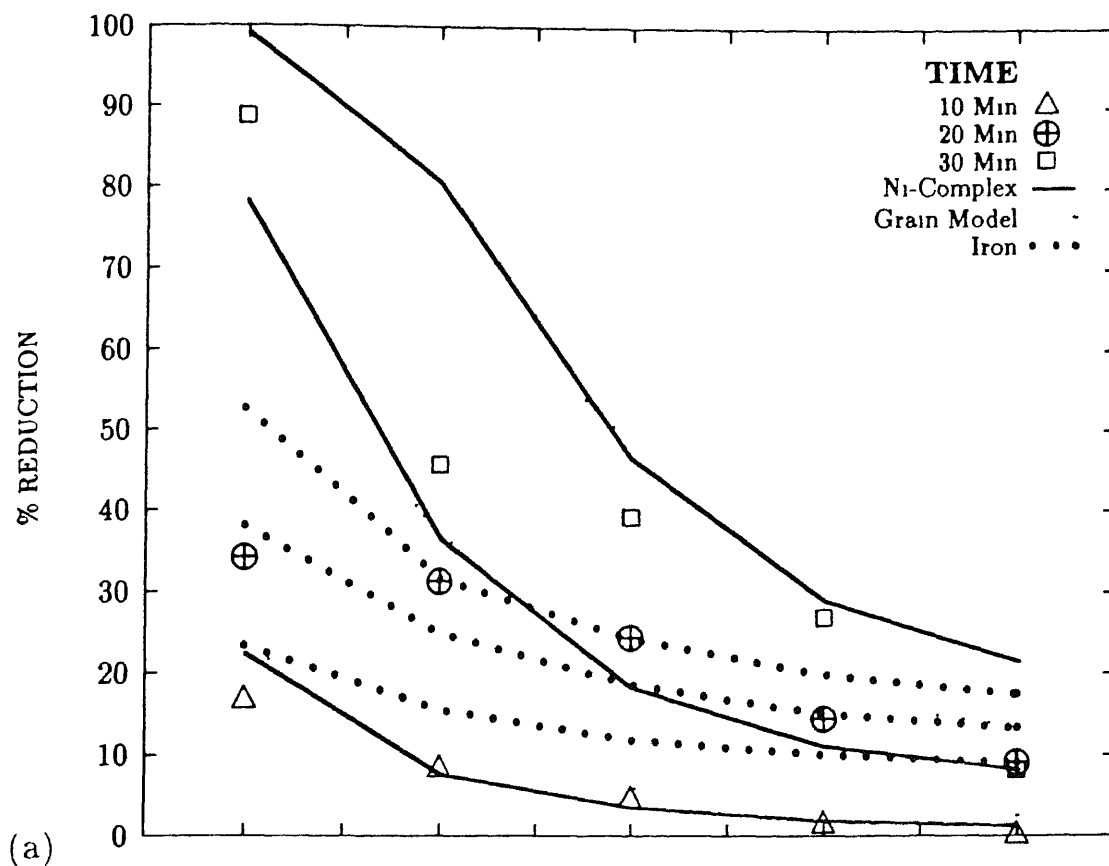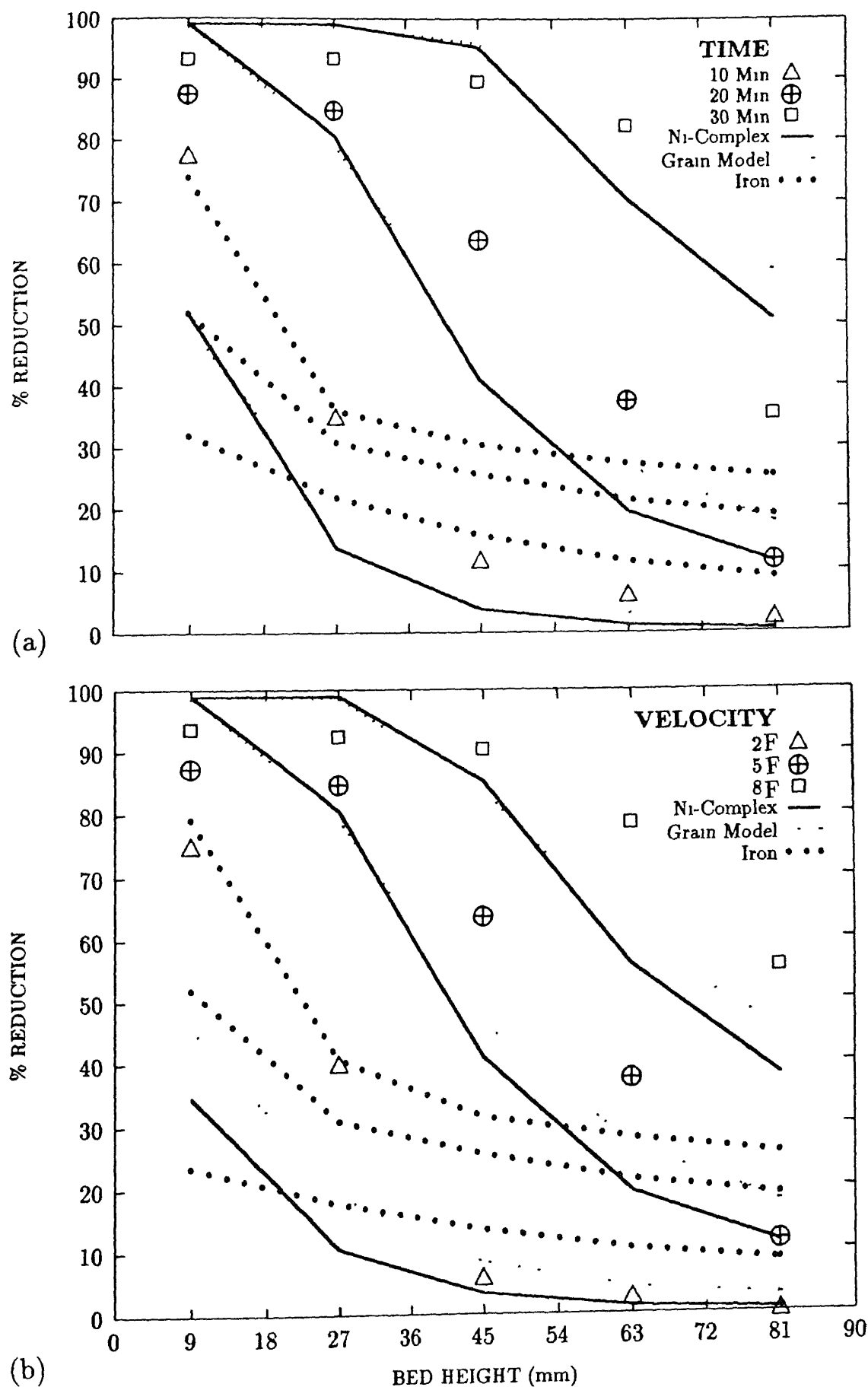
Figure 5.8 Experimental and predicted variation of reduction profile at 1000 K with : (a) Time

deviation from the predicted curves, and inconsistency with the general trends. These may be due to various difficulties and limitations of the experimental techniques The possible reason for error are as follows :

1 Oxygen entry from atmosphere during the removal of the reaction chamber from the furnace when the gas inlet and outlet tubes were temporarily removed.

2 The presence of residual hydrogen in the reaction chamber after the experiments

3. There may be some non-uniformity in packing, or in pellet size giving rise to flow maldistribution in the layers

5.7.3   Reproducibility and Grid Independence Test

The results for reproducibility and grid independence test are shown in figure 5 9 Reproducibility of the experimental results were checked by conducting a second experiment at 1000 K for 20 minutes with 5F gas velocity, and the results showed that the maximum error involved in the experimental measurements are in the range of 10 % nickel reduction The computational grid independence test was done by reducing the grid size and time step by half, and the results showed a maximum difference of about 1-2 % for nickel reduction.

5.7.4   Process Dynamics

Dynamic properties of the process is studied by plotting the values of various parameters at the central position of the layers as a function of time. This will give us an idea about the progress of the process from its initial condition. Figure 5 10 shows the percentage reduction *vs.* time plot for nickel and iron at 900 K and 1000 K The plots showed very similar trend but faster reduction rate at 1000 K. In all the cases nickel reduction rate is very slow initially, while the iron reduction rate is much faster. With progress in time iron reduction rate slows down considerably, while the nickel reduction rate increases sharply. The reason behind this is as mentioned before, due to faster reduction of hematite and magnetite and subsequent slower reduction rate of wüstite. Nickel reduction rate picks up after it gets unlocked from the complex oxide structure. For the reduction of iron in the bottom layer at 1000 K there is a small increase in slope after 15 minute reduction, this may be due to completion of nickel reduction after 15 minutes and so water vapor formation due to nickel reduction is not there, which makes it possible for purer hydrogen to
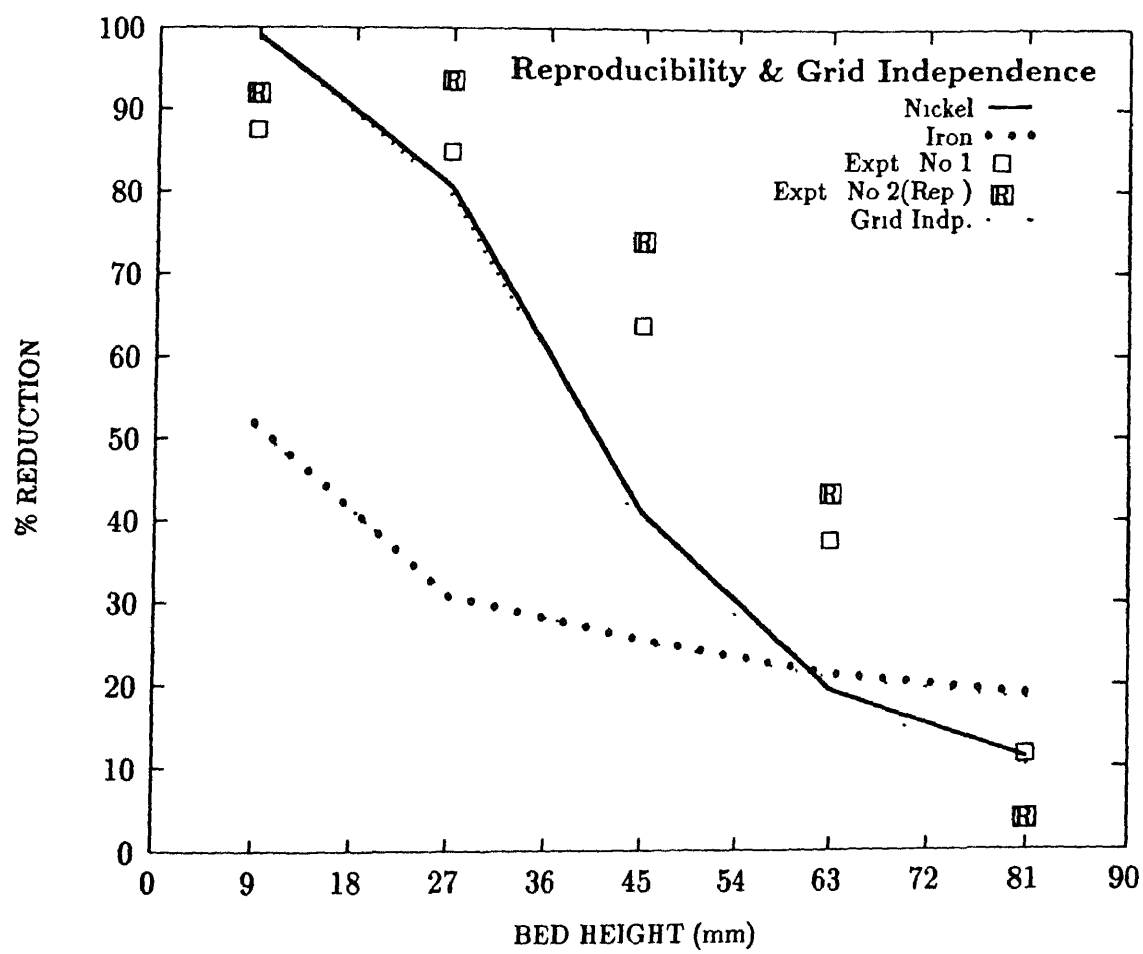
Figure 5.9   Reproducibility and grid independence test for the results of 15 minutes reduction at 1000 K

react with wüstite giving rise to higher reduction rate for iron The reduction kinetics of iron is manifested in the gas composition *vs.* time plot shown in figure 5.11. The initial gas concentration is much lower since the hematite and magnetite reduction rates are much faster, and also due to the fact that equilibrium partial pressure of water vapor is much higher for hematite and magnetite than wüstite As wüstite formation reaches completion gas concentration in the bed gradually increases and then remains more or less constant reaching a dynamic equilibrium with wüstite reduction rate The gas and solid temperature in the three layers are shown in figure 5 12 when the initial gas temperature was 1000 K and solid temperature was 800 K. The 9 cm bed depth is found to be quite sufficient for the gas-solid heat exchange and the temperature difference dropped from more than 40 K in the bottom layer to less than 4 K in the topmost layer The rise in solid temperature is very slow and gradual in the middle and top layers, although there is some sharp rise in temperature initially in the bottom layer.

5.7.5 Contour Plots

Contour plots for various parameters are plotted for the longitudinal cross section of the cylindrical reactor. The plots showed both the lateral and longitudinal variation of the parameters in the reactor. The effect of gas velocity profile in the bed can be visualized by the lateral variation of the contour plots. All the contour plots studied were for 20 minute reduction with 5F gas velocity Figure 5 13 shows the percentage nickel reduced at 900 K and 1000 K. Complete reduction (above 97 %) is observed in the lower regions, and it is much larger for 1000 K than for 900 K reduction. The change in percentage reduction is also very fast in the bottom layers as indicated by the close association of contour lines. The percentage iron reduced at 900 K and 1000 K is shown in figure 5 14. The iron reduction rate is faster in the lower layers, and particularly so for the 1000 K plot, and very slow in the upper layers Gas composition profile (figure 5 15) shows a very gradual change in gas composition from lower to upper layers. For 900 K the gas composition is below 65 % in the top position and it is below 57 % for 1000 K reduction, indicating that utilization of the reactant gas is better at 1000 K The gas and solid temperature profile for reduction at 1000 K is shown in figure 5 16. The initial temperature for gas and solid temperature was 1040 K. The temperature drops shown in the figure is due to the endothermic nature of the reduction reaction with hydrogen. The temperature difference between gas and solid is maximum at the lower layers where the gas is entering at 1040 K and the solid temperature is about 1020 K. At the top layer the gas-solid temperature difference is about 4 K.
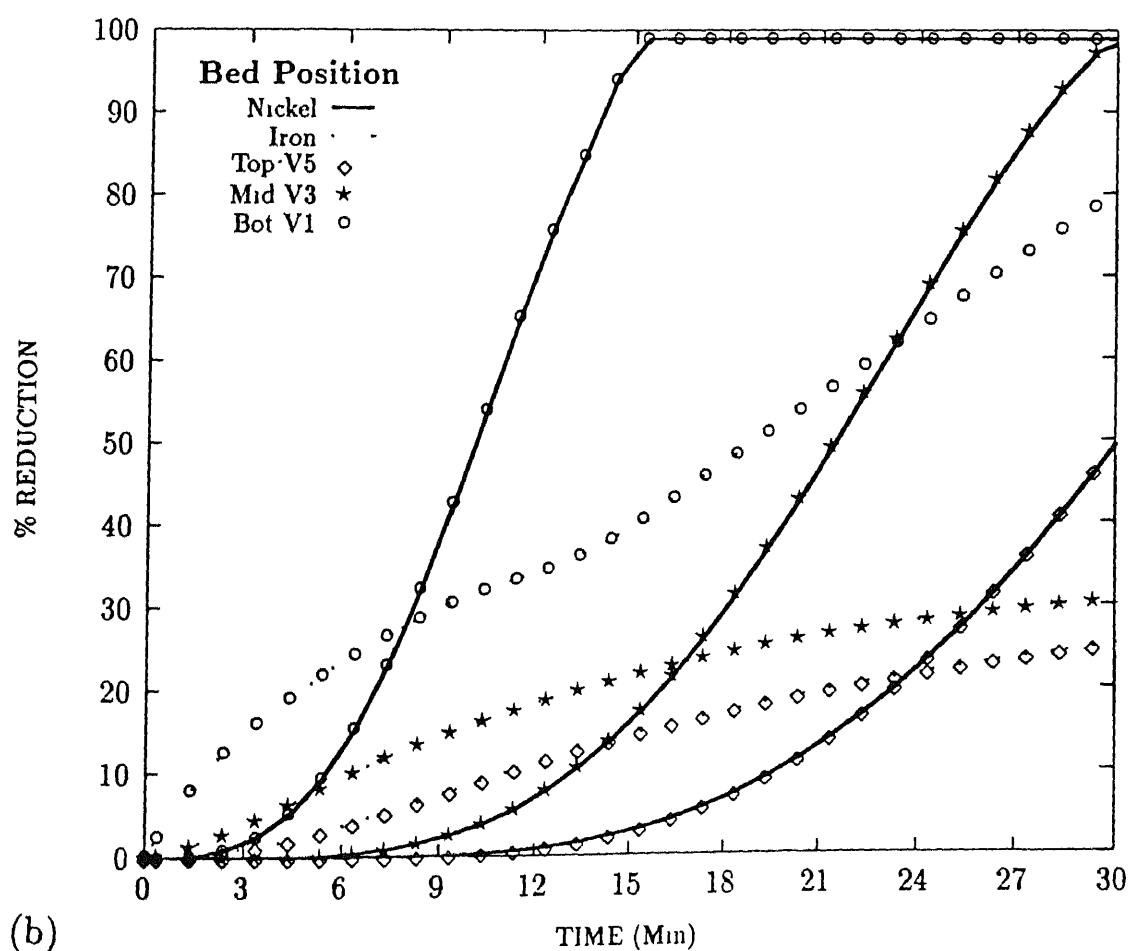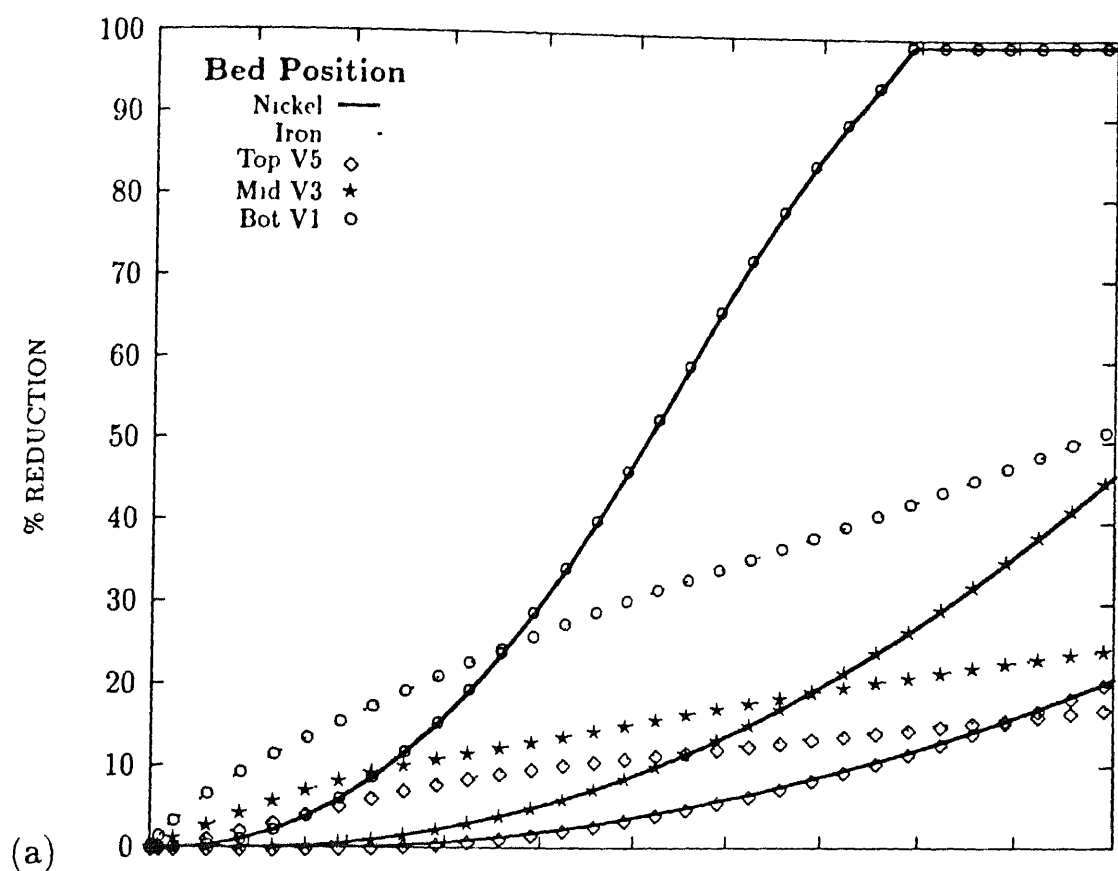
Figure 5 10· Reduction rate of nickel and iron in the top, middle and bottom layers at : (a)
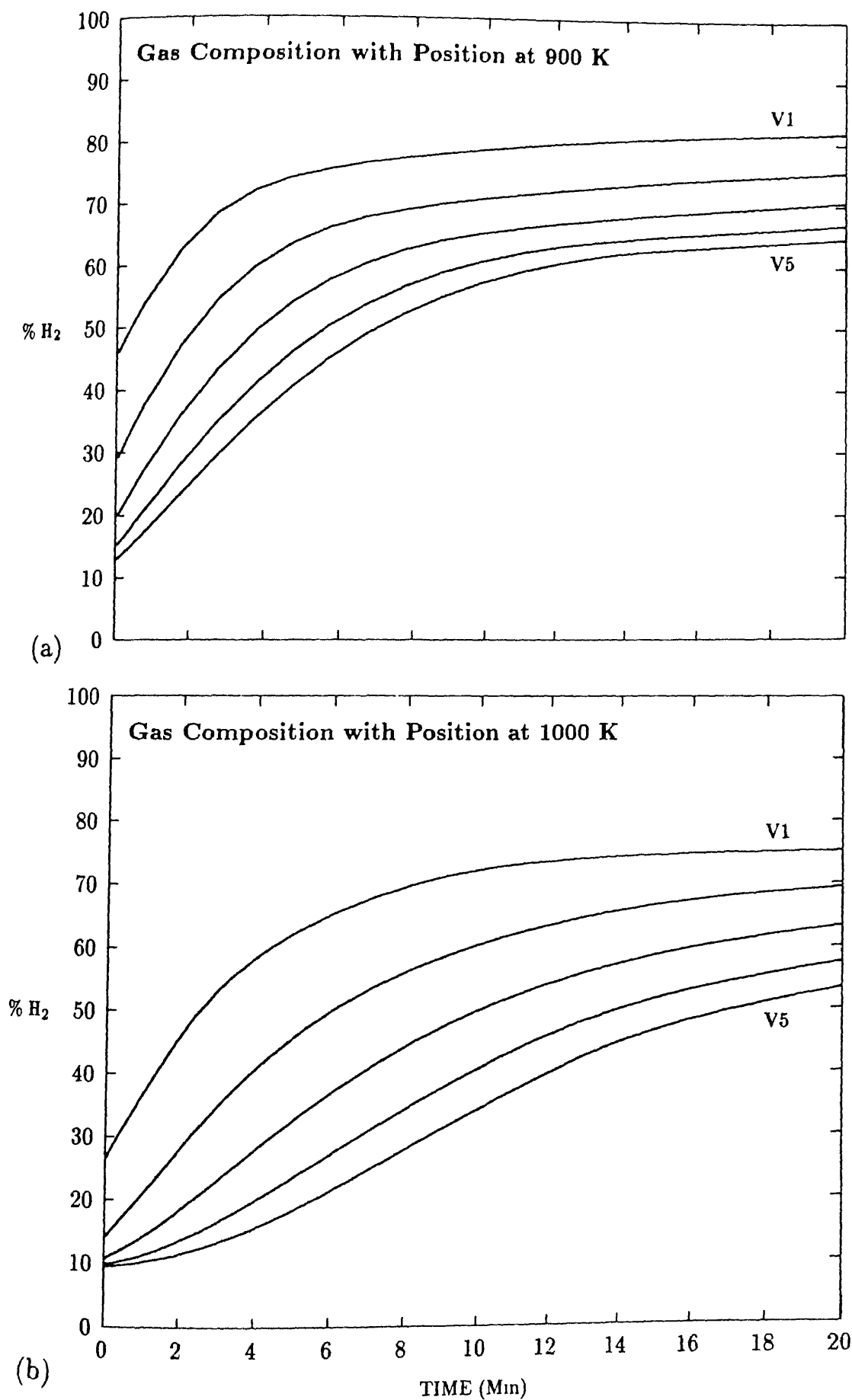
Figure 5 11· Gas concentration variation in the five layers with time at : (a) 900 K and (b) 1000 K
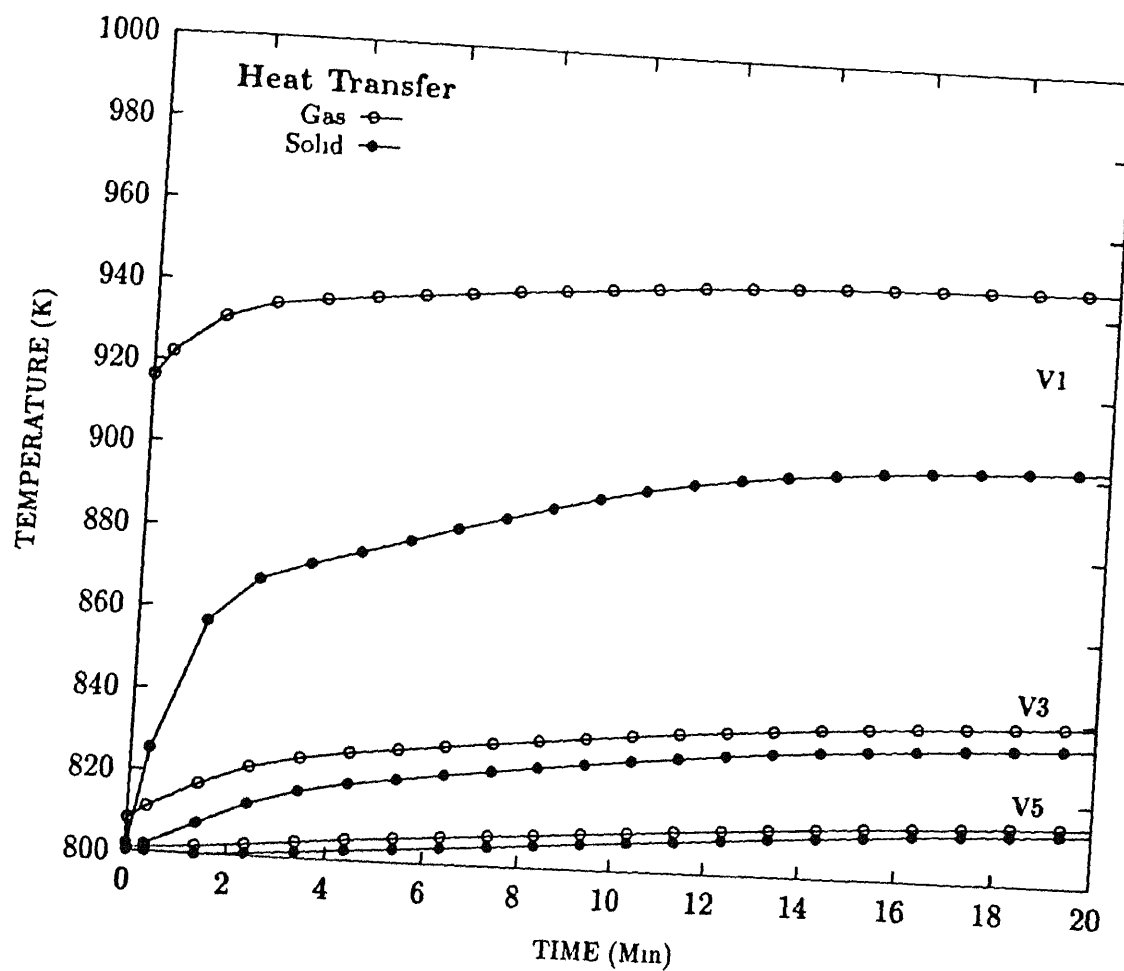
Figure 5 12· Gas and Solid temperature variation with time at the top, middle and bottom layers, for initial gas temperature of 1000 K and solid temperature of 800 K.

In general the parameters like percentage reduction, gas composition and temperature have lower values in the central region and higher value near the walls This is expected since gas velocity is higher near the cylinder wall The lateral variation of the parametric values are not very significant in the present case. This may be due to the fact that the diameter of the cylinder is only 4 cm, and the diffusivity of hydrogen is very high. The effect may be significant for larger diameter packed beds as used in industrial packed beds, and for reduction with carbon monoxide which has much lower diffusivity than hydrogen.

5.7.6 Parametric Study

The effect of parameters like pellet size and gas composition is studied computationally for 20 minutes reduction at 900 K and 1000 K. The effect of pellet size on the reduction profile is shown in figure 5.17 The effect was found to be, not very significant for the selected size range It is relatively more significant for nickel which has higher reduction rate, and in the bottom layer where pure hydrogen comes in contact with the pellets. In the upper layers the effect is insignificant for both nickel and iron reduction.

Figure 5 18 shows the effect of inert gas like nitrogen on the reduction profile. The trend in the reduction profiles for nickel and iron remained the same and the decrease in percentage reduction is also more or less proportional with the decrease in hydrogen concentration. The effect is more prominent in nickel at 1000 K

The effect of water vapor, which is the product gas formed during the reduction process is studied next, and shown in figure 5.19. Significant decrease in percentage reduction is observed for both iron and nickel reduction profiles. The effect is more prominent in the lower regions and gradually diminishes in the upper regions, where the gas always contains considerable amount of water vapor With the addition of 20 % water vapor iron reduction rate remained slow through out the bed without showing any sharp rise in the bottom layers, giving rise to good selective reduction at 1000 K. The iron reduction at the bottom position dropped from 80 % to about 33 %, and although there is some drop in nickel reduction rate, the over all selectivity for nickel reduction improved.

For the 900 K reduction, the drop in percent reduction for nickel is very sharp from about 100 % to 43 % in the lower most position, and although there is a similar decrease from more than 50 % to about 25 % for iron reduction, the selective reduction is not better due to the sharp fall in nickel reduction
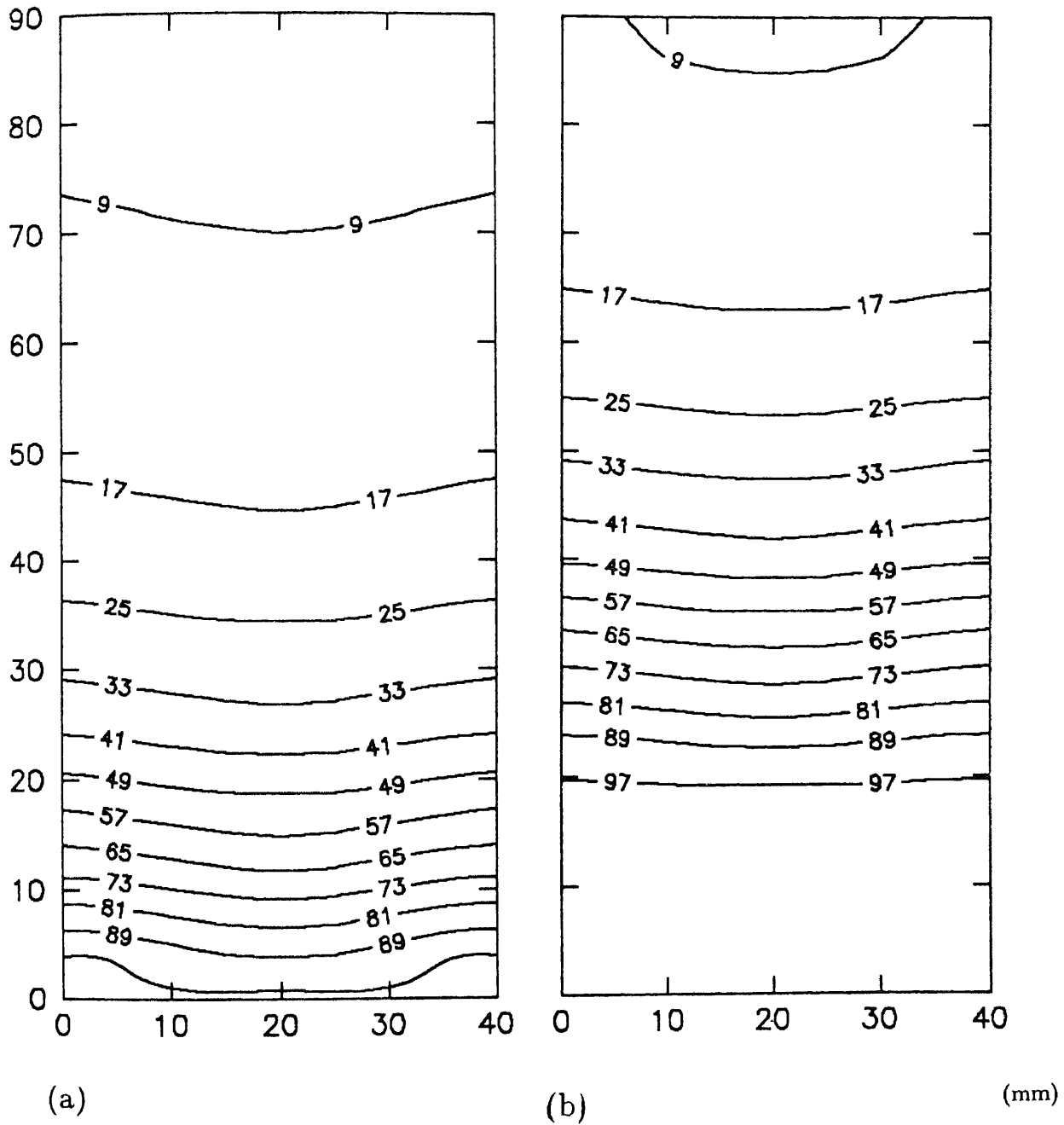
Figure 5 13: Contour plots for nickel reduced for 20 min under vertical gas flow condition at (a) 900 K and (b) 1000 K

(a)   (b)   (mm)
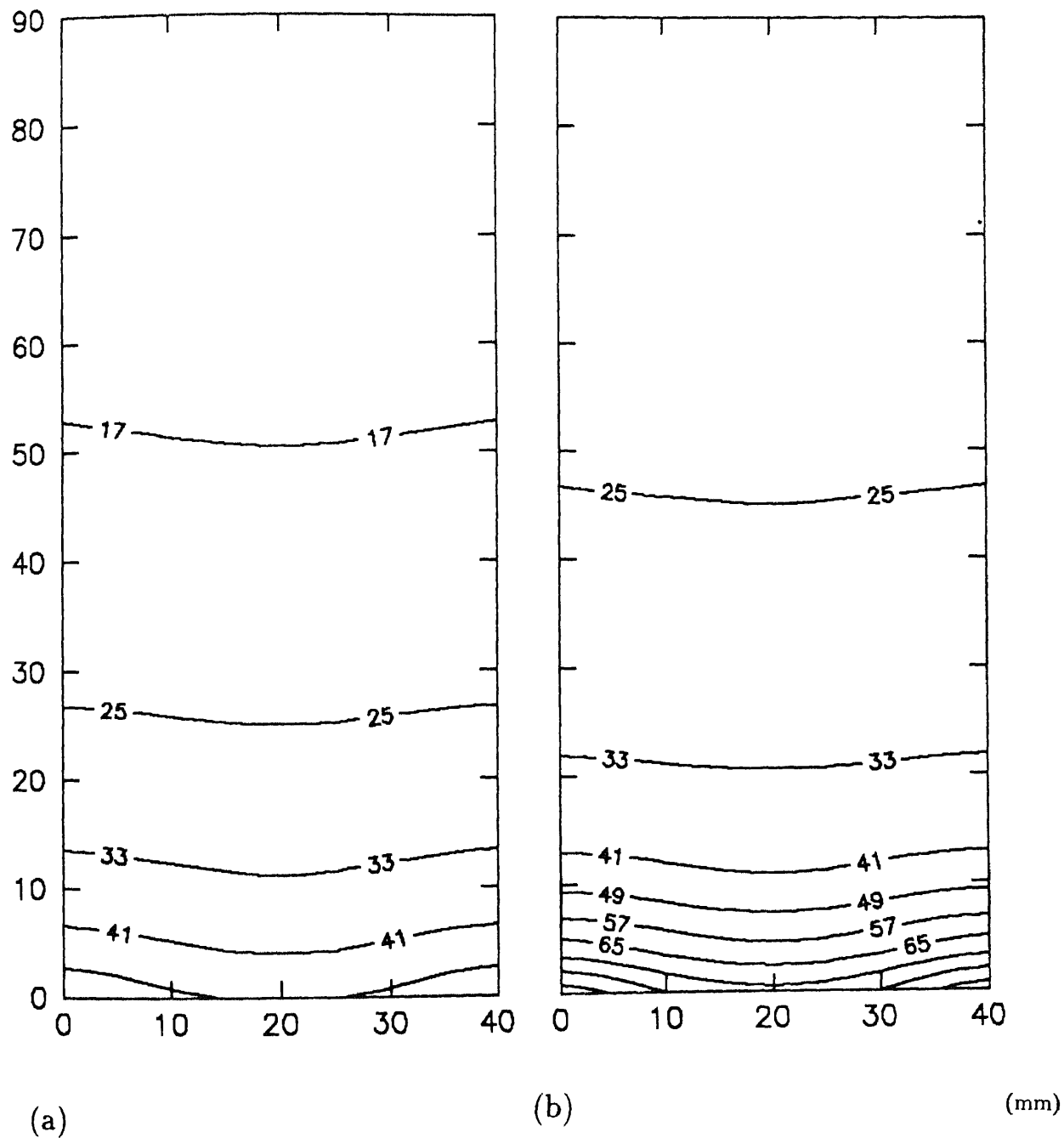
Figure 5.14: Contour plots for iron reduced for 20 min. under vertical gas flow condition at · (a) 900 K and (b) 1000 K.
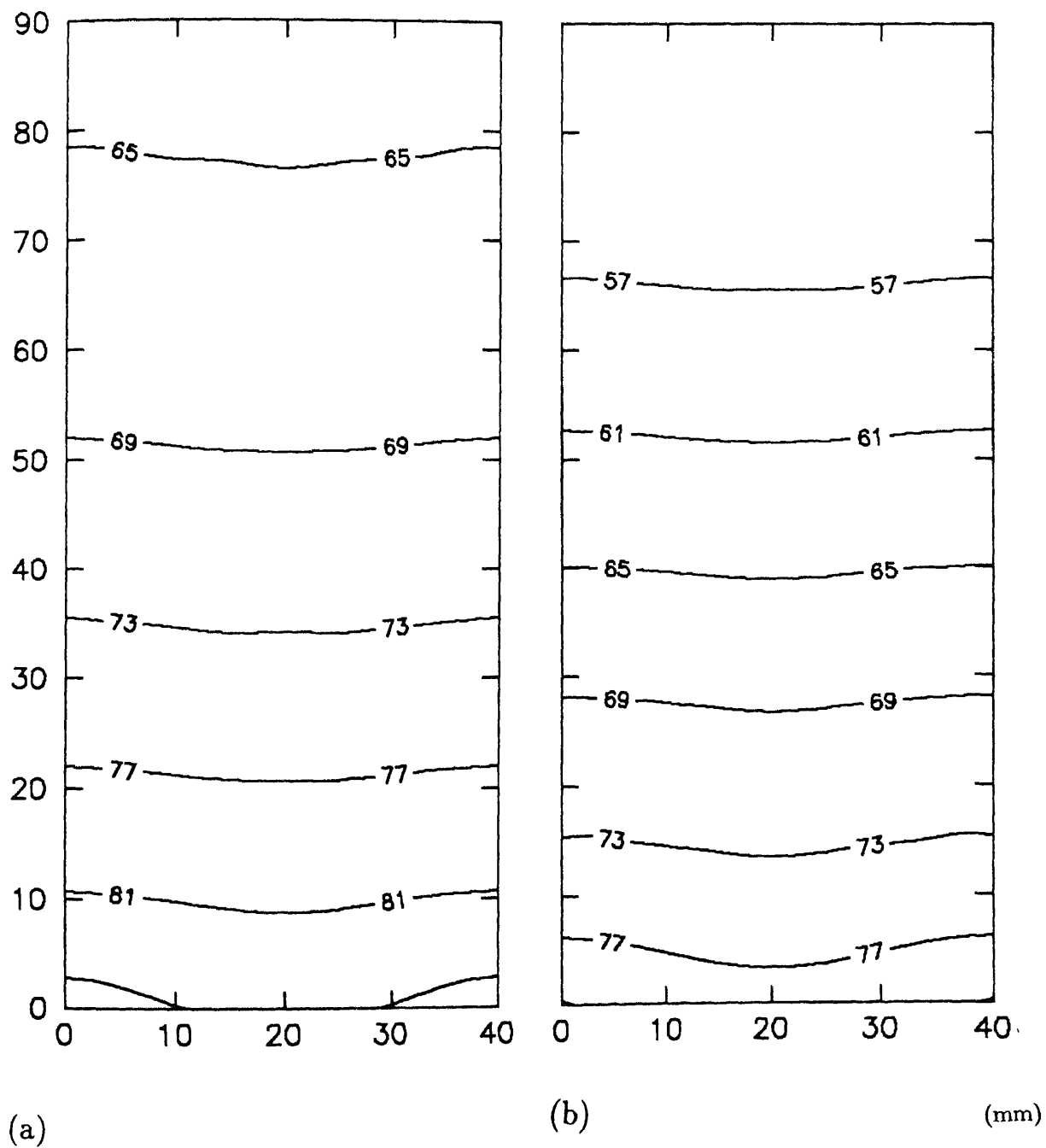
Figure 5 15. Contour plots for hydrogen concentration after 20 min. reduction at : (a) 900 K and (b) 1000 K
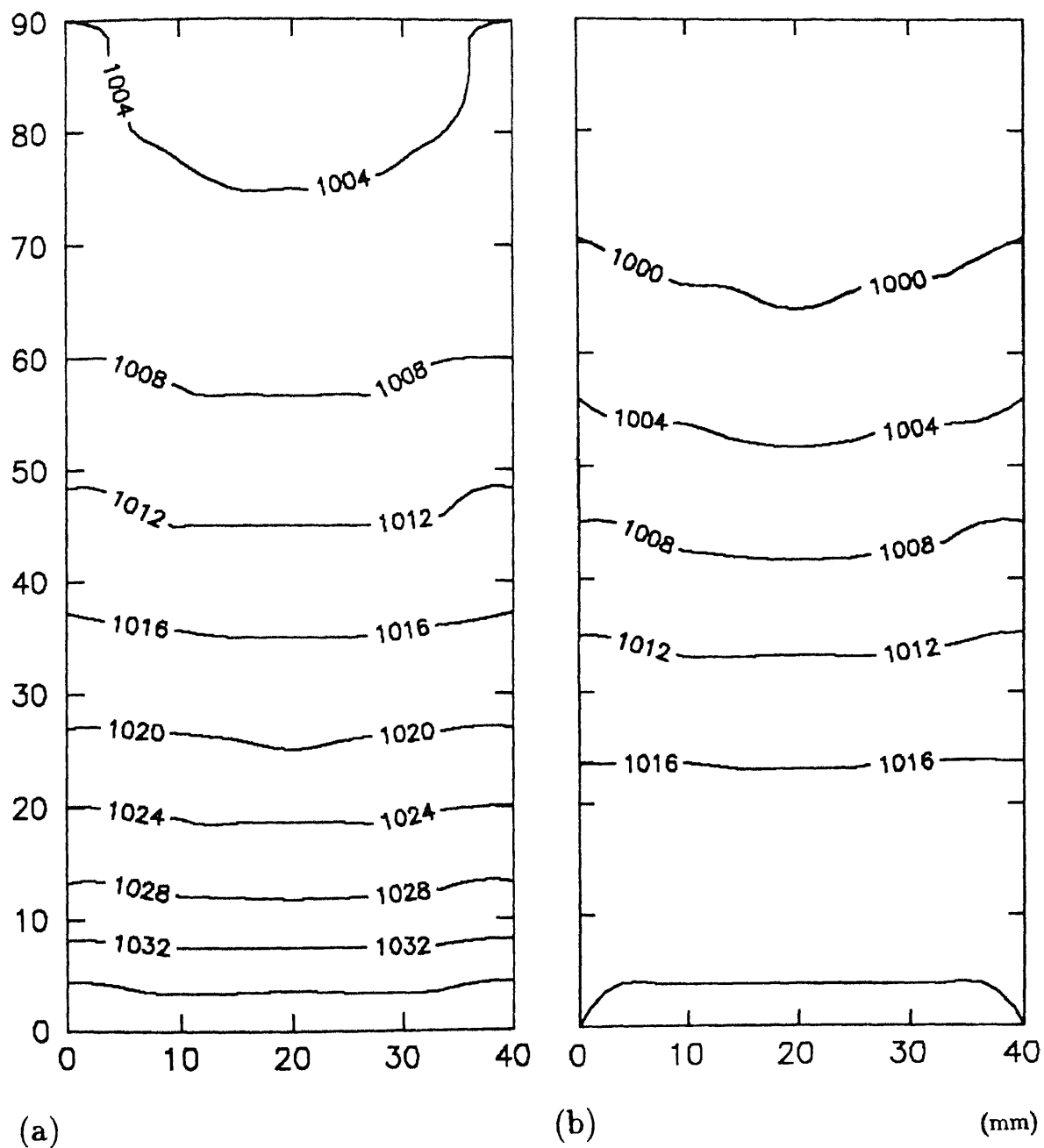
Figure 5 16: Contour plots for the gas and solid temperature after 20 min. reduction. The initial gas and solid temperature is 1040 K (a) gas (b) Solid

From this observation we can say that drop in iron reduction rate after wüstite formation is mainly due to the low equilibrium partial pressure of water vapor for wüstite reduction. Under industrial conditions the reducing gas always contains some water vapor, and so reduction becomes very slow at 900 k Therefore roasting operations are generally conducted at around 1000 K. With proper understanding of the process, the small amount of initial water vapor concentration can be used advantageously for getting better selective reduction for nickel

5.8 Concluding Remarks

The experimental and simulation study of the reduction process under vertical gas flow condition gave us a good understanding about the process, and the effect of some of the important process parameters. The salient features of the process can be summarized as given below.

1. The experimental and simulation study showed reasonably good matching establishing the validity and applicability of the model for studying the process.

2. Both the mixed oxide mechanism and complex oxide mechanism predicted very similar trends for nickel reduction, and any one of them can be used for the simulation study of the process. In the present study complex oxide mechanism is employed due to its better predictions at some particular positions like, the topmost layer where reduction is minimum.

3. The effect of velocity profile for the present conditions is found to be not very significant. The reasons may be, high diffusivity of hydrogen and much smaller diameter of the cylindrical reactor compared to the industrial shaft furnace

4. Reduction rate of iron is initially much faster due to the higher rate of reduction of hematite and magnetite and higher equilibrium concentration of water vapor than wüstite. After the wüstite formation iron reduction rate falls significantly mainly due to the low equilibrium water vapor concentration for wüstite reduction. Nickel reduction increases sharply after the formation of wüstite when it is unlocked from the complex oxide structure.

5. The effect of pellet size is not very significant for the size range of 2 to 8 mm, and it is relatively more significant for nickel in the lower layers where reduction rate is faster.

(a)

(b)

BED HEIGHT (mm)
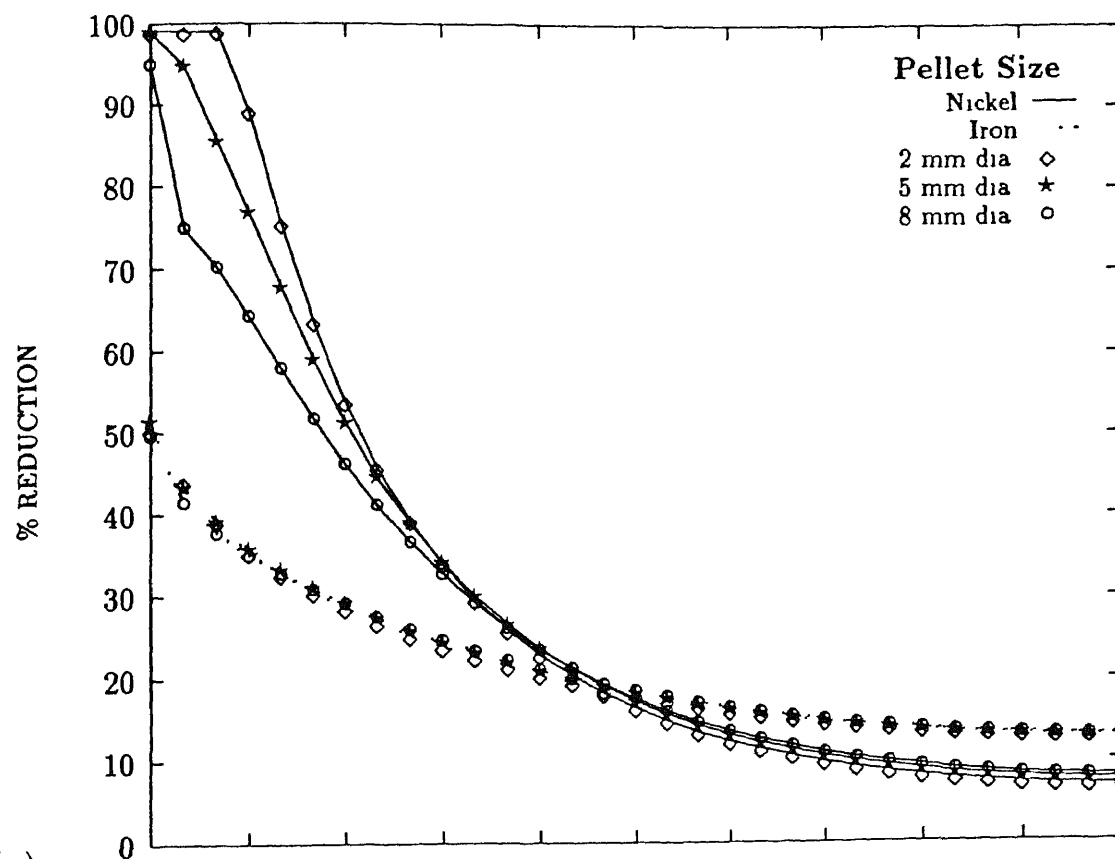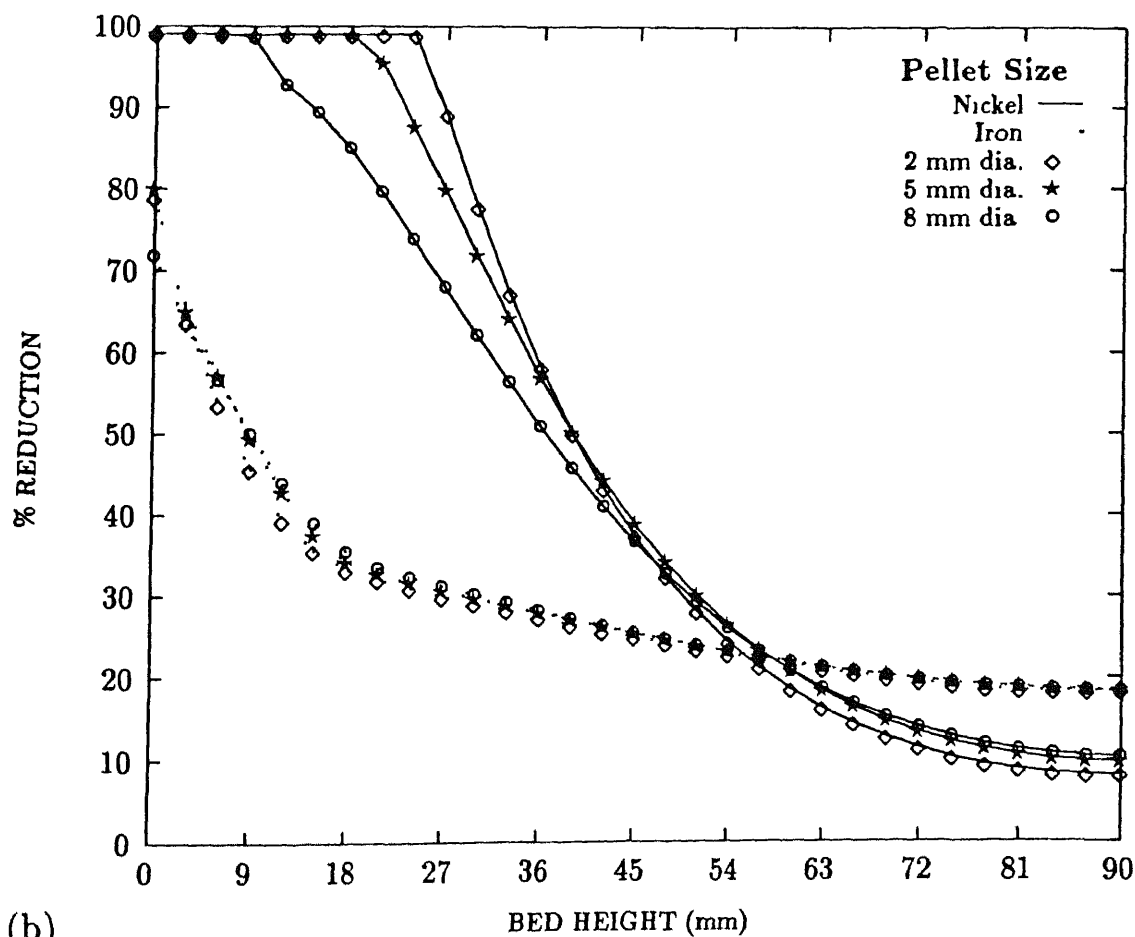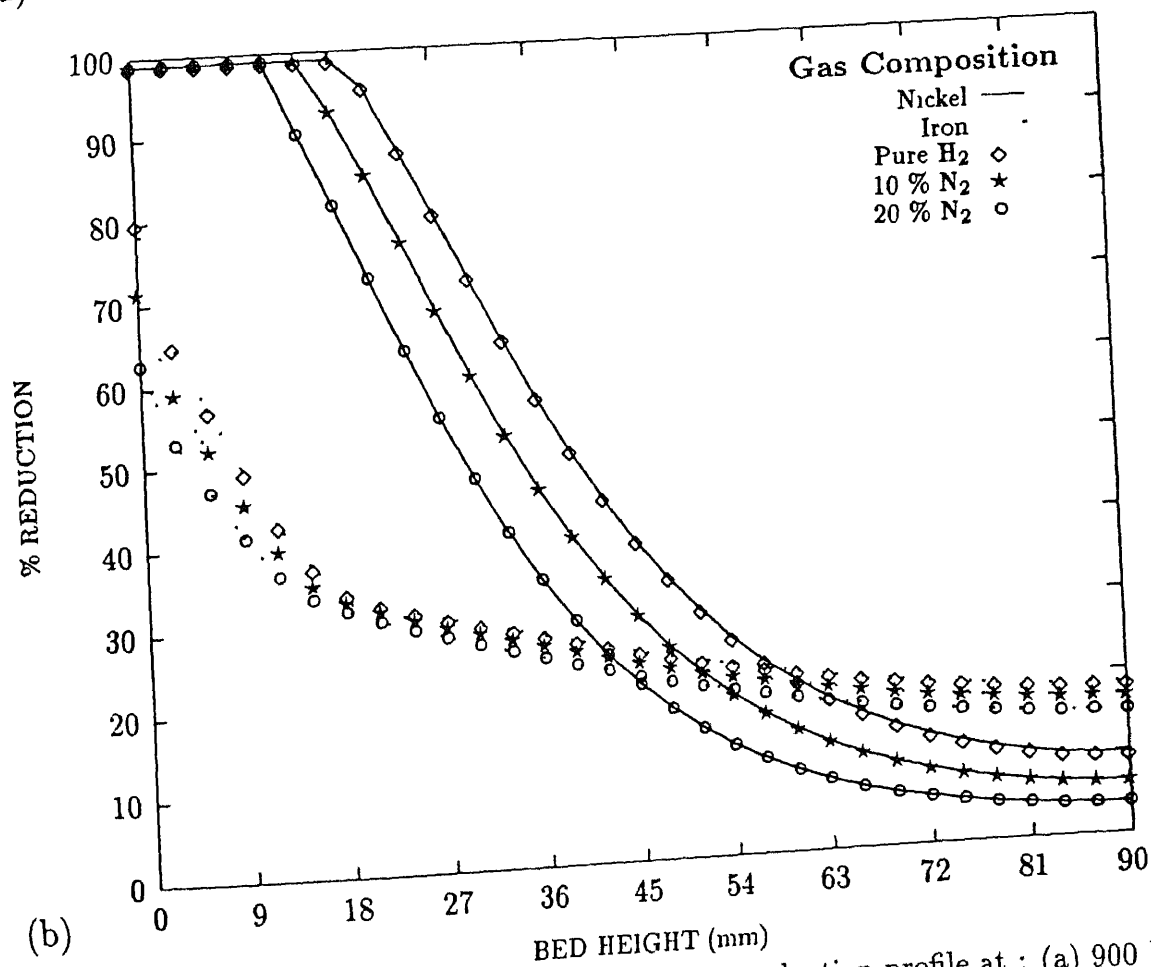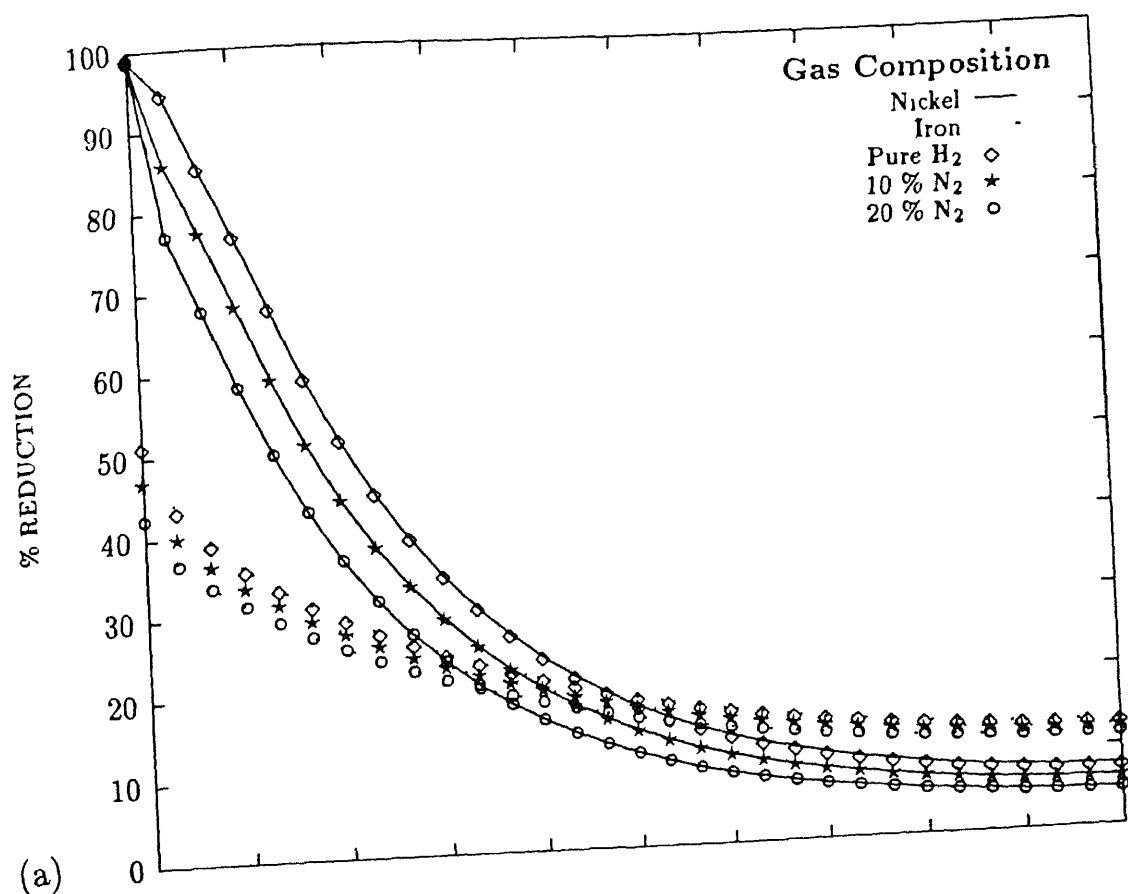
Figure 5.18 Effect of inert gas like nitrogen on 20 min. reduction profile at : (a) 900 K and (b)
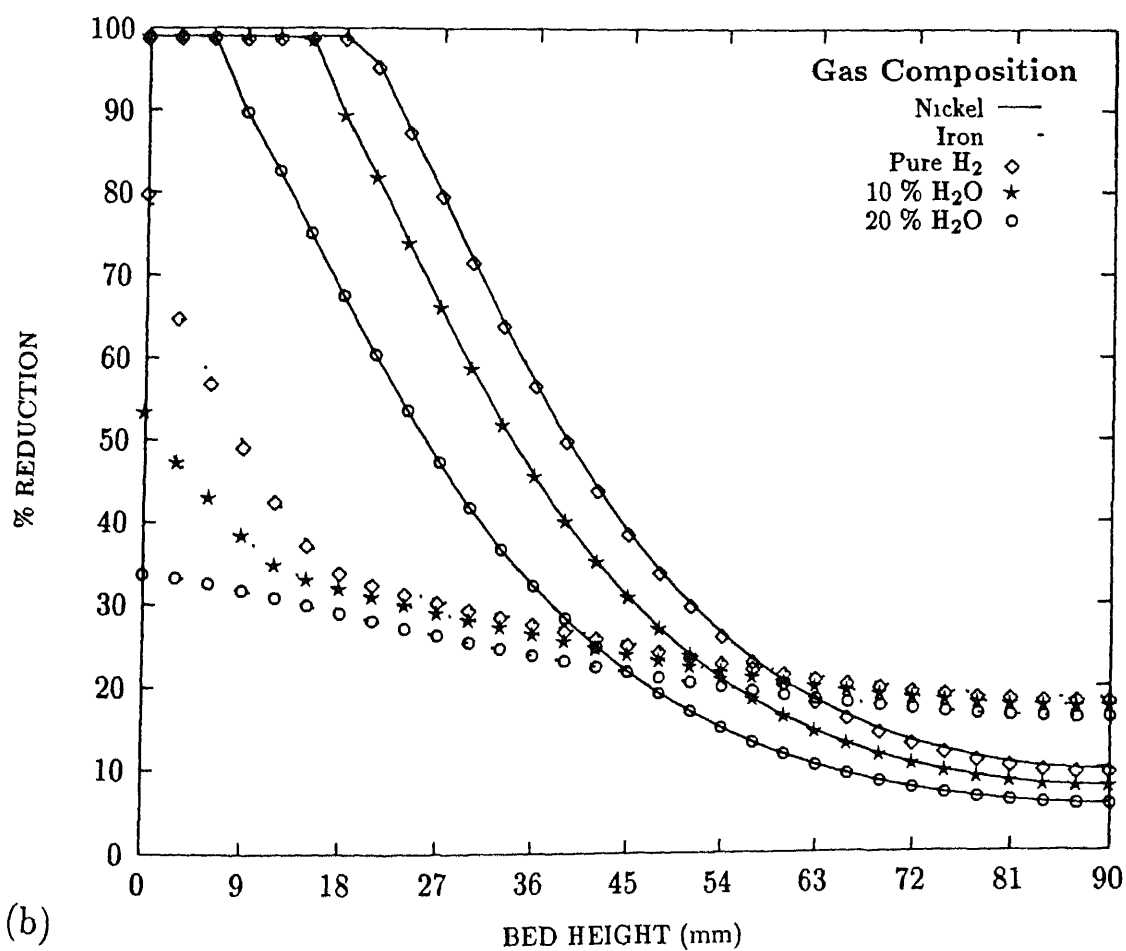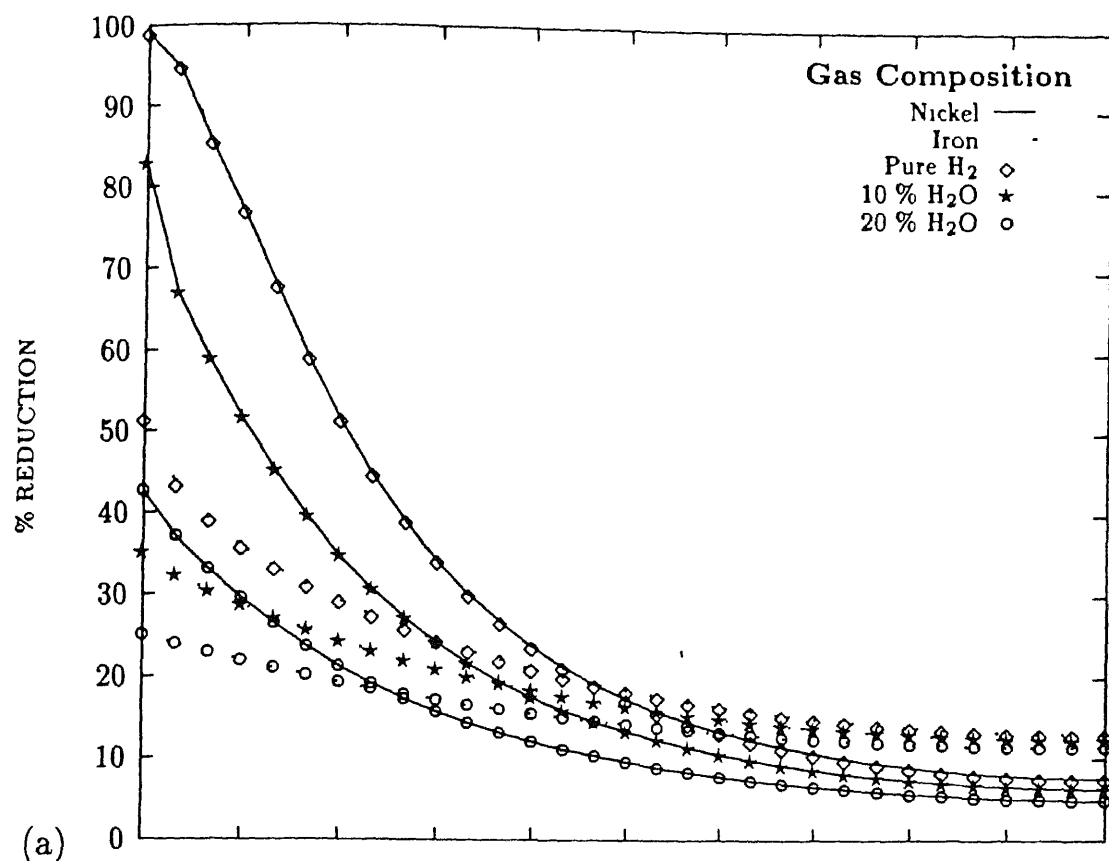
Figure 5.10. Effect of water vapor on 20 min. reduction profile at · (a) 900 K and (b) 1000 K

6 The effect of inert gas like nitrogen is proportional with the decrease in hydrogen concentration, and the reduction profile of both nickel and iron remains more or less the same

7 There is a strong effect of water vapor concentration on both iron and nickel reduction and it is more prominently visible in the lower layers where gas first comes in contact with the pellet. The lowering of reduction rate is relatively stronger in iron than in nickel at 1000 K, giving rise to good selective reduction of nickel At 900 K, reduction rate of both iron and nickel decreased considerably giving rise to an overall poor reducibility.

8 The model can be easily extended for the moving bed reactors like shaft furnaces shown in figure 2.21, by considering a moving bed or solid velocity, as described in Chapter 7 for MHF model, which has moving beds in horizontal direction.

Chapter 6

REDUCTION IN A FIXED BED REACTOR WITH GAS FLOWING HORIZONTALLY OVER THE BED

Reduction in a fixed bed reactor with gas flowing horizontally over the bed was studied next to get a complete picture of the reduction process in fixed bed reactors The most common examples of this type of gas solid contact is in multiple hearth furnace (MHF), and in rotary kiln, although the bed is moving in these industrial furnaces. The effect of time and temperature was studied experimentally by measuring the nickel reduction percentage in different bed depths or layers. The experimental results were then compared with the computationally simulated results to verify the reliability and applicability of the model

6.1   Experimental Setup and Procedure

Experiments were conducted in a rectangular stainless steel box with arrangements for gas inflow from one side and out flow from another side as shown in figure 6.1. The stainless tubes for gas inlet and outlet and were passed through a hole from the back of the muffle furnace The gas inlet was from the more distant side of the hole in the furnace so that the gas travels a longer distance through the inlet tube inside the furnace, to have sufficient time for attaining the furnace temperature The reactor was filled with five layers of pellets separated by wire mesh having a total bed height of about 6 cm as shown in figure 6.1. The box was made air tight to avoid atmospheric oxidation by using a mixture of white cement, asbestos wool and

water. The whole assembly was then inserted in the muffle furnace and heated to the desired temperature and flushed with nitrogen before passing hydrogen for conducting the experiments. The arrangements for passing gas and temperature control were similar to the single pellet experimental arrangement shown in figure 3 5. After conducting the reduction experiment the box was taken out and cooled to room temperature, under stagnant H_2-H_2O atmosphere About 3 5 grams of the reduced pellet sample were then taken from each layer to analyze the amount of nickel reduced.

6.2 Formulation for Modeling the Fixed Bed Reactor

For simulating the reduction process in the rectangular reactor two dimensional Cartesian coordinate system was chosen considering negligible lateral gas velocity . Mass transfer from the bulk gas to the solid surface depends on the velocity profile of the gas over the bed. For computing the gas velocity profile, steady state stream function - vorticity formulation was employed, since the total number of moles are conserved in the reduction reaction This velocity profile can be used throughout the reduction process, leading to a quasi-steady state formulation.

For describing the reduction process four set of transient differential equations are solved simultaneously as given below :

- Solid phase thermal energy balance

- Gaseous phase thermal energy balance

- Solid phase mass or species balance

- Gaseous phase mass or species balance

The equations were solved by using Crank Nicholson technique, and first order upwinding for the convective terms.

6.3 Parameter Values for the Process

The dimensions of the reactor, gas velocity and value of the parameters used in the process simulation are given in table 6 1. The manometer calibration for gas velocity is shown in figure

A.1 and table A.7 The reaction kinetic parameters like rate constant values are given in table A 22, and the values for diffusivity, heat of reaction, gas-solid heat transfer coefficient values *etc* are taken from table A.24, A.17 and A 27 respectively of Appendix A

Table 6 1. Reactor dimensions and parameter values for horizontal gas flow condition.

PARAMETER	VALUE	UNIT
Reactor Dimensions		(in mm)
Length (x-direction)	60	
Cross wise length (z-direction)	84	
Packed Bed Height (y-direction)	60	
Gas flow zone (y-direction)	24	
No. of Layers	5	
Pellet diameter	5	mm
Average Gas Velocity	8.41	cm/sec at 1000 K
Reynolds number	4 06	
Biot Number at		
900 K	0 21	
1000 K	0 23	
Grid Size		
$\triangle x$	0.3	cm
$\triangle y$	0 2	cm
No. of grid points I_{Max}, J_{Max}	48, 20	
$\triangle t$ (for 900 K)	0.50	sec
$\triangle t$ (for 1000 K)	0.25	sec

6.4   Computational Domain

The computational domain for simulating the reduction process under horizontal gas flow condition is shown in figure 6.2. The solid circles or dots signify the packed bed region, and the empty circles above this zone shows the pure gas phase zone. The gas solid boundary is denoted by GS. The gas entry and exit is shown by EN and EX respectively The solid wall boundaries are denoted by W1, W2, W3 and W4. The bed height and width is 6 cm and the height of the gas flow region is 2 cm.

The boundary regions in the computational domain in terms of grid points can be summarized
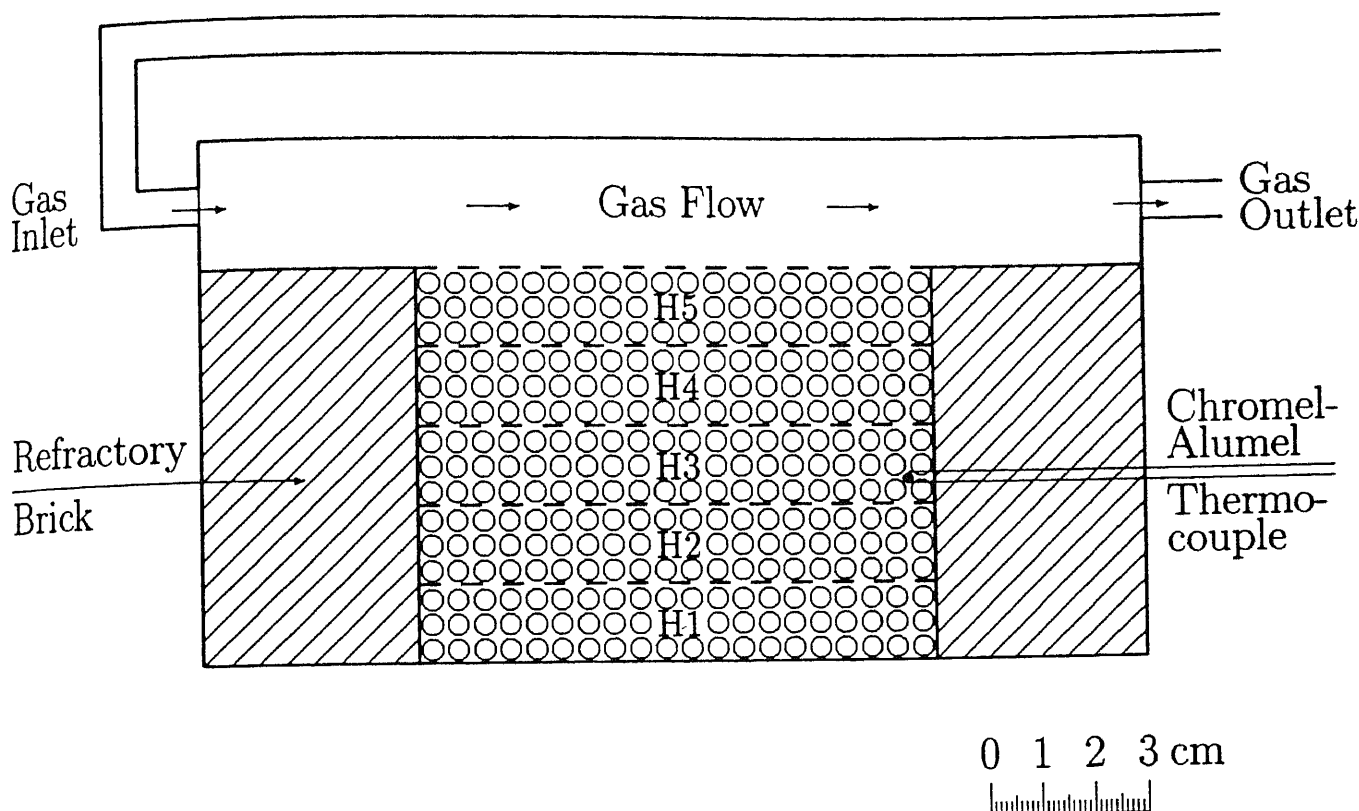
Figure 6 1: Set up for the Horizontal gas flow experiment.
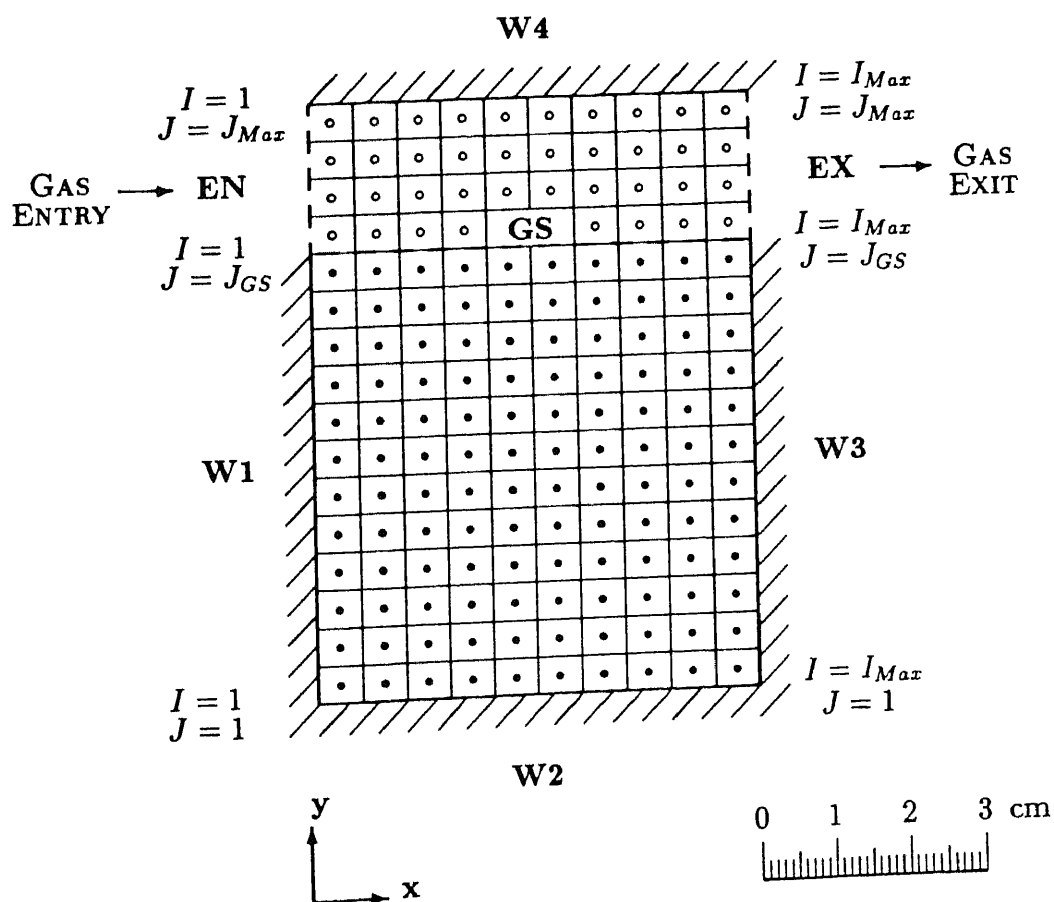
as follows :

W1   Left side Wall $i = 1,\ 1 \leq j \leq J_{GS}$

W3 · Right side Wall $i = I_{Max},\ 1 \leq j \leq J_{GS}$

W2 : Bottom boundary : $1 \leq i \leq I_{Max},\ J = J_{Max}$

W4 : Upper boundary : $1 \leq i \leq I_{Max},\ J = J_{Max}$

GS · Gas-Solid boundary · $1 \leq i \leq I_{Max};\ J = J_{GS}$

EN   Gas Entry . $i = 1,\ J_{GS} \leq j \leq J_{Max}$

EX · Gas Exit : $i = I_{Max};\ J_{GS} \leq j \leq J_{Max}$

6.5   Governing Equations

The gas velocity profile over the bed was solved for steady state conditions, since the total no of moles remained conserved during the reduction process, as mentioned in the previous Chapter. All the other parameters were evaluated for transient conditions. The equations were non-dimensionalized for simplification and easy scale up for the model, and the non-dimensional terms are defined in the list of non-dimensional terms in table 4 2 of Chapter 4. The boundary conditions are implemented by virtual point method coupled with the main equation in most of the cases. The initial condition for the parameters are summarized below :

For $t = 0;\quad (1 \leq i \leq I_{Max};\ 1 \leq j \leq J_{Max})$

1. $T_{s(i,j)} = T_{s,int} = T_{s,w}$

2. $T_{g(i,j)} = T_{g,int}$

3. $G_{H(i,j)} = G_{H,int}$

4 $X_{i(i,j)} = 0$

6.5.1 Gas Flow Field by Stream function and Vorticity method

The gas flow field over the horizontal bed in the computational domain is denoted by the open circles in figure 6 2, and is solved by stream function - vorticity method. The gas velocity inside the packed bed is considered to be zero

The governing equations of motion in two dimensional Cartesian coordinate system are as mentioned before in Chapter 4. The four set of simultaneous equations given by eqn.(4.21), (4 22) and (4 19) are solved for evaluating ψ, ω, V_x and V_y

Boundary Conditions

The computational domain for gas velocity is denoted by open circles in figure 6.2. There is solid boundary at the upper and lower positions (W4 and GS), and the inlet and outlet is denoted by EN and EX.

W4 and GS : Upper and Lower Boundaries

Considering no slip condition at the upper and lower boundaries we get :

$$\left.\begin{array}{rcl} V_{x(i,j)} &=& 0 \\ V_{y(i,j)} &=& 0 \end{array}\right\} \tag{6.1}$$

Solid boundaries always have constant stream function value, and any value can be chosen for one of them, while the others will be dependent on it. In this problem stream functions were taken as :

$$\left.\begin{array}{rcl} \psi_{(i,J_{GS})} &=& 0 \\ \psi_{(i,J_{Max})} &=& (J_{Max} - J_{GS}) \, \Delta \, y V_{x,av} \end{array}\right\} \tag{6.2}$$

The wall vorticity is an extremely important evaluation. At no slip boundaries, vorticity (ω) is produced. It is the diffusion and subsequent advection of the wall produced vorticity which governs the physics of the process The stream function value remains constant under no slip boundary condition in the lower and upper surfaces along x–direction (which means $\frac{\partial^2 \psi}{\partial x^2} = \frac{\partial V_y}{\partial x} = 0$) Therefore from eqn (4.21) at the lower and upper surface, by virtual point method we get ·

$$\omega_s = \frac{\partial V_x}{\partial y} = \frac{\partial^2 \psi}{\partial y^2} \quad = \frac{2}{\Delta y^2} \left\{ \psi_{(1,J_{GS}+1)} - \psi_{(1,J_{GS})} \right\} \quad \left.\begin{matrix} \\ \end{matrix}\right\}$$
$$= \frac{2}{\Delta y^2} \left\{ \psi_{(1,J_{Max}-1)} - \psi_{(1,J_{Max})} \right\} \quad \tag{6.3}$$

EN : Inlet Boundary Condition

The inlet boundary condition (at EN) will depend on the physical situation For the axial velocity V_x, uniform or parabolic or any possible profile can be taken Uniform inlet velocity is taken in the present case ·

$$\left.\begin{matrix} V_{x(1,j)} = & V_{av,x} \\ V_{y(1,j)} = & 0 \end{matrix}\right\} \tag{6.4}$$

The stream function at the inlet can be obtained from the axial velocity profile as given below

$$\psi_{(1,j)} = \int_{y_{GS}}^{y_{Max}} V_{x(1,j)} dy \tag{6 5}$$

Vorticity also depends on the inlet velocity profile Greenspan [77] fixed up $\psi(I_{min}, j)$ from the axial velocity profile and assumed $\frac{\partial V_y}{\partial x} = 0$, which results in

$$\omega_{(1,j)} = \frac{\partial V_x}{\partial y} = \frac{\partial^2 \psi}{\partial y^2} \tag{6.6}$$

EX : Outflow Boundary Condition

Outflow boundary conditions cannot be known beforehand, but we can prescribe or set some gradients at the outlet which are physically meaningful We can imagine about continuitive outflow conditions which will ensure smooth transition through the outlet boundary.

For the axial and normal velocities, we have to impose less restrictive type conditions, which are

$$\frac{\partial V_x}{\partial x} = \frac{\partial V_y}{\partial x} = 0 \tag{6.7}$$

Thoman and Szewczyk [78] developed outflow boundary conditions through setting :

$$\frac{\partial \omega}{\partial x} = 0 \qquad (6.8)$$

Then, from $\frac{\partial V_x}{\partial x} = 0$ they derived $\frac{\partial^2 \psi}{\partial x^2} = 0$. For the present condition, this gives :

$$\omega_{(I_{Max},J)} = \omega_{(I_{Max}-1,J)} \qquad (6.9)$$

$$\psi_{(I_{Max},J)} = 2\psi_{(I_{Max}-1,J)} - \psi_{(I_{Max}-2,J)} \qquad (6.10)$$

Solution Procedure

1. The values of stream function (ψ) and vorticity (ω) are initialized at the interior points Taking initial value of zero for vorticity is usually acceptable. For x-direction a uniform value of V_x is taken which is equal to the average velocity in x-direction, and for y-direction the initial guess value is taken to be zero i.e. $V_y = 0$.

   The value of stream function (ψ) is constant at the walls and is taken as zero at the lower boundary, and $V_x dx.J_{Max}$ for the upper boundary For the interior points the initial guess value can be taken as :

   $$\psi = \int_0^h u \, dy \qquad (6.11)$$

2. The appropriate boundary conditions for V_x, V_y, ψ and ω are applied

3. The stream function (ψ) is then calculated everywhere using eqn.(4.21). Under-relaxation type calculation is done, for example .

   $$\psi_{(i,j)}^{n+1} = \psi_{(i,j)}^n + F\left(\psi_{(i,j)}^{n+1} - \psi_{(i,j)}^n\right) \qquad (6.12)$$

   Where, $\psi_{(i,j)}^n$ is the value from previous calculation, $\psi_{(i,j)}^{n+1}$ is the most recent value, and F ($0 < F < 1$) is the under relaxation factor. For the present set of calculations the under relaxation factor is taken as 0.5.

4. V_x and V_y is calculated at all the internal grid points using eqns.(4.19).

5. In a subsequent step vorticity (ω) is calculated at all the interior mesh points using eqn (4.22). Line-by-line method of solution is used by employing a tridiagonal matrix solver [74].

6. The computation process is repeated from step 4 to step 6 until the desired degree of convergence is achieved

6.5.2   Solid Phase Thermal Energy Balance

Solid phase thermal energy balance was solved to consider the non-isothermal nature of the reduction process and also to consider the gas-solid heat exchange   The thermal conductivity of solid is taken equal to the thermal conductivity of the bed   The non-dimensional equation in the packed bed is given by .

$$\frac{\partial T_s}{\partial t} = \left(\frac{\partial^2 T_s}{\partial x^2} + \frac{\partial^2 T_s}{\partial y^2} \right) + Nu(T_g - T_s) + \sum_{i=1}^{i=2} R_{T,i} \frac{\partial X_i}{\partial t} \tag{6.13}$$

Boundary Conditions

W1 and W3 : Zero temperature gradient for solid ·

$$\frac{\partial T_s}{\partial x} = 0 \tag{6 14}$$

W2 and GS : By neglecting the y-direction conductivity we get :

$$\frac{\partial T_s}{\partial t} = \frac{\partial^2 T_s}{\partial x^2} + Nu(T_g - T_s) + \sum_{i=1}^{i=2} R_{T,i} \frac{\partial X_i}{\partial t} \tag{6 15}$$

The boundary conditions are implemented by virtual point method.

6.5.3   Gaseous Phase Thermal Energy Balance

For considering the non-isothermal reduction process and gas-solid heat exchange gaseous phase thermal energy balance also have to be solved along with solid phase energy balance. The gaseous phase is continuous through out the computational domain, and the overall non-dimensional equation applicable throughout the domain is given by :

$$\frac{\partial T_g}{\partial t} + Pe_{T_g} \left(V_x \frac{\partial T_g}{\partial x} + V_y \frac{\partial T_g}{\partial y} \right) = \left(\frac{\partial^2 T_g}{\partial x^2} + \frac{\partial^2 T_g}{\partial y^2} \right) + Nu(T_s - T_g) \tag{6.16}$$

The gas-solid heat transfer term will be absent over the bed, and the convective terms are neglected in the packed bed region. Gas Conductivity in the packed bed region is taken equal to the bed conductivity.

Boundary Conditions

W1 and W3 . Known wall or solid temperature $(T_{s(i,j)} = T_{s,int})$:

$$\frac{\partial T_g}{\partial x} = 0$$

W2 and W4 . Known wall or solid temperature $(T_{s(i,j)} = T_{s,int})$.

$$\frac{\partial T_g}{\partial y} = 0$$

GS No boundary condition is applied here, since the gas phase is continuous along this surface.

EN : Temperature is defined :

$$T_{g(i,j)} = T_{g,int} \tag{6 17}$$

EX Continuity of gas temperature :

$$\frac{\partial T_g}{\partial x} = 0 \tag{6.18}$$

6.5.4 Gaseous Phase Mass or Species Balance

The gaseous phase mass or species balance will determine the gas concentration profile in the reactor which will then determine the reduction rate of the solid The gas phase is continuous through out the computational domain, and the equation in its non-dimensional form is given by ·

$$\frac{\partial G_H}{\partial t} + Pe_G \left(V_x \frac{\partial G_H}{\partial x} + V_y \frac{\partial G_H}{\partial y} \right) = \left(\frac{\partial^2 G_H}{\partial x^2} + \frac{\partial^2 G_H}{\partial y^2} \right) + \sum_{i=1}^{n} R_{G,i} \frac{\partial X_i}{\partial t} \tag{6.19}$$

The gas-solid reaction term is absent above the packed bed, and in the packed bed region the convective terms are neglected since there is no gas velocity. Diffusivity in the packed bed region is less than the molecular diffusion by an amount proportional to the void fraction.

Boundary Conditions

W1 and W3 . Zero flux condition :

$$\frac{\partial G_H}{\partial x} = 0 \qquad (6.20)$$

W2 and W4 : Zero flux condition ·

$$\frac{\partial G_H}{\partial y} = 0 \qquad (6.21)$$

GS : No boundary condition is applied here, since the gas phase is continuous along this surface.

EN : Known concentration of the gaseous phase :

$$G_{H(i,j)} = G_{H,int} \qquad (6.22)$$

EX : Continuity of gas composition :

$$\frac{\partial G_H}{\partial x} = 0 \qquad (6.23)$$

6.5.5 Solid Phase Mass or Species Balance by Grain Model

Grain model is used for predicting the reduction rate of solid due to its simplicity and good accuracy of prediction. The gas concentration at the reaction interface is estimated by using eqn.(3.41), for calculating the reaction rate constant.

$$\frac{dX}{dt} = \frac{k_{/rg}C_A}{C_{Bo}\left[1 + 2\sigma^2\left\{\frac{1}{(1-X)^{1/3}} - 1\right\}\right]} \qquad (6.24)$$

6.6 Computational Procedure

The grid size and the time steps were first estimated by using the Von Neuman stability analysis. The main program and the subroutines used are described, and given in Appendix C. The computations were done in a local area network of HP 9000 Series miniframe systems, and the computation time (real time) is about 8 minutes per 1000 time steps.

6.7 Results and Discussion

Experiments were conducted at two different temperatures for three different time periods and matched with the simulated results obtained from the model developed. Gas velocity profile over the bed has to be obtained first since it will primarily determine the mass transfer of the reducing gas from the bulk phase to the packed bed surface, and also the heat transfer between the gas and solid phase. Process dynamics, contour plots and parametric study of some of the important parameters were done subsequently to evaluate the basic mechanism and kinetics of the process

6.7.1 Gas Velocity Profile

The velocity profile of the gaseous phase over the bed is shown in figure 6.3 The figure shows, fully developed velocity profile is attained within a very short distance from the uniform inlet velocity profile, giving a more or less similar velocity profile over the bed.

6.7.2 Matching between Experimental and Simulated results

The experimental and predicted results at 900 K and 1000 K is shown in figure 6.4 for nickel by grain model, and the modified grain model for the complex oxide mechanism. The predicted iron reduction values are also plotted and shown by large dotted curves. The experimental data points for nickel reduction are given in table A.16 in Appendix A

Very small amount of nickel reduction is observed in the two lower most layers for 900 K reduction The predicted values by grain model is much higher for nickel reduction at those regions, but there is a considerable decrease in the predicted nickel reduction by the complex oxide mechanism which compares well with the experimental results. Iron reduction in the lower layers is below the wüstite formation value of 33 % and so most of the nickel is not available for reduction leading to a very low amount of nickel reduction. In the other regions the trend for experimental and predicted results are very similar for both the mechanisms and the matching is within the experimental error range. For the further study of the process complex oxide mechanism is chosen due to its better prediction of 900 K results in the bottom layers.

The probable source of error in the experimental results may be due to the following reasons
:
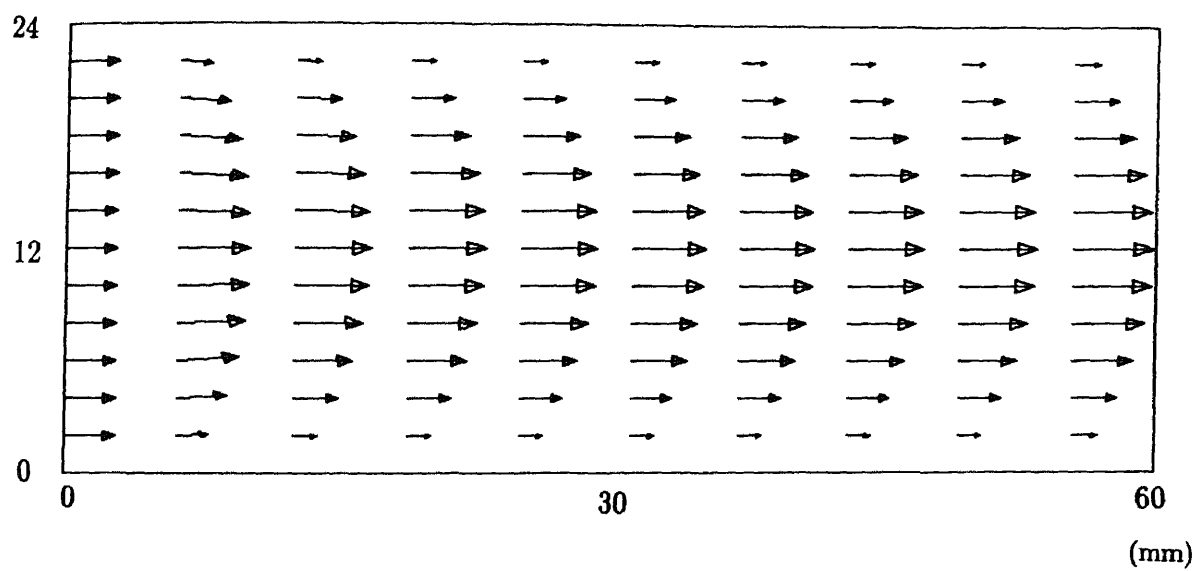
Figure 6.3: Vector plot for the gas velocity profile over the bed.
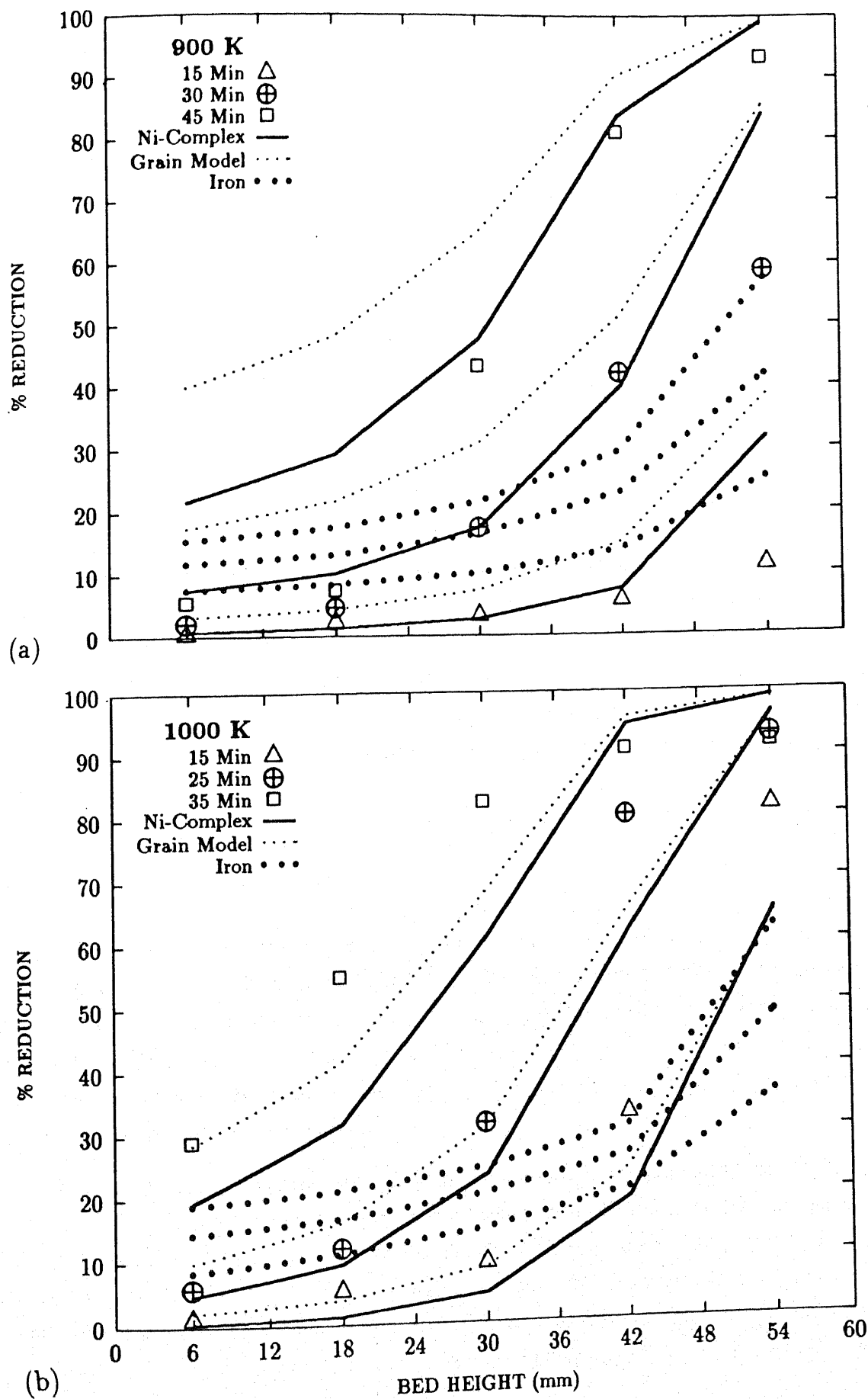
Figure 6.4: Experimental results for nickel reduction and the computationally predicted nickel and iron reduction at : (a) 900 K and (b) 1000 K.

1 Oxygen entry from the atmosphere during removal of the reactor from the furnace Error due to this effect is less here than vertical flow condition since there is a large gaseous phase over the packed bed where the oxygen will get diluted and form water vapor with the residual hydrogen.

2 The presence of residual hydrogen in the reaction chamber after the experiments

3. The representative samples analyzed may vary slightly from the average composition of that layer.

6.7.3 Reproducibility and Grid Independence Test

The results for reproducibility and grid independence test are shown in figure 6 5. Reproducibility of the experimental results were checked by conducting a second experiment at 1000 K for 15 minutes of reduction, and the results showed good agreement among them in general, although at 42 mm bed height the deviation is about 15 %. The computational grid independence test was done by reducing the grid size and time step by half, and the results showed a difference of about 2-3 % for nickel reduction in the upper most layers and the error is even less in the lower layers.

6.7.4 Process Dynamics

Process dynamics can be studied by plotting the change in parametric values at the middle of the layers Figure 6.6 shows the rate of reduction of nickel and iron at the top, middle and bottom layers. The rate of reduction of iron is faster initially and slower afterwards while nickel reduction is very slow initially and increases very rapidly afterwards, particularly in the top layers. The reduction rate in the lower layers is considerably slower since the gas has to diffuses through the upper layers to reach the lower layers.

The gas composition variation with time in the five layers are shown in figure 6.7. During the initial stage of reduction, hydrogen gas concentration is much lower and it increases gradually with time, since hematite and magnetite has faster reduction rate and higher equilibrium partial pressure for water vapor. The overall hydrogen gas concentration is less for identical positions for the 1000 K reduction than at 900 K, indicating that utilization of reactant gas is better at 1000 K than at 900 K. Gas solid heat transfer rate under horizontal flow condition can be observed
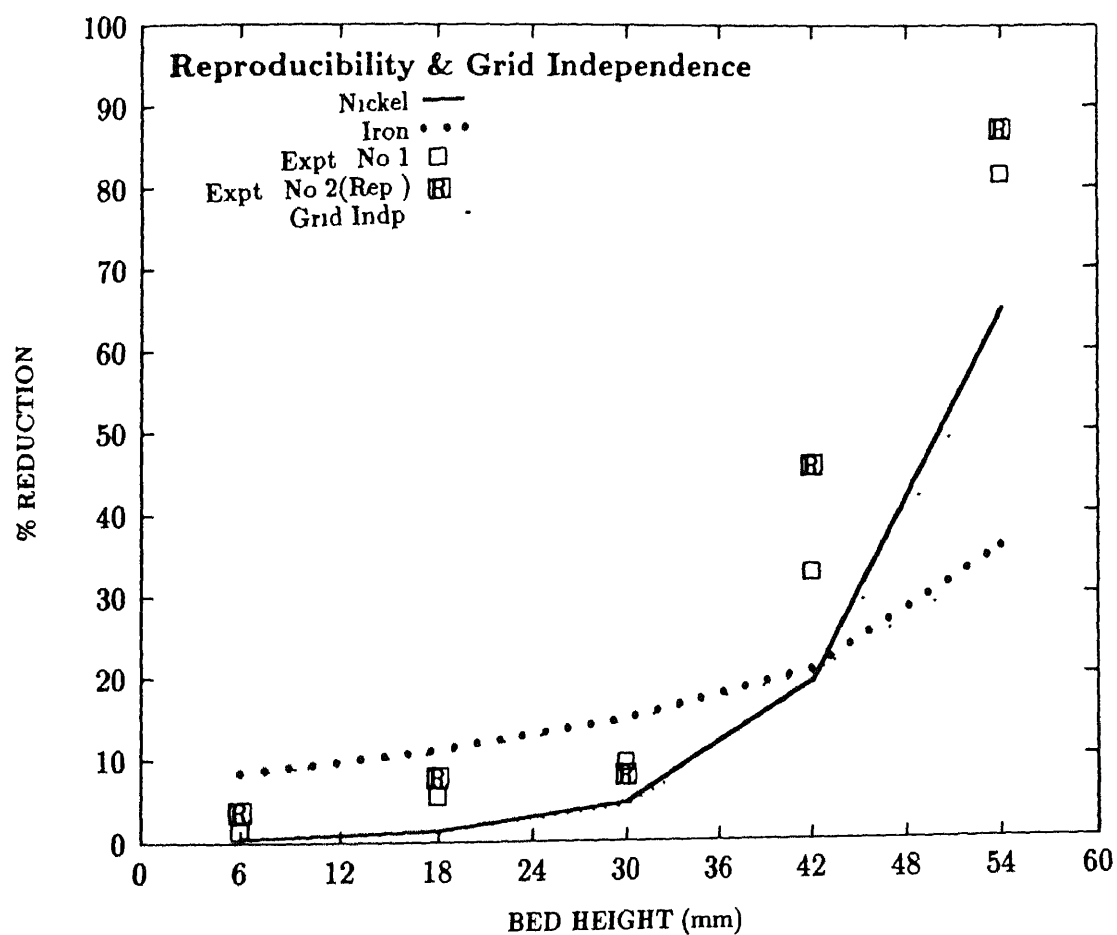
Figure 6.5: Experimental reproducibility and grid independence test for the results of 15 minutes reduction at 1000 K.
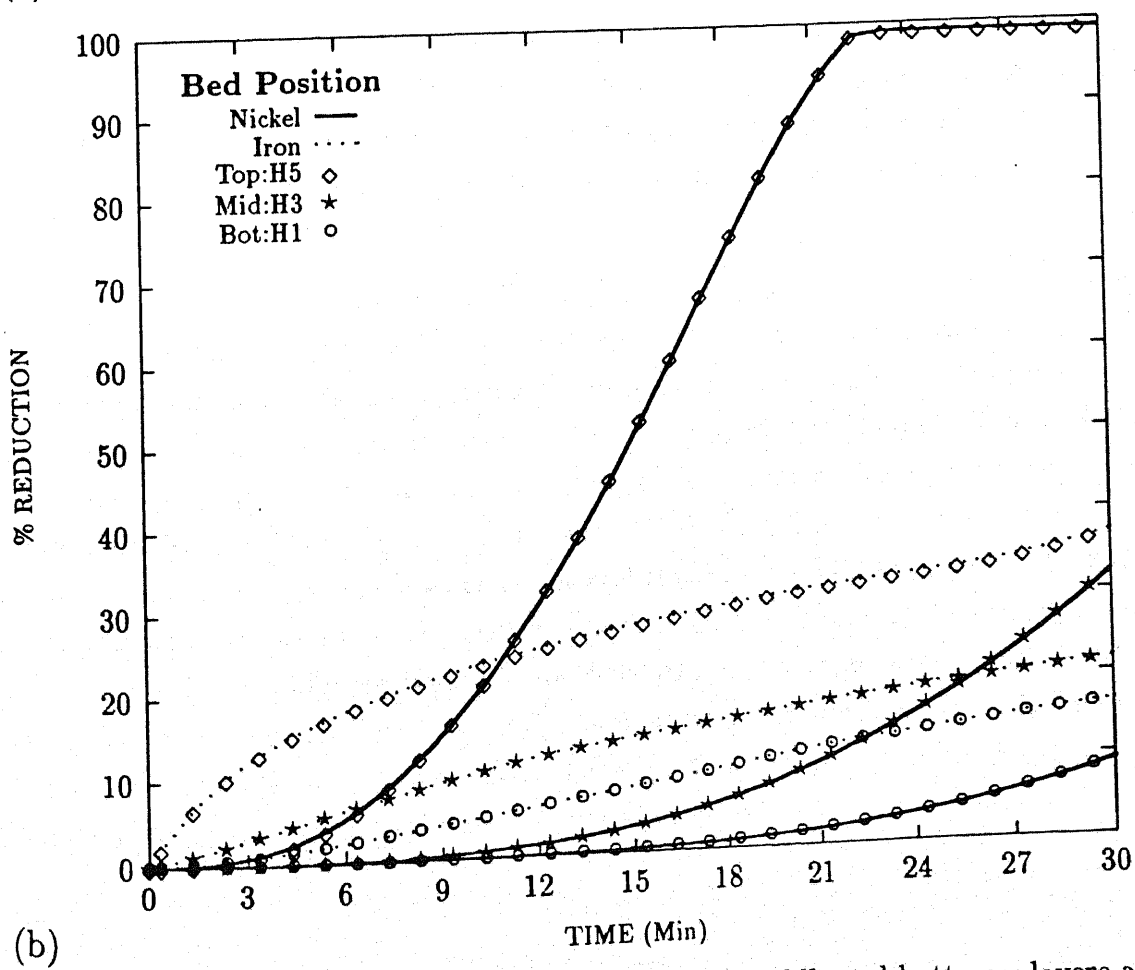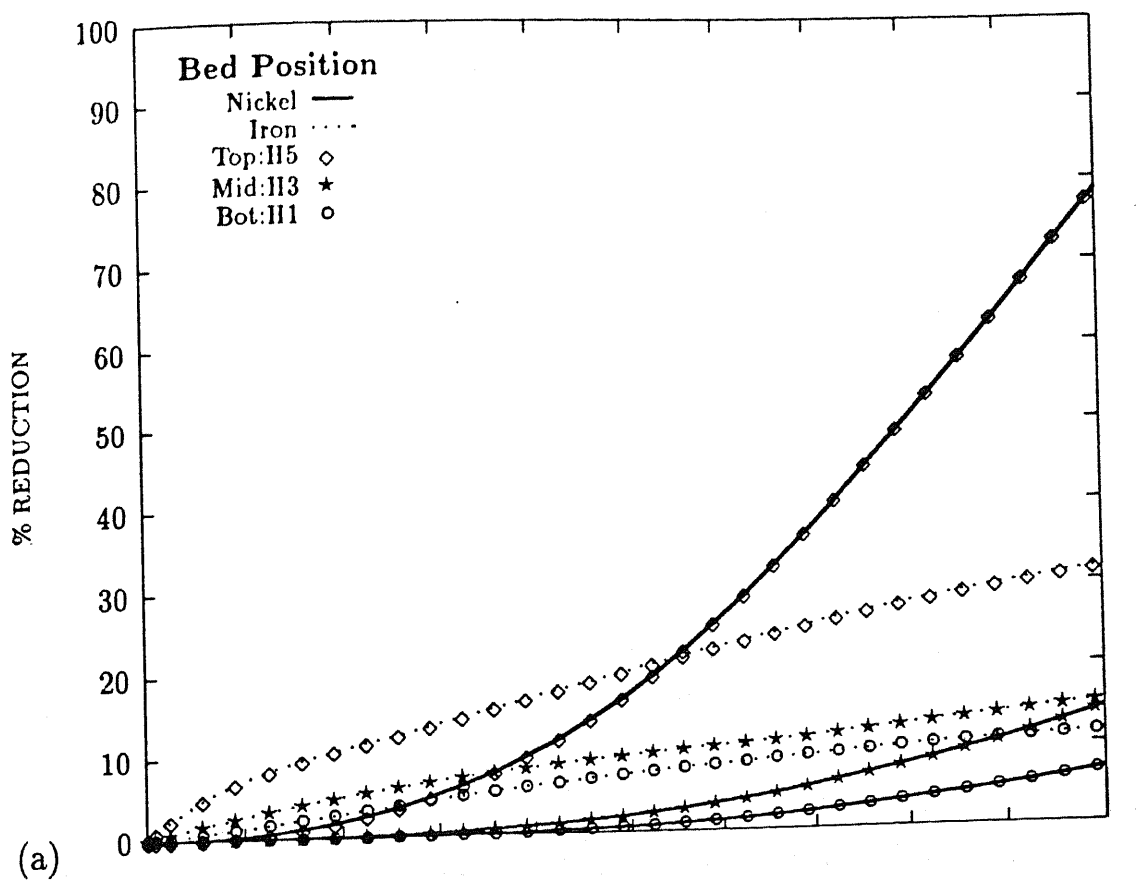
Figure 6.6: Reduction rate of nickel and iron in the top, middle and bottom layers at : (a) 900 K and (b) 1000 K

from figure 6 8. The initial solid temperature taken was 800 K and the gas temperature was 1000 K to observe clearly the effect of gas and solid heat transfer. There is a significant drop in gas temperature from the initial temperature of 1000 K to about 860-880 K and the increase in solid temperature is very slow and gradual from 800 K to about 855 K in the top most layer The temperatures are still lower in the bottom layers The gas solid temperature difference also decreases gradually in the lower layers.

6.7.5 Contour Plots

Contour plots for the whole computational domain were done for the 20 minutes reduction condition for the parameters like percentage reduction of nickel and iron, gas composition, gas and solid temperature.

Figure 6 9 shows the percentage reduction of nickel at 900 and 1000 K. The reduction proceeds from the top left corner of the packed bed, where the gas entry takes place. Reduction is complete (above 97 %) in the top most layer and the change in percentage reduction is very fast in a narrow range below the completely reduced zone as indicated by the large number of contour lines in that range. Reduction has proceeded a greater distance downwards at 1000 K than at 900 K. The reduction of iron also follows a similar trend as can be seen from figure 6.10, but complete reduction is not observed in this case

The contour plot for gas composition is shown in figure 6 11. The contour line tends to become vertical in the gas flow zone over the packed bed due to convection effect. Inside the packed bed the contour lines are almost horizontal, since mass transfer is dominated by diffusion inside the packed bed. Gas concentration in the lower most level is about 56 % at 900 K, where as it is 34 to 40 % at 1000 K, indicating that reactant gas utilization is much better at 1000 K. The gas solid temperature profile for reduction at 1000 K is shown in figure 6.12. Since the side wall temperature has been taken as constant and equal to the initial temperature of 1040 K, the zone of minimum temperature is in the lower bottom part of the solid bed forming a semicircular region. The solid temperature ranges from 1016-1012 in the upper layers and 1012-1008 in the most of the lower regions. The gas solid temperature difference is about 4 K for most of the packed bed region. The convective effect of the gas flow can be observed in the gas flow zone, by the gradual change in contour lines in vertical direction.
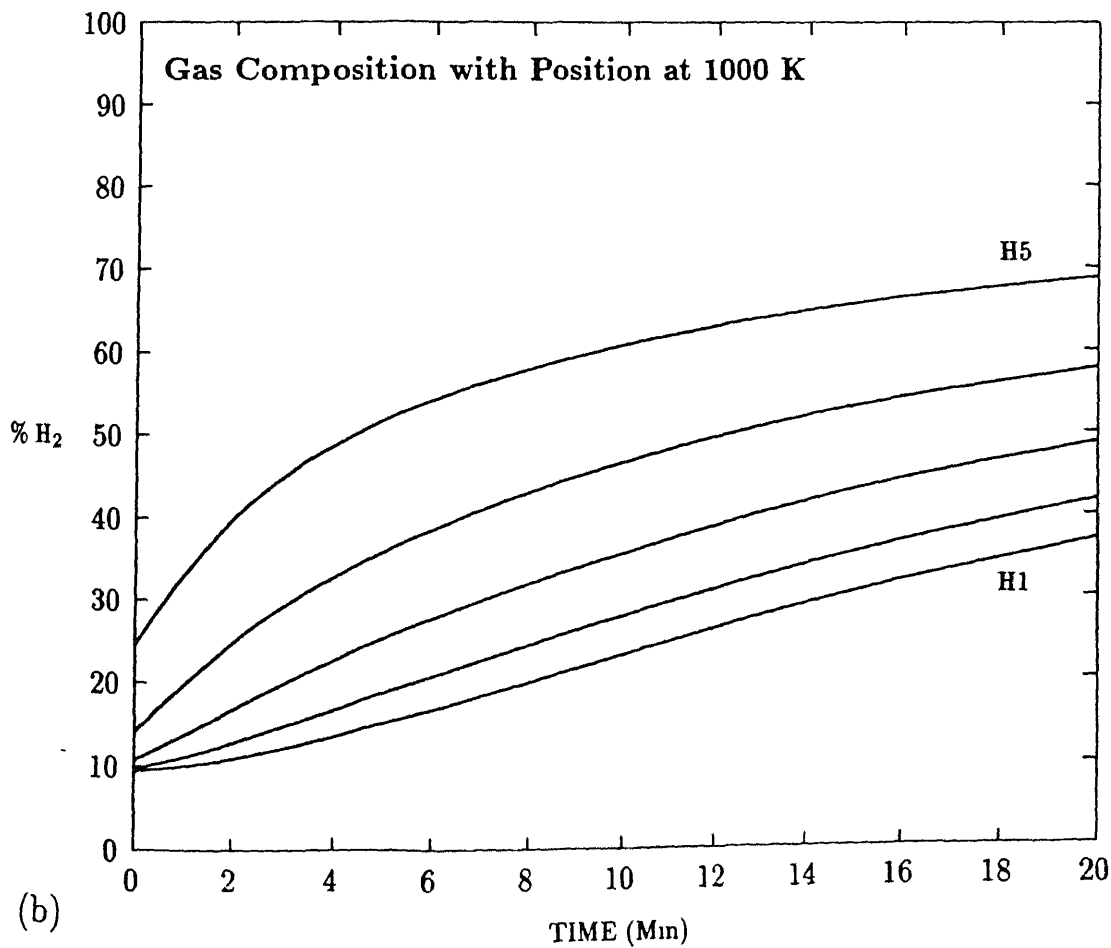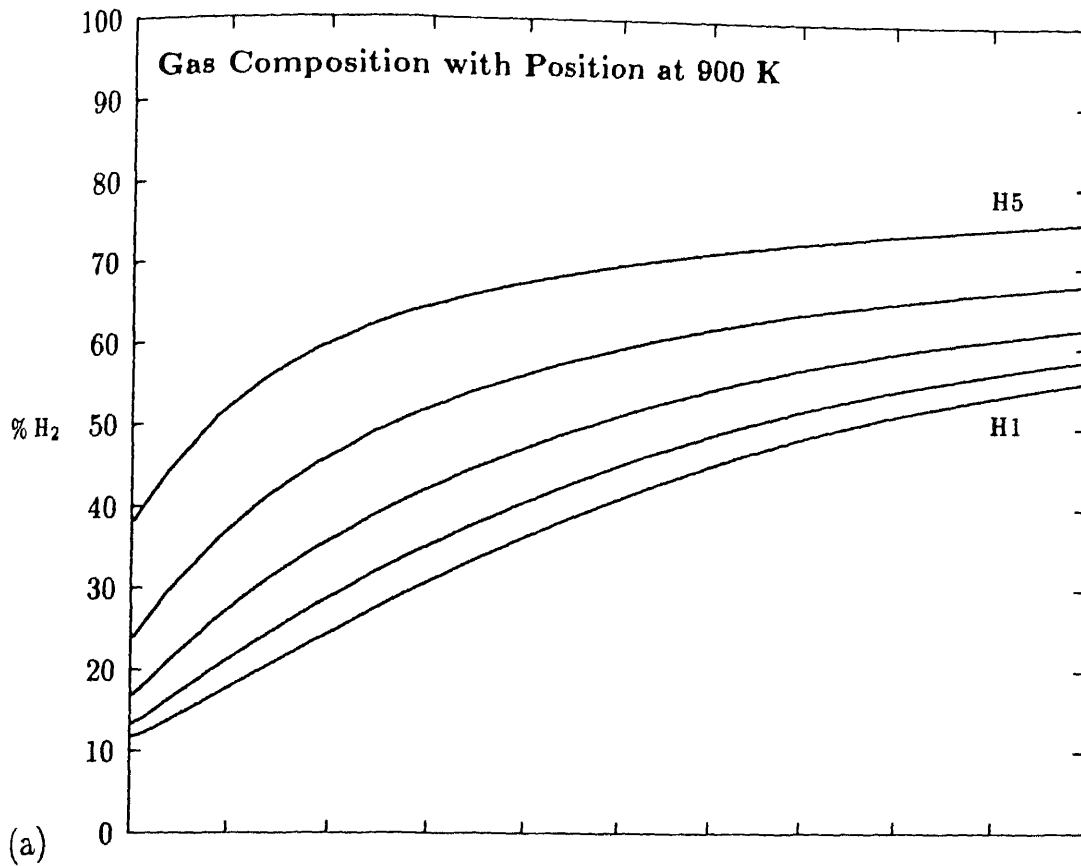
Figure 6 7: Gas concentration variation under horizontal flow condition in the five layers with
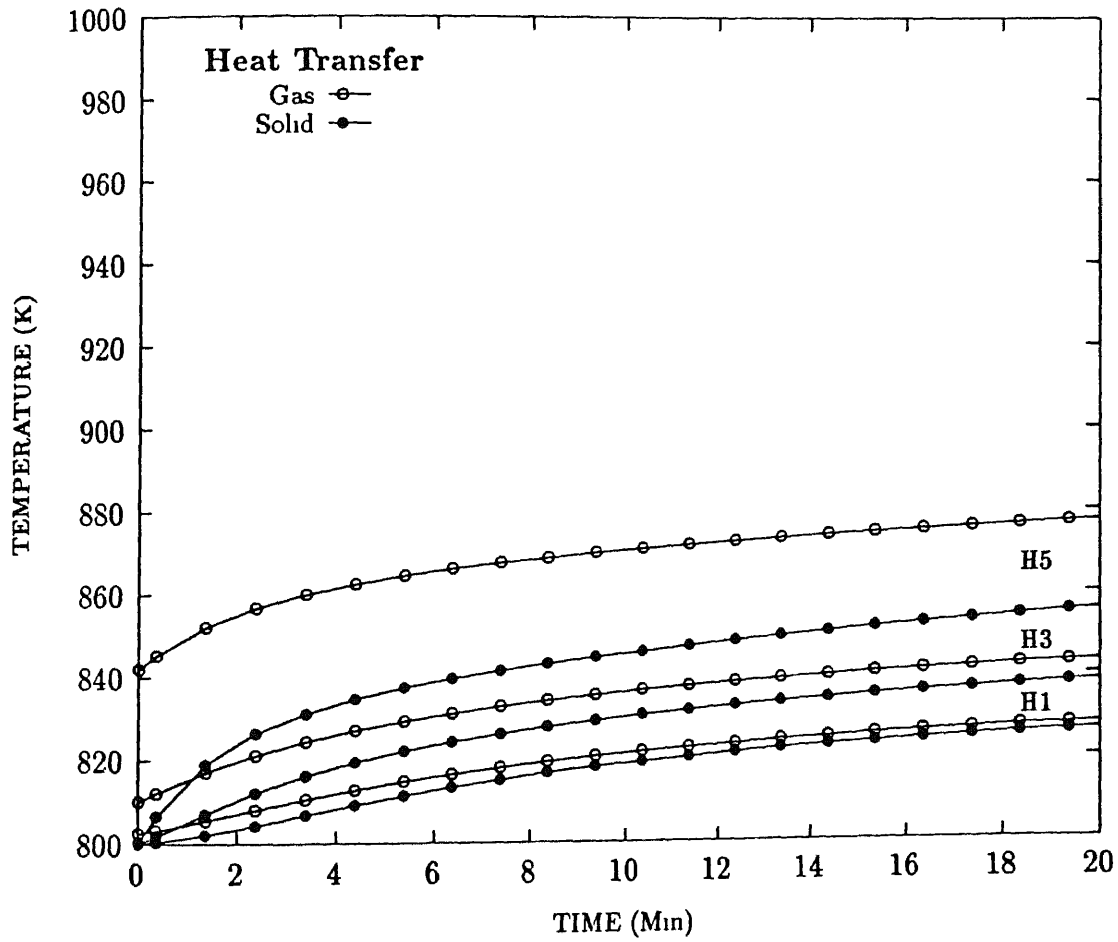
Figure 6.8: Gas and Solid temperature at the top, middle and bottom layers, when the initial gas temperature is 1000 K and solid temperature is 800 K.

170
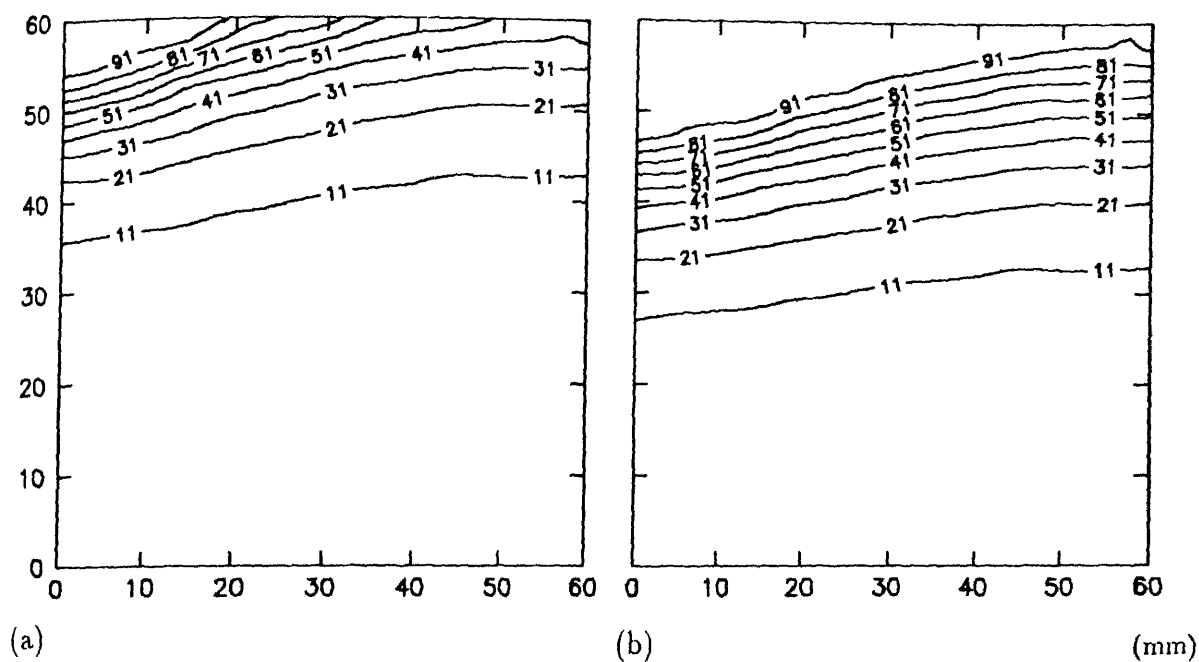
Figure 6 9: Contour plots after 20 minute reduction under horizontal gas flow condition for nickel at · (a) 900 K and (b) 1000 K
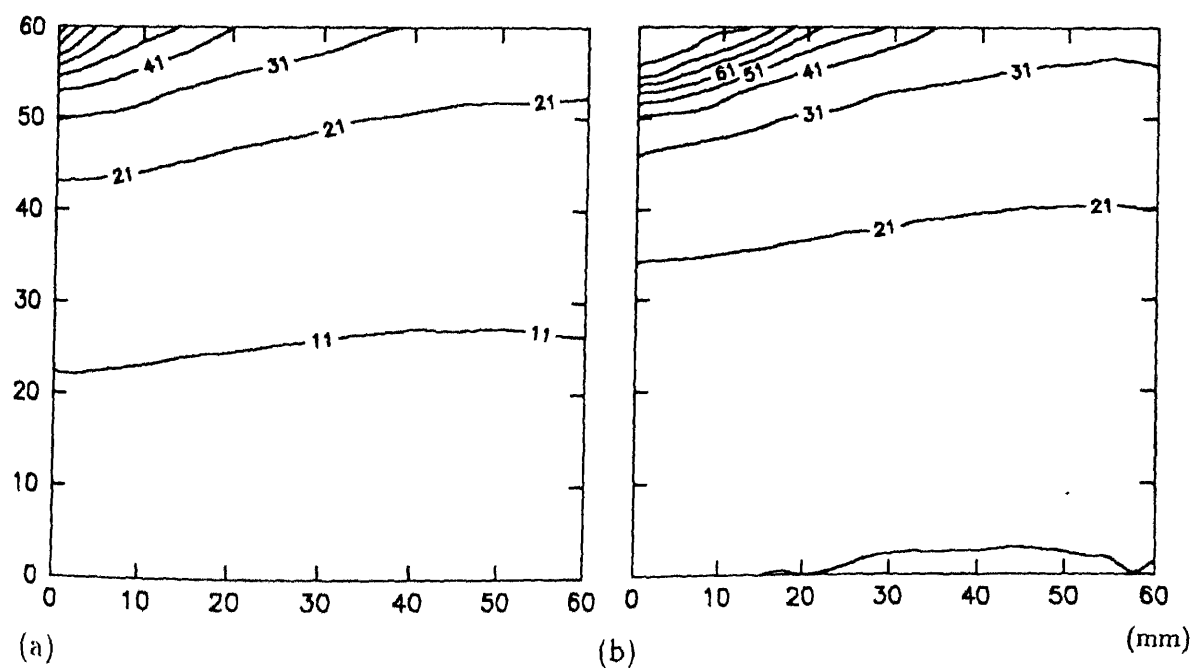
Figure 6.10: Contour plots after 20 min. reduction under horizontal gas flow condition for iron at : (a) 900 K and (b) 1000 K
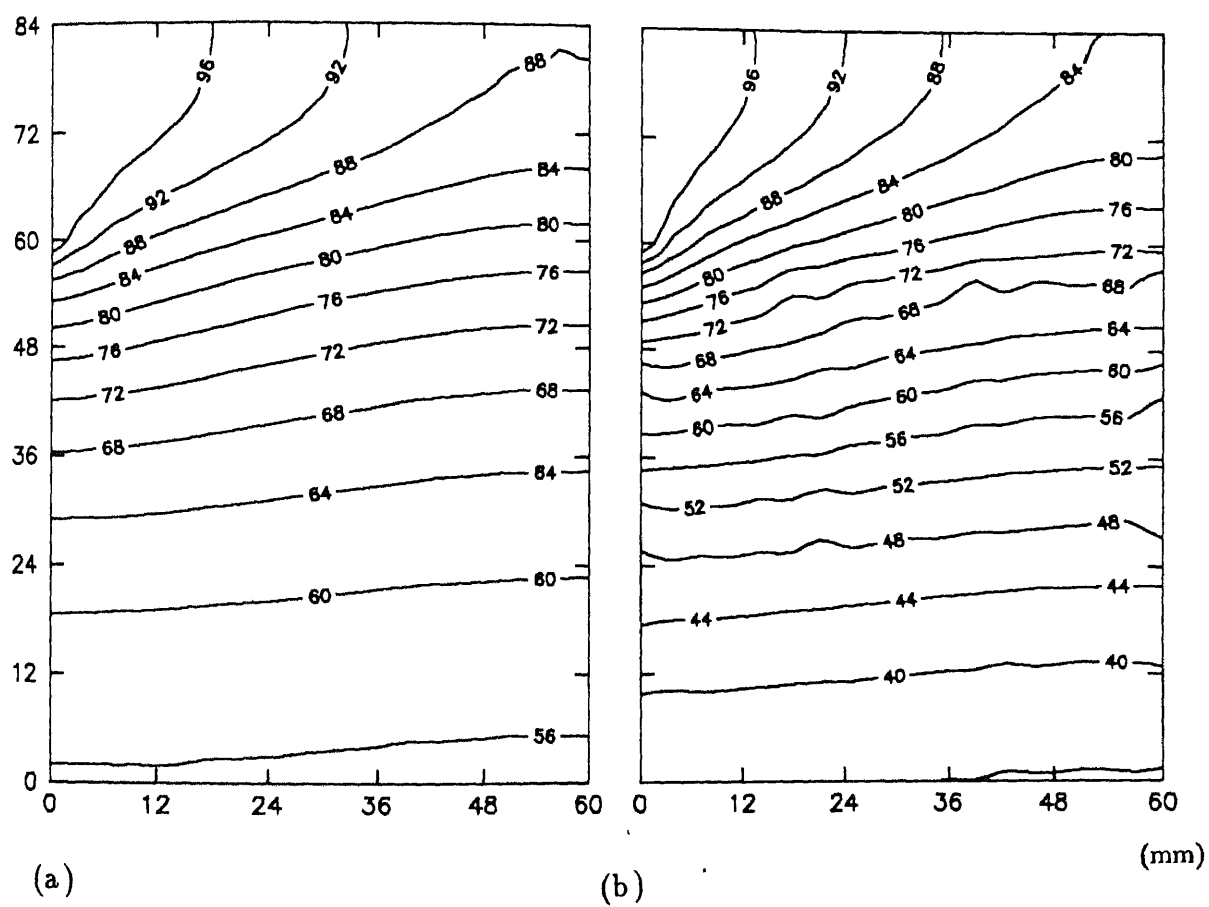
Figure 6.11: Contour plots for hydrogen concentration after reduction for 20 minutes at : (a) 900 K and (b) 1000 K
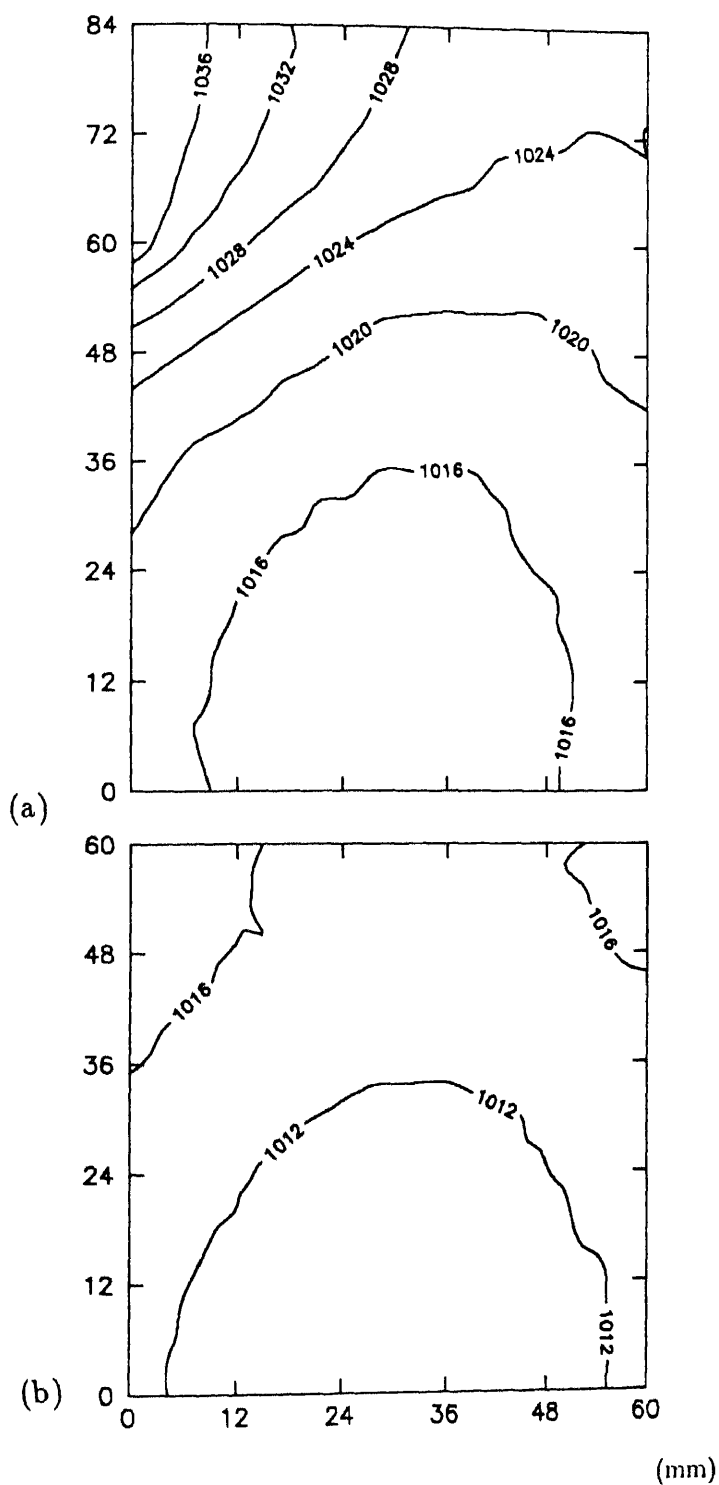
Figure 6.12. Contour plots for the gas and solid temperature after reduction for 20 minutes. The initial gas and solid temperature is 1040 K. (a) gas (b) solid

6.7.6 Parametric Study

The effect of some of the important parameters under horizontal gas flow condition, like gas velocity, pellet size and gas composition were studied computationally to understand their role in the process performance, which will help in evaluating the optimum conditions for the operation.

The effect of gas velocity is shown in figure 6.13. The effect is more significant in the top layers where the heat and mass transfer from the bulk gas phase to the solid surface is dominated by convection The effect is almost negligible in the lower regions where transportation is governed by diffusion The increase in percentage reduction for the increase in gas velocity is more for 5 to 10 cm/s than for 10 to 15 cm/s increment in gas velocity. This indicates that the effect of gas velocity is nearing its saturation limit, and any further increase in gas velocity will not produce proportional increase in reduction rate

The effect of pellet size shown in figure 6 14 also shows more prominent effect in the top surface, where the reaction is faster and intra pellet pore diffusion played a more distinctive role. In the lower layers there is no perceptible change in percentage reduction due to pellet size . This indicates that intra pellet pore diffusion in the individual pellets is not rate limiting factor and macroscopic or inter pellet diffusion in the bed is the rate limiting factor in the lower layers

The effect of inert gas like nitrogen is shown in figure 6.15. Higher nitrogen concentration produced a proportional decrease in the percentage reduction, although the trend or profile remained the same.

The effect of water vapor is studied next and shown in figure 6 16 Equal percentage of water vapor produced much more severe effect on the reduction profiles of both nickel and iron than nitrogen. The sharp rise in percentage reduction of iron in the upper most regions is diminished by both 10 % and 20 % water vapor addition The corresponding drop in nickel reduction is also very sharp for 900 K reduction, while for 1000 K, the nickel reduction still remained high in the top layers So with the addition of about 10 % water vapor in the reducing gas we can expect good selective reduction of nickel at 1000 K.

6.8 Concluding Remarks

The reduction process under horizontal gas flow condition is studied in this Chapter, after studying the process for vertical flow condition in the previous Chapter, to understand the whole
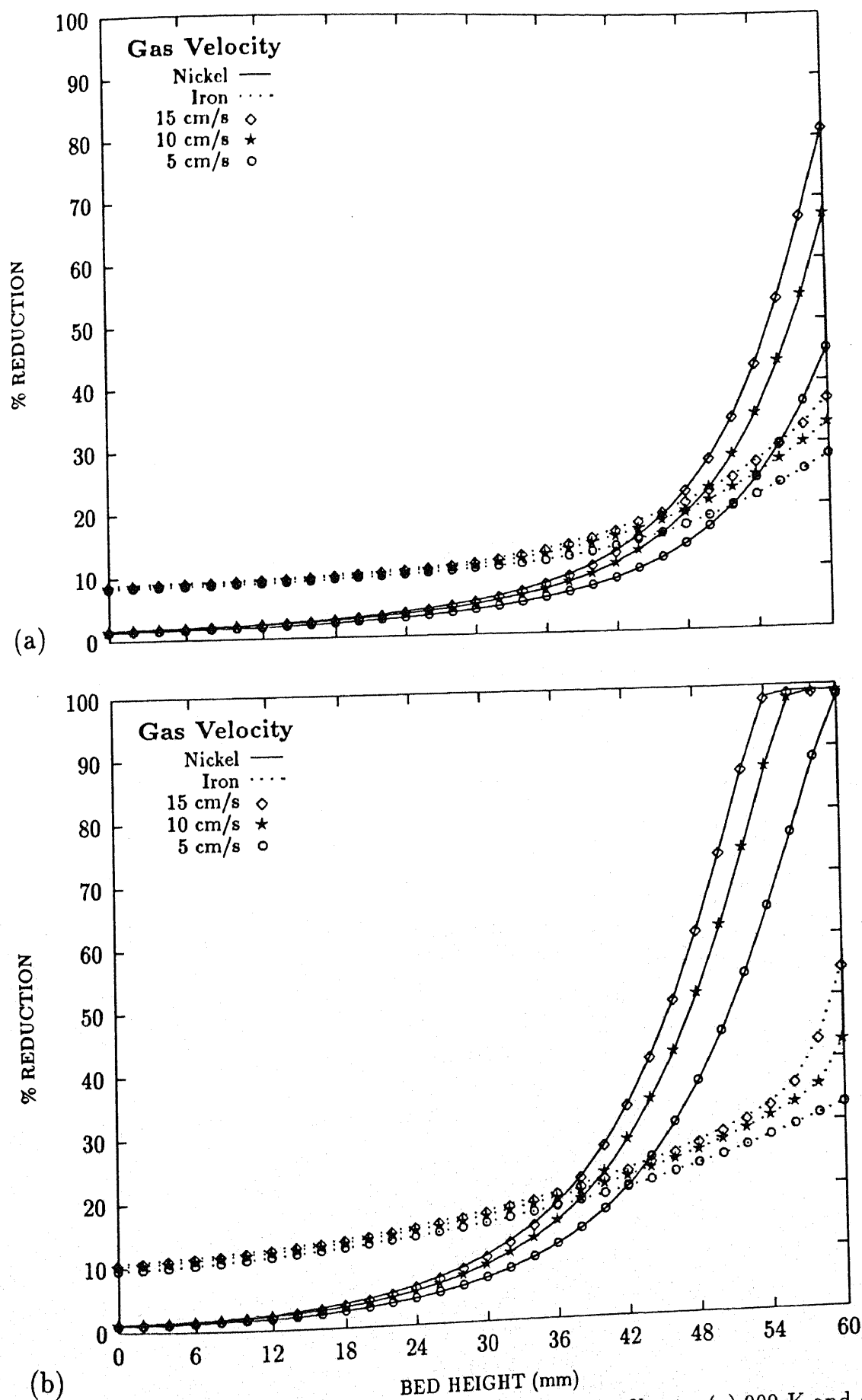
Figure 6.13: Effect of gas velocity on 20 minute reduction profile at : (a) 900 K and (b) 1000 K.
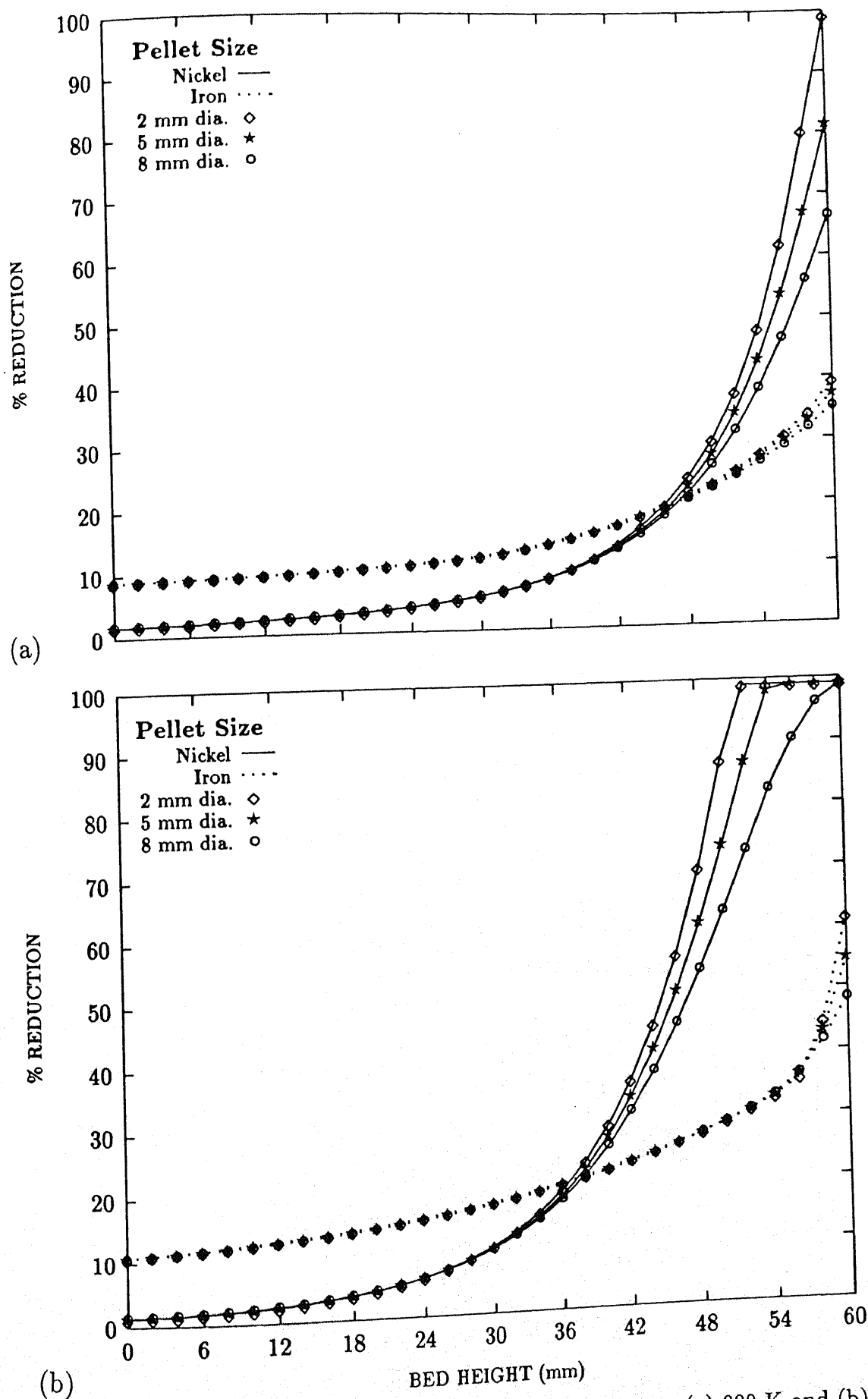
Figure 6.14: Effect of pellet size on 20 minute reduction profile at : (a) 900 K and (b) 1000 K.
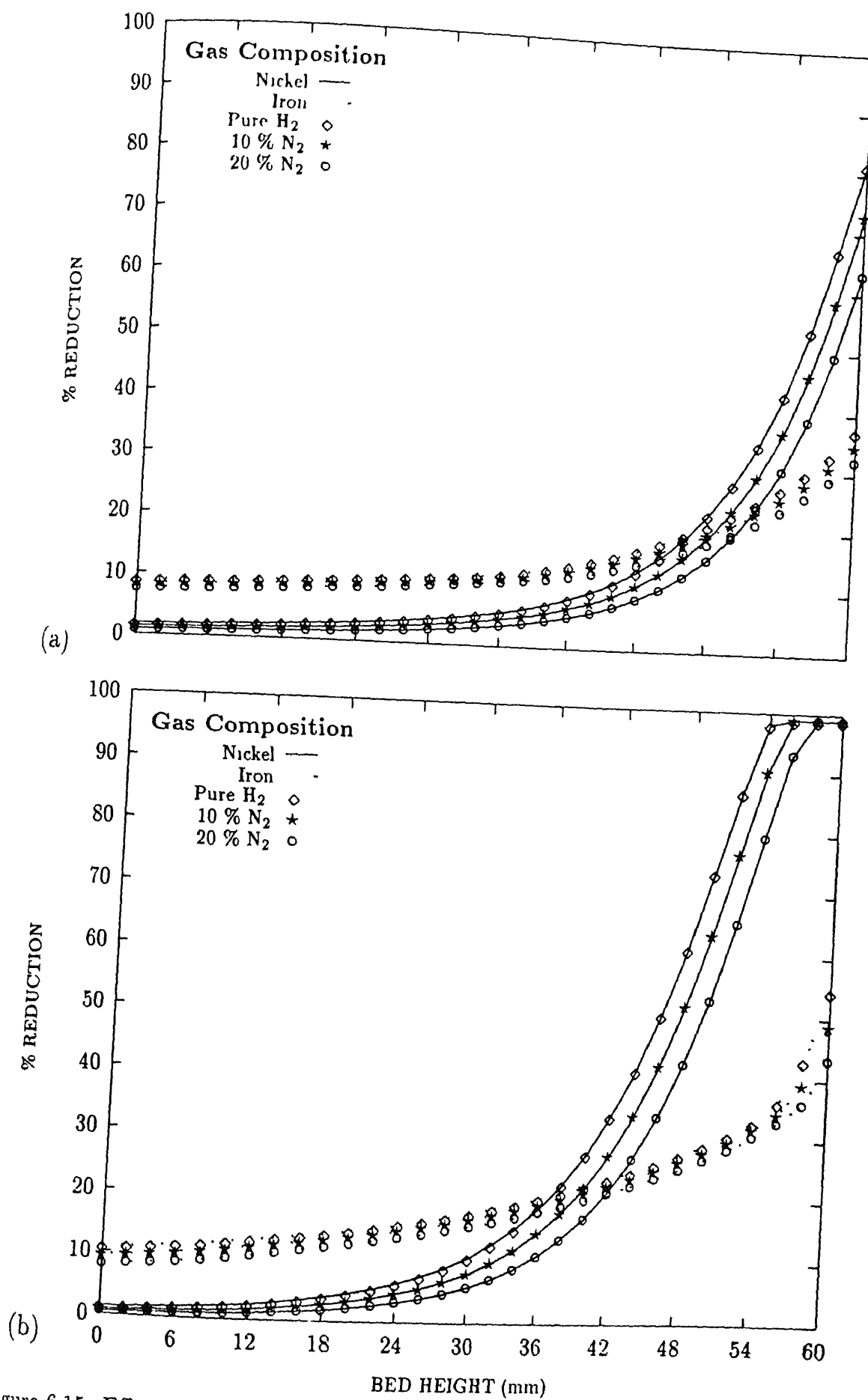
Figure 6.15: Effect of inert gas like nitrogen on 20 minute reduction profile at : (a) 900 K and
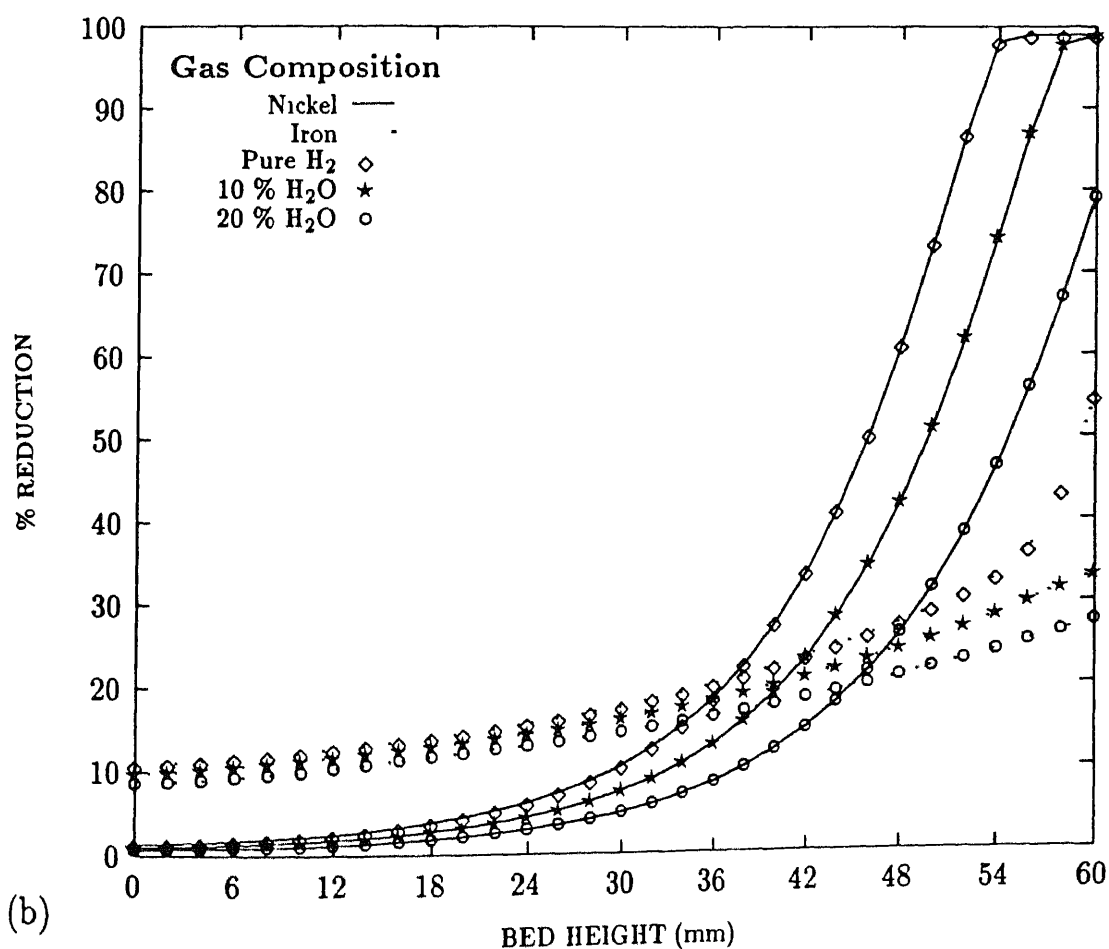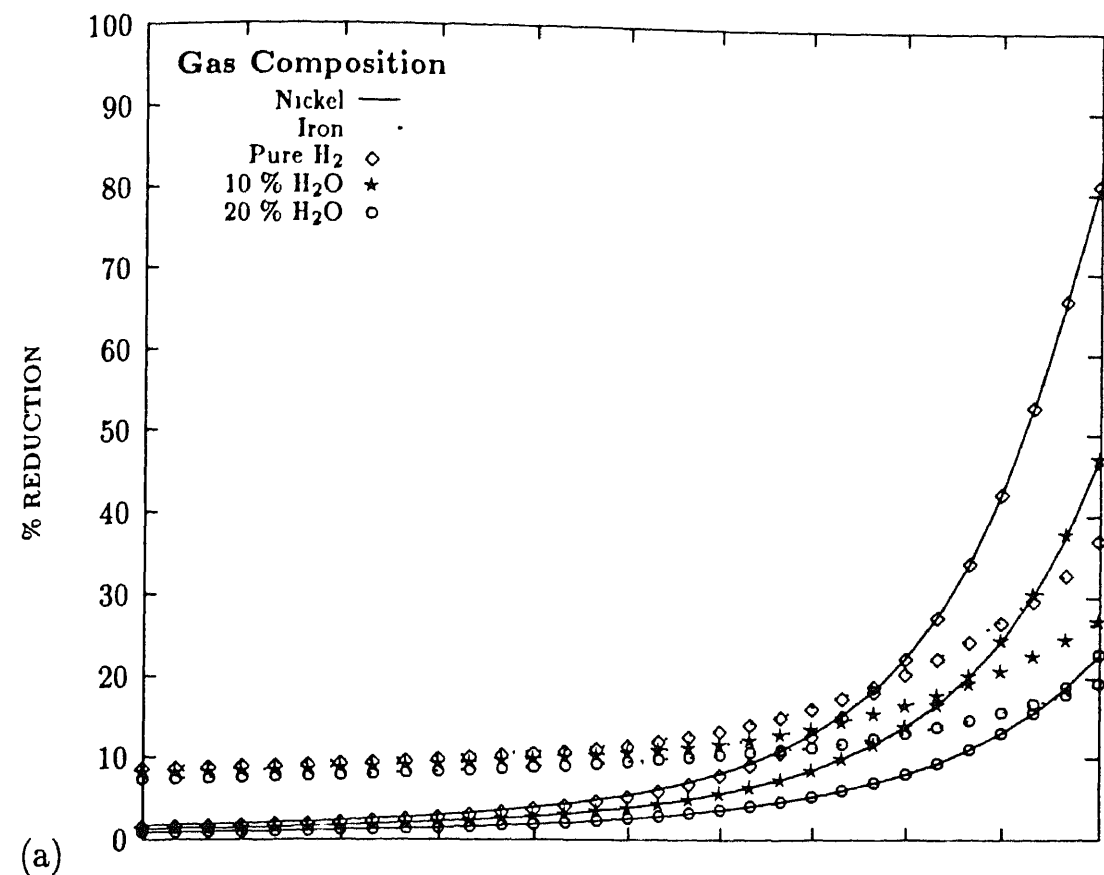
Figure 6.16: Effect of water vapor on 20 minute reduction profile at : (a) 900 K and (b) 1000 K

process of fixed bed reduction under different conditions The important observations can be summerized as given below :

1. The matching between the experimental and simulated results are reasonably good considering the complexities of the process.

2. The experimental results for 900 K showed very low reduction of nickel in the lower layers for all the three time periods The results predicted by grain model showed much higher reduction of nickel at those positions. The nickel reduction predicted by the complex oxide mechanism are much lower and thus much closer to the experimental results.

3. The process dynamics showed the reduction of iron is fast initially and becomes slow gradually, while nickel reduction is slow initially and becomes fast in the later stages. This is due to the faster reduction rates of hematite and magnetite than wüstite, and unlocking of nickel oxide after the formation of wüstite according to the mixed oxide mechanism.

4 The contour plot for gas composition showed almost horizontal contour lines in the lower regions indicating diffusion control mechanism, while the lines are almost vertical in nature showing the change in gas concentration as it moves forward due to gas velocity, indicating mass transfer is controlled by convection in the fluid flow zone. Similar trend is also observed for gas temperature profile.

5. The effect of gas velocity over the bed is found to be not very significant around the selected range, indicating that the gas flow rate is sufficiently high for the experiments.

6. The effect of pellet size is observed prominently for nickel reduction in the upper layers, while it is negligible in the lower regions of the bed.

7. The effect of water vapor is much stronger than the effect of same quantity of inert gas like nitrogen.

8. The understanding of the reduction process in a fixed bed reactor under horizontal gas flow condition provides the necessary background for modeling the process for moving bed conditions prevailing in the industrial furnaces like multiple hearth furnace discussed in the next Chapter.

Chapter 7

MATHEMATICAL MODELING OF REDUCTION ROASTING PROCESS IN MULTIPLE HEARTH FURNACE

After studying the reduction process in fixed bed reactors, we can now model the reduction process in a typical moving bed reactor. Among the reactors used for roasting purpose of laterite ores, MHF is considered to be best suited for the reduction of limonitic ores containing high percentage of iron. The optimum temperature of reduction of this type of ore is in the range of 1000 to 1050 K. Below this temperature range incomplete reduction takes place and above this range nickel may become locked in olivine structure, or excess reduction of iron may take place leading to difficulties in the subsequent leaching step. For this reason good control of temperature and gas composition is needed in the furnace. The initial reduction rate of nickel is slow since it remains locked in the complex oxide structure before the formation of wüstite. After the formation of wüstite also, the condition is kept such that the wüstite reduction rate is very slow and only nickel gets reduced to get a good selective reduction for nickel; and so the condition cannot be strongly reducing, giving rise to an overall slow kinetics of the process. Temperature and gas composition control is much simpler and more accurate in MHF, since the conditions can be controlled in different hearth regions. The furnace also gives best efficiency for slow kinetic systems, and therefore considered to be most suitable for the reduction of nickeliferrous ore.

Mathematical models for MHF were earlier developed by Gupta et al. [51], and Saharoy et al [52], for sulfide roasting systems. Saharoy et al have considered a three dimensional cylindrical coordinate system and assumed uniform gas velocity or plug flow condition. In the present study cylindrical axisymmetric condition is assumed, since there is very little variation

in the angular direction, and also to avoid excessive time of computation for a three dimensional simulation Fluid flow or gas velocity profile will play a very important role in the process, since the heat and mass transfer between the gas and solid phase will be primarily controlled by gas convection. Therefore the gas velocity profile in the different hearth levels are evaluated in the present study by stream function - vorticity formulation. The dimensions of the MHF modeled is approximately based on the reported dimensions of the MHF used for this purpose in Regional Research Laboratory, Bhubaneswar [2, 53] Industrially hydrocarbon fuels like pulverized coal, natural gas or fuel oil is used for producing the reducing gas as well as for providing the thermal energy. The reducing gas therefore will contain both hydrogen and carbon monoxide In the present study the kinetic parameters for reduction with hydrogen is experimentally determined as described in Chapter 3, and the kinetic parameters for carbon monoxide are taken from literature as given in table A.23 of Appendix A.

7.1 Description of the Process

The schematic diagram of the MHF modeled for the reduction roasting process is shown in figure 7.1. The number of hearths in a MHF can vary to a large extent, and the prevailing conditions in different hearths can be controlled much more efficiently in MHF. The heat and mass transfer between the gas and solid phase takes place in counter current fashion, and the ore enters at the top hearth through a hopper and follows a tortuious path from the circumference to the center in the odd numbered hearths, and from the center to the circumference in the even numbered hearths. The time of fall of the solid ore from one hearth to the next lower hearth is considered negligible compared to the total residence time of solids. Each hearth can be considered as a unit system and computed individually. The solid output of one hearth is taken as the input of the next lower hearth. The gas also moves in a similar fashion counter current to the solid, and so the output of one hearth is taken as the input of the next upper hearth By this process all the hearths can be interlinked for computing the whole MHF. This will also help in simulating the performance of any particular hearth or region consisting of one or more hearths.
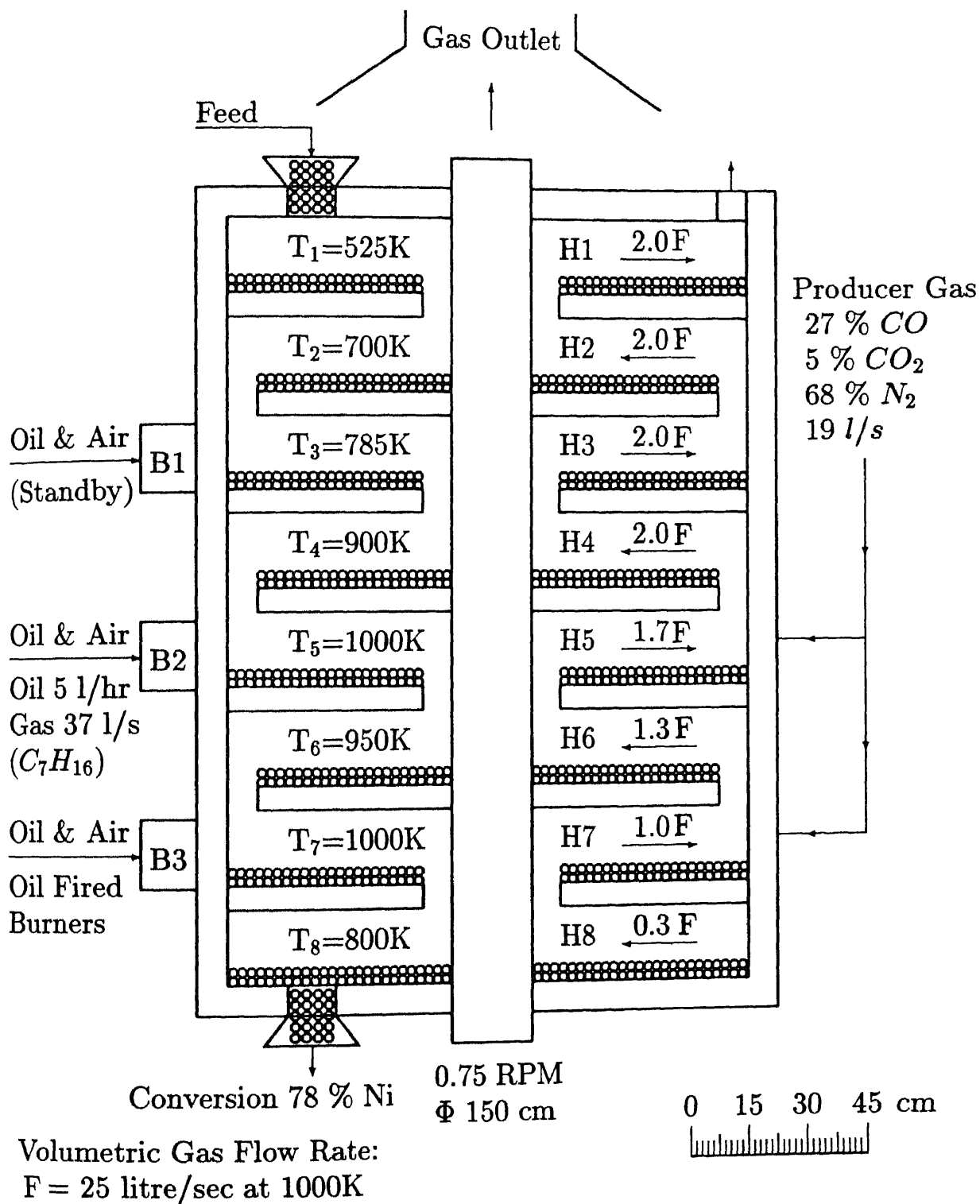
Figure 7.1: Schematic diagram of the Multiple Hearth Furnace

7.2 Formulation for the MHF model

Cylindrical axisymmetric coordinate system is chosen for the MHF model considering negligible θ-direction variation Steady state stream function and vorticity formulation was used for the solving gas velocity profile over the packed bed since the total number moles remained conserved in the reduction process as discussed in the previous Chapters. All other process phenomena were solved for transient conditions and so it can be termed as quasi-steady state formulation. The set of equations solved for the process simulation are as given below .

- Gas velocity profile in the hearths

- Solid phase thermal energy balance.

- Gaseous phase thermal energy balance.

- Solid phase mass or species balance

- Gaseous phase mass or species balance.

The equations were solved by using Crank Nicholson technique, and first order upwinding for the convective terms.

7.3 Parameter Values for the Process

The dimensions of the MHF, gas velocity and value of the parameters used for the process simulation are given in table 7.1. The temperature profile and the gas composition shown in figure 7.1 are based on the plant data of RRL Bhubaneswar, provided by Banerjee et al., Das and Dey [2, 53]. The initial conditions are not taken exactly from the diagram since they are steady state profiles and not the initial conditions. The maximum Reynold's number for the gas velocity near the central shaft region is 107, which is in the laminar zone, well below the turbulence Reynold's number of about 2000 or above for channel flow condition. The rate constant values for reduction with H_2 and CO, and heat and mass transfer parameters, used for the present calculations are given in table A.22, A.23 and A.27 respectively in Appendix A.

Table 7.1· Dimensions and parameter values used for MHF modeling.

PARAMETER	VALUE	UNIT
MHF Dimensions		(in cm)
Central shaft diameter	30	
Outer diameter	110	
Packed Bed Height	2 5	
Height of the gas flow region	15	
Gap width	8	
Pellet diameter	5 mm	
Packed Bed density	1000	kg/m^3
Solid Input Rate	70	kg/hr
Residence Time		
Total	120	Min
Odd Hearths	16.8	Min
Even Hearths	13.4	Min
For the three Hearths studied	43.6	Min
Gas Velocity in 4th, 5th, 6th hearths	1.3F, 1.7F and 2 0F	
Where F (Volumetric Flow)	25	liter/s at 1000 K
or F (Velocity near the shaft)	17.7	cm/s at 1000 K
Reynolds number for 2V	107	
Biot Number in the three hearths 4th; 5th; 6th	0.16, 0.20, 0.30	
Grid Size		
Δr	1.0	cm
Δz	0.5	cm
No. of grid $I_{Max} - I_{Min}$, J_{Max}	40, 35	
Δt	0.15	sec

7.4 Computational Domain

The computational domain of the odd numbered hearths ($k = 1, 3, 5 \cdots$) and even numbered hearths ($k = 2, 4, 6 \cdots$) are shown in figure 7.2. The nodal points in the packed bed region is indicated by solid circles and the nodes in the gaseous phase is indicated by hollow circles. The figure is only schematic and the actual number of grid points in the vertical direction of the packed bed is five. The details of the grid size, number of grids and time step taken for the computation are given in table (7.1). The gas solid boundary is denoted by GS. The gas entry and exit boundary is denoted by EN and EX respectively, and the solid walls are denoted W1, W2, W3 and W4.

The boundary regions in terms of grid positions can be summarized as given below :

EN : Gas Entry ($I_{Min} \leq i \leq I_{Min+ng}$, for odd k, $I_{Min+nh} \leq i \leq I_{Max}$, for even k; $j = 1$)

EX · Gas Exit ($I_{Min+nh} \leq i \leq I_{Max}$, for odd k; $I_{Min} \leq i \leq I_{Min+ng}$, for even k; $j = 1$)

W1 : Central Wall ($i = I_{Min}$; $1 \leq j \leq J_{Max}$)

W3 . Outer Wall ($i = I_{Max}$; $1 \leq j \leq J_{Max}$)

W2 · Lower Wall ($I_{Min+ng} \leq i \leq I_{Max}$, for odd k; $I_{Min} \leq i \leq I_{Min+nh}$, for even k; $j = 1$)

W4 . Upper Wall ($I_{Min} \leq i \leq I_{Min+nh}$, for odd k; $I_{Min+ng} \leq i \leq I_{Max}$, for even k; $j = J_{Max}$)

SEN . Solid Entry ($i = I_{Max}$, for odd k; $i = I_{Min}$ for even k; $1 \leq j \leq J_{GS}$)

SEX : Solid Exit ($i = I_{Min+ng}$, for odd k, $i = I_{Min+nh}$ for even k; $1 \leq j \leq J_{GS}$)

7.5 Governing Equations

The governing equations were non-dimensionalized for simplification and easy scaleup of the model, and the non-dimensional terms are given in table (4.2) of Chapter 4. The gas and solid conductivity were taken equal to the overall conductivity of the bed. The gas diffusivity inside the packed bed region was taken proportional to the bed porosity or void fraction. The initial condition for the parameters are summarized below :

GAS EXIT

W4 $I = I_{Min} + nh$

EX

$I = I_{Min}$
$J = J_{Max}$

$I = I_{Max}$
$J = J_{Max}$

ODD HEARTHS

K= 1, 3, 5 $\cdots$

W1

W3

$\circ$GS$\circ$

$J = J_{GS}$

$I = I_{Min}$
$J = 1$

EN

$I = I_{Min} + ng$

W2

$I = I_{Max}$
$J = 1$

GAS ENTRY

GAS EXIT

EX

$I = I_{Min} + ng$ W4

$I = I_{Min}$
$J = J_{Max}$

$I = I_{Max}$
$J = J_{Max}$

EVEN HEARTHS

K= 2, 4, 6 $\cdots$

W1

W3

$J = J_{GS}$

$\circ$GS$\circ$

$I = I_{Min}$
$J = 1$

W2 $I = I_{Min} + nh$ EN

$I = I_{Max}$
$J = 1$

GAS ENTRY

z

r

0   5   10   15 cm
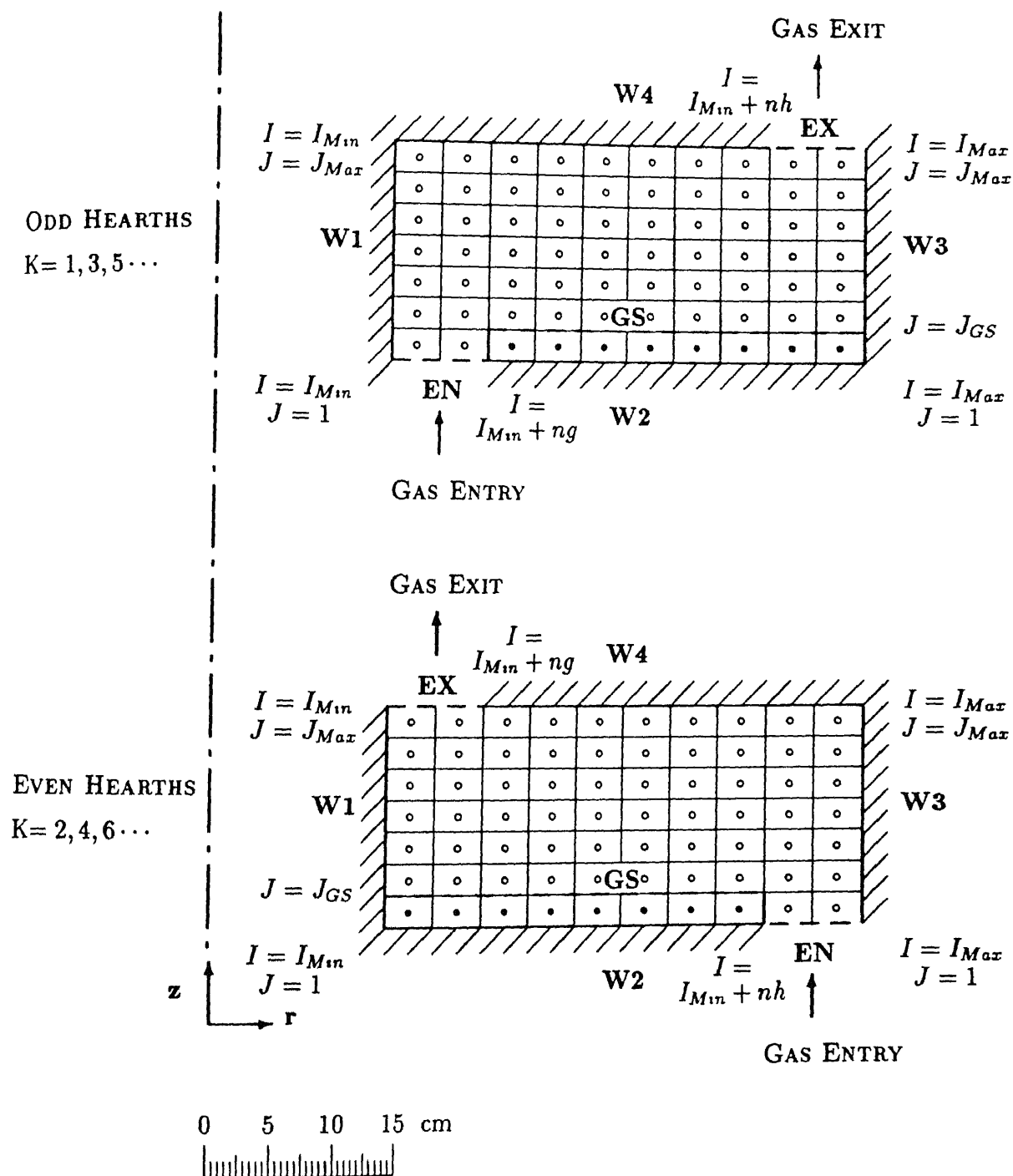
Figure 7.2: Computational domain for the odd and even hearths

For $t = 0$; $(1 \leq i \leq I_{Max};\ 1 \leq j \leq J_{Max})$

1. $T_{s(i,j)} = T_{s,int} = T_{s,w}$

2. $T_{g(i,j)} = T_{g,int}$

3. $G_{H(i,j)} = G_{H,int}$

4. $X_{i(i,j)} = 0$

First order upwinding method is used for discretizing the equations, since the gas velocity is quite high, and there are many changes in flow direction in the computational domain.

7.5.1 Gas Velocity Profile by Stream Function and Vorticity method

For describing the convective heat and mass transfer from the bulk gas phase to the reactive packed bed surface gas velocity profile has to be known. For this purpose the velocity profile was solved by using stream function and vorticity formulation. The gas velocity inside the packed bed region is considered to be zero. The set of non-dimensional equations used are given below :

Velocity in r and z direction :

$$V_{r(i,j)} = \frac{1}{r} \frac{\partial \psi}{\partial z} = \frac{\psi_{(i,j+1)} - \psi_{(i,j-1)}}{2r \, \triangle z} \tag{7.1}$$

$$V_{z(i,j)} = -\frac{1}{r} \frac{\partial \psi}{\partial r} = -\frac{\left\{ \psi_{(i+1,j)}(nr - 1) + (-1)^{nr}\psi_{(i,j)} + nr\psi_{(i-1,j)} \right\}}{r \, \triangle r} \tag{7.2}$$

Definition of Vorticity (ω) : Coupling between vorticity and stream function.

$$\omega_{(i,j)} = \frac{\partial V_r}{\partial z} - \frac{\partial V_z}{\partial r} = \frac{1}{r} \left(\frac{\partial^2 \psi}{\partial r^2} - \frac{1}{r} \frac{\partial \psi}{\partial r} + \frac{\partial^2 \psi}{\partial z^2} \right) \tag{7.3}$$

By using first order upwinding in r-direction and central in z-direction, and rearranging the terms we get .

$$\psi_{(i,j)} = \frac{\psi_{(i-1,j)} \left\{ \frac{1}{\Delta r^2} + \frac{(1-nr)}{r\Delta r} \right\} + \psi_{(i+1,j)} \left\{ \frac{1}{\Delta r^2} - \frac{nr}{r\Delta r} \right\} + \frac{1}{\Delta z^2} \left\{ \psi_{(i,j-1)} + \psi_{(i,j+1)} \right\} - \omega_{(i,j)} r}{\frac{2}{\Delta r^2} + \frac{2}{\Delta z^2} + \frac{(-1)^{nr}}{r\Delta r}} \quad (7.4)$$

Vorticity transport equation ·

$$\frac{1}{r}\frac{\partial \psi}{\partial z}\frac{\partial \omega}{\partial r} - \frac{1}{r}\frac{\partial \psi}{\partial r}\frac{\partial \omega}{\partial z} - \frac{\omega}{r^2}\frac{\partial \psi}{\partial z} = \frac{1}{R_e}\left\{ \frac{\partial^2 \omega}{\partial r^2} + \frac{1}{r}\frac{\partial \omega}{\partial r} - \frac{\omega}{r^2} + \frac{\partial^2 \omega}{\partial z^2} \right\} \quad (7.5)$$

Solution Procedure

The four set of simultaneous equations given by eqns.(7.4), (7 5), (7 1) and (7.2) are solved in a similar fashion as described in Chapter 6, to evaluate the four unknowns ψ, ω, V_r and V_z respectively.

Initialization of Velocity and Stream function values

The initial guess velocity for the gas can be set as follows :

$$\text{Velocity in the radial direction} : \quad V_r(i,j,k) = \frac{vol}{2\pi(J_{Max} - J_{GS})dr\,dz} \quad (7.6)$$

$$\text{Velocity in the Central gap} : \quad V_{z(cen)} = \frac{vol}{\pi\left((I_{Min+ng})^2 - (I_{Min})^2\right)dr^2} \quad (7.7)$$

$$\text{Velocity in the Perifery} : \quad V_{z(per)} = \frac{vol}{\pi\left((I_{Max})^2 - (I_{Min+nh})^2\right)dr^2} \quad (7.8)$$

Initial guess value for stream function (ψ) :

$$\psi = -\int_{r1}^{r2} rV_z dr \quad (7.9)$$

$$\psi = \int_{0}^{h} rV_r dz \quad (7.10)$$

Boundary Conditions for the Vorticity Transport equation

W1 and W3 : Vertical wall boundary conditions

For no slip condition at the wall boundaries, stream function values are constant, and so at the central and outer wall boundaries stream function is constant along the $z-$direction Therefore from eqn.(7.3) we can get the boundary condition as .

$$\omega = \frac{1}{r}\frac{\partial^2\psi}{\partial r^2} - \frac{1}{r^2}\frac{\partial\psi}{\partial r} \tag{7.11}$$

From which we can get the boundary conditions in discretized form by virtual point method for W1 and W3 as follows :

$$\omega_{(i,j)} = \frac{2}{r\,\triangle\,r^2}\left\{\psi_{(i+1,j)} - \psi_{(i,j)}\right\} - \frac{1}{r^2\,\triangle\,r}\left\{\psi_{(i+1,j)} - \psi_{(i,j)}\right\} \tag{7.12}$$

$$\omega_{(i,j)} = \frac{2}{r\,\triangle\,r^2}\left\{\psi_{(i-1,j)} - \psi_{(i,j)}\right\} - \frac{1}{r^2\,\triangle\,r}\left\{\psi_{(i,j)} - \psi_{(i-1,j)}\right\} \tag{7.13}$$

GS and W4 : Horizontal boundary conditions

Similarly for the upper and lower wall boundaries stream function is constant along the $r-$direction. Therefore from eqn.(7.3) we can get the boundary condition as :

$$\omega = \frac{1}{r}\frac{\partial^2\psi}{\partial z^2} \tag{7.14}$$

which on discretization for the upper and lower boundaries (GS and W4) becomes :

$$\omega_{(i,j)} = \frac{2}{r\,\triangle\,z^2}\left\{\psi_{(i,j+1)} - \psi_{(i,j)}\right\} \tag{7.15}$$

$$\omega_{(i,j)} = \frac{2}{r\,\triangle\,z^2}\left\{\psi_{(i,j-1)} - \psi_{(i,j)}\right\} \tag{7 16}$$

EN and EX : Inlet and Outlet boundary conditions

EN · According to Greenspan's boundary condition [77], which assumes $\frac{\partial V_r}{\partial z} = 0$, as discussed in Chapter 6. Therefore from eqn.(7 3) we get :

$$\omega = -\frac{\partial V_z}{\partial r} \tag{7.17}$$

EX . By using Thoman and Szewczyk's [78] boundary condition as discussed in Chapter 6 :

$$\omega_{(\iota,J)} = \omega_{(\iota,J-1)} \tag{7.18}$$

The solution procedure for the equations are similar to the procedure followed and described in Chapter 6 for gas velocity calculations.

7.5.2 Solid Velocity

The variables for the velocity of the moving bed of solid particles or pellets are as follows :

1 Height of the packed bed.

2. Rate of solid input

3 Residence time of the solid (or solid velocity in radial direction).

If any two of the three variables are defined or specified, the other one can be easily calculated. For the present case rate of solid input and height of the packed bed is defined and so the solid velocity (in radial direction) and residence time of the solid can be evaluated as.

$$V_s(\iota) = \frac{R_{kg}}{2\pi\rho_{s(b)}.\iota.\,\Delta\,rJ_{GS}.\,\Delta\,z} \tag{7.19}$$

$$\text{Residence Time}\quad Rs_t = \frac{B_{Vol}}{2\pi V_{s(I_{Min})}I_{Min}.\,\Delta\,r.J_{GS}.\,\Delta\,z} \tag{7.20}$$

7.5.3 Solid Phase Thermal Energy Balance

As mentioned before the solid phase thermal energy balance is solved to consider the non-isothermal reduction process and gas-solid heat exchange. The equation in its non-dimensional form is given by :

$$\frac{\partial T_s}{\partial t} + Pe_{T_s} V_s \frac{\partial T_s}{\partial r} = \left[\frac{1}{r}\frac{\partial}{\partial r}\left(r\frac{\partial T_s}{\partial r}\right) + \frac{\partial^2 T_s}{\partial z^2}\right] + Nu(T_g - T_s) + \sum_{i=1}^{n} R_{T,i}\frac{\partial X_i}{\partial t} \qquad (7.21)$$

Boundary Conditions

The boundary conditions were implemented by virtual point method.

W2 and GS . By neglecting the z-direction conductivity we get .

$$\frac{\partial T_s}{\partial t} + Pe_{T_s} V_s \frac{\partial T_s}{\partial r} = \frac{1}{r}\frac{\partial}{\partial r}\left(r\frac{\partial T_s}{\partial r}\right) + + Nu(T_g - T_s) + \sum_{i=1}^{n} R_{T,i}\frac{\partial X_i}{\partial t} \qquad (7.22)$$

SEN : The output solid temperature from the upper hearth will be the input temperature of the lower hearth. The rate of input will depend on the solid velocity or the convective term. For odd hearths :

$$T_{s(i+1,j,k)} = T_{s,av(k-1)} \qquad (7.23)$$

For even hearths :

$$T_{s(i-1,j,k)} = T_{s,av(k-1)} \qquad (7.24)$$

SEX : Continuity boundary condition :

$$\frac{\partial T_s}{\partial r} = 0 \qquad (7.25)$$

7.5.4 Gaseous Phase Thermal Energy Balance

As discussed in the previous Chapters gaseous phase thermal energy balance has to be solved along with the solid phase thermal energy balance to evaluate the non-isothermal reduction

process and gas-solid heat exchange Under industrial conditions the gas produced by sub-stoicheometric combustion of the fuel provides both heat energy and reducing atmosphere, and so for evaluating the thermal efficiency of the process, solution of this equation becomes essential. The equation in its non-dimensional form is given by :

$$\frac{\partial T_g}{\partial t} + Pe_{T_g}\left(V_r\frac{\partial T_g}{\partial r} + V_z\frac{\partial T_g}{\partial z}\right) = \left[\frac{1}{r}\frac{\partial}{\partial r}\left(r\frac{\partial T_g}{\partial r}\right) + \frac{\partial^2 T_g}{\partial z^2}\right] + Nu(T_s - T_g) \qquad (7\ 26)$$

The gas phase is continuous throughout the computational domain and conductivity in the packed bed region is taken equal to the bed conductivity. The gas-solid heat transfer term will be absent over the bed and the convective terms are neglected in the packed bed region.

Boundary Conditions

The boundary conditions which are in differential equation form are implemented by virtual point method.

W1 and W3 .

$$\frac{\partial T_g}{\partial x} = 0 \qquad (7.27)$$

W2 and W4 :

$$\frac{\partial T_g}{\partial x} = 0 \qquad (7.28)$$

where, Nusselt's number for thermal resistance of the wall is $= \frac{k_w}{k^\dagger l_w{}^2}$

(Where, $k^\dagger = k_b$ or, k_g)

EN : Temperature is defined :

$$T_{g(i,j,k)} = T_{g,av(k+1)} \qquad (7\ 29)$$

EX : Continuity of gas temperature :

$$\frac{\partial T_g}{\partial z} = 0 \qquad (7.30)$$

7.5.5 Gaseous Phase Mass or Species Balance

The reactant gas concentration profile in the reactor for the gas-solid reaction will be obtained by solving the gaseous phase mass or species balance The gas phase is continuous through out the computational domain, and the equation in its non-dimensional form is given by :

$$\frac{\partial G_H}{\partial t} + Pe_G \left(V_r \frac{\partial G_H}{\partial r} + V_z \frac{\partial G_H}{\partial z} \right) = \left[\frac{1}{r} \frac{\partial}{\partial r} \left(r \frac{\partial G_H}{\partial r} \right) + \frac{\partial^2 G_H}{\partial z^2} \right] + \sum_{i=1}^{n} R_{G,i} \frac{\partial X_i}{\partial t} \quad (7.31)$$

In the gas flow zone above the packed bed there is no solid phase and so the gas-solid reaction term will be absent. In the packed bed region the convective terms are absent since gas velocity is neglected in this region. Diffusivity in the packed bed region is less than the gas flow zone, and is proportional to the void fraction of the packed bed.

Boundary Conditions

The boundary conditions in differential equation form are implemented by virtual point method.

W1 and W3 : Zero flux condition ·

$$\frac{\partial G_H}{\partial r} = 0 \quad (7.32)$$

W2 and W4 : Zero flux condition :

$$\frac{\partial G_H}{\partial z} = 0 \quad (7.33)$$

EN : Gas composition is known :

$$G_{H(i,j,k)} = G_{H,av(k+1)} \quad (7.34)$$

EX : Continuity of gas composition :

$$\frac{\partial G_H}{\partial z} = 0 \quad (7.35)$$

7.5.6 Solid Phase Mass or Species Balance by Grain Model

Grain Model is used for predicting the solid phase mass or species balance as in the previous two Chapters. In the present case the solid is not static but moving and so the solid velocity also have to be taken under consideration with the help of a convective term, and the reaction rate at that position obtained by using grain model will act as a source term. Therefore the final equation becomes :

$$\frac{\partial X}{\partial t} + V_s \frac{\partial X}{\partial r} = \frac{DX}{Dt} \tag{7.36}$$

Where,

$$\frac{DX}{Dt} = \frac{k_{/rg} C_A}{C_{Bo} \left[1 + 2\sigma^2 \left\{ \frac{1}{(1-X)^{1/3}} + \frac{1}{N_{Sh}} - 1 \right\} \right]} \tag{7.37}$$

Boundary Conditions

SEN   Output composition from the upper hearth :

For odd k : $X_{(i+1,j,k)} = X_{av(k-1)}$ \hspace{2cm} (7.38)

For even k : $X_{(i-1,j,k)} = X_{av(k-1)}$ \hspace{2cm} (7.39)

SEX · Continuity boundary condition :

$$\frac{\partial X}{\partial r} = 0 \tag{7.40}$$

7.6   Computational Procedure

The grid size and time step were first estimated on the basis of Von Neuman stability analysis for the Crank Nicholson scheme used for the discretization. The parameters are initialized for the given input conditions by a main program, which then calls the subroutines for different process phenomena. The time difference between two consecutive set of solutions are in the range of 0.15 to 0.20 second, which is considered to be small enough to assume the solution of the equations

as simultaneous The equations were solved by line-by-line method by using a tridiagonal matrix solver [74]. The time of computation (real time) is in the range of 36 minutes for 1000 time steps, in the HP 9000 series miniframe systems The description of the program and the code developed for the process simulation are given in the Appendix C

7.7   Results and Discussion

Since the conditions in the hearths are not known we have to set some initial conditions, and since the gas and solid is moving counter current to each other they will reach a steady state after some time depending on the total residence time in the hearths. The total residence time for solid in the three hearths is about 44 minutes, and the results after 100 minutes of reduction are plotted, when all the parameter values have reached steady state condition Computation is done for the three middle hearths (4th, 5th and 6th), since the time for computation of steady condition is very high.

7.7.1   Gas Velocity

The gas velocity profile will play a very important role in mass transfer of the gaseous reactant from the bulk phase to the solid surface. The convective gas solid heat transfer will also be governed by gas velocity. Therefore the vector plot and streamline diagram of the gas flow is plotted, along with the contour plots for gas composition and temperature. Process dynamics of the system is studied next by plotting the change in parameter values with time. Parametric study for some of the important parameters like, the effect of temperature, gas composition and mixing of solid pellets by rabble arms were done to ascertain their relative importance.

Figure 7 3 shows the vector plot for the gas velocity profile in the three hearths. The increase in vector length in the identical positions indicate the relative increase in the gas velocity due to addition of reducing gases in that hearth. In figure 7.4 the stream line diagram for the gas flow is shown, and the increase in gas velocity from the lower hearth to the upper dearth is indicated by the increase in the number of stream lines.
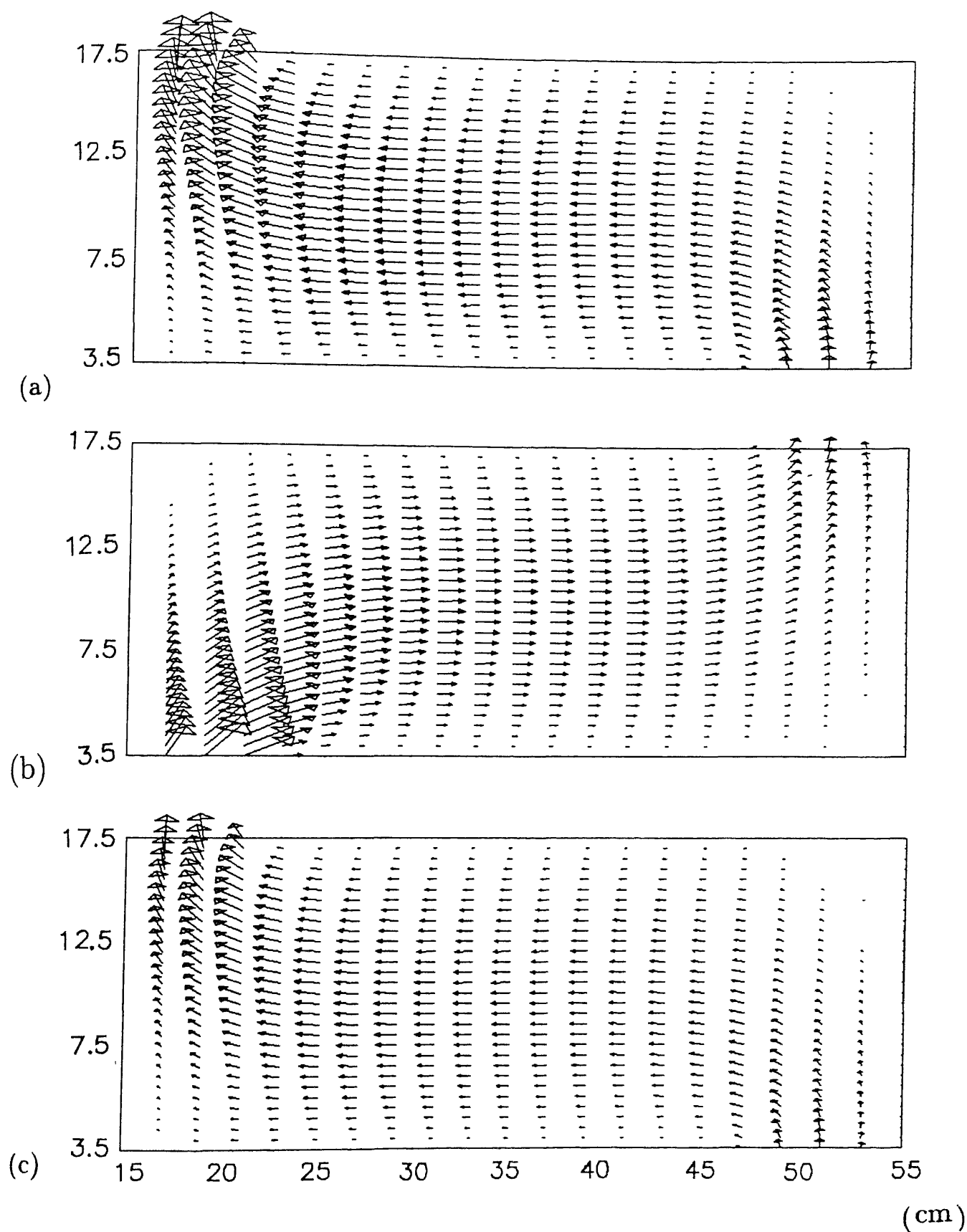
Figure 7 3. Vector plot for the gas velocity profile in the (a) 4th, (b) 5th, and (c) 6th hearths
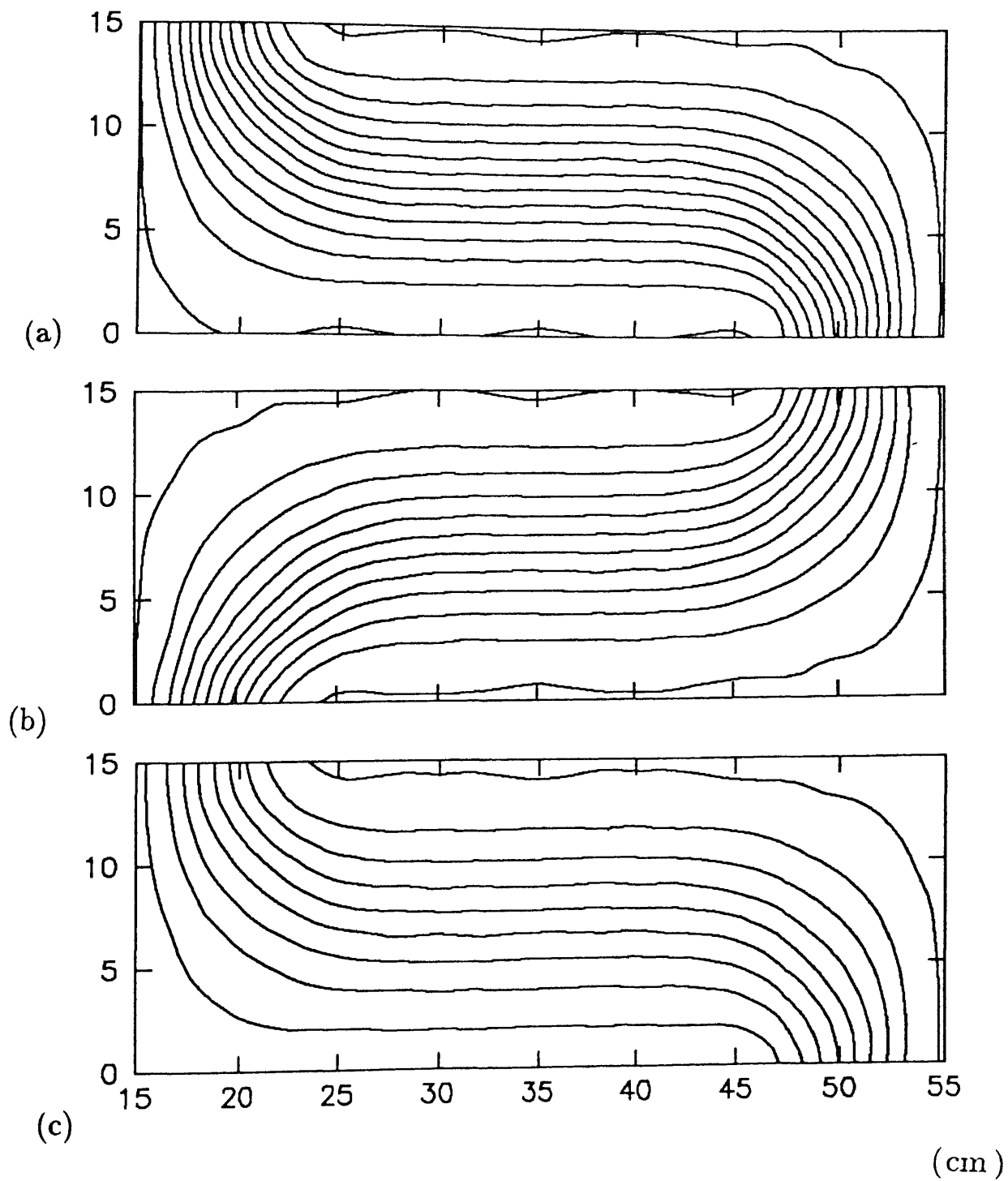
Figure 7.4: Stream lines for gas flow in the : (a) 4th, (b) 5th, (c) and 6th hearths.

7.7.2 Contour Plots

Contour plots for gas composition is shown in figure 7.5. The diagram showed very similar trend as shown by the stream line diagram for the gas flow, indicating that the gas-solid mass transfer is dominated by convection The change in gas composition is maximum in the 4^{th}th hearth as indicated by the number of contour lines. This is due to the reason that, unreduced gas enters the 4^{th}th hearth and initial reduction rate of iron is much higher due to the presence of hematite and magnetite which has much higher equilibrium partial pressure for water vapor than wüstite, which is the predominant phase in the next two hearths

Figure 7 6 shows the contour plot for gas temperature The gas is entering in the 6th hearth at 1040 K, while the temperature of the solid entering from top of the 4th hearth is 940 K The gas solid heat transfer is very fast in the 6th hearth indicated by the large number of contour lines in the gas entry position Here also the gas temperature follows the trend of the gas flow stream lines. Although there is some effect of heat transfer through the top walls.

7.7.3 Process Dynamics

Process dynamics of the system can be studied from figure 7.7, showing the change in percentage reduction of iron and nickel in the solid phase coming out from the lower (6th) hearth, and the composition of the gas coming out from the upper hearth (4th). Residence time of the solid pellets in the three hearths is about 44 minutes. From figure 7.7 it can be seen that approximate steady state composition for nickel is reached in about 66 minutes, after which it increases very slowly. From this we can roughly estimate that the time for attainment of steady state composition of the solid phase is about one and half the residence time of the solid in the hearths. The time for attainment of steady state in iron and gas composition is not very clearly demarkable since the reduction rate of iron is itself very slow in that region.

7.7.4 Parametric Study

There are various process parameters which can be studied by this model to understand their relative importance and optimize the conditions for efficient and economic operation. Some of the important parameters like effect of temperature, solid mixing in the hearths, and the effect of other reducing gases like carbon monoxide (CO) is studied in the present investigation.
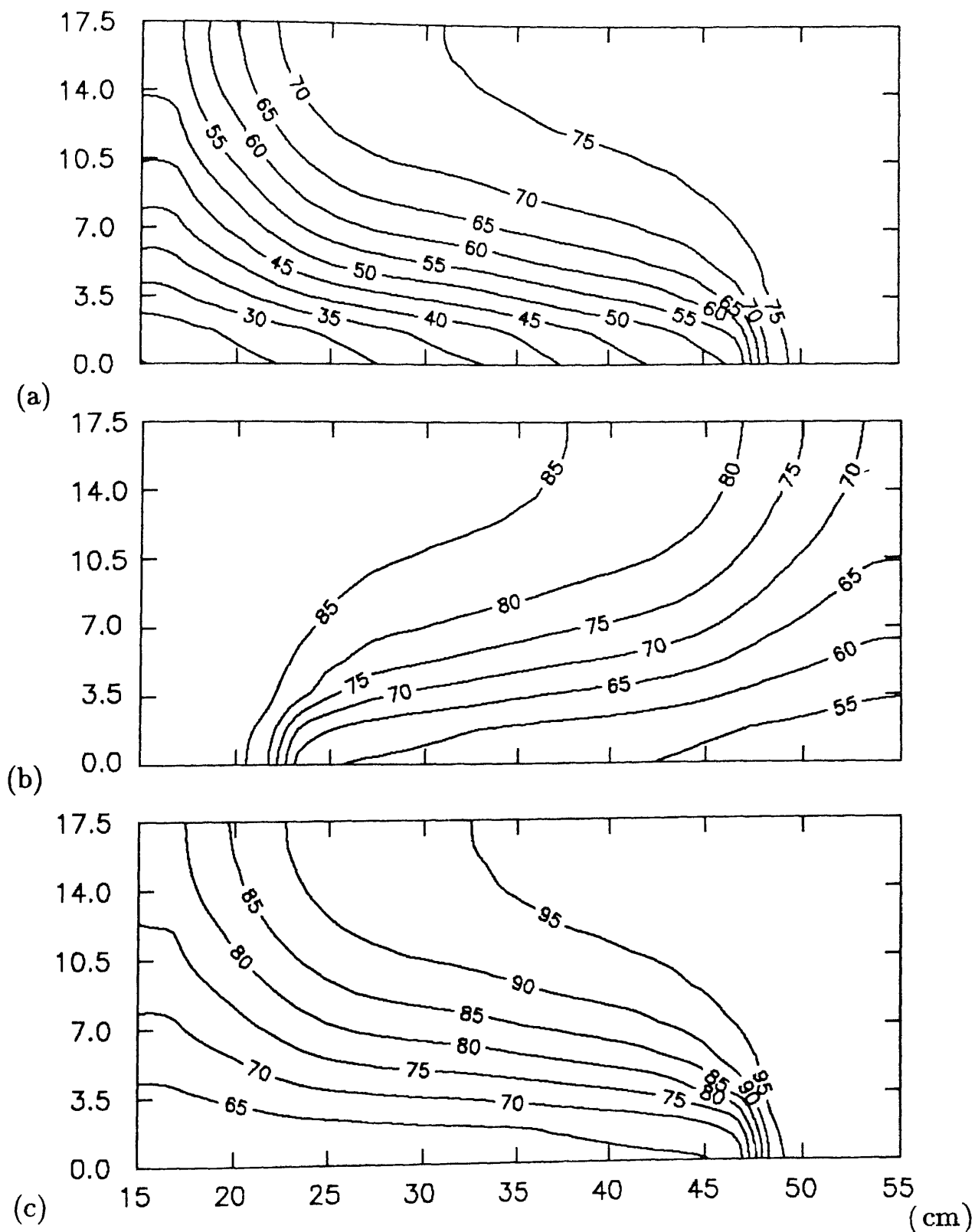
Figure 7.5: Contour plot for gas composition in the (a) 4th, (b) 5th, and (c) 6th hearths
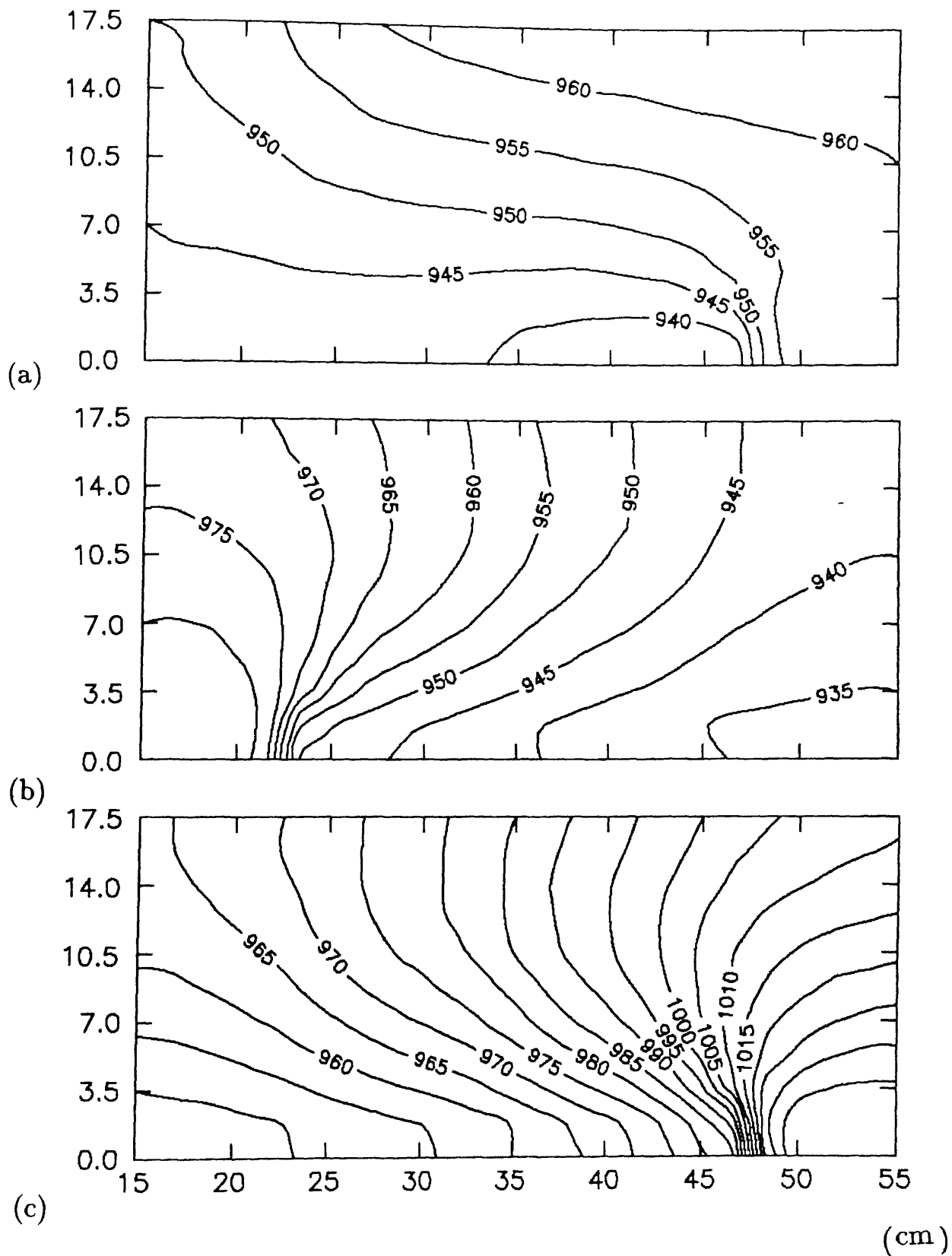
Figure 7 6· Contour plot for gas temperature in the (a) 4th, (b) 5th, and (c) 6th hearths.
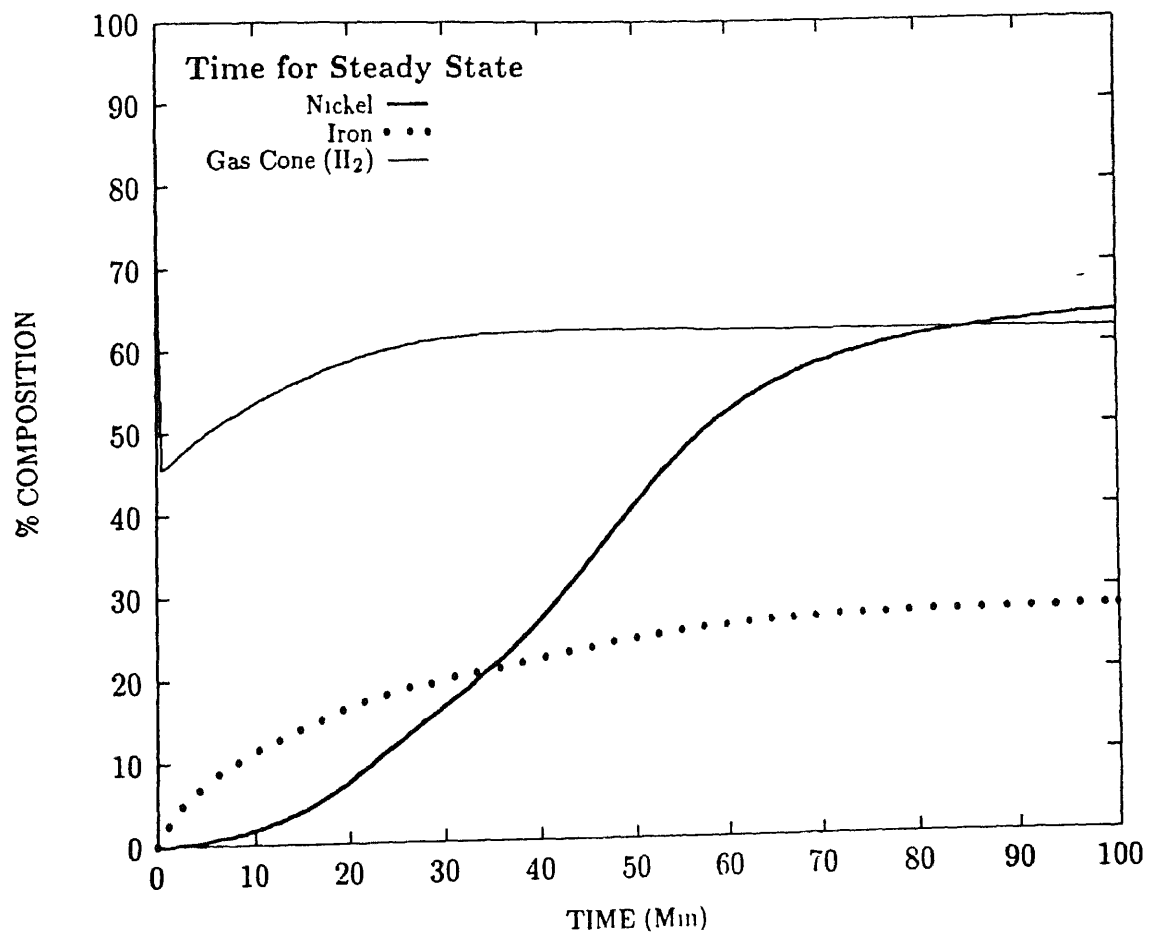
Figure 7 7: Attainment of steady state composition of exit gas from the 4th hearth and solid output from the 6th hearth.

The effect of temperature on reduction profile is shown in figure 7.8 The initial solid temperature for the two cases were 900 K and 940 K and the gas temperature were 1000 K and 1040 K, i.e , the overall difference in temperature for the two cases is 40 K. The result showed, the trend in reduction profile for the two cases remained more or less the same, and the final output concentration of nickel increased from about 46 % to about 62 % for the higher temperature condition.

The solid pellets in the hearths were continuously pushed by the rotating rabble arms and so mixing of the pellets bed takes place. The average angular velocity of the rabble arms were kept in the range of 1-3 RPM and the rate of mixing may vary to a large extent according to the RPM and shape of the rabble arms. No quantitative relationship for this mixing rate is available. However, its effect can be computationally studied by considering some mixing rate. In the present study 0 %, 25 % and 50 % solid mixing per minute is considered .The mixing condition is incorporated as follows .

$$X_{(i,j)} = (1 - M_x)X_{(i,j)} + M_x X_{i,av} \qquad (7.41)$$

Where $M_x = \frac{\%Mix}{100} dt$ and
$X_{i,av}=$Average Solid bed composition in the ith position in the $r-$direction.

The effect of mixing on the steady state reduction profile in the three hearths were shown in figure 7.9 For 0 to 25 % mixing there is an increase of about 6 % reduction of nickel in the final product, however the improvement in nickel reduction diminished to about 1-2 % for the further increase in mixing by another 25 %. This indicates the effect of mixing decreases gradually above 25 % mixing of the pellet bed. The effect of mixing is apparently not very significant in the present situation. This may be due to the reason that the bed thickness of 2.5 cm is not very high, and hydrogen having high diffusivity can easily diffuse inside the packed bed.

In the industrial furnaces reducing atmosphere is generated by substoichiometric combustion of hydrocarbon fuels like natural gas, fuel oil or coal. The hydrocarbon fuels were used for producing both thermal energy for the process and for the reduction operation; and the gaseous phase always contains hydrogen and carbon monoxide almost in equal proportions, as shown in table 2 2 reported in literature [3, 4] The kinetic parameters for carbon monoxide is taken from literature and may not be very accurate for the complex ore under investigation. Nevertheless, it will give us an first hand idea on its effect over the reduction process. The initial gas compositions chosen are 60 % H_2 , 30 % H_2 and 30 % CO, and 60 % CO, and their effect on the reduction
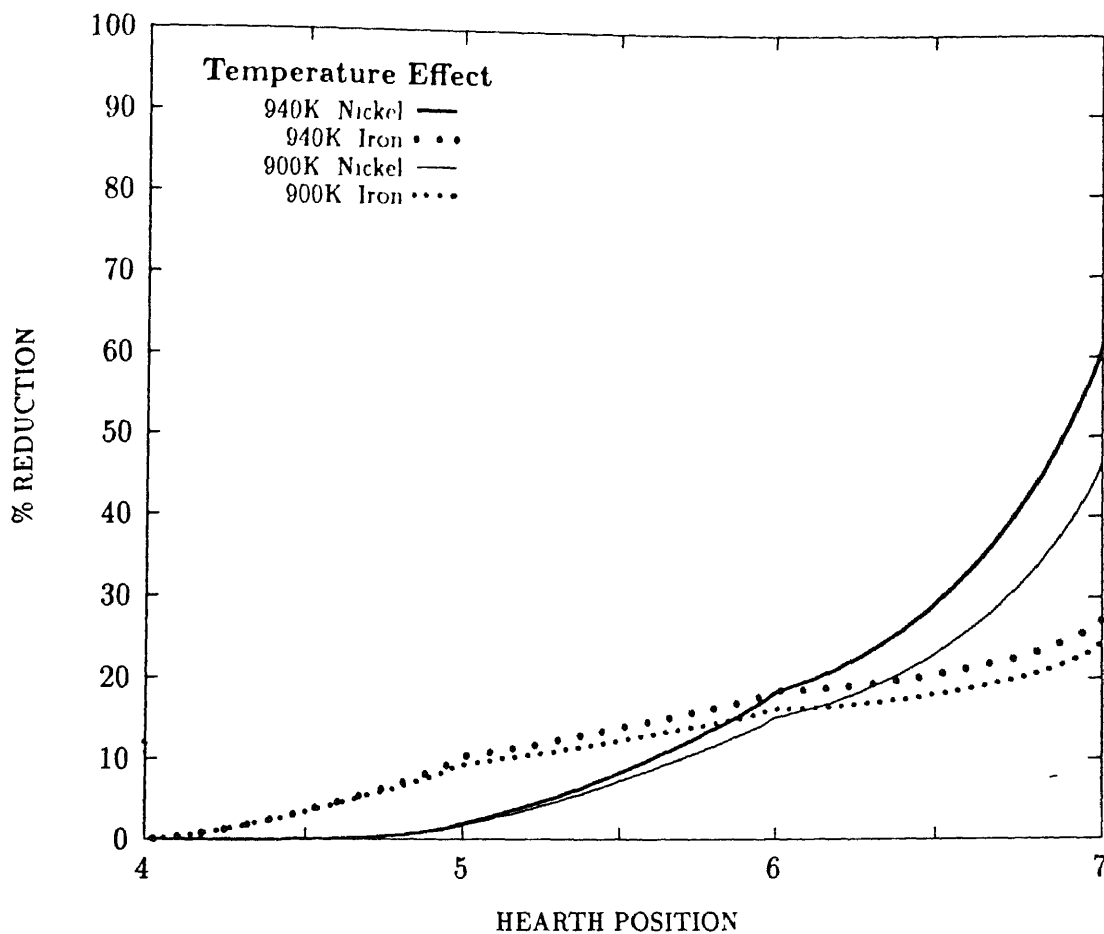
Figure 7.8 Effect of temperature on the steady state reduction profile in the hearths.
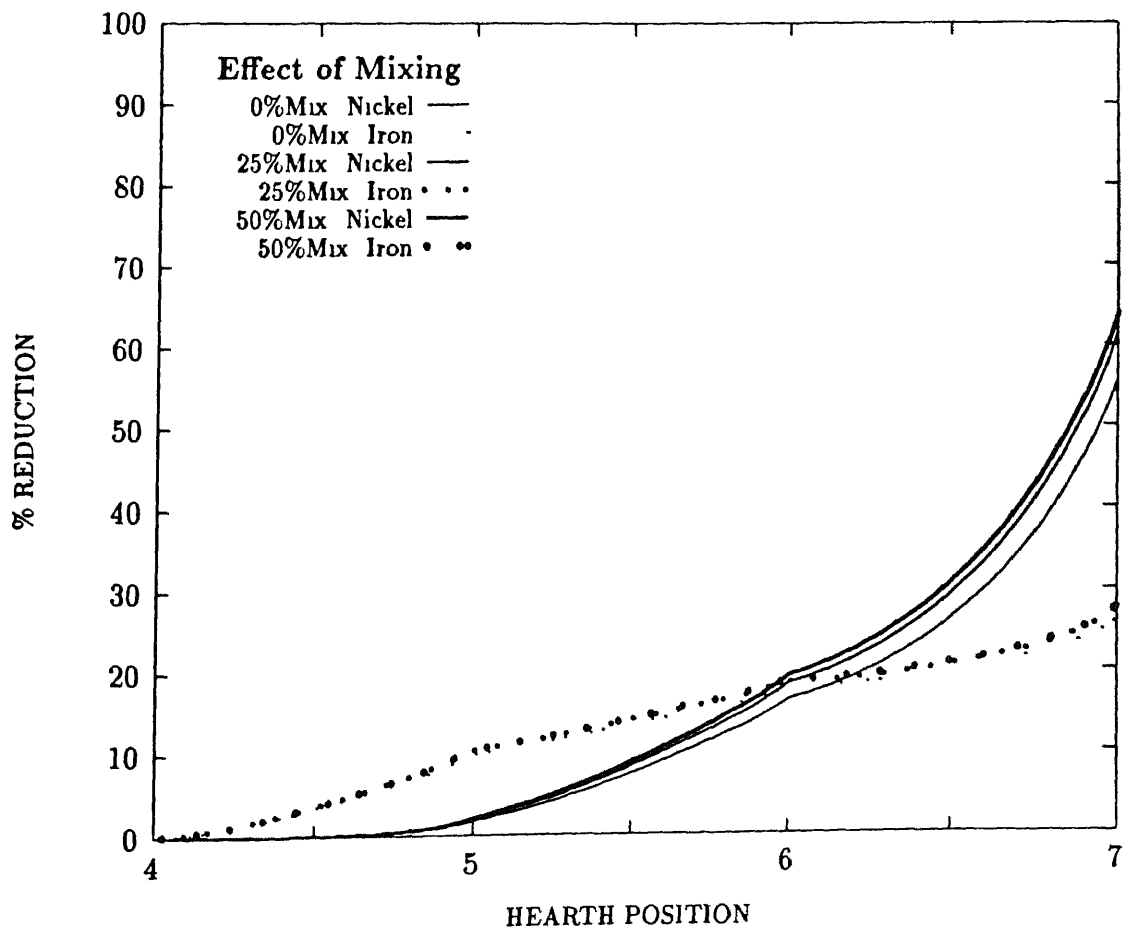
profile is shown in figure 7.10 The figure shows pure carbon monoxide is not a very strong reducing agent under the operating conditions, but the mixture of CO and H_2 has much better reducibility and good selective reducivity for nickel This is in agreement with the experimental findings reported by Singh et al. [4] for this type of ores. Therefore, mixture of hydrogen and carbon monoxide can be used advantageously for the reduction process under industrial conditions. The solid temperature profile for the three gas compositions mentioned before is plotted in figure 7 11. The initial solid and gas temperature is 940 K and 1040 K respectively. The profile shows there is a remarkable increase in solid temperature when carbon monoxide is used for the reduction. This is due to the exothermic nature of the reduction process with CO and endothermic nature with H_2. Therefore, the presence of carbon monoxide is also beneficial for the thermal efficiency of the process

7.8   Concluding Remarks

The salient features of the mathematical model developed for the MHF can be summarized below

1 The model for MHF developed in the present study is based on the experimental and computational study of the fixed bed reactors. This is done to improve the reliability and applicability of the simulated results.

2. Cylindrical axi-symmetric equations are considered for this purpose, since there is negligible angular variation in the furnace.

3. All the important phenomena like fluid flow, gas solid heat and mass transfer, and reaction kinetics of the nickeliferrous ore pellets are taken into consideration.

4. The results showed the heat and mass transfer between the gas and solid phases is dominated by convection.

5 The time for attainment of steady state composition of the solid product is approximately one and half times the residence time of the solid in the hearths

6. The effect of mixing is not very significant for the present operating conditions.

7. Although pure carbon monoxide is a poor reducing agent under the operating conditions; the mixture of CO and H_2 is found to have good reducibility for nickel.
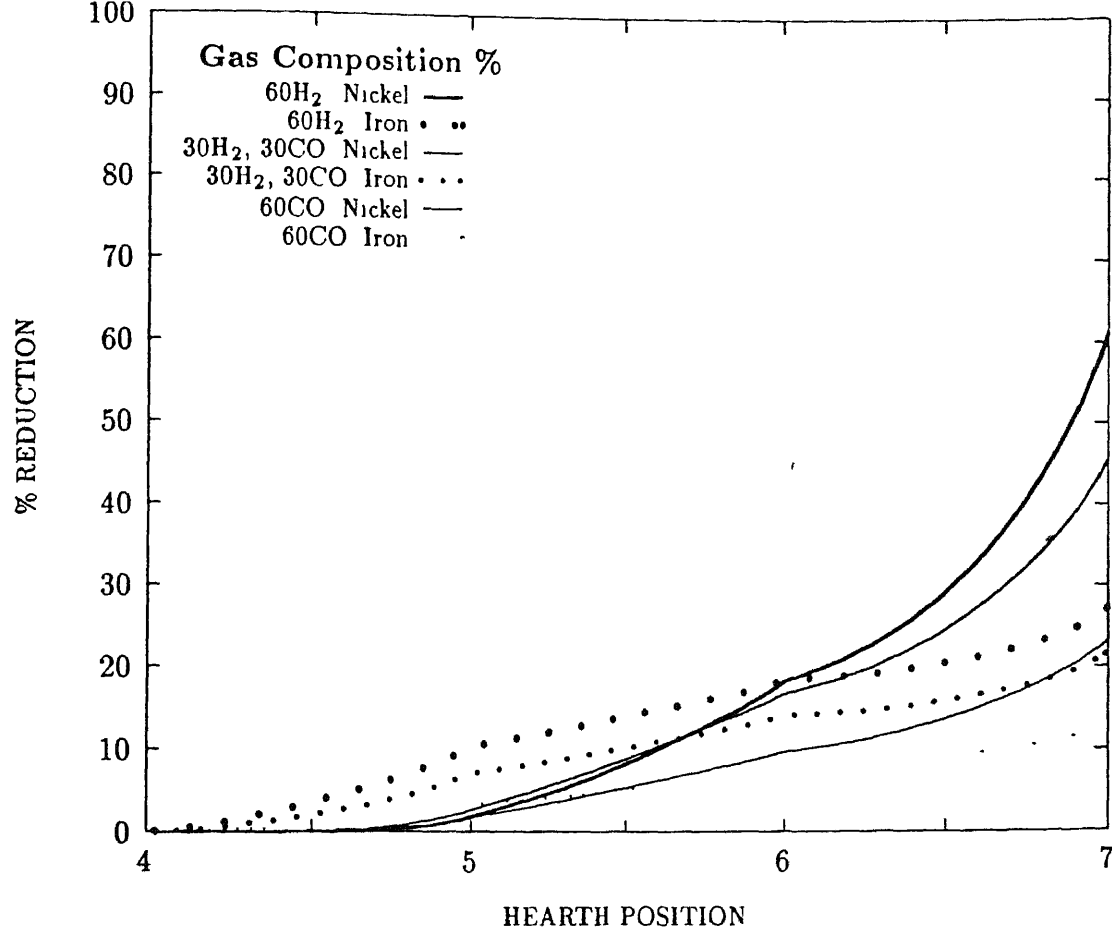
Figure 7.10: Effect of gas composition on the steady state reduction profile.
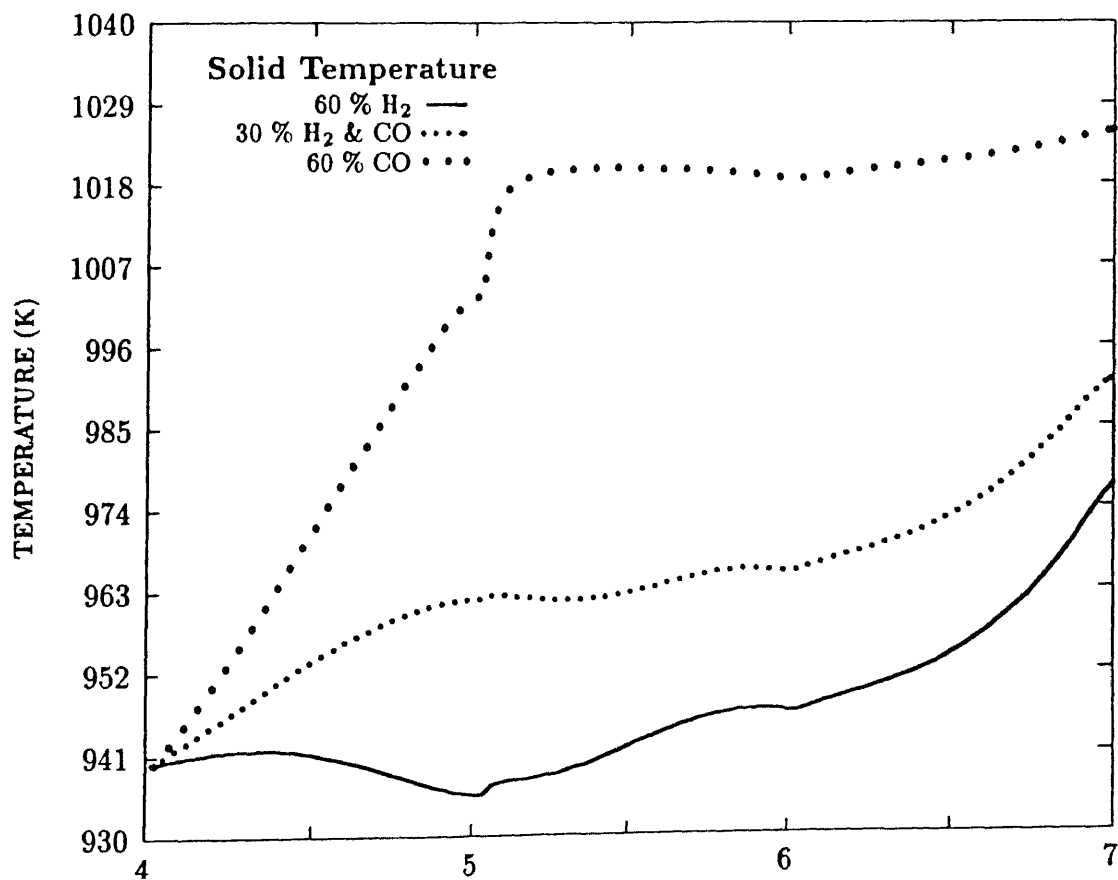
8 Temperature profile for solid increases appreciably for the reduction with CO, since the reduction of nickel and iron is exothermic with CO and endothermic with H_2.

Chapter 8

SUMMARY AND CONCLUSION

Considering the importance of nickel as a economically and strategically important metal, its extraction process is studied in this investigation Economic recovery of nickel from the low grade lateritic ore poses a considerable challenge for extractive metallurgy due to the energy intensive roasting operation involved in the process. The reduction mechanism of this type of ore is also not well established, and the reduction kinetics of nickel present in the ore varies considerably from the pure nickel oxide. To address these problems we have systematically studied the reduction roasting process of a typical low grade high iron containing nickel ore found in India. The procedure followed and the findings of the present investigation can be summarized as given below .

1. Single pellet reduction kinetics study with hydrogen was conducted in the range of 800 to 1000 K, in which the reduction roasting operation of this type of ores are generally conducted The study showed good reducibility of 90 % or more for nickel at 900 K and 1000 K, but 50 % or less at 800 K.

2. The experimental results were then analyzed by established gas solid reaction models to evaluate the kinetic parameters and to understand the mechanism of reduction The results showed gradual decrease in the rate constant value with reduction time. This is explained to be due to the product gas formation and non-isothermal reduction

3. It is known that nickel is present as solid solution with iron in the goethite phase of the nickel ore, and its reducibility is much less than the pure NiO. Due to this reason a complex oxide reduction mechanism is proposed.

4. Industrially reduction operations are conducted in roasting furnaces with moving bed of ore pellets or briquetes. The reactant gas flow may be vertically through the bed as in shaft furnace or over the bed as in multiple hearth furnace and rotary kiln To evaluate the reduction process under such conditions, fixed bed pellet reduction experiments were conducted for both the types of gas flow

5. Quasi-steady state models were then developed for the fixed bed reduction conditions and matched with the experimental results to verify the models The matching were found to be satisfactory considering the difficulties and limitations of experimental technique. The models were then used further to study the effect of some of the important parameters like pellet size, gas composition etc.

6. The experimental results were compared with the predictions made by the mixed oxide mechanism (which is used generally), and the proposed complex oxide mechanism. The predictions are similar for most of the cases, except for the conditions where reduction is less, and complete wüstite formation has not taken place Under such conditions complex oxide mechanism for nickel reduction gave better results and so for the parametric study this mechanism is used.

7 The effect of water vapor on reducibility was found to be more significant at 900 K than at 1000 K, and due to this reason reduction kinetics under packed bed conditions is much faster at 1000 K than at 900 K.

8 The effect of pellet size is not very significant under the packed bed conditions, indicating that the diffusion inside the pellet is not rate controlling.

9. An axisymmetric model for multiple hearth furnace was then developed using quasi-steady state formulation as used for the fixed bed reactor models. In the model each hearth is considered as a separate entity and output of one hearth is the input for the next hearth. By this method we can compute all the hearths together, or few selected hearths of importance.

10. MHF results showed gas solid heat transfer is quite fast, and high gas temperature is required to heat the ore bed.

11 Although Pure CO is not a very good reducing agent at the operating temperatures, but mixture of CO and H_2 was found to be a good reducing agent with better selective reducibility of nickel than pure H_2.

12 The MHF model can be easily scaled up for larger industrial furnaces, for nickel ore reduction, and it can also be adopted for other roasting systems provided the reaction kinetics of the system is known.

Chapter 9

SUGGESTION FOR FUTURE WORK

Based on the experience gained by this study few suggestions can be made for the future investigation of the process :

1. Similar experimental study can be conducted for reduction with carbon monoxide as the reducing agent, since under industrial conditions hydrocarbon fuels are used for providing both thermal energy and reducing atmosphere containing H_2 and CO in almost equal proportions.

2. The MHF model can be scaled up and used for comparing with industrial data, and for process control.

3. Similar models can be developed for other types of industrial furnaces like shaft furnace, rotary kiln etc., and compared with the MHF results to quantitatively determine their performance and advantages under different conditions.

Appendix A

Experimental data and Parameter values

A.1 X-Ray Powder Diffraction Data

X-ray powder diffraction study is done to characterize the ore and its reduced product. The powder diffraction charts and the identified phases are shown in figure 3.2 and 3 9 of Chapter 3 The peak angles and their intensities are measured from those charts and given in a tabular form in this section

The measured values of the peak angles and intensities for the gangue mineral, run of mine ore, and the heated and dehydrated ore (shown in figure 3.2), is given in table A.1. Table A.2 showed the similar results for the reduced ore (shown in figure 3 9) Powder diffraction data cards [54] are used to identify the phases by matching the characteristic peak positions or $d-$spacings. The characteristic $d-$spacings and their peak intensities for the phases identified in the present study are shown in table A.3, A.4, A.5 and A.6.

Table A 1 The characteristic peaks and phase identified for the ore, gangue and dehydrated ore.

(Gangue)		< Reducible Oxide >			
(1) SiO_2		<4> $(Fe_{2/3}Ni_{1/3})OOH$			
(2) Al_2SiO_5		<5> $FeOOH$			
(3) SiO_2		<6> $\gamma - Fe_2O_3$			
		<7> $(FeCr_2O_4$			
Angle	d Å	Gangue Mineral I/I_{Max}	As Received Ore I/I_{Max}	Dried at : 850 K I/I_{Max}	Phase Identified Code No.
19.80	6.662	15	0	4	(2)
26.55	4.988	0	8	0	<5>
31.60	4 253	50	65	21	(1) <5>
36 40	3.668	6	0	17	(3) <6>
40.09	3.342	100	100	63	(1,2) <5>
50.26	2 697	10	28	51	<5,6>
51.68	2.628	0	6	0	(3)
54.25	2.513	0	0	45	<6,7>
55.53	2.459	20	42	15	(1) <5>
60.22	2.283	10	0	4	(1)
61.52	2.240	10	10	0	(1) <4,5>
63.01	2.192	0	10	12	<5,6>
65.26	2.124	19	7	4	(1)
70.60	1.982	10	0	4	(1)
77.04	1.839	0	0	18	<7>
78.00	1.820	22	12	25	(1)
79.01	1.801	0	6	0	<5>
83.77	1.716	0	19	0	<5>
85.26	1.691	3	0	30	<6,7>
86.26	1.676	10	0	0	(1)
91 25	1.603	0	3	7	<6>
94.19	1.564	0	8	0	<5>
95.68	1 545	25	7	9	(1)
98.82	1.508	0	6	0	<5>
100.87	1.486	0	0	15	<6>
104.01	1.454	6	13	25	(3) <6>
111.88	1.383	12	5	7	(1,2)
112.82	1.375	26	8	17	(1)
122.29	1.308	0	0	10	<6>

Table A 2· The characteristic peaks and phase identified for the ore reduced at 800 K, 900 K and 1000 K

(Gangue Mineral)		< Reducible Oxide >		{Partially Reduced Oxide}	[Reduced Metal]
(1) SiO_2		< 4 > $(Fe_{2/3}Ni_{1/3})OOH$		{8} Fe_3O_4	[10] α-Fe
(2) Al_2SiO_5		< 5 > $FeOOH$		{9} FeO	[11] Ni
(3) SiO_2		< 6 > $\gamma - Fe_2O_3$			
		< 7 > $FeCr_2O_4$			
		Reduction Temperature			Phase
		800 K	900 K	1000 K	Identified
Angle	d Å	I/I_{Max}	I/I_{Max}	I/I_{Max}	Code No.
27.35	4.845	8	4	4	< 7 > {8}
31.25	4.253	24	24	22	(1)
40 01	3.348	83	85	85	(1,2)
45.84	2.941	12	12	4	< 6,7 > {8}
54.25	2.513	45	37	17	< 6,7 > {8,9}
55.53	2.459	15	10	10	(1)
60 22	2.283	8	6	8	(1)
61 52	2.240	3	5	4	(1)
65.26	2.124	9	5	6	(1)
66.81	2.081	11	5	0	< 6,7 >
68.80	2.029	0	75	100	[10,11]
70.60	1.982	5	5	2	(1)
78 00	1.820	10	14	14	(1)
86.26	1.676	0	3	5	(1)
90 65	1.611	14	0	0	< 6,7 >
91 25	1.603	0	9	5	{8}
95.68	1.545	9	13	9	(1){9}
102 10	1.473	22	16	5	< 7 > {8}
105.85	1.436	0	8	20	[10]
111.88	1.383	6	5	10	(1,2)
112.82	1.375	10	8	20	(1){9}

Table A.3: X-Ray Powder Diffraction Datafile for · (Gangue Mineral)

(1) SiO_2 Alpha Quartz 5-0490		(2) Al_2SiO_5 Aluminium Silicate 11-46,46a		(3) $Mg - Al - Si - O$ Serpentine 11-386	
d Å	I/I_{Max}	d Å	I/I_{Max}	d Å	I/I_{Max}
4 260	35	6.70	5	7.25	60
3.343	100	4 30	25	4.61	20
2 458	12	3.77	20	3.62	60
2.282	12	3.35	65	2 503	100
2.237	6	3 18	100	2.148	35
2 128	9	3.02	15	1 788	15
1.980	6	2.947	20	1 541	25
1.817	17	2.727	10	1.507	20
1.672	7	2.699	25	1.496	15
1 659	3	2.694	25	1 312	10
1.541	15	2.520	30	1 299	5
1.453	3	2.509	20	1.274	5
1.375	11	2.355	30		
1.372	9	2 350	30		
1.288	3	1.962	55		
		1.935	50		
		1.930	50		
		1.377	75		

Table A.4: X-Ray Powder Diffraction Datafile for : <Reducible Oxide>

< 4 > $(Fe_{2/3}Ni_{1/3})OOH$ Iron Nickel Hydroxide 14-556		< 5 > $FeOOH$ Goethite 17-536		< 6 > $\gamma - Fe_2O_3$ Hematite 4-0755		< 7 > $FeCr_2O_4$ Chromite 4-075a	
d Å	I/I_{Max}	d Å	I/I_{Max}	d Å	I/I_{Max}	d Å	I/I_{Max}
2.565	100	4.98	10	2.95	34	4.83	50
2.240	70	4.18	100	2.78	19	2.95	50
1.710	50	3.38	10	2.52	100	2.51	100
1.480	70	2.69	30	2 08	24	2.08	50
		2.49	16	1.70	12	1.91	75
		2.452	25	1 61	33	1.71	25
		2 252	10	1 48	53	1.61	75
		2.192	20	1.27	11	1.49	75
		1.721	20			1.28	50
		1.564	16				

Table A 5 X-Ray Powder Diffraction Datafile for {Partially Reduced Oxide}

{8} Fe_2O_3 Magnetite 19-629		{9} FeO Wüstite 6-0615	
d Å	I/I_{Max}	d Å	I/I_{Max}
4.852	8	2.49	80
2 967	30	2 153	100
2 532	100	1.523	60
2.424	8	1.299	25
2 099	20		
1.7146	10		
1.6158	30		
1.4845	40		
1.2807	10		

Table A.6· X-Ray Powder Diffraction Datafile for : [Reduced Metal]

[10] $\alpha - Fe$ Iron (α phase) 6-0696		[11] Ni Nickel 4-0850	
d Å	I/I_{Max}	d Å	I/I_{Max}
2.0268	100	2.034	100
1 4332	20	1.762	42
1.1702	30	1.246	21
		1.0624	20

A.2 Reduction Experiment Results and Data

A.2.1 Manometer Calibration

The hydrogen gas flow rate for the experiments were measured and controlled by gas flow manometers. The manometer pressure or height difference is first calibrated for the gas flow rates by soap bubble flow measuring tube. Flow rates are measured for different height differences and a second order curve is fitted through the points to get the relation between flow rate and height difference. The manometer calibration data is given in table A.7, and the fitted curve and the selected flow rates for the three set of experiments, are shown in figure A.1.

Table A 7. Manometer calibration for the flow rate measurements of hydrogen in the single pellet, and fixed bed reduction experiments.

Serial No.	Single Pellet		Vertical Flow		Horizontal Flow	
	Height diff. (cm)	Flow Rate (cc/s)	Height diff. (cm)	Flow Rate (cc/s)	Height diff. (cm)	Flow Rate (cc/s)
1	1.9	3.796	4.5	4 725	1.9	6.49
2	4.7	8 538	7.0	7.106	4.2	13.02
3	8.7	12.445	8.6	8.704	5.5	16.28
4	11.0	15 44	11.1	11.275	8.6	23.39
5	17.4	21.186	13.0	13.014	11.9	33.30
6	18.4	21.952	15.7	15.285	19.6	49.38
7			18.3	17.519		
Flow Rate :	$1.396 + 1.48 h_d - 0.0195 h_d^2$		$0\ 082 + 1.062 h_d - 0.006 h_d^2$		$0\ 982 + 2.91 h_d - 0.022 h_d^2$	
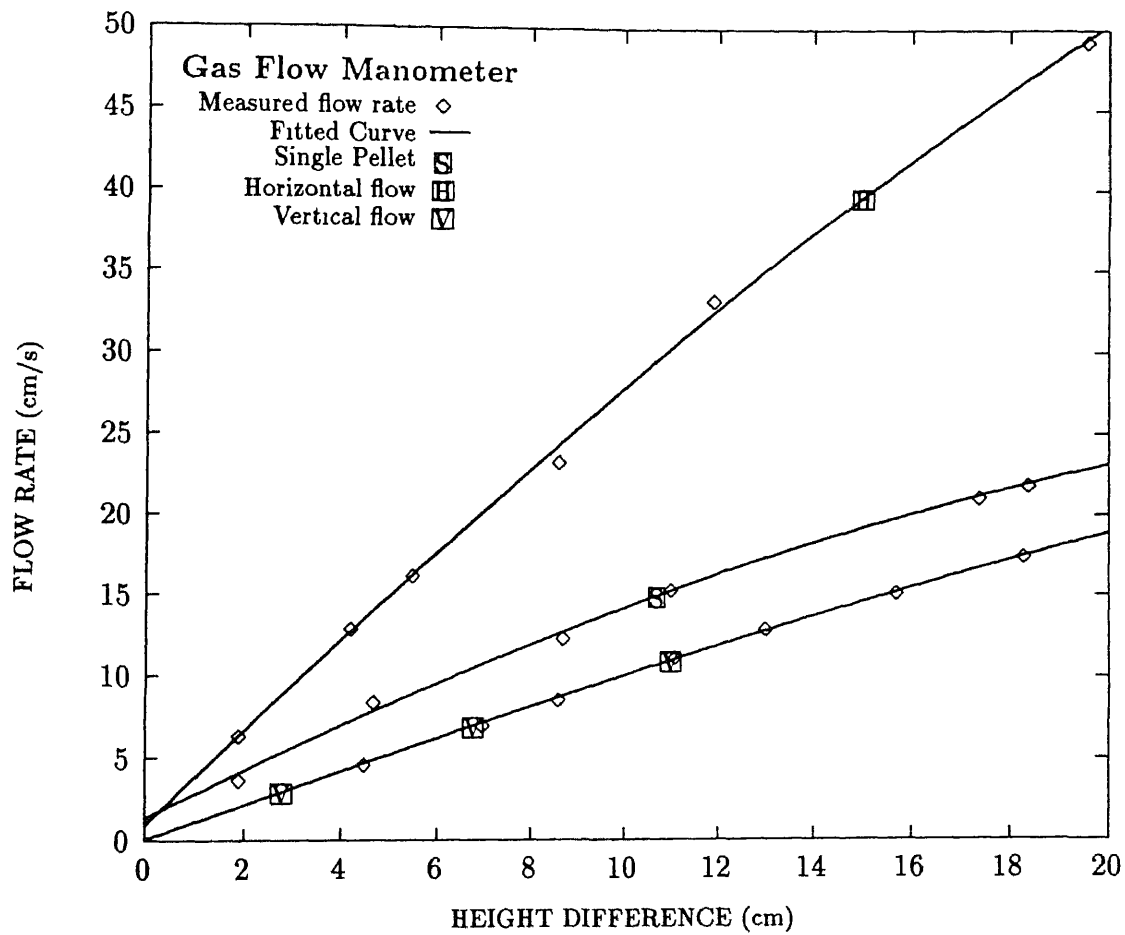
Figure A 1: Manometer calibration and selected gas flow rates of hydrogen.

A.2.2 Single Pellet Reduction Data

The single pellet reduction experiment data shown in figure 3.8 of Chapter 3 is given in tabular form for nickel and iron reduction in tables A 8, A.9, A.10, and tables A 11, A.12, A.13 respectively.

Table A.8. Single pellet reduction data for nickel at 800 K.

Serial	Small		Medium		Large	
No.	Time (Min)	% Ni Reduced	Time (Min)	% Ni Reduced	Time (Min)	% Ni Reduced
1	5.0	18 18	5.0	16.44	6.0	15.78
2	10.0	28 49	10 0	24 97	8 0	18 91
3	15 0	36 34	18.0	35 74	15.0	29.07
4	24.0	43 62	25 0	41.13	20.0	35.55
5	34 0	49.96	33.0	45.63	30.0	40.55
6			40.0	47 98	40.0	44.27

Table A.9. Single pellet reduction data for nickel at 900 K.

Serial	Small		Medium		Large	
No.	Time (Min)	% Ni Reduced	Time (Min)	% Ni Reduced	Time (Min)	% Ni Reduced
1	5.0	37.10	7 5	42.53	8.0	38.10
2	8.0	54.85	10.0	52.45	11.0	48.15
3	10.0	65.77	15.0	72.92	12.5	55.85
4	18.0	84.76	25.0	86.27	19.0	69.20
5	30.0	91.50	32.0	91.09	30.0	80.61

Table A.10: Single pellet reduction data for nickel at 1000 K

Serial	Small		Medium		Large	
No.	Time (Min)	% Ni Reduced	Time (Min)	% Ni Reduced	Time (Min)	% Ni Reduced
1	4.0	56.26	5.0	51.25	5.0	47.98
2	8 0	77.89	10 0	77.72	10 0	67.93
3	12.0	85.50	15.0	83.95	15.0	78 80
4	15 0	88.52	20.0	89.18	24.0	86.80
5	20.0	91.36	26.0	91.16	28 0	89.37

Table A.11: Single pellet reduction data for iron at 800 K.

Small		Medium		Large	
Time (Min)	% Fe Reduced	Time (Min)	% Fe Reduced	Time (Min)	% Fe Reduced
1.0	7 049	0.5	2.632	2.0	7.848
2.5	14.361	1 5	6.239	4.0	13 325
4.0	17.413	2.5	10 518	7.0	15.205
5.0	19.075	3.5	14.967	10 0	16.904
7.0	20.701	5.5	16.383	11.0	17.474
9.0	22.627	10.5	19 892	15.0	19.173
11.0	24.279	19.5	24.391	20.0	20 482
12.0	25 109	29.5	27 608	26.0	21.806
14.0	26.490	33.5	28.573	28.0	22.187
17.0	27.862	35.0	28.895	31.0	22.762
21.0	30.369	40.0	29 875	34.0	23.340
23 0	31.200			40.0	24.102
30 0	34.257				
34.0	35.512				

Table A 12· Single pellet reduction data for iron at 900 K

Small		Medium		Large	
Time (Min)	% Fe Reduced	Time (Min)	% Fe Reduced	Time (Min)	% Fe Reduced
1 5	7 531	1.0	5.398	1.0	5.764
2.5	17 435	2 0	10 486	2 0	10 588
3.5	20 755	3.0	14 479	3 0	12.961
4.5	23.511	4 0	16 588	4 0	15.903
5 5	25 702	6 0	19 878	8 0	21.101
6 5	28.187	7 0	22.946	10 0	23 909
8.5	32 606	8 0	24 760	13 0	26 984
10 5	38 484	9 0	26 579	15.0	29 144
12 5	41.522	10 0	28.402	17.0	30.579
14.5	43.436	11.0	29.600	19.0	32.120
16.5	45.658	12 5	31.718	21 0	33 710
17.5	46.918	14.0	35.105	24.0	36.123
20 5	50 438	15.0	36.633	27.0	38.292
24 5	52.837	19.0	40 892	29.0	39.882
26 5	54 982	20 0	41.807	30 0	40.254
27 5	55.842	23.0	44.571		
30.0	56.848	27.0	47.472		
		30.0	48.994		
		32.0	50.468		

Table A.13: Single pellet reduction data for iron at 1000 K

Small		Medium		Large	
Time (Min)	% Fe Reduced	Time (Min)	% Fe Reduced	Time (Min)	% Fe Reduced
1.0	18 076	1.0	16.636	1.0	13.025
2.0	27.152	2.0	25.766	2.0	19.465
3.0	36.808	4.5	42.257	3.0	27.582
4 0	43.841	5.0	44.712	4.0	34.250
5.0	50.908	6.0	48.561	5.0	40.110
6.0	55.074	7.0	52.355	6.0	45.104
7.0	57.398	10.0	61.022	7.0	47.743
8.0	61.337	11.0	62 997	9.0	53.130
9.0	63.293	12.0	65 123	10.0	57.308
10.0	65 791	16.0	71.511	11.0	59.656
12 0	69.660	18.0	73.280	12.0	61.276
16.0	74.204	21.0	75.756	15.0	67 814
20 0	76.840	22.0	76 464	16.0	68.897
		25.0	78.600	20.0	72.321
		26.0	79 036	23.0	75.766
				26.0	77.200
				28.0	77.555

A.2.3 Nickel Reduction Data for Vertical gas flow condition

Representative samples from the five layers of ore pellets separated by wire mesh is collected and leached to estimate the amount of nickel reduced The experimental nickel reduction data points are shown in figure 5.7 and 5 8 for reduction at 900 K and 1000 K Those results are given in tabular form in this section in table A.14 and A 15 respectively

Table A.14· Experimental results for nickel reduction under vertical gas flow at 900 K

Velocity :	5V	5V	5V	2V	8V
Time .	10 Min	20 Min	30 Min	20 Min	20 Min
Bed Position					
V1	16 68	34.18	78.63	8 68	62 61
V2	8 20	31.28	45.53	4 25	49.68
V3	4 43	24 41	39.07	1.29	32 18
V4	1.39	14.51	26.81	0 00	23.54
V5	0 00	9 05	8.08	0 00	12.68

Table A 15· Experimental results for nickel reduction under vertical gas flow at 1000 K.

Velocity :	5V	5V	5V	2V	8V	5V : Reproducibility
Time :	10 Min	20 Min	30 Min	20 Min	20 Min	20 Min
Bed Position						
V1	77.11	87 36	93.12	74.62	93.67	92 27
V2	34.67	84.69	93 27	39.68	92.39	93.91
V3	11.41	63.70	89.42	5.58	90.32	74.35
V4	5.72	37 53	82 14	2.31	78.44	43.70
V5	2.05	11.53	35 33	0.00	55.39	4.13

A.2.4 Nickel Reduction Data for Horizontal gas flow condition

The experimental results for nickel reduction under horizontal gas flow condition at 900 K and 1000 K is shown in figure 6.1. Those results are given in tabular form in this section in table A 16

Table A 16· Experimental results for nickel reduction under horizontal gas flow condition.

Bed Position	Temperature 900 K			Temperature 1000 K			Reproducibility 1000 K
	Time 15 Min	Time 30 Min	Time 45 Min	Time 15 Min	Time 25 Min	Time 35 Min	Time 15 Min
H1	0.50	2.1	5.4	1.30	5.95	29.12	4.10
H2	2.48	4.62	7.34	5 40	12 12	54 91	8.13
H3	3.33	17.35	43.21	9 40	31.56	82.45	8.31
H4	5 64	42.14	81 03	32 64	80 20	90.80	46.07
H5	11.22	58.84	93 2	81 42	93 12	91.60	87.42

A.3 Thermodynamic Data

A.3.1 Free Energy change due to reaction

Free energy change of the relevant reactions are take from literature [79] and is given in table A.17. The heat of reaction ($q = - \Delta H^o$) is also taken from the thermodynamic data. The equilibrium constant values for magnetite, and wüstite reduction are also evaluated from the thermodynamic data, while for hematite to magnetite reduction it is approximately taken as ten, since the thermodynamic value is too high, which is not supported by experimental observations reported literature [80], and also for computational stability. The value is still much higher than the magnetite and wüstite reduction as shown in figure 3.12 indicating much lesser effect of water vapor

Table A 17 Standard state free energy change of the reactions and the equilibrium constant values used in the present study

REACTION	$\triangle G° = \triangle H° - T \triangle S°$ $(J/Mole)$	Equilibrium Constant (K_{eq})
$< C > +2(H_2) = (CH_4)$	$-75180 + 81.73T$	
$2 < C > +3(H_2) = (C_2H_6)$	$-84840 + 173\ 33T$	
$< C > +(O_2) = (CO_2)$	$-395640 + 0.84T$	
$< C > +0.5(O_2) = (CO)$	$-112140 + 88.00T$	
$(CO) + 0.5(O_2) = (CO_2)$	$-283500 + 87.15T$	
$(H_2) + 0.5(O_2) = (H_2O)$	$-247380 + 55.02T$	
$< NiO >=< Ni > +0.5(O_2)$	$240660 - 94.42T$	
$< NiO > +(CO) =< Ni > +(CO_2)$	$-42840 - 7.27T$	(Neglected)
$< NiO > +(H_2) =< Ni > +(H_2O)$	$-6720 - 39.40T$	(Given below)[†]

[†] Plushkel et al. [21] $\left(1 - \dfrac{R_h}{K_{eq}}\right) = \dfrac{1}{\sqrt{P_{H_2}}\left(1 + 2.71 \times 10^{-2}\exp(5838/T)R_h{}^2\right)}$

Equilibrium Constant
(Approximated from above eqn) : $K_{eq} = 518\exp(-5838/T)$

$3 < Fe_2O_3 >= 2 < Fe_3O_4 > +0.5(O_2)$	$250404 - 141.20T$	
$< Fe_3O_4 >= 3 < FeO > +0.5(O_2)$	$313404 - 125.60T$	
$< FeO >=< Fe > +0.5(O_2)$	$265902 - 65.60T$	
Combustion		
$< C_7H_{16} > +11O_2 = 8(H_2O) + 7(CO_2)$	-4455700	
Step Wise Reduction .		
$3 < Fe_2O_3 > +(H_2) = 2 < Fe_3O_4 > +(H_2O)$	$3024 - 86.18T$	10^*
$3 < Fe_2O_3 > +(CO_2) = 2 < Fe_3O_4 > +(CO_2)$	$-33096 - 54.05T$	10^*
$< Fe_3O_4 > +(H_2) = 3 < FeO > +(H_2O)$	$66024 - 70.56T$	$4821\exp(-66024/RT)$
$< Fe_3O_4 > +(CO) = 3 < FeO > +(CO_2)$	$29904 - 38.43T$	$100\exp(-29904/RT)$
$< FeO > +(H_2) =< Fe > +(H_2O)$	$18522 - 10.58T$	$3.684\exp(-18522/RT)$
$< FeO > +(CO) =< Fe > +(CO_2)$	$-17598 + 21.55T$	$0.0756\exp(-17598/RT)$
Water Gas Reaction :		
$< CO > + < H_2O >= (H_2) + (CO_2)$	$-36120 + 32.13T$	

* Approximated

A.3.2 Reaction Kinetic Parameters

The activation energy and rate constant values for the reduction reactions of nickel and iron, as reported by various investigators, and the experimentally determined kinetic parameters for hydrogen is given in this section. The activation energies for nickel and iron reduction with hydrogen is given in table A.18 and A.19, and with carbon monoxide is given in table A.20 and A.21 respectively. The experimentally determined rate constant values for reduction with hydrogen, which is used for the present calculations are given in table A.22, and the rate constant values used for estimating the reduction rate with CO is given in table A.23.

Table A.18 Activation Energy of Nickel Oxide Reduction with Hydrogen

Reference	KJ/mole	Temperature Range (K)
Kivnick and Hixson [81]	42.8	450 - 673
Parravano [82]	110.9	428 - 473
Bandrowski et al [20]	52.1 - 60.5	534 - 576
Fretty [83]	52 1 - 60.5	534 - 576
Chiesa and Rigaud [84]	110.5	453 - 523
	47.5	523 - 573
Szekely et al [18]	133.6	497 - 532
	44.5	532 - 581
Szekely, Evans [17]	57.5	- below 630
	53.3	- above 630
Szekely, Hastaoglu [27]	53.7	670 - 550
Present Work	57.4	800 - 1000

Table A 19. Activation Energy of Iron Oxide Reduction with Hydrogen.

Reference	Oxide Phase	KJ/mole	Temperature Range (K)
Hockings [85]	Hematite(Fe_2O_3)	49.35	below 823
McKewan [80]	Hematite	60.06	above 823
Themelis and Gauvin [86]	Hematite	34.86	above 873
Shehata and Ezz [86]	Hematite	53.76	below 873
Szekely and Hastaoglu [27]	Hematite	53.68	550 - 670
Ranade and Evans [36]	Hematite	39.90	above 873
McKewan [63]	Magnetite(Fe_3O_4)	57 2	670 - 830
Yu and Gillis [87]	Hematite-Magnetite	63.30	above 773
	Magnetite-Wüstite	73.30	above 773
	Wüstite-Iron	113.00	above 773
Warner [64]	Wüstite(Fe_xO)	63.84	900 - 1250
Hayes [88]	Wüstite	69.30	750 - 1250
Present Work	Hematite	26 37	800 - 900
		76.80	900 - 1000
	Magnetite	17.28	800 - 900
		96 28	900 - 1000
	Wüstite	75.53	800 - 1000

Table A.20: Activation Energy of Nickel Oxide Reduction with Carbon monoxide.

Reference	KJ/mole	Temperature Range (K)
Szekely, Lin [22]	16.8	1080 - 1400
Vorontsov and Suikovskaya [89]	93 18	800 - 950
Karasuk and Smith [90]	112.14	800 - 950
	0 0	above-950

Table A.21: Activation Energy of Iron Oxide Reduction with Carbon monoxide

Reference	Oxide Phase	KJ/mole	Temperature Range (K)
Hayes [88]	overall	103.90	750 - 1250
Benesch et al. [91]	Hematite(Fe_2O_3)	64.73	950 - 1100
Et-tabirou et al. [92]	Magnetite(Fe_3O_4)		
	Small Crystal	74 46	850 - 1250
	Large Crystal	62.81	850 - 1250
Yu and Gillis [87]	Hematite-Magnetite	69.20	above 773
	Magnetite-Wustite	70.80	above 773
	Wüstite-Iron	91.70	above 773
Bicknese and Clark [93]	Wüstite(FeO)	58.30	1200 - 1470
Hayes [88]	Wüstite(FeO)	66.03	750 - 1250

Table A 22: Rate constant for hydrogen reduction estimated by the experimental study.

Oxides	Rate Constant value (Sec^{-1})	Temperature range (K)
Nickel Oxide (NiO)	$k = 6132 \exp(-57391/RT)$	800 - 1000
Hematite (Fe_2O_3)	$k = 69\,228 \exp(-26374/RT)$	800 - 900
Hematite (Fe_2O_3)	$k = 58157 \exp(-76795/RT)$	900 - 1000
Magnetite (Fe_3O_4)	$k = 15\,85 \exp(-17284/RT)$	800 - 900
Magnetite (Fe_3O_4)	$k = 604825 \exp(-96279/RT)$	900 - 1000
Wüstite (FeO)	$k = 36435 \exp(-75534/RT)$	800 - 1000
For NiO in Complex Oxide NiO in $(Fe_{1-x}Ni_x)_2O_3$	$k = 9132 \exp(-57391/RT)$	800 - 1000

Table A.23: Rate constant for reduction with CO estimated from literature data.

Oxides	Rate Constant value (Sec^{-1})	Temperature range
Hematite (Fe_2O_3)	$k = 22000 \exp(-77792/RT)$	800 - 1000
Magnetite (Fe_3O_4)	$k = 5100 \exp(-68640/RT)$	800 - 1000
Wüstite (FeO)	$k = 3184 \exp(-66027/RT)$	800 - 1000
For NiO in Complex Oxide NiO in $(Fe_{1-x}Ni_x)_2O_3$	$k = 481800 \exp(-93184/RT)$	800 - 950

A.4   Diffusivity and Estimation of Diffusion Coefficients

For binary mixture of gases at constant pressure Interdiffusion coefficient (or Molecular Diffusion coefficient) is given by the Chapman and Enskog correlation [59] :

$$D_{AB} = 0.018583 \frac{\sqrt{T^3 \left(\frac{1}{M_A} + \frac{1}{M_B} \right)}}{P\sigma_{AB}^2 \Omega_{D,AB}} \quad (cm^2/s) \tag{A.1}$$

Where σ_{AB} and $\Omega D, AB$ are Lenard-Jones parameter and their values can be obtained from literature for various gases. σ_{AB} is Collision diameter in Å

$\Omega_{D,AB}$ is a dimensionless function

$\varepsilon_{AB} = \sqrt{\varepsilon_A \varepsilon_B}$ Characteristics energy of interaction

$\sigma_{4B} = 0.5(\sigma_A + \sigma_B)$

$\Omega_{D,AB}$ vs $\frac{kT}{\varepsilon_{AB}}$ charts are taken from Bird et al. [59].

Diffusion of A in a gas mixture of A,B,C,D ·

$$D_{Am} = \frac{1 - X_A}{\frac{X_B}{D_{AB}} + \frac{X_C}{D_{AC}} + \frac{X_D}{D_{AD}}} \tag{A.2}$$

Molecular diffusivity of various binary gas mixtures are given in table A 24.

Diffusion in Capillaries

$r_g > 10\lambda$ ÅMolar Diffusivity predominant.

$r_g < 0.1\lambda$ ÅKnudsen Diffusivity predominant.

Where λ = Mean free path of gas molecules 100 Å

Knudsen diffusion of species A is given by

$$D_K = \frac{r_g}{(1 - e)(1 + \frac{\pi}{8}) \left(\frac{8M_A}{\pi R} T \right)^{1/2}} \tag{A.3}$$

In the transient region where effect of both are contributing $r > 100$ ÅDetermined by Mercury porosimetry

$r < 100$ ÅDetermined by BET surface area

The pores are considered to be cylindrical in shape Since the pores are numerous in shape and zig-zag in nature, a factor Known as tortuosity factor τ is defined whose value varies from 1.4 to 2 5.

Therefore the effective diffusivity D_e inside the pores of the solid for the gas species A is given by.

$$\frac{1}{D_e} = \frac{\tau}{p\left(\frac{1}{D_K} + \frac{1}{D_{AB}}\right)} \tag{A.4}$$

For Knudsen diffusion the equations in table are used only to estimate the diffusivity at 800 K and for higher temperatures, stronger dependence on temperature is used by using temperature dependence of $T^{2.334}$ as reported by other investigators like Ranade and Evans [36]. The knudsen diffusivity is dependent on various parameters like grain size, pellet porosity and shape of the pores which is taken care of by tortuosity factor (which is a adjustable parameter). These parameters are not accurately measurable and keep on changing with reduction temperature. Since porosity is higher when reduced at higher temperature, and so knudsen diffusivity also increases at higher rate with temperature than suggested by eqn.(A.3). The knudsen diffusivity used in the present study are :

$$\left.\begin{array}{ll} D_{k,H} & = \dfrac{1.202 \times 10^{-15} T^{3.33}}{(1-p)}, \qquad (m^2/s) \\[2mm] D_{k,CO} & = \dfrac{3.046 \times 10^{-16} T^{3.33}}{(1-p)}, \qquad (m^2/s) \end{array}\right\} \tag{A.5}$$

Table A.24: Molecular diffusivity of gas mixtures.

Gas Mixture	kT/ε_{AB}	$\Omega_{D,AB}$	Power of T	σ_{AB}	$D_{AB}\ cm^2/s$
CO/CO_2	5.534 6.225 6.917	0.8263 0.8073 0.7915	0.193	3.793	$1.040 \times 10^{-5} T^{1.693}$
H_2/H_2O	7.348 8.266 9.184	0.7832 0.7671 0.7532	0.175	2.808	$6.953 \times 10^{-5} T^{1.675}$
CO/H_2	13.218 14.870 16.523	0.7172 0.7042 0.6913	0.165	3.279	$5.856 \times 10^{-5} T^{1.665}$
CO/H_2O	4.043 4.548 5.053	0.8815 0.8590 0.8406	0.213	3.120	$1.575 \times 10^{-5} T^{1.713}$
CO/N_2	7.974 8.971 9.968	0.7717 0.7561 0.7428	0.171	3.636	$1.552 \times 10^{-5} T^{1.671}$
H_2/CO_2	10.058 11.315 12.572	0.7419 0.7321 0.7222	0.120	3.482	$6.697 \times 10^{-5} T^{1.62}$
H_2/CO_2	14.493 16.305 18.116	0.7072 0.6930 0.6788	0.184	3.325	$5.082 \times 10^{-5} T^{1.684}$

A.5 Physical Parameters of Gas and Solid

The physical properties of the gas and solid taken from literature [79, 60, 59, 56]. The composition of the ore estimated by chemical and EDAX analysis, and the properties of solid and gases involved are given in table A.25 and A 26 respectively. The thermal properties of gas and gas-solid heat transfer parameters are given in table A 27

Table A 25. Composition of the ore considered in the present study and their properties.

Components	Wt %	Dry Wt %	Density (gm/cc)	Molecular Wt.	Cp (J/Mole.K)	No. of Moles (Dry Wt)
NiO	0 76	1.22	6 75	74.71	$47 0 + 8.5 \times 10^{-3}T$	0.01633
Fe_2O_3	33.83	54.65	5.20	154 70	151.2	0 34220
Cr_2O_3	1.57	2.54	5.00	152 00	$118 6 + 9.2 \times 10^{-3}T$	0.01671
GANGUE						
SiO_2	19.45	31.42	2 72	60 09	$43.5 + 1.0 \times 10^{-3}T$	0.52290
Al_2O_3	5.30	8.56	2.42	101.96	$105.0 + 17.9 \times 10^{-3}T$	0.08395
MgO	1.00	1.63	3.58	40 31	$48.0 + 3 2 \times 10^{-3}T$	0.04044
DRY ORE	61.9	100.00	3.74	-	$88.0 + 2 4 \times 10^{3}T$	1.02253
Moisture ·						
Free	28.60	-	1.00	18.0	75.7(+Latent ht)	-
Combined	9.50	-	1.00	18 0	75.7(+Latent ht)	-

Table A.26: Properties of the gas involved in the process.

Gas	Mol. Wt	Cp (J/Mole.K)	K. Viscosity ν (m^2/s)
H_2	2	$27.47 + 3 28 \times 10^{-3}T$	$8 858 \times 10^{-9}T^{1.656}$
H_2O	18	$33.60 + 7 77 \times 10^{-3}T$	$1.213 \times 10^{-9}T^{2 04}$
CO	28	$28.77 + 4.20 \times 10^{-3}T$	$1.057 \times 10^{-9}T^{1.689}$
CO_2	44	$44.10 + 9.07 \times 10^{-3}T$	$3.426 \times 10^{-9}T^{1 779}$
N_2	28	$29.23 + 3 78 \times 10^{-3}T$	$1.716 \times 10^{-9}T^{1 612}$

Table A.27· Thermal properties of gas and solid.

PARAMETERS	VALUES	IN SI UNITS	REF.
Thermal Conductivity		(in $W/m.K$)	
Solid	$K_s = 0.655 \times 10^{-3} T^{0.6}$		[59]
Gas Mixture	$K_g = \dfrac{\sum_i n_i k_i M_i^{1/3}}{\sum_i n_i M_i^{1/3}}$		[56]
Hydrogen	$K_H = 0.758 \exp(-544/T)$		
Nitrogen	$K_N = 0.114 \exp(-570/T)$		
Steam	$K_{H2O} = 0.175 \exp(-869/T)$		
CO$_2$	$K_{CO2} = 0.151 \exp(-754/T)$		
CO	$K_{CO} = 0.09 \exp(-420/T)$		
Gas-Solid Heat transfer	$h_v = \dfrac{398 V_{av}^{0.9} T^{0.3}}{R_p^{0.75}}$	$(J/m^3 K)$	[56]

Appendix B

Gas-Solid Reaction Kinetic Models

The derivations of the model equations used for the gas-solid reaction kinetics are briefly discussed here for easy reference by the reader.

B.1 Grain Model : Diffusion Control kinetics for Spherical Pellets $(\sigma \rightarrow \infty)$

The equation used in the grain model for diffusion control kinetics is also known as shrinking core model, which is well documented by Habasi [33]. The derivation of the equation for the spherical pellets are briefly discussed here.

$$\frac{\partial}{\partial r}\left(\frac{r^2\partial C_A}{\partial r}\right) = 0 \tag{B.1}$$

Eqn (B 1) indicates that rate of diffusion through a spherical shell is constant. Integrating eqn.(B.1) we get :

$$\int \frac{\partial}{\partial r}\left(\frac{r^2\partial C_A}{\partial r}\right) = 0 \tag{B.2}$$

$$\frac{r^2\partial C_A}{\partial r} = K \tag{B.3}$$

$$\int_{C_A}^{C_{Ab}} dC = \int_r^{r_o} K\frac{dr}{r^2} \tag{B.4}$$

$$C_{Ab} - C_A = K \left(\frac{1}{r} - \frac{1}{R_p} \right) \tag{B 5}$$

Number of moles of gas passing through the spherical shell

$$\dot{n} = 4\pi r^2 D \left(\frac{dC}{dr} \right) \tag{B.6}$$

$$\frac{dC}{dr} = \frac{\dot{n}}{4\pi r^2 D} \tag{B.7}$$

From eqn (B 3) and eqn (B 7) . $K = \frac{n}{4\pi D}$
And from eqn (B.5) .

$$C_{Ab} - C_A = \frac{n}{4\pi D} \left(\frac{R_p - r}{R_p r} \right) \tag{B.8}$$

Again, $\dot{n} = \alpha \dfrac{dN}{dt} = \alpha \dfrac{dN}{dr} \dfrac{dr}{dt}$

Where, $N = \dfrac{4\pi r^3 \rho_m}{3}$ and $\alpha = (1 - e)$ i.e , the solid fraction present in the ore.

$$[\dot{n} =] \quad -\frac{\alpha(\frac{4}{3}\pi r^3 \rho_m)}{dr} \frac{dr}{dt} = \frac{4\pi D R_p r(C_{Ab} - C_A)}{(R_p - r)}$$

Integrating for reaction progress from R_p to r in time t ·

$$-\frac{\alpha \rho_s}{DR_p} \int_{R_p}^{r} r(R_p - r)dr = \int_0^t (C_{Ab} - C_A)dt \tag{B.9}$$

$$-\frac{6\alpha \rho_s}{DR_p}(3R_p r^2 - 2r^3 - R_p{}^3) = (C_{Ab} - C_A)t \tag{B.10}$$

Fraction reacted X can be written as :

$$X = \frac{\frac{4}{3}\pi R_p{}^3 - \frac{4}{3}\pi r^3}{\frac{4}{3}\pi R_p{}^3} = 1 - \left(\frac{r}{R_p}\right)^3 \tag{B.11}$$

$$r = R_p(1 - X)^{1/3} \tag{B.12}$$

Putting the value of r in eqn (B 10) we get ·

$$1 - 3(1 - X)^{2/3} + 2(1 - X) = \frac{6D(C_{Ab} - C_A)t}{\alpha R_p^2 \rho_s} \tag{B 13}$$

Where, $C_{Ab} \rightarrow = (C_{Ab} - C_A) \rightarrow C_{Ab}$; as $C_A \rightarrow 0$ in gm.moles/cc

ρ_m = Gram atomic density of removable oxygen per cc of solid . The above eqn.(B 13) is equivalent to the eqn.(2 9) given in Chapter 2 and 3.

B.2   Two Layer Model

The two layer model have been developed by Rao [39], Ishida and Wen [37], and Aushman and Watson [38] The derivations of the equations are given in Y K Rao's notes which is not published. Therefore the derivation of the equations are briefly discussed here for the convenience of the reader.

Let the gas solid reaction in a porous solid is represented by :

$$(A)+ < B >= (C)+ < G > \tag{B.14}$$
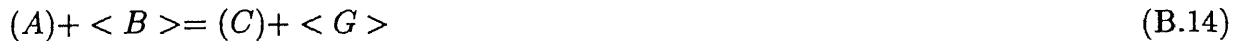
Where the reactant gas A and product gas C counter diffuse through the pores in equimolar proportions :

$$N_A = -D_e \left(\frac{dC_A}{dr}\right) \quad moles/cm^2.sec \tag{B.15}$$

$$\text{and,} \quad N_A = -N_B \tag{B.16}$$

At the pellet exterior there is some resistance to mass transfer of A. Let K_f denote the mass transfer coefficient. Thus rate of transfer of A $= 4\pi R_p^2 k_f(C_{Ab} - C_{As})$ $mole/sec$

At any point within the porous solid, the gas A is brought in by diffusion and is simultaneously consumed by the surface reaction At the steady state condition we can perform mass balance on a elemental section at radius 'r' and thickness 'dr'.

$$\left\{\begin{matrix}\text{Rate of diffusion of} \\ \text{A inwards at r+dr}\end{matrix}\right\} + \left\{\begin{matrix}\text{Rate of diffusion} \\ \text{of A outwards at r}\end{matrix}\right\} = \left\{\begin{matrix}\text{Rate of} \\ \text{Reaction}\end{matrix}\right\}$$

$$4\pi(r+dr)^2 \left\{ N_A + \frac{dN_A}{dr}dr \right\} - 4\pi r^2 N_A = 4\pi r^2 dr S_o k'_A C_A$$

Where, S_o is the internal surface area of the solid per unit volume in cm^2/cm^3, and k'_A in cm/sec is the first order reaction rate constant. Volumetric reaction rate constant is defined as $k_A = S_o k'_A$ in sec^{-1}. Substituting for N_A in terms of C_A from eqn (B 15) and rearranging we get ·

$$\frac{d^2 C_A}{dr^2} + \frac{2}{r}\frac{dC_A}{dr} = -\frac{k_A C_A}{D_e}$$

$$\Rightarrow \qquad \frac{d^2(rC_A)}{dr^2} = \frac{k_A r C_A}{D_e} \qquad\qquad\qquad (B.17)$$

The boundary conditions are deduced from the physical picture :
(i) At the porous solid exterior .

$$k_f(C_{As} - C_{Ab}) = -D_e \left(\frac{dC_A}{dr} \right)_{r=R_p} \qquad\qquad (B.18)$$

(ii) At the center .

$$\left(\frac{dC_A}{dr} \right)_{r=0} = 0 \qquad\qquad\qquad (B\ 19)$$

A general solution of eqn.(B.17) is given by :

$$rC_A = C_1 e^{mr} + C_2 e^{-mr} \ ; \quad \text{Where, } m = \sqrt{\frac{k_A}{D_e}} \qquad (B.20)$$

Using the second boundary condition, we find ·

$$C_1 = -C_2 \qquad\qquad\qquad (B.21)$$

Substitution in eqn.(B.20) gives :

$$C_A = \frac{2C_1}{r} \sinh mr = \frac{2C_1}{r} \sinh\left(\frac{\phi r}{R_p} \right) \qquad\qquad (B.22)$$

Where, $\phi = R_p m = R_p \sqrt{\dfrac{k_A}{D_e}}$ equivalent to the term σ used in the grain model.

At $r = R_p$, the concentration of A is C_{As}

$$C_{As} = \frac{2C_1}{R_p} \sinh \phi \tag{B 23}$$

We now make use of eqn.(B 18) to determine the value of C_1.

$$\left(\frac{dC_A}{dr}\right)_{r=R_p} = -\frac{2C_1}{R_p^2} \sinh \phi + \frac{2C_1 \phi}{R_p^2} \cosh \phi \tag{B.24}$$

$$\Rightarrow \quad C_{Ab} = C_{As} + \frac{2D_e C_1}{k_f R_p^2}(\phi \cosh \phi - \sinh \phi)$$

Substituting the value of C_{As} from eqn.(B.23) in the above equation we can get the value of integration constant C_1 .

$$C_1 = \frac{C_{Ab} R_p}{2 \sinh \phi \left[1 + \frac{D_e}{R_p k_f}(\phi \coth \phi - 1)\right]} \tag{B.25}$$

Thus the concentration profile of gas inside the pellet is obtained by putting the value of C_1 in eqn.(B.22) :

$$C_A = \frac{C_{Ab} \sinh(\phi \varepsilon)}{\varepsilon \sinh \phi \left[1 + \frac{1}{N_{Sh}}(\phi \coth \phi - 1)\right]} \tag{B.26}$$

Where, $N_{Sh} = \frac{R_p k_f}{D_e}$ is the Nusselt's number for mass transfer from the bulk gas phase to the pellet surface and $\varepsilon = \frac{r}{R_p}$ is the non-dimensional pellet radius. The above eqn.(B.26) is same as eqn (3.47) given in Chapter 3 and is used for computing the gas concentration profile inside the pellet in the initial stages below the critical time t_c.

By putting $r = R_p$ we can get the gas concentration at the pellet surface .

$$C_{As} = \frac{C_{Ab}}{1 + \frac{1}{N_{Sh}}(\phi \coth \phi - 1)} \tag{B.27}$$

B.2.1 Observed Rate of Reaction

The observed rate of reaction may be determined by computing the rate of mass transfer of A to the surface of the pellet.

$$R_{obs} = -4\pi R_p^2 k_f(C_{As} - C_{Ab}) \tag{B.28}$$

Substituting the value of C_{As} from eqn.(B.25) in the above equation gives :

$$R_{obs} = \frac{4\pi R_p D_e C_{Ab}(\phi \coth \phi - 1)}{1 + \frac{1}{N_{Sh}}(\phi \coth \phi - 1)} \tag{B.29}$$

The above eqn (B 29) is same as eqn (3.26) used in Chapter 3 for calculating the reaction rate below the critical time

B.2.2 Rate of Change of Solid Reactant

For the rate of change of solid reactant concentration B we obtain :

$$-\left(\frac{\partial C_B}{\partial t}\right) = k_A C_A \tag{B.30}$$

The concentration of solid reactant B is a function of positional coordinate 'r' and time elapsed 't' Integrating eqn.(B.30) we get :

$$C_B = C_{Bo} - \int_o^t k_A C_A dt \tag{B.31}$$

Substituting the value of C_A from eqn.(B.26) :

$$\left(\frac{C_B}{C_{Bo}}\right) = 1 - \frac{C_{Ab} k_A \sinh(\phi\varepsilon)t}{C_{Bo}\varepsilon \sinh \phi \left[1 + \frac{1}{N_{Sh}}(\phi \coth \phi - 1)\right]} \tag{B 32}$$

Eqn (B 32) is equivalent to eqn.(3.48) used in Chapter 3 for computing the solid concentration profile
The fractional conversion of solid reactant X is given by :

$$X = 1 - \frac{\int_o^{r_o} 4\pi r^2 C_B dr}{\int_o^{r_o} 4\pi r^2 C_{Bo} dr} \tag{B 33}$$

Putting the value of C_B from eqn.(B.32) and integrating we have :

$$X = \frac{3k_A C_{Ab} t(\phi \coth \phi - 1)}{C_{Bo} \phi^2 \left[1 + \frac{1}{N_{Sh}}(\phi \coth \phi - 1)\right]}$$ (B 34)

Eqn (B 34) for fraction reacted is given by eqn.(3 25) in Chapter 3.

B.2.3 Time Constant t_c

The progress of reaction is faster at the surface and slower inside. Let t_c be the time required for full conversion at the surface :

$t = t_c$, When $C_B = 0$ at $r = R_p$ Substitution in eqn (B 32) gives

$$t_c = \frac{C_{Bo} \left[1 + \frac{1}{N_{Sh}}(\phi \coth \phi - 1)\right]}{k_A C_{Ab}}$$ (B.35)

If the reaction is continued beyond t_c (given by eqn.(3.23)) a distinct layer of product 'G' is formed with diffusivity say D'_e, and no further reaction occurs in this layer and it acts only as a diffusion barrier. The pellet structure before, at and after the product layer formation is shown in figure 3.14

Material balance for A leads to the following relationships ·

In the Product G Layer $(R_p > r > r_m)$

$$\frac{2}{r} N'_A + \frac{dN'_A}{dr} = 0$$ (B.36)

$$-N'_A \mid_{r=R_p} = D'_e \left(\frac{dC'_A}{dr}\right)_{r=R_p} = k_f (C_{Ab} - C_{As})$$ (B.37)

$$N'_A = -D'_e \left(\frac{dC'_A}{dr}\right)$$ (B.38)

Nusselt's number in the product layer is given by : $N'_{sh} = \dfrac{R_p k_f}{D'_e}$

In the Partially-Reacted inner Core $(r_m > r > 0)$

$$\frac{2}{r} N_A + \frac{dN_A}{dr} = k_A C_A \tag{B.39}$$

$$\left(\frac{dC_A}{dr}\right)_{r=0} = 0 \tag{B.40}$$

At the Boundary between the Layers $(r = r_m)$

$$C'_A = C_A \tag{B.41}$$

$$D'_e \left(\frac{dC'_A}{dr}\right) = D_e \left(\frac{dC_A}{dr}\right) \tag{B.42}$$

Concentration profile of A is obtained by solving eqn.(B.36) through (B.42).

By integrating eqn.(B.36) and putting the value of N'_A from eqn.(B.38) we get :

$$C'_A = a_1 + \frac{a_2}{r} \tag{B.43}$$

Where, a_1 and a_2 are the integration constants.

Using eqn.(B.37) we get :

$$C'_A = C_{Ab} - \frac{a2}{R_p} \left(1 - \frac{D'_e}{R_p k_f}\right) + \frac{a_2}{r} \tag{B.44}$$

The general solution of eqn.(B.39) coupled with the boundary condition given by eqn.(B.40) provides :

$$C_A = \frac{2a_3}{r} \sinh(\phi \varepsilon) \tag{B.45}$$

Where, a_3 is the integration constant.

By using eqn.(B.41) and (B.42) at the boundary between the unreacted and reacted (G) core, i.e. at $r = r_m$ we have :

$$a_3 = \frac{r_m C_{Am}}{2 \sinh(\phi_m)} \tag{B.46}$$

$$a_2 = -C_{Am} r_m \frac{D_e}{D'_e} (\phi_m \coth \phi_m - 1) \tag{B.47}$$

Where, $\phi_m = \phi \varepsilon_m$ and $\varepsilon_m = \frac{r_m}{R_p}$

From eqn (B.44) at the boundary ε_m we find ·

$$C_{Am} = \frac{C_{Ab}}{1 + \frac{D_e}{D'_e} (\phi_m \coth \phi_m - 1) \left(1 - \varepsilon_m + \frac{\varepsilon_m}{N'_{Sh}}\right)} \tag{B.48}$$

This gives the gas concentration at the reaction interface given by eqn.(3.49). Substituting eqn.(B 48) in eqn.(B 44) gives .

$$C'_A = C_{Am} + C_{Am} \frac{D_e}{D'_e} (\phi_m \coth \phi_m - 1)(1 - \frac{\varepsilon_m}{\varepsilon}) \tag{B.49}$$

Using eqn.(B.48) we can show that gas concentration in the product layer ($\varepsilon_m \leq \varepsilon \leq 1$) is :

$$C'_A = \frac{C_{Am} \varepsilon_m \left(1 - \varepsilon + \frac{\varepsilon}{N'_{Sh}}\right) + C_{Ab}(\varepsilon - \varepsilon_m)}{\varepsilon \left(1 - \varepsilon_m + \frac{\varepsilon_m}{N'_{Sh}}\right)} \tag{B.50}$$

Which is given by eqn (3.50) in Chapter 3.
In the core ($\varepsilon_m \geq \varepsilon \geq 0$) region, we have from eqn (B 45 & B.46) .

$$C_A = C_{Am} \varepsilon_m \frac{\sinh(\phi \varepsilon)}{\sinh(\phi_m)} \tag{B.51}$$

(Eqn (3 51) of Chapter 3)
Mass balance on the solid reactant B provides :

$$-\left(\frac{\partial C_B}{\partial t}\right) = k_A C_A \tag{B.52}$$

Integration leads to :

$$C_B = C_{BI} - \int_{t_c}^{t} k_A C_A dt \tag{B.53}$$

Where C_{BI} is the concentration of the solid B at $t = t_c$.

$$C_{BI} = C_{Bo}\left(1 - \frac{\sinh(\phi\varepsilon)}{\varepsilon \sinh \phi}\right) \qquad (B.54)$$

This result was obtained by substituting for t_c from eqn (B 35) into eqn (B 32) which gives eqn (3 52).

$$C_B = C_{Bo}\left[1 - \frac{\sinh(\phi\varepsilon)}{\varepsilon \sinh \phi}\right] + \int_{t_c}^{t} \frac{k_A C_{Ab}\varepsilon_m \sinh(\phi\varepsilon)dt}{\sinh \phi_m \left[1 + \frac{D_e}{D_e^l}(\phi_m \coth \phi_m - 1)\left(1 - \varepsilon_m + \frac{\varepsilon_m}{N_{Sh}^l}\right)\right]} \qquad (B.55)$$

To evaluate the above integral, the nature of $\varepsilon_m - t$ relationship must be ascertained first. This can be accomplished as.

Let $\varepsilon = \varepsilon_m$ for $t \geq t_c$, we have two specific relations.

(i) $C_B = 0$ at $\varepsilon = \varepsilon_m$
(ii) $dC_B = 0$ at $\varepsilon = \varepsilon_m$

Since C_B, in general is a function of both 'ε' and 't' we can write :

$$dC_B = \left(\frac{\partial C_B}{\partial t}\right)_r dt + \left(\frac{\partial C_B}{dr}\right)_t dr \qquad (B.56)$$

The partial differentials are evaluated in the normal manner. For C_B the concentration of reactant B at the position ε and at time t :

$$\left(\frac{\partial C_B}{\partial t}\right)_r = -\frac{k_A C_A \sinh(\phi\varepsilon)\varepsilon_m}{\sinh \phi_m \left[1 + \frac{D_e}{D_e^l}(\phi_m \coth \phi_m - 1)\left(1 - \varepsilon_m + \frac{\varepsilon_m}{N_{Sh}^l}\right)\right]} \qquad (B.57)$$

and,
$$\left(\frac{\partial C_B}{\partial \varepsilon}\right)_t = -\frac{C_{Bo}}{\varepsilon_m}(\phi_m \coth \phi_m - 1) \qquad (B.58)$$

Since $dC_B = 0$ at $\varepsilon = \varepsilon_m$, putting the value of the differentials from eqn.(B.57) and (B.58) in eqn.(B.56) we have :

$$0 = \frac{k_A C_{Ab}dt}{1 + \frac{D_e}{D_e^l}(\phi_m \coth \phi_m - 1)\left(1 - \varepsilon_m + \frac{\varepsilon_m}{N_{Sh}^l}\right)} + \frac{C_{Bo}}{\varepsilon_m}(\phi_m \coth \phi_m - 1)d\varepsilon_m$$

$$\Rightarrow \left(\frac{dt}{d\varepsilon_m}\right) = -\frac{C_{Bo}(\phi_m \coth \phi_m - 1)}{k_A C_{Ab}\varepsilon_m}\left[1 + \frac{D_e}{D_e^l}(\phi_m \coth \phi_m - 1)\left(1 - \varepsilon_m + \frac{\varepsilon_m}{N_{Sh}^l}\right)\right] \qquad (B.59)$$

Combining eqn (B 55) and (B 59), we can get the expression for the concentration of solid B at any position ε .

$$C_B = C_{Bo}\left[1 - \frac{\sinh(\phi\varepsilon)}{\varepsilon\sinh\phi}\right] + \frac{C_{Bo}\sinh(\phi\varepsilon)}{\varepsilon}\int_{\varepsilon_m}^1 \frac{(\phi_m\coth\phi_m - 1)d\varepsilon_m}{\sinh\phi_m} \qquad (B.60)$$

$$\Rightarrow \quad C_B = C_{Bo}\left[1 - \frac{\varepsilon_m\sinh(\phi\varepsilon)}{\varepsilon\sinh\phi_m}\right] \qquad (B\,61)$$

Separating the terms of eqn (B 59) and integrating we get eqn (3 27) of Chapter 3 :

$$\int_{t_c}^t \frac{k_A C_{Ab}dt}{C_{Bo}} = \int_{\varepsilon_m}^1 \frac{(\phi_m\coth\phi_m - 1)}{\varepsilon_m}\left[1 + \frac{D_e}{D_e'}(\phi_m\coth\phi_m - 1)\left(1 - \varepsilon_m + \frac{\varepsilon_m}{N_{Sh}'}\right)\right]d\varepsilon_m$$

$$\Rightarrow \quad \frac{k_A C_{Ab}t}{C_{Bo}} = 1 + \left(1 - \frac{D_e}{D_e'}\right)\ln\left(\frac{\varepsilon_m\sinh\phi}{\sinh\phi_m}\right) + \frac{D_e}{D_e'}(\phi_m\coth\phi_m - 1)\left(1 - \varepsilon_m + \frac{\varepsilon_m}{N_{Sh}'}\right)$$
$$+ \frac{D_e\phi^2}{6D_e'}\left\{(1 - \varepsilon_m)^2(1 + 2\varepsilon_m) + \frac{2}{N_{Sh}'}(1 - \varepsilon_m{}^3)\right\} \qquad (B.62)$$

B.2.4 fractional Conversion X for $t \geq t_c$

The fractional conversion of B is deduced as follows :

$$X = 1 - \frac{\int_0^{\varepsilon_m} 4\pi\varepsilon^2 C_B d\varepsilon}{\int_0^1 4\pi\varepsilon^2 C_{Bo}d\varepsilon} \qquad (B.63)$$

By putting the value of C_B from eqn (B 61) and integrating we get eqn.(3 28) of Chapter 3 .

$$X = 1 - \varepsilon_m{}^3 + \frac{3\varepsilon_m}{\phi^2}(\phi_m\coth\phi_m - 1) \qquad (B.64)$$

B.2.5 Observed Rate of Reaction R_{obs} for $t \geq t_c$

The observed rate of reaction is given by :

$$R_{obs} = 4\pi R_p{}^2 k_f(C_{Ab} - C_{As}) \qquad (B\,65)$$

From eqn (B 48) and (B 49) we can get eqn.(3 29) of chapter-3 .

$$R_{obs} = \frac{4\pi D_e R_m C_{Ab}(\phi_m\coth\phi_m - 1)}{1 + \frac{D_e}{D_e'}\left(1 - \varepsilon_m + \frac{\varepsilon_m}{N}\right)(\phi_m\coth\phi_m - 1)} \qquad (B\,66)$$

Appendix C

Flow Chart and Computer Program Listing

The computer programs developed for the process simulation and the solution procedure adopted are briefly discussed in this section. The programs have been written in FORTRAN-77, and consists of several subroutines each of which has a set of specific tasks to carry out. The main program and its subroutines are written in the form of modules. Flow charts for the programs are shown in figure C.1, C.2 and C 3. The operational sequence of the various subroutines with their major communication links with the main program are shown in the flow charts. A short description of the indices and the main functions of the subroutines are given below, and the program listings are also included behind for any reference purpose.

C.1 Single Pellet Reduction Kinetics

The single pellet experimental results were first analyzed to evaluate the rate constant values by grain model and two layer model. A program is then developed to predict the pellet reduction rate considering the effect of non-isothermal reduction and product gas formation. The concentration profiles of the product phase such as metallic nickel and iron for solid and water vapor for the gaseous phase inside the pellet are also computed. The flow chart for the program is shown in figure C 1. Brief description of, some of the accessory programs and the Reaction Kinetics programs are listed below

Accessory Programs

TRIDAG · Tridiagonal matrix solver.

GFIT A generalized curve fitting program

KRG · Evaluation of rate constant and other parameters by grain model

NRK . Evaluation of rate constant by two layer model.

PDATA and PPLOT : Datafile generation and plotting of pellet structure

Prediction of Single Pellet Reduction Rate and Concentration Profile

RKMain : The main program for estimating the single pellet reduction It initializes the parameters, predicts the reduction rate by grain model, and also calculates the non-isothermal effect.

RKA : The subroutine calculates the reduction rate by two layer model

RKSC : Calculates the solid concentration profile in the pellet at any particular instant.

RKWV : Calculates the water vapor concentration profile in the pellet at any particular instant.

RKFX : Calculates the water vapor correction factor or gas concentration at the reaction interface
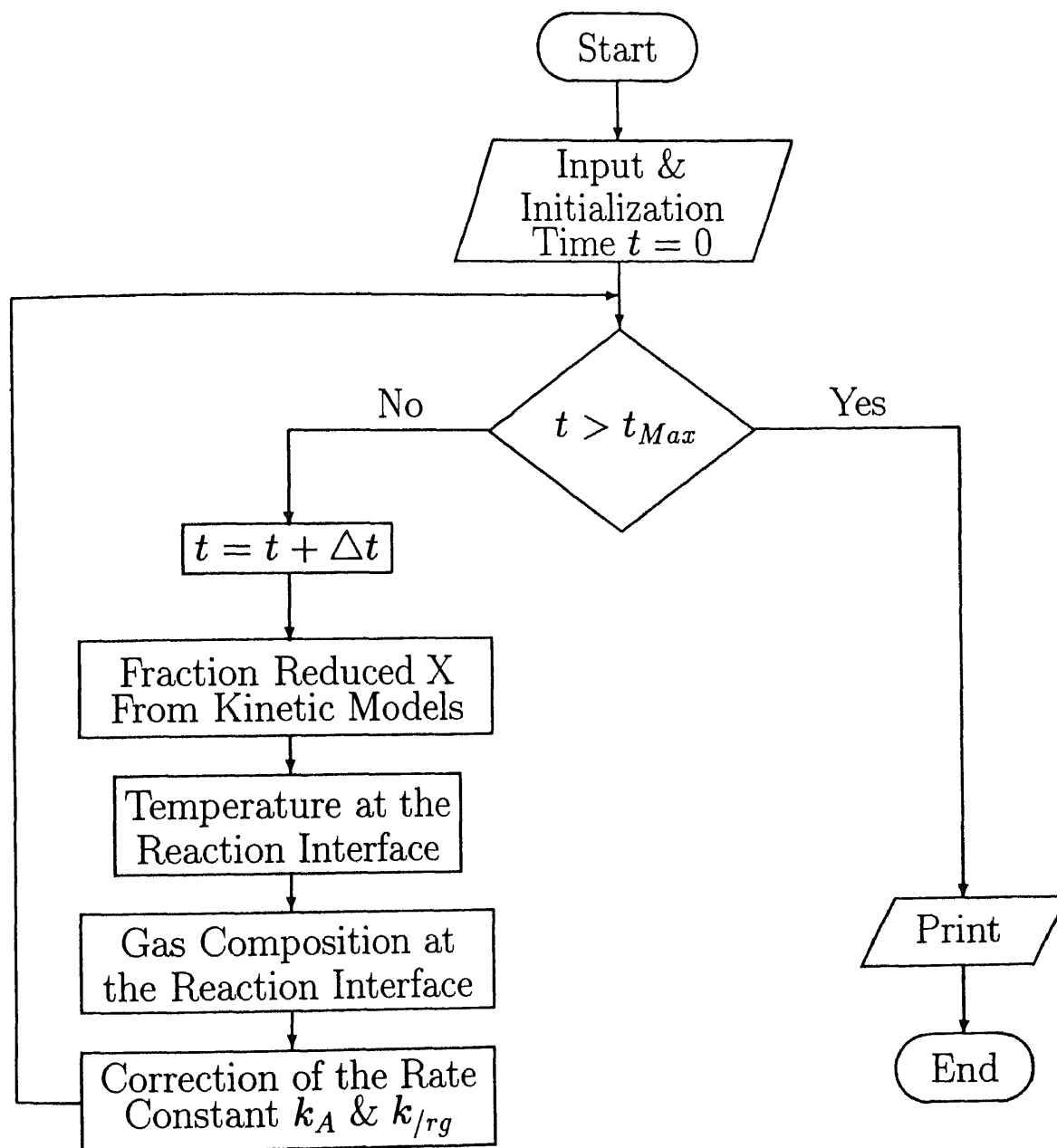
Figure C 1· Computer flow chart the single pellet calculations.

C.2 Fixed Bed Reactor Models

The solution procedure adopted for the fixed bed reduction kinetics studies for flow through the bed and flow over the bed are very similar, and so they are discussed together in this section. The flow chart for the solution procedure is shown in figure (C.2) The gas velocity profiles are solved for steady state conditions and the rest of the parameters are evaluated for transient conditions by Cranck Nicholson method The main program and its subroutines are described below

VFMain and HFMain · The main program reads the input conditions specified and initializes all the parameters It also calls all the subroutines used

VFVelo and HFVelo · Steady state formulation for gas velocity profile through the bed by using Ergun's equation and for flow over the bed by using stream function and vorticity method.

VFTs and HFTs : Solid phase thermal energy balance

VFTg and HFTg . Gaseous phase thermal energy balance

VFRK and HFRK . Solid phase mass or species balance by using grain model.

VFGH and HFGH : Gaseous phase mass or species balance

VFAv and HFAv : For calculating the average parameter values in each layer (to compare with the experimental results).

```
                    ┌─────────────┐
                    │    Start    │
                    └─────────────┘
                           │
                           ▼
                 ╱─────────────────╲
                ╱    Input &        ╲
               ╱   Initialization    ╲
               ╲    Time t = 0       ╱
                ╲───────────────────╱
                           │
                           ▼
                 ┌──────────────────┐
                 │ Velocity Profile │
                 └──────────────────┘
                           │
                           ▼
                        ╱─────╲
              No      ╱         ╲      Yes
         ◄───────────   t > t_Max   ───────────►
                       ╲         ╱
                        ╲─────╱
```

$t > t_{Max}$

$t = t + \triangle t$

Solid Temperature

Gas Temperature

Reduction Kinetics

Gas Composition

Print

End
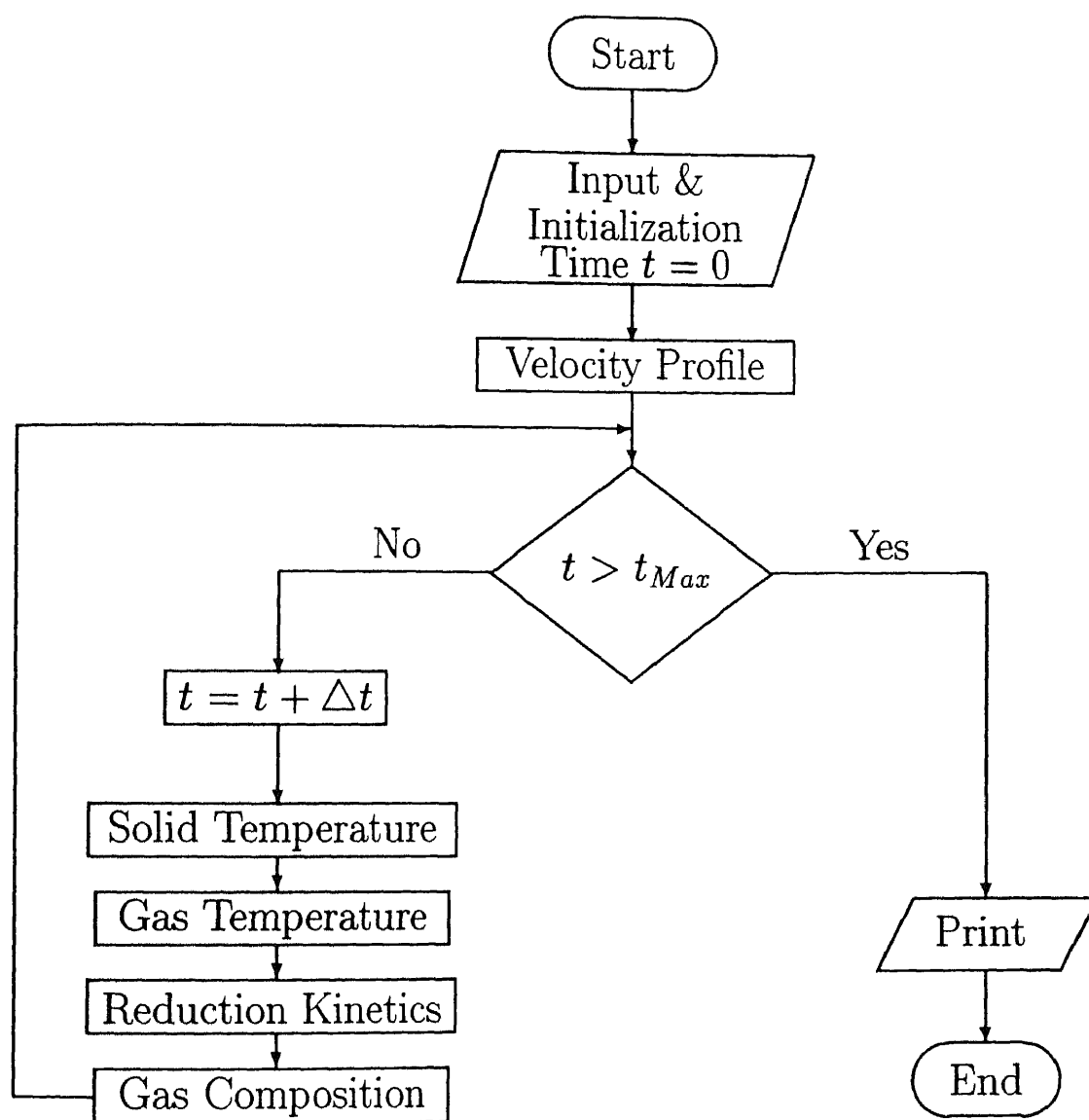
Figure C 2· Flow chart for the fixed bed reactor models.

C.3 Multiple Hearth Furnace Model

The solution strategy for modeling the reduction process in the MHF is shown in figure (C 3) The solution of each hearth were done separately. The gas and solid velocity is counter current to each other and the direction of the gas and solid velocity is reverse in the odd and even numbered hearths To take into account this flow reversal a term NPM is defined such that its value is '1' for odd numbered hearths and '-1' for the even numbered hearths The solution of each hearth were done separately and the output of one hearth is the input for the next upper hearth for the gas phase and input for the next lower hearth for the solid phase according to the gas and solid velocity Some extra gas addition in the hearths (according to burner position) were also mixed with the output gas of the lower hearth and the final gas phase properties become the input for the next upper hearth. Description of the main program and the subroutines are given below and the codes developed are also attached behind for easy reference

MHMain . The main program initializes all the parameters according to the input conditions, and calls the subroutines made for specific purpose

MHVelo : Gas velocity is solved for steady state conditions by using a stream function and vorticity formulation.

MHTs · Solid phase thermal energy balance

MHTg : Gaseous phase thermal energy balance.

MHRK : Solid phase mass or species balance by using grain model.

MHGH · Gaseous phase mass or species balance for H_2.

MHGCO : Gaseous phase mass or species balance for CO.

MHParam : The output of each hearth is averaged to set the conditions for the next lower hearth for the solid and the next upper hearth for the gas phase For the gas phase any extra gas addition is also added with the output to set the conditions for the next upper hearth.
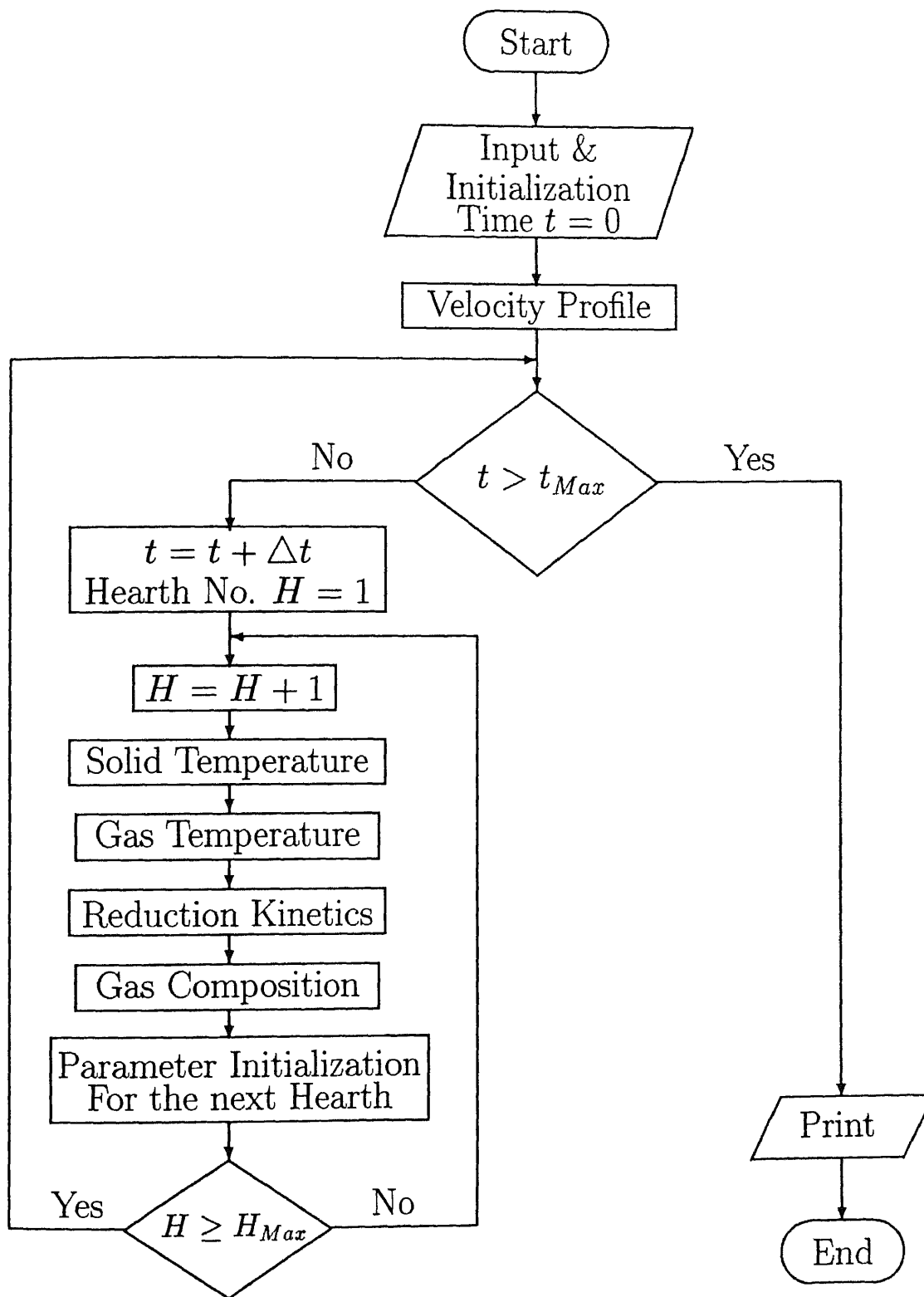
Figure C 3: Flow chart for the MHF model.

GFIT

C.4 Fortran Program Listing

C.4.1 Accessory Programs

```
C ********************************************************
C    GFIT F  MULTIPLE FIT FOR GENERAL PURPOSE
C ********************************************************
C    KINETIC DATA INTERPRETATION
C    TIME IN MINUTES OR SECONDS & WT LOSS IN WT %
      IMPLICIT REAL*8(A-H,O-Z)
      PARAMETER(N=150,NP=4)
      COMMON/AREA1/TM(N),Y(N),PN,NA,NS,NT,ND,YZ(N)
      COMMON/AREA2/AA(NP,NP+1),XN(NP),YY(N)
      INTEGER NS,NT
      DIMENSION A(NP,NP+1)
      DIMENSION X(N,NP),B(NP,NP),Z(NP)
C     OPEN(UNIT=65,FILE='GP IN')
C     OPEN(UNIT=35,FILE='GP1 OUT')
C     OPEN(UNIT=36,FILE='G1P OUT')
      READ(65,*)NDS
      DO 300 J=1,NDS
      READ(65,*)PN,NA
      WRITE(35,5)NP-1,PN NA
5     FORMAT(72('-')/5X,'T(MIN)',5X,'YY=',I2,9X,'Y',8X,
2    'SLOPEY'/72('-')/2X,F5 2,X,I3)
      DO 200 I=1,NA
      READ(65,*)TM(I),Y(I)
200   ENDDO
      NS=TM(1)
      NT=TM(NA)
      ND=NT-NS+1
      CALL CURVE
      ER=0 0
      DO 250 I=1,NA
      SL1=0 0
      DO K=2,NP
      SL1=SL1+FLOAT(K-1)*XN(K)*TM(I)**(K-2)
      ENDDO
      WRITE(35,7)TM(I),YY(I),Y(I),SL1
7     FORMAT(F9 4,3(3X,F9 4))
      ER=ER+(Y(I)-YY(I))**2
250   ENDDO
      WRITE(36,18)J,ND,PN
18    FORMAT(4X,I4/4X,I4/4X,F5 1)
C     DO 25 K=1,NT+1
      DO 25 K=NT+1,1,-2
      TC=K-1
      WRITE(36,8)TC,YZ(K)
8     FORMAT(F7 1,3X,F9 4)
25    ENDDO
      RME=ER**0 5/NA
      WRITE(35,17)(X.N'(I),I=1,NP)
17    FORMAT(72('-')/4(2X,'A(I)=',E14 8))
      WRITE(35,19)RME
19    FORMAT(3X,'RMS ERROR =',E12 4/72('-'))
300   ENDDO
      STOP
      END

C     SUBROUTINE CURVE
C     PROGRAM FOR CUBIC CURVE FITTING
      IMPLICIT REAL*8(A-H,O-Z)
      PARAMETER(N=150,NP=4)
      COMMON/AREA1/TM(N),Y(N),PN,NA,NS,NT,ND,YZ(N)
      COMMON/AREA2/AA(NP,NP+1),XN(NP),YY(N)
      INTEGER NS,NT
      DIMENSION A(NP,NP+1)
      DIMENSION X(N,NP),B(NP,NP),Z(NP)
```

TRIDAG

```
C ********************************************************
      SUBROUTINE TRIDAG(A,B,C,D,V,M,N)
C ********************************************************
      IMPLICIT REAL*8(A-H,O-Z)
      DIMENSION A(N),B(N),C(N),D(N),V(N),BETA(N),GAMA(N)
C     COMPUTE INTERMEDIATE ARRAYS BETA & GAMA
      BETA(M)=B(M)
      GAMA(M)=D(M)/BETA(M)
      IFP1=M+1
      DO 1 I=IFP1,N
      BETA(I)=B(I)-A(I)*C(I-1)/BETA(I-1)
      GAMA(I)=(D(I)-A(I)*GAMA(I-1))/BETA(I)
1     CONTINUE
C     COMPUTE FINAL SOLUTION V
      V(N)=GAMA(N)
      LAST=N-M
      DO 2 K=1,LAST
      I=N-K
      V(I)=GAMA(I)-C(I)*V(I+1)/BETA(I)
2     CONTINUE
      RETURN
      END
```

KRG

```
C **************************************************************
C KRG F INPUT FROM MFIT F 1 F FROM BEST FIT VALUES
C **************************************************************
C DETERMINATION OF KINETIC PARAMETERS & MECHANISMS
      IMPLICIT REAL*8(A-H,O-Z)
      PARAMETER (N=50,NS=18)
      CHARACTER*7 Q
      DIMENSION TM(N),Y1(N),Y2(N),Y3(N),Y4(N),Y5(N) PN(NS),RGKL(N)
      OPEN(UNIT=28,FILE='KRG OUT')
      OPEN(UNIT=29,FILE='MKP')
      OPEN(UNIT=30,FILE='KRG IN')
      OPEN(UNIT=31,FILE='GKND OUT')
C RHO  MOLAR DENSITY OF SOLID PER CC WRT [O]
      FG=1 0
      PP=0 5645
      RG=2 0E-6
      RHO=0 03874*(1-PP)
      DO 100 I=1,NS
      READ(30,*)PN(I),PW,SN,ND,Q
      WRITE(28,8)Q,PN(I),PW,SN,FG
8     FORMAT(128('-')/4X,'PS & PN =',A3 F5 2 1X, PW = F4 1 1X
1     'SN=',F4 0,3X,'FG=',F4 1/2X,'TIME ,5X 'FR,6X Y1 ,5X, kRGC
2     5X,'SI',5X,'Y2',5X,'KRGS',5X,'S2',6X,'Y4 6X,'DF' 6X S4 ,5X
3     'KGRM',6X,'Y5',6X,'KRGML',5X,'DPCL'/128('-'))
      WRITE(29,81)PN(I),PW,SN,ND
81    FORMAT(80('-')/4X,F5 2,12X,F8 4 4X,F4 0,3X 14/4X, TIME  5X,
1     'FC',9X,'Y1',9X,'Y2',9X,'Y3',9X,'Y4',9X,'Y5'/80('-'))
      IF(ABS(PN(I)-PN(I-1)) LE 0 01)THEN
61    FORMAT(3X,F5 2,3X,I3)
      TM(0)=TM(N)
      Y1(0)=Y1(N)
      Y2(0)=Y2(N)
      Y4(0)=Y4(N)
      ELSE
      TM(0)=0 0
      Y1(0)=0 0
      Y2(0)=0 0
      Y4(0)=0 0
      ENDIF
      IF(PN(I) LE 1 8)THEN
      FPN=PN(I)-1 0
      RP=(2 1087E-2*PW)**0 333
      ELSEIF((PN(I) GE 2 0) AND (PN(I) LE 2 8))THEN
      FPN=PN(I)-2 0
      RP=(4 0204E-2*PW)**0 333
      ELSEIF((PN(I) GF 3 0) AND (PN(I) LE 1 8))THEN
      FPN=PN(I)-3 0
      RP=(7 3806E-2*PW)**0 333
      ELSEIF(PN(I) GE 3 8)THEN
      FPN=PN(I)-4 0
      RP=0 50
      ENDIF
C **************************************************************
      IF(FPN LE 0 56) THEN
      T=800
      ELSEIF((FPN GE 0 56) AND (FPN LE 0 67))THEN
      T=900
      ELSEIF(FPN GE 0 67)THEN
      T=1000
      ENDIF
C   MOLAR DENSITY OF GAS PER CC
      C=1 21875D-2/T
      UM=3 633D 4*DEXP( 580/T)
      DFO=286*EXP(-4200/T)
      DII=6 698E-5*T**1 68
      Dk=(5 89D-6*RG*T**3 33)/(1-PP)
      DE=PP**2/((1/DII+1/DK)
      DEO=DFO*DE
      RE=10*RP*C/UM
```

```
      FNDDO
      DO 10 J=2,NP
      DO 20 I=1 NA
      X(1 1)=1 0
      X(I J)=X(I,2)**(J-1)
20    PRINT*,X(I,1),X(.,I.',J,)=,X(I,J)
      ENDDO
10    FNDDO
      DO 300 k=1 NP
      DO 100 J=1,NP
      B(K,J)=0 0
      Z(J)=0 0
200   FNDDO
      B(K J)=B(K J)+X(I k)*X(I J)
      Z(J)=Z(J)+X(I,J)*Y(I)
      AA(J k)=B(k,J)
      AA(J,NP+1)=Z(J)
      A(J k)=B(k J)
      A(J NP+1)=Z(J)
100   FNDDO
300   FNDDO
      DO J=1,NP
      PRINT*,('B(',K ',',J,')=',B(K,J),k=1,NP)
      PRINT*, Z(',J,,)=',Z(J)
      ENDDO
C ****************************************************
C DIAGONALIZATION STARTS
C ****************************************************
      DO I=1 NP
      IF(I LT NP) THEN
      DO K=I+1,NP
      DO J=I+1,NP+1
      A(K,J)=A(K J) A(K I)*A(I J)/A(I 1)
      ENDDO
      ENDDO
      ENDIF
      IF(I GT 1) THEN
      DO K=I-1,1,-1
      DO J=I+1,NP+1
      A(K,J)=A(K,J)-A(1,K J)*A(I,J)/A(I,I)
      ENDDO
      ENDDO
      ENDIF
      DET=1
      DO I=1 NP
      A(I NP+1)=A(I,NP+1)/A(I I)
      XN(I)=A(I NP+1)
      PRINT*,'XN(',I,') = ',XN(I)
      DFT=A(I,I)*DFT
      ENDDO
      PRINT*,'DETERMINANT = ',DET
      DO J=1,NA
      YY(J)=0 0
      DO I=1,NP
      YY(J)=YY(J)+XN(I)*X(J,2)**(I-1)
      FNDDO
      FNDDO
      DO J=1 NT+1
      Y(J)=0 0
      TC =FLOAT(J 1)
      DO I=1,NP
      Y7(J)=Y7(J)+XN(I)*TC**(I 1)
      FNDDO
      FNDDO
      RFTURN
      FND
```

```
NRK

C *********************************************************
C NRK F   PROGRAM FOR REDUCTION KINETICS VERIFICATION
C         BY NEWTON RAPHSON METHOD
C *********************************************************
      IMPLICIT REAL *8(A-H,O-Z)
      PARAMETER(N=50)
      DIMENSION TM(N),TI(N),TFI(N) XNP(N),XFP(N)
      OPEN(UNIT=44,FILE='RK IN')
      OPEN(UNIT=45,FILE='NRK OUT')
      PP=0 5645
      TO=1/PP
      RHO=0 03874**(1-PP)
      RG=2D-6
      FG=1 0
C **** RELAXATION FACTOR RFN,RFE=1  MEANS NO RELAXATION ****
      RFN=0 70
      RFE=0 70
      PRINT *,IJ
      DO 1000 IJ=1,9
      PRINT *,IJ
      READ(44,*)PN,PW,SN,ND
      IF(PN LE 2)THEN
      F1=PN-1 0
      ELSEIF((PN GE 2 0) AND (PN LE 3 0))THEN
      F1=PN-2 0
      ELSEIF((PN GE 3 0) AND (PN LE 4 0))THEN
      F1=PN-3 0
      ENDIF
      IF(PN LE 2 0)THEN
      RP=(2 1087D-2*PW)**0 333
      ELSEIF((PN GE 2 0) AND (PN LE 3 0))THEN
      RP=(4 9204D-2*PW)**0 333
      ELSEIF((PN GE 3 0) AND (PN LE 4 0))THEN
      RP=(7 3806D-2*PW)**0 333
      ENDIF
      IF(F1 LE 0 56)THEN
      TS=800 0
      ELSEIF((F1 GE 0 56) AND (F1 LE 0 67))THEN
      TS=900 0
      ELSEIF((F1 GE 0 67) AND (F1 LE 0 78))THEN
      TS=1000 0
      ENDIF
      CG=1 210D-2/TS
      UM=3 633D-4*DEXP(-589/TS)
      DFO=286*DEXP(-4200/TS)
      Dk=(5 89D-6*RG*TS**3 33)/(1-PP)
      DII=6 698D 5*TS**1 08
      DE=PP/((TO*(1/DK+1/DII))
      DEO=DE*DFO
      DR=DE/DEO
      TFI(4)=600 0
      RE,SC,FK,DNS  REYNOLD S,SCHIMIDT S NO,FILM MIC 1/NSII
      RE=10*RP*CG/UM
      SC=UM/(2*CG*DII)
      FK=(DII/(2*RP))*(2+0 6*RE**0 5*SC**0 333)
      DNS=DEO/((RP*FK)
      DNI=DE/((RP*FK)
      READ(44,*)TM(J),XNP(J),XFP(J),J=1,ND)
C ***************** DATA I,ND A WRITE *******************
      WRITE(45,5)PN,TS,RP,RG,DI ,DII,RF SC,DNS
```

```
      SC=UM/(2*C*DII)
      FK=(DII/(2*RP))*(2+0 6*RE**0 5*SC**0 333)
      DNS=DEO/((RP*FK)
      PRINT * DNS,DFO RP FK
      IF(PN(I) I E 1 8)THEN
      RP=(2 1087E-2*PW)**0 333
      ELSF IF((PN(I) GE 2 0) AND (PN(I) LF 2 8))THEN
      RP=(4 9204F 2*PW)**0 333
      ELSF IF((PN(I) GF 3 0) AND (PN(I) I E 3 8))THEN
      RP=(7 3806E-2*PW)**0 333
      FLSEIF(PN(I) GE 3 8)THEN
      RP=0 50
      ENDIF
      RGKL(2)=2 0
      DO 200 J=1 ND
      READ(70 *),TM(J),FC
      X=F C/100
      XP=F C/1000
      TI=60*TM(J)
      Y1(J)=1-(1-X)**0 5
      S1=(Y1(J) Y1(J-1))/(TM(J)-TM(J-1))
      RGC=(Y1(J)*RHO)/(C *TI)
      Y2(J)=1-(1-X)**0 3331
      S2=(Y2(J)-Y2(J-1))/(TM(J)-TM(J-1))
      RGS=(Y2(J)*RHO)/(C*TI)
      Y3(J)=1-(1-X)**(1/FG)
      S3=(Y3(J)-Y3(J-1))/(TM(J)-TM(J-1))
      RG3=(Y3(J)*RHO)/(C*TI)
      IF(PN(I) GE 4 0)THIFN
      Y4(J)=X+(1-X)*DLOG(1-X)
      S4=(Y4(J)-Y4(J-1))/(TM(J)-TM(J-1))
      DM=(RHO*RP**2*Y4(J))/(6*C*TI)
      FI SE
      Y4(J)=3 -2*X-3*(1-X)**0 667
      S4=(Y4(J) Y4(J 1))/(TM(J) TM(J-1))
      DM=(RHO*RP**2*Y4(J))/(6*C*TI)
      ENDIF
      RGK=Y3(J)/((TI*C)/RHO-(Y4(J)*RP**2))/(6*DE))
      DPC=(Y4(J)*RP**2)/(6*(TI*C)/RHO)-Y3(J)/RGK)
      RGKL(J)=Y3(J)/((TI*C)/RHO-((Y4(J)+2*X*DNS)*RP**2))/(6*DE))
      DPCL=((Y4(J)+2*X*DNS)*RP**2)/(6*((TI*C)/RHO)-Y3(J)/RGK))
      Y5(J)=Y3(J)+((RGKL(2)*RP**2)/6*DE)*(Y4(J)+2*X*DNS)
C ***** 1FROM /1 RG INTERPOLATED DATA *****
      IF(F1 OAT(J) I F 1 1)THEN
      IF(FPN LF 0 52)THEN
      RGKL(1)=69 228*DEXP(-3170/T)
      ELSEIF(FPN GE 0 52) AND (FPN LE 0 58))THEN
      RGK1(1)=6151*EXP(-6894/T)
      ELSEIF((FPN GE 0 58) AND (FPN LE 0 62))THEN
      RGKL(1)=69 228*DEXP(-3170/T)
      FLSEIF((FPN GF 0 62) AND (FPN LE 0 68))THEN
      RGK1(1)=6151*EXP( 6894/1)
      ELSF1F((FPN GF 0 68) AND (FPN LF 0 72))THFN
      RGKL(1)=58157*EXP(-9230 2/T)
      ELSEIF(FPN GF 0 72)THEN
      RGKL(1)=6151*EXP(-6894/T)
      ENDIF
      ENDIF
      GKND=1 0-RGK1(J)/RGK1(1)
      WRITE(28 11)TM(J),X Y1(J),RGC,S1,Y2(J),RGS,S2,
    1 Y4(J),DM S4 RGK,Y5(J),RGKL(J),DPCL
   11 FORMAT(F5 1,3X 11(X F7 4))
      WRITE(29 91)TM(J) X Y1(J),Y2(J) Y3(J),Y4(J),Y5(J)
   91 FORMAT(F6 1 1X 6(F9 3 2*X))
      WRITE(71,62)X,GKND
   62 FORMAT(3X,F8 4,3X,F8 4)
  200 ENDDO
      WRITE(28 22)DF,RP RG,C,RHO
   22 FORMAT(128(' ')/3X,'DE=',F7 3,3X 'RP=',F6 1,3X,'RG=',F10 2,
    1 3X 'C= E12 4,3X,'RHO=',3,12 3/128(' '))
  100 ENDDO
      STOP
      END
```

```fortran
5     FORMAT(128('-')/3X,'PN=',F5 2,3X,'T K=',F6 1,3X,'RP=',F6 4,
1     3X,'RG=',E9 2,3X,'DE=',F8 5,3X,'DH=',F8 4,3X,'RE=',
2     F8 4,3X,'SC=',F6 3,3X,'1/NSH=',F6 3,5X,'TMIN',6X,'XN',8X,
3     'XF',8X,'AKN',8X,'AKF',8X,'RMN',8X,'RMF'/128('-'))
      *********************** GUESS VALUE ***********************
C
      IF(FLOAT(IJ) LE 3 5)THEN
      AK=6 1
      AKF=8 9
      ELSEIF((FLOAT(IJ) GE 3 5) AND (FLOAT(IJ) LE 6 5))THEN
      AK=7 1
      AKF=11 0
      ELSE
      AK=11 6
      AKF=10 5
      ENDIF
      IF((FLOAT(IJ) GE 5) AND (FLOAT(IJ) LE 9 6))THEN
C     ************** COMPUTATION START ***********************
      DO 200 J=1,ND
      IF(TM(J) GT 0 1)THEN
      T=60*TM(J)
      XN=(XNP(J)-XNP(1))/100
      XF=(XFP(J)-XPP(1))/100
      RM=RP
      RMF=RP
      P=RP*(AK/DE)**0 5
      PM=RM*(AK/DE)**0 5
C     ************** NIO REDUCTION KINETICS ***************
      DO 300 ITER=1,20
      TI(J)=(RHO*(1+DNI*(P/DTANH(P)-1)))/(AK*CG)
      IF(T LE TI(4))THEN
      P=P-((3*DE*CG*T*(P/DTANH(P)-1)-XN*RHO*RP**2*(1+DNI*
1     (P/DTANH(P)-1)))*(1+DNI*(P/DTANH(P)-1)))/(3*DE*CG*T*
2     (1/DTANH(P)-P/DSINH(P)**2))
      AK=AK*(1-RFN)+RFN*DE*(P/RP)**2
      ELSE
      EM=RM/RP
      FKA=1+(1-DR)*DLOG((EM*DSINH(P))/DSINH(PM))+DR*(PM/DTANH(PM)-1)*
1     (1-EM+EM*DNS)+((DR*P*P)/6)*((1-EM**3)*(2*DNS+1)-3*EM*EM*(1-EM))
2     -(P**2*DE*CG*T)/(RHO*RP**2)
      FX=1-EM**3+((3*EM)/P**2)*(PM/DTANH(PM)-1)-XN
      AKP=(1-DR)*(1/DTANH(P)-EM/DTANH(PM))+DR*EM*(1-EM+EM*DNS)*
1     (1/DTANH(PM)-PM/((DSINH(PM))**2))+((DR*P)/3)*((1-EM**3)*
2     (2*DNS+1)-3*EM*EM*(1-EM))-(2*CG*T*DE*P)/(RHO*RP**2)
      BKM=(1/EM-P/DTANH(PM))*(1-DR+EM*DR-EM*DR*DNS+(DR*PM*(1-EM+
1     EM*DNS))/DTANH(PM))+((DR*P**2)/6)*(1+2*DNS)
      CXP=((3*EM)/P**3)*(2-PM/DTANH(PM)-(PM/DSINH(PM))**2)
      DXM=-(3/P**2)*(PM/DTANH(PM)-1)**2
      DEN=AKP*DXM-BKM*CXP
      P=P-(DXM*FKA-BKM*FX)/DEN
      EM=EM-(AKP*FX-CXP*FKA)/DEN
      AK=AK*(1-RFN)+RFN*DE*(P/RP)**2
      RM=RP*EM
      RMF=RM*(1-RFN)+RFN*RP*EM
      PM=RM*(AK/DE)**0 5
      ENDIF
      ENDDO
300   ENDDO
C     ************** FE2O3 REDUCTION KINETICS ***************
      DO 400 ITER=1,20
      TFI(J)=(RHO*(1+DNI*(P/DTANH(P)-1)))/(AKF*CG)

      IF(T LE TFI(4))THEN
      P=P-((3*DE*CG*T*(P/DTANH(P)-1)-XF*RHO*RP**2*(1+DNI*
1     (P/DTANH(P)-1)))*(1+DNI*(P/DTANH(P)-1)))/(3*DE*CG*T*
2     (1/DTANH(P)-P/DSINH(P)**2))
      AKF=AKF*(1-RFE)+RFE*DE*(P/RP)**2
      ELSE
      EM=RMF/RP
      FKA=1+(1-DR)*DLOG((EM*DSINH(P))/DSINH(PM))+DR*(PM/DTANH(PM)-1)*
1     (1-EM+EM*DNS)+((DR*P*P)/6)*((1-EM**3)*(2*DNS+1)-3*EM*EM*(1-EM))
2     -(P**2*DE*CG*T)/(RHO*RP**2)
      FX=1-EM**3+((3*EM)/P**2)*(PM/DTANH(PM)-1)-XF
      AKP=(1-DR)*(1/DTANH(P)-EM/DTANH(PM))+DR*EM*(1-EM+EM*DNS)*
1     (1/DTANH(PM)-PM/((DSINH(PM))**2))+((DR*P)/3)*((1-EM**3)*
2     (2*DNS+1)-3*EM*EM*(1-EM))-(2*CG*T*DE*P)/(RHO*RP**2)
      BKM=(1/EM-P/DTANH(PM))*(1-DR+EM*DR-EM*DR*DNS+(DR*PM*(1-EM+
1     EM*DNS))/DTANH(PM))+((DR*P**2)/6)*(1+2*DNS)
      CXP=((3*EM)/P**3)*(2-PM/DTANH(PM)-(PM/DSINH(PM))**2)
      DXM=-(3/P**2)*(PM/DTANH(PM)-1)**2
      DEN=AKP*DXM-BKM*CXP
      P=P-(DXM*FKA-BKM*FX)/DEN
      EM=EM-(AKP*FX-CXP*FKA)/DEN
      AKF=AKF*(1-RFE)+RFE*DE*(P/RP)**2
      RMF=RMF*(1-RFE)+RFE*RP*EM
      PM=RMF*(AKF/DE)**0 5
      ENDIF
      ENDDO
400   ENDDO
      ELSE
      RM=RP
      RMF=RP
      IF(F1 LE 0 56)THEN
      AK=6151 7*EXP(-6893 9/TS)
      AKF=69 228*EXP(-3170/TS)
      ELSEIF(F1 GE 0 56) AND (F1 LE 0 67))THEN
      AK=6151 7*EXP(-6893 9/TS)
      AKF=69 228*EXP(-3170/TS)
      ELSEIF((F1 GE 0 67) AND (F1 LE 0 78))THEN
      AK=6151 7*EXP(-6893 9/TS)
      AKF=58157*EXP(-9230 2/TS)
      ENDIF
      ENDIF
      WRITE(45,6)TM(J),XNP(J),XFP(J),AK,AKF,RM,RMI
6     FORMAT(3X,F5 1,δ(2X,F8 4))
200   ENDDO
1000  ENDDO
      STOP
      END
```

```
C     ************************************************
C     DATA FILE GENERATION FOR PELLET STRUCTURE
C     ************************************************
      IMPLICIT REAL *8(A-H,O-Z)
      PARAMETER(NR=64,NX=128)
      DIMENSION CH(NR),CF(NR),CN(NR),NSH(NX+1,NX+1),LB(NX+2)
      OPEN(UNIT=33,FILE='PC IN')
      OPEN(UNIT=34,FILE='PELS OUT')
      DO 1000 KI=1,3
      READ(33,*)
      READ(33,*)
      READ(33,*)
      DO J=1,NX+1
      LB(J)=84
      ENDDO
39    WRITE(34,39)(LB(J),J=1,NX+1)
      FORMAT(129(I3))
      DO K=1,NR
      READ(33,*)CH(K),CN(K),CF(K)
      ENDDO
      DO 100 I=1,NR
      PT=0 0
      DO 200 J=NR+1,NX
      SC=((NR-I)**2+(NR-J)**2)**0 5
      PL=ABS(FLOAT(NR-J)/FLOAT(NR-I))
C     PRINT *,PL,SC
      IF((SC GE NR) AND (SC LE NR+1))THEN
      NSH(I,J)=84
      ELSEIF(SC GT NR+1)THEN
      NSH(I,J)=12
      ELSEIF((PL GE 0 57) AND (PT LE 0 58))THEN
      NSH(I,J)=84
      PT=1 0
      ELSEIF(PL GT 0 58)THEN
      DO 10 K=1,NR
      IF((SC GE (K-1)) AND (SC LE K))THEN
      NSH(I,J)=98*CH(K)
      ENDIF
10    ENDDO
      ELSEIF(PL LT 0 57)THEN
      DO 20 K=1,NR
      IF((SC GE (K-1)) AND (SC LE K))THEN
      NSH(I,J)=98*CN(K)
      ENDIF
20    ENDDO
200   ENDIF
100   ENDDO
      DO 300 J=NR+1,NX
      PT=0 0
      DO 400 J=NR+1,NX
      SC=((NR-I)**2+(NR-J)**2)**0 5
      PL=ABS(FLOAT(NR-J)/FLOAT(NR-I))
      IF((SC GE NR) AND (SC LE NR+1))THEN
      NSH(I,J)=84
      ELSEIF(SC GT NR+1)THEN
      NSH(I,J)=12
      ELSEIF((PL GE 0 57) AND (PT LE 0 58))THEN
      NSH(I,J)=84
      PT=1 0
      ELSEIF(PL GT 0 58)THEN
      DO 30 K=1,NR
      IF((SC GE (K-1)) AND (SC LE K))THEN
      NSH(I,J)=98*CH(K)
      ENDIF
30    ENDDO
      ELSEIF(PL LT 0 57)THEN
      DO 40 K=1,NR
      IF((SC GE (K-1)) AND (SC LE K))THEN
      NSH(I,J)=98*CF(K)
      ENDIF
40    ENDIF
      ENDDO
400   ENDDO
300   ENDDO
      DO 500 I=1,NR
      DO 600 J=1,NR
      SC=((NR-I)**2+(NR-J)**2)**0 5
      IF((SC GE NR) AND (SC LE NR+1))THEN
      NSH(I,J)=84
      ELSEIF(SC GT NR+1)THEN
      NSH(I,J)=12
      ELSEIF(I GT NR-1)THEN
      NSH(I,J)=84
      ELSE
      DO 50 K=1,NR
      IF((SC GE (K-1)) AND (SC LE K))THEN
      NSH(I,J)=98*CN(K)
      ENDIF
50    ENDDO
      ENDIF
600   ENDDO
500   ENDDO
      DO 700 I=NR+1,NX
      DO 800 J=1,NR
      SC=((NR-I)**2+(NR-J)**2)**0 5
      IF((SC GE NR) AND (SC LE NR+1))THEN
      NSH(I,J)=84
      ELSEIF(SC GT NR+1)THEN
      NSH(I,J)=12
      ELSE
      DO 60 K=1,NR
      IF((SC GE (K-1)) AND (SC LE K))THEN
      NSH(I,J)=98*CF(K)
      ENDIF
60    ENDDO
      ENDIF
800   ENDDO
700   ENDDO
      DO J=1,NX-1
      WRITE(34,66)(LB(J),(NSH(I,J),I=1,NX-1),LB(J))
66    FORMAT(129(I3))
      ENDDO
      WRITE(34,49)(LB(J),J=1,NX+1)
49    FORMAT(129(I3))
1000  ENDDO
      STOP
      END
```

PPLOT

```c
#INCLUDE <STARBASE C H>
#INCLUDE <STDIO H>
#DEFINE EDGE FALSE
#DEFINE BOLDSANSSERIF    6
#DEFINE BOLDSERIF        8
#DEFINE SIMPLEXSANSSERIF 4
/* #DEFINE GRAY(LV1) LV1,LV1,LV1 */
#DEFINE ENDOFLINE FALSE

MAIN()
{
INT FILDES,
INT COLORMAPENTRIES,
    STATIC FLOAT WHITE[3] = {1 0,1 0,1 0},
INT I,J,II,III,II2,JJ1,JJ2,
INT ITIMES,IDEVC,IPTS,DATA[500][500],
FLOAT SCALE,X1,X2,Y1,Y2,XT1,YT1,XT2,RR,
FLOAT X,Y,W1,W2,W3,W4,
CHAR TITLE[50],DEVNAME[10],DATFILE[10],
FLOAT DMY[6],TXC,
FILE    *DATAFILE, *FOPEN(),

PRINTF("\33H\33J"), FFLUSH(STDOUT),
PRINTF("\N GIVE THE DEVICE NO  1 FOR HP98550 OR O FOR HP98721 \N"),
        SCANF("%D",&IDEVC),
        DEVNAME=="HP98550",
        IF(IDEVC == 0){ DEVNAME=="HP98720", }
IF ((FILDES = GOPEN("/DEV/CRT", OUTDEV, DEVNAME ,INIT)) == -1)
    {
FPRINTF(STDERR, "ERROR  GOPEN FAILED USING ENVIRONMENT"),
EXIT(-1),
    }
TXC=0 5,
SCANF("%S",DATFILE),
SCANF("%D",&ITIMES),
SCANF("%F %F %F",&W1,&W2,&W3,&W4),
DATAFILE = FOPEN("TITLE IN","R"),

VDC_EXTENT(FILDES,0 0,0 0,0,1 25,1 0,0 0),
VIEW_PORT(FILDES,0 1,0 1,0 8,0 8),
CLEAR_VIEW_SURFACE(FILDES),
TEXT_COLOR(FILDES,TXC,TXC,TXC),
LINE_COLOR_INDEX(FILDES,0 5),
INTERIOR_STYLE(FILDES,INT_SOLID, EDGE),
TEXT_FONT_INDEX(FILDES, BOLDSERIF),
TEXT_ALIGNMENT(FILDES, TA_CENTER, TA_TOP, 0 0, 0 0),
CHARACTER_HEIGHT(FILDES, 0 086),
TEXT_ORIENTATION2D(FILDES, -1 0, 0 0, 0 0, 1.0),
FCLOSE(DATAFILE)

INQUIRE_SIZES(FILDES,DMY,DMY,DMY,DMY,&COLORMAPENTRIES),
FOR (I = 1, I < COLORMAPENTRIES, I++)
    DEFINE_COLOR_TABLE(FILDES,I,1,WHITE),
FILL_DITHER(FILDES,16),
DATFILE = FOPEN(DATFILE,"R"),
VIEW_WINDOW(FILDES,W1,W2,W3,W4),

FOR (IJ=1, IJ<= ITIMES , IJ++){
SCANF("%D", &IPTS),
SCANF("%F", &SCALE),
SCANF("%D%D%D%D", &II1,&II2,&JJ1,&JJ2),
FOR (I=II1, I<= II2, I++){
FOR (J=JJ1, J<= JJ2, J++){
FSCANF(DATAFILE,"%D%N", &DATA[I][J]), }}
    FOR (I=II1; I<= II2; I++){
    FOR (J=JJ1, J<= JJ2, J++){

xi=j
Y1=I,
}
ELSE IF (IJ == 2 ) {
X1=J+91,
Y1=I+91,
}
ELSE IF (IJ == 3 ) {
X1=J+202,
Y1=I+202,
}
ELSE IF (IJ > 3 6) {
X1=J+(IJ-1)*IPTS,
Y1=I+(IJ-1)*IPTS,
}
X2=X1+1,
Y2=Y1+1,
XT1=(X1+X2)/2 0,
YT1=(Y1+Y2)/2 0,
RR=DATA[I][J]/SCALE,
FILL_COLOR(FILDES,RR,RR,RR),
RECTANGLE(FILDES,X1,Y1,X2,Y2),
}}
FCLOSE(DATAFILE),
/* **************************************CHANGE****************************************** */
TEXT_ORIENTATION2D(FILDES, 0 0, 1 0, 0 0),
    VIEW_PORT(FILDES,0 84,0 2,0 9,0 85),
TEXT_COLOR(FILDES,0 5,0 5,0 5),
INTERIOR_STYLE(FILDES,INT_SOLID, EDGE),
TEXT_FONT_INDEX(FILDES, BOLDSERIF),
TEXT_ALIGNMENT(FILDES, TA_CENTER, TA_TOP, 0 0, 0 0),
CHARACTER_HEIGHT(FILDES, 0 040),
TEXT2D(FILDES, 0 287, 0 312,"H2 H20", VDC_TEXT, ENDOFLINE),
TEXT2D(FILDES, 0 527, 0 575,"H2 H20", VDC_TEXT, ENDOFLINE),
TEXT2D(FILDES, 0 833, 0 924,"H2 H20", VDC_TEXT, ENDOFLINE),
TEXT2D(FILDES, 0 287, 0 084,"SMALL", VDC_TEXT, ENDOFLINE),
TEXT2D(FILDES, 0 527, 0 300,"MEDIUM", VDC_TEXT, ENDOFLINE),
TEXT2D(FILDES, 0 833, 0 583,"LARGE", VDC_TEXT, ENDOFLINE),
TEXT_ORIENTATION2D(FILDES, -1 0, 0 0, 0 0, 1 0),
TEXT2D(FILDES, 0 160, 0 178,"N10 N1", VDC_TEXT, ENDOFLINE),
TEXT2D(FILDES, 0 368, 0 418,"N10 N1", VDC_TEXT, ENDOFLINE),
TEXT2D(FILDES, 0 629, 0 715,"N10 N1", VDC_TEXT, ENDOFLINE),
TEXT2D(FILDES, 0 378, 0 178,"Fe203 Fe", VDC_TEXT, ENDOFLINE),
TEXT2D(FILDES, 0 641, 0 418,"Fe203 Fe", VDC_TEXT, ENDOFLINE),
TEXT2D(FILDES, 0 890, 0 716,"Fe203 Fe", VDC_TEXT, ENDOFLINE),
TEXT2D(FILDES, 001, 616, "PRODUCT PHASE CONE  --->", VDC_TEXT, ENDOFLINE),
/* **************************************CHANGE****************************************** */
VIEW_PORT(FILDES,0 84,0 12,0 9,0 86),
LINE_COLOR_INDEX(FILDE,1),
INTERIOR_STYLE(FILDES,INT_SOLID, TRUE),
    Y2=15 0*16 0,
    VIEW_WINDOW(FILDES,10 0,0 0,20 0,Y2),
    X1=122 0,
    X2=-110 0,

INQUIRE_SIZES(FILDES,DMY,DMY,DMY,DMY, &COLORMAPENTRIES),
FOR (I = 1, I < COLORMAPENTRIES, I++)
    DEFINE_COLOR_TABLE(FILDES,I,1,WHITE),
FILL_DITHER(FILDES,16),

FOR (I = 1, I <= 17, I++){
    RR=(I-1)/16 0,
Y1=(I-1)*16 0-9 0,
Y2=(I*16.0)-9 0,
FILL_COLOR(FILDES,RR,RR,RR),
RECTANGLE(FILDES,X1,Y1,X2,Y2),
}
BITMAP_TO_FILE(FILDES,1,0,0,"HP1",1,0,0,0,1),
GCLOSE(FILDES)}
```

C.4.2 Program for Single Pellet reduction study

COM.RK

```
f77 RKMain f TRIDAG f RKA f RKWV f RKFX f RKSC f
f77 RKMain o TRIDAG o RKA o RKWV o RKFX o RKSC o
f77 RKMain o TRIDAG o RKA o RKWV o RKFX o RKSC o -o run
run
```

COVER.RK

```
IMPLICIT REAL *8(A-H,O-Z)
PARAMETER (N=50,KT=64)
COMMON/A1/TXF,TXN,RP,TS,DZI,SK,RHO,CG,DT,ND,NTS,ARN,ARF
COMMON/A2/DE,DEO,DR,DNS,DNI,FK,CFE,CFN,XCAW,XCAW1
COMMON/A3/DXN(N),DXF(N),DKN(N),DKF(N)
COMMON/A4/EFA(N),EFGM(N),EFTM(N),EFNA(N),EFNGM(N),EFNTM(N)
COMMON/A5/EKN(N),EKF(N),EMS(N),EMSN(N)
COMMON/A6/TX(N),TI(N),TJ(N),TM(N),THS(N),TKS(N)
COMMON/A7/XXC1(N),XXC2(N),XX(N),XX1(N),XX2(N),XP(N),XN(N)
COMMON/A8/XNP(N),XFP(N),XWV(N),XZ1(N),XZ2(N)
COMMON/A9/FEX(N),FNX(N),GKN(N),GKF(N),OKN(N),OKF(N)
COMMON/A10/PFX(N),PME(N),HF(N),YRH(N),YRW(N)
COMMON/A11/WVC(N),WVC1N(N),WRH(N),RF(N),RIW(N),RIWN(N)
COMMON/A12/CAW(KT),CAW1(KT),RWH(KT),RWP(KT),RWS(KT),ZI(KT)
COMMON/A13/SNTC(KT),SFTC(KT),SNT3(KT),SFT3(KT),SNT1(KT),SFT1(KT)
COMMON/A14/TP(KT),TSC(KT),TZ(KT),TH(N,KT),TK(N,KT)
```

```
C   ********************************************************
C   RKMain F  PROGRAM FOR REDUCTION KINETICS VERIFICATION
C   MAIN  RKMain F/SUB  RKA/RKFX/RKWV/RKSC
C   UNITS  CGS  JOULE FOR ENERGY
C   EFNA(J),EFA(J) EFFECTIVENESS FACTOR FOR NICKEL AND IRON
C   1 FOR NICKEL, 2 FOR IRON
C   ********************************************************
      $INCLUDE 'COVER RK'
      DIMENSION TR(KT),TST(N)
      DIMENSION ERN(N),ERNA(N),ERF(N),ERFA(N),WFT(N),WFT1(N)
      CHARACTER*1 Q
      OPEN(UNIT=44,FILE='RK IN')
      OPEN(UNIT=45,FILE='RKZM OUT')
      OPEN(UNIT=47,FILE='RKPC D')
      OPEN(UNIT=48,FILE='RKT D')
      OPEN(UNIT=49,FILE='RKTT D')
      PP=0 5645
      TO=1/PP
      RHO=0 03874*(1-PP)
      RG=2D-6
      FG=1 0
      PH=0 999
      PH2O=1-PH
      RH=PH2O/PH
      HN=6720
      H1F=-3024
      H2F=-66024
      H3F=-18522
      SK=0 0063
      CFN=0 016
      CFE=0 984
      DO 1000 IJ=1,3
      WRITE(46,29)
29    FORMAT(6X,'12')
      DO 100 I=1,3
      PRINT *,I
      ERRN=0 0
      ERRNA=0 0
      ERRF=0 0
      ERRFA=0 0
      READ(44,*)PN,PW,SN,ND,Q
      IF(PN LE 2)THEN
      F1=PN-1 0
      ELSEIF((PN GE 2 0) AND (PN LE 3 0))THEN
      F1=PN-2 0
      ELSEIF((PN GE 3 0) AND (PN LE 4 0))THEN
      F1=PN-3 0
      ENDIF
      IF(PN LE 2 0)THEN
      RP=(2 1087D-2*PW)**0 333
      ELSEIF((PN GE 2 0) AND (PN LE 3 0))THEN
      RP=(4 9204D-2*PW)**0 333
      ELSEIF((PN GE 3 0) AND (PN LE 4 0))THEN
      RP=(7 3806D-2*PW)**0 333
      ENDIF
      IF(F1 LE 0 56)THEN
      TS=800 0
      ELSEIF((F1 GE 0 56) AND (F1 LE 0 67))THEN
      TS=900 0
      ELSEIF((F1 GE 0 67) AND (F1 LE 0 78))THEN
      TS=1000 0
      ENDIF
```

```
      UM=3 633D-4*DEXP(-589/TS)
      CG=1 219D-2/TS
      DFO=994*EXP(-5197/TS)
      DK=(5 89D-6*RG*TS**3 33)/(1-PP)
      DH=6 953D-5*TS**1 675
      DE=PP/(TO*(1/DK+1/DH))
      DEO=DFO*DE
      DR=DE/DEO
      RE=10*RP*CG/UM
      SC=UM/(2*CG*DH)
      FK=(DH/(2*RP))*(2+0 6*RE**0 5*SC**0 333)
      DNS=DEO/(RP*FK)
      DNI=DE/(RP*FK)
      PPN=(PH**0 5)/((1+2 71D-2*DEXP(5837 9/TS)*RH**2)
      X1=0 001
      X2=0 001
      DX1=0 0001
      DX2=0 0001
      TC=TS
      TNC=TS
      DO 93 K=1,KT
      TR(K)=TS
      TP(K)=TS
      TSC(K)=TS
      ENDDO
93    DT=5 0
      NTS=60/DT
C     ********** CONSTANT FOR TEMPERATURE CORRECTION ********
      CTC=(RHO*RP**2)/(6*SK)
C     ********** READ & WRITE *********************
      WRITE(49,39)PN,TS
39    FORMAT(8X,'TC',F3 1/5X,'0 0',3X,F8 3/80('-')/5X,'TM',8X,'TX'
     1 ,7X,'TST',7X,'TKS',7X,'THSC'/80('-'))
      WRITE(47,33)PN,TS
33    FORMAT(80('-')/2X,'PN=',F4 1,2X,'TS=',F6 1/80('-'))
      WRITE(48,34),KT,XCAW,XCAW1,Q,PN
34    FORMAT(5X,13/5X,13/5X,'XCAW=',F7 4,5X,'XCAW1=',F7 4
     1 /4X,A,F3 1,7X,'TR',7X,'TP',6X,'TKSC',6X,
     2 'T2',6X,'TH',6X,'RWH',6X,'RWS',6X,'RWP',6X,'CAW',6X,'CAW1')
      READ(44,*)(TM(J),XNP(J),XFP(J),J=1,ND)
      DO 150 J=1,ND
      XN(J)=XNP(J)/100 0
      XF(J)=XFP(J)/100 0
150   ENDDO
      WV=0 0
      DO J=1,ND
      GKF(J)=0 55
      TX(J)=TS
      ENDDO
C     **********************************************************
      DZI=1/(FLOAT(KT)-1)
      DO 22 J=1,ND
      DXN(J)=DT*(XN(J)-XN(J-1))/60 0
      DXF(J)=DT*(XF(J)-XF(J-1))/60 0
      IF(XF(J) LE 0 111)THEN
      HF(J)=H1F+9*XF(J)*(H2F-H1F)
      ELSEIF((XF(J) GE 0 111) AND (XF(J) LE 0 333))THEN
      HF(J)=H2F+4 5*(H3F-H2F)*(XF(J)-0 111)
      ELSEIF(XF(J) GE 0 333)THEN
      HF(J)=H3F
      ENDIF
22    CONTINUE
```

```
C     ***********************************************************
      OKN(1)=6132*EXP(-6898/TS)
      IF(TS LE 900)THEN
      OKF(1)=69 228*EXP(-3170/TS)
      ELSE
      OKF(1)=58157*EXP(-9230 2/TS)
      ENDIF
      XX(1)=0 0
      EMS(1)=1 0
      EMSN(1)=1 0
C     DO 200 J=2,ND
      TIS=60*TM(J)
      IF(X2 LE 0 99)THEN
      TS1=TNC
      DO 120 K=1,NTS
C     ********** WATER VAPOR CORRECTION BY Y K RAO MODEL **************
      XX(J)=X1*CFN+X2*CFE
      EMS(J)=(1-XX(J))**0 333
      EMSN(J)=(1-X1)**0 333
      PM=RP*EMS(J)*(OkF(J)/DE)**0 5
      PW=RP*(OKF(J)/DE)**0 5
      IF(F1 LE 0 56)THEN
      TCF=44 0
      ELSE
      TCF=(RHO/(60*OKF(J)*CG))*(1+DNI*(PW/TANH(PW)-1))
      ENDIF
      IF(J LE TCF)THEN
      YH=1/(1+(PM/TANH(PM)-1)*(1-EMS(J)+EMS(J)*DNI)'
      ELSE
      YH=1/(1+(PM/TANH(PM)-1)*(1-EMS(J)+EMS(J)*DNI))
      ENDIF
      YRW(J)=ABS((1-YH)/YH)
C     ********** WATER VAPOR CORRECTION BY DIFFUSION CALCULATION ******
      RW=(RHO/(DT*CG))*(DX2*CFE+DX1*CFN)
      TW=(RW*RP**2)/(6*DE)
      XWV(J)=TW*(1-EMSFJ)**2)
      WRH(J)=XWV(J)/(1-XWV(J))
C     ********** WATER VAPOR CORRECTION FROM K-VARIATION ******
      RH=(0 06+0 24*X2+0 16*X2**2)*(RP+1)
      WFT(J)=RH/(1+RH)
      WVC(J)=1-YH
C     **** 1ST STEP OF IRON OXIDE REDUCTION FE2O3 -> FE3O4 -> FEO ****
      IF(X2 LE 0 111)THEN
      HF(J)=H1F+9*X2*(H2F-H1F)
      TXF=(CTC*CFE*DXF(J)*HF(J))/DT
      TC=TS1-TXF*((1-XF(J))**0 667-1)
      EK1=10 0
      EK2=4698*DEXP(-7911 4/TX(J))
      PPF1=1-RH/EK1
      PPF2=1-RH/EK2
      IF(PPF2 LE 0 04)THEN
      PPF2=0 025/RP
      ENDIF
      IF(TS LE 900)THEN
      RK1=69 228*DEXP(-3170/TX(J))
      RK2=15 85*DEXP(-2077 4/TX(J))
      R1=RK1*PPF1
      R2=RK2*PPF2
      ELSE
```

```fortran
      RK1=5815.7*EXP(-9230 2/TX(J))
      RK2=604825*EXP(-11572/TX(J))
      R1=RK1*PPF1
      R2=RK2*PPF2
      ENDIF
      EKF(J)=1/(1/EK1+9*X2*(1/EK2-1/EK1))
      GKF(J)=R1+9*X2*(R2-R1)
      OKF(J)=RK1+9*X2*(RK2-RK1)
***** 2ND STEP OF IRON OXIDE REDUCTION FE3O4 --> FEO --> FE *****
      ELSEIF((X2 GE 0 111) AND (X2 LE 0 333))THEN
      HF(J)=H2F+4 5*(H3F-H2F)*(X2-0 111)
      TXF=(CTC*CFE*DXF(J)*HF(J))/DT
      TC=TS1-TXF*((1-XF(J))**0 667-1)
      EK2=4698*DEXP(-7911 4/TX(J))
      EK3=3 684*DEXP(-2226/TX(J))
      PPF2=1-RH/EK2
      PPF3=1-RH/EK3
      IF(PPF2 LE 0 04)THEN
      PPF2=0 025/RP
      ENDIF
      IF(PPF3 LE 0 04)THEN
      PPF3=0 025/RP
      ENDIF
      IF(TS LE 900)THEN
      RK2=15 85*DEXP(-2077 4/TX(J))
      ELSE
      RK2=604825*EXP(-11572/TX(J))
      ENDIF
      R2=OKF(J)*PPF2
      RK3=36435*DEXP(-9078 6/TX(J))
      R3=RK3*PPF3
      EKF(J)=1/(1/EK2+4 5*(1/EK3-1/EK2)*(X2-0 11))
      GKF(J)=R2+4 5*(R3-R2)*(X2-0 11)
      OKF(J)=RK2+4 5*(RK3-RK2)*(X2-0 11)
********* 3RD STEP OF IRON OXIDE REDUCTION FEO --> FE **********
      ELSEIF(X2 GE 0 333)THEN
      HF(J)=H3F
      TXF=(CTC*CFE*DXF(J)*HF(J))/DT
      TC=TS1-TXF*((1-XF(J))**0 667-1)
      EK3=3 684*DEXP(-2226/TX(J))
      PPF3=1-RH/EK3
      IF(PPF3 LE 0 04)THEN
      PPF3=0 025/RP
      ENDIF
      EKF(J)=EK3
      OKF(J)=36435*DEXP(-9078 6/TX(J))
      GKF(J)=OKF(J)*PPF3
      ENDIF
********* KINETIC CALCULATION BY GRAIN MODEL **************
      SH2=RP*(GKF(J)/(6*DE))**0 5
      FH2=1/(FG*(1-X2)**(1-1/FG))+2*SH2**2*(1/((1-X2)**0 333)-1+DNS)
      DX2=((CG*GKF(J))/(RHO*FH2))*DT
      X2=X2+DX2
      EFGM(J)=(DX2*RHO)/(DT*OKF(J)*CG)
      ENDDO
      TX(J)=TC
      XX2(J)=100*X2
      ELSE
      XX2(J)=99 99
      ENDIF
      ERF(J)=XX2(J)-XFP(J)
```

```fortran
      ERRF=ERRF+ERF(J)
      PRINT *,'TCF--YH--X2=',TCF,YH,X2
***********************************************
C     CALCULATION FOR NIO REDUCTION KINETICS
***********************************************
      DO 110 K=1,NTS
********* WATER VAPOR CORRECTION FOR NICKEL ********
      EM1N=(1-X1)**0 333
      PW1N=RP*(OKF(J)/DE)**0 5
      PM1N=RP*EM1N*(OKF(J)/DE)**0 5
      IF(J LE TCF)THEN
      YH1N=1/(1+(PM1N/TANH(PM1N)-1)*(1-EMIN+EMIN*DNI))
      ELSE
      YH1N=1/(1+(PM1N/TANH(PM1N)-1)*(1-EMIN+EMIN*DNI))
      ENDIF
      WVC1N(J)=1-YH1N
********* WATER VAPOR CORRECTION FROM K-VARIATION *********
      WFT1(J)=RH/(1+RH)
      FT=2 71D-2*DEXP(5838/TX(J))
      PPN=1/(PH**0 5*(1+FT*RH**2))
      EKN(J)=518*EXP(-5838/TX(J))
***********************************************
      OKN(J)=6132*DEXP(-6898/TX(J))
      GKN(J)=OKN(J)*PPN
      SHI=RP*(GKN(J)/(6*DE))**0 5
      FH1=1/(FG*(1-X1)**(1-1/FG))+2*SHI**2*(1/((1-X1)**0 333)-1+DNS)
      DX1=((CG*GKN(J))/(RHO*FH1))*DT
***********************************************
      EFNGM(J)=(DX1*RHO)/(DT*OKN(J)*CG)
      IF(X1 LE 0 99)THEN
      X1=X1+DX1
      ELSE
      X1=0 9999
      ENDIF
      TXN=(CTC*CFN*DXN(J)*IIN)/DT
      TNC=TC-TXN*((1-XN(J))**0 667-1)
      TX(J)=TNC
      TST(J)=TS+2*(TXF+TXN)*((1-XF(J))**(-0 333)-1)
      ENDDO
      XX1(J)=100*X1
      ERN(J)=XX1(J)-XNP(J)
      ERRN=ERRN+ERN(J)
***********************************************
C     TEMPERATURE PROFILE FOR HOMOGENEOUS REACTION
***********************************************
      IF((TM(J) GE 1 5) AND (TM(J) LE 2 5))THEN
      DTR=0 0
      DO 400 K=1,KT
      ZI(K)=1 0-DZI*FLOAT(K-1)
      DTR=(TXF+TXN)**2*(1-ZI(K)**2)
      TR(K)=TR(K)+DTR
400   CONTINUE
      DNO=(CFE*ABS(HF(J))+CFN*IIN)
      ZEM=(1-(XF(J)*CFE*ABS(HF(J))+XN(J)*CFN*IIN)/DNO)**0 333J
      ENDIF
      ENDDO
***********************************************
      GKN(1)=6132*EXP(-6898/TS)
      IF(TS LE 900)THEN
      GKF(1)=(69 228*EXP(-3170/TS)+GKF(2))/2 0
      ELSE
```

```fortran
        GKF(1)=(58157*EXP(-9230 2/TS)+GKF(2))/2 0
        ENDIF
C       ***********************************************
        CALL RKA
        CALL RKSC
        CALL RKWV
        CALL RKFX
        ERFA(J)=XXC2(J)-XFP(J)
        ERRFA=ERRFA+ERFA(J)
        ERNA(J)=XXC1(J)-XNP(J)
        ERRNA=ERRNA+ERNA(J)
        PRINT *,PPF1,PPF2,PPF3
C
        DO 94 K=1,KT
        WRITE(48,4)ZI(K),TR(K),TP(K),TKS(K),TZ(K),TH(15,K),RWH(K),
     1  RWS(K),RWP(K),CAW(K),CAW1(K)
4       FORMAT(2X,F7 3,5(2X,F7 2),5(2X,F7 4))
94      ENDDO
        DO L=KT,1,-1
C       WRITE(47,11)CAW(L),SNT3(L),SFT3(L),CAW1(L)
        WRITE(47,11)ZI(L),CAW(L),SNT3(L),SFT3(L)
11      FORMAT(2X,4(F9 5))
        ENDDO
        DO L=1,KT
        WRITE(47,42)ZI(L),CAW(L),SNT3(L),SFT3(L)
42      FORMAT(2X,4(F9 5))
        ENDDO
        WRITE(45,5)PN,TS,RP,RG,DE,KRG1,KRG2,SH1,SH2
5       FORMAT(128('-')/3X,'PN=',F5 2,3X,'T K=',F6 1,3X,'RP=',F6 4,
     1  3X,'RG=',E9 2,3X,'DE=',F8 5,3X,'KRG1=',F8 4,3X,'KRG2=',
     2  F8 4,3X,'SH1=',F6 3,3X,'SH2=',F6 3/2X,'TMIN',4X,'XN',6X,
     3  'XP',6X,'X1',6X,'X2',5X,'XC1',5X,'XC2',4X,'WFNX',5X,'WFEX',
     4  4X,'WVC1N',4X,'WVC',5X,'R1W',5X,'WFT1',4X,'WFT',5X,'KNO',5X,
     5  'GKN'/128('-'))
        DO J=1,ND
        WFNX=FNX(J)/(1+FNX(J))
        WFEX=FEX(J)/(1+FEX(J))
        WRITE(49,77)TM(J),TX(J),TST(J),TKS(J),THS(J)
77      FORMAT(2X,F6 1,4(2X,F8 2))
        WRITE(45,6)TM(J),XNP(J),XFP(J),XX1(J),XX2(J),XXC1(J),XXC2(J),
     1  WFNX,WFEX,WVC1N(J),WVC(J),R1W(J),WFT1(J),WFT(J),OKN(J),GKN(J)
6       FORMAT(F5 1,6(X,F7 3),9(X,F7 4))
        ENDDO
        PRINT *,ERRN,ERRF
        PRINT *,ERRNA,ERRFA
100     ENDDO
1000    ENDDO
        STOP
        END

C
C       RKA F  REDUCTION KINETICS BY Y K RAO MODEL
C       MAIN  RKMan F /SUB  RTP/ZIK/RKFX/RKA/RKWV
C       ***********************************************
        SUBROUTINE RKA
$INCLUDE 'COVER RK'
        REAL KNA(N),KFA(N)
        XC1=0 0
        XC2=0 0
        DO 200 J=2,ND
        T=60*TM(J)
C       ********** TWO LAYER MODEL FOR FE2O3 REDUCTION ***************
        DO 120 K=1,NTS
        IF(XC2 LE 0 99)THEN
        RH=(0 06+0 24*XC2+0 16*XC2**2)*(RP+1)
C       ******** 1ST STEP FOR IRON OXIDE REDUCTION FE2O3 --> FE3O4 ********
        IF(XC2 LE 0 111)THEN
        EKI=10 0
        EK2=4698*DEXP(-7911 4/TX(J))
        PPF1=1-RH/EK1
        PPF2=1-RH/EK2
        IF(PPF2 LE 0 04)THEN
        PPF2=0 025/RP
        ENDIF
        IF(TS LE 900)THEN
        RK1=69 228*DEXP(-3170/TX(J))
        RK2=15 85*DEXP(-2077 4/TX(J))
        R1=RK1*PPF1
        R2=RK2*PPF2
        ELSE
        RK1=58157*EXP(-9230 2/TX(J))
        RK2=604825*DEXP(-11572/TX(J))
        R1=RK1*PPF1
        R2=RK2*PPF2
        ENDIF
        AKF=R1+9*XC2*(R2-R1)
        KFA(J)=RK1+9*XC2*(RK2-RK1)
C       ******** 2ND STEP FOR IRON OXIDE REDUCTION I L3O4 --> I LO ********
        ELSEIF(XC2 GE 0 111) AND (XC2 LE 0 3J3))THEN
        EK2=4698*DEXP(-7911 4/TX(J))
        EK3=3 684*DEXP(-2226/TX(J))
        PPF2=1-RH/EK2
        PPF3=1-RH/EK3
        IF(PPF2 LE 0 04)THEN
        PPF2=0 025/RP
        ENDIF
        IF(PPF3 LE 0 04)THEN
        PPF3=0 025/RP
        ENDIF
        IF(TS LE 900)THEN
        RK2=15 85*DEXP(-2077 4/TX(J))
        ELSE
        RK2=604825*DEXP(-11572/TX(J))
        ENDIF
        R2=RK2*PPF2
        RK3=30435*DEXP(-9078 6/TX(J))
        R3=RK3*PPF2
        AKF=R2+4 5*(R3-R2)*(XC2-0 111)
        KFA(J)=RK2+4 5*(RK3-RK2)*(XC2-0 111)
```

```fortran
C     ******** 3RD STEP FOR IRON OXIDE REDUCTION FEO -> FE ********
      ELSEIF(XC2.GE.0.333)THEN
      EK3=3.525*DEXP(-2000/TX(J))
      EK3=3.684*DEXP(-2226/TX(J))
      PPF3=1-RH/EK3
      IF(PPF3.LE.0.04)THEN
      PPF3=0.025/RP
      ENDIF
      KFA(J)=36435*DEXP(-9078.6/TX(J))
      AKF=KFA(J)*PPF3
      ENDIF
C     ******** REDUCTION KINETICS OF BY Y.K RAO MODEL/T.L.M *********
      P=RP*(AKF/DE)**0.5
      PM=RM*(AKF/DE)**0.5
      TI(J)=(RHO/(AKF*CG))*(1+DNI*(P/TANH(P)-1))
      IF(T.LE.TI(1))THEN
      XC2=(3*AKF*CG*T*(P/TANH(P)-1))/(RHO*P*P*(1+DNI*(P/TANH(P)-1)))
      RM=RP*(1-XC2)**0.333
      PM=RM*(AKF/DE)**0.5
      EFTM(J)=(3/P**2)*(P/TANH(P)-1)/(1+DNI*(P/TANH(P)-1))
      EFA(J)=(DXF(J)*RHO)/(DT*KFA(J)*CG)
      ELSE
C     ******************************************************
C     METHOD 1  AKF SHOULD BE CORRECTED ONLY FOR TEMP TX & WATER
C     VAPOR COMP FACTOR BUT NOT TOTAL EFFECTIVE PH2,PM,EM COMMON
C     EFTM  ISOTHERMAL EFF FACTOR/EFA  EXPERIMENTAL EFF FACTOR
C     ******************************************************
      ROBS=(12.566*DE*RM*CG*(PM/TANH(PM)-1))/(1+DR*(1-EM+EM*DNS)
    1 *(PM/TANH(PM)-1))
      DXC2=(ROBS*DT)/(4.1888*RP**3*RHO)
      XC2=XC2+DXC2
      RM=RP*(1-XC2)**0.333
      PM=RM*(AKF/DE)**0.5
      EM=RM/RP
      EN=RN/RP
      EFTM(J)=ROBS/(4.1888*RM**3*KFA(J)*CG)
      ENDIF
      T=T+DT
      XXC2(J)=100*XC2
      ELSE
      XXC2(J)=99.99
      ENDIF
      EFA(J)=(DXF(J)*RHO)/(DT*KFA(J)*CG)
120   ENDDO
C     ********** TWO LAYER MODEL FOR NIO REDUCTION **************
      DO 110 K=1,NTS
      IF(XC1.LE.0.99)THEN
      RH=(0.06+0.24*XC1+0.16*XC1**2)*(RP+1)
      PH=1/(1+RH)
      FT=2.71D-2*DEXP(5838/TX(J))
      PPN=1/(PH**0.5*(1+FT*RH**2))
      EKN(J)=518*EXP(-5838/TX(J))
      AKN(J)=6132*DEXP(-6898/TX(J))
      AKN=KNA(J)*PPN
      P1=RP*(AKN/DE)**0.5
      PN=RN*(AKN/DE)**0.5
      TJ(J)=(RHO/(AKN*CG))*(1+DNI*(P1/TANH(P1)-1))
      PRINT*,TI(J),TJ(J)
      IF(T.LE.TJ(1))THEN
      XC1=(3*AKN*CG*T*(P1/TANH(P1)-1))/(RHO*P1**2*(1+DNI*
    1 (P1/TANH(P1)-1)))
      RN=RP*(1-XC1)**0.333
      PN=RN*(AKN/DE)**0.5
      EFNTM(J)=(3/P1**2)*(P1/TANH(P1)-1)/(1+DNI*(P1/TANH(P1)-1))
      EFNA(J)=(DXN(J)*RHO)/(DT*KNA(J)*CG)
      ELSE
      RN=RP*(1-XC1)**0.333
      PN=RN*(AKN/DE)**0.5
C     ********************************************************
C     METHOD  AKN SHOULD BE CORRECTED ONLY FOR TEMP TC & WATER
C     VAPOR COMPO FACTOR BUT NOT TOTAL EFFECTIVE PH2,PM,EM COMMON
C     EFNTM  ISOTHERMAL EFF FACTOR/EFNA  EXPERIMENTAL EFF FACTOR
C     ********************************************************
      ROBS=(12.566*DE*RN*CG*(PN/TANH(PN)-1))/(1+DR*(1-EN+EN*DNS)
    1 *(PN/TANH(PN)-1))
      DXC1=(ROBS*DT)/(4.1888*RP**3*RHO)
      XC1=XC1+DXC1
      RN=RP*(1-XC1)**0.333
      PN=RN*(AKN/DE)**0.5
      EN=RN/RP
      EFNTM(J)=ROBS/(4.1888*RN**3*KNA(J)*CG)
      ENDIF
      T=T+DT
      XXC1(J)=100*XC1
      ELSE
      XXC1(J)=99.99
      ENDIF
      EFNA(J)=(DXN(J)*RHO)/(DT*KNA(J)*CG)
      ENDDO
      PRINT*,TI(J),TJ(J)
200   ENDDO
      RETURN
      END
```

```fortran
C     *********************************************************
C     RKSC F  SUBROUTINE FOR CALCULATION OF SOLID CONE IN THE PELLET
C     *********************************************************
      SUBROUTINE RKSC
$INCLUDE 'COVER RK'
      DIMENSION AKN(N),AKF(N),PNX(N),RHOF(N),RN(N)
      OPEN(UNIT=66,FILE='NRK OUT')
      OPEN(UNIT=67,FILE='RKSOL D')
      READ(66,*)
      READ(66,*)
      READ(66,*)
      READ(66,*)
      TCN=TJ(2)/60 0
      TCF=TI(2)/60 0
77    FORMAT(100('-')/3X,'TMP=',F6 0,3X,'TCNI=',F5 1,3X,'TCFE=',
     1 F5 1,3X,'RP=',F5 3,3X,'DE=',E9 2/6X,'ZI',5X,'SNT1',5X,'SNTC',5X,
     2 'SNT3',5X,'SFT1',5X,'SFTC',5X,'SFT3'/100('-'))
      RNM=0 0
      RFM=0 0
      DO K=1,KT
      SNT1(K)=0 0
      SNTC(K)=0 0
      SNT3(K)=0 0
      SFT1(K)=0 0
      SFTC(K)=0 0
      SFT3(K)=0 0
      ENDDO
      DO 100 J=1,ND
      READ(66,*)A,A,A,AKN(J),AKF(J),RN(J),RF(J)
C     ************ PXN,PXF  EXPERIMENTAL PHI VALUES ************
      PNX(J)=RP*(GKN(J)/DE)**0 5
      PME(J)=RP*(AKF(J)/DE)**0 5
      PFX(J)=RP*(GKF(J)/DE)**0 5
      RTNF=XNP(J)/XPP(J)
      IF(RTNF GE 1 0)THEN
      RHOF(J)=RHO*RTNF
      ELSE
      RHOF(J)=RHO
      ENDIF
      IF(RN(J) GE RNM)THEN
      RNM=RN(J)
      ENDIF
      IF(RF(J) GE RFM)THEN
      RFM=RF(J)
      ENDIF
      RN(J)=(RN(J)/RNM)*RP
      RF(J)=(RF(J)/RFM)*RP
      ENDDO
100   ARN=RN(15)
      ARF=RF(15)
      WRITE(67,77)TS,TCN,TCF,RP,DE
C     ********** CALCULATION FOR NIO REDUCTION ***********
C     *************      AT T < TC, ****************
      XNT1=0 0
      MT1=5
      DO 200 K=1,KT
      DO 210 J=1,MT1
C     SNT1(K)=1-(60*GKN(J)*CG*TM(I)*SINH(PNX(J)*ZI(K)))/(ZI(K)*RHO*
      SNT1(K)=SNT1(K)+(60*GKN(J)*CG*SINH(PNX(J)*ZI(K)))/(ZI(K)*
     1 RHO*SINH(PNX(J))*(1+DNI*(PNX(J)/TANH(PNX(J))-1)))
      ENDDO
210   IF(SNT1(K) GE 1 0)THEN
      SNT1(K)=1 0
      ENDIF
      XNT1=XNT1+(ZI(K)**3-ZI(K+1)**3)*SNT1(K)
      ENDDO
200
C     *************      AT T=TC, ****************
      XNTC=0 0
      MTC=TCN
      DO 300 K=1,KT
      DO 310 J=1,MTC
      SNTC(K)=SNTC(K)+(60*GKN(J)*CG*SINH(PNX(J)*ZI(K)))/(ZI(K)*
     1 RHO*SINH(PNX(J))*(1+DNI*(PNX(J)/TANH(PNX(J))-1)))
      ENDDO
310   IF(SNTC(K) GE 1 0)THEN
      SNTC(K)=1 0
      ENDIF
      XNTC=XNTC+(ZI(K)**3-ZI(K+1)**3)*SNTC(K)
      ENDDO
300
C     *************      AT T > TC, ****************
      IF(TCN LT 15)THEN
      XNT3=0 0
      MT3=15
      MT=MT3-TCN
      DO 400 K=1,KT
      DO 410 J=1,MT
      PNM=PNX(J)*RN(J)/RP
      SNT3(K)=SNT3(K)+(GKN(J)*CG*RN(J)*SINH(PNX(J)*ZI(K))*60)/
     1 (RP*ZI(K)*RHO*SINH(PNM)*(1+(PNM/TANH(PNM)-1)*DR*(1-RN(J)/RP+
     2 RN(J)*DNI/RP)))
      ENDDO
410   SNT3(K)=SNT3(K)+SNTC(K)
      IF(SNT3(K) GE 1 0)THEN
      SNT3(K)=1 0
      ARN=ZI(K-1)*RP
      ENDIF
      IF((SNT3(K) GE 0 99) AND (ARN LE RN(J)))THEN
      RN(J)=ARN
      ENDIF
      XNT3=XNT3+(ZI(K)**3-ZI(K+1)**3)*SNT3(K)
      ENDDO
400   CONTINUE
C     *************      AT T=15, ****************
      ELSEIF(TCN GE 15)THEN
      XNT3=0 0
      MT3=15
      DO 450 K=1,KT
      DO 460 J=1,MT3
      SNT3(K)=SNT3(K)+(60*GKN(J)*CG*SINH(PNX(J)*/I(K)))/(ZI(K,*
     1 RHO*SINH(PNX(J))*(1+DNI*(PNX(J)/TANH(P^X(J))-1)))
      ENDDO
460   IF(SNT3(K) GE 1 0)THEN
      SNT3(K)=1 0
      ARN=ZI(K)*RP
      IF(SNT3(K) GE 1 0) AND (ARN LE RN(J)))THEN
      RN(J)=ARN
      ENDIF
      XNT3=XNT3+(ZI(K)**3-ZI(K+1)**3)*SNT3(K)
      ENDDO
450   ENDIF
```

```
C      ******************** CALCULATION FOR FE2O3 REDUCTION ****************
C      ****************          AT T < TC,  ********************************
C      ***********************************************************************
       XFT1=0 0
       MT1=5
       DO 500 K=1,KT
       DO 510 J=1,MT1
       SFT1(K)=SFT1(K)+(60*GKF(J)*CG*SINH(PFX(J)*ZI(K)))/(ZI(K)*RHOF(J))
     1 *SINH(PFX(J))*(1+DNI*(PFX(J)/TANH(PFX(J))-1)))
510    ENDDO
       IF(SFT1(K) GE 1 0)THEN
       SFT1(K)=1 0
       ENDIF
       XFT1=XFT1+(ZI(K)**3-ZI(K+1)**3)*SFT1(K)
500    ENDDO
C      ************************          AT T=TC,  **********************
       XFTC=0 0
       MTFC=TCF
       DO 600 K=1,KT
       DO 610 J=1,MTFC
       SFTC(K)=SFTC(K)+(60*GKF(J)*CG*SINH(PFX(J)*ZI(K)))/(ZI(K)*RHOF(J))
     1 *SINH(PFX(J))*(1+DNI*(PFX(J)/TANH(PFX(J))-1)))
610    ENDDO
       IF(SFTC(K) GE 1 0)THEN
       SFTC(K)=1 0
       ENDIF
       XFTC=XFTC+(ZI(K)**3-ZI(K+1)**3)*SFTC(K)
600    ENDDO
C      ******************          AT T > TC,  *******************************
       IF(TCF LT 15)THEN
       XFT3=0 0
       MT3=15
       MT=MT3-TCF
       DO 700 K=1,KT
       DO 710 J=1,MT
       PFM=PFX(J)*RF(J)/RP
       SFT3(K)=SFT3(K)+(GKF(J)*CG*RF(J)*SINH(PFX(J)*ZI(K))*60)/
     1 (RP*ZI(K)*RHOF(J)*SINH(PFM)*(1+(PFM/TANH(PFM)-1)*DR*(1-RF(J)/RP
     2 +RF(J)*DNI/RP)))
710    ENDDO
       SFT3(K)=SFT3(K)+SFTC(K)
       IF(SFT3(K) GE 1 0)THEN
       SFT3(K)=1 0
       ARF=ZI(K-1)*RP
       RF(J)=ARF
       ENDIF
       IF((SFT3(K) GE 0 99) AND (ARF LE RF(J)))THEN
       RF(J)=ARF
       ENDIF
       XFT3=XFT3+(ZI(K)**3-ZI(K+1)**3)*SFT3(K)
700    CONTINUE
C      ************************************************************
       ELSEIF(TCF GE 15)THEN
       XFT3=0 0
       MT3=15
       DO 550 K=1,KT
       DO 560 J=1,MT3
       SFT3(K)=SFT3(K)+(60*GKF(J)*CG*SINH(PFX(J)*ZI(K)))/(ZI(K)*RHOF(J))
     1 *SINH(PFX(J))*(1+DNI*(PFX(J)/TANH(PFX(J))-1)))
560    ENDDO

       IF(SFT3(K) GE 1 0)THEN
       SFT3(K)=1 0
       ENDIF
       XFT3=XFT3+(ZI(K)**3-ZI(K+1)**3)*SFT3(K)
550    ENDDO
       ENDIF
C      ***********************************************************************
       PRINT *,'GKN-XN',GKN(9),XNT3
       ENDDO
       DO K=1,KT
       WRITE(67,7)ZI(K),SNT1(K),SNTC(K),SNT3(K),SFT1(K),SFTC(K),SFT3(K)
7      FORMAT(7(F9 4))
       ENDDO
       WRITE(67,8)MT1,MT3,XNT1,XNTC,XNT3,XFT1,XFTC,XFT3
8      FORMAT(100('-'),1X,'TMT1=',F4 0,2X,'TMT3=',F4 0,2X,'XNT1=',F6 4,
     1 2X,'XNTC=',F6 4,2X,'XNT3=',F6 4,2X,'XFT1=',F6 4,2X,'XFTC=',F6 4,
     2 2X,'XFT3=',F6 4/100('-'))
       RETURN
       END
```

```fortran
C     ***** RKWV F SUBROUTINE FOR CALCULATING WATER VAPOR CONE
C     ***************************************************
C     SUBROUTINE RKWV
$INCLUDE 'COVER RK'
      DIMENSION CA(KT),PM(N)
C     ***************************************************
C     WATER VAPOR CONCENTRATION PROFILE WITHIN A PELLET FOR
C     HOMOGENEOUS REACTION AT A PARTICULAR INSTANT
C     ***************************************************
      IF((TM(I) GE 14 5) AND (TM(I) LE 15 5))THEN
      B=3
      RM=RP*EMS(I)
      RWH(1)=0 0
      PTC=TW/(EMS(I)*(1+0 6*B))
      XCAW=0 0
      DO 400 K=1,KT
      CAW(K)=1-SINH(PME(I)*ZI(K)))/(ZI(K)*SINH(PME(I))*(1+DNI*PME(I)/
    1 TANH(PME(I))-1))
      DWV=TW*(1-ZI(K)**2)
      RWH(K)=RWH(K)+DWV
      IF(ZI(K-1) GE EMS(I))THEN
      RWP(K)=((2*PTC*EMS(I))/ZI(K))*(1+0 6*B)*(1-ZI(K))
      RWS(K)=2*TW*(1/ZI(K)-1)
      RSF=RWS(K)
      ELSE
      RWS(K)=RSF
      RWP(K)=PTC*((1-(ZI(K)/EMS(I))**2)+0 3*B*(1-(ZI(K)/EMS(I))**4)+
    1 (2+1 2*B)*(1-EMS(I)))
      ENDIF
      XCAW=XCAW+(ZI(K)**3-ZI(K+1)**3)*CAW(K)
400   CONTINUE
      PRINT *,'RF=',ARF,RP
      IF(RF(I) LT RP)THEN
      EMF=ARF/RP
      PHM=PME(I)*EMF
      CAM=CG/(1-DR*(1-EMF+EMF*DNI)*(1-PHM/TANH(PHM)))
      XCAW1=0 0
      DO 500 K=1,KT
      IF(ZI(K) GE EMF)THEN
      CA(K)=(CAM*EMF*(1-ZI(K)+ZI(K)*DNS)+CG*(ZI(K)-EMF)/
    1 (ZI(K)*(1-EMF+EMF*DNS))
      ELSEIF(ZI(K) LT EMF)THEN
      CA(K)=(CAM*EMF*SINH(PME(I)*ZI(K))/(ZI(K)*SINH(PHM))
      ENDIF
      CAW1(K)=1-CA(K)/CG
      XCAW1=XCAW1+(ZI(K)**3-ZI(K+1)**3)*CAW1(K)
500   ENDDO
      ENDIF
      ENDIF
C     ***********WATER VAPOR CONE IN THE REACTION INTERFACE *****
      EMF=RF(I)/RP
      PHM=PM(I)*EMF
      IF(I LE TI(2))THEN
      RIW(I)=1-(SINH(PM(I)*EMS(I)))/(EMS(I)*SINH(PM(I))*
    1 (1+DNI*PM(I)/TANH(PM(I))-1))
      RIWN(I)=1-(SINH(PM(I)*EMSN(I)))/((EMSN(I)*SINH(PM(I))*
    1 (1+DNI*PM(I)/TANH(PM(I))-1))
      ELSE
      RCAM=1/(1-DR*(1-EMF+FMF*DNI)*(1-PHM/TANH(PHM)))
      RIW(I)=1-(RCAM*EMF*SINH(PM(I)*EMS(I)))/(EMS(I)*SINH(PHM))
      RIWN(I)=1-(RCAM*EMF*SINH(PM(I)*EMSN(I)))/((EMSN(I)*SINH(PHM))
      ENDIF
100   CONTINUE
      RIW(1)=0 0
      RIWN(1)=0 0
      RETURN
      END
```

```fortran
C     ***** RKFX F CALCULATION FOR WATER VAPOR CORRECTION F(X)
C     ***** MAIN RKMain F/SUB RTP/ZIK/RKA/RKFX/RKWV
C     ***************************************************
      SUBROUTINE RKFX
      REAL NKE
      DIMENSION GMKN(N),GMKF(N),XXN(N),XXF(N)
      OPEN(UNIT=55,FILE='DIFK IN')
      OPEN(UNIT=56,FILE='WV OUT')
      FG=1 0
      READ(55,*)
      WRITE(56,8)
8     FORMAT(80('-')/5X,'TMIN',7X,'BRHN',7X,'BRHF',8X,'WRH',8X
    1 'YRH',8X,'FNX',8X,'FEX'/80('-'))
      DO 100 J=1,ND
      XXN(J)=XX1(J)/100
      XXF(J)=XX2(J)/100
      READ(55,*)A,GMKN(J),C,GMKF(J)
      DKN(J)=(OKN(J)-GMKN(J))/OKN(J)
      DKF(J)=(OKF(J)-GMKF(J))/OKF(J)
      PM=RP*(OKF(J)/DE)**0 5
      YH=SINH(PM*EMS(J))/((EMS(J))*SINH(PM))*(1+DNI*(PM/TANH(PM)-1)))
      YRH(J)=(1-YH)/YH
      BRHN=DKN(J)*EKN(J)
      BRHF=DKF(J)*EKF(J)
      TIS=60*TM(J)
      GFN=1-(1-XXN(J))**(1/FG)
      GFE=1-(1-XXF(J))**(1/FG)
      FNP=3-2*XXN(J)-3*(1-XXN(J))**0 667
      FEP=3-2*XXF(J)-3*(1-XXF(J))**0 667
C     ************************* FE2O3  -> FE3O4 ************
      IF(XXF(J) LE 0 111)THEN
      EK1=10 0
      EK2=4698*DEXP(-7911 4/TX(J))
      FKE=1/((1/EK1+0*XXF(J)*(1/EK2-1/EK1))
C     ************************* FE3O4  -> FEO *************
      ELSEIF((XXF(J) GE 0 111) AND (XXF(J) LE 0 333))THEN
      EK2=4698*DEXP(-7911 4/TX(J))
      EK3=3 684*DEXP(-2226/TX(J))
      FKE=1/((1/EK2+4 5*(1/EK3-1/EK2)*(XXF(J)-0 111))
C     ************************* FEO  -> FE ****************
      ELSEIF(XXF(J) GE 0 333)THEN
      FKE=3 684*DEXP(-2226/TX(J))
      ENDIF
      NKE=518*DEXP(-5838/TX(J))
      IF(J LE 1)THEN
      FNX(J)=0 0
      FEX(J)=0 0
      ELSE
```

```fortran
      FNX(J)=ABS(NKE*(1-GFN/((OKN(J)*(CG*TIS/RHO-(RP**2/(6*DE)))
    1 *(FNP+2*XXN(J)*DNS)))))
      FEX(J)=ABS(FKE*(1-GFE/((OKF(J)*(CG*TIS/RHO-(RP**2/(6*DE)))
    1 *(FEP+2*XXF(J)*DNS)))))
      ENDIF
      WRITE(56,6)TM(J),BRHN,BRHF,WRH(J),YRH(J),FNX(J),FEX(J)
6     FORMAT(3X,F6 2,6(3X,F8 4))
100   ENDDO
      RETURN
      END
```

VFMain

```
C     **************************************************************
C     MODEL FOR NON-ISOTHERMAL GAS-SOLID REDUCTION IN A FIXED BED
C     REACTOR UNDER VERTICAL GAS FLOW CONDITION USING GRAIN MODEL
C     FOR SPHERICAL PELLETS BY H2/H2O//CO/CO2//N2 GAS MIXTURE
C     **************************************************************
C     VFMan F  NON-DIMENSIONAL CRANCK-NICHOLSON SCHEME FRCY3 IS THE
C     SUBROUTINES FOR REACTION KINETICS ACCORDING TO GRAIN MODEL
C     **************************************************************
C     SUBROUTINE DESCRIPTION -
C     TRIDAG  TRI-DIAGONAL MATRIX SOLVER
C     VVelo   GAS VELOCITY PROFILE THROUGH THE REDUCING PELLET BED
C     VFTg    GAS PHASE ENERGY BALANCE
C     VFTs    SOLID PHASE ENERGY BALANCE
C     VFRK    REDUCTION KINETICS FOR SPHERICAL PELLETS
C     VFGCO   GAS PHASE SPECIES(MASS) BALANCE FOR CO
C     VFGH2   GAS PHASE SPECIES(MASS) BALANCE FOR H2
C     **************************************************************
C     FOR A FIXED BED OF ORE HAVING BED HEIGHT OF 14CM ,REDUCED BY
C     CO GAS, POROSITY P= 72,S1 UNITS,MOLE
C     TS,TG=TEMP OF SOLID & GAS,F1,F2=FRACTION OF NIO & FE2O3 REDUCED
C     G,GH=DIMENSIONLESS CONE  OF CO AND H2
C     DF1,DF2,DF1H,DF2H=INCREMENT IN FRACTION REDUCTION OF NIO & FE2O3
C     FP,FG=>STRUCTURE FACTOR FOR PELLETS
C     PARAMETERS CPG,ROG,VAZ,RP,H,RG,FP,FG,HT,FCO,FAG,CO,H2,TSI,TGI
C     **************************************************************
$INCLUDE 'COVER VF'
C     **************************************************************
      OPEN(UNIT=51,FILE='VFPUT')
      OPEN(UNIT=53,FILE='V1 OUT')
      OPEN(UNIT=54,FILE='V2 OUT')
      OPEN(UNIT=55,FILE='V3 OUT')
      OPEN(UNIT=56,FILE='VGRZ')
      OPEN(UNIT=57,FILE='TGH CVF')
      OPEN(UNIT=58,FILE='FTS CVF')
      OPEN(UNIT=61,FILE='AVVF')
C     **************************************************************
      NBED=1
C     NS,NG=>NO OF GRID POINTS OF SOLID & GAS
C     ********STANDARD VALUES FOR NONDIMENSIONALIZING***************
      VO=0 1
      SLO=0 1
      WKHO=10 0
      WKCO=10 0
C     **************************************************************
      DO 300 JV=1,1
      TM=0 0
C     FAG=>FRACTION OF ADDITIONAL GAS ADDED BETWEEN HEARTHS
      FAG=0 1
C     H=>OTHER DIMENSION OF CYLINDRICAL OR PLATE PELLET
      TIS,TIG=>INITIAL KRG VALUE INITIAL TEMP OF SOLID & GAS
      READ(51,*)TIG,TIS,IID,RP,ITER,DLTS
C     *******HD MANOMETER HEIGHT DIFFERENCE, FR FLOW RATE (CC/S*****
      FR=0 082+1 062*IID 017E-3*IID**2
      PRINT *,FR,FR
      T=1
C     DR & DZ  R & Z DIRECTION GRID SIZE
      DR=0 02
      DZ=0 015
C     **************************************************************
```

C.4.3 Program for Vertical Gas Flow condition

COM.VF

```
f77 +O3 VFMan f TRIDAG f VFTs f VFTg f VFRK f VFVelo f VFAv f VFGH2 f
f77 +O3 VFMan o TRIDAG o VFTs o VFTg o VFRK o VFVelo o VFAv o VFGH2 o
f77 +O3 VFMan o TRIDAG o VFTs o VFTg o VFRK o VFVelo o VFAv o VFGH2 o -o run
run
```

VFPUT

```
0.915,0 915,6 8,0 25,66,0 5
0 915,0 915,2 8,0 25,46,0 5
0 915,0 915,11 0,0 25,46,0 5
1 04,1 04,6 8,0 25,126,0 25
1 04,1 04,2 8,0 25,86,0 25
1 04,1 04,11 0,0 4,86,0 25
(TIG TIS MANOR RP ITER DELT= VFPUT)
```

COVER.VF

```
      IMPLICIT REAL*8(A-H,O-Z)
      PARAMETER(NP=70,NS=60,NG=10,IM=10,NV=5)
      PARAMETER(NP=140,NS=120,NG=10,IM=20,NV=5)
      COMMON/A1/DELT,DR,DZ,HT,N1,N2,VGO,FP,S1,S2,SH1,SH2
      COMMON/A2/RP,RG,FCO,FH2,FAG,VAZ,PP,H2O,CO2,SBR,HTS
      COMMON/A3/KRGN,KRGF,HKRGN,HKRGF,DK,DKH,DE,DEH,GI,GHI
      COMMON/A4/FXC1(IM),FXC2(IM),FXH1(IM),FXH2(IM),VF(IM),P(IM)
      COMMON/A5/TS(IM,NP),TG(IM,NP),G(IM,NP),GH(IM,NP),RHM(IM)
      COMMON/A6/DF1(IM,NP),DF2(IM,NP),DF1H(IM,NP),DF2H(IM,NP)
      COMMON/A7/F1(IM,NP),F2(IM,NP),RD(9),WF(9),Z(NP),AG(NV),GA
      COMMON/A8/VR(IM,NP),VZ(IM,NP),HF(IM,NP),CF(IM,NP),X(NP),Y(NP)
      COMMON/A9/TM,M,LS,LG,SK,AKB,AKG,SLO,VO,TIG,TIS,RTO,RAD1
      COMMON/A10/ZP(NV),AF1(NV),AF2(NV),AGH(NV),ATS(NV),ATG(NV)
      COMMON/A11/AVZ,F1A,F2A,GHA,TSA,TGA,KFO,KNO,WKHO,WKCO
      REAL N1,N2,KRGN,KRGF,KFO,KNO
C
```

```
        IF(TIS LE 0 900)THEN
        HKRGF=69 228*EXP(-3 17/TIS)
        ELSE
        HKRGF=58157*EXP(-9 2302/TIS)
        ENDIF
        KRGF=798*EXP(-8 25/TIS)
        HKRGN=613*EXP(-6 898/TIS)
        IF(TIS LE 950)THEN
        KRGN=48180*EXP(-11 2/TIS)
        ELSE
        KRGN=3*EXP(-2/TIS)
        ENDIF
C  *****************************************************
        RG=6 7D-7
        FP=3 0
C  VF VOID FRACTN OF BED, PP PELLET POROSITY
C  P TOTAL POROSITY, E SOLID FRACTION
        PP=0 5645
C  *****************************************************
        RTO=10*IM*DR/RP
        RADI=RTO/FLOAT(IM)
        DO 110 I=1,IM
        RADP=RTO-FLOAT(I)*RADI
        VF(I)=(0 479- 0 0381*RADP+3 234E-4*RADP**2-1 897E-6*RADP**3)*0 9
        P(I)=(1-VF(I))*PP+VF(I)
        RHM(I)=37977*(1-P(I))
        PRINT *,'VF(',I,')',VF(I)
110     ENDDO
C  *****************************************************
C  RS DENSITY OF SOLID 3714 KG/CU M
C  RHM ORE BED DENSITY IN MOLE/CU M
C  RP RADIUS OF PELLET(0 1 TO 0 2 CM)
C  RG RADIUS OF GRAINS IN PELLET(6 E-5 TO 1E-3 CM)
C  N1,N2 NO  OF MOLES OF [O] IN NIO & FE3O4 PER MOLE OF ORE
        N1=0 01597
        N2=1 004
C  FCO & FH2 FRACTION OF REDUCING GAS CO & H2, IN THE GAS
C  GHI GI INITIAL H2 & CO CONCENTRATION OR PURITY (H2 H2O/CO CO2)
        FCO=0 000001
        FH2=0 999
        GHI=1 0
        GI=1 0
        FHK=0 667*FH2
C  ***********CONDUCTIVITY OF GAS AND SOLID***********
        SK=0 67*TIS**0 6
        AKG=(0 955*EXP(- 544/TIG)*FHK+0 459*EXP(- 869/TIG)*(1-FHK))/
     1  (1 26*FHK+(1-FHK)*2 62)
        AKB=(1-VF(2))*SK+VF(2)*AKG
C  ***********CONSIDERING 40 % VOIDAGE AND 1 65 CM RCYL***********
        N=NBED*NS+(NBED-1)*NG+1
        VAZ=FR*TIG/23 35
        VO=2 13*RP**2*VF(2)**3*VAZ/(1-VF(2))**2
        DO 10 IJK=1,NBED
        M=1+(IJK-1)*(NS+NG)
        LS=M+NS
        LG=M+NS
        DO 20 I=1,IM
        DO 30 J=M,LG
        Z(J)=DZ*FLOAT(J-1)*100 0
        TG(I,J)=TIG
        TS(I,J)=TIS

        F1(I,J)=0 00
        F2(I,J)=0 00
        DF1(I,J)=0 000000
        DF1H(I,J)=0 00000
        DF2(I,J)=0 000000
        DF2H(I,J)=0 00000
        G(I,J)=GI
        GH(I,J)=GHI
        VR(I,J)=0 0
        VZ(I,J)=VAZ
30      CONTINUE
20      CONTINUE
10      CONTINUE
C  ********* MOLECULAR GAS DIFFUSIVITY SH F 0 9 IN MKS UNITS **********
        DH=7 365D-4*TIG**1 675
        DC=1 2475D-4*TIG**1 693
C  HT GAS SOLID HEAT TRANSFER COEFF  AT TEMP TG(1)
        HTS=(3159*(VAZ/VF(2)**0 9*TIG**0 3)/RP**0 75
        HT=HTS
        WRITE(53,65)HT,RP,GHI,DR,DZ,FH2
65      FORMAT(128('-')/2X,'HT=',F7 1,2X,'RP=',F6 4,2X,
     1  'GHI=',F5 2,2X,'DR=',F6 4,2X,'DZ=',F6 4,2X,'FH2=',F4 1/128('-')/
     2  2X,'TIME',2X,'TG6',4X,'TS6',3X,'TG18',3X,'TS18',3X,'TG30',3X,
     3  'TS30',3X,'TG42',3X,'TS42',3X,'TG54',3X,'TS54',2X,'DF1/1',3X,
     4  'DF1H1',3X,'DF2/1',3X,'DF2H1'/128('-'))
        WRITE(54,77)VAZ,RP,TIS,FCO,FH2,TIG
77      FORMAT(128('-')/1X,'PARAMETERS',2X,'VAZ=',F8 6,2X,'RP=',
     1  F6 4,2X,'TIS=',F6 3,2X,'FCO=',F5 3,2X,'FH2=',
     2  F6 4,2X,'TIG=',F6 3/128('-')/2X,'TIME',3X,'F1/6',2X,'T1/18',
     3  2X,'F1/30',2X,'F1/42',2X,'F1/54',3X,'F2/6',2X,'F2/18',2X,'T2/30',
     4  2X,'F2/42',2X,'F2/54',4X,'G30',4X,'GH16',3X,'GH18',3X,'GH30',3X,
     5  'GH42',3X,'GH54'/128('-'))
        DO 600 JK=1,NBED
        M=1+(JK-1)*(NS+NG)
        LS=M+NS
        LG=M+NS+NG
        CALL VFVelo
        PRINT *,'VZ=',VZ(5,18)
600     ENDDO
        DO 32 J=M,LS,10
        WRITE(56,67)(VZ(I,J),I=1,IM)
67      FORMAT(20(F6 3))
32      CONTINUE
        WRITE(56,46)
46      FORMAT(128('-'))
        DO 34 J=M,LS,10
        WRITE(56,68)(VR(I,J),I=1,IM)
68      FORMAT(20(F6 3))
34      CONTINUE
        WRITE(56,47)
47      FORMAT(128('-'))
        DO 35 J=M,LS
        DO 36 I=1,IM
36      ENDDO
35      ENDDO
        PRINT *,'HTS,HT',HTS,HT
        DO 200 KKK=1,ITER
        IF(KKK LE 5) THEN
        DELT=0 1*DLTS*FLOAT(KKK)
        ELSE
        DELT=DLTS
        ENDIF
```

```fortran
      PRINT *,'DT=',DELT
      WRITE(53,5)TM,TG(5,6),TS(5,6),TG(5,18),TS(5,18),TG(5,30),
     1 TS(5,30),TG(5,42),TS(5,42),TG(5,54),TS(5,54),
     2 DF1(5,M),DF1H(5,M),DF2(5,M),DF2H(5,M)
5     FORMAT(F6 2,10(F7 4),4(E8 2))
      WRITE(54,7)TM,F1(5,6),F1(5,18),F1(5,30),F1(5,42),F1(5,54),
     1 F2(5,6),F2(5,18),F2(5,30),F2(5,42),F2(5,54),G(5,30),
     2 GH(5,6),GH(5,18),GH(5,30),GH(5,42),GH(5,54)
7     FORMAT(F6 2,16(F7 4))
      DO 100 KK=1,120
      DO 400 IJK=1,NBED
      M=1+(IJK-1)*(NS+NG)
      LS=M+NS
      LG=M+NS+NG
      CALL VFTs
      CALL VFTg
      IF(TS(9,M+2) GT 0 623) THEN
      CALL VFRK
      CALL VFGCO
      CALL VFGH2
      ENDIF
400   CONTINUE
      TM=TM+DELT/60 0
100   CONTINUE
      PRINT *,'TM TG TS GHI GH5 GHIM ',TM,TG(9,LS),TS(9,LS),
     1 GH(1,M),GH(5,30),GH(1M,LS)
      CALL VFAv
71    FORMAT(120('-')/2X,'TS='F6 3,2X,'TM=',F6 2,2X,'AVZ=',F6 4,2X,
     1 'F1A=',F6 4,2X,'F2A=',F6 4,2X,'GHA=',F6 4,2X,'TSA=',F6 3,2X,
     2 'TGA=',F6 3,2X,'VAZ=',F6 3/120('-')/6X,'ZP',7X,'AF1',6X,'AF2'
     3 ,6X,'AGH',6X,'AG',7X,'ATS',6X,'ATG'/120('-'))
      FORMAT(F9 2,F9 4,F9 4,F9 4,F9 4,F9 4)
88    FORMAT(128('-')/4X,'TIME=',F7 3,3X,'DELT=',F5 3,3X,'VAZ=',F5 3,
     1 3X,'RP=',F6 4,3X,'GHI=',F5 2,3X,'S1=',F6 3,3X,'S2=',F6 3,3X,
     2 'FH2=',F4 2,3X,'TS=',F7 3/128('-')/5X,'Z',6X,'ZP',7X,'Z',6X,'TS',6X,
     3 'F1',6X,'F2',6X,'DF1',6X,'DF1H',5X,'DF2',6X,'DF2H',8X,'G',7X,
     4 'GH'/128('-'))
      FORMAT(F8 2,F8 4,F8 4,F8 5,E9 2,E9 2,E9 2,E9 2,F9 5,F9 5)
8     IF((TM GE 9 9) AND (TM LE 10 3))THEN
      WRITE(61,71)TIS,TM,AVZ,F1A,F2A,GHA,TSA,TGA,VAZ
      WRITE(61,6)(ZP(L),AF1(L),AF2(L),AGH(L),AG(L),ATS(L),ATG(L),L=1,NV)
      WRITE(55,88)TM,DELT,VAZ,RP,GHI,S1,S2,FH2,TIS
      WRITE(55,8)(Z(J),TG(5,J),TS(5,J),F1(5,J),F2(5,J),DF1(5,J),
     1 DF1H(5,J),DF2(5,J),DF2H(5,J),G(5,J),GH(5,J),J=1,LS)
      ELSEIF((TM GE 19 9) AND (TM LE 20 3))THEN
      WRITE(57,51)TM,TIG
51    FORMAT(45('-'),X,'TIME=',F5 1,3X,'*TG*=',F6 3,X,45('-'))
      DO J=M,LS
      WRITE(57,52)(TG(1,J),I=1,IM)
52    FORMAT(20(F6 3))
      ENDDO
      WRITE(57,53)TM,TIG
53    FORMAT(45('-'),X,'TIME=',F5 1,3X,'*GH*',3X,'TG=',F6 3,X,45('-'))
      DO J=M,LS
      WRITE(57,54)(GH(1,J),I=1,IM)
54    FORMAT(20(F6 3))
      ENDDO
      WRITE(58,55)TM,TIS
55    FORMAT(45('-'),X,'TIME=',F5 1,3X,'*F1*',3X,'TG=',F6 3,X,45('-'))
      DO J=M,LS
      WRITE(58,56)(F1(1,J),I=1,IM)
56    FORMAT(20(F6 3))
      ENDDO
      WRITE(58,57)TM,TIS
57    FORMAT(45('-'),X,'TIME=',F5 1,3X,'*F2*',3X,'TS=',F6 3,X,45('-'))
      DO J=M,LS
      WRITE(58,58)(F2(1,J),I=1,IM)
58    FORMAT(20(F6 3))
      ENDDO
      WRITE(58,59)TM,TIS
59    FORMAT(45('-'),X,'TIME=',F5 1,3X,'*TS*=',F6 3,X,45('-'))
      DO J=M,LS
      WRITE(58,70)(TS(1,J),I=1,IM)
70    FORMAT(20(F6 3))
      ENDDO
      WRITE(61,71)TIS,TM,AVZ,F1A,F2A,GHA,TSA,TGA,VAZ
      WRITE(61,6)(ZP(L),AF1(L),AF2(L),AGH(L),AG(L),ATS(L),ATG(L),L=1,NV)
      WRITE(55,88)TM,DELT,VAZ,RP,GHI,S1,S2,FH2,TIS
      WRITE(55,8)(Z(J),TG(5,J),TS(5,J),F1(5,J),F2(5,J),DF1(5,J),
     1 DF1H(5,J),DF2(5,J),DF2H(5,J),G(5,J),GH(5,J),J=1,LS)
      ELSEIF((TM GE 29 9) AND (TM LE 30 3))THEN
      WRITE(61,71)TIS,TM,AVZ,F1A,F2A,GHA,TSA,TGA,VAZ
      WRITE(61,6)(ZP(L),AF1(L),AF2(L),AGH(L),AG(L),ATS(L),ATG(L),L=1,NV)
      WRITE(55,88)TM,DELT,VAZ,RP,GHI,S1,S2,FH2,TIS
      WRITE(55,8)(Z(J),TG(5,J),DF2H(5,J),G(5,J),GH(5,J),J=1,LS)
     1 DF1H(5,J),DF2(5,J),DF2H(5,J),G(5,J),GH(5,J),J=1,LS)
      ENDIF
200   CONTINUE
555   WRITE(61,71)TIS,TM,AVZ,F1A,F2A,GHA,TSA,TGA,VAZ
      WRITE(61,6)(ZP(L),AF1(L),AF2(L),AGH(L),AG(L),A1s(L),A1G(L),L=1,NV)
      WRITE(55,88)TM,DELT,VAZ,RP,GHI,S1,S2,FH2,TIS
      WRITE(55,8)(Z(J),TG(5,J),TS(5,J),F1(5,J),F2(5,J),DF1(5,J),
     1 DF1H(5,J),DF2(5,J),DF2H(5,J),G(5,J),GH(5,J),J=1,LS)
      WRITE(53,33)SBR,S1,S2,KRGN,KRGF,DA,DC,DE,IIT,RP
33    FORMAT(128('-')/2X,'SBR=',F4 0,3X,'S1=',F6 3,2X,'S2=',F6 3,
     1 3X,'KRGN=',F6 3,2X,'KRGF=',F6 3,2X,'DK=',E8 2,2X,'DC=',E8 2,
     2 2X,'DE=',E8 2,3X,'HT=',F7 1,3X,'RP=',E8 2/128('-'))
      WRITE(54,22)SH1,SH2,HKRGN,IIKRGF,DKII,DII,DEII
22    FORMAT(128('-')/2X,'SH1=',F6 3,2X,'SH2=',F6 3,
     1 3X,'HKRGN=',F6 2,2X,'HKRGF=',F5 2,3X,'DKII=',E8 2,2X 'DII=',E8 2,
     2 2X,'DEII=',E8 2/128('-'))
300   CONTINUE
      STOP
      END
```

VFVelo

```fortran
C *******************************************************
C     ERGUN  SOLUTION OF ERGUN'S EQUATION FOR AXI-SYMMETRIC
C     FLOW THROUGH A POROUS BED
C *******************************************************
C
      SUBROUTINE VFVelo
C *******************************************************
$INCLUDE 'COVER VF'
      DIMENSION S(IM+2,LG),SN(IM+2,LG),RI(IM+2,LG),R2(IM+2,LG),EV(IM,LG)
      DIMENSION A(LS+2),B(LS+2),C(LS+2),D(LS+2),V(LS+2)
C ***************INPUT CONDITIONS***************
C     TIS N D TEMP, DP DIA OF CENTRAL & OUTER PELLETS (M),
C     RTO RATIO OF CYLINDER DIA/PELLET DIA, VEL GAS VELOCITY (M/S),
C     CYL CYLINDER DIA (M), GAS GAS MOLECULAR WEIGHT,
C     WFS WEIGHTAGE FACTOR, VK KINEMATIC VISCOSITY (M**2/S),
C ********************************************
      WFS=0 9
      VKH=8 228D-4*TIS**1 656
      VKW=1 702D-4*TIS**2 049
      VKN=1 168D-4*TIS**1 611
      VK=(0 5*VKH+0 45*VKW+0 05*VKN)/SLO**2
      ROG=0 128*SLO**3/TIS
      GMU=ROG*VK
      DP=RP/(50*SLO)
      DO 100 I=1,IM
      RADP=RTO-FLOAT(I)*RADI
      DO 100 J=1,LS
      EV(I,J)=VF(I)
      ENDDO
100   DO 11 I=1,IM
      DO 11 J=1,LS
      R1(I,J)=(150*GMU*(1-EV(I,J))**2)/(DP**2*EV(I,J)**3)
      R2(I,J)=(1 75*ROG*(1-EV(I,J)))/(DP*EV(I,J)**3)
      S(I,J)=-VAZ*(FLOAT(I)*DR)**2/2.0
      SN(I,J)=S(I,J)
      ENDDO
11
C *******I/R DIRECTION SWEEP SYMMETRY AT CENTER**************
      DO 1000 K=1,200
      DO 15 J=1,LS
      DO 15 I=1,IM
      S(I,J)=SN(I,J)
      ENDDO
15
C *******CENTRAL IN R/BACKWARD IN Z ******************
      DO 200 J=2,LS-1
      A(1)=0 0
      B(1)=1 0
      C(1)=0 0
      D(1)=S(1,J)
C *******CENTRAL IN R/BACKWARD IN Z ******************
      DO 300 I=2,IM
      SR=((S(I+1,J)-S(I-1,J))/(2*DR))**2
      SZ=((S(I,J)-S(I,J-1))/DZ)**2
      F1R=((R1(I+1,J)-R1(I-1,J))/(2*DR))
      F2R=((R2(I+1,J)-R2(I-1,J))/(2*DR))
      F1Z=((R1(I,J)-R1(I,J-1))/DZ)
      F2Z=((R2(I,J)-R2(I,J-1))/DR)
      SRZ=(S(I+1,J)-S(I+1,J-1)-S(I-1,J)+S(I-1,J-1))/(2*DR*DZ)
      F11=R1(I,J)
      F12=R2(I,J)
      RI=FLOAT(I)*DR
      A(I)=(F1Z/DR**2+F11/(2*DR*RI))*RI*(SR+SZ)**0 5+SR*
     1 (2*F12/DR**2+F12/(2*DR*RI))-F1R/(2*DR)*F12/DR**2+F12/(DR*RI))-
     2 F2R/(2*DR))-(F12*SRZ*(S(I,J)-S(I,J-1)))/(DR*DZ)

      B(I)=(F1Z/DZ-2*F11/DR**2-2*F11/DZ**2)*RI*(SR+SZ)**0 5+SR*(F2Z/DZ-
     1 4*F12/DR**2-2*F12/DZ**2)+SZ*(F2Z/DZ-2*F12/DR**2)*RI*(SR+SZ)**0 5+SR*(F2Z/DZ**2)
      C(I)=(F1R/(2*DR)+F11/DR**2-F11/(2*DR*RI))*RI*(SR+SZ)**0 5+SR*
     1 (F2R/(2*DR)+2*F12/DR**2-F12/(RI*DR))+SZ*(F2R/(2*DR)+F12/DR**2-
     2 F12/(RI*DR))+F12*((F(S(I,J)-S(I,J-1))*SRZ)/(DR*DZ)
      D(I)=S(I,J-1)*((F1Z/DZ-F11/DZ**2)*RI*(SR+SZ)**0 5+SR*(F2Z/DZ-
     1 F12/DZ**2)+SZ*(F2Z/DZ-2*F12/DZ**2))-S(I,J+1)*(F11*RI*
     2 (SR+SZ)**0 5)/DZ**2+(2*SZ*F12)/(DZ**2))
      ENDDO
300   ENDDO
C ***********CONSTANT STREAM FUNCTION VALUE AT THE WALL***********
      A(IM)=0 0
      B(IM)=1 0
      C(IM)=0 0
      D(IM)=S(IM,J)
C
      CALL TRIDAG(A,B,C,D,V,1,IM)
      DO 20 I=1,IM
      S(I,J)=V(I)
      SN(I,J)=(1-WFS)*SN(I,J)+WFS*S(I,J)
      ENDDO
20    ENDDO
200
C ***********J/Z DIRECTION SWEEP IMAGE POINT AT INLET & OUTLET***********
      DO 400 I=2,IM-1
      SR=((S(I+1,1)-S(I-1,1))/(2*DR))**2
      SZ=0 0
      F1R=((R1(I+1,1)-R1(I-1,1))/(2*DR))
      F2R=((R2(I+1,1)-R2(I-1,1))/(2*DR))
      F11=R1(I,1)
      F12=R2(I,1)
      RI=FLOAT(I)*DR
      A(1)=0 0
      B(1)=(2*F11/DR**2+F11/DZ**2)*RI*(SR+SZ)**0 5-
     1 SR*(4*F12/DR**2+F12/DZ**2)
      C(1)=(F11*RI*(SR+SZ)**0 5)/DZ**2+(2*SZ*F12)/DZ**2+(2*SZ*F12)/DZ**2
      D(1)=S(I-1,1)*((F1R/(2*DR)-F11/(2*DR*RI)/(2*DR*RI))*RI*(SR+SZ)**0 5
     1 +SR-SR*((2*F12/DR**2-F12/(2*DR*RI))-F2R/(2*DR))-SZ*(F12/DR**2+
     2 F12/(DR*RI))-F2R/(2*DR)-S(I+1,1)*((F1R/(2*DR)+F11/DR**2-F11/
     3 (2*DR*RI))*RI*(SR+SZ)**0 5+SR*(F2R/(2*DR)+F12/DR**2-F12/
     4 (RI*DR))+SZ*(F2R/(2*DR)+F12/DR**2-F12/(RI*DR)))
      ENDDO

      DO 500 J=2,LS
      SR=((S(I+1,J)-S(I-1,J))/(2*DR))**2
      SZ=((S(I,J)-S(I,J-1))/DZ)**2
      F1R=((R1(I+1,J)-R1(I-1,J))/(2*DR))
      F2R=((R2(I+1,J)-R2(I-1,J))/(2*DR))
      F1Z=((R1(I,J)-R1(I,J-1))/DZ)
      F2Z=((R2(I,J)-R2(I,J-1))/DR)
      SRZ=(S(I+1,J)-S(I+1,J-1)-S(I-1,J)+S(I-1,J-1))/(2*DR*DZ)
      F11=R1(I,J)
      F12=R2(I,J)
      RI=FLOAT(I)*DR
      A(J)=(F1Z/DZ**2-F12/DZ)*RI*(SR+SZ)**0 5+SR*(F2Z/DZ**2-F12/DZ)+
     1 SZ*(2*F12/DZ-2*F2Z/DZ)-(F12*(S(I+1,J)-S(I-1,J))*RI*(2*SZ/DZ)+
      B(J)=(F1Z/DZ-2*F11/DR**2-2*F11/DZ**2)*RI*(SR+SZ)**0 5+SR*(F2Z/DZ-
     1 4*F12/DR**2-2*F12/DZ**2)+SZ*(F2Z/DZ-2*F12/DR**2-2*F12/DZ**2)+
      2 (F12*SRZ*(S(I+1,J)-S(I-1,J))/(DR*DZ)
      C(J)=(F11*RI*(SR+SZ)**0 5)/DZ**2+(2*SZ*F12)/DZ**2+(2*SZ*F12)/DZ**2
      D(J)=S(I-1,J)*((F1R/(2*DR)-F11/(2*DR*RI))*RI*(SR+SZ)**0 5+SR*0 5
     1 *RI-S(I-1,J)*((F1R/(2*DR)-F11/(2*DR*RI))*RI*(SR+SZ)-SZ*(F12/DR**2+
     2 F12/(DR*RI)-F2R/(2*DR))-S(I+1,J)*((F1R/(2*DR)+F11/DR**2-F11/
     3 (2*DR*RI))*RI*(SR+SZ)**0 5+SR*(F2R/(2*DR)+2*F12/DR**2-F12/
     4 (RI*DR))+SZ*(F2R/(2*DR)+F12/DR**2-F12/(RI*DR)))
```

```fortran
C      ************************************************************
       SUBROUTINE VFTs
C      ************************************************************
$INCLUDE 'COVER VF'
       DIMENSION A(LS),B(LS),C(LS),D(LS),V(LS)
       CS=88+2 44*TIS
       CN=42840 0
       HN=6720 0
       TC=(SLO**2*RHM(2)*CS)/AKB
       DT=DELT/TC
       AR=DT/(2*DR*DR)
       AZ=DT/(2*DZ*DZ)
       SNU=(HT*SLO**2*DT)/(2*AKB)
       R1=N1*CN/(1000*CS)
       RH1=N1*HN/(1000*CS)
       DO 13 I=1,IM
C      -----LOWER BOUNDARY CONDITION/KNOWN TEMPERATURE-----
       ARI=AR/(2*FLOAT(I))
       R2=N2*CF(I,M)/(1000*CS)
       RH2=N2*HF(I,M)/(1000*CS)
       A(M)=0 0
       C(M)=-AZ
       IF(I LE 1)THEN
       B(M)=1+AR+ARI+AZ+SNU
       D(M)=(1-AR-ARI-AZ-SNU)*TS(I,M)+TS(I,M+1)*AZ+2*TS(I+1,M)*(AR+ARI)
     1 +2*SNU*TIG+R1*DF1(I,M)+R2*DF2(I,M)+RH1*DF1H(I,M)+RH2*DF2H(I,M)
       ELSEIF(I GE IM)THEN
       B(M)=1+AR+AZ-ARI+SNU
       D(M)=(1-AR-AZ+ARI-SNU)*TS(I,M)+TS(I,M+1)*AZ+2*TS(I-1,M)*(AR-ARI)
     1 +2*SNU*TIG+R1*DF1(I,M)+R2*DF2(I,M)+RH1*DF1H(I,M)+RH2*DF2H(I,M)
       ELSE
       B(M)=1+2*AR+AZ+SNU
       D(M)=(1-2*AR-AZ-SNU)*TS(I,M)+TS(I,M+1)*AZ+
     1 2*SNU*TIG+2*TS(I-1,M)*(AR-ARI)+2*TS(I+1,M)*(AR+ARI)+
     2 R1*DF1(I,M)+R2*DF2(I,M)+RH1*DF1H(I,M)+RH2*DF2H(I,M)
       ENDIF
C      -----CRANK NICHOLSON/CENTRAL IN SPACE-----
       DO 11 J=M+1,LS
       R2=N2*CF(I,J)/(1000*CS)
       RH2=N2*HF(I,J)/(1000*CS)
       A(J)=-AZ
       C(J)=-AZ
       IF(I LE 1)THEN
       B(J)=1+AR+ARI+2*AZ+SNU
       D(J)=(1-AR-ARI-2*AZ-SNU)*TS(I,J)+TS(I,J+1)*AZ+TS(I,J-1)*AZ
     1 +2*TG(I,J)*SNU+2*TS(I+1,J)*(AR+ARI)+
     2 R1*DF1(I,J)+R2*DF2(I,J)+RH1*DF1H(I,J)+RH2*DF2H(I,J)
       ELSEIF(I GE IM)THEN
       B(J)=1+AR-ARI+2*AZ+SNU
       D(J)=(1-AR+ARI-2*AZ-SNU)*TS(I,J)+TS(I,J+1)*AZ+TS(I,J-1)*AZ
     1 +2*TIS*SNU+2*TS(I-1,J)*(AR-ARI)+
     2 R1*DF1(I,J)+R2*DF2(I,J)+RH1*DF1H(I,J)+RH2*DF2H(I,J)
       ELSE
       B(J)=1+2*AR+2*AZ+SNU
       D(J)=(1-2*AR-2*AZ-SNU)*TS(I,J)+TS(I,J+1)*AZ+TS(I,J-1)*AZ
     1 +2*TG(I,J)*SNU+2*TS(I-1,J)*(AR-ARI)+2*TS(I+1,J)*(AR+ARI)+
     2 R1*DF1(I,J)+R2*DF2(I,J)+RH1*DF1H(I,J)+RH2*DF2H(I,J)
       ENDIF
11     CONTINUE
500    ENDDO
C      *********IMAGE POINT ***********************************
       A(LS)=0 0
       B(LS)=1 0
       C(LS)=0 0
       D(LS)=S(I,LS-1)
C      ****************************************************
       CALL TRIDAG(A,B,C,D,V,1,LS)
       DO 40 J=1,LS
       S(I,J)=V(J)
40     ENDDO
400    ENDDO
1000   ENDDO
       DO 60 J=1,LS
       DO 70 I=1,IM
       VR(I,J)=(S(I,J+1)-S(I,J-1))/(2*FLOAT(I)*DR**2)
       VZ(I,J)=(S(I-1,J)-S(I+1,J))/(2*FLOAT(I)*DR**2)
70     ENDDO
60     ENDDO
       SUM=0 0
       DO I=1,IM
       SUM=SUM+FLOAT(I)*DR**2*VR(I,30)
       ENDDO
       FS=IM*DR*VAZ/SUM
       DO 66 J=1,LS
       DO 77 I=1,IM
       VR(I,J)=VR(I,30)
       VZ(I,J)=VZ(I,30)
77     ENDDO
       VR(IM,J)=VR(IM-1,30)
       VZ(IM,J)=VZ(IM-1,30)
66     ENDDO
       RETURN
       END
```

VFTg

```
C     ***************************************************
      SUBROUTINE VFTg
C     ***************************************************
$INCLUDE 'COVER.VF'
      DIMENSION A(LS),B(LS),C(LS),D(LS),V(LS)
      ROG=12 1875/TIG
      CPG=29 5+4 78*TIG
      TC=(SLO**2*ROG*CPG)/AKB
      DT=DELT/TC
      AZ=DT/(2*DZ*DZ)
      AR=DT/(2*DR*DR)
      GNU=(HT*SLO**2*DT)/(2*AKB)
      DO 200 I=1,IM
C     ------LOWER BOUNDARY CONDITION------
      A(M)=0 0
      B(M)=1 0
      C(M)=0 0
      D(M)=TIG
C     ------DISCRETIZED BY CRANK NICHOLSON TECH
      DO 500 J=M+1,LS-1
      ROG=12 1875/TG(I,J)
      ARI=AR/(2*FLOAT(I))
      PER=(VO*SLO*ROG*CPG*VR(I,J)*DT)/(4*AKB*DR)
      PEZ=(VO*SLO*ROG*CPG*VZ(I,J)*DT1)/(2*AKB*DZ)
      A(J)=-PEZ-AZ
      C(J)=AZ
      IF(I LE 1)THEN
      B(J)=1+PEZ+2*AZ+AR+ARI-PER+GNU
      D(J)=TG(I,J)*(1-PEZ-2*AZ-AR-ARI-PER-GNU)+TG(I+1,J)*2*(AR+ARI-PER)
     1+TG(I,J-1)*(PEZ+AZ)+TG(I,J+1)*AZ+2*GNU*TS(I,J)
      ELSEIF(I GE IM)THEN
      B(J)=1+PEZ+2*AZ+AR+ARI+PER+GNU
      D(J)=TG(I,J)*(1-PEZ-2*AZ-AR-ARI-PER-GNU)+TG(I-1,J)*2*(AR+PER-ARI)
     1+TG(I,J-1)*(PEZ+AZ)+TG(I,J+1)*AZ+2*GNU**TIS
      ELSE
      B(J)=1+PEZ+2*AZ+2*AR+GNU
      D(J)=TG(I,J)*(1-PEZ-2*AZ-2*AR-GNU)+2* TG(I-1,J)*(AR+PER-ARI)+
     1 2*TG(I+1,J)*(AR+ARI-PER)+TG(I,J-1)*(PEZ+AZ)+
     2 TG(I,J+1)*AZ+2*GNU* TS(I,J)
      ENDIF
500   CONTINUE
C
      A(LS)=0 0
      B(LS)=1 0
      C(LS)=0 0
      D(LS)=TG(I,LS-1)
C
      CALL TRIDAG(A,B,C,D,V,M,LS)
      DO 30 J=M,LS
      TG(I,J)=V(J)
30    CONTINUE
200   CONTINUE
C1000  CONTINUE
      RETURN
      END
```

```
C     ------UPPER SURFACE BOUNDARY/DEFINED HT-TRANSFER COEFFICIENT------
      R2=N2*CF(I,LS)/(1000*CS)
      RH2=N2*HF(I,LS)/(1000*CS)
      A(LS)=-AZ
      C(LS)=0 0
      IF(I LE 1)THEN
      B(LS)=1+AR+ARI+AZ+SNU
      D(LS)=(1-AR-ARI-AZ-SNU)*TS(I,LS)+2*TG(I,LS)*SNU+
     1 TS(I,LS-1)*AZ+2*TS(I+1,LS)*(AR+ARI)+
     2 R1*DF1(I,LS)+R2*DF2(I,LS)+RH1*DF1H(I,LS)+RH2*DF2H(I,LS)
      ELSEIF(I GE IM)THEN
      B(LS)=1+AR-ARI+AZ+SNU
      D(LS)=(1-AR+ARI-AZ-SNU)*TS(I,LS)+2*TIS*SNU+
     1 TS(I,LS-1)*AZ+2*TS(I-1,LS)*(AR-ARI)+
     2 R1*DF1(I,LS)+R2*DF2(I,LS)+RH1*DF1H(I,LS)+RH2*DF2H(I,LS)
      ELSE
      B(LS)=1+2*AR+AZ+SNU
      D(LS)=(1-2*AR-AZ-SNU)*TS(I,LS)+2*TG(I,LS)*SNU+TS(I,LS-1)*AZ
     1 +2*TS(I-1,LS)*(AR-ARI)+2*TS(I+1,LS)*(AR+ARI)+
     2 R1*DF1(I,LS)+R2*DF2(I,LS)+RH1*DF1H(I,LS)+RH2*DF2H(I,LS)
      ENDIF
C
      CALL TRIDAG(A,B,C,D,V,M,LS)
      DO 12 J=M,LS
      TS(I,J)=V(J)
12    CONTINUE
13    CONTINUE
      RETURN
      END
```

VFRK

```fortran
C  ***********************************************
C     FOR SPHERICAL PELLETS
C  ***********************************************
      SUBROUTINE VFRK
$INCLUDE 'COVER VF'
C     RHO NO OF MOLES OF [O] PER CC OF NIO & FE3O4 PRESENT IN ORE
      RHO=0 0374*(1-PP)
      DT=DELT
C     TO TORTUOSITY FACTOR
      TO=1/PP
      FG=1 0
      HN=6720 0
      HF1=-3024 0
      HF2=-66024 0
      HF3=-18522 0
      CN=42840 0
      CF1=33100 0
      CF2=-29900 0
      CF3=17600 0
      DO 50 I=1,IM
      DO 30 J=M,LS
C     GC,GG  NO  OF GM MOLES OF CO & H2 PER CU CM
      GC=1 21875D-5*G(I,J)*FCO/TG(I,J)
      GG=1 21875D-5*GH(I,J)*FH2/TG(I,J)
      DKH=(1 175D-1*TS(I,J)**3 333)/(1-PP)
      DK=(2 977D-2*TS(I,J)**3 333)/(1-PP)
      DH=7 365*TS(I,J)**1 675
      DC=1 2475*TS(I,J)**1 693
      DE=PP/(TO*(1/DK+1/DC))
      DEH=PP/(TO*(1/DKH+1/DH))
      DF1(I,J)=0 000000001
      DF2(I,J)=0 000000001
      DF1H(I,J)=0 00000001
      DF2H(I,J)=0 00000001
      PCO=G(I,J)*FCO
      H2=GH(I,J)*FH2
      PCO2=(1-G(I,J))*FCO
      H2O=(1-GH(I,J))*FH2
      RH=H2O/H2
      RC=PCO2/PCO
      DNS=DEH/DH
      RDE=1 006D-3*EXP(5 197/TS(I,J))
      RDE=1 0
      WKHO=10 0
C     REDUCTION KINETICS FOR IRON OXIDE   (2)
C     HK1,HK2,HK3 KINETIC CONSTANT FOR H2 REDUCTION
C     CK1,CK2,CK3 KINETIC CONSTANT FOR CO REDUCTION
C     WH1,WH2,WH3,WC1,WC2,WC3 EFFECT OF PRODUCT GAS H2O & CO2
C  ***********************************************
      IF(F2(I,J) LE 0 99)THEN
      WH1=10 0
      WH2=4821*EXP(-7 936/TS(I,J))
      WH3=3 684*EXP(-2 226/TS(I,J))
      WC1=10 0
      WC2=100*EXP(-3 583/TS(I,J))
      WC3=0 07564*EXP(2 1087/TS(I,J))
      IF(TS(I,J) LE 0 900)THEN
      HK1=69 228*EXP(-3 17/TS(I,J))
      HK2=15 85*EXP(-2 0774/TS(I,J))
      ELSE

      HK1=58157*EXP(-9 2302/TS(I,J))
      HK2=604825*EXP(-11 572/TS(I,J))
      ENDIF
      HK3=36435*EXP(-9 0786/TS(I,J))
      CK1=22000*EXP(-9 35/TS(I,J))
      CK2=5100*EXP(-8 25/TS(I,J,K))
      CK3=3184*EXP(-7 936/TS(I,J,K))
C  ****** 1ST STEP OF IRON OXIDE REDUCTION FE2O3 -> FE3O4 ********
      IF(F2(I,J) LE 0 111)THEN
      HF(I,J)=HF1+9*F2(I,J)*(HF2-HF1)
      CF(I,J)=CF1+9*F2(I,J)*(CF2-CF1)
      KFO=HK1+9*F2(I,J)*(HK2-HK1)
C  ********* WATER VAPOR CORRECTION ***********************
      S2=RP*(KRGF/DE)**0 5
      SH2=RP*(HKRGF/DEH)**0 5
      ESCF=(1-F2(I,J))**0 333
      SH2M=SH2*ESCF
      H2N=GH(I,J)/(1+RDE*(SH2M/TANH(SH2M)-1)*(1-ESCF+1SCF*DN5))
      RH=(1-H2N)/H2N
C  ********* WATER VAPOR CORRECTION ***********************
      WKHO=1/(1/WH1+9*F2(I,J)*(1/WH2-1/WH1))
      HKRGF=HK1*(1-RH/WH1)+9*F2(I,J)*(HK2*(1-RH/WH2)-HK1*(1-RH/WH1))
      KRGF=CK1*(1-RC/WC1)+9*F2(I,J)*(CK2*(1-RC/WC2)-CK1*(1-RC/WC1))
      IF(HKRGF LE 0 0001)THEN
      HKRGF=0 0001
      ENDIF
      IF(KRGF LE 0 0001)THEN
      KRGF=0 0001
      ENDIF
C  ****** 2ND STEP OF IRON OXIDE REDUCTION FE3O4 -> FEO *********
      ELSEIF((F2(I,J) GE 0 111) AND (F2(I,J) LE 0 333))THEN
      HF(I,J)=HF2+(4 5*F2(I,J)-0 5)*(HF3-HF2)
      CF(I,J)=CF2+(4 5*F2(I,J)-0 5)*(CF3-CF2)
      KFO=HK2+(4 5*F2(I,J)-0 5)*(HK3-HK2)
C  ********* WATER VAPOR CORRECTION ***********************
      S2=RP*(KRGF/DE)**0 5
      SH2=RP*(HKRGF/DEH)**0 5
      ESCF=(1-F2(I,J))**0 333
      SH2M=SH2*ESCF
      H2N=GH(I,J)/(1+RDE*(SH2M/TANH(SH2M)-1)*(1-SCF+I SCF*1DN5))
      RH=(1-H2N)/H2N
C  ********* WATER VAPOR CORRECTION ***********************
      WKHO=1/(1/WH2+(4 5*F2(I,J)-0 5)*(1/WH3 1/WH2))
      HKRGF=HK2*(1-RH/WH2)+(4 5*F2(I,J)-0 5)*(HK3*(1-RH/WH3)
     1                     -HK2*(1-RH/WH2))
      KRGF=CK2*(1-RC/WC2)+(4 5*F2(I,J)-0 5)*(CK3*(1-RC/WC3)
     1                     -CK2*(1-RC/WC2))
      IF(HKRGF LE 0 0001)THEN
      HKRGF=0 0001
      ENDIF
      IF(KRGF LE 0 0001)THEN
      KRGF=0 0001
      ENDIF
C  ****** 3RD STEP OF IRON OXIDE REDUCTION FEO -> FE **********
      ELSEIF(F2(I,J) GE 0 333)THEN
      HF(I,J)=HF3
      CF(I,J)=CF3
      KFO=HK3
C  ********* WATER VAPOR CORRECTION ***********************
      S2=RP*(KRGF/DE)**0 5
      SH2=RP*(HKRGF/DEH)**0 5
      ESCF=(1-F2(I,J))**0 333
      SH2M=SH2*ESCF
      H2N=GH(I,J)/(1+RDE*(SH2M/TANH(SH2M)-1)*(1-FSCF+I SCF*1DN5))
      RH=(1-H2N)/H2N
```

260

VFGH2

```
C     ***************************************************
      WKHO=WH3
      KRGF=CK3*(1-RC/WC3)
      HKRGF=HK3*(1-RH/WH3)
      IF(HKRGF LE 0 0001)THEN
      HKRGF=0 0001
      ENDIF
      IF(KRGF LE 0 0001)THEN
      KRGF=0 0001
      ENDIF
      ENDIF
C     ********** REDUCTION KINETICS BY GRAIN MODEL **************
      S2=RP*(KRGF/DE)**0 5
      SH2=RP*(HKRGF/DEH)**0 5
      P2=(1-F2(I,J))**(1/FG-1)/FG+((S2*S2)/3)*((1-F2(I,J))**(- 333)-1)
      PH2=(1-F2(I,J))**(1/FG-1)/FG+(SH2**2/3)*((1-F2(I,J))**(- 333)-1)
      IF(F2(I,J) GE 0 95)THEN
      DIVF=1+100*(F2(I,J)-0 95)
      DF2(I,J)=((GC*KRGF)/(DIVF*RHO*P2))*DT
      DF2H(I,J)=((GG*HKRGF)/(DIVF*RHO*PH2))*DT
      ELSE
      DF2(I,J)=((GC*KRGF)/(RHO*P2))*DT
      DF2H(I,J)=((GG*HKRGF)/(RHO*PH2))*DT
      ENDIF
      F2(I,J)=F2(I,J)+DF2(I,J)+DF2H(I,J)
      ENDIF
C     ***************************************************
C     REDUCTION KINETICS FOR NICKEL OXIDE (1)
C     ***************************************************
      IF(F1(I,J) LE 0 99) THEN
      KNO=6132*DEXP(-6 898/TS(I,J))
      KNO=9132*DEXP(-6 898/TS(I,J))
      IF(TS(I,J) LT 0 950)THEN
      KRGN=481800*DEXP(-11 2/TS(I,J))
      ELSE
      KRGN=30*DEXP(-2/TS(I,J))
      ENDIF
      IF(HKRGN LE 0 0001)THEN
      HKRGN=0 0001
      ENDIF
C     ********** WATER VAPOR CORRECTION *****************
      S1=RP*(KRGN/DE)**0 5
      SH1=RP*(HKRGN/DEH)**0 5
      ESC=(1-F1(I,J))**0 333
      SH1M=SH1*ESC
      H2N=GH(I,J)/(1+RDE*(SH2*ESC/TANH(SH2*ESC)-1)*(1-ESC+ESC*DNS))
      RH=(1-H2N)/H2N
      PPN=1/((H2**0 5*(1+2 71D-2*DEXP(5 838/TS(I,J))*RH**2))
      HKRGN=KNO*PPN
C     ********** MECHANISM FOR COMPLEX OXIDE REDUCTION *******
      P1=(1-F1(I,J))**(1/FG-1)/FG+(S1*S1/3)*((1-F1(I,J))**(- 333)-1)
      PH1=(1-F1(I,J))**(1/FG-1)/FG+(SH1**2/3)*((1-F1(I,J))**(- 333)-1)
      DF1(I,J)=((GC*KRGN)/(RHO*P1))*DT
      DF1H(I,J)=((GG*HKRGN)/(RHO*PH1))*DT
      IF(F2(I,J) LE 0 333)THEN
      DF1(I,J)=DF1(I,J)*F2(I,J)/0 333
      DF1H(I,J)=DF1H(I,J)*F2(I,J)/0 333
      ENDIF
      F1(I,J)=F1(I,J)+DF1(I,J)+DF1H(I,J)
      ENDIF
C     ***************************************************
30    CONTINUE
50    CONTINUE
      RETURN
      END
```

```
C     ***************************************************
C     GAS CONE OF H2   CENTRAL IN R, BACKWARD IN Z
C     ***************************************************
      SUBROUTINE VFGH2
C     ***************************************************
$INCLUDE 'COVER VF'
C
      DIMENSION A(LG),B(LG),C(LG),D(LG),V(LG)
      DO 1000 KIT=1,2
      DO 100 I=1,IM
      DH=7 365D-4*TG(I,M)**1 675
      DML=DH*P(I)
      TC=SLO**2/DH
      DT=DELT/TC
      AZ=DT/(2*DZ**2)
      AR=DT/(2*DR**2)
      ARI=AR/(2*FLOAT(I))
      ROG=12 1875/TG(I,M)
      RGN=RHM(I)*N1/(ROG*FH2)
      RGF=RHM(I)*N2/(ROG*FH2)
      HNU=VZ(I,LS)*VO*SLO*DT/(2*DZ*DH)
      PER=(VO*SLO*VR(I,M)*DT)/(4*DR*DH)
C     ----LOWER BOUNDARY CONDITION FLUX OR GAS VLLOCI1Y ----
      A(M)=0 0
      C(M)=-AZ
      IF(I LE 1)THEN
      B(M)=1+AR+ARI-PER+AZ+HNU
      D(M)=GH(I,M)*(1-AR-ARI-PER+AZ-IINU)+GH(I,M+1)*AZ+
    1   2*GH(I+1,M)*(AR+ARI-PER)-RGN*DF1H(I,M)-RGF*DI 2H(I,M)+2*HNU*GHI
      ELSEIF(I GE IM)THEN
      B(M)=1+AR+ARI+PER+AZ+HNU
      D(M)=GH(I,M)*(1-AR+ARI-PER-AZ-HNU)+GH(I,M+1)*AZ+
    1   2*GH(I-1,M)*(AR+PER-ARI)-RGN*DF1H(I,M)-RGI *DI 2H(I M)+2*HNU*GHI
      ELSE
      B(M)=1+2*AR+AZ+HNU
      D(M)=GH(I,M)*(1-2*AR-AZ-HNU)+GH(I,M+1)*AZ+
    1   2*GH(I+1,M)*(AR+ARI-PER)+2*GH(I-1,M)*(AR+PER-ARI)
    2   -RGN*DF1H(I,M)-RGF*DF2II(I,M)-2*HNU*GHI
      ENDIF
C     ---- DISCRETIZED BY CRANK NICHOLSON CEN IN R BW IN Z -
      DO 300 J=M+1,LS
      DH=7 365D-4*TG(I,J)**1 675
      DML=DH*P(I)
      TC=SLO**2/DML
      DT=DELT/TC
      AR=DT/(2*DR**2)
      AZ=DT/(2*DZ**2)
      ARI=AR/(2*FLOAT(I))
      PER=(VO*SLO*VR(I,J)*D1)/(4*DR*DML)
      PEZ=(VO*SLO*VZ(I,J)*D1)/(2*DZ*DML)
      A(J)=-PEZ-AZ
      C(J)=-AZ
      IF(I LE 1)THEN
      B(J)=1+PEZ+AR+ARI-PER+2*AZ
      D(J)=GH(I,J)*(1-PEZ-AR-ARI+PER-2*AZ)+2*GH(I+1,J)*(AR+ ARI-PER)+
    1   GH(I,J-1)*(PEZ+AZ)+GH(I,J+1)*AZ-RGN*DF1H(I,J) RGF*DF2H(I,J)
      ELSEIF(I GE IM)THEN
      B(J)=1+PEZ+AR-ARI+PER+2*AZ
      D(J)=GH(I,J)*(1-PEZ-AR+ARI-PER-2*AZ)+2*GH(I-1,J)*(AR+PER-ARI)+
    1   GH(I,J-1)*(PEZ+AZ)+GH(I,J+1)*AZ-RGN*DF1H(I,J)-RGF*DF2H(I,J)
      ELSE
      B(J)=1+PEZ+2*AR+2*AZ
```

```
      D(J)=GH(I,J)*(1-PEZ-2*AR-2*AZ)+2*GH(I+1,J)*(AR+ARI-PER)+
     1 2*GH(I-1,J)*(AR+PER-ARI)+GH(I,J-1)*(PEZ+AZ)+GH(I,J+1)*AZ
     2 -RGN*DF1H(I,J)-RGF*DF2H(I,J)
      ENDIF
  300 CONTINUE
C         --------OUTLET BOUNDARY CONDITION--------
      A(LS)=-PEZ-AZ
      C(LS)=0 0
      IF(I LE 1)THEN
      B(LS)=1+PEZ+AR+ARI-PER+AZ
      D(LS)=GH(I,LS)*(1-PEZ-AR-ARI+PER-AZ)+2*GH(I+1,LS)*(AR+ARI-PER)+
     1 GH(I,LS-1)*(AZ+PEZ)-RGN*DF1H(I,J)-RGF*DF2H(I,J)
      ELSEIF(I GE IM)THEN
      B(LS)=1+PEZ+AR-ARI+PER+AZ
      D(LS)=GH(I,LS)*(1-PEZ-AR+ARI-PER-AZ)+2*GH(I-1,LS)*(AR+PER-ARI)+
     1 GH(I,LS-1)*(AZ+PEZ)-RGN*DF1H(I,J)-RGF*DF2H(I,J)
      ELSE
      B(LS)=1+PEZ+2*AR+AZ
      D(LS)=GH(I,LS)*(1-PEZ-2*AR-AZ)+2*GH(I+1,LS)*(AR+ARI-PER)+
     1 GH(I,LS-1)*(AZ+PEZ)+2*GH(I-1,LS)*(PER+AR-ARI)+
     2 -RGN*DF1H(I,J)-RGF*DF2H(I,J)
      ENDIF
C
      CALL TRIDAG(A,B,C,D,V,M,LS)
      DO 42 J=M,LS
      GH(I,J)=V(J)
      IF(GH(I,J) LE 0 015)THEN
      GH(I,J)=0 015
      ENDIF
   42 CONTINUE
  100 CONTINUE
C1000 CONTINUE
      RETURN
      END

C ***************************************************************
C  CALCULATION OF VOLUME AVERAGE VALUES AT DIFFERENT POSITIONS
C ***************************************************************
      SUBROUTINE VFAv
C ***************************************************************
$INCLUDE 'COVER VF'
      ZP(1)=0 0
      F1A=0 0
      F2A=0 0
      GHA=0 0
      TSA=0 0
      TGA=0 0
      DO 10 K=1,NV
      AVZ=0 0
      AGH(K)=0 0
      AG(K)=0 0
      AF1(K)=0 0
      AF2(K)=0 0
      ATS(K)=0 0
      ATG(K)=0 0
      NZ1=M+(NS/NV)*(K-1)
      NZ2=M+(NS/NV)*K
      NZD=NZ2-NZ1+1
      ZP(K)=100*(FLOAT(K)-0 5)*(NZD-1)*DZ
      DO 11 I=1,IM
      AVZ=AVZ+(2*I-1)*VZ(I,LS)
      DO 11 J=NZ1,NZ2
      AGH(K)=AGH(K)+(2*I-1)*GH(I,J)
      AG(K)=AG(K)+(2*I-1)*G(I,J)
      AF1(K)=AF1(K)+(2*I-1)*F1(I,J)
      AF2(K)=AF2(K)+(2*I-1)*F2(I,J)
      ATS(K)=ATS(K)+(2*I-1)*TS(I,J)
      ATG(K)=ATG(K)+(2*I-1)*TG(I,J)
   11 CONTINUE
      AGH(K)=AGH(K)/(IM**2*NZD)
      AG(K)=AG(K)/(IM**2*NZD)
      AF1(K)=AF1(K)/(IM**2*NZD)
      AF2(K)=AF2(K)/(IM**2*NZD)
      ATS(K)=ATS(K)/(IM**2*NZD)
      ATG(K)=ATG(K)/(IM**2*NZD)
      F1A=F1A+AF1(K)
      F2A=F2A+AF2(K)
      GHA=GHA+AGH(K)
      GA=GHA+AG(K)
      TSA=TSA+ATS(K)
      TGA=TGA+ATG(K)
      ENDDO
   10 F1A=F1A/FLOAT(NV)
      F2A=F2A/FLOAT(NV)
      GHA=GHA/NV
      TSA=TSA/NV
      TGA=TGA/NV
      AVZ=AVZ/IM**2
      RETURN
      END
```

HFMain

C.4.4   Program for Horizontal Gas Flow condition

The subroutine for reaction kinetics HFRK is same as VFRK, so HFRK is not given here

COM.HF

```
f77 +O3 HFMain f TRIDAG f HFVelo f HFTs f HFTg f HFRK f HFAv f HFGH2 f
f77 +O3 HFMain o TRIDAG o HFVelo o HFTs o HFTg o HFRK o HFAv o HFGH2 o
f77 +O3 HFMain o TRIDAG o HFVelo o HFTs o HFTg o HFRK o HFAv o HFGH2 o -o run
run
```

HFPUT

```
0 915,0 915,15 0,0 25,96,0 5
1 04,1 04,15 0,0 25,146,0 25
(TIG TIS MANOR RP ITER DELT=HFPUT)
```

COVER.HF

```
      IMPLICIT REAL*8(A-H,O-Z)
      PARAMETER(NP=50,NS=36,NG=12,IM=20,NH=6)
      PARAMETER(NP=100,NS=72,NG=24,IM=40,NH=6)
      COMMON/A1/DELT,DX,DY,HT,N1,N2,VGO,FP,S1,S2,SH1,SH2,GI,GHI
      COMMON/A2/RP,RG,FCO,FH2,FAG,VAX,PP,P(NP),H2O,CO2,SBR,HTS
      COMMON/A3/KRGN,KRGF,HKRGN,HKRGF,DK,DKH,DE,DEH,VF(NP),TFR
      COMMON/A4/FXC1(IM),FXC2(IM),FXH1(IM),FXH2(IM),S(IM,NP)
      COMMON/A5/TIS(IM,NP),TG(IM,NP),G(IM,NP),GH(IM,NP)
      COMMON/A6/DF1(IM,NP),DF2(IM,NP),DF1II(IM,NP),DF2H(IM,NP)
      COMMON/A7/F1(IM,NP),F2(IM,NP),RD(9),WF(9),Y(NP),X(IM)
      COMMON/A8/VX(IM,NP),VY(IM,NP),HF(IM,NP),CF(IM,NP)
      COMMON/A9/TM,M,LS,LG,SK,AKB,AKG,SLO,VO,RHM(NP),TIG,TIS
      COMMON/A10/AGH(NII),AF1(NII),AF2(NII),ATS(NII),ATG(NII),YP(NII)
      COMMON/A11/F1A,F2A,GHA,TSA,TGA,FLXTS,FLXTG
      COMMON/A12/TSEC,WKHO,WKCO,KFO,KNO
      REAL N1,N2,KRGN,KRGF,KFO,KNO
```

C

C   ***
C   MODEL FOR NON-ISOTHERMAL GAS-SOLID REDUCTION IN A FIXED
C   BED REACTOR UNDER HORIZONTAL GAS FLOW CONDITION USING
C   GRAIN MODEL, BY H2/H2O//CO/CO2//N2 GAS MIXTURE
C   ***
C   HFMain F   NON-DIMENSIONAL CRANCK-NICHOLSON SCHEME FOR
C   AXI-SYMMETRIC MODEL
C   ***
C   SUBROUTINE DESCRIPTION -
C   TRIDAG   TRI-DIAGONAL MATRIX SOLVER
C   HFVelo   GAS VELOCITY PROFILE OVER THE REDUCING PELLET BED
C   HFTg   GAS PHASE ENERGY BALANCE
C   HFTs   SOLID PHASE ENERGY BALANCE
C   HFRK   REDUCTION KINETICS FOR SPHERICAL PELLETS
C   HFFCO   GAS PHASE SPECIES(MASS) BALANCE FOR CO
C   HFGH2   GAS PHASE SPECIES(MASS) BALANCE FOR H2
C   ***
C   FOR A FIXED BED OF ORE HAVING BED HEIGHT OF 7 ¿ CM ,REDUCED BY
C   CO GAS, POROSITY P= 72,S1 UNITS,MOLE
C   TS,TG=TEMP OF SOLID & GAS,F1,F2=FRACTION OF NIO & FE2O3 REDUCED
C   G,GH=DIMENSIONLESS GAS CONE OF CO AND H2
C   DF1,DF2=INCREMENT IN FRACTION REDUCTION OF NIO & FL2O3 BY (O
C   DF1H,DF2H=INCREMENT IN FRACTION REDUCTION OF NIO & FE2O3 BY H2
C   FP,FG=>STRUCTURE FACTOR FOR PELLETS & GRAINS=1,2,3
C   PARAMETERS CPG,ROG,VGO,RP,H,NG,FP,FG,H1,FCO,FAG,CO,H2,1S1,1G1
C   ***
C
$INCLUDE 'COVER HF'
C   ***
C
      OPEN(UNIT=71,FILE='HFPUT')
      OPEN(UNIT=73,FILE='H1 OUT')
      OPEN(UNIT=74,FILE='H2 OUT')
      OPEN(UNIT=75,FILE='H3 OUT')
      OPEN(UNIT=76,FILE='VGXY')
      OPEN(UNIT=77,FILE='TGH CNT')
      OPEN(UNIT=78,FILE='TTS CNT')
      OPEN(UNIT=79,FILE='RK')
      OPEN(UNIT=80,FILE='VXYS')
      OPEN(UNIT=81,FILE='AVHF')
C   ***
C
      NBED=1
C
      NS,NG=>NO OF GRID POINTS OF SOLID & GAS
C   ***********STANDARD VALUES FOR NONDIMENSIONALIZING************
      VO=0 1
      SLO=0 1
C   ***
C
      M=1
      LS=M+NS
      LG=M+NS+NG
      WKHO=10 0
      WKCO=10 0
      DO 300 JV=1,1
      TM=0 0
C
      FAG=>FRACTION OF ADDITIONAL GAS ADDED BETWEEN HEARTHS
      FAG=0 1
C
      H=>OTHER DIMENSION OF CYLINDRICAL OR PLATE PELLET
      TIS,TIG=>INITIAL TEMP OF SOLID & GAS
      READ(71,*)TIG,TIS,HD,RP,ITER,DELT
      IF(TIS LE 0 900)THEN
      HKRGF=69 228*EXP(-3 17/TIS)
      ELSE
      HKRGF=58187*EXP(-9 2302/TIS)
      ENDIF
      KRGF=708*EXP(-8 25/TIS)
      HKRGN=6132*EXP(-6 898/TIS)
```

```fortran
      IF(TIS LE 960) THEN
      KRGN=48180*EXP(-11 2/TIS)
      ELSE
      KRGN=3*DEXP(-2/TIS)
      ENDIF
C     ****** HD  MANOMETER HEIGHT DIFFERENCE, FR  FLOW RATE CC/S******
      FR=-0 6223+4 66*HD-0 101*HD**2+1 539E-3*HD**3
      FR=0 9818+2 907*HD-0 02198*IID**2
C     T,DELT TIME & TIME INCREMENT
      T=1
C     DX X-DIRECTION INCREMENT
C     DY Y-DIRECTION INCREMENT
      DX=0 03
      DY=0 02
C     ***************************************************
C     VGOI,VGO GAS VELOCITY AT TG(1)(0 006 TO 0 2 M/S)
      VGOI=0 00001
      VGO=0 00001
      RG=6 7D-7
      FP=3 0
C     VF VOID FRACTN OF BED, PP PELLET POROSITY
C     P TOTAL POROSITY, E SOLID FRACTION
      PP=0 5645
      DO J=M,LS
      VF(J)=0 36
      P(J)=(1-VF(J))*PP+VF(J)
      RHM(J)=3797*(1-P(J))
      ENDDO
C     RS DENSITY OF SOLID 3714 KG/CU M
C     RHM ORE BED DENSITY IN MOLE/CU M
C     RP RADIUS OF PELLET(0 1 TO 0 2 CM)
C     RG RADIUS OF GRAINS IN PELLET(6 E-5 TO 1E-3 CM)
C     N1,N2 NO  OF MOLES OF [O] IN NIO & FE3O4 PER MOLE OF ORE
      N1=0 01597
      N2=1 004
C     FCO & FH2 FRACTION OF REDUCING GAS CO & H2, IN THE GAS
C     GHI,GI INITIAL H2 & CO PURITY (H2 H2O & CO CO2)
      FCO=0 000001
      FH2=0 999
      GHI=1 0
      GI=1 0
      FHK=0 667*FH2
      SK=0 67*TIS**0 6
C     ********CONDUCTIVITY OF GAS AND SOLID AKG  GEIGER P********
      AKG=(0 955*EXP(-544/TIG)*FHK+0 469*EXP(-869/TIG)*(1-FHK))/
     1 (1 28*FHk+(1-FHK)**2 02)
      AKB=(1-VF(20))*SK+VF(20)*AKG
C     ***************************************************
      N=NBED*NS+(NBED-1)*NG+1
      VAX=0 25
      VAX=FR*TIG/49 0
      VO=2 13*RP**2*VF(20)**3*VAX/(1-VF(20))**2
      M=1+(IJK-1)*(NS+NG)
      LS=M+NS
      LG=M+NS+NG
      DO 20 I=1,IM
      DO 30 J=M,LG
      Y(J)=DY*FLOAT(J-1)*100 0
      X(I)=DX*FLOAT(I-1)*100 0
      TG(I,J)=TIG
      TS(I,J)=TIS
      F1(I,J)=0 00
      F2(I,J)=0 00
      DF1(I,J)=0 000000
      DF1H(I,J)=0 00000
      DF2(I,J)=0 000000
      G(I,J)=G1
      GH(I,J)=GHI
      VX(I,J)=0 0
      VY(I,J)=0 0
   30 CONTINUE
      DO 40 J=1,LS,LG
      VX(I,J)=VAX
   40 CONTINUE
   20 CONTINUE
   10 CONTINUE
C     **** MOLECULAR GAS DIFFUSIVITY & HT TR SH F 0 9  MKS UNITS ****
      DH=7 365D-4*TIG**1 675
      DC=1 2475D-4*TIG**1 693
C     HT GAS SOLID HEAT TRANSFER COEFF  AT TEMP TG(1)
      HTS=(3159*VAX**0 9*TIG**0 3)/RP**0 75
      HT=HTS
      WRITE(73,65)VGOI,IIT,RP,RG,DY,FP,TIS
   65 FORMAT(128('-')/2X,'VGOI=',F8 6,2X,'IIT=',F7 1,2X,'RP=',F6 4,2X,
     1 'RG=',E9 2,2X,'DY=',F6 4,2X,'FP=',F4 1,2X,'TS=',16 3/128('-')/2X
     2 'TIME',3X,'TG9',4X,'TS9',4X,'TG15',3X,'TS15',4X,'TG21',3X,
     3 'TS21',3X,'TG27',3X,'TS27',3X,'TG33',3X,'TS33',3X,'DT1'/',3X,
     4 'DF1H1',3X,'DF2/1',3X,'DF2H1'/128('-'))
      WRITE(74,77)VGOI,RP,RG,FCO,FH2,FP,TIS
   77 FORMAT(128('-')/1X,'PARAMETERS',2X,'VGOI=',18 6,2X,'RP=',
     1 F6 4,2X,'RG=',E8 2,2X,'FCO=',F5 3,2X,'FH2=',F6 4,2X,'FP=',F4 1,
     2 2X,'TS=',F6 3/128('-')/2X,'TIME',3X,'F1'/3',2X,'F 1/9',
     3 2X,'F1/15',2X,'F1/21',2X,'F2/27',4X,'F2/3',3X,'F2/9',2X,'F2/15',
     4 2X,'F2/21',2X,'F2/27',4X,'G15',4X,'GH3',3X,'GH9',4X,'GH15',3X,
     5 'GH15',3X,'GH27'/128('-'))
      DO 600 JK=1,NBED
      M=1+(JK-1)*(NS+NG)
      LS=M+NS
      LG=M+NS+NG
      CALL HFVelo
      PRINT *,'VX=',VX(10,LS+9)
  600 ENDDO
      DO 32 J=LS,LG
      WRITE(76,67)(VX(I,J),I=1,IM)
   67 FORMAT(20(F6 3))
   32 CONTINUE
      WRITE(76,46)
   46 FORMAT(128('-'))
      DO 34 J=LS,LG
      WRITE(76,68)(VY(I,J),I=1,IM)
   68 FORMAT(20(F6 3))
   34 CONTINUE
      WRITE(76,47)
   47 FORMAT(128('-'))
      DO 35 I=1,IM
      WRITE(80,28)X(I),Y(J),VX(I,J),VY(I,J)
   28 FORMAT(2(1X,F6 2),2(3X,F8 4))
   35 ENDDO
      PRINT *,'HTS,HT',HTS,IIT
      TSEC=0 0
      DO 200 KKK=1,ITER
      IF(KKK LE 5) THEN
      DELT=0 1*DLTS*FLOAT(KKK)
      ELSE
      DELT=DLTS
      ENDIF
      TSEC=TSEC+DELT
      PRINT *,'DT=',DELT
      WRITE(73,5)TM,TG(10,9),TS(10,9),TG(10,15),TS(10,15),IG(10,21),
     1 TS(10,21),TG(10,27),TS(10,27),TG(10,33),TS(10,33),
     2 DF1(10,NS),DF1H(10,NS),DF2(10,NS),DF2H(10,N5)
    5 FORMAT(F6 2,10(F7 4),4(E8 2))
```

// DF2H(i,j) = 0.0000 ↑

```fortran
      WRITE(74,7)TM,F1(10,9),F1(10,15),F1(10,21),F1(10,27),F1(10,33),
     1 F2(10,9),F2(10,15),F2(10,21),F2(10,27),F2(10,33),G(10,21),
     2 GH(10,9),GH(10,15),GH(10,21),GH(10,27),GH(10,33)
    7 FORMAT(F6 2,16(F7 4))
      DO 100 KK=1,120
      VGO=VGOI
      DO 400 IJK=1,NBED
      M=1+(IJK-1)*(NS+NG)
      LS=M+NS
      LG=M+NS+NG
      CALL HFTs
      CALL HFTg
      IF(TS(9,M+2) GT 0.623) THEN
      CALL HFRK
    C CALL HFGCO
      CALL HFGH2
      ENDIF
  400 CONTINUE
      TM=TM+DELT/60 0
  100 CONTINUE
      PRINT *, 'TM-TG TS GH DF1H DF2H ',TM,TG(9,16),TS(9,15),
     1 GH(9,LS),DF1H(9,LS),DF2H(9,LS)
      DO I=1,IM
      DO J=M,LG
      STBL=GH(I,J)-GHI
      IF(STBL GE 0 15)GO TO 555
      ENDDO
      ENDDO
      CALL HFAv
    C ************ FORMATTING ****************************
   61 FORMAT(99('-')/2X,'TS=',F6 3,2X,'TM=',F7 3,2X,'F1A=',F6 4,2X,
     1 'F2A=',F6 4,2X,'GHA=',F6 4,2X,'TSA=',F6 4,2X,'TGA=',F6 4/99('-')
     2 /6X'YP',7X,'AF1',6X,'AF2',6X,'AGH',6X,'ATS',6X,'ATG'/99('-'))
   71 FORMAT(F9 2,F9 4,F9 4,F9 4,F9 4,F9 4)
   88 FORMAT(128('-')/4X,'TIME=',F7 3,3X,'DELT=',F5 3,3X,'VGO=',F5 3
     1 ,3X,'RP=',F6 4,3X,'FH2=',F6 3,3X,'S1=',F6 3,3X,'S2=',F6 3,3X,
     2 'FP=',F4 1,2X,'TS=',F6 3/128('-')/5X,'Y',6X,'TG',6X,'TS',6X,
     3 'F1',6X,'F2',6X,'DF1H',5X,'DF2',6X,'DF2H',8X,'G',7X,
     4 'GH'/128('-'))
    8 FORMAT(F8 2,F8 4,F8 4,F8 5,F8 5,E9 2,E9 2,E9 2,F9 5,F9 5)
    C ************ FORMATTING ****************************
      IF((TM GE 9 9) AND (TM LE 10 3))THEN
      WRITE(81,61)TIS,TM,F1A,F2A,GHA,TSA,TGA
      WRITE(81,71)(YP(L),AF1(L),AF2(L),AGH(L),ATS(L),ATG(L),L=1,NH)
      WRITE(75,88)TM,DELT,VGO,RP,FH2,S1,S2,FP,TIS
      WRITE(75,8)(Y(J),TG(10,J),TS(10,J),F1(10,J),F2(10,J),DF1(10,J),
     1 DF1H(10,J),DF2(10,J),DF2H(10,J),G(10,J),GH(10,J),J=1,NS+NG)
      ELSEIF(TM GE 14 9) AND (TM LE 15 3))THEN
      WRITE(81,61)TIS,TM,F1A,F2A,GHA,TSA,TGA
      WRITE(81,71)(YP(L),AF1(L),AF2(L),AGH(L),ATS(L),ATG(L),L=1,NH)
      WRITE(75,88)TM,DELT,VGO,RP,FH2,S1,S2,FP,TIS
      WRITE(75,8)(Y(J),TG(10,J),TS(10,J),F1(10,J),F2(10,J),DF1(10,J),
     1 DF1H(10,J),DF2(10,J),DF2H(10,J),G(10,J),GH(10,J),J=1,NS+NG)
      ELSEIF((TM GE 19 9) AND (TM LE 20 3))THEN
      WRITE(77,51)TM,TIG
   51 FORMAT(45('-'),X,'TIME=',F5 1,3X,'*TG*=',F6 3,X,45('-'))
      DO J=M,LG
      WRITE(77,52)(TG(I,J),I=1,IM)
   52 FORMAT(20(F6 3))
      ENDDO
      WRITE(77,53)TM,TIG
   53 FORMAT(45('-'),X,'TIME=',F5 1,3X,'*GH*',3X,'TG*=',F6 3,X,45('-'))
      DO J=M,LG
      WRITE(77,54)(GH(I,J),I=1,IM)
   54 FORMAT(20(F6 3))

      ENDDO
      WRITE(78,55)TM,TIS
   55 FORMAT(45('-'),X,'TIME=',F5 1,3X,'*F1*',3X,'TG=',F6 3,X,45('-'))
      DO J=M,LS
      WRITE(78,56)(F1(I,J),I=1,IM)
   56 FORMAT(20(F6 3))
      ENDDO
      WRITE(78,57)TM,TIS
   57 FORMAT(45('-'),X,'TIME=',F5 1,3X,'*F2*',3X,'TS=',F6 3,X,45('-'))
      DO J=M,LS
      WRITE(78,58)(F2(I,J),I=1,IM)
   58 FORMAT(20(F6 3))
      ENDDO
      WRITE(78,59)TM,TIS
   59 FORMAT(45('-'),X,'TIME=',F5 1,3X,'*TS*=',F6 3,X,45('-'))
      DO J=M,LS
      WRITE(78,60)(TS(I,J),I=1,IM)
   60 FORMAT(20(F6 3))
      ENDDO
      WRITE(81,61)TIS,TM,F1A,F2A,GHA,TSA,TGA
      WRITE(81,71)(YP(L),AF1(L),AF2(L),AGH(L),ATS(L),ATG(L),L=1,NH)
      WRITE(75,88)TM,DELT,VGO,RP,FH2,S1,S2,FP,TIS
      WRITE(75,8)(Y(J),TG(10,J),TS(10,J),F1(10,J),F2(10,J),DF1(10,J),
      DF1H(10,J),DF2(10,J),DF2H(10,J),G(10,J),GH(10,J),J=1,NS+NG)
      ELSEIF((TM LE 24 9) AND (TM LE 25 3))THEN
      WRITE(81,61)TIS,TM,F1A,F2A,GHA,TSA,TGA
      WRITE(81,71)(YP(L),AF1(L),AF2(L),AGH(L),ATS(L),A1G(I 1),L=1,NH)
      WRITE(75,88)TM,DELT,VGO,RP,FH2,S1,S2,FP,TIS
      WRITE(75,8)(Y(J),TG(10,J),TS(10,J),F1(10,J),F2(10,J),DF1(10,J),
      DF1H(10,J),DF2(10,J),DF2H(10,J),G(10,J),GH(10,J),J=1,NS+NG)
      ELSEIF((TM GE 34 9) AND (TM LE 35 3))THEN
      WRITE(81,61)TIS,TM,F1A,F2A,GHA,TSA,TGA
      WRITE(81,71)(YP(L),AF1(L),AF2(L),AGH(L),ATS(L),A1G(L),L=1,NH)
      WRITE(75,88)TM,DELT,VGO,RP,FH2,S1,S2,FP,TIS
      DF1H(10,J),DF2(10,J),DF2H(10,J),G(10,J),GH(10,J),J=1,NS+NG)
      ELSEIF((TM GE 29 9) AND (TM LE 30 3))THEN
      WRITE(81,61)TIS,TM,F1A,F2A,GHA,TSA,TGA
      WRITE(81,71)(YP(L),AF1(L),AF2(L),AGH(L),ATS(L),A1G(L),L=1,NH)
      WRITE(75,88)TM,DELT,VGO,RP,FH2,S1,S2,FP,TIS
      WRITE(75,8)(Y(J),TG(10,J),TS(10,J),F1(10,J),F2(10,J),DF1(10,J),
      DF1H(10,J),DF2(10,J),DF2H(10,J),G(10,J),GH(10,J),J=1,NS+NG)
      ELSEIF((TM GE 44 9) AND (TM LE 45 3))THEN
      WRITE(81,61)TIS,TM,F1A,F2A,GHA,TSA,TGA
      WRITE(81,71)(YP(L),AF1(L),AF2(L),AGH(L),ATS(L),A1G(L),I -1,NH)
      WRITE(75,88)TM,DELT,VGO,RP,FH2,S1,S2,FP,TIS
      DF1H(10,J),DF2H(10,J),G(10,J),GH(10,J),J=1,NS+NG)
      ENDIF
  200 CONTINUE
  555 WRITE(75,88)TM,DELT,VGO,RP,FH2,S1,S2,FP,TIS
      WRITE(75,8)(Y(J),TG(10,J),TS(10,J),F1(10,J),F2(10,J),DF1(10,J),
      DF1H(10,J),DF2(10,J),DF2H(10,J),G(10,J),GH(10,J),J=1,NS+NG)
      WRITE(81,61)TIS,TM,F1A,F2A,GHA,TSA,TGA
      WRITE(81,71)(YP(L),AF1(L),AGH(L),ATS(L),A1G(L),L=1,NH)
      WRITE(73,33)SBR,S1,S2,KRGN,KRGF,DK,DC,DE,H I',RP
   33 FORMAT(128('-')/2X,'SBR=',F4 0,3X,'S1=',F5 3,2X,'S2=',F5 3,
     1 3X,'KRGN=',F6 3,2X,'KRGF=',F6 3,3X,'DK=',E8 2,2X,'DC =',E8 2,
     2 2X,'DE=',E8 2,3X,'HTS=',F7 1,3X,'RP=',F8 2/128(' '))
      WRITE(74,22)SH1,SH2,HKRGN,HKRGF,DKH,DEH,DH
   22 FORMAT(128('-')/2X,'SH1=',F5 3,2X,'SH2=',F5 3,3X,'HKRGN=',F6 3,
     1 2X,'HKRGF=',F6 3,3X,'DKH=',E8 2,2X,'DEH=',E8 2,2X,'DH=',
     2 E8 2/128('-'))
  300 CONTINUE
      STOP
      END
```

```fortran
C **************************************************
C STREAM FUNCTION VORTICITY FORMULATION FOR HORIZONTAL
C GAS FLOW OVER THE BED IN X-Y COORDINATE   STEADY STATE
C BACKWARD IN X  FIRST ORDER UPWINDING IN Y
C **************************************************
C
      SUBROUTINE HFVelo
C **************************************************
$INCLUDE 'COVER HF'
      DIMENSION A(LG),B(LG),C(LG),D(LG),V(LG),DI(LG),VLX(IM,LG)
      DIMENSION VLY(IM,LG),W(IM,LG)
      VKH=8 228D-4*TIG**1 656
      VKW=1 702D-4*TIG**2 049
      VKN=1 168D-4*TIG**1 611
      VK=0 9*VKH+0 09*VKW+0 01*VKN
      WFV=0 5
      REN=(VO*SLO)/VK
      AX=1/DX**2
      AY=1/DY**2
C ------- STREAM FUNCTION INITIALIZATION -------
      DO 11 I=1,IM
      DO 12 J=LS,LG
      W(I,J)=0 0
      S(I,J)=FLOAT(J-LS)*DY*VAX
12    ENDDO
11    ENDDO
      DO 1000 KT=1,250
      DO 13 I=1,IM
      DO 14 J=LS,LG
      VLX(I,J)=VX(I,J)
      VLY(I,J)=VY(I,J)
14    ENDDO
      VLX(I,LS)=0 0
      VLX(I,LG)=0 0
13    ENDDO
C ----- STREAM FUNCTION OF INTERIOR POINTS  CENTRAL DIFF ---
      DO 200 J=LS+1,LG-1
      DO 77 I=2,IM-1
      S(I,J)=(AX*(S(I-1,J)+S(I+1,J))+AY*(S(I,J-1)+S(I,J+1))-W(I,J))/
     (2*AX+2*AY)
77    CONTINUE
      S(IM,J)=2*S(IM-1,J)-S(IM-2,J)
200   ENDDO
C ------- VELOCITY CALCULATION -------
      DO 87 I=2,IM
      DO 210 J=LS+1,LG-1
      IF(I GE IM)THEN
      VLY(I,J)=(S(I-1,J)-S(I,J))/DX
      ELSE
      VLY(I,J)=(S(I-1,J)-S(I+1,J))/(2*DX)
      ENDIF
      VLX(I,J)=(S(I,J+1)-S(I,J-1))/(2*DY)
210   CONTINUE
87    CONTINUE
C ------ 1/X-DIRECTION SWEEP FOR VORTICITY TRANSPORT ------
      DO 97 I=2,IM
      A(LS)=0 0
      B(LS)=1 0
      C(LS)=0 0
      D(LS)=2*AY*(S(I,LS+1)-S(I,LS))
C
      DO 300 J=LS+1,LG-1
      PEX=VLX(I,J)*REN/DX
      PEY=VLY(I,J)*REN/DY
      IF(VLY(I,J) GE 0 0)THEN
      NY=0
      NY=1
      ENDIF
      A(J)=(NY-1)*PEY-AY
      C(J)=NY*PEY-AY
      IF(I GE IM)THEN
      B(J)=AX+2*AY+PEX+(-1)**NY*PEY
      D(J)=W(I-1,J)*(PEX+AX)
      ELSE
      B(J)=2*(AX+AY)+PEX+(-1)**NY*PEY
      D(J)=W(I-1,J)*(PEX+AX)+W(I+1,J)*AX
      ENDIF
300   ENDDO
C
      A(LG)=0 0
      B(LG)=1 0
      C(LG)=0 0
      D(LG)=2*AY*(S(I,LG-1)-S(I,LG))
      CALL TRIDAG(A,B,C,D,V,LS,LG)
      DO 20 J=LS,LG
      W(I,J)=V(J)
      VLX(I,J)=WFV*VLX(I,J)+(1-WFV)*VX(I,J)
      VLY(I,J)=WFV*VLY(I,J)+(1-WFV)*VY(I,J)
20    CONTINUE
97    CONTINUE
C ------- INLET VORTICITY -------
      DO 88 J=LS+1,LG-1
      A(1)=0 0
      B(1)=1 0
      C(1)=0 0
      D(1)=(VLX(1,J+1)-VLX(1,J-1))/(2*DY)
C ------- X-DIRECTION MARCHING -------
      DO 500 I=2,IM
      PEX=VLX(1,J)*REN/DX
      PEY=VLY(1,J)*REN/DY
      IF(VLY(1,J) GE 0 0)THEN
      NY=0
      ELSE
      NY=1
      ENDIF
      A(1)=-AX-PEX
      B(1)=2*AX+2*AY+PEX+(-1)**NY*PEY
      C(1)=-AX
      D(1)=W(1,J-1)*(AY-(NY-1)*PEY)+W(1,J+1)*(AY-NY*PI Y)
500   CONTINUE
C ------- OUT FLOW CONDITION ---
      A(IM)=0 0
      B(IM)=1 0
      C(IM)=0 0
      D(IM)=W(IM-1,J)
      CALL TRIDAG(A,B,C,D,V,1,IM)
      DO 40 I=1,IM
      W(I,J)=V(I)
40    CONTINUE
88    CONTINUE
      DO 23 I=1,IM
      DO 24 J=LS,LG
      VX(I,J)=WFV*VLX(I,J)+(1-WFV)*VX(I,J)
      VY(I,J)=WFV*VLY(I,J)+(1-WFV)*VY(I,J)
24    ENDDO
23    ENDDO
1000  CONTINUE
      PRINT *,'S---VX---W',S(9,LS+5),VLX(9,LS+5),W(9,LS+5)
      DO J=LS,LG
      VY(1,J)=0 0
      ENDDO
      RETURN
      END
```

```fortran
C  *********************************************************
   SUBROUTINE HFTs
C  *********************************************************
$INCLUDE 'COVER HF'
   DIMENSION A(LG),B(LG),C(LG),D(LG),V(LG)
   CS=88+2.44*TIS
   CN=42840.0
   HN=6720.0
   R1=N1*CN/(1000*CS)
   RH1=N1*HN/(1000*CS)
   DO 13 I=1,IM
C        ----LOWER BOUNDARY CONDITION/KNOWN TEMPERATURE----
   TC=(SLO**2*RHM(M)*CS)/AKB
   DT=DELT/TC
   SNU=(HT*SLO**2*DT)/(2*AKB)
   AX=DT/(2*DX*DX)
   AY=DT/(2*DY*DY)
   A(M)=0.0
   C(M)=-AY
   IF(I.LE.1)THEN
   B(M)=1+AX+AY+SNU
   D(M)=(1-AX-AY-SNU)*TS(I,M)+TS(I,M+1)*AY+2*AX*TS(I+1,M)+2*SNU*TIS
   ELSEIF(I.GE.IM)THEN
   B(M)=1+AX+AY+SNU
   D(M)=(1-AX-AY-SNU)*TS(I,M)+TS(I,M+1)*AY+2*AX*TS(I-1,M)+2*SNU*TIS
   ELSE
   B(M)=1+2*AX+AY+SNU
   D(M)=(1-2*AX-AY-SNU)*SNU+2*AX*(TS(I-1,M)+TS(I+1,M))
 2 2*TG(I,M)*SNU+2*AX*(TS(I-1,M)+TS(I+1,M))
   ENDIF
C           ----CRANK NICHOLSON/CENTRAL IN SPACE----
   DO 11 J=M+1,LS-1
   TC=(SLO**2*RHM(J)*CS)/AKB
   DT=DELT/TC
   SNU=(HT*SLO**2*DT)/(2*AKB)
   AX=DT/(2*DX*DX)
   AY=DT/(2*DY*DY)
   R2=N2*CF(I,J)/(1000*CS)
   RH2=N2*HF(I,J)/(1000*CS)
   A(J)=-AY
   C(J)=-AY
   IF(I.LE.1)THEN
   B(J)=1+AX+2*AY+SNU
   D(J)=(1-AX-2*AY-SNU)*TS(I,J)+TS(I,J+1)*AY+TS(I,J-1)*AY+
 1 2*AX*TS(I+1,J)+2*SNU*TIS+R1*DF1(I,J)+R2*DF2(I,J)
 2 +RH1*DF1H(I,J)+RH2*DF2H(I,J)
   ELSEIF(I.GE.IM)THEN
   B(J)=1+AX+2*AY+SNU
   D(J)=(1-AX-2*AY-SNU)*TS(I,J)+TS(I,J+1)*AY+TS(I,J-1)*AY+
 1 2*AX*TS(I-1,J)+2*SNU*TIS+R1*DF1(I,J)+R2*DF2(I,J)
 2 +RH1*DF1H(I,J)+RH2*DF2H(I,J)
   ELSE
   B(J)=1+2*AX+2*AY+SNU
   D(J)=(1-2*AX-2*AY-SNU)*TS(I,J)+TS(I,J+1)*AY+TS(I,J-1)*AY+
 1 2*TG(I,J)*SNU+2*AX*(TS(I-1,J)+TS(I+1,J))+R1*DF1(I,J)+R2*DF2(I,J)
 2 +RH1*DF1H(I,J)+RH2*DF2H(I,J)
   ENDIF
11 CONTINUE

C     ---- UPPER SURFACE BOUNDARY/DEFINED HT-TRANSFER COL... CLN 1 ----
   TC=(SLO**2*RHM(LS)*CS)/AKB
   DT=DELT/TC
   AX=DT/(2*DX*DX)
   AY=DT/(2*DY*DY)
   R2=N2*CF(I,LS)/(1000*CS)
   RH2=N2*HF(I,LS)/(1000*CS)
   SNU=(HTS*SLO**2*DT)/(2*AKB)
   A(LS)=-AY
   C(LS)=0.0
   IF(I.LE.1)THEN
   B(LS)=1+AX+AY+SNU
   D(LS)=(1-AX-AY-SNU)*TS(I,LS)+2*TG(I,LS)*SNU+TS(I,LS-1)*AY
 1 +2*AX*TS(I+1,LS)+R1*DF1(I,LS)+R2*DF2(I,LS)+
 2 RH1*DF1H(I,LS)+RH2*DF2H(I,LS)
   ELSEIF(I.GE.IM)THEN
   B(LS)=1+AX+AY+SNU
   D(LS)=(1-AX-AY-SNU)*TS(I,LS)+2*TG(I,LS)*SNU+TS(I,LS-1)*AY
 1 +2*AX*TS(I-1,LS)+R1*DF1(I,LS)+R2*DF2(I,LS)+
 2 RH1*DF1H(I,LS)+RH2*DF2H(I,LS)
   ELSE
   B(LS)=1+2*AX+AY+SNU
   D(LS)=(1-2*AX-AY-SNU)*TS(I,LS)+2*TG(I,LS)*SNU+TS(I,LS-1)*AY
 1 +2*AX*(TS(I-1,LS)+TS(I+1,LS))+R1*DF1(I,LS)+R2*DF2(I,LS)+
 2 RH1*DF1H(I,LS)+RH2*DF2H(I,LS)
   ENDIF
C
   CALL TRIDAG(A,B,C,D,V,M,LS)
   DO 12 J=M,LS
   TS(I,J)=V(J)
12 CONTINUE
13 CONTINUE
   RETURN
   END
```

HFTg

```fortran
C     ********************************************
      SUBROUTINE HFTg
C     ********************************************
$INCLUDE 'COVER HF'
      DIMENSION A(LG),B(LG),C(LG),D(LG),V(LG)
      CPG=29 5+4 78*TIG
      DO 1000 KT=1,2
      DO 200 I=1,IM
C     ------LOWER BOUNDARY CONDITION------
      ROG=12 1875/TG(1,M)
      TC=(SLO**2*ROG*CPG)/AKB
      DT=DELT/TC
      AY=DT/(2*DY*DY)
      AX=DT/(2*DX*DX)
      GNU=(HT*SLO**2*DT)/(2*AKB)
      A(M)=0 0
      C(M)=-AY
      IF(I LE 1)THEN
      B(M)=1+AX+AY+GNU
      D(M)=TG(1,M)*(1-AX-AY-GNU)+TG(I+1,M)*2*AX+TG(1,M+1)*AY+2*GNU*TIS
      ELSEIF(I GE IM)THEN
      B(M)=1+AX+AY+GNU
      D(M)=TG(1,M)*(1-AX-AY-GNU)+TG(I-1,M)*2*AX+TG(1,M+1)*AY+2*GNU*TIS
      ELSE
      B(M)=1+2*AX+AY+GNU
      D(M)=TG(1,M)*(1-2*AX-AY-GNU)+TG(I-1,M)*2*AX+
     1  TG(I+1,M)*2*AX+TG(1,M+1)*AY+2*GNU*TIS
      ENDIF
C     ------DISCRETIZED BY CRANK NICHOLSON TECH------
      DO 300 J=M+1,LS
      ROG=12 1875/TG(I,J)
      TC=(SLO**2*ROG*CPG)/AKB
      DT=DELT/TC
      AY=DT/(2*DY*DY)
      AX=DT/(2*DX*DX)
      IF(J EQ LS)THEN
      GNU=(HTS*SLO**2*DT)/(2*AKB)
      ELSE
      GNU=(HT*SLO**2*DT)/(2*AKB)
      ENDIF
      A(J)=-AY
      C(J)=-AY
      IF(I LE 1)THEN
      B(J)=1+AX+2*AY+GNU
      D(J)=TG(I,J)*(1-AX-2*AY-GNU)+
     1  TG(I+1,J)*2*AX+TG(I,J-1)*AY+TG(I,J+1)*AY+2*GNU*TIS
      ELSEIF(I GE IM)THEN
      B(J)=1+AX+2*AY+GNU
      D(J)=TG(I,J)*(1-AX-2*AY-GNU)+TG(I-1,J)*2*AX+
     1  TG(I,J-1)*AY+TG(I,J+1)*AY+2*GNU*TIS
      ELSE
      B(J)=1+2*AX+2*AY+GNU
      D(J)=TG(I,J)*(1-2*AX-2*AY-GNU)+TG(I-1,J)*2*AX+
     1  TG(I+1,J)*2*AX+TG(I,J-1)*AY+TG(I,J+1)*AY+2*GNU*TS(I,J)
      ENDIF
300   CONTINUE
C     ------GAS SOLID INTERFACE------
      DO 500 J=LS,LG
      ROG=12 1875/TG(I,J)
      TC=(SLO**2*ROG*CPG)/AKG
      DT=DELT/TC
      AY=DT/(2*DY*DY)
      AX=DT/(2*DX*DX)
      PEX=(VO*SLO*ROG*CPG*VX(I,J)*DT)/(2*AKG*DX)
      PEY=(VO*SLO*ROG*CPG*VY(I,J)*DT)/(2*AKG*DY)
      IF(VY(I,J) GE 0 0)THEN
      NY=0
      ELSE
      NY=1
      ENDIF
      A(J)=(NY-1)*PEY-AY
      C(J)=NY*PEY-AY
      IF(I LE 1)THEN
      A(J)=0 0
      B(J)=1 0
      C(J)=0 0
      D(J)=TIG
      ELSEIF(I GE IM)THEN
      A(J)=0 0
      B(J)=1 0
      C(J)=0 0
      D(J)=TG(IM-1,J)
      ELSE
      B(J)=1+PEX+(-1)**NY*PEY+2*AY+2*AX
      D(J)=TG(I,J)*(1-PEX-(-1)**NY*PEY-2*AY-2*AX)+TG(I-1,J)*2*(AX+PI X)
     1  +TG(I+1,J)*2*AX+TG(I,J-1)*(AY-(NY-1)*PEY)+TG(I,J+1)*(AY-NY*PEY)
      ENDIF
500   CONTINUE
C
      A(LG)=(NY-1)*PEY-AY
      C(LG)=0 0
      IF(I LE 1)THEN
      A(LG)=0 0
      B(LG)=1 0
      D(LG)=TIG
      ELSEIF(I GE IM)THEN
      A(LG)=0 0
      B(LG)=1 0
      D(LG)=TG(I-1,LG)
      ELSE
      B(LG)=1+PEX+(NY+(-1)**NY)*PEY+AY+2*AX+GNU
      D(LG)=TG(I,LG)*(1-PEX-(NY+(-1)**NY)*PEY-AY-2*AX-GNU)+2*GNU*TIG+
     1  TG(I-1,LG)*2*(AX+PEX)+TG(I+1,LG)*2*AX+TG(I,LG-1)*(AY-(NY-1)*PEY)
      ENDIF
C
      CALL TRIDAG(A,B,C,D,V,M,LG)
      DO 30 J=M,LG
      TG(I,J)=V(J)
30    CONTINUE
200   CONTINUE
C1000  CONTINUE
      RETURN
      END
```

```fortran
C ***************************************************
C HYDROGEN GAS CONCENTRATION  BACKWARD IN X, UPWINDING IN Y
C ***************************************************
      SUBROUTINE HFGH2
C ***************************************************
$INCLUDE 'COVER HF'
      DIMENSION A(LG),B(LG),C(LG),D(LG),V(LG)
      NX=0
      DO 100 I=1,IM
      DH=7 365D-4*TG(I,M)**1 675
      DML=DH*P(M)
      TC=SLO**2/DML
      DT=DELT/TC
      AY=DT/(2*DY**2)
      AX=DT/(2*DX**2)
      ROG=12 1875/TG(I,M)
      RGN=RHM(M)*N1/(ROG*FH2)
      RGF=RHM(M)*N2/(ROG*FH2)
C ------LOWER BOUNDARY CONDITION ZERO FLUX OR IMAGE POINT----
      A(M)=0 0
      C(M)=-AY
      IF(I LE.1)THEN
      B(M)=1+AY+AX
      D(M)=GH(1,M)*(1-AY-AX)+2*AX*GH(I+1,M)+
    1 GH(I,M+1)*AY-RGN*DF1H(1,M)-RGF*DF2H(I,M)
      ELSEIF(I GE IM)THEN
      B(M)=1+AY+AX
      D(M)=GH(I,M)*(1-AY-AX)+2*AX*GH(I-1,M)+
    1 GH(I,M+1)*AY-RGN*DF1H(I,M)-RGF*DF2H(I,M)
      ELSE
      B(M)=1+AY+2*AX
      D(M)=GH(I,M)*(1-AY-2*AX)+2*AX*(GH(I-1,M)+GH(I+1,M))+
    1 GH(I,M+1)*AY-RGN*DF1H(I,M)-RGF*DF2H(I,M)
      ENDIF
C ------DISCRETIZED BY CRANK NICHOLSON BW IN X,FW IN Y ----
      DO 40 J=M+1,LS
      DH=7 365D-4*TG(I,J)**1 675
      DML=DH*P(J)
      TC=SLO**2/DML
      DT=DELT/TC
      AX=DT/(2*DX**2)
      AY=DT/(2*DY**2)
      ROG=12 1875/TG(I,J)
      RGN=RHM(J)*N1/(ROG*FH2)
      RGF=RHM(J)*N2/(ROG*FH2)
      A(J)=-AY
      C(J)=-AY
      IF(I LE 1)THEN
      B(J)=1+2*AY+AX
      D(J)=GH(I,J)*(1-2*AY-AX)+2*AX*GH(I+1,J)+
    1 GH(I,J-1)*AY+GH(I,J+1)*AY-RGN*DF1H(I,J)-RGF*DF2H(I,J)
      ELSEIF(I GE IM)THEN
      B(J)=1+2*AY+AX
      D(J)=GH(I,J)*(1-2*AY-AX)+2*AX*GH(I-1,J)+
    1 GH(I,J-1)*AY+GH(I,J+1)*AY-RGN*DF1H(I,J)-RGF*DF2H(I,J)
      ELSE
      B(J)=1+2*AY+2*AX
      D(J)=GH(I,J)*(1-2*AY-2*AX)+2*AX*(GH(I-1,J)+GH(I+1,J))+
    1 GH(I,J-1)*AY+GH(I,J+1)*AY-RGN*DF1H(I,J)-RGF*DF2H(I,J)
      ENDIF
   40 CONTINUE
C
C ------ SURFACE BOUNDARY CONDITION ----
      DO 300 J=LS,LG
      DH=7 365D-4*TG(I,J)**1 675
      TC=SLO**2/DH
      DT=DELT/TC
      AX=DT/(2*DX**2)
      AY=DT/(2*DY**2)
      PEX=(VO*SLO*VX(I,J)*DT)/(2*DX*DH)
      PEY=(VO*SLO*VY(I,J)*DT)/(2*DY*DH)
      IF(VY(I,J) GE 0 0)THEN
      NY=0
      ELSE
      NY=1
      ENDIF
      A(J)=PEY*(NY-1)-AY
      C(J)=PEY*NY-AY
      IF(I LE 1)THEN
      A(J)=0 0
      B(J)=1 0
      C(J)=0 0
      D(J)=GH
      ELSEIF(I GE IM)THEN
      A(J)=0 0
      B(J)=1 0
      C(J)=0 0
      D(J)=GH(IM-1,J)
      ELSE
      B(J)=1+PEX*(-1)**NX+PEY*(-1)**NY+2*AX+2*AY
      D(J)=GH(I,J)*(1-PEX*(-1)**NX-PEY*(-1)**NY-2*AX-2*AY)+
    1 2*GH(I-1,J)*(AX-PEX*(NX-1))+2*GH(I+1,J)*(AX-PEX*NX)+
    2 GH(I,J-1)*(AY-PEY*(NY-1))+GH(I,J+1)*(AY-PEY*NY)
      ENDIF
  300 CONTINUE
C ------OUTLET BOUNDARY CONDITION------
      A(LG)=PEY*(NY-1)-AY
      C(LG)=0 0
      IF(I LE 1)THEN
      A(LG)=0 0
      B(LG)=1 0
      C(LG)=0 0
      D(LG)=GH
      ELSEIF(I GE IM)THEN
      B(LG)=1+PEX*(NX+(-1)**NX)+PEY*(NY+(-1)**NY)+AX+AY
      D(LG)=GH(I,LG)*(1-PEX*(NX-(-1)**NX)-PEY*(NY+(-1)**NY)-AX-AY)+
    1 2*GH(I-1,LG)*(AX-PEX*(NX-1))+GH(I,LG-1)*(AY P1 Y*(NY-1))
      ELSE
      B(LG)=1+PEX*(-1)**NX+PEY*(NY+(-1)**NY)+2*AX+AY
      D(LG)=GH(I,LG)*(1-PEX*(-1)**NX-PEY*(NY+(-1)**NY)-2*AX-AY)+
    1 2*GH(I-1,LG)*(AX-PEX*(NX-1))+2*GH(I+1,LG)*(AX-PEX*NX)+
    2 GH(I,LG-1)*(AY-PEY*(NY-1))
      ENDIF
C
      CALL TRIDAG(A,B,C,D,V,M,LG)
      DO 42 J=M,LG
      GH(I,J)=V(J)
      IF(GH(I,J) LE 0 015)THEN
      GH(I,J)=0 015
      ENDIF
   42 CONTINUE
  100 CONTINUE
      RETURN
      END
```

```
C     **************************************************************
C     CALCULATION OF VOLUME AVERAGE VALUES AT DIFFERENT POSITIONS
C     **************************************************************
C     **************************************************************
$INCLUDE 'COVER.HF'
      SUBROUTINE HFAv
      YP(1)=0 0
      F1A=0 0
      F2A=0 0
      GHA=0 0
      TSA=0 0
      TGA=0 0
      DO 10 K=1,NH
      AGH(K)=0 0
      AF1(K)=0 0
      AF2(K)=0 0
      ATS(K)=0 0
      ATG(K)=0 0
      NY1=M+(NS/NH)*(K-1)
      NY2=M+(NS/NH)*K
      NYD=NY2-NY1+1
      YP(K)=100*(FLOAT(K)-0 5)*(NYD-1)*DY
      DO 11 I=1,IM
      DO 11 J=NY1,NY2
      AGH(K)=AGH(K)+GH(I,J)
      AF1(K)=AF1(K)+F1(I,J)
      AF2(K)=AF2(K)+F2(I,J)
      ATS(K)=ATS(K)+TS(I,J)
      ATG(K)=ATG(K)+TG(I,J)
   11 CONTINUE
      AGH(K)=AGH(K)/(IM*NYD)
      AF1(K)=AF1(K)/(IM*NYD)
      AF2(K)=AF2(K)/(IM*NYD)
      ATS(K)=ATS(K)/(IM*NYD)
      ATG(K)=ATG(K)/(IM*NYD)
      F1A=F1A+AF1(k)
      F2A=F2A+AF2(K)
      GHA=GHA+AGH(K)
      TSA=TSA+ATS(K)
      TGA=TGA+ATG(K)
      ENDDO
   10 F1A=(F1A-AF1(1))/(NH-1)
      F2A=(F2A-AF2(1))/(NH-1)
      GHA=(GHA-AGH(1))/(NH-1)
      TSA=(TSA-ATS(1))/(NH-1)
      TGA=(TGA-ATG(1))/(NH-1)
      RETURN
      END
```

4.5 Program for Multiple Hearth Furnace

The subroutine for gas phase mass or species balance MHGH and MHCO are exactly same, only the parameters like diffusivity are different So the subroutine for CO MHGCO is given since diffusion parameters can be seen from the previous subroutines VFGH and HFGH

COM.MH

```
f77 MHMan f TRIDAG f MHVelo f MHTs f MHTg f MHRK f MHGCO f MHGH2 f MHParam f
f77 MHMan o TRIDAG o MHVelo o MHTs o MHTg o MHRK o MHGCO o MHGH2 o MHParam o
f77 MHMan o TRIDAG o MHVelo o MHTs o MHTg o MHRK o MHGCO o MHGH2 o MHParam o -o run
run
```

MHPUT

```
1 0,0 9,70,0 25,256,0 2
1 04,0 94,70,0 25,256,0 15
(TIG TIS RKG RP ITER DELT=MHPUT)
```

COVER.MH

```
      IMPLICIT REAL*8(A-H,O-Z)
      PARAMETER(IS=30,IG=16,IH=64,IM=110,NP=115,NS=10,NG=60,NH=8)
      PARAMETER(IS=15,IG=8,IH=32,IM=55,NP=60,NS=5,NG=30,NH=8)
      COMMON/A1/DELT,DR,DZ,N1,N2,VGO,FP,S1,S2,SH1,SH2,ADV(NH)
      COMMON/A2/RP,RG,FCO,FH2,FAG,VAV(NH),VF,PP,P,E,HT(NH),HTS(NH)
      COMMON/A3/KRGN,KRGF,HKRGN,HKRGF,DK,DKH,DE,DEH,DF2H(NP,NP,NH)
      COMMON/A4/DF1(NP,NP,NH),DF2(NP,NP,NH),DF1H(NP,NP,NH)
      COMMON/A5/TS(NP,NP,NH),TG(NP,NP,NH),G(NP,NP,NH),GH(NP,NP,NH)
      COMMON/A6/F1(NP,NP,NH),F2(NP,NP,NH),RD(9),WF(9),Z(IM)
      COMMON/A7/VR(NP,NP,NH),VZ(NP,NP,NH),HF(NP,NP,NH),CF(NP,NP,NII)
      COMMON/A8/TM,M,LS,LG,SK,AKB,AKG,SLO,VO,RHM,VS(IM),VOL(NII)
      COMMON/A9/AF1(NP,NII),AF2(NP,NII),ATS(NP,NII),AGH(NII),AG(NII),AVZ(NH)
      COMMON/A10/F1O(NH),F2O(NH),TSH(NII),NPM(NH)
      COMMON/A11/ATG(NII),IA,IB,K TIS,TIG,GI,GHI,KNO,KFO,WKHO,WKCO
      REAL N1,N2,KRGN,KRGF,KNO,KFO
```

```
C ****************************************************
C MODEL FOR REDUCTION IN MULTIPLE HEARTH FURNACE USING
C GRAIN MODEL BY H2/H2O//CO/CO2//N2 GAS MIXTURE
C ****************************************************
C MHMan F  NON-DIMENSIONAL AXI-SYMMETRIC EQUATIONS IN
C CYLINDRICAL COORDINATE USING CRANCK NICHOLSON SCHEME &
C FIRST ORDER UPWINDING FOR CONVECTIVE TERMS
C ****************************************************
C SUBROUTINE DESCRIPTION -
C TRIDAG  TRI-DIAGONAL MATRIX SOLVER
C MHVelo  GAS FLOW BY STREAMFUNCTION VORTICITY METHOD
C MHTs  SOLID PHASE ENERGY BALANCE
C MHTg  GAS PHASE ENERGY BALANCE
C MHRK  REDUCTION KINETICS FOR SPHERICAL PELLETS
C MHGCO  GAS PHASE SPECIES(MASS) BALANCE FOR CO
C MHGH2  GAS PHASE SPECIES(MASS) BALANCE FOR H2
C MHParam  AVERAGE VALUE OF PARAMETERS IN EACH HEARTH
C ****************************************************
C FOR A MOVING BED OF ORE HAVING BED HEIGHT OF 2 5 CM ,REDUCED BY
C H2/CO GAS,S1 UNITS
C TS,TG=TEMP OF SOLID & GAS,F1,F2=FRACTION OF NIO & FE2O3 REDUCED
C G=DIMENSIONLESS CONE OF REDUCING GAS
C DF1,DF2=INCREMENT IN FRACTION REDUCTION OF NIO & FE2O?
C FP,FG=>STRUCTURE FACTOR FOR PELLETS & GRAINS=1,2,3
C PARAMETERS CPG,ROG,VAV,RP,II,RG,FP,FG,H1,F,CO,1,AG,CO,II2,TSI,1GI
C ****************************************************
$INCLUDE 'COVER.MH'
C ****************************************************
      DIMENSION VGR(IM,NP,NH),VGZ(IM,NP,NH)
C
      OPEN(UNIT=71,FILE='MHPUT')
      OPEN(UNIT=73,FILE='M1 OUT')
      OPEN(UNIT=74,FILE='M2 OUT')
      OPEN(UNIT=75,FILE='M3 OUT')
      OPEN(UNIT=76,FILE='VMRZ')
      OPEN(UNIT=77,FILE='TGH CMT')
      OPEN(UNIT=78,FILE='TTS CMT')
      OPEN(UNIT=80,FILE='AVMH')
      OPEN(UNIT=81,FILE='VMH')
C
C     NS,NG=>NO  OF GRID POINTS OF SOLID & GAS
      M=1
      LS=M+NS
      LG=M+NS+NG
C ********STANDARD VALUES FOR NONDIMENSIONALIZING********
      VO=0 1
      SLO=0 1
      WKHO=10 0
      WKCO=10 0
C ****************************************************
      DO 300 JV=1,1
      TM=0 0
C     FAG=>FRACTION OF ADDITIONAL GAS ADDED BETWEEN HEARTHS
      FAG=0 1
C     H=>OTHER DIMENSION OF CYLINDRICAL OR PLAH PELLET
C     TIS,TIG=>INITIAL TEMP OF SOLID & GAS
      READ(71,*)TIG,TIS,RKG,RP,ITER,DELTS
C     T,DELT TIME & TIME INCREMENT
      T=.1
C     DR & DZ  R & Z DIRECTION GRID SIZE
      DR=0 10
      DZ=0 05
```

```
C
************************************************
      IF(TIS LE 0 900)THEN
      HKRGF=69 228*EXP(-3 17/TIS)
      ELSEIF(TIS LE 1 0)THEN
      HKRGF=58157*EXP(-9 2302/TIS)
      ELSE
      HKRGF=58157*EXP(-9 2302)
      ENDIF
      KRGF=798*EXP(-8 25/TIS)
      HKRGN=6132*EXP(-6 898/TIS)
      IF(TIS LE 950)THEN
      KRGN=48180*EXP(-11 2/TIS)
      ELSE
      KRGN=3*DEXP(-2/TIS)
      ENDIF
C
************************************************
      RG=6 7D-7
      FP=3 0
C     VF VOID FRACTN OF BED, PP PELLET POROSITY
C     P TOTAL POROSITY, E SOLID FRACTION
      VF=0 4025
      PP=0 5645
      P=(1-VF)*PP+VF
      E=1-P
C     RS DENSITY OF SOLID 3714 KG/CU M
C     RHM ORE BED DENSITY IN MOLE/CU M
      RHM=37977*E
C     RP RADIUS OF PELLET(0 1 TO 0 2 CM)
C     RG RADIUS OF GRAINS IN PELLET(6 E-5 TO 1E-3 CM)
C     N1,N2 NO OF MOLES OF [O] IN NIO & FE3O4 PER MOLE OF ORE
      N1=0 01597
      N2=1 004
C     FCO & FH2 FRACTION OF REDUCING GAS CO & H2, IN THE GAS
C     GHI GI INITIAL H2 & CO CONCENTRATION OR PURITY (H2 H2O/CO CO2)
      FCO=0 0000001
      FH2=0 600
      GHI=1 0
      GI=1 0
C     ************CONDUCTIVITY OF GAS AND SOLID AKG  GEIGER P*********
      SK=0 67*TIS**0 6
      AKG=(0 955*EXP(-544/TIG)*FH2+0 272*EXP(-42/TIG)*FCO+
     0 346*EXP(-57/TIG)*(1-FH2-FCO))/(1 26*FH2+(1-FH2)*3 04)
      AKB=(1-VF)*SK+VF*AKG
C     ************************************************
C     VS SOLID VELOCITY
      DO 10 I=IS,IM
      VS(I)=4 42D-5*RKG/(FLOAT(NS*I)*DR*DZ)
      ENDDO
      RSDT=DR*(IM+IS)*(IM-IS-IG)/(15*VS(IS)*IS)
      RSDT1=DR*IH*(IM+IS+IG)/(120*VS(IS)*IS)
      RSDT2=DR*IH*(IM+IS-IG)/(120*VS(IS)*IS)
      PRINT *,'VS,RSDT,RSDT1/2=',VS(IS),RSDT,RSDT1,RSDT2
C     ************************************************
      DO 10 K=1,NH
      DO 20 I=IS,IM
      DO 20 J=M,LG
      Z(J)=DZ*FLOAT(J-1)*100 0
      TG(I,J,K)=TIG
      TS(I,J,K)=TIS
      F1(I,J,K)=0 00
      F2(I,J,K)=0 00

      DF1(I,J,K)=0 000000
      DF1H(I,J,K)=0 00000
      DF2(I,J,K)=0 000000
      DF2H(I,J,K)=0 00000
      G(I,J,K)=GI
      GH(I,J,K)=GHI
      VR(I,J,K)=0 0
      ATS(I,K)=TIS
      AF1(I,K)=0 00
      AF2(I,K)=0 00
20    CONTINUE
      TSH(K)=TIS
      F1O(K)=0 0
      F2O(K)=0 0
      AG(K)=GI
      AGH(K)=GHI
      ATG(K)=TIG
10    CONTINUE
C
************************************************
      SVOL=25 0
      ADV(1)=0 0
      ADV(2)=0 0
      ADV(3)=0 0
      ADV(4)=0 30*SVOL*TIG
      ADV(5)=0 40*SVOL*TIG
      ADV(6)=0 30*SVOL*TIG
      ADV(7)=0 70*SVOL*TIG
      ADV(8)=0 30*SVOL*TIG
      DO K=NH,1,-1
      GASVOL=GASVOL+ADV(K)
      VOL(K)=GASVOL
      ENDDO
C
      DO K=1,NH
      NPM(K)=-(1)**K
      VAV(K)=0 31831*VOL(k)/(IM*NG*DR*DZ)
      IF(NPM(K) GE 0 0)THEN
      AVZ(K)=0 31831*VOL(K)/(DR**2*IG*(2*IM-IG))
      ELSE
      AVZ(K)=0 31831*VOL(K)/(DR**2*IG*(2*IS+IG))
      ENDIF
C     ********** MOLECULAR GAS DIFFUSIVITY IN MKS UNITS ***************
      DH=7 365D-4*TIG**1 675
      DC=1 2475D-4*TIG**1 603
C     HT GAS SOLID HEAT TRANSFER COEFF AT TEMP TG(1)
      HTS(K)=(1755*VAV(K)**0 9*TIG**0 3)/RP**0 75
      HT(K)=HTS(K)
      ENDDO
      WRITE(74,77)VAV(3),HT(3),RP,RG,TCO,FH2,DH,DZ,k
77    FORMAT(128('-')/2X,'VAV=',F6 3,2X,'HT=',F7 1,2X,'RP=',
     1 F6 4,2X,'RG=',E8 2,2X,'TCO=',F5 3,2X,'FH2=',F6 1,2X,'DH=',
     2 F6 4,2X,'DZ=',F6 4,2X,'k=',I4/128('-')/2X,'TIM',5X,'I11',1X,
     3 'F15',3X,'F16',5X,'F24',3X,'F25',4X,'F2G',5X,'F54',3X,'I55',
     4 3X,'TS6',5X,'TG4',3X,'TG5',3X,'TG6',5X,'GH4',3X,'GH5',3X,
     5 'GH6',5X,'G4',4X,'G5',4X,'G6'/128('-'))
      IF(NPM(K) GE 0 0)THEN
      IA=IS+IG
      ELSE
      IA=IS
      ENDIF
```

```fortran
        IB=IA+IH
        CALL MHVelo
        DO 32 J=M,LG
        WRITE(76,67)(VR(I,J,K),I=IS,IM,2)
67      FORMAT(21(F6 2))
32      CONTINUE
        WRITE(76,46)K
46      FORMAT(60('-'),1X,'VR=',I3,1X,60('-'))
        DO 34 J=M,LG
        WRITE(76,68)(VZ(I,J,K),I=IS,IM,2)
68      FORMAT(21(F6 2))
34      CONTINUE
        WRITE(76,47)K
47      FORMAT(60('-'),1X,'VZ=',I3,1X,60('-'))
        VVZ=0 0
        DO 350 J=IS,LG
        VVZ=VVZ+DZ
        VVR=0 0
        DO 350 I=IS,IM,2
        VVR=VVR+DR
        WRITE(81,87)VVR,VVZ,VVR(I,J,K),VZ(I,J,K)
87      FORMAT(2(3X,F8 3),2(3X,F8 4))
        VGR(I,J,K)=VR(I,J,K)
        VGZ(I,J,K)=VZ(I,J,K)
350     ENDDO
        WRITE(81,89)K
89      FORMAT(30('**'),3X,'K=',I4,3X,30('**'))
600     ENDDO
        PRINT *,'HTS,HT',HTS(3),HT(3)
        DO 200 KKK=1,ITER
        IF(KKK LE 6) THEN
        DELT=0 1*DLTS*FLOAT(KKK)
        ELSE
        DELT=DLTS
        ENDIF
        PRINT *,'DT=',DELT
        DO 150 K=2,7
        DO 150 I=IS,IM
        DO 150 J=IS,LG
        VR(I,J,K)=VGR(I,J,K)*ATG(K)/TIG
        VZ(I,J,K)=VGZ(I,J,K)*ATG(K)/TIG
        ENDDO
150     WRITE(74,7)TM,AF1(47,4),AF1(23,5),AF1(47,6),
1       AF2(47,4),AF2(23,5),AF2(47,6),ATS(47,4),
2       ATS(23,5),ATS(47,6),TG(19,34,4),TG(51,34,5),
3       TG(19,34,6),GH(19,34,4),GH(51,34,5),GH(19,34,6),
4       G(19,34,4),G(51,34,5),G(19,34,6)
7       FORMAT(F5.1,2X,6(2X,3(F6 3)))
        DO 100 KK=1,1
        DO 400 K=4,6
        IF(NPM(K) GE 0 0)THEN
        IA=IS+IG
        ELSE
        IA=IS
        ENDIF
        IB=IA+IH
        CALL MHTs
        CALL MHTg
        IF(TS(IM,LS,K) GT 0 600)THEN
        CALL MHRK
        CALL MHGCO
        CALL MHGH2
        CALL MHParam

        ENDIF
400     CONTINUE
        TM=TM+DELT/60 0
100     CONTINUE
        DO K=4,6
        PRINT *,'IT K TM GHIM GIM ',KKK,K,TM,GH(IM,LS,K)
        ENDDO
        DO 45 I=1,IM
        DO 45 J=M,LG
        STBL=GH(I,J,K)-1 0
        IF(STBL GE 0 15)GO TO 555
        ENDDO
45      CONTINUE
61      FORMAT(89('-')/2X,'TIME=',F6 2,2X,'TG=',F6 3,2X,'TS=',F6 3,2X,
1       'K=',I3/89('-')/6X,'AVZ',6X,'AG',6X,'AGH',6X,'ATG',6X,'ATS',
2       6X,'AF1',6X,'AF2'/89('-'))
62      FORMAT(89('-')/2X,'TIME=',F6 2,2X,'TG=',F6 3,2X,'TS=',F6 3,2X,
1       'K=',I3,3X,'NPM=',I3,3X,'FIO=',F7 4,3X,'F2O=',F7 4/89('-')/3X,
2       'T',6X,'AF1',6X,'AF2',6X,'ATS'/89('-'))
6       FORMAT(F9 4,F9 4,F9 4,F9 4,F9 4,F9 4)
9       FORMAT(I5,F9 4,F9 4,F9 4)
88      FORMAT(128('-')/4X,'TIME=',F7 3,3X,'DELT=',F5 3,3X,'VAV=',F5 3,
1       3X,'RP=',F6 4,3X,'GH=',F5 2,3X,'FH2=',F5 2,3X,'SH=',I6 3,3X,
2       'SH2=',F6 3,3X,'TS=',F7 3,3X,'K=',I3/128('-')/5X,'Z',6X,'TG',
3       6X,'TS',6X,'F1',6X,'F2',6X,'DF1',6X,'DF1H',5X,'DF2',6X,
4       'DF2H',8X,'G',7X,'GH'/128('-'))
8       FORMAT(F8 2,F8 4,F8 4,F8 5,F8 5,E9 2,E9 2,E9 2,F9 5,F9 5)
51      FORMAT(40('-'),'TIME=',F5 1,2X,'*TG*',F6 3,3X,'k=',I3,40('-'))
52      FORMAT(21(F6 3))
53      FORMAT(40('-'),'TIME=',F5 1,3X,'*TS*',F6 3,3X,'k=',I3,40('-'))
55      FORMAT(40('-'),'TIME=',F5 1,3X,'*GH',3X,'TG=',I6 3,3X,
1       'K=',I3,40('-'))
56      FORMAT(40('-'),'TIME=',F5 1,3X,'*F1*',3X,'TG=',F6 3,3X,
1       'K=',I3,40('-'))
57      FORMAT(40('-'),'TIME=',F5 1,3X,'*F2*',3X,'TG=',F6 3,3X,
1       'K=',I3,40('-'))
        DO 450 K=4,6
        IF((TM GE 10 0) AND (TM LE 10 2))THEN
        WRITE(73,62)TM,TIG,TIS,K,NPM(K),F1O(K),F2O(k)
        WRITE(73,9)(AF1(I,K),AF 2(I,K),AIS(1,K),I=IS,IM)
        WRITE(80,61)TM,TIG,TIS,K
        WRITE(80,6)AVZ(K),AG(k),AGH(K),ATG(K),TSH(k),F1O(k),F2O(K)
        WRITE(75,88)TM,DELT,VAV(3),RP,GH1,FH2,SH1,SH2,11S,K
        WRITE(75,8)(Z(J),TG(35,J,K),TS(35,J K),F1(35,J,k),1 2(35,J,k),
1       DF1(35,J,K),DF1H(35,J,K),DF2(35,J,k),DF2H(35,J,k),G(35,J,k),
2       GH(35,J,K),J=M,LS+NG)
        ELSEIF((TM GE 30 0) AND (TM LE 30 2))THEN
        WRITE(73,62)TM,TIG,TIS,K,NPM(K),F1O(k),F2O(k)
        WRITE(73,9)(AF1(I,K),Ak 2(I,k),ATS(I,K),I=IS,IM)
        WRITE(77,51)TM,TIG,K
        DO J=M,LG
        WRITE(77,52)(TG(I,J,K),I=IS,IM,2)
        ENDDO
        WRITE(77,55)TM,TIG,K
        DO J=M,LG
        WRITE(77,52)(GH(I,J,K),I=IS,IM,2)
        ENDDO
        WRITE(78,56)TM,TIS,K
        DO J=M,LS
        WRITE(78,52)(F1(I,J,K),I=IS,IM,2)
        ENDDO
        WRITE(78,57)TM,TIS,K
        DO J=M,LS
        WRITE(78,52)(F2(I,J,K),I=IS,IM,2)
        ENDDO
```

MHVelo

```fortran
C  **************************************************************
C  STREAM FUNCTION VORTICITY METHOD FOR HORIZONTAL GAS FLOW OVER
C  THE BED IN R-Z COORDINATE FOR STEADY STALL CONDITION
C  **************************************************************
C  HERE  W = VORTICITY*R = ω × R TO SIMPLIFY THE EQUATIONS
C  **************************************************************
C  SUBROUTINE MHVelo
C  **************************************************************
$INCLUDE 'COVER MH'
      DIMENSION A(IM),B(IM),C(IM),D(IM),V(IM),VLR(IM,LG)
      DIMENSION VLZ(IM,LG),S(IM,LG),W(IM,LG),VAR(IM)
      OPEN(UNIT=21,FILE='VGR D')
C     OPEN(UNIT=23,FILE='VGS D')
C     OPEN(UNIT=24,FILE='VGC D')
      VKH=8 228D-4*TIG**1 656
      VKW=1 702D-4*TIG**2 049
      VKN=1 168D-4*TIG**1 611
      VK=(0 5*VKH+0 45*VKW+0 05*VKN)/SLO**2
      WFV=0 9
      SMX=0 159155**VOL(K)
      DO 100 I=IS,IM
      DO 100 J=LS,LG
      VAR(I)=0 5*NPM(K)*VAV(K)*FLOAT(IM)/FLOAT(I)
      VR(1,J,K)=6*VAR(I)*FLOAT((J-LS)*(LG-J))/FLOAT((LG-LS)**2)
      VZ(I,J,K)=0 0
      VR(I,LS,K)=0 0
      VR(I,LG,K)=0 0
      VR(IS,J,K)=0 0
      VR(IM,J,K)=0 0
      ENDDO
100   IF(NPM(K) GE 0 0)THEN
      LGS=LS
      LGM=LG
      NR=0
      ELSE
      LGS=LG
      LGM=LS
      NR=1
      ENDIF
      DO 150 I=IS,IS+IG
      VR(I,LGS,K)=0 0
      VIS=0 31831*VOL(K)/(DR**2*IG*((IG+2*IS))
      RK=FLOAT(IS)/FLOAT(IS+IG)
      RKI=FLOAT(I)/FLOAT(IS+IG)
      VZ(I,LGS,K)=(2*VIS*(1-RKI**2+((1-RK**2)/DLOG(1/RK))*
     1 DLOG(RKI))/(1+RK**2)-(1-RK**2)/DLOG(1/RK))
      IF(NPM(K) GE 0 0)THEN
      DO J=M,LS
      VZ(1,J,K)=0 0
      VZ(I,J,K)=VZ(I,LGS,K)
      ENDDO
      ENDIF
      ENDDO
      DO 250 I=IS+III,IM
      VR(I,LGM,K)=0 0
      VIM=0 31831*VOL(K)/(DR**2*IG*(2*IM-IG))
      RKI=FLOAT(IS+III)/FLOAT(IM)
      VZ(I,LGM,K)=(2*VIM*(1-RKI**2+((1-RK**2)/DLOG(1/RK))*
     1 DLOG(RKI))/(1+RK**2)-(1-RK**2)/DLOG(1/RK))
```

```fortran
      DO J=M,LS
      WRITE(78,52)(TS(1,J,K),I=IS,IM,2)
      ENDDO
      WRITE(80,61)TM,TIG,TIS,K
      WRITE(80,6)AVZ(K),AG(K),AGH(K),ATG(K),TSH(K),F1O(K),F2O(K)
      WRITE(75,88)TM,DELT,VAV(3),RP,GH,FH2,SH1,SH2,TIS,K
      WRITE(75,8)(Z(J),TG(35,J,K),TS(35,J,K),F1(35,J,K),F2(35,J,K),
     1 DF1(35,J,K),DF1H(35,J,K),DF2(35,J,K),DF2H(35,J,K),G(35,J,K),
     2 GH(35,J,K),J=M,LS+NG)
      ELSEIF((TM GE 20 0) AND (TM LE 20 2))THEN
      WRITE(73,62)TM,TIG,TIS,K,NPM(K),F1O(K),F2O(K)
      WRITE(73,9)(1,AF1(1,K),AF2(1,K),ATS(I,K),I=IS,IM)
      WRITE(80,61)TM,TIG,TIS,K
      WRITE(80,6)AVZ(K),AG(K),AGH(K),ATG(K),TSH(K),F1O(K),F2O(K)
      WRITE(75,88)TM,DELT,VAV(3),RP,GH,FH2,SH1,SH2,TIS,K
      WRITE(75,8)(Z(J),TG(35,J,K),TS(35,J,K),F1(35,J,K),F2(35,J,K),
     1 DF1(35,J,K),DF1H(35,J,K),DF2(35,J,K),DF2H(35,J,K),G(35,J,K),
     2 GH(35,J,K),J=M,LS+NG)
      ENDIF
450   CONTINUE
200   CONTINUE
      DO 550 K=4,6
      WRITE(73,62)TM,TIG,TIS,K,NPM(K),F1O(K),F2O(K)
      WRITE(73,9)(1,AF1(1,K),AF2(1,K),ATS(I,K),I=IS,IM)
      WRITE(77,51)TM,TIG,K
      DO J=M,LG
      WRITE(77,52)(TG(1,J,K),I=IS,IM,2)
      ENDDO
      WRITE(77,55)TM,TIG,K
      DO J=M,LG
      WRITE(77,52)(GH(1,J,K),I=IS,IM,2)
      ENDDO
      WRITE(78,56)TM,TIS,K
      DO J=M,LS
      WRITE(78,52)(F1(1,J,K),I=IS,IM,2)
      ENDDO
      WRITE(78,57)TM,TIS,K
      DO J=M,LS
      WRITE(78,52)(F2(1,J,K),I=IS,IM,2)
      ENDDO
      WRITE(78,53)TM,TIS,K
      DO J=M,LS
      WRITE(78,52)(TS(1,J,K),I=IS,IM,2)
      ENDDO
      WRITE(80,61)TM,TIG,TIS,K
      WRITE(80,6)AVZ(K),AG(K),AGH(K),ATG(K),TSH(K),F1O(K),F2O(K)
      WRITE(75,88)TM,DELT,VAV(3),RP,GH,FH2,SH1,SH2,TIS,K
      WRITE(75,8)(Z(J),TG(35,J,K),TS(35,J,K),F1(35,J,K),F2(35,J,K),
     1 DF1(35,J,K),DF1H(35,J,K),DF2(35,J,K),DF2H(35,J,K),G(35,J,K),
     2 GH(35,J,K),J=M,LS+NG)
      ENDDO
550   WRITE(74,33)S1,S2,KRGN,KRGF,DK,DC,DE,IIT(3)
33    FORMAT(128('-')/2X,'S1=',F6 3,2X,'S2=',F6 3,
     1 3X,'kRGN=',F6 3,2X,'KRGF=',F6 3,2X,'DK=',E8 2,2X,'DC=',E8 2,
     2 2X,'DE=',E8 2,3X,'IIT=',I7 1)
      WRITE(74,22)SH1,SH2,HKRGN,IIKRGF,DKII,DII,DEII
22    FORMAT(128('-')/2X,'SH1=',F6 3,2X,'SH2=',F6 3,
     1 3X,'HKRGN=',F6 2,2X,'IIKRGF=',F5 2,3X,'DKII=',E8 2,2X,'DII=',E8 2,
     2 2X,'DEH=',E8 2/128('-'))
300   CONTINUE
555   STOP
      END
```

```fortran
      IF(NPM(K) LE 0 0)THEN
      DO J=M,LS
      VR(I,J,K)=0 0
      VZ(I,J,K)=VZ(I,LGM,K)
      ENDDO
      ENDIF
250   ENDDO
      DO 200 I=IS,IM
      DO 200 J=LS,LG
      S(I,J)=SMX*NR+VAR(I)*DR*DZ*FLOAT(I*(J-LS))**2*(3*LG-LS-2*J))/
1     (FLOAT((LG-LS)**2))
200   CONTINUE
      SDY1=0 0
      DO 233 I=IS,IS+IG
      SDY1=SDY1+VZ(I,LGS,K)*FLOAT(I)*DR**2
      S(I,LGS)=SMX-SDY1
233   ENDDO
      SDY=0 0
      DO I=IS+IH,IM
      SDY=SDY+VZ(I,LGM,K)*FLOAT(I)*DR**2
      S(I,LGM)=SMX-SDY
      ENDDO
      DO J=LS,LG
      S(IS,J)=SMX
      S(IM,J)=0 0
      ENDDO
      REN=(VO*SLO)/VK
      AR=1/DR**2
      AZ=1/DZ**2
      DO 17 I=IS,IM
      DO 17 J=LS,LG
      W(I,J)=0 0
17    ENDDO
C  ------- STREAM FUNCTION INITIALIZATION -------
      DO 14 I=IS,IM
      DO 14 J=LS,LG
      VLR(I,J)=VR(I,J,K)
      VLZ(I,J)=VZ(I,J,K)
14    ENDDO
      DO 1000 KT=1,9
C  ------- STREAM FUNCTION OF INTERIOR POINTS  CENTRAL DIFF -------
      DO 77 I=IS+1,IM-1
      DO 77 J=LS+1,LG-1
      ARI=AR/FLOAT(I)
      IF(VR(I,J,K) GE 0 0)THEN
      NR=0
      ELSE
      NR=1
      ENDIF
      S(I,J)=(S(I-1,J)*(AR+ARI*(1-NR))+S(I+1,J)*(AR-ARI*NR)+
1     AZ*(S(I,J-1)+S(I,J+1))-W(I,J))/(2*AR+2*AZ+ARI*(-1)**NR)
77    ENDDO
      IF(NPM(K) GE 0 0)THEN
      NR=0 0
      ELSE
      NR=1
      ENDIF
C  ------- VELOCITY CALCULATION -------
      DO 87 I=IS+1,IM-1
      DO 210 J=LS,LG
      IF(J LE LS)THEN
      VLR(I,J)=(S(I,J+1)-S(I,J))/(FLOAT(I)*DR*DZ)
      ELSEIF(J GE LG)THEN
      VLR(I,J)=(S(I,J)-S(I,J-1))/(FLOAT(I)*DR*DZ)
      ELSE
      VLR(I,J)=(S(I,J+1)-S(I,J-1))/(2*FLOAT(I)*DR*DZ)
      ENDIF
      VLZ(I,J)=-(S(I+1,J)-S(I-1,J))/(2*FLOAT(I)*DR*DR)
210   CONTINUE
87    CONTINUE
C  ------- I/R-DIRECTION SWEEP FOR VORTICITY TRANSPORT -------
      DO 97 I=IS,IM
      A(LS)=0 0
      B(LS)=1 0
      C(LS)=0 0
      IF(I LE IS+IG)THEN
      IF(I LE IS)THEN
      D(LS)=-FLOAT(I)*(VLZ(I+1,LS)-VLZ(I,LS))
      ELSE
      D(LS)=-0 5*FLOAT(I)*(VLZ(I+1,LS)-VLZ(I-1,LS))
      ENDIF
      ELSE
      D(LS)=2*AZ*(S(I,LS+1)-S(I,LS))
      ENDIF
C
      DO 300 J=LS+1,LG
      PER=VR(I,J,K)*REN/DR
      PERI=PER/FLOAT(I)
      PEZ=VZ(I,J,K)*REN/DZ
      ARI=AR/FLOAT(I)
      IF(VR(I,J,K) GE 0 0)THEN
      NR=0
      ELSE
      NR=1
      ENDIF
      IF(VZ(I,J,K) GE 0 0)THEN
      NZ=0
      ELSE
      NZ=1
      ENDIF
      A(J)=-AZ+(NZ-1)*PEZ
      B(J)=2*(AR+AZ-PERI)+(-1)**NR*(ARI+PER)+(-1)**NZ*PEZ
      C(J)=-AZ+NZ*PEZ
      IF(I LE IS)THEN
      D(J)=W(I+1,J)*(AR-NR*(PER+ARI))
      B(J)=2*(AZ-PERI)+(NR-1+(-1)**NR)*(ARI+PER)+(-1)**NZ*PEZ/+AR
      ELSEIF(I GE IM)THEN
      D(J)=W(I-1,J)*(AR-(NR-1)*(PER+ARI))
      B(J)=2*(AZ-PERI)+(NR+(-1)**NR)*(ARI+PER)+(-1)**NZ*PEZ+AR
      ELSE
      D(J)=W(I-1,J)*(AR-(NR-1)*(PER+ARI))+W(I+1,J)*(AR-NR*(PER+ARI))
      ENDIF
      ENDDO
300   
C
      A(LG)=0 0
      B(LG)=1 0
      C(LG)=0 0
      IF(I LE IS+IH)THEN
      D(LG)=2*AZ*(S(I,LG)-S(I,LG-1))
      ELSE
      D(LG)=W(I,LG-1)
      ENDIF
```

```fortran
C
      CALL TRIDAG(A,B,C,D,V,LS,LG)
      DO 20 J=LS,LG
      W(I,J)=V(J)
20    CONTINUE
97    CONTINUE
      DO 88 I=IS+1,IM-1
      DO 88 J=LS+1,LG-1
      ARI=AR/FLOAT(I)
      IF(VR(I,J,K) GE 0 0)THEN
      NR=0
      ELSE
      NR=1
      ENDIF
      S(I,J)=(S(I-1,J)*(AR+ARI*(1-NR))+S(I+1,J)*(AR-ARI*NR)+
1     AZ*(S(I,J-1)+S(I,J+1))-W(I,J))/(2*AR+2*AZ+ARI*(-1)**NR)
      ENDDO
88    DO 219 I=IS+1,IM-1
      DO 219 J=LS,LG
      IF(J LE LS)THEN
      VLR(I,J)=(S(I,J+1)-S(I,J))/(FLOAT(I)*DR*DZ)
      ELSEIF(J GE LG)THEN
      VLR(I,J)=(S(I,J)-S(I,J-1))/(FLOAT(I)*DR*DZ)
      ELSE
      VLR(I,J)=(S(I,J+1)-S(I,J-1))/(2*FLOAT(I)*DR*DZ)
      ENDIF
      VLZ(I,J)=(S(I+1,J)-S(I-1,J))/(2*FLOAT(I)*DR*DR)
      VLR(I,J)=WFV*VLR(I,J)+(1-WFV)*VR(I,J,K)
      VLZ(I,J)=WFV*VLZ(I,J)+(1-WFV)*VZ(I,J,K)
219   CONTINUE
C          ------- CENTRAL WALL -------
      DO 99 J=LS,LG
      A(IS)=0 0
      B(IS)=1 0
      C(IS)=0 0
      D(IS)=2*AR*(S(IS+1,J)-S(IS,J))-AR*(S(IS+1,J)-S(IS,J))/FLOAT(IS)
C          ------- R-DIRECTION MARCHING -------
      DO 500 I=IS+1,IM
      PER=VLR(I,J)*REN/DR
      PERI=PER/FLOAT(I)
      PEZ=VLZ(I,J)*REN/DZ
      ARI=AR/FLOAT(I)
      IF(VLR(I,J) GE 0 0)THEN
      NR=0
      ELSE
      NR=1
      ENDIF
      IF(VLZ(I,J) GE 0 0)THEN
      NZ=0
      ELSE
      NZ=1
      ENDIF
      A(I)=-AR+(NR-1)*(PER+ARI)
      C(I)=-AR+NR*(PER+ARI)
      IF(J LE LS)THEN
      D(I)=W(I,J+1)*(AZ-NZ*PEZ)
      B(I)=2*(AR-PERI)+(-1)**NR*(ARI+PER)+(NZ-1+(-1)**NZ)*PEZ+AZ
      ELSEIF(J GE LG)THEN
      D(I)=W(I,J-1)*(AZ-(NZ-1)*PEZ)
      B(I)=2*(AR-PERI)+(-1)**NR*(ARI+PER)+(NZ+(-1)**NZ)*PEZ+AZ
      ELSE

      D(I)=W(I,J-1)*(AZ-(NZ-1)*PEZ)+W(I,J+1)*(AZ-NZ*PEZ)
      B(I)=2*(AR+AZ-PERI)+(-1)**NR*(ARI+PER)+(-1)**NZ*PEZ
      ENDIF
500   CONTINUE
C          ------- OUT FLOW CONDITION -------
      A(IM)=0 0
      B(IM)=1 0
      C(IM)=0 0
      D(IM)=-2*AR*(S(IM,J)-S(IM-1,J))-ARI*(S(IM,J)-S(IM-1,J))
C
      CALL TRIDAG(A,B,C,D,V,IS,IM)
      DO 40 I=IS,IM
      W(I,J)=V(I)
40    CONTINUE
99    CONTINUE
      DO 23 I=IS,IM
      DO 24 J=LS,LG
      VR(I,J,K)=WFV*VLR(I,J)+(1-WFV)*VR(I,J,K)
      VZ(I,J,K)=WFV*VLZ(I,J)+(1-WFV)*VZ(I,J,K)
24    ENDDO
23    ENDDO
1000  ENDDO
      PRINT *,'S---V---W',S(IS+5,LS+5),VLR(IS+5,LS+5),W(IS+5,LS+5)
      IF(NPM(K) GE 0 0)THEN
      ENDIF
      DO 12 J=M,LS-1
      DO 12 I=IA,IB
      VZ(I,J,K)=0 0
      VR(I,J,K)=0 0
12    ENDDO
      FORMAT(21(F6 2))
61    FORMAT(60('-'),2X,'k=',I2,2X,60('-'))
74    DO J=M,LG,2
      WRITE(21,61)(VR(I,J,K),I=IS,IM,4)
      ENDDO
      WRITE(21,74)K
      DO J=M,LG,2
      WRITE(21,61)(VZ(I,J,K),I=IS,IM,4)
      ENDDO
      WRITE(21,74)K
      DO J=LS,LG,2
      WRITE(21,61)(S(I,J),I=IS,IM,4)
      ENDDO
      WRITE(21,74)K
      RETURN
      END
```

```fortran
C     ******************************************************
C     SUBROUTINE MHTs
C     ******************************************************
$INCLUDE 'COVER MH'
      DIMENSION A(IM),B(IM),C(IM),D(IM),V(IM)
      CS=88+2 44**TIS
      CN=42840 0
      HN=6720 0
      TC=(SLO**2*RHM*CS)/AKB
      DT=DELT/TC
      AR=DT/(2*DR*DR)
      AZ=DT/(2*DZ*DZ)
      SNU=(HT(K)*SLO**2*DT)/(2*AKB)
      R1=N1*CN/(1000*CS)
      RH1=N1*HN/(1000*CS)
      IF(NPM(K) GE 0 0)THEN
      NR=1
      ELSE
      NR=0
      ENDIF
      DO 13 I=IA,IB
C     -----LOWER BOUNDARY CONDITION/KNOWN TEMPERATURE-----
      ARI=AR/FLOAT(I)
      R2=N2*CF(I,M,K)/(1000*CS)
      RH2=N2*HF(I,M,K)/(1000*CS)
      PER=(VO*SLO*RHM*CS*VS(I)*DT)/(2*AKB*DR)
      A(M)=0 0
      IF(I LE IA)THEN
      IF(NPM(K) GE 0 0)THEN
      B(M)=1+AR+((-1)**NR+NR-1)*(PER-ARI)+AZ+SNU
      C(M)=-AZ
      D(M)=(1-AR-((-1)**NR+NR-1)*(PER-ARI)-AZ-SNU)*TS(I,M,K)+
     2 TS(I,M+1,K)*AZ+2*TS(I+1,M,K)*(AR-NR*(PER-ARI))+2*SNU*TG(I,M,K)
     2 +R1*DF1(I,M,K)+R2*DF2(I,M,K)+RH1*DF1H(I,M,K)+RH2*DF2H(I,M,K)
      ELSE
      B(M)=1 0
      C(M)=0 0
      D(M)=TSH(K-1)
      ENDIF
      ELSEIF(I GE IB)THEN
      IF(NPM(K) GE 0 0)THEN
      B(M)=1 0
      C(M)=0 0
      D(M)=TSH(K-1)
      ELSE
      B(M)=1+2*AR+(-1)**NR*(PER-ARI)+AZ+SNU
      C(M)=-AZ
      D(M)=(1-2*AR-(-1)**NR*(PER-ARI))-AZ-SNU)*TS(I,M,K)+
     1 TS(I,M+1,K)*AZ+2*TS(I-1,M,K)*(AR-(NR-1)*(PER-ARI))+2*SNU*TG(I,M,K)
     2 +2*TS(I+1,M,K)*(AR-NR*(PER-ARI))+2*TG(I,M,K)*SNU+
     3 R1*DF1(I,M,K)+R2*DF2(I,M,K)+RH1*DF1H(I,M,K)+RH2*DF2H(I,M,K)
      ENDIF

C     -----CRANK NICHOLSON/CENTRAL IN SPACE-----
      DO 11 J=M+1,LS
      R2=N2*CF(I,J,K)/(1000*CS)
      RH2=N2*HF(I,J,k)/(1000*CS)
      IF(I LE IA)THEN
      IF(NPM(K) GE 0 0)THEN
      A(J)=-AZ
      C(J)=-AZ
      B(J)=1+AR+((-1)**NR+NR-1)*(PER-ARI)+2*AZ+SNU
      D(J)=(1-AR-((-1)**NR+NR-1)*(PER-ARI)-2*AZ-SNU)*TS(I,J,K)+
     1 TS(I,J+1,K)*AZ+2*TS(I+1,J,K)*AZ-2*TS(I+1,J,K)*(AR-NR*(PER-ARI))+
     2 2*SNU*TG(I,J,K)+R1*DF1(I,J,K)+R2*DF2(I,J,K)+RH1*DF1H(I,J,K)+
     3 RH2*DF2H(I,J,K)
      ELSE
      A(J)=0 0
      B(J)=1 0
      C(J)=0 0
      D(J)=TSH(K-1)
      ENDIF
      ELSEIF(I GE IB)THEN
      IF(NPM(K) GE 0 0)THEN
      A(J)=0 0
      B(J)=1 0
      C(J)=0 0
      D(J)=TSH(K-1)
      ELSE
      A(J)=-AZ
      C(J)=-AZ
      B(J)=1+AR+((-1)**NR+NR)*(PER-ARI)+2*AZ+SNU
      D(J)=(1-AR-((-1)**NR+NR)*(PER-ARI)-2*AZ-SNU)*TS(I,J,K)+
     1 TS(I,J+1,K)*AZ+2*TS(I-1,J,K)*AZ+2*TS(I-1,J,K)*(AR-(NR-1)*(PER-ARI))
     2 +2*SNU*TG(I,J,K)+R1*DF1(I,J,K)+R2*DF2(I,J,K)+RH1*DF1H(I,J,k)+
     3 RH2*DF2H(I,J,K)
      ENDIF
      ELSE
      A(J)=-AZ
      C(J)=-AZ
      B(J)=1+2*AR+(-1)**NR*(PER-ARI)+2*AZ+SNU
      D(J)=(1-2*AR-(-1)**NR*(PER-ARI))-2*AZ-SNU)*TS(I,J,k)+
     1 TS(I,J+1,K)*AZ+2*TS(I-1,J,K)*AZ+2*TS(I-1,J,K)*(AR-(NR-1)*(PER-ARI))+
     2 +2*TS(I+1,J,K)*AZ+2*TG(I,J,K)*SNU+
     3 R1*DF1(I,J,K)+R2*DF2(I,J,K)+RH1*DF1H(I,J,k)+RH2*DF2H(I,J,K)
      ENDIF
   11 CONTINUE
C     ----- UPPER SURFACE BOUNDARY/DEFINED HT-TRANSFER COEFFICIENT ---
      R2=N2*CF(I,LS,K)/(1000*CS)
      RH2=N2*HF(I,LS,k)/(1000*CS)
      C(LS)=0 0
      IF(I LE IA)THEN
      IF(NPM(K) GE 0 0)THEN
      A(LS)=-AZ
      B(LS)=1+AR+((-1)**NR+NR-1)*(PER-ARI)+AZ+SNU
      D(LS)=(1-AR-((-1)**NR+NR-1)*(PER-ARI)-AZ-SNU)*TS(I,LS,K)+
     1 TS(I,LS-1,K)*AZ+2*SNU*TG(I,LS,K)+2*TS(I+1,LS,k)*(AR-NR*(PER-ARI))
     2 +R1*DF1(I,LS,K)+R2*DF2(I,LS,K)+RH1*DF1H(I,LS,k)+RH2*DF2H(I,LS,k)
      ELSE
      A(LS)=0 0
      B(LS)=1 0
      D(LS)=TSH(K-1)
      ENDIF
      ELSEIF(I GE IB)THEN
```

```fortran
C
C
      SUBROUTINE MHTg
C
      ****************************************************************
$INCLUDE 'COVER MH'
      DIMENSION A(IM),B(IM),C(IM),D(IM),V(IM)
      REAL LW
C
      ROG=12 1875/TIG
      CPG=32 8+5 67*TIG
C
      TOUT=0 3
      TOUT=TIG
      LW=1 0
C
      DO 1000 KT=1,2
      TC=(SLO**2*ROG*CPG)/AKB
      DT=DELT/TC
      AZ=DT/(2*DZ*DZ)
      AR=DT/(2*DR*DR)
      GNU=(HT(K)*SLO**2*DT)/(2*AKB)
      WNU=(SK*DT)/(2*AKB*LW*DR)
      IF(NPM(K) GE 0 0)THEN
      NR=1
      ELSE
      NR=0 0
      ENDIF
      DO 200 I=IS,IM
C     -----LOWER BOUNDARY CONDITION-----
      ROG=12 1875/TG(I,M,K)
      ARI=AR/FLOAT(I)
      A(M)=0 0
      C(M)=-AZ
      IF((I GE IA) AND (I LE IB))THEN
      IF(I LE IA)THEN
      B(M)=1-((-1)**NR+NR-1)*ARI+AZ+AR+WNU
      D(M)=TG(I,M,K)*(1+((-1)**NR+NR-1)*ARI-AZ-AR-WNU)+
     1 2*TG(I+1,M,K)*(AR+NR*ARI)+TG(I,M+1,K)*AZ+2*WNU*TG(I,LG,K+1)
      ELSEIF(I GE IB)THEN
      B(M)=1-((-1)**NR+NR)*ARI+AZ+AR+WNU
      D(M)=TG(I,M,K)*(1+((-1)**NR+NR)*ARI-AZ-AR-WNU)+
     1 2*TG(I-1,M,K)*(AR+(NR-1)*ARI)+TG(I,M+1,K)*AZ+2*WNU*TG(I,LG,K+1)
      ELSE
      B(M)=1-((-1)**NR*ARI+AZ+AZ-2*AB+WNU
      D(M)=TG(I,M,K)*(1+((-1)**NR*ARI-AZ-2*AR-WNU)+2* TG(I-1,M,K)
     1 *(AR+(NR-1)*ARI)+2*TG(I+1,M,K)*(AR+NR*ARI)
     2 +TG(I,M+1,K)*AZ+2*WNU*TG(I,LG,k+1)
      ENDIF
      ELSE
      B(M)=1 0
      C(M)=0 0
      D(M)=ATG(K+1)
      ENDIF
C     -----DISCRETIZED BY CRANK NICHOLSON TECH ---- -
      DO 500 J=M+1,LS-1
      ROG=12 1875/TG(I,J,K)
      ARI=AR/FLOAT(I)
      A(J)=-AZ
      C(J)=-AZ
      IF((I GE IA) AND (I LE IB))THEN
      IF(I LE IA)THEN
      B(J)=1-((-1)**NR+NR-1)*ARI+2*AZ+AR+GNU
      D(J)=TG(I,J,K)*(1+((-1)**NR+NR-1)*ARI-2*AZ-AR GNU)+AZ*TG(I,J-1,K)
     1 +TG(I,J+1,K)*AZ+2*TG(I+1,J,K)*(AR+NR*ARI)+2*GNU*TS(I,J,K)
```

```fortran
      IF(NPM(K) GE 0 0)THEN
      A(LS)=0 0
      B(LS)=1 0
      D(LS)=TSH(K-1)
      ELSE
      A(LS)=-AZ
      B(LS)=1+AR+((-1)**NR+NR)*(PER-ARI)+AZ+SNU
      D(LS)=(1-AR-((-1)**NR+NR)*(PER-ARI)-AZ-SNU)*TS(I,LS,K)+
     1 TS(I,LS-1,K)*AZ+2*TS(I-1,LS,K)*(AR-(NR-1)*(PER-ARI))+
     2 2*SNU*TG(I,LS,K)+R1*DF1(I,LS,K)+R2*DF2(I,LS,K)+RH1*DF1H(I,LS,K)
     3 +RH2*DF2H(I,LS,K)
      ENDIF
      ELSE
      A(LS)=-AZ
      B(LS)=1+2*AR+(-1)**NR*(PER-ARI)+AZ+SNU
      D(LS)=(1-2*AR-(-1)**NR*(PER-ARI)-AZ-SNU)*TS(I,LS,K)+
     1 TS(I,LS-1,K)*AZ+2*TS(I-1,LS,K)*(AR-NR*(PER-ARI))
     2 +2*TS(I+1,LS,K)*(AR-NR*(PER-ARI))+2*TG(I,LS,K)*SNU+
     3 R1*DF1(I,LS,K)+R2*DF2(I,LS,K)+RH1*DF1H(I,LS,K)+RH2*DF2H(I,LS,K)
      ENDIF
C
      CALL TRIDAG(A,B,C,D,V,M,LS)
      DO 12 J=M,LS
      TS(I,J,K)=V(J)
      IF(NPM(K) GE 0 0)THEN
      TS(IB,J,K)=TSH(K-1)
      ELSEIF(NPM(K) LE 0 0)THEN
      TS(IA,J,K)=TSH(K-1)
      ENDIF
12    CONTINUE
13    CONTINUE
      RETURN
      END
```

287

```fortran
      ELSEIF(I GE IB)THEN
      B(J)=1-((-1)**NR+NR)*ARI+2*AZ+AR+GNU
      D(J)=TG(I,J,K)*(1+((-1)**NR+NR)*ARI-2*AZ-AR-GNU)+AZ*TG(I,J-1,K)
     1 +AZ*TG(I,J+1,K)+2*TG(I-1,J,K)*(AR+(NR-1)*ARI)+2*GNU*TS(I,J,K)
      ELSE
      B(J)=1-(-1)**NR*ARI+2*AZ+2*AR+GNU
      D(J)=TG(I,J,K)*(1+(-1)**NR*ARI-2*AZ-2*AR-GNU)+AZ*TG(I,J-1,K)+
     1 AZ*TG(I,J+1,K)+2*TG(I-1,J,K)*(AR+(NR-1)*ARI)+
     2 2*TG(I+1,J,K)*(AR+NR*ARI)+2*GNU*TS(I,J,K)
      ENDIF
      ELSE
      A(J)=0 0
      B(J)=1 0
      C(J)=0 0
      D(J)=ATG(K+1)
      ENDIF
500   CONTINUE
C
      DO 600 J=LS,LG-1
      IF(VR(I,J,K) GE 0 0)THEN
      NR=0 0
      ELSE
      NR=1
      ENDIF
      IF(VZ(I,J,K) GE 0 0)THEN
      NZ=0 0
      ELSE
      NZ=1
      ENDIF
      ROG=12 1875/TG(I,J,K)
      TC=(SLO**2*ROG*CPG)/AKG
      DT=DELT/TC
      AZ=DT/(2*DZ*DZ)
      AR=DT/(2*DR*DR)
      WNU=(Sk*DT)/(2*AKG*LW*DR)
      ARI=AR/FLOAT(I)
      PER=(VO*SLO*ROG*CPG*VR(I,J,K)*DT)/(2*AKG*DR)
      PEZ=(VO*SLO*ROG*CPG*VZ(I,J,K)*DT)/(2*AkG*DZ)
      A(J)=PEZ*(NZ-1)-AZ
      C(J)=NZ*PEZ-AZ
      IF(I LE IS)THEN
      B(J)=1+((-1)**NR+NR-1)*(PER-ARI)+(-1)**NZ*PEZ+2*AZ+AR
      D(J)=TG(I,J,K)*(1-((-1)**NR+NR-1)*(PER-ARI)-(-1)**NZ*PEZ-2*AZ-AR)
     1 +2*TG(I+1,J,K)*(AR-NR*(PER-ARI))+TG(I,J-1,K)*(AZ-(NZ-1)*PEZ)+
     2 TG(I,J+1,K)*(AZ-NZ*PEZ)
      ELSEIF(I GE IM)THEN
      B(J)=1+((-1)**NR+NR)*(PER-ARI)+(-1)**NZ*PEZ+2*AZ+AR+WNU
      D(J)=TG(I,J,K)*(1-((-1)**NR+NR)*(PER-ARI)-(-1)**NZ*PEZ-2*AZ-AR-
      WNU)+2*TG(I-1,J,K)*(AR-(NR-1)*(PER-ARI))+TG(I,J+1,K)*(AZ-NZ*PEZ)
     1 +TG(I,J-1,K)*(AZ-(NZ-1)*PEZ)+TG(I,J+1,K)*(AZ-NZ*PEZ)
      ELSE
      B(J)=1+(-1)**NR*(PER-ARI)+(-1)**NZ*PEZ+2*AZ+2*AR
      D(J)=TG(I,J,K)*(1-(-1)**NR*(PER-ARI)-(-1)**NZ*PEZ-2*AZ-2*AR)+
     1 2*TG(I-1,J,K)*(AR-(NR-1)*(PER-ARI))+2*TG(I+1,J,K)*(AR-NR*
     2 (PER-ARI))+TG(I,J-1,K)*(AZ-(NZ-1)*PEZ)+TG(I,J+1,K)*(AZ-NZ*PEZ)
      ENDIF
600   ENDDO

C
      IAT=IA-NPM(K)*IG
      IBT=IAT+IH
      A(LG)=PEZ*(NZ-1)-AZ
      C(LG)=0 0
      IF((I GE IAT) AND (I LE IBT))THEN
      IF(I LE IS)THEN
      B(LG)=1+((-1)**NR+NR-1)*(PER-ARI)+((-1)**NZ+NZ)*PEZ+AZ+AR
      D(LG)=TG(I,LG,K)*(1-((-1)**NR+NR-1)*(PER-ARI)-((-1)**NZ+NZ)*PEZ-
     1 AZ-AR)+2*TG(I+1,LG,K)*(AR-NR*(PER-ARI))+
     2 TG(I,LG-1,K)*(AZ-(NZ-1)*PEZ)
      ELSEIF(I GE IM)THEN
      B(LG)=1+((-1)**NR+NR)*(PER-ARI)+((-1)**NZ+NZ)*PEZ+AZ+AR+WNU
      D(LG)=TG(I,LG,K)*(1-((-1)**NR+NR)*(PER-ARI)-(-1)**NZ+NZ)*PEZ-
     1 AZ-AR-WNU)+2*TG(I-1,LG,K)*(AR-(NR-1)*(PER-ARI))+
     2 TG(I,LG-1,K)*(AZ-(NZ-1)*PEZ)+2*WNU*TG(I,J,K)
      ELSE
      B(LG)=1+(-1)**NR*(PER-ARI)+((-1)**NZ+NZ)*PEZ+AZ+2*AR+WNU
      D(LG)=TG(I,LG,K)*(1-(-1)**NR*(PER-ARI)-((-1)**NZ+NZ)*PEZ-AZ-2*AR
     1 -WNU)+2*TG(I-1,LG,K)*(AR-(NR-1)*(PER-ARI))+2*TG(I+1,LG,K)*(AR-NR*
     2 (PER-ARI))+TG(I,LG-1,K)*(AZ-(NZ-1)*PEZ)+TG(I,LG+1,A)*(AZ-NZ*PEZ)
     3 +2*WNU*TG(I,M,K-1)
      ENDIF
      ELSE
      A(LG)=0 0
      B(LG)=1 0
      D(LG)=TG(I,LG-1,K)
      ENDIF

C
      CALL TRIDAG(A,B,C,D,V,M,LG)
      DO 30 J=M,LG
      TG(I,J,K)=V(J)
30    CONTINUE
200   CONTINUE
C1000 CONTINUE
      RETURN
      END
```

MHRK

```fortran
C  *********************************************************
C     FOR SPHERICAL PELLETS,
C  *********************************************************
      SUBROUTINE MHRK
$INCLUDE 'COVER MH'
C     RHO NO OF MOLES OF [O] PER CC OF NIO & FE3O4 PRESENT IN ORE
      RHO=0 0374*(1-PP)
      DT=DELT
C     TO TORTUOSITY FACTOR
      TO=1/PP
      FG=1 0
      HN=6720 0
      HF1=-3024 0
      HF2=-66024 0
      HF3=-18522 0
      CF1=33100 0
      CF2=-29900 0
      CF3=17600 0
      DO 50 I=IA,IB
      DO 30 J=M,LS
C     GC,GG  NO  OF GM MOLES OF CO & H2 PER CU CM
      GC=1 21875D-5*G(I,J,K)*FCO/TG(I,J,K)
      GG=1 21875D-5*GH(I,J,K)*FH2/TG(I,J,K)
      DKH=(1 175D-1*TS(I,J,K)**3 333)/(1-PP)
      DK=(2 977D-2*TS(I,J,K)**3 333)/(1-PP)
      DH=7 365*TS(I,J,K)**1 675
      DC=1 2475*TS(I,J,K)**1 693
      DE=PP/(TO*(1/DK+1/DC))
      DEH=PP/(TO*(1/DKH+1/DH))
      DF1(I,J,K)=0 000000001
      DF2(I,J,K)=0 000000001
      DF1H(I,J,K)=0 00000001
      DF2H(I,J,K)=0 00000001
      IF(GH(I,J,K) LE 0 01)THEN
      H2=0 001*FH2
      ENDIF
      PCO=G(I,J,K)*FCO
      H2=GH(I,J,K)*FH2
      PCO2=(1-G(I,J,K))*FCO
      H2O=(1-GH(I,J,K))*FH2
      RH=H2O/H2
      RC=PCO2/PCO
      DNS=DEH/DH
      RDE=1 006D-3*EXP(5 197/TS(I,J,K)) ****** DIFF  RATIO *****
      RDE=1 0
      WKHO=5 0
      PER=-NPM(K)*VS(I)*DT/DR
      IF(NPM(K) GE 0 0)THEN
      IF(I GE 1M)THEN
      F1(I+1,J,K)=F1O(K-1)
      F2(I+1,J,K)=F2O(K-1)
      ENDIF
      NR=1
      ELSE
      IF(I LE 1S)THEN
      F1(I-1,J,K)=F1O(K-1)
      F2(I-1,J,K)=F2O(K-1)
      ENDIF
      NR=0
      ENDIF


C  *********************************************************
C     REDUCTION KINETICS FOR IRON OXIDE
C     HK1,HK2,HK3,CK1,CK2,CK3 KINETIC CONSTANT FOR H2 & CO REDUCTION
C     WH1,WH2,WH3,WC1,WC2,WC3 EFFECT OF PRODUCT GAS H2O & CO2
C  *********************************************************
      IF(F2(I,J,K) LE 0 99)THEN
      WH1=5 0
      WH2=-4821*EXP(-7 936/TS(I,J,K))
      WH3=-3 684*EXP(-2 226/TS(I,J,K))
      WC1=5 0
      WC2=100*EXP(-3 583/TS(I,J,K))
      WC3=0 07564*EXP(2 1087/TS(I,J,K))
      IF(TS(I,J,K) LE 0 900)THEN
      HK1=69 228*EXP(-3 17/TS(I,J,K))
      HK2=15 85*EXP(-2 0774/TS(I,J,K))
      ELSE
      HK1=58157*EXP(-9 2302/TS(I,J,K))
      HK2=604825*EXP(-11 572/TS(I,J,K))
      ENDIF
      HK3=36435*EXP(-9 0786/TS(I,J,K))
      CK1=22000*EXP(-9 35/TS(I,J,K))
      CK2=5100*EXP(-8 25/TS(I,J,K))
      CK3=3184*EXP(-7 936/TS(I,J,K))
C ******* 1ST STEP OF IRON OXIDE REDUCTION FE2O3 -> FE3O4 *******
      IF(F2(I,J,K) LE 0 111)THEN
      HF(I,J,K)=HF1+9*F2(I,J,K)*(HF2-HF1)
      CF(I,J,K)=CF1+9*F2(I,J,K)*(CF2-CF1)
      KFO=HK1+9*F2(I,J,K)*(HK2-HK1)
C ********** WATER VAPOR CORRECTION ***********************
      S2=RP*(KRGF/DE)**0 5
      SH2=RP*(HKRGF/DEH)**0 5
      ESCF=(1-F2(I,J,K))**0 333
      SH2M=SH2*ESCF
      H2N=GH(I,J,K)/(1+RDE*(SH2M/TANH(SH2M)-1)*(1-ESCF+ESCF*DNS))
      RH=(1-H2N)/H2N
C ****************************************************
      WKHO=1/(1/WH1+9*F2(I,J,K)*(1/WH2-1/WH1))
      HKRGF=HK1*(1-RH/WH1)+9*F2(I,J,K)*(HK2*(1-RH/WH2) HK1*(1-RH/WH1))
      KRGF=CK1*(1-RC/WC1)+9*F2(I,J,K)*(CK2*(1-RC/WC2)-CK1*(1-RC/WC1))
      IF(HKRGF LE 0 0001)THEN
      WH2=0 0001
      ENDIF
      IF(KRGF LE 0 0001)THEN
      WC2=0 0001
      ENDIF
C ****** 2ND STEP OF IRON OXIDE REDUCTION FF3O1 -> FEO *********
      ELSEIF(F2(I,J,K) GE 0 111) AND (F2(I,J,K) LE 0 333))THEN
      HF(I,J,K)=HF2+(4 5*F2(I,J,K)-0 5)*(HF3-HF2)
      CF(I,J,K)=CF2+(4 5*F2(I,J,K)-0 5)*(CF3-CF2)
      KFO=HK2+(4 5*F2(I,J,K)-0 5)*(HK3-HK2)
C ********** WATER VAPOR CORRECTION ***********************
      S2=RP*(KRGF/DE)**0 5
      SH2=RP*(HKRGF/DEH)**0 5
      ESCF=(1-F2(I,J,K))**0 333
      SH2M=SH2*ESCF
      H2N=GH(I,J,K)/(1+RDE*(SH2M/TANH(SH2M)-1)*(1-ESCF+ESCF*DNS))
      RH=(1-H2N)/H2N
C ****************************************************
      WKHO=1/(1/WH2+(4 5*F2(I,J,K)-0 5)*(1/WH3-1/WH2))
      HKRGF=HK2*(1-RH/WH2)+(4 5*F2(I,J,K)-0 5)*(HK3*(1-RH/WH3)-
     1 HK2*(1-RH/WH2))
```

```fortran
1     KRGF=CK2*(1-RC/WC2)+(4 5*F2(I,J,K)-0 5)*(CK3*(1-RC/WC3)-
      CK2*(1-RC/WC2))
      IF(HKRGF LE 0 0001)THEN
      HKRGF=0 0001
      ENDIF
      IF(KRGF LE 0 0001)THEN
      KRGF=0 0001
      ENDIF
C     ********* 3RD STEP OF IRON OXIDE REDUCTION FEO -> FE *********
      ELSEIF(F2(I,J,K) GE 0 333)THEN
      HF(I,J,K)=HF3
      CF(I,J,K)=CF3
      KFO=HK3
C     ********* WATER VAPOR CORRECTION *********
      S2=RP*(KRGF/DE)**0 5
      SH2=RP*(HKRGF/DEH)**0 5
      ESCF=(1-F2(I,J,K))**0 333
      SH2M=SH2*ESCF
      H2N=GH(I,J,K)/(1+RDE*(SH2M/TANH(SH2M)-1)*(1-ESCF+ESCF*DNS))
      RH=(1-H2N)/H2N
C     *********
      WKHO=WH3
      KRGF=CK3*(1-RC/WC3)
      HKRGF=HK3*(1-RH/WH3)
      IF(HKRGF LE 0 0001)THEN
      HKRGF=0 0001
      ENDIF
      IF(KRGF LE 0 0001)THEN
      KRGF=0 0001
      ENDIF
      ENDIF
C     ********* REDUCTION KINETICS BY GRAIN MODEL *********
      S2=RP*(KRGF/DE)**0 5
      SH2=RP*(HKRGF/DEH)**0 5
      P2=1/(FG*(1-F2(I,J,K))**(1-1/FG))+(S2*S2/3)*
1     (1/((1-F2(I,J,K))** 333)-1)
      PH2=1/(FG*(1-F2(I,J,K))**(1-1/FG))+(SH2*SH2/3)*
1     (1/((1-F2(I,J,K))** 333)-1)
      DIVF=1+100*(F2(I,J,K)-0 95)
      IF(F2(I,J,K) GE 0 95)THEN
      DF2(I,J,K)=((GC*KRGF)/(DIVF*RHO*P2))*DT
      DF2H(I,J,K)=((GG*HKRGF)/(DIVF*RHO*PH2))*DT
      ELSE
      DF2(I,J,K)=((GC*KRGF)/(RHO*P2))*DT
      DF2H(I,J,K)=((GG*HKRGF)/(RHO*PH2))*DT
      ENDIF
      F2(I,J,K)=F2(I,J,K)+DF2(I,J,K)+DF2H(I,J,K)
      F2(I,J,K)=DF2(I,J,K)+DF2H(I,J,K)-PER*(NR-1)*F2(I-1,J,K)+
      (1-(-1)**NR*PER)*F2(I,J,K)-NR*PER*F2(I+1,J,K)
      ENDIF
C     REDUCTION KINETICS FOR NICKEL OXIDE (1)
C     *********
      IF(F1(I,J,K) LE 0 99) THEN
      KNO=6132*DEXP(-6 898/TS(I,J,K))
      KNO=9132*DEXP(-6 898/TS(I,J,K))
      IF(TS(I,J,K) LT 0 950)THEN
      kRGN=48180O*DEXP(-11 2/TS(I,J,K))
      ELSE
      KRGN=30*DEXP(-2/TS(I,J,K))
      ENDIF


      IF(HKRGN LE 0 0001)THEN
      HKRGN=0 0001
      ENDIF
C     ********* WATER VAPOR CORRECTION *********
      S1=RP*(KRGN/DE)**0 5
      SH1=RP*(HKRGN/DEH)**0 5
      ESC=(1-F1(I,J,K))**0 333
      SH1M=SH1*ESC
      H2N=GH(I,J,K)/(1+RDE*(SH2*ESC/TANH(SH2*ESC)-1)*(1-ESC+ESC*DNS))
      RH=(1-H2N)/H2N
      PPN=1/(H2**0 5*(1+2 71D-2*DEXP(5 838/TS(I,J,K))*RH**2))
      HKRGN=KNO*PPN
C     ********* REDUCTION KINETICS BY GRAIN MODEL *********
      S1=RP*(KRGN/DE)**0 5
      SH1=RP*(HKRGN/DEH)**0 5
      P1=1/(FG*(1-F1(I,J,K))**(1-1/FG))+(S1*S1/3)*
      (1/((1-F1(I,J,K))** 333)-1)
      PH1=1/(FG*(1-F1(I,J,K))**(1-1/FG))+((SH1**2)/3)*
      (1/((1-F1(I,J,K))** 333)-1)
      DF1(I,J,K)=((GC*KRGN)/(RHO*P1))*DT
      DF1H(I,J,K)=((GG*HKRGN)/(RHO*PH1))*DT
C     ********* MECHANISM FOR COMPLEX OXIDE REDUCTION *********
      IF(F2(I,J,K) LE 0 333)THEN
      DF1(I,J,K)=DF1(I,J,K)*F2(I,J,K)/0 333
      DF1H(I,J,K)=DF1H(I,J,K)*F2(I,J,K)/0 333
      ENDIF
      F1(I,J,K)=DF1(I,J,K)+DF1H(I,J,K)-PER*(NR-1)*F1(I-1,J,K)+
      (1-(-1)**NR*PER)*F1(I,J,K)-NR*PER*F1(I+1,J,k)
      ENDIF
30    CONTINUE
50    CONTINUE
      RETURN
      END
```

MHGCO

```
C
C
C
C
      ***************************************************
      GAS CONC. OF CO  CENTRAL IN R  BACKWARD IN Z
      ***************************************************
      ***************************************************
      SUBROUTINE MHGCO

$INCLUDE COVER.MH
      DIMENSION A(IM),B(IM),C(IM),D(IM),V(IM)
      DO 1000 K1=1,2
      DO 100 I=IS,IM
      DC=1.2475D-4*TG(I,M,K)**1.693
      DMI=DC*P
      TC=SLO**2/DMI
      DT=DELT/TC
      AZ=DT/(2*DZ**2)
      AR=DT/(2*DR**2)
      ARI=AR/(2*FLOAT(I))
      ROG=12.1R75/TG(I,M,K)
      RGN=RIIM*N1/(ROG*FCO)
      RGF=RIIM*N2/(ROG*FCO)
C                 ─────LOWER BOUNDARY CONDITION ZERO FLUX OR IMAGE POINT───
      A(M)=0.0
      IF((I.GE.1A).AND.(I.LF.1B))THEN
      C(M)=-AZ
      IF(I.LE.1A)THEN
      B(M)=1+ARI+AR+AZ
      D(M)=G(I,M,K)*(1-ARI-AR-AZ)+G(I,M+1,K)*AZ+
     1 2*G(I+1,M,K)*(AR+ARI)-RGN*DF1(I,M,K) RGF*DF2(I,M,K)
      F1SFIF(I.GE.IB)THEN
      B(M)=1-ARI+AR+AZ
      D(M)=G(I,M,K)*(1+ARI-AR-AZ)+G(I,M+1,K)*AZ+2*G(I-1,M,K)*(AR-ARI)
     1-RGN*DF1(I,M,k) RGF*DF2(I,M,k)
      FLSE
      B(M)=1+2*AR+AZ
      D(M)=G(I,M,k)*(1-2*AR-AZ)+G(I,M+1,K)*AZ+2*G(I-1,M,K)*(AR-ARI)
     1+2*G(I+1,M,K)*(AR+ARI) RGN*DF1(I,M,K)-RGF*DF2(I,M,k)
      ENDIF
      11SF
      B(M)=1.0
      C(M)=0.0
      D(M)=AG(k+1)
      ENDIF
C       ─── DISCRETIZED BY CRANK NICHOLSON CEN IN R,BW IN Z ───
      DO 300 J=M+1,LS
      DC=1.2475D-4*TG(I,J,K)**1.693
      DML=DC*P
      TC=SLO**2/DML
      DT=DELT/TC
      AR=DT/(2*DR**2)
      AZ=DT/(2*DZ**2)
      ARI=AR/(2*FLOAT(I))
      IF((I.GE.1A).AND.(I.LF.1B))THEN
      A(J)=-AZ
      C(J)=-AZ
      IF(I.LF.1A)THEN
      B(J)=1+ARI+AR+2*AZ
      D(J)=G(I,J,K)*(1-ARI AR-2*AZ)+
     1 2*(-(I+1,J.K)*(AR+ARI)+G(I,J-1,k)*AZ+G(I,J+1,K)*AZ
      R(N*DF1(I,J,K),IIGF*DF2(I,J,K)
      F1SEIF(I.GE.IB)THEN
      B(J)=1 ARI+AR+2*AZ
      D(J)=G(I,J,k)*(1+ARI-AR-2*AZ)+
     1 2*(-(I-1,J,k)*(AR ARI)+G(I,J-1,K)*AZ+G(I,J+1,K)*AZ
     2 RGN*DF1(I,J,k) RGF*DF2(I,J,k)
      FLSE
      B(J)=1+2*AR+2*AZ
      D(J)=G(I,J,k)*(1-2*AR-2*AZ)+
     1 2*G(I-1,J.k)*(AR-ARI)+2*G(I+1,J,k)*(AR+ARI)+
     2 G(I,J-1,k)*AZ+G(I,J+1,k)*AZ RGN*DF1(I,J,K) RGF*DF2(I,J,K)
```

```
      ENDIF
      ELSE
      A(J)=0.0
      B(J)=1.0
      C(J)=0.0
      D(J)=AG(K+1)
      ENDIF
300   CONTINUE
C                 ─────────── GAS PHASE MASS BALANCE ──────────
      DO 400 J=1,LS,LG
      IF(VR(I,J,K).GT.0.0)THEN
      NR=0
      ELSE
      NR=1
      ENDIF
      IF(VZ(I,J,K).GT.0.0)THEN
      NZ=0
      ELSE
      NZ=1
      ENDIF
      DC=1.2475D-4*TG(I,J,K)**1.693
      TC=SLO**2/DC
      DT=DELT/TC
      AR=DT/(2*DR**2)
      AZ=DT/(2*D7**2)
      ARI=AR/(2*FLOAT(I))
      PER=(VO*SLO*VR(I,J,K)*DT)/(2*DR*DM1)
      PEZ=(VO*SLO*VZ(I,J,K)*DT)/(2*DZ*DML)
      A(J)=(NZ-1)*PEZ-AZ
      C(J)=NZ*PEZ-AZ
      IF(I.LE.IS)THEN
      B(J)=1+(-1)**NR+NR-1)*(PFR-ARI)+(-1)**NZ*PFZ+AR+2*AZ
      D(J)=G(I,J,K)*(1-(-(-1)**NR+NR-1)*(PFR-ARI) ( )**N/*PI./-AR 2*A/)
     1+2*G(I+1,J,K)*(AR+ARI)+G(I,J-1,k)*(A/  PI./*(N/ 1))+
     2 G(I,J+1,K)*(AZ-N7*PEZ)
      ELSEIF(I.GE.IM)THEN
      B(J)=1+(-1)**NR+NR)*(PER-ARI)+(-1)**NZ*PFZ+AR+2*A7
      D(J)=G(I,J,K)*(1-(-1)**NR+NR)*(PER-ARI) ( )**N/*PEZ 2*AR+2*A7)+
     1 2*G(I-1,J,K)*(AR-ARI)*(PER-ARI)+G(I,J-1,k)*(AZ PFZ*(NZ-1))+
     2 G(I,J+1,K)*(AZ-NZ*PEZ)
      ELSE
      B(J)=1+(-1)**NR*(PFR-ARI)+(-1)**NZ*PFZ+2*AR+2*A7
      D(J)=G(I,J,K)*(1-(-1)**NR*(PFR-ARI) (-1)**N/*PEZ 2*AR-2*AZ)+2*
     1+G(I-1,J,K)*(AR (NR-1)*(PER-ARI))+2*G(I+1.J.k)*(AR NR*(PI R ARI))
     2 +G(I,J-1,K)*(AZ-PEZ*(NZ-1))+G(I,J+1,A)*(AZ N7*PI./))
      ENDIF
400   CONTINUE
C
      IF((I.LE.IS).OR.(I.GE.IM))THEN
      A(LG)=0.0
      B(LG)=1.0
      C(LG)=0.0
      D(LG)=G(I,LG-1,K)
      ELSE
      A(LG)=(NZ-1)*PEZ-AZ
      C(LG)=V(J)
      B(LG)=1+(-1)**NR*(PER-ARI)+((-1)**NZ+NZ)*PLZ+2*AR+AZ
      D(LG)=G(I,LG,K)*(1-(-1)**NR*(PER-ARI)-((-1)**NZ+N7)*PEZ-2*AR AZ)
     1+2*G(I-1,LG,K)*(AR-(NR-1)*(PER-ARI))+2*G(I+1 G.K)*
     2 (AR-NR*(PER-ARI))+G(I,LG-1 K)*(AZ-PEZ*(NZ-1))
      ENDIF
C
      CALL TRIDAG(A,B,C,D,V,M,LG)
      DO 42 J=M,LG
      G(I,J,K)=V(J)
      IF(G(I,J,K).LE.0.0)THEN
      G(I,J,K)=0.1
      ENDIF
42    CONTINUE
100   CONTINUE
      RETURN
      END
```

MHParam

```fortran
C   ****************************************************************
C      CALCULATION OF VOLUME AVERAGE VALUES AT DIFFERENT POSITIONS
C   ****************************************************************
C   ****************************************************************
      SUBROUTINE MHParam
$INCLUDE 'COVER MH'
      PMX=0 5*DELT/60 0
      ATG(K)=0 0
      AVZ(K)=0 0
      AGH(K)=0 0
      AG(K)=0 0
      DO I=IS,IM
      AF1(I,K)=0 0
      AF2(I,K)=0 0
      ATS(I,K)=0 0
      ENDDO
C   **************** FOR ODD HEARTHS ****************
      IF(NPM(K) GE 0 0)THEN
      DO 10 I=IS,IH+1,IM
      CNF=0 7854*(VZ(I-1,LG,K)+VZ(I,LG,K))*FLOAT(2*I-1)*DR**2
      ATG(K)=ATG(K)+CNF*(TG(I-1,LG,K)+TG(I,LG,K))
      AG(K)=AG(K)+CNF*(G(I-1,LG,K)+G(I,LG,K))
      AGH(K)=AGH(K)+CNF*(GH(I-1,LG,K)+GH(I,LG,K))
      AVZ(K)=AVZ(K)+2*CNF
      ENDDO
10    ATG(K)=ATG(K)/AVZ(k)
      AG(K)=AG(K)/AVZ(K)
      AGH(K)=AGH(K)/AVZ(K)
      AVZ(k)=0 31831*AVZ(K)/(DR**2*FLOAT(IG*(2*IM-IG)))
C   ****************************************************************
      DO 25 I=IA,IB
      DO J=M,LS
      AF1(I,K)=AF1(I,K)+F1(I,J,K)/(LS-M+1)
      AF2(I,K)=AF2(I,K)+F2(I,J,K)/(LS-M+1)
      ATS(I,K)=ATS(I,K)+TS(I,J,K)/(LS-M+1)
      ENDDO
      F1O(K)=AF1(IA,K)
      F2O(K)=AF2(IA,K)
      TSH(K)=ATS(IA,K)
      DO J=M,LS
      F1(I,J,K)=F1(I,J,K)*(1-PMX)+PMX*AF1(I,K)
      F2(I,J,K)=F2(I,J,k)*(1-PMX)+PMX*AF2(I,K)
      TS(I,J,K)=TS(I,J,K)*(1-PMX)+PMX*ATS(I,K)
      ENDDO
      ENDDO
25 C
      ATG(K)=(ATG(K)*VOL(K)+TIG*ADV(K-1))/VOL(K-1)
      AGH(K)=(AGH(K)*VOL(K)+GHI*ADV(K-1))/VOL(K-1)
      AG(K)=(AG(K)*VOL(K)+GI*ADV(K-1))/VOL(K-1)
C   ************ FOR EVEN HEARTHS ****************
      ELSE
      DO 30 I=IS+1,IS+IG
      CNF=0 7854*(VZ(I-1,LG,K)+VZ(I,LG,K))*(2*I-1)*DR**2
      ATG(K)=ATG(K)+CNF*(TG(I-1,LG,K)+TG(I,LG,K))
      AG(K)=AG(K)+CNF*(G(I-1,LG,K)+G(I,LG,K))
      AGH(K)=AGH(K)+CNF*(GH(I-1,LG,K)+GH(I,LG,K))
      AVZ(K)=AVZ(K)+2*CNF
      ENDDO
30    ATG(K)=ATG(K)/AVZ(K)
      AG(K)=AG(K)/AVZ(K)
      AGH(K)=AGH(K)/AVZ(K)
      AVZ(K)=0 31831*AVZ(K)/(DR**2*IG*(2*IS+IG))

C
      DO 35 I=IA,IB
      DO J=M,LS
      AF1(I,K)=AF1(I,K)+F1(I,J,K)/(LS-M+1)
      AF2(I,K)=AF2(I,K)+F2(I,J,K)/(LS-M+1)
      ATS(I,K)=ATS(I,K)+TS(I,J,K)/(LS-M+1)
      ENDDO
      F1O(K)=AF1(IB,K)
      F2O(K)=AF2(IB,K)
      TSH(K)=ATS(IB,K)
      DO J=M,LS
      F1(I,J,K)=F1(I,J,K)*(1-PMX)+PMX*AF1(I,K)
      F2(I,J,K)=F2(I,J,K)*(1-PMX)+PMX*AF2(I,K)
      TS(I,J,K)=TS(I,J,K)*(1-PMX)+PMX*ATS(I,K)
      ENDDO
      ENDDO
35 C
      ATG(K)=(ATG(K)*VOL(K)+TIG*ADV(K-1))/VOL(K-1)
      AGH(K)=(AGH(K)*VOL(K)+GHI*ADV(K-1))/VOL(K-1)
      AG(K)=(AG(K)*VOL(K)+GI*ADV(K-1))/VOL(K-1)
      ENDIF
      RETURN
      END
```

Bibliography

[1] J. C Nayak. *Trans Ind. Inst Metall.*, 44(3) 195, 1991.

[2] G N. Banerjee, H. K. Tripathy, J N. Mohanty, D. K Dey, A. K. Jouhari, and D N. Dey *Trans Ind. Inst. Metall*, 47(1)·21, 1994.

[3] M G. Bodas and D. D Akerkar. *Trans Ind. Inst Metall*, 44(6):433, 1991.

[4] B N Singh, M S Mohanty, D D Akerkar, and V A. Altekar. *Trans. Ind. Inst Metall*, 35(4).357, 1982.

[5] M O. Pearce. *Int. J. of Min Processing*, 19(1 to 2) 5, 1987.

[6] T. Watanabe, S. Ono, S. Arai, and T. Matsumori *Int. J. of Min. Processing*, 19(1 to 2):173, 1987.

[7] K. Yamada and T. Hiyama *Int. J. of Min. Processing*, 19(1 to 2):215, 1987.

[8] J. G. Reid Hydrometall research development and plant practice. In K. Osseo-Asare and J. D. Miller, editors, *3rd Int Symposium on Hydrometall., SME/AIME*, page 109, Atlanta, Gorgia, 1983.

[9] H. S. Ray, R. Sridhar, and K P Abraham *Extraction of Nonferrous Metals*. EWP Affiliated East-West Press, New Delhi, 1985

[10] T Utigard and R. A Bergman RA *Metall. Trans. B*, 23B:271, 1992.

[11] J Onodera, T. Inoue, and T. Imaizumi *Int J. of Min. Processing*, 19(1 to 2):25, 1987.

[12] A Cores, A. Formoso, M T Larrea, and J. Ortiz. *Ironmaking and Steelmaking*, 16(6):446, 1989.

[13] C. H P Lupis. *Chemical Thermodynamics of Materials*. Elsevier Sci. Pub., North - Holland, 1983.

[14] S Samanta, R. N Misra, and P P Bhatnagar *Trans. Ind. Inst. Metall.*, 21(3)·5, 1968.

[15] J O Edström *J Iron Steel Inst*, 175·289, 1953.

[16] T E Dancy *Scand J Metall*, 22.100, 1993

[17] J Szekely and J W Evans. *Metall. Trans.*, 2.1699, 1971

[18] J. Szekely, C I. Lin, and H. Y Sohn. *Chem Engng. Sci*, 28:1975, 1973.

[19] H. Y Sohn and D. Kim. *Metall. Trans. B*, 15B 403, 1984.

[20] J. Bandrowski, C R Bickling, K. H. Yang, and O. A Hougen. *Chem. Engng Sci. 1962*, 17 379, 1962.

[21] W. Pluschkell, Drtmund, and B. V. S Sarma. *Arch Eisenhuttenewes*, 45.23, 1974.

[22] J Szekely and C. I. Lin *Metall. Trans. B*, 7B 493, 1976.

[23] E T. Turkdogan and J. V Vinters. *Metall. Trans B*, 2·3175, 1971.

[24] W. M. Mckewan. *Trans Met. Soc. AIME.*, 218:2, 1960.

[25] A J. Wilhelem and G. R S Piere. *Trans. Met. Soc. AIME.*, 221.1186, 1961

[26] N J. Themelis and W H Gauvin. *A.I Ch.E. J.*, 8(4):437, 1962.

[27] J. Szekely and A. Hastaoglu *Inst. Min. and Metall*, page C78, 1976.

[28] D. S. Clark and W. R. Varney *Physical Metallurgy for Engineers* EWP an East-West Edition, New Delhi, 1962

[29] V Raghavan. *Materials Science and Engineering* Prentice Hall of India Pvt.Ltd, New Delhi-110001, 1990.

[30] M. Kawahara, J. M Toguri, and R A. Bergman. *Metall Trans. B*, 19B:181, 1988.

[31] F T. D. Silva. *Min Proc. Extr. Metall Rev.*, 9:97, 1992

[32] H Y. Sohn HY and J. Szekely. *Chem. Engng. Sci*, 27:763, 1972

[33] F. Habasi. *Principles of Extractive Metallurgy*, volume 1. Gordon and Breach Sci. Pub., New York, 1969.

[34] H. Y Sohn. *Metall. Trans. B*, 9B·89, 1978.

[35] J W Evans and M. G. Ranade *Chem. Engng. Sci.*, 35 1261, 1980.

[36] M G Ranade and J. W Evans *Ind. Eng. Chem Process Des. Dev.*, 19:118, 1980

[37] M Ishida and C. Y Wen *A I.Ch E J*, 14(2) 311, 1968.

[38] J. M Ausman and C C Watson *Chem Engng Sci · 1*, 17 323, 1962.

[39] Y K Rao Gas solid reaction Unpublished Lecture Notes, 1982

[40] D. Bandyopadhyay, N. Chakraborti, and A. Ghosh *Steel Res.*, 59·537, 1988

[41] D. Bandyopadhyay, N. Chakraborti, and A. Ghosh. *Steel Res.*, 62:143, 1991

[42] M H. Caron *J of Metals, Trans AIME· 1950·*, 188 67, 1950.

[43] R Schrader, D Loewe, and C Sehmenn. *Neue Huette*, 11(5)·263, 1966

[44] J Jandova and M. Pedlik *Hydrometallurgy*, 35:123, 1994

[45] I. N. Bhattacharya, S. Anand, S. C Das, and R. P. Das *Trans. Ind. Inst. Metall.*, 42(4)·385, 1989.

[46] Johnston JD : U Im SJ. *Extractive Metallurgy Recent Advances* Noyes Data Corporation, Park Ridge, New Jersey, USA, 1976

[47] Im SJ Dubeck M *Extractive Metallurgy Recent Advances.* Noyes Data Corporation, Park Ridge, New Jersey, USA, 1976.

[48] J W. Evans and S. Song. *Ind Eng. Chem. Process Des Dev*, 13(2):146, 1974.

[49] R. F Benenati and C B Brosilow. *A.I Ch.E J.*, 8(3)·359, 1962.

[50] J Szekely and J. J. Poveromo. *A I.Ch E J.*, 21(4):769, 1975.

[51] G S. Gupta, N. Chakraborti, and T Sundararajan. *Metall. Trans. B*, 20B:925, 1989

[52] S. Saharoy, B. Sarma, T. Sundararajan, and N. Chakraborti *Scand. J Metall.*, 21:27, 1992.

[53] R. P. Das and D. N. Dey. Private Communication, 1992.

[54] Joint committee on powder Diffraction Standards. *Powder Diffraction file. Inorganic volume* JCPDS, International Center for Diffraction Data, 1601 Park Lane, Swarthmore, Pennsylvania - 19081, 1974.

[55] D Bandhyopadhyay PhD thesis, Indian Inst. Tech , Kanpur, 1988.

[56] H G. Geiger and D. R Poirier. *Transport Phenomena in Metallurgy.* Addison-Wesley, Massachusetts, California, 1973.

[57] A I Vogel *Quantitative Inorganic Analysis*. ELBS Pub., London, 1961

[58] J M. Quests, M E. Wadsworth ME, and J. R. Lewis. *Trans. Met Soc. AIME.*, 221:1186, 1961

[59] R B Bird, W. E Stewart, and E N. Lightfoot *Transport Phenomena* John Wiley, New York, 1963

[60] J R. Welty, C. E. Wicks, and R. E. Wilson. *Fundamentals of Momentum, Heat and Mass Transfer· John Wiley & Sons: 1984*. Mass Transfer: John Wiley & Sons· 1984, New York, 1984.

[61] H. Y Sohn and J. Szekely *Chem. Engng. Sci.*, 29 630, 1974.

[62] S Srinivasan and L I Staffanson. *Scand. J. Metall* , 17 281, 1988

[63] W M. McKewan. *Trans Met Soc AIME* , 221:140, 1961

[64] N A Warner. *Trans Met. Soc AIME·*, 230 163, 1964

[65] G. Bitsianes and T L Joseph. *Transactions AIME Dec*, page 1641, 1953.

[66] J Szekely *Metall. Trans B*, 19B.525, 1988.

[67] S. Ergun *Chem Eng. Prog* , 48 89, 1952

[68] S Irmay *Trans. Am Geophys Union*, 39·702, 1958.

[69] I Muchi, S. Asai, and M. Kuwabara *Memoirs of the Faculty of Engng., Nagoya University*, 39(1).92, 1987.

[70] J. Radestock and R. Jeschar. *Stahl Eisen.*, 22·1249, 1970.

[71] V Stanek and J. Szekely *A.I Ch E. J.*, 20(5).974, 1974.

[72] J Szekely. *Fluid Flow Phenomena in Metals Processing*. Academic Press, New York, 1979.

[73] A. Das, D. J. Kinneberg, N. Chakraborti, and J. D Miller. *Scand. J Metall.*, 21:27, 1992

[74] W H. Press, S. A. Teukolsky, W T Vitterling, and B P Flannery. *Numerical Receipies in Fortran* Cambridge University Press, 1992

[75] Y Jaluria and K. E. Torrance *Computational Heat transfer* Hemisphere Pub Corp., Washington, 1986.

[76] C W. Hirt. *J. of Comp. Physics*, 2 339, 1968

[77] D Greenspan *The Computer J.*, 12.88, 1969

[78] D. C Thoman and A A Szewczyk. Technical report, Indiana USA, 1966

[79] O Kubaschewski and C B Alcock *Metallurgical Thermochemistry* Pergamon Press, Oxford, UK, 1979

[80] W M McKewan *Trans Met. Soc AIME.*, 224.2, 1962.

[81] A Kivnick and A N Hixon. *Chem. Eng Prog*, 48·394, 1952.

[82] G Parravano *J. Am Chem. Soc.*, 74·1194, 1952

[83] D. Fretty PhD thesis, Universiti de Lyon, 1969

[84] F. Chiesa and M Rigaud *Can. J. Chem. Engng*, 49 617, 1971

[85] W. Hockings. In *Proceedings AIME Blast Furnace, Coke Oven and Raw Materials Conference*, volume 19, page 170, 1960.

[86] K Shehata and S. Ezz. *Trans Inst. Min. Met.*, 82:C38, 1973.

[87] K O. Yu and P. P. Gills *Metall Trans B, Vol*, 12B:111, 1981.

[88] P. C Hayes. *Metall. Trans. B*, 10B:211, 1979

[89] E S. Vorontsov and V. D. Suikovskaya *Izv. Vissh Ucheb Zaved Chern Met.*, 12(5), 1969.

[90] J H. Krasuk and J. M. Smith. *A I.Ch E. J.*, 18(3) 506, 1972.

[91] R. Benesch, M. Janowski, and A Ledzki. *Scand. J Metall.*, 3:236, 1974.

[92] M. Et-Tabirou, B. Dupre, and C Gleitzer. *Metall. Trans B*, 19B 311, 1988.

[93] E Bicknese and R. Clark *Trans. Met. Soc. AIME.*, 236:2, 1966.